Claudio Mancuso
Cristina Jommi
Francesca D'Onza
Editors

Unsaturated Soils: Research and Applications 1

Springer

Unsaturated Soils: Research and Applications

Claudio Mancuso, Cristina Jommi,
and Francesca D'Onza (Eds.)

Unsaturated Soils: Research and Applications

Volume 1

Springer

Editors
Claudio Mancuso
Department of Hydraulic, Geotechnical and Environmental Engineering
Università degli Studi di Napoli Federico II
Napoli
Italy

Francesca D'Onza
Department of Hydraulic, Geotechnical and Environmental Engineering
Università degli Studi di Napoli Federico II
Napoli
Italy

Cristina Jommi
Department of Structural Engineering
Politecnico di Milano
Milano
Italy

ISBN 978-3-642-31115-4 e-ISBN 978-3-642-31116-1
DOI 10.1007/978-3-642-31116-1
Springer Heidelberg New York Dordrecht London

Library of Congress Control Number: 2012940418

Printed on acid-free paper

Springer is part of Springer Science+Business Media (www.springer.com)

Preface

These volumes contain the proceedings of the Second European Conference on Unsaturated Soils, E-UNSAT 2012, held in Napoli, Italy, in June 2012. The event is the second of a series of European conferences, born on initiative of the researchers involved in the EU FP6 MUSE – Mechanics of Unsaturated Soils for Engineering – Research and Training Network, and follows the first successful one, organised in Durham, UK, in 2008. The conference series was then supported by Technical Committee 106 of the International Society of Soil Mechanics and Geotechnical Engineering on Unsaturated Soils, which is very active in promoting new opportunities to bring together researchers and practitioners to share advances in unsaturated soils mechanics and related engineering applications.

A collection of more than one hundred papers is included in these volumes, addressing the three thematic areas *experimental*, including advances in testing techniques and soil behaviour, *modelling*, covering theoretical and constitutive issues together with numerical and physical modelling, and *engineering*, focusing on approaches, case histories and geo-environmental themes. The areas of application of the papers embrace most of the geotechnical problems related to unsaturated soils. Increasing interest in geo-environmental problems, including chemical coupling, marks new perspectives in unsaturated soil mechanics. We hope this book will provide a valuable up-to-date reference across the subject for both researchers and practitioners.

The published contributions, coming from fourteen European countries and another fourteen countries all around the world, were selected after a careful peer-review process. We would like to acknowledge the work done by the reviewers, for their fundamental contribution in assuring the quality of the published papers. We also gratefully acknowledge our colleagues from the Organising and the Technical Advisory Committees and the Authors for the valuable help they provided towards the outcome of the Conference. Special thanks are due to Dr. Marco Caruso, who took charge of the final layout of the publication.

The Conference has been endorsed by the Università di Napoli Federico II, and by the Politecnico di Milano. We thank the Italian Geotechnical Society – AGI –for supporting the initiative in the National and the International community.

It is, with a sort of romantic attitude, that we acknowledge valued contributions from all the continents, which reminds us of the role played by Napoli in joining cultures and peoples during its long lasting history of more than twenty-eight centuries.

Claudio Mancuso
Cristina Jommi
Francesca D'Onza

Committees

Conference Chair

Claudio Mancuso	Università degli Studi di Napoli Federico II
Cristina Jommi	Politecnico di Milano

Organizing Committee

Marco Caruso	Politecnico di Milano
Manuela Cecconi	Università degli Studi di Perugia
Gabriele Della Vecchia	Politecnico di Milano
Anna D'Onofrio	Università degli Studi di Napoli Federico II
Francesca D'Onza	Università degli Studi di Napoli Federico II
Marco V. Nicotera	Università degli Studi di Napoli Federico II
Luca Pagano	Università degli Studi di Napoli Federico II
Giacomo Russo	Università degli Studi di Cassino
Anna Scotto di Santolo	Università degli Studi di Napoli Federico II
Giuseppe Sorbino	Università degli Studi di Salerno
Donatella Sterpi	Politecnico di Milano
Gianfranco Urciuoli	Università degli Studi di Napoli Federico II
Roberto Vassallo	Università degli Studi della Basilicata

International Advisory Committee

Eduardo Alonso	Spain
Michael Bardanis	Greece
Geoff E. Blight	South Africa
Leonardo Cascini	Italy
Robert Charlier	Belgium
Yu-Jun Cui	France
Tacio M.P. de Campos	Brazil
Pierre Delage	France

Augusto Desideri	Italy
Aldo Evangelista	Italy
Delwyn G. Fredlund	Canada
Domenico Gallipoli	U.K.
Kazimierz Garbulewski	Poland
Behrouz Gatmiri	France
Antonio Gens	Spain
Ghassem Habibagahi	Iran
Laureano Hoyos	U.S.A.
Emoke Imre	Hungary
Nasser Khalili	Australia
Suhail A.A. Khattab	Iraq
Lyesse Laloui	Switzerland
Fernando Marinho	Brazil
David Mašín	Czech Republic
Farimah Masrouri	France
Gerald A. Miller	U.S.A.
Charles Ng	China
Luciano Oldecop	Argentina
Luciano Picarelli	Italy
Harianto Rahardjo	Singapore
Enrique Romero	Spain
Marcelo Sanchez	U.S.A.
Tom Schanz	Germany
Daichao Sheng	Australia
Sarah M. Springman	Switzerland
Alessandro Tarantino	U.K.
David G. Toll	U.K.
Hirofumi Toyota	Japan
Sai K. Vanapalli	Canada
Jean Vaunat	Spain
Simon Wheeler	U.K.
Tony L.T. Zhan	China

TC 106 COMMITTEE ON UNSATURATED SOILS

The TC106 Committee of the ISSMGE plays a leading role in the promotion of the series of international and regional UNSAT conferences, assisting with technical programs. The Committee promotes cooperation and exchange of knowledge in unsaturated soils including compacted, expansive, collapsible, arid, and residual soils.

Organised by:

Under the auspices of:

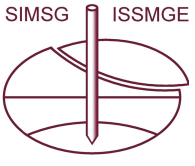

Contents

Experimental

Advances in Testing Techniques

Microstructure and Hydraulic Behaviour

EXPERIMENTAL

Advances in Testing Techniques

A Double Cell Triaxial System for Unsaturated Soils Testing

Joao Mendes, David G. Toll, and Fred Evans

Abstract. The presence of different pore fluids present in unsaturated soils (water and air) complicates the measurement of sample volume change. Since volume change of the air phase is difficult due to the compressibility of the fluid, it becomes necessary to measure sample volume change by measuring the change in volume of water in the surrounding triaxial cell. This paper introduces and assesses a new double cell triaxial cell developed by Wykeham Farrance. The design of the new triaxial system is similar to the Wheeler modified triaxial cell (Wheeler, 1988) but uses a glass inner cell wall, to avoid problems of absorption of water by Perspex. Furthermore, the cell has been designed to use a high capacity suction probe that can be fitted through the base pedestal. Issues of de-airing the cell and the accuracy of volumetric measurements that can be achieved are discussed in the paper.

Keywords: unsaturated soils, volume measurements, soil suction.

1 Introduction

The traditional method for sample volume change used in triaxial testing of saturated soils involves measuring the pore fluid that leaves or enters the sample. This is no longer sufficient in an unsaturated soil as water volume and sample volume

Joao Mendes
The University of Newcastle, Newcastle, Australia
e-mail: Joao.Mendes@newcastle.edu.au

David G. Toll
Durham University, Durham, UK
e-mail: d.g.toll@durham.ac.uk

Fred Evans
Wykeham Farrance Division, Controls Testing Equipment Ltd, Tring, UK
email: Fred.Evans@controlstesting.co.uk

are not linked. To monitor volume change of unsaturated samples the simplest arrangement is to monitor the volume of the fluid (i.e. water) that leaves or enters the triaxial cell (Bishop & Donald, 1961). If a single wall Perspex cell, i.e. the traditional triaxial system, is used this indirect method to monitor the volume of fluid is not reliable due to volume variations in the Perspex part of the cell. These changes are due to cell volume changing with cell pressure, water absorption and thermal expansion (Wheeler, 1988) as well as creep of the cell under constant cell pressure. Although small, these changes still impose significant errors. In this paper a new double cell triaxial system is presented that can be used for triaxial testing of unsaturated soils.

2 The Design of the New Double Cell Triaxial Cell

To overcome the difficulties when using a traditional triaxial cell, a double cell is preferred, such as is shown in Figure 1, developed by the Wykeham Farrance Division of Controls Testing Equipment Ltd. The cell volume resulting from changes in cell pressure is greatly reduced by having two cells since the inner cell is subject to equal pressures on both sides of the cell wall. The Wykeham Farrance (WF) design is similar to the Wheeler cell (Wheeler, 1988). However, the WF double cell system differs from the Wheeler cell by having an interior cell wall made of glass instead of Perspex; with the intention to eliminate the water absorption by the wall of the inner cell. The WF equipment is double celled (rather than doubled walled), meaning that the top cap of the inner cell is also subjected to equal pressures inside and out. In earlier designs a double walled cell was trialled, where a common top cap was used for inner and outer cells. It was found that extensions of the tiebars produced volume changes that could affect results.

The biggest difference between the new system and other testing systems found in the literature is the ability to install a DU-WF high capacity suction probe in the pedestal in order to measure matric suction, as shown in figure 2. Since suction probes can cavitate during testing, the pedestal was designed to allow the user to remove/insert the probe while a test is underway. Information on the suction probe design and operation can be found in Lourenco et al (2006) with specific information about the use with the new double cell triaxial cell given in Mendes (2011).

The dimensions of the double cell triaxial cell are presented in table 1 and the cell components are shown in Figure 1b) and c). The inner cell can accomodate samples with diameters from 38mm up to 100mm. The loading ram passes through both outer and inner cell tops; there is no need for separate outer and inner ram arrangements, as is needed in some other systems.

Table 1. Dimensions of the double cell triaxial cell.

Height	41.6	cm
Inner cell inner diameter	19	cm
Inner cell outer diameter	20	cm
Outer cell inner diameter	22.35	cm
Volume of water in the inner cell	11795	cm^3
Volume of water in the outer cell	3252	cm^3

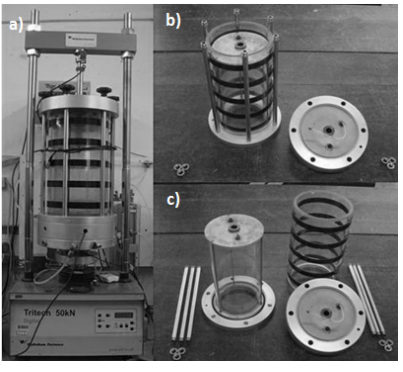

Fig. 1. Wykeham Farrance double cell triaxial system a) fully assembled, b) without outer cell top cap and c) view of the inner cell.

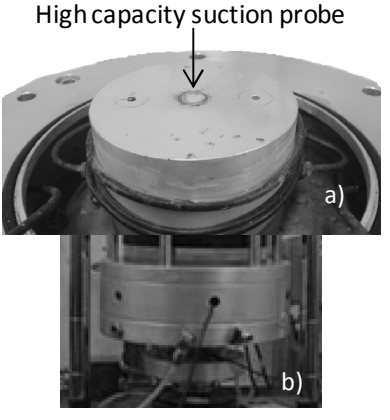

Fig. 2. a) Close up view of the 100mm pedestal on the triaxial frame, b) Access to remove/insert the probe below the cell base

3 Calibration of the New Double Cell Triaxial Cell

Calibrations were preformed on the WF double cell triaxial cell for creep under a constant pressure. The inner and outer cells were filled with de-aired water and afterwards a constant pressure of 600kPa was applied in both cells. The pressure was maintained for an extended period (weeks) to observe and quantify possible creep of the inner cell. Later, pressure cycles were performed to verify the volume changes due to pressure changes. A volume gauge of the rolling bellofram type device developed at Imperial College was used for the measurement of volume water exchanges in the inner cell (Maswoswe, 1985), while the confining pressure was imposed by a stepper motor driven hydraulic pump built by Wykeham Farrance. No specimen was used during testing.

A full view of the test can be observed in figure 3. During the tests it was observed that at a constant pressure of 600 kPa there was a small flow of water entering the inner cell ranging between 0.0016 to 0.0027 cm^3/hour and during the total duration of the test (almost 3 months) a total volume increase of 2.5cm^3 was observed inside the inner cell.

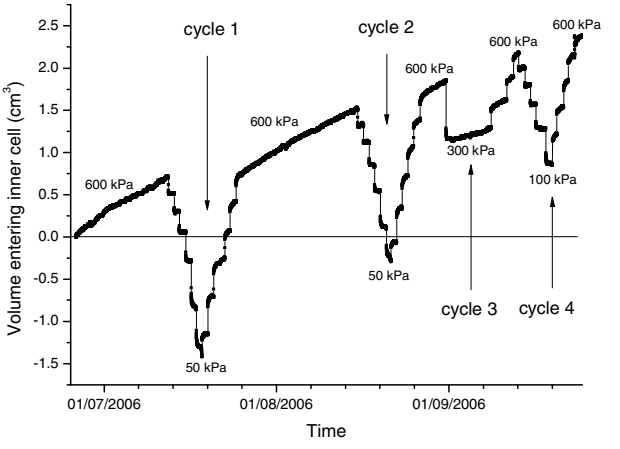

Fig. 3. Volume changing of the inner cell as a response to pressure.

Pressure cycles were performed by changing the pressure initially starting from 600 kPa, then decreasing in increments of 100 kPa down to 100 kPa with a further reduction of 50 kPa and then increasing back to 600 kPa at the same rate. These cycles had the intention of observing the reaction of the cell to pressure changes but also to attempt to estimate the flow rates for other pressures. During the pressure cycles a fixed flow rate was not achieved as the cell did not reach an equilibrium state; however, the flow rates generated were extremely low reaching a maximum 0.0042 cm^3/hour for a confining pressure of 400kPa during the 4^{th} cycle. Nevertheless, the creep effect observed on the double cell triaxial cells was found to be minimal, as low as 0.0008 cm^3/hour reaching a maximum of 0.0042 cm^3/hour. During triaxial testing this creep effect would have: during 3 months of testing at constant pressure a maximum increase of the measurement by 9 cm^3 and, during 24 hours (such as a shearing stage) a maximum increase by 0.1 cm^3. When compared with the volume of sample with 100mm in diameter by 200mm in height (1571 cm^3) this represents an error of 0.6% for the period of 3 months and as low as 0.006% for 24 hours.

The calibration also included the effect of volume changing due to the penetration of the loading shaft into the inner cell. The piston was pushed inside the inner cell increasing its volume inside the inner cell. The load cell was lowered by 8mm inside the inner cell at a rate of 0.05 mm/min and maintaining a constant pressure of 1500 kPa, as presented graphically in Figure 4. This meant that, considering the diameter of the shaft of the load cell as 25 mm, where each millimetre of travel from part of the piston represents an increase 0.49 cm^3, a displacement of 3.93 cm^3 of water exiting the inner cell should have been observed. In fact, the measured volume was slightly higher, 4.24 cm^3, resulting in a difference of 0.31 cm^3.

The volume was measured using a volume gauge using a bellofram seal where, for a good operation of this system, it is necessary to ensure that no air bubbles are trapped inside. It is possible that the differences between measured and expected values in Figure 4 could be related with the performance of the volume gauge

itself, perhaps due to poor de-airing. Another factor could be the change in direction of the volume gauge. When the cell is being pressurised, the water flow will be entering the cell. However, when the loading piston is entering the inner cell at a constant pressure, the flow of water will be exiting the cell and this change could explain why the volume gauge lags in response. In summary, the change in direction of the water flow could possibly result in the differences between the predicted and measured values. In any case, the observed changes in volume were minimal.

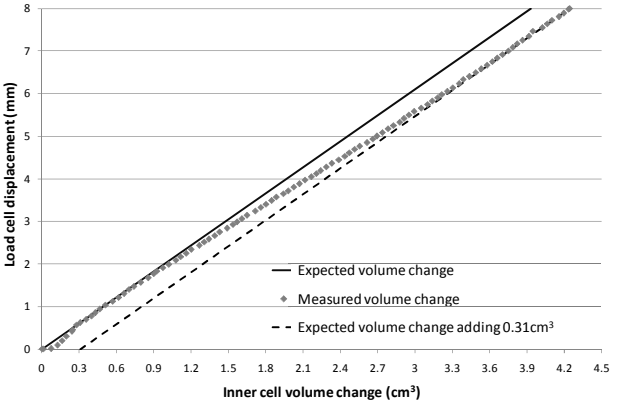

Fig. 4. Volume change originated by the displacement of the load cell entering the inner cell.

4 Other Observations about the WF Double Cell

One important deficiency encountered while testing with the WF double cell was the design of the top caps in both the inner and outer cells. It was found that a substantial volume of air was always trapped in the top of both cells when filling the cell. Applying a small vacuum at the top of the inner cell during filling can help with removing air bubbles, but it does not remove them entirely. Since the volumetric measurement is made indirectly, having air bubbles trapped will affect greatly the obtained results. However, if the cell is pressurised the air bubbles are compressed and eventually dissolve in the water. The effect of the air bubbles was observed during calibration. In Figure 3 the volume was still changing inside the cell at a constant pressure of 600 kPa even after a month period. This could mean that the air bubbles were still being compressed into solution even after such a long equalisation period. Nevertheless, providing the pressure remains constant through the test the effects of initial air bubbles on the volumetric measurement can be neglected. To overcome the problem of air being trapped an intermediate solution is to pressurise the cell while maintaining the sample net stress close to zero so no deformation (consolidation) of the sample can occur.

Initially it was intended to use only one hydraulic pump to pressurise both cells. However, some increase in pressure in the outer cell was observed when the load cell was entering the inner cell. This increase in pressure in the outer cell, while maintaining the pressure constant in the inner cell endangered the glass wall of the inner cell. To avoid failure of the glass wall, both cells were separated by a valve and a second pump was installed. The cause of the pressure rise in the outer cell was not fully identified, but it was thought to be due to sticking of the volume gauge allowing a differential pressure to build up between the pressure at the base of the gauge (feeding the outer cell) and the top (feeding the inner cell).

5 Conclusions

In this work a new double cell triaxial system developed by Wykeham Farrance (Controls Equipment Testing Ltd) was assessed. The double cell arrangement enables more accurate measurement of the volume change of samples when carrying out tests on unsaturated soils. The observed creep developed at constant pressure was found to be minimal for long and short duration triaxial tests as was the influence of the volume changes generated by the load cell movement inside the inner cell. However, problems were encountered with the design of top caps of both cells (inner and outer) where air can be easily trapped; this can be minimized by pressurizing the cell and sample (so net stress remains equal to zero) in order to dissolve the air into water.

Two features makes the Double Cell Triaxial System a suitable piece of equipment to carry out triaxial tests on unsaturated samples: (i) the wall of the inner cell being made in glass eliminated the water absorption problem identified in cell walls built in Perspex and (ii) the placement of a high capacity suction probe in the pedestal enabled pore water pressure measurements directly in the sample which could be replaced during testing if the device cavitated.

References

Bishop, A.W., Donald, I.B.: The experimental study of partly saturated soils in the triaxial apparatus. In: Proc. 5th Int. Conf. Soil Mech. Found. Engng, Paris, vol. 1, pp. 13–21 (1961)

Lourenço, S.D.N., Gallipoli, D., Toll, D.G., Evans, F.D.: Development of a commercial tensiometer for triaxial testing of unsaturated soils. In: 4th Int. Conf. on Unsaturated Soils, Carefree-USA, Geotechnical Special Publication No. 14, vol. 2, pp. 1875–1886. ASCE, Reston (2006)

Maswoswe, J.: Stress path for a compacted soil during collapse due to wetting. PhD thesis, Imperial College, London (1985)

Mendes, J.: Assessment of the Impact of Climate Change on an Instrumented Embankment: An unsaturated soil mechanics approach. PhD thesis, Durham University (2011)

Wheeler, S.: The Undrained Shear Strength of Soils Containing Large Gas Bubbles. Geotechnique 38(3), 397–413 (1988)

Performances of Two High Capacity Tensiometers

Claudio Mancuso, Marco V. Nicotera, and Raffaele Papa

Abstract. Two High Capacity Tensiometers (HCT) have been developed at the University of Napoli Federico II (UNINA) using a design layout similar to that of Ridley and Burland (1993). One of the HCT includes a O-ring sealing and a high air-entry value disk (HAEV) to protect a water-saturated measurement chamber from desaturation. The second one eliminates the O-ring in the attempt to enhance the time-response and improve the mechanical design for the calibration in the "negative" pressure range. Two different pre-conditioning devices have been developed to water-saturate the HAEV and the measurement chamber. The HCT may also be calibrated in the same chamber by applying positive values of water pressure to the first prototype, and positive value of air pressure, to the second prototype, for 'negative' calibration. A number of free evaporation tests and matric suction measurements against preconditioned soil samples are presented in the paper and discussed in order to highlight the performances of the two HCTs.

Keywords: HCT, suction measurement, unsaturated soils, calibration, evaporation tests.

1 Introduction

The main factors that qualify the performance of a High Capacity Tensiometer (HCT) are the measurement duration and the maximum value of suction reached

Claudio Mancuso
Università di Napoli Federico II, Napoli, Italy
e-mail: mancuso@unina.it

Marco V. Nicotera
Università di Napoli Federico II, Napoli, Italy
e-mail: nicotera@unina.it

Raffaele Papa
Università di Napoli Federico II, Napoli, Italy
e-mail: rafpapa@unina.it

prior to cavitation. The elements that govern these factors are strongly linked: the measuring chamber (size, absence of superficial irregularities on the chamber wall, level of saturation); the porous stone (at least 5 bar AEV, perfect saturation); the materials used to manufacture the instrument. It has been shown by Ridley & Burland (1993) that the maximum sustainable suction of a HCT is strictly a function of the air entry value of the ceramic disk provided the ceramic disk is adequately saturated. If this is not the case, there are other sub-experimental factors that make the tensiometer difficult to set-up. Therefore, the mechanical design of HCT plays a crucial role because it influences its robustness, sensitivity, ease of saturation, speed of response and the sustainability of large suction measurements (Take & Bolton, 2003).

2 First Prototype of UniNa HCT

The first prototype of High Capacity Tensiometer (Rojas et al., 2008) has been developed at University of Naples Federico II using a design layout similar to that initially proposed by the Imperial College of London (Ridley & Burland, 1993), with the introduction of some modifications. The instrument was composed of (Fig. 1): an interchangeable filter cup containing a HAEV ceramic disk of 6.0 mm in height inserted into stainless steel housing; a water reservoir of 3 mm^3 in volume; an integral strain-gauged diaphragm embedded in a brass housing; a vented waterproof sheathing to protect the electrical connections.

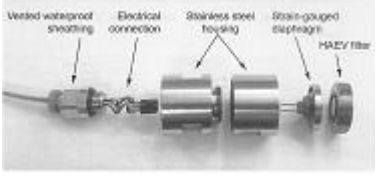

Fig. 1. First prototype of Unina High capacity tensiometer, (Rojas et al., 2008).

The measuring chamber was inspectable and this allowed to eliminate a greater number of imperfections; one stainless steel housing was used to hold the diaphragm and the other one was used to provide a support and isolate the electrical connectors; the shape of the filter holder permitted the HAEV disk to be easily replaced if multiple measurements were required.

The strain-gauge measurements were acquired through a bridge amplifier static strain indicator and stored in a digital data logger. The strain gauge was connected to the acquisition system through appropriate input terminals.

The saturation procedure used for the first prototype was in part based on the information provided by Take & Bolton (2003). In particular, a conditioning

system was designed to calibrate and pre-pressurize the HCT. The system developed, Fig.2a, allowed the combined application of high temperatures and vacuum pressures, in order to improve the effectiveness of the drying phase of the porous stone and also of the measuring chamber. The conditioning procedure consisted of the following phases: application of vacuum with simultaneous heating, chamber c2, to improve the porous stone drying (16 hours); submersion of HCT with deaired water (4 hours); c2 chamber filling and application of a pressure of 800 kPa (72 hours).

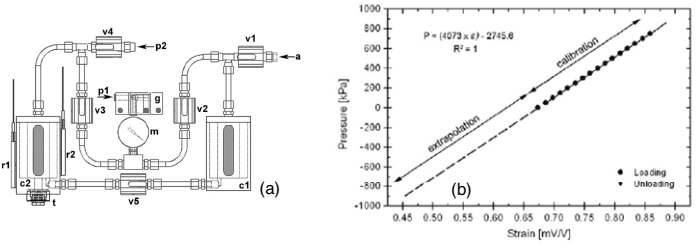

Fig. 2. a) Saturation system; b) tensiometer calibration curve (Rojas et al., 2008).

The tensiometer was then calibrated in the chamber c2 by varying pressure p2 from 0 to 800 kPa. The response of the HCT during the loading unloading process showed a linear response without appreciable hysteresis (Fig.2b). The calibration curve in the negative pressure range was extrapolated from the calibrated positive range (Fig.2b). A this point the instrument was ready and further tests were performed to verify its ability to rapidly and efficiently measure high suction values. These tests will be described later along with the new prototype.

3 New HCT Prototype

The main changes of the new HCT essentially concern the mechanical parts. In particular a more quick and functional assembly of components was realized (Fig.3). In this way, the HCT performance were less affected by setting up procedures and resulted more easily constructable.

The possibility of inspecting the measuring chamber was sacrificed to achieve different goals (Fig.3). The housing for the porous stone was machined in the same metal body that was used to manufacture the sensitive membrane; as a consequence it was possible to eliminate the O-ring seal that likely gave rise to some mechanical hysteresis affecting the response of the first prototype along a suction cycle. Moreover it was decided to reduce the upper bound of the measuring range to 500 kPa; this upper bound was considered a good compromise accordingly to the suction values expected in laboratory and in situ for possible future applications. Hence the membrane thickness was reduced to achieve an

adequate sensitivity as compared to the new measuring range (Fig.3). Obviously the 1.5 MPa AEV filter was substituted with a 500 kPa AEV; this resulted in a faster and easier saturation of the device.

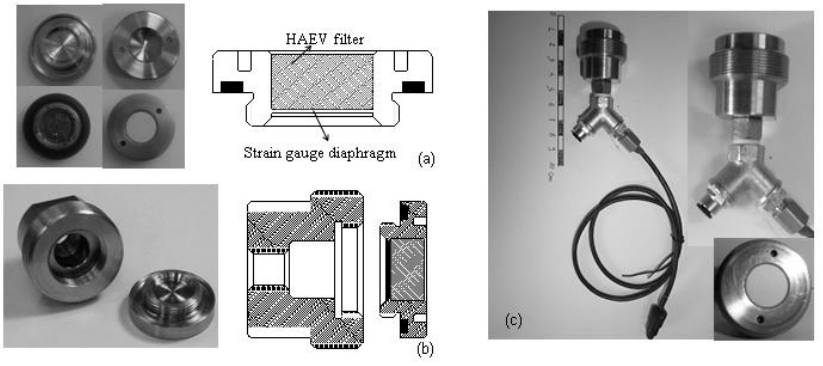

Fig. 3. Second prototype of Unina high capacity tensiometer. a) strain gauge diaphragm; b) total body; c) HCT assembled.

If compared with the first prototype, significant modifications to the external structure may be noticed (Fig. 3c). In particular there is vent for the application of air pressure to the back of the membrane, through which the back chamber of the instrument can be pressurized in order to perform calibration in the "negative pressure range". Therefore under these conditions the membrane is deflected in the same direction of suction measurements and then the calibration is obtained directly without the need of extrapolating it from the calibration in the positive pressure range. Another visible change is the presence of a thread outside the body of HCT to allow easy, installation into other equipment.

4 Experimental Procedures

In addition to the mechanical improvements also the system of saturation and the conditioning procedure were changed. The new device for saturation was smaller and capable of reaching pressure values much higher than the previous one (about 2.0 MPa). This device was also cheaper and easier to be assembled. As regards the modifications to the procedure of saturation, they were related to various issues and in particular:

- the initial phase of heating was eliminated, since it seemed to produce irreversible deformation of the resin used for gluing the strain gauge on the deformable membrane;
- the pressurization to saturate the HAEV disk and the water reservoir was performed by applying a positive water pressure of about 1.3 MPa in the

measuring chamber and an air pressure of about 800 kPa behind the membrane; thereby during pressurization (72 hours) the membrane was subjected to a differential pressure of about 500 kPa; therefore, its deformations are kept in the elastic range;

- pressurization cycles were repeated for the purpose of deflecting the diaphragm in both directions in order to minimize any hysteresis in its response.

5 HCT Calibration and First Results

The calibration of the HCT was performed initially by progressively increasing the water pressure in the measuring chamber (calibration for positive water pressure) and subsequently by rising air pressure in the posterior chamber (calibration for positive air pressure).

The diagram in Fig. 4 shows that the instrument response was perfectly linear and, moreover, that the calibration curve was independent of the sign of the diaphragm deflection. This result confirms that, with the design adopted, it is possible to extrapolate the calibration performed in positive pressure to negative pressures without making significant errors.

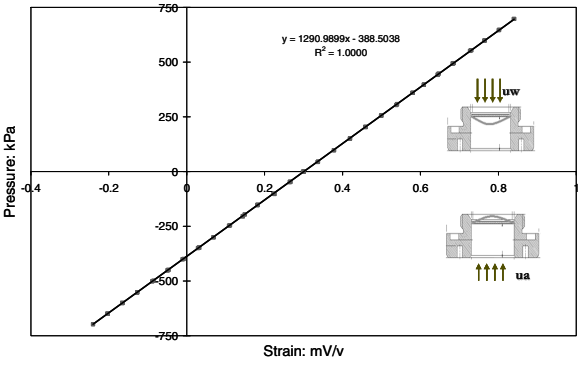

Fig. 4. Calibration curve of new HCT.

The HCT ability to measure rapid suction changes was investigated by means of cyclic evaporation tests. Fig. 5 shows several evaporation tests, consisting in free evaporation stages up to prescribed suction values (i.e. lower than the nominal filter AEV) and stages in which the water pressure inside the chamber was reduced to the atmospheric value by submerging the tensiometer tip in a water reservoir. The new adopted saturation procedure provided excellent results. In fact, few seconds (about 7-8 s) were enough to reach zero suction regardless of its initial value. The maximum value of suction measured up to cavitations was always greater than 500 kPa (nominal filter AEV about 500 kPa).

Long lasting measurements were conducted to estimate the response time of the tensiometer and to verify its ability to sustain high suction for a long time. The results are showed in Fig. 6. The equalization time of the tensiometer was examined by using silty-sand samples. Matric suction of about 350 kPa was generated in the sample of this material by using a modified Wissa oedometer working under the axis translation technique. A thin layer of the soil paste was used to improve the contact between the soil sample and the HCT. During the measurement the sample remained isolated to avoid large suction changes associated with the environmental conditions.

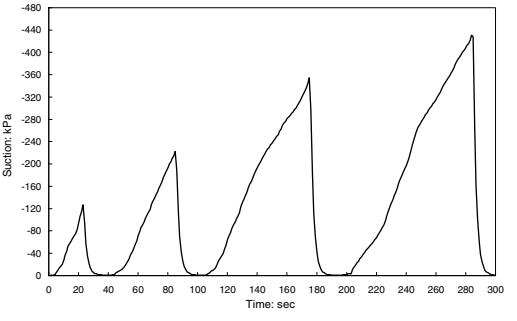

Fig. 5. Evaporation tests of new HCT.

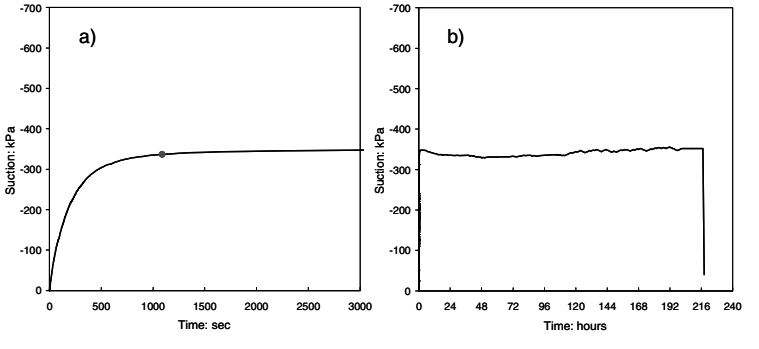

Fig. 6. Long time suction measurement on soil sample.

As it can be observed in Fig. 6a, about 1100 seconds were needed for the measurement to equalize (the response time was evaluated according to the procedure suggested by Oliveira and Marinho, 2008). The measurement remained stable for about 10 days (Fig. 6b), after which it was interrupted due to an electrical failure in the laboratory.

6 Conclusions and Future Developments

The results obtained from preliminary testing show satisfactory performance of the new prototype in terms of readiness and stability of measurement and seem very promising for future use of the instrument in the laboratory and in the field.

References

Oliveira, O.M., Marinho, F.A.M.: Suction equilibration time for a high capacity tensiometer. Geotechnical Testing Journal 31(1), 1–5 (2008)

Ridley, A.M., Burland, J.B.: A new instrument for the measurement of soil moisture suction. Geotechnique 43, 321–324 (1993)

Rojas, J.C., Pagano, L., Zingariello, M.C., Mancuso, C., Giordano, G., Passeggio, G.: A new high capacity tensiometer: first results. In: First European Conference on Unsaturated Soils, Durham, July 2-4 (2008)

Take, W.A., Bolton, M.D.: Tensiometer saturation and the reliable measurement of soil suction. Geotechnique 53(2), 159–172 (2003)

A Local Monitoring of Water Content in Unsaturated Soil Triaxial Testing

José Muñoz-Castelblanco, Pierre Delage, Jean-Michel Pereira, and Yu-Jun Cui

Abstract. Advanced triaxial testing in unsaturated soils includes local strain and suction measurements. However, in unsaturated soils, the complete local determination of the state of the specimen also requires the monitoring of local changes in water content. To this aim, a new electrical resistivity probe, composed of two pairs of electrodes was developed. Some experimental data on the changes in resistivity with the degree of saturation were obtained by carrying out calibration tests in specimens of natural unsaturated loess from Northern France. Two resistivity models were also used to analyze the obtained data. Results are finally discussed with respect to the loess's water retention properties.

Keywords: resistivity, water content, loess, triaxial, new probe.

1 Introduction

To investigate in the laboratory the relationship between water content and electrical resistivity, Gupta & Hanks (1972) and Rhoades et al. (1976) tested compacted specimens by using circular four-probe resistivity cells, a device also utilized by

José Muñoz-Castelblanco
Ecole des Ponts ParisTech, now in Cathie Associates SARL, Nanterre, France
e-mail: jose.munoz@cathie-associates.com

Pierre Delage
Ecole des Ponts ParisTech, Paris, France
e-mail: delage@cermes.enpc.fr

Jean-Michel Pereira
Ecole des Ponts ParisTech, Paris, France
e-mail: pereira@cermes.enpc.fr

Yu-Jun Cui
Ecole des Ponts ParisTech, Paris, France
e-mail: cui@cermes.enpc.fr

Kalinski and Kelly (1993). Other resistivity measurements were made by Fowles (1980) on compacted specimens, McCarter (1984) on remoulded clays, Fukue et al. (1999) on remoulded and natural clays and Chen et al. (2007) on expansive soils. As quoted by Kalinski and Kelly (1993), the resistivity of saturated soils depends on the particle size distribution, mineralogy, specific clay surface, porosity, pore size distribution, connectivity of pores, water content, salt concentration and temperature.

In unsaturated soils, the changes in degree of saturation are derived from the changes in both sample volume and water content. Local strain measurements in unsaturated triaxial soil testing should hence preferably be coupled with local measurements of the changes in water content. In this paper, a new resistivity probe to measure the local water content variation in a triaxial system was tested on an unsaturated natural loess from Northern France. Results are analyzed by means of two theoretical models.

2 Basic Concepts

In unsaturated soils, the electrical resistance depends on the resistance of the solid phase R_s, of air R_a and of water R_w. Since the air phase is an electrical insulator, and since water has a significantly higher electrical conductivity than solids, the electrical current mainly flows through water. In saturated soils, Archie (1942) proposed a simple empirical model (equation 1) relating the soil electrical resistivity ρ, that of the pore water ρ_w to the porosity n. This law was adapted for unsaturated soils (Archie 1942) by introducing the degree of saturation S_r as presented in equation 2, where a and b are experimental parameters.

$$\rho / \rho_w = (n)^{-a} \tag{1}$$

$$\rho / \rho_w = (n)^{-a} (S_r)^{-b} \tag{2}$$

Fukue et al. (1999) proposed a more sophisticated model accounting for the combined effects of the serial and parallel transmission of the electric current in the three phases (air, water and solids). They defined a structural coefficient F to separate the parallel flux (related to $1 - F$ and mainly occurring in water) and the serial one (related to F and influenced by the insulating properties of solids and air) giving the following expression of the electric resistivity ρ through a cylinder of radius r:

$$\rho = \frac{\pi r}{w G_s n} \Gamma ; \quad \Gamma = \frac{\rho_w}{(1-F)} \tag{3}$$

where w is the gravimetric water content, G_s is the specific solid density and n the soil porosity. F has a dimension of length and depends on the structure of the soil. The value of parameter Γ is related to the soil state.

3 Resistivity Probe

A small sized electric resistivity probe (11 mm in diameter) was developed to measure the water content at the mid-height of the triaxial specimen. It was inspired from the concept of concentric and surface probe developed by Maryniak et al. (2003). The probe is composed of four circular electrodes of diameter 1.5 mm disposed in a squared-grid (inter electrodes distance of 6 mm) as presented in Fig. 1.

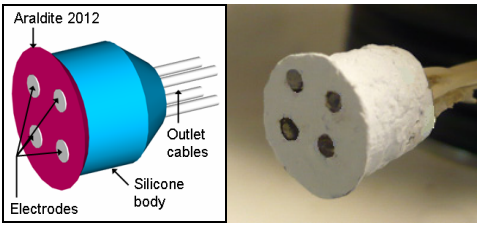

Fig. 1. Cermes resistivity probe.

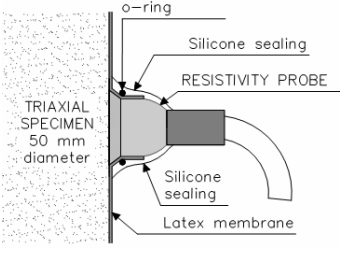

Fig. 2. Holding system

A hydrophobic dielectric matrix (Araldite 2012 epoxy resin) was used to accommodate the electrodes with proper electric isolation. Fig. 2 shows how the resistivity probe is fixed on the lateral side of the triaxial sample. Two input electrodes are supplied by a voltage source of 10 V and the output signal is received by two output electrodes.

4 Experimental Results

Tests were carried out on samples of a natural unsaturated loess of low plasticity, high porosity with an open structure that result in a significant collapse susceptibility (Cui et al. 2004, Delage et al. 2005, Yang et al. 2008, Karam et al. 2009, Munoz-Castelblanco et al. 2011a). To investigate the relationship between water content and the soil resistivity, five triaxial specimens (three from 1m deep and two from 3.3 m deep) of height 100 mm and diameter 50 mm were used. Samples were submitted to controlled wetting and drying processes while measuring their electrical resistivity at mid-height with the new gauge.

Fig. 3 shows the data obtained on the samples from 1m and 3.3 m depth along both the wetting and drying paths (whole range in a semi log plot in Fig. 3a and a zoom in linear plot between 0 and 100 Ωm in Fig. 3b). A fairly good compatibility between the data from the different samples is observed along both the wetting and drying paths.

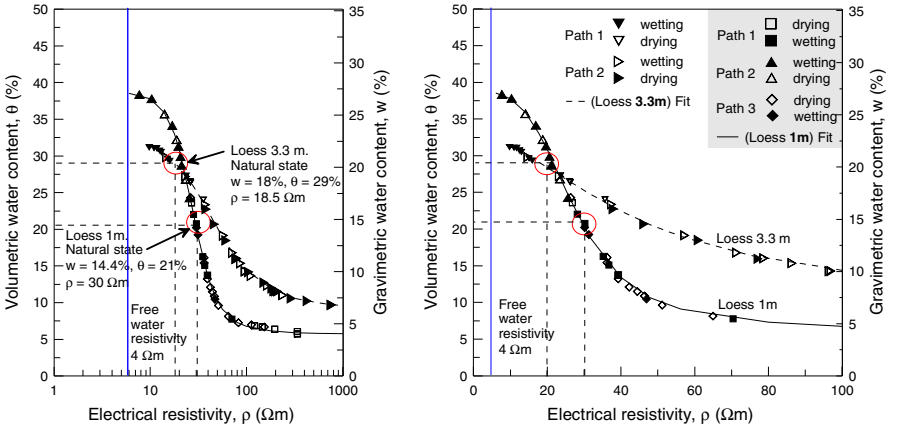

Fig. 3. Calibration curves of the resistivity probe for samples from 1m and 3.3 m depth. (a) Resistivity values in log-scale. (b) Zoom in true scale

At 1 m depth, the slope of the curve indicates that a reasonable estimation can be made for gravimetric water contents between w = 24 and 5%. For a drier sample with w < 5%, the resistivity rapidly reaches values higher than 100 Ωm and the changes become too tiny. The curve of the 3.3 m sample appears to be less steep than that of the 1 m sample, allowing better determination of the water content between θ = 13% and 31% (w between 8% and 22%).

5 Analysis

The data from both soils are also presented in a ρ/ρ_w versus S_r plot in Fig. 4 and compared to the modified Archie's law and to the model proposed by Fukue et al. (1999). Archie's curves agree reasonably well at degrees of saturation between 15 and 70% for the 1m deep specimen and between 30 and 70% for the 3.3 m deep specimen. Thanks to their concave shape, Fukue's curves appear to better agree with the data than Archie's model. This shape is due to the non-linear variation of the $(1 - F)$ value with respect to the degree of saturation. The coefficient $(1 - F) / (1 - F_{sat})$ of the 1m deep sample is almost equal to 1 for degrees of saturation higher than 20% (w = 10%) and it sharply increases below this value. This large resistivity increase is suspected to be due to discontinuities into the water phase at low water contents, specifically in soils containing some clay (Fukue et al. 1999).

F_{sat} values are 0.94 m and 0.97 m for the 1m and 3.3 m deep specimens, respectively. They correspond to Γ_{sat} values of 297 Ω and 366 Ω respectively. Whereas there is no particular physical meaning of the F parameter, Fukue et al. (1999) stated that parameter Γ was an indicator of the soil state, Γ values close to or higher than 300 Ω indicating undisturbed specimens. The values obtained here confirm the good quality of the extraction and sampling procedures followed.

Fig. 5 represents in the same graph the changes in relative resistivity with respect to the degree of saturation together with the water retention curve of the 1m depth sample, taken from Muñoz-Castelblanco et al. (2011b).

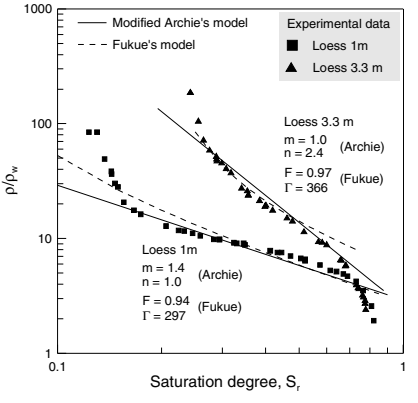

Fig. 4. Comparison of experimental data with both the modified Archie's law expression and Fukue's model.

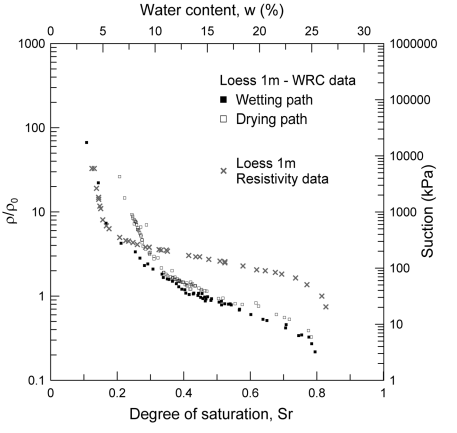

Fig. 5. Comparison between resistivity changes and the water retention properties.

The water retention curve exhibits, in a standard fashion, a hysteresis whereas the resistivity curve doesn't. Both curves are comparable, confirming the predominant role of water in the electrical transfer. The absence of hysteresis is due to the fact that resistivity is mainly related to the amount of water and not to its energetic potential. It is favourable for water content measurements, since they are independent of the hydraulic path previously followed by the sample.

6 Conclusions

The measurement of the electrical resistivity of a natural unsaturated loess from Northern France under various water contents showed a deviation from Archie's law at low degrees of saturation, related to the clay fraction and to possible changes in microstructure during drying. Fukue's model appeared to better fit at low degrees of saturation thanks to the structural factor F that depends on the degree of saturation. It is suspected that the electrical conduction through the soil can be divided into two regimes: one related to a continuous water phase in the range of high water contents and the other to a discontinuous water phase within the clay fraction, in the range of lower water contents. Compared to the water retention curve, the changes in resistivity with respect to the degree of saturation do not exhibit any hysteresis, making easier the determination of the water content.

References

Archie, G.E.: The electrical resistivity log as an aid in determining some reservoir characteristics. Trans. AM. Inst. Min. Metall. Pet. Eng. 146, 54–62 (1942)

Cui, Y.J., Marcial, M., Terpereau, J.M., Delage, P., Antoine, P., Marchadier, G., Ye, W.M.: A geological and geotechnical characterisation of the loess of Northern France. In: A.W. Skempton Memorial Conference, vol. 1, pp. 417–428 (2004)

Delage, P., Cui, Y.J., Antoine, P.: Geotechnical Problems related with Loess deposits in Northern France. In: Proceedings of International Conference on Problematic Soils, pp. 517–540 (2005)

Fowles, D.: Soil Resistivity Measurements. Report prepared by the Ductile Iron Pipe Research Institute, Oak Brook, US (1980)

Fukue, M., Minato, T., Horibe, H., Taya, N.: The micro-structures of clay given by resistivity measurements. Engineering Geology 54, 43–53 (1999)

Guéguen, Y., Palciauskas, V.: Introduction to the Physics of Rocks, 294 p. Princeton University Press, Princeton (1994)

Gupta, S.C., Hanks, R.J.: Influence of Water Content on Electrical Conductivity of the Soil. Soil Sci. Soc. Am. J. 36, 855–857 (1972)

Kalinski, R., Kelly, W.: Estimating Water Content of Soils from Electrical Resistivity. Geotechnical Testing Journal 16(3), 323–329 (1993)

Karam, J.P., Cui, Y.J., Tang, A.M., Terpereau, J.-M., Marchadier, G.: Experimental study on the cyclic resistance of a natural loess from Northern France. Soils and Foundations 49(3), 421–429 (2009)

Maryniak, W., Uehara, T., Noras, M.: Surface Resistivity and Surface Resistance Measurements Using a Concentric Ring Probe Technique. TREK, INC. Trek Application Note Number 1005 (2003)

McCarter, W.J.: Electrical resistivity characteristics of compacted clays. Géotechnique 34(2), 263–267 (1984)

Muñoz-Castelblanco, J., Delage, P., Pereira, J.M., Cui, Y.J.: Some aspects of the compression and collapse behaviour of an unsaturated natural loess. Géotechnique Letters (2011a), doi:10.1680/geolett.11.00003

Muñoz-Castelblanco, J., Pereira, J.M., Delage, P., Cui, Y.J.: The water retention properties of a natural unsaturated loess from Northern France. Géotechnique 61 (2011b) (in press), doi:10.1680/geot.2011.61.00.1

Rhoades, J.D., Raats, P.A.C., Prather, R.J.: Effects of Liquid-phase Electrical Conductivity, Water Content, and Surface Conductivity on Bulk Soil Electrical Conductivity. Soil Sci. Soc. Am. J. 40, 651–655 (1976)

Yang, C., Cui, Y.J., Pereira, J.M., Huang, M.S.: A constitutive model for unsaturated cemented soils under cyclic loading. Computers and Geotechnics 35(6), 853–859 (2008)

Effect of Intermediate Stress on Collapse Behaviour of a Compacted Clayey Silt

Octavio E. Cárdenas, Enrique Romero, Antonio Lloret, and Josep Suriol

Abstract. There are few experimental results on the influence of the intermediate principal stress on the behaviour of unsaturated soils. Particularly, the effect of intermediate stress on the collapse response of a soil subjected to a suction reduction path has not been studied in depth. This paper describes soaking tests performed in a hollow cylinder device, in which specimens of a compacted clayey silt have been saturated under constant mean and deviatoric stresses but at different intermediate stresses. The descriptions of sample preparation, testing device characteristics, test procedures and interpretation methods are presented. Preliminary analyses of the results seem to indicate that collapse is larger when the intermediate stress coincides with the minor one, i.e. under conventional axi-symmetric triaxial stress state.

Keywords: hollow cylinder, intermediate principal stress, collapse.

1 Introduction

The influence of the intermediate principal stress on the behaviour of saturated soils has been widely studied. On the contrary, studies performed on unsaturated

Octavio E. Cárdenas Díaz
Universidad Autónoma de Coahuila
e-mail: ecardenas@mail.uadec.mx

Enrique Romero Morales
Universitat Politècnica de Catalunya
e-mail: enrique.romero-morales@upc.edu

Antonio Lloret Morancho
Universitat Politècnica de Catalunya
e-mail: antonio.lloret@upc.edu

Josep Suriol Castellví
Universitat Politècnica de Catalunya
e-mail: jose.suriol@upc.edu

soils are still limited due to experimental difficulties, mainly associated with the precise determination of the volume change response. Hoyos (1998) and Matsuoka et al. (2002) used a true triaxial apparatus, whereas Toyota et al. (2001) and Toyota et al. (2004) a hollow cylinder device, to perform tests under constant suction to study the influence of this constitutive stress variable on soil behaviour under three-dimensional stress conditions. The effect of the principal intermediate stress is by no means an academic issue, since it has been taken into account in modeling earthwork constructions (see for instance, Zerfa & Loret, 2003). Despite its importance, the effects of this intermediate stress on collapse response originated during saturation increase are rather unknown.

Particularly, the present work aims at studying the influence of the intermediate principal stress on the collapse response upon soaking of a statically compacted clayey silt tested in a hollow cylinder device.

2 Testing Apparatus and Tested Material

The sample installed in the hollow cylinder apparatus (see for instance, Bilé Serra and Hooker, 2011) features 50 mm of external radius r_0, 30 mm in inner radius r_i, and 200 mm in height H_o. The capacity of the axial load cell and the torque cell are 10 kN and 100 Nm, respectively. The principal stress parameter $b = (\sigma_2-\sigma_3)/(\sigma_1-\sigma_3)$ (Bishop 1966), can be automatically controlled during the tests (σ_i are principal stresses, being σ_1 and σ_3 the major and minor ones). Both the base and top caps have conventional porous discs. Three pressure / volume controllers were used for the application and control of the pressures, as well as for the measurement of the water volume changes. Figure 1 shows a scheme of the stress state of the soil with the definition of the deviatoric stress (q) and a picture of a sample after the test. The procedure to obtain the principal stress values from the applied forces and pressures has been described in Hight et al. (1983).

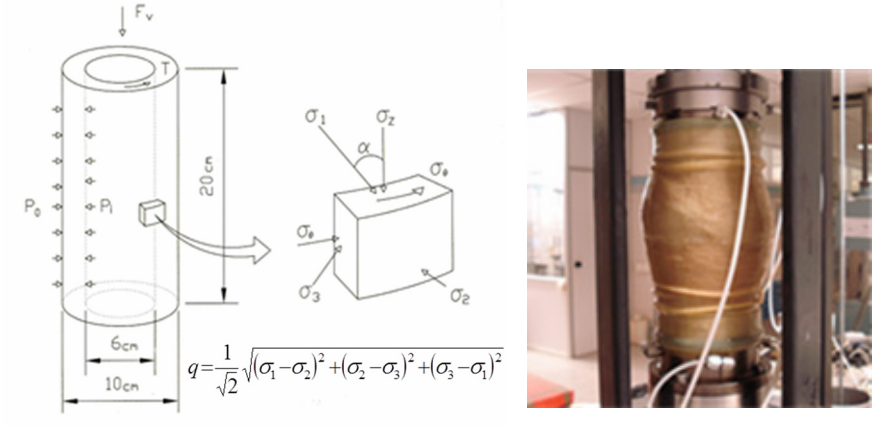

Fig. 1. Stress state in the hollow cylinder device and a picture of a tested specimen.

The soil used is the result of the mixture of two materials: fine sand of Castelldefells (Barcelona) and Barcelona silty clay (w_L = 34%, PI = 18%). The mixing ratio was studied to find a suitable combination of shear strength, water permeability and collapsibility properties. Finally, a mixture of 30% sand and 70% silty clay by dry mass was selected. The mixture with a water content of 4% was statically compacted up to a dry density of (1.55 ± 0.01) Mg/m^3 (void ratio $e \approx 0.74$, degree of saturation $S_r \approx 0.15$).

3 Testing Procedure

The specimen was compacted inside a set of two concentric cylindrical moulds: an inner mould with diameter 60 mm and split up into four parts and an external split mould of 100 mm in diameter. The static compaction was carried out by a hydraulically driven press at a displacement rate of 0.2 mm/min up to a maximum vertical stress around 200 kPa. The assembly of the specimen in the cell was carefully carried out due to the low strength of the mixture. Once the sample was installed, the inner and outer chambers were filled with water. Once the filling was finished, the external pressure was fixed at 10 kPa in the pressure controller to maintain certain confinement on the sample.

To determine the effect of the intermediate principal stress σ_2 on collapse, three tests were performed by changing the value of the parameter b, which was set to 0, 0.5 and 0.8. The tests were carried out by maintaining constant the mean and deviatoric stresses during the saturation stage. The tests started with an isotropic compression stage by applying approximately the same inner and outer chamber pressures up to a maximum mean net stress $p = (\sigma_1+\sigma_2+\sigma_3)/3$=200 kPa under constant water content conditions and atmospheric air pressure. A rate of 2.5 kPa/hour was selected for the application of the external P_o and internal P_i pressures during isotropic compression. After this initial stage, a small increase of deviatoric stress q = 30 kPa was applied before setting the parameter b. Afterwards, the value of q was increased at a rate of 15 kPa/hour up to 200 kPa by maintaining p = 200 kPa and a constant b parameter. Once the target stresses were reached, the samples were soaked under constant stress state by setting a small water pressure at the base. Figure 2 shows the stress paths followed at different b values.

The axial strain ε_z was evaluated directly from the vertical displacements controlled by the stepper motor and the initial height of the sample. Nevertheless, the most important limitation was the lack of local instrumentation in the sample for volumetric strain ε_v measurement. It was necessary to obtain this strain from alternative recorded values (change in sample height ΔH and the volume changes of inner ΔV_i and outer ΔV_0 chambers). The measurement of the final water content and the initial and final dry densities of the sample allowed better assessing volumetric strain measurement.

The evaluation of volumetric ε_v, radial ε_r, and circumferential ε_θ strains need the knowledge of the magnitude of the changes in the internal and external radius u_i and u_o, respectively (see for instance, Hight et al., 1983). These changes can be evaluated from inner and outer chamber volume changes together with height changes:

$$u_i = \Delta r_i = \sqrt{\frac{\pi r_i^2 H_o + \Delta V_i}{\pi\left(H_o + \Delta H\right)}} - r_i \;\; ; \;\; u_o = \Delta r_o = \sqrt{\frac{\pi r_o^2 H_o + \Delta V_i - \Delta V_o}{\pi\left(H_o + \Delta H\right)}} - r_o \qquad (1)$$

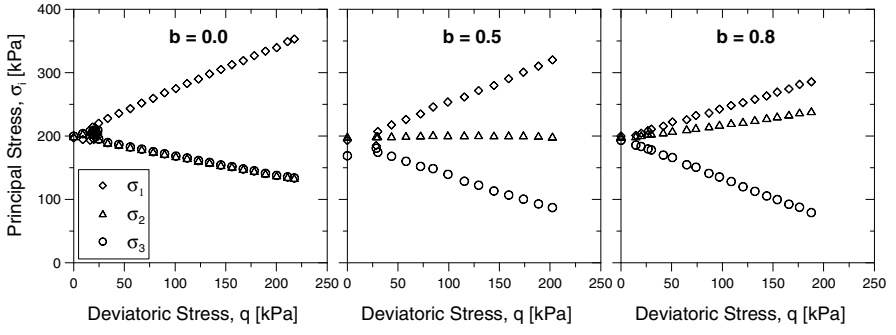

Fig. 2. Principal stress paths followed at different b values.

4 Results

The paths in terms of principal strains ε_1, ε_2 and ε_3 followed during the shearing stages are shown in Figure 3. It should be remarked that values of ε_2 changed from negative (expansion) for the case of $b = 0$, to positive (compression) for $b = 0.8$. This behaviour is equivalent to the one observed by Hoyos (1998) in tests performed using a true triaxial equipment.

Figure 4 shows the behaviour of the volumetric strain ε_v for different values of b, both along the shearing and saturation stages, and plotted against the deviatoric stress q. It can be observed that during the deviatoric stress stage, volumetric strains attain values around 2%. The maximum volumetric strain during this shearing stage was measured at $b = 0.5$. On the other hand, during the saturation stage at constant $q = 200$ kPa and $p = 200$ kPa, important collapse strains were recorded along the three soaking tests. Final ε_v values of 14%, 11% and 8% were measured at the end of these soaking stages for values of $b = 0.0$, $b = 0.5$ and $b = 0.8$, respectively. These results indicate that collapse is larger when the intermediate principal stress σ_2 coincides with the minor one σ_3, as in conventional axisymmetric triaxial conditions ($b = 0$; $\sigma_2 = \sigma_3$). As the intermediate principal stress σ_2 tends to σ_1, collapse strains progressively decrease.

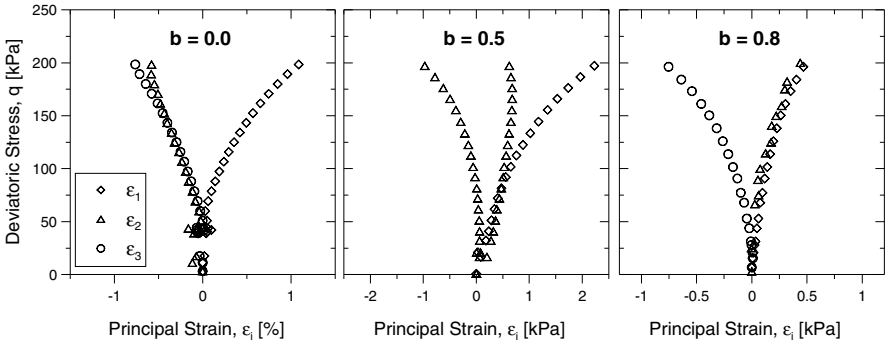

Fig. 3. Principal strain paths followed during the shearing stages for different values of parameter *b*.

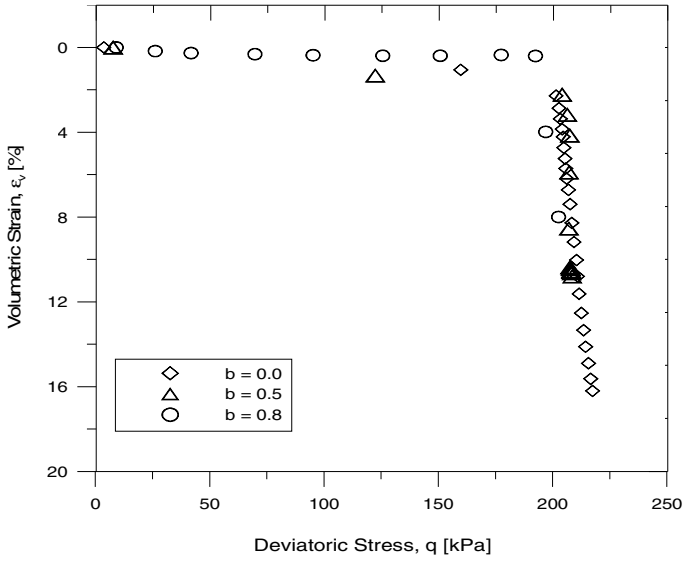

Fig. 4. Volumetric strain versus deviatoric stress for different values of parameter *b* (shearing stage and soaking stage at constant deviatoric and mean net stresses).

5 Conclusions

A laboratory test program was carried out aimed at studying the influence of intermediate principal stress on the collapse behaviour of unsaturated (compacted) clayey silt. A conventional hollow cylinder device can be a suitable equipment to perform these tests, if changes in inner and outer diameters of the specimen are correctly evaluated from volume changes of inner and outer chambers and by taking into account the initial and final dry densities of the material. During shearing,

intermediate strain ε_2 changed from negative (expansion) for $b = 0$, to positive (compression) for $b = 0.8$. During this stage, the major principal strain ε_1 remained always positive (compression) independently of the value of b; and the minor principal strain ε_3 always negative (expansion).

Collapse on soaking at constant mean and deviatoric stresses is influenced by the intermediate principal stress σ_2. Test results indicated that collapse was larger when the intermediate principal stress σ_2 coincided with the minor one σ_3, as in conventional axi-symmetric triaxial conditions ($\sigma_2 = \sigma_3$). A progressive and systematic decrease of collapse strain was detected as the intermediate principal stress σ_2 tended to σ_1.

Acknowledgements. This work is part of a research project financed by the Spanish Ministry of Science and Innovation (Project CGL2005-03677).

References

Bilé Serra, J.P., Hooker, P.: A new computer controlled hollow cylinder torsional shear apparatus (2011), http://www.docstoc.com/docs/77287577/A-New-Computer-Controlled-Hollow-Cylinder-Torsional-Shear-Apparatus

Bishop, A.W.: The strength of soils as engineering materials. 6th Rankine Lecture. Géotechnique 16(2), 91–128 (1966)

Hight, D.W., Gens, A., Symes, M.J.: The development of a new hollow cylinder apparatus for investigating the effects of principal stress rotation in soils. Géotechnique 33(4), 355–383 (1983)

Hoyos, L.R.: Experimental and computational modeling of unsatured soil behavior under true triaxial stress state. PhD Thesis, Georgia Institute of Technology, Atlanta (1998)

Matsuoka, H., Sun, D., Kogane, A., Fukuzawa, N., Ichihara, W.: Stress-strain behaviour of unsatured soil in true triaxial test. Canadian Geotechnical Journal 39, 608–619 (2002)

Toyota, H., Nakamura, K., Sakai, N., Nakamura, T.: Effect of the stress history due to unsaturation and drainage condition on shear properties of unsaturated cohesive soil. Soils and Foundations 41(1), 13–24 (2001)

Toyota, H., Nakamura, K., Sramoon, W.: Failure criterion of unsaturated soil considering tensile stress under three-dimensional stress conditions. Soils and Foundations 44(5), 1–14 (2004)

Zerfa, F.Z., Loret, B.: Coupled dynamic elastic–plastic analysis of earth structures. Soil Dynamics and Earthquake Engineering 23, 435–454 (2003)

Unsaturated Soil Response under Plane Strain Conditions Using a Servo/Suction-Controlled Biaxial Apparatus

José A. Cruz, Laureano R. Hoyos, and Arcesio Lizcano

Abstract. The engineering response of a vast majority of geotechnical infrastructure, including earth slopes, embankments, tunnels and pavements, may be most accurately modelled using plane strain analyses, given the particular geometries, stress paths and boundary conditions that such geosystems normally feature or undergo in the field. Biaxial devices allow for direct testing of soils under truly plane strain conditions, facilitating a more accurate assessment of shear banding phenomena and stress-strain-strength parameters under these conditions. However, most conventional biaxial devices reported to date only allow for soil testing under dried or saturated conditions. This paper introduces a suction-controlled biaxial apparatus that is suitable for soil testing under controlled-suction states via axis-translation technique. The design of its core system is based upon the original Vardoulakis type of biaxial apparatus. In this work, biaxial specimens are prepared by uniaxial consolidation of a slurry mixture, made of 75% silty sand and 25% kaolin clay, into an acrylic custom-made biaxial consolidation mold. The results from a short series of constant-suction tests reflect the important role played by matric suction in the stress-strain response of unsaturated soils under plane strain conditions.

Keywords: unsaturated soil, matric suction, axis-translation, plane strain analysis, biaxial apparatus.

José A. Cruz
Visiting Research Scholar, University of Texas at Arlington, Texas 76019
e-mail: jacruz@uta.edu

Laureano R. Hoyos
Associate Professor, University of Texas at Arlington, Texas 76019
e-mail: lhoyos@uta.edu

Arcesio Lizcano
Professor, Universidad de los Andes, Bogotá, Colombia
e-mail: alizcano@uniandes.edu.co

1 Introduction

The engineering response of a vast majority of geotechnical infrastructure, including earth slopes, embankments, tunnels and pavements, may be most accurately modelled using plane strain analyses, given the particular geometries, stress paths and boundary conditions that such geosystems normally feature or undergo in the field. Biaxial devices allow for direct testing of soils under truly plane strain conditions, facilitating a more accurate assessment of shear banding phenomena and stress-strain-strength parameters under these conditions. However, most conventional biaxial devices reported to date only allow for soil testing under dried or saturated conditions, including Wood (1958), Vardoulakis & Goldscheider (1981), Vardoulakis & Graf (1985), Dresher et al. (1990), Lizcano et al. (1997), and Alshibli et al. (2004). Recently, few attempts have been made at testing unsaturated soils under both plane strain shearing and controlled-suction states, including the works by Schanz & Alabdullah (2007) and Fauziah & Nikraz and (2008). These results, however, are far from conclusive and the corresponding devices offer ample room for further development, refinement and elaboration.

This paper introduces a suction-controlled biaxial apparatus that is suitable for soil testing under controlled-suction states via the axis-translation technique (Hilf 1956). The design of its core system is based on the original Vardoulakis type of biaxial apparatus (Vardoulakis & Goldscheider 1981). In the present work, biaxial specimens are prepared via uniaxial consolidation of a slurry mixture, made of 75% silty sand and 25% kaolin clay, into a custom-made biaxial consolidation mold. The range of induced matric suction states (50-100 kPa) from a short series of tests is shown to have a critical influence on the stress-strain-strength response of unsaturated soils under plane strain conditions.

2 Servo/Suction-Controlled Biaxial Apparatus: Key Features

The core system of the biaxial apparatus introduced in this work was designed and manufactured at the geotechnical laboratories of the University of the Andes, Bogotá, Colombia (Ruiz 2003), and was adapted for suction-controlled testing at the University of Texas at Arlington. The apparatus allows for the assessment of all of the following: (1) Pre/post-failure soil behavior; (2) Peak strength and evolution of strength parameters with time; (3) Soil response under combined direct and biaxial shearing; (4) Angle of dilatancy; and (5) Orientation of failure plane and formation of spontaneous shear bands.

Fig. 1 shows a detailed schematic of the fully assembled apparatus, including a numbered outline of all its main components. Fig. 2 shows actual photographs of the core system and the partly assembled apparatus. The device allows measurements of normal stresses between the soil sample and two lateral rigid walls, as well as soil volumetric changes during shearing. A detailed description of its calibration, using a neoprene spring rubber block, is given by Cruz et al. (2011).

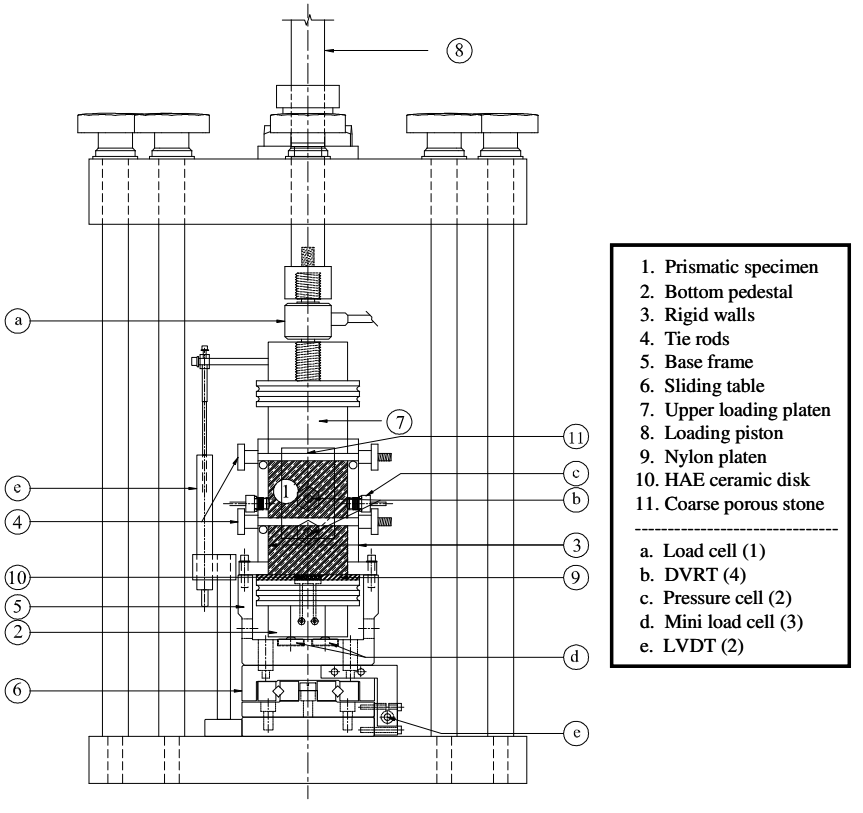

Fig. 1. Schematic of fully assembled suction-controlled biaxial apparatus and main components.

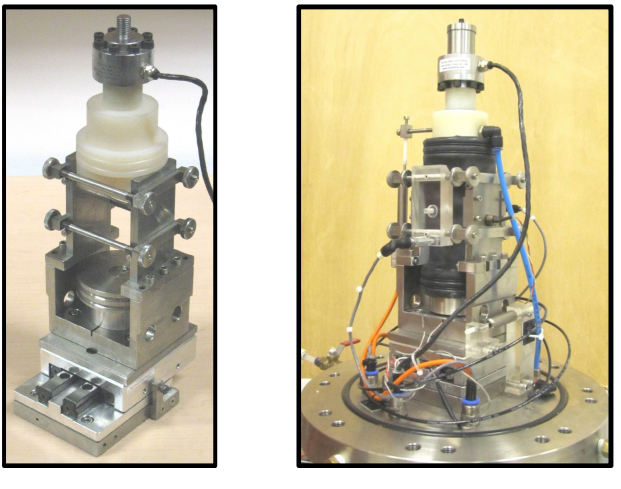

Fig. 2. Photographs of core system and partly assembled suction-controlled biaxial apparatus.

3 Test Soil and Sample Preparation

The soil material tested in this work is an artificially mixed soil made of silty sand (SM) and kaolin clay (CH). The silty sand soil yields a specific gravity, $G_s = 2.63$; while the kaolin clay yields a specific gravity, $G_s = 2.58$. Atterberg limits tests on kaolin clay yield liquid limit, LL = 57.1%, and plastic limit, PL = 45.8%. The soil-water characteristic curve (SWCC) of the artificially mixed soil is shown in Fig. 3, including data from pressure plate extractor, Tempe cell, and chilled mirror based techniques, and best-fitting model curves by van Genuchten (1980) and Fredlund & Xing (1994). The mixed soil still classifies as SM according to the USCS.

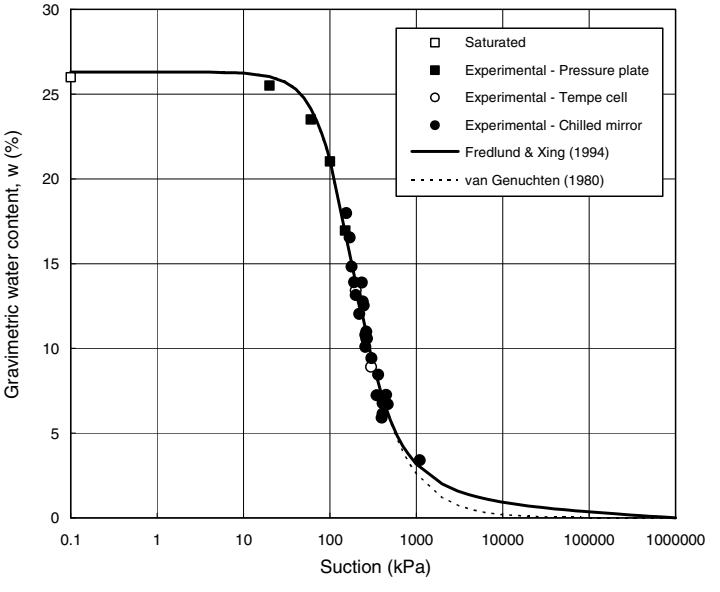

Fig. 3. Soil-water characteristic curve of SM soil using data from various techniques.

As previously mentioned, a typical biaxial specimen in this work is prepared by uniaxial consolidation of a slurry mixture (75% silty sand and 25% kaolin) into an acrylic custom-made biaxial mold, as shown in Fig. 4(a). The slurry is prepared with an initial water content that is about twice that corresponding to its liquid limit, LL = 25.3% (i.e., 1500 g of dry sand-kaolin thoroughly mixed with deaired-deionized water). The biaxial mold has an 80 x 80 mm square section and a 200 mm height. An incremental vertical load is applied to the slurry mixture through a squared acrylic plate featuring an affixed coarse porous stone at its bottom surface. The load is applied via a pneumatic actuator: Fig. 4 (a).

During uniaxial consolidation, the axial deformations are measured with a dial gauge while the expelled water, from within the slurry, is collected in a graduated cylinder: Fig. 4(a). The initial height of the slurry mix is 190 mm, and

it is consolidated to final target dimensions of 80 mm x 80 mm x 135 mm. Load increments of 12.5, 25, 50, 100, 200, and 400 kPa are typically applied, with each load increment acting on the slurry mix until no further vertical deformation or change in expelled water volume, whichever is achieved last, is observed (normally after 90% of primary consolidation, t_{90}). This consolidation process yields an average saturated unit weight of about 20 kN/m^3.

The compacted 80 x 80 x 135 mm sample is then gently removed from the consolidation mold, from which two soil specimens can be trimmed for plane-strain testing in the biaxial apparatus, as shown in Fig. 4(b). Prior to plane strain testing, two specimens, having a final average mass of about 323.3 g, are trimmed to final dimensions, d_{10} = 90 mm, d_{20} = 60 mm and d_{30} = 30 mm, as shown in Fig. 5.

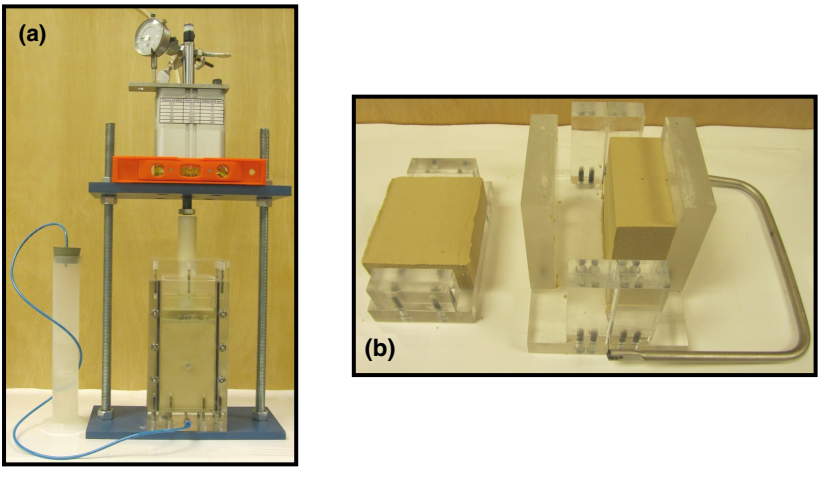

Fig. 4. Biaxial sample preparation: (a) consolidation of slurry mixture, (b) split sample trimming.

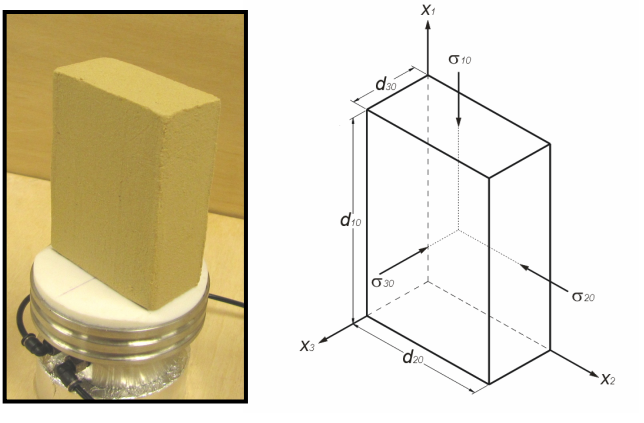

Fig. 5. Fully trimmed 90 mm x 60 mm x 30 mm sample for testing in the biaxial apparatus.

4 Results from Suction-Controlled Plane-Strain Tests on SM Soil

In this work, two identically prepared samples of compacted SM soil were tested in the fully assembled biaxial apparatus (Fig. 1) under net confining pressure, $p = (\sigma_3 - u_a) = 50$ kPa; and matric suction states, $s = u_a = 50$ kPa and 100 kPa, respectively. The axis-translation technique was implemented via a 15.87 mm diameter, 3-bar ceramic disk (i.e., HAEV = 300 kPa) located at the bottom pedestal, as illustrated in Fig. 1.

The suitable pore-fluid equalization time, for the typical biaxial specimen used in this work, was found to be about 144 hrs (6 days). Upon completion of pore-fluid equalization stage, the sample was sheared at a constant vertical deformation rate of 0.004 mm/min (i.e., 4.44×10^{-5}% strain/min), which is considered to be low enough to prevent sudden increases in pore pressure during shearing (Fredlund & Rahardjo 1993). Thorough flushing of diffused-air underneath the 3-bar ceramic disk was performed every 24 hrs.

The applied axial stress vs. axial strain response of SM soil from both suction-controlled tests is shown in Fig. 6. Peak stress values of 724.8 kPa and 309 kPa, corresponding to axial strain values of 6.16% and 6.42%, were attained under matric suction states, s = 100 kPa and 50 kPa, respectively. Peak strength is followed by a sharp drop in stress until an apparent residual state is achieved at maximum axial strain values of 8.32% and 8.83%, respectively. The results reflect the important role played by matric suction in the stress-strain-strength response of unsaturated soils under plane strain conditions.

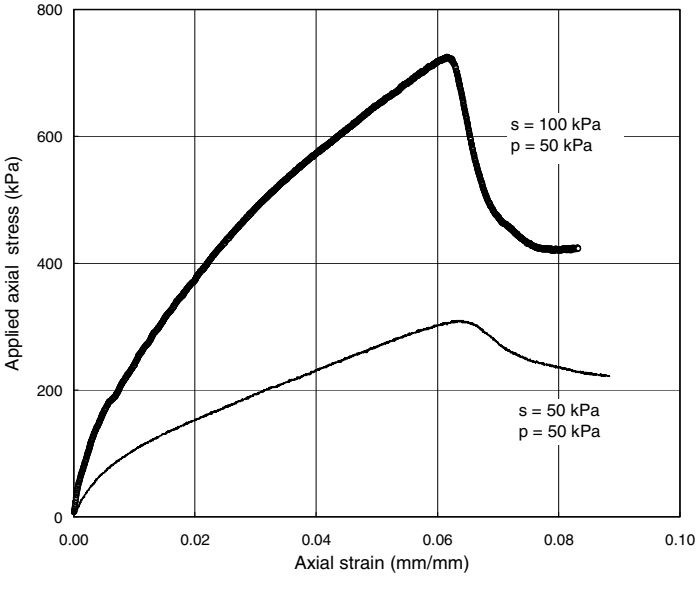

Fig. 6. SM soil response from biaxial tests under constant matric suction s = 50 kPa and 100 kPa.

Fig. 7 shows actual photographs of soil samples failed under plane strain shearing at constant matric suction states, s = 100 kPa (left photo) and s = 50 kPa (right photo). A fully developed failure surface, making a 65° angle with the horizontal, can be readily identified for the sample failed at s = 100 kPa. Likewise, a failure surface, making a 61° angle with the horizontal, can be identified for the sample failed at s = 50 kPa, which further substantiates the results observed in Fig. 6.

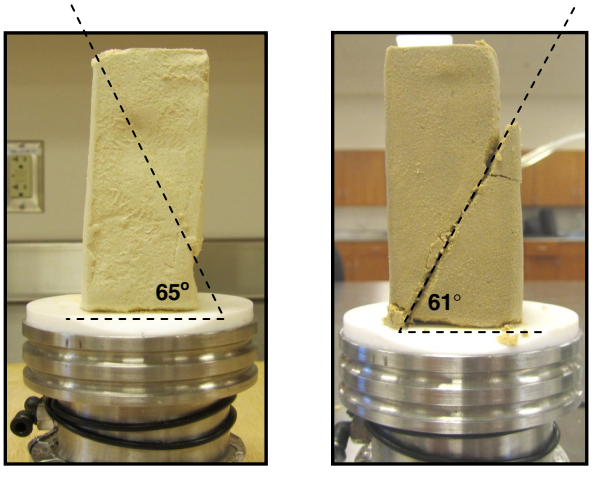

Fig. 7. SM soil specimens failed under biaxial shearing at s = 100 kPa (left) and 50 kPa (right).

5 Concluding Remarks

A suction-controlled biaxial apparatus for soil testing under controlled-suction states has been introduced. Results show that the apparatus is suitable for testing soils under controlled-suction states via the axis-translation technique. Two identically prepared samples of SM soil were tested in the biaxial apparatus under net confining pressure of 50 kPa and matric suction states of 50 and 100 kPa, respectively. Test results reflect the important role played by matric suction in the stress-strain-strength response of unsaturated soils under plane strain conditions. The operational apparatus will continue to play a fundamental role in future research related to the calibration and validation of constitutive models postulated for unsaturated soils under plane strain conditions, as well as the effects of suction on stress localization phenomenon in compacted soils subjected to plane-strain stress states.

Acknowledgements. The suction-controlled biaxial apparatus was developed under sponsorship of COLCIENCIAS ("Departamento Administrativo de Ciencia, Tecnología e Innovación"), Bogotá, Colombia; and CEIBA ("Centro de Estudios Interdisciplinarios Básicos y Aplicados en Complejidad"), University of the Andes, Bogotá, Colombia. This support is gratefully acknowledged. Any findings, conclusions, or recommendations expressed in this material are those of the authors and do not necessarily reflect the views of COLCIENCIAS or CEIBA.

References

Alshibli, K.A., Godbold, D.L., Hoffman, K.: The Louisiana plane strain apparatus for soil testing. Geotechnical Testing Journal, ASTM 27(4), 337–346 (2004)

Cruz, J.A., Hoyos, L.R., Lizcano, A.: A novel suction-controlled biaxial apparatus for unsaturated soils. In: Proc., 5th Asia-Pacific Conference on Unsaturated Soils, Pattaya, Thailand, February 29-March 2 (in press, 2012)

Drescher, A., Vardoulakis, I., Han, C.: A biaxial apparatus for testing soils. Geotechnical Testing Journal, ASTM 13, 226–234 (1990)

Fauziah, M., Nikraz, H.R.: The behaviour of unsaturated compacted clay under plane strain condition. In: Proc., 3rd International Conference on Evolution, Monitoring, Simulation, Management and Remediation of the Geological Environment and Landscape Evolution III, New Forest, UK, pp. 77–85 (June 2008)

Fredlund, D.G., Rahardjo, H.: Soil Mechanics for Unsaturated Soils. John Wiley & Sons (1993)

Fredlund, D.G., Xing, A.: Equations for the soil-water characteristic curve. Canadian Geotechnical Journal 31(3), 521–532 (1994)

Hilf, J.W.: An investigation of pore water pressure in compacted cohesive soils. Technical Memorandum No. 654, United States Department of Interior, Bureau of Reclamation, Design and Construction Division, Denver, CO (1956)

Lizcano, A., Vardoulakis, I., Goldscheider, M.: Biaxial test on normally, anisotropically consolidated kaolin clay. In: Asaoka, A., Adachi, T., Oka, F. (eds.) Deformation and Progressive Failure in Geomechanics, Pergamon, UK, pp. 223–227 (1997)

Ruiz, W.: Diseño de un aparato biaxial. Proyecto de grado de Magíster en Ingeniería Civil. Universidad de los Andes, Bogotá (2003)

Schanz, T., Alabdullah, J.: Testing unsaturated soil for plane strain conditions: A new double wall biaxial device. In: Experimental Unsaturated Soil Mechanics, pp. 169–178. Springer (2007)

van Genuchten, M.T.: A closed-form equation for prediction of the hydraulic conductivity of unsaturated soils. Soil Sci. Soc. Am. J. 44, 892–898 (1980)

Vardoulakis, I., Goldscheider, M.: Biaxial apparatus for testing shear bands in soils. In: Proc., 10th International Conference on Soil Mechanics and Foundation Engineering, Stockolm, vol. 4, pp. 819–824 (1981)

Vardoulakis, I., Graf, B.: Calibration of constitutive models for granular materials using data from biaxial experiments. Géotechnique 35(3), 299–317 (1985)

Wood, C.C.: Shear strength and volume change characteristics of compacted soil under conditions of plane strain. Ph.D. dissertation, University of London, UK (1958)

Behaviour of Compacted Clayey Silty Sand under Suction-Controlled Ring Shear Testing

Laureano R. Hoyos, Claudia L. Velosa, and Anand J. Puppala

Abstract. Assessment of residual shear strength parameters of soils at relatively low net normal stresses and suction states is of critical importance in slope stability analyses that involve potentially shallow failures triggered by rainfall at relatively high degrees of saturation. To date, however, there is limited experimental evidence of soil behaviour under large deformations, and the corresponding residual shear strength properties, for soils subjected to controlled-suction states. In this work, a series of suction-controlled ring shear tests were conducted on statically compacted samples of clayey silty sand. The tests were accomplished in a newly developed servo/suction-controlled ring shear apparatus that is suitable for testing unsaturated soils via axis-translation technique. Results reflect the important role played by matric suction on residual shear strength properties of unsaturated soils.

Keywords: unsaturated soil, residual shear strength, ring shear testing.

1 Introduction

Assessment of residual shear strength parameters of soils at relatively low net normal stresses and suction states, as reflected by the range of experimental variables considered in this work, is of critical importance in slope stability analyses that involve potentially shallow failures triggered by rainfall at relatively high degrees of saturation. To date, however, there is limited experimental

Laureano R. Hoyos
Associate Professor, University of Texas at Arlington, Texas 76019
e-mail: lhoyos@uta.edu

Claudia L. Velosa
Staff Engineer, Fugro Geoconsulting, Houston, Texas 77081
e-mail: clilianav@hotmail.com

Anand J. Puppala
Professor, University of Texas at Arlington, Texas 76019
e-mail: anand@uta.edu

evidence of unsaturated soil behaviour at large deformations, and the corresponding residual shear strength properties, for soils subjected to controlled-suction states. It is in this context that a suction-controlled ring shear apparatus would play a fundamental role.

Recent efforts, including Vaunat et al. (2006) and Infante Sedano et al. (2007), have focused on adapting existing Bromhead-type devices (Bromhead 1979) for unsaturated soil testing using vapor-transfer or axis-translation techniques. Despite their crucial findings, highlighting the key role played by soil suction, additional experimental efforts have yet to be undertaken in order to assess a thorough set of suction-dependent residual failure envelopes for soils tested at relatively low suction states (0-100 kPa). The present work is motivated by these research needs.

2 Suction-Controlled Ring Shear (RS) Apparatus

The RS apparatus used herein allows for application of vertical loads up to 8 kN, monotonic torque up to 113 N-m, and unlimited angular rotation. It features three main modules: (1) Main cell with pneumatic actuator for normal loads, and electromechanical rotary actuator for torque loads; (2) DA/PC system with data reduction software for calculation of normal and shear stresses, and average linear and angular displacements; and (3) PCP-15U suction control panel for implementation of the axis-translation technique. An orderly step-by-step setting-up procedure was established as follows:

1. A small piece of wet filter paper is placed over the top of each HAE disk, prior to soil compaction, in order to ensure phase continuity between the pore-water in the soil and the water in the saturated disk: Fig. 1(a).
2. A 15-mm (0.59-in) thick sample is statically compacted into the bottom annular platen: Fig. 1(b). The sample is transferred to the RS frame and the platen tightly fixed onto the bottom base plate: Fig. 1(c).
3. The vertical load shaft is brought up via a servo controller and the upper annular platen affixed to the top of the piston shaft: Fig. 1(c). A vertical sitting load of 25 N is applied to bring the upper platen in full contact with the soil.
4. All drainage and flushing lines are filled with de-aired water and flushed several times to avoid any trapped air in the whole system.
5. The main RS cell is set into place and the top cover plate affixed to the main cell: Fig. 1(d). A pore-air pressure line, from the PCP-15U panel, is connected to the cover plate via a quick connector.
6. Readings of the load-torque transducers are reset, and the LVDT and angular deformation sensors are re-zeroed, prior to RS testing.
7. The sample is then subject to a suction-controlled multi-stage RS test using the $s = u_a$ testing concept ($u_w = 0$).
8. Finally, the induced failure surface is thoroughly examined via microscopic digital imaging (Velosa 2011).

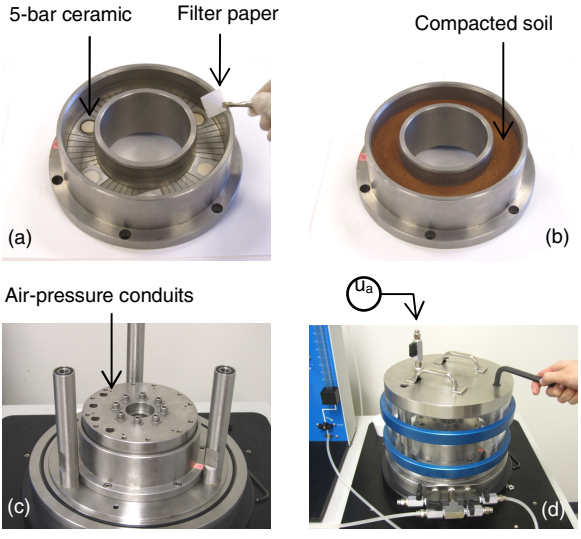

Fig. 1. RS assembly: (a) lower platen, (b) test sample, (c) top platen, (d) main cell.

3 Soil Properties and Test Procedures

The soil classifies as silty clayey sand (SC-SM) according to the USCS; with 60% sand, 34.05% silt, and 5.95% clay; OMC = 26%; and $\gamma_{d\text{-}max}$ = 1.33 g/cm^3. The fine-grained fraction yields LL = 26.4% and PI = 6.2%. The soil was selected because of its poor gradation and relatively low plasticity, thus reducing the time required for pore-fluid equalization during suction-controlled RS testing. A significant content of fine-grained material is expected to minimize the potential for wall-friction effects. All samples were prepared directly into the lower annular platen, using in-place static compaction, to a target dry unit weight of 95% of $\gamma_{d\text{-}max}$.

The first stage of a multi-stage suction-controlled RS test requires bringing the soil to an initial net normal stress, $(\sigma_n - u_a)$ = 25 kPa, and matric suction state, s = u_a = 25, 50, or 100 kPa. A vertical load is first monotonically applied via the upper annular platen to induce a normal stress 25 kPa greater than the target value of soil suction, and the soil allowed to consolidate. The pore-air pressure u_a is then raised in the main cell, as shown in Fig. 1(d), to the desired suction state, s = u_a. The vertical load is adjusted accordingly to keep the net normal stress constant at 25 kPa. The time required for consolidation-equalization ranged from 74 to 116 hrs.

A total of 4 suction-controlled RS tests were performed on an equal number of samples of SC-SM soil, under saturated (s = 0) and constant-suction states (s = 25, 50, or 100 kPa), by following a multi-stage scheme in which residual strength assessments were made at three or more net normal stresses, $(\sigma_n - u_a)$ = 25, 50, 75, 100, or 200 kPa. All tests were conducted at an equivalent horizontal displacement rate of 0.025 mm/min, which corresponds to a rotational speed of 0.023°/min.

4 Soil Response under Suction-Controlled RS Testing

Fig. 2(a) shows the effect of matric suction on both the position and slope of all residual failure envelopes assessed from multi-stage suction-controlled RS testing on compacted SC-SM soil. It can be readily observed that the final positioning of the envelopes is greatly influenced by suction, with a considerably higher position for s = 100 kPa. Suction also has a significant effect on the residual apparent cohesion, with the lowest value close to 17.5 kPa, for s = 0. For the range of suction states considered in this work, the residual failure envelopes are observed to be essentially linear and reasonably parallel, with $R^2 = 0.954$ to 0.999.

Fig. 2(b) shows the effect of net normal stress on residual failure envelopes projected onto the residual shear stress versus matric suction plane. Results show a high nonlinearity with respect to matric suction. The data have been fitted by second-degree polynomial functions with coefficients of determination, $R^2 = 0.985$ to 1.0. It can also be readily noticed that the nonlinearity of the residual failure envelopes increases with increasing net normal stress. This appears to confirm the direct correspondence between the nonlinear nature of residual shear strength envelopes, with respect to increasing suction, and the soil-water characteristic curve, as illustrated in Fig. 3.

To better appreciate the effect of matric suction over the residual shear strength of compacted SC-SM soil, the change of residual beta angle (ϕ_r^b) with suction, for different net normal stresses, has been plotted in Fig. 3 (top). In this case, the data have also been fitted by second-degree polynomial functions. Residual beta angles start at a constant value of 22.09° ($\phi_r^b = \phi_r$) under fully saturated state, s = 0; then increase ($\phi_r^b > \phi_r'$) until a suction value close to the air-entry value of the very soil, s = 28 kPa, according to the SWCC shown in Fig. 3 (bottom); and finally decrease gradually ($\phi_r^b < \phi_r'$) to as low as zero, or even negative values, for higher suction values. This decrease is more dramatic at higher levels of net normal stress, with a considerable reduction for net normal stress, $(\sigma_n - u_a) = 100$ kPa.

Vanapalli et al. (1996) and Lu & Likos (2004) have documented that there is a direct correspondence between the nonlinear nature of the peak shear strength envelope, with respect to increasing matric suction, and the SWCC. Within the regime of relatively low suction, and prior to the air-entry pressure of the soil, the soil pores remain essentially saturated, the shear strength envelope is reasonably linear, and the residual beta angle (ϕ_r^b) is effectively equal to the residual friction angle (ϕ_r').

As the soil becomes unsaturated, the reduction in the volume of pore-water within this regime effectively reduces the contribution of matric suction toward increasing shear strength. This effect is more noticeable as the net normal stress increases. This particular feature of the hydro-mechanical behavior of unsaturated soils might provide the most rational basis for understanding the patterns observed in Figs. 2 and 3 with respect to residual shear strength parameters of compacted clayey silty sand.

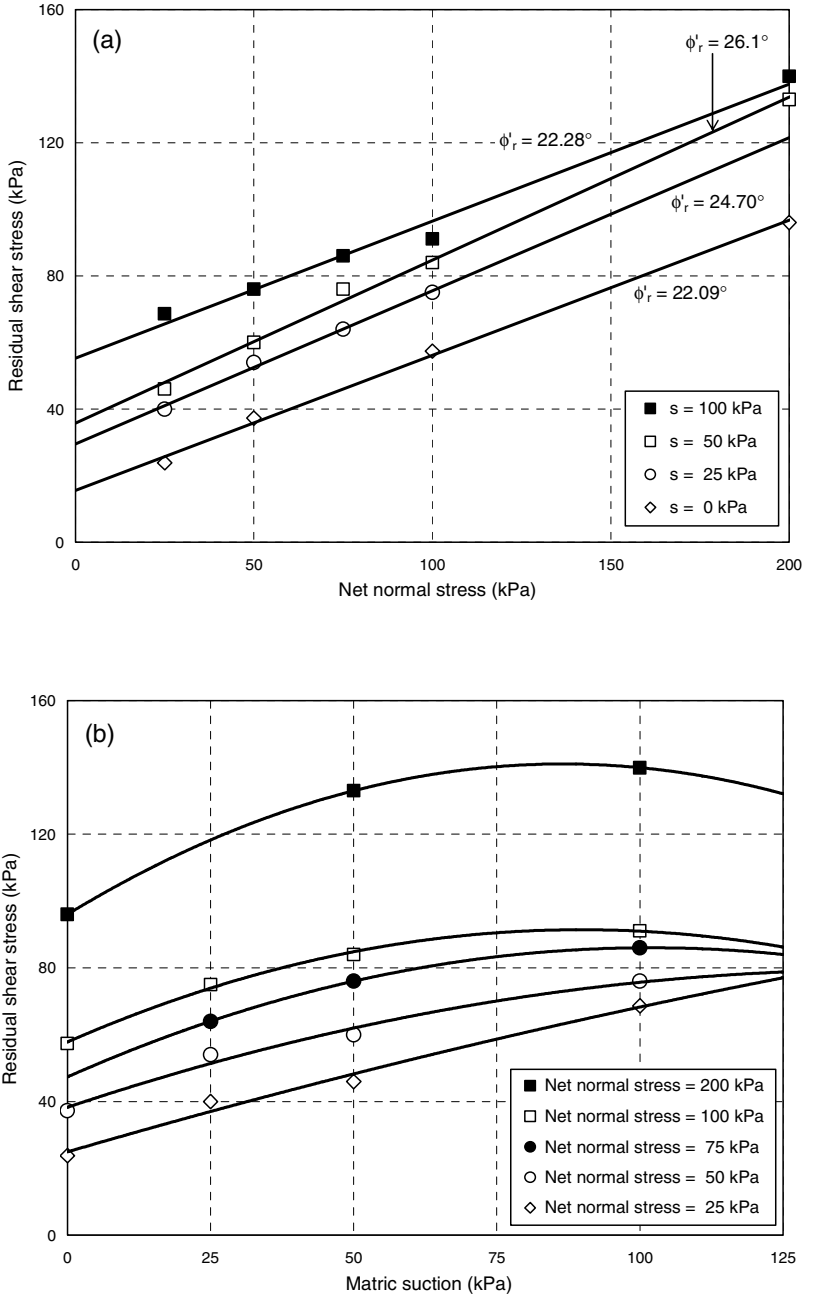

Fig. 2. Residual failure envelopes: (a) effect of matric suction, (b) effect of net normal stress.

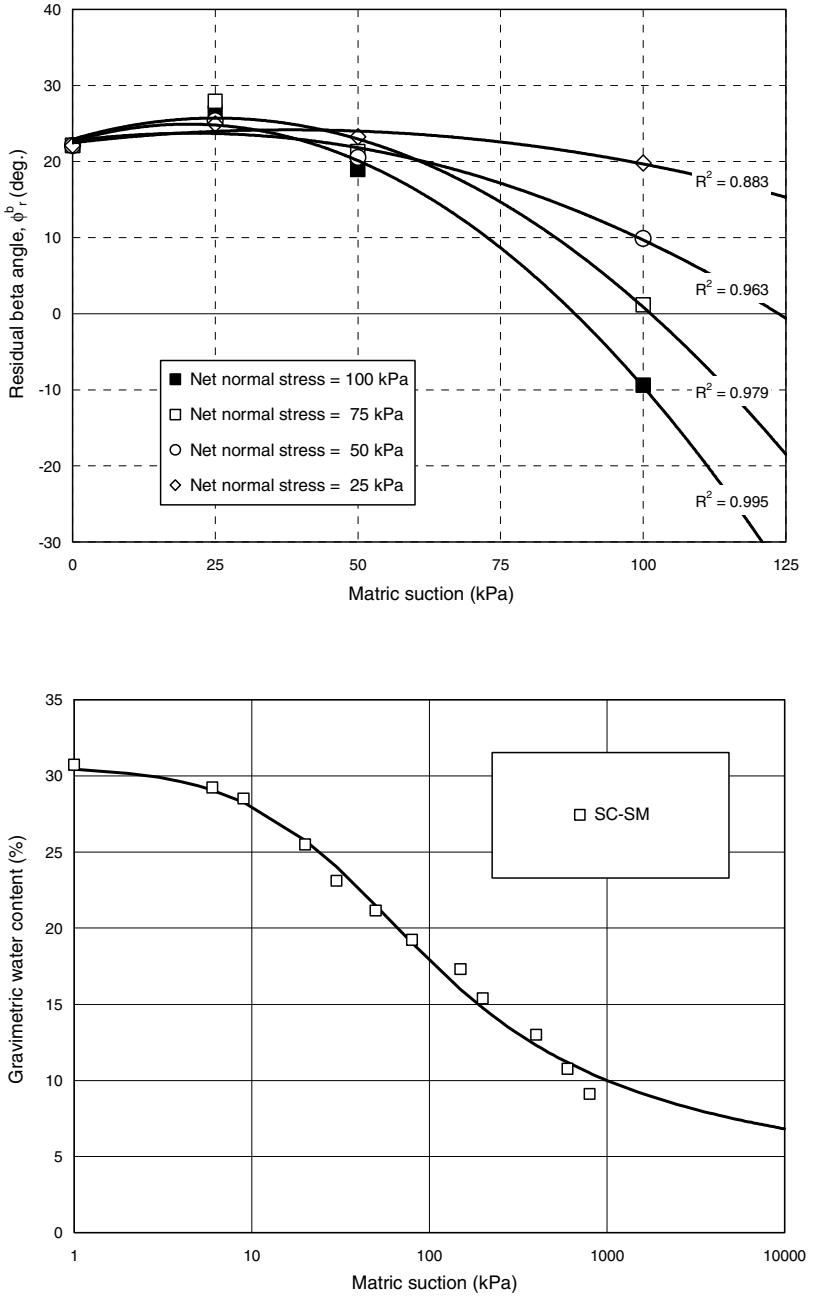

Fig. 3. Correspondence between the nonlinear residual beta angle (top) and the SWCC (bottom).

5 Typical Failure Surface: Key Features

Key features of a typical failure surface induced by shearing on SC-SM soil are shown in Fig. 4. A microscopic digital image of the initial top soil surface, after compaction, is shown in Fig. 4(a). A similar image of the induced failure plane is shown in Fig. 4(b), which is characterized by a polished and bright surface, indicating a reorientation of the plately clayey minerals (mica) along the plane; hence the development of slickensides along which residual strength is measured.

Furthermore, a thorough inspection of both the top and bottom annular platens shows that, in most cases, the induced failure plane was within the thickness of the sheared sample, about 2.0-mm deep on average: Figs. 4(c)-(d). It is worth noting that the rough-surfaced disk adapted to the top platen is a custom-made, sintered-bronze porous disk manufactured by Geotest Instrument Corp. Although the actual roughness index of the disk was not provided, its roughness was made considerably higher than that of the top disk used in a conventional Bromhead device.

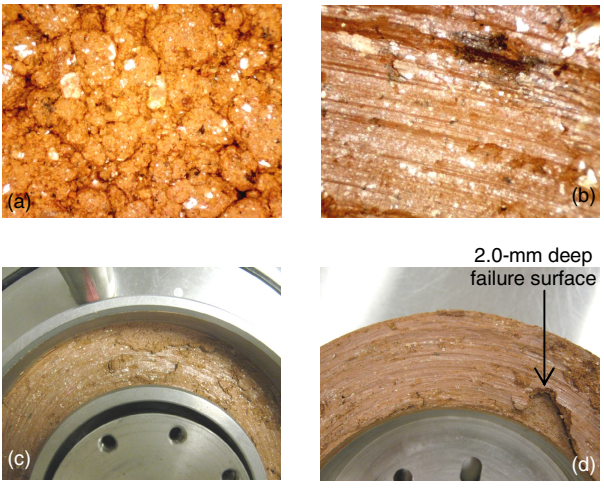

Fig. 4. Typical failure surface induced by ring shearing in compacted SC-SM soil.

6 Concluding Remarks

Results from a series of suction-controlled RS tests on statically compacted samples of SC-SM soil suggest that a conceptual residual shear strength framework for unsaturated soils, similar to that postulated for peak shear strength, can eventually be devised as more experimental evidence of this kind is made available. The authors are currently embarked on a thorough experimental effort involving low-plasticity clay using both the axis-translation and the vapor-transfer techniques. Results will be eventually shared with the geotechnical community in due time.

Acknowledgements. The core system of the RS apparatus used in this experimental effort was developed under U.S. National Science Foundation Award # CMS-0626090. This support is gratefully acknowledged. Any findings, conclusions or recommendations expressed in this material are those of the authors and do not necessarily reflect the views of the U.S. National Science Foundation.

References

Bromhead, E.N.: A simple ring shear apparatus. Ground Engineering 12(5), 40–44 (1979)

Infante Sedano, J.A., Vanapalli, S.K., Garga, V.K.: Modified ring shear apparatus for unsaturated soil testing. Geotechnical Testing Journal, ASTM 30(1), 1–9 (2007)

Lu, N., Likos, W.J.: Unsaturated soil mechanics. John Wiley & Sons, Hoboken (2004)

Vanapalli, S.K., Fredlund, D.G., Pufahl, D.E., Clifton, A.W.: Model for the prediction of shear strength with respect to soil suction. Canadian Geotechnical Journal 33(3), 379–392 (1996)

Vaunat, J., Amador, C., Romero, E., Djeren-Maigre, I.: Residual strength of a low plasticity clay at high suctions. In: Proceedings of Fourth International Conference on Unsaturated Soils, Carefree, Arizona, vol. 1, pp. 1279–1289 (2006)

Velosa, C.L.: Unsaturated soil behavior under large deformations using a fully servo/suction-controlled ring shear apparatus. Ph.D. dissertation. University of Texas at Arlington, Texas, 192 p. (2011)

Estimating the Retention Curve of a Compacted Soil through Different Testing and Interpretation Methods

Osvaldo Bottiglieri, Francesco Cafaro, and Federica Cotecchia

Abstract. The paper reports the results of a study about the hydraulic properties of a self-weight compacted medium-grained soil. The investigation was based on both physical modelling and element volume testing, using different suction measurement techniques. The paper shows the efficacy in the assessment of the soil retention properties of the use of the filter paper technique and of low capacity tensiometers to measure the soil suction in different suction ranges.

Keywords: Retention curve, inverse numerical analysis, suction measurement.

1 Introduction

The hydraulic behaviour of partially saturated compacted soils is usually characterized through the assessments of both the retention curve and the conductivity function. An extensive experimental investigation has been recently carried out in order to deduce the hydraulic properties of a partially saturated medium-grained soil (Bottiglieri 2009; Bottiglieri et al. 2008), based upon soil element volume tests and physical modelling of seepage through the soil, under controlled boundary conditions.

The grain size distribution of the soil subjected to testing is shown in Fig.1a (continuous line). The soil is a mixture of two different natural soils. 30% of the soil (soil S1) is an illitic clay, part of the Subappennine Blue Clays, whose grain

Osvaldo Bottiglieri
Politecnico di Bari, Bari, Italy
e-mail: o.bottiglieri@poliba.it

Francesco Cafaro
Politecnico di Bari, Bari, Italy

Federica Cotecchia
Politecnico di Bari, Bari, Italy

size distribution is shown in Figure 1. 70% of the soil is a quartz sand (S2), also shown in Figure 1 and classified as SP (Unified Soil Classification System - ASTM 2006). The liquid and plastic limits of portion S1 are 55% and 27%, respectively. The specific gravity of the whole soil has been measured to be Gs=2.65.

It is well known that the water retention curve (WRC) of a soil, thus its air entry value and desaturation rate, depend not only on the soil composition (i.e. grain size distribution and index properties; Fredlund 2006), but also on its initial state (Salager et al. 2010). Recent studies are also demonstrating how it depends also on the soil hardening history and achieved structure (Cafaro & Cotecchia 2005). In the present study, the state of the soil subjected to investigation was achieved through a non-routine procedure. The soil was air-dried for several days and set through static *self-weight compaction*, as illustrated in detail later. In order to assess soil states that, being achieved through routine compaction energies, could be of reference for comparison with the *self-weight* compacted states, the mixed soil was subjected to a Standard Proctor Compaction Test (Fig.2). The results in Figure 2 show that the optimum water content of the mixed soil is 10% and corresponds to a dry density of γ_d=19.8 kN/m^3. The *self-weight* compacted state of the soil is also shown in Figure 2. The soil has a quite open fabric (low dry unit weight) on the dry side of optimum; therefore it may be expected to experience a volumetric collapse under wetting (Tadepalli & Fredlund, 1991).

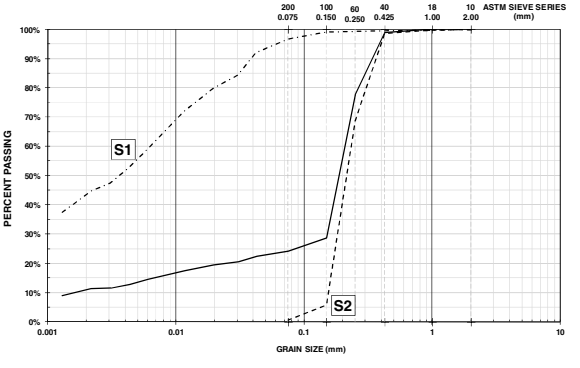

Fig. 1. Grain size distribution of S1, S2 and their mixture.

The experimental programme was designed to derive the WRC and the conductivity function(k(s)) through inverse numerical analysis (Kodesová 2003) of the physical model test data (Cafaro et al. 2008), as well as by means of direct measurements of the soil state during drying and wetting element volume tests. In these latter tests the initial soil state was the same as that of the soil in the

physical model, being achieved through static compaction procedure (Bottiglieri et al. 2008).The experimental and numerical procedures employed to derive the soil hydraulic properties are briefly outlined in the following, along with the test results.

Specific aim of the paper is to provide evidence of the usefulness of combining filter paper test suction measurements with measurements achieved by means of standard low capacity tensiometers (suction range of 0-100 kPa) in deriving the soil water retention law even for medium-grained soils.

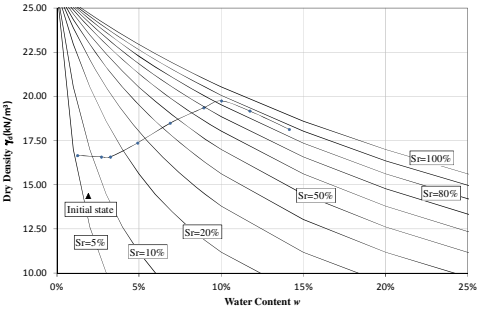

Fig. 2. Standard Proctor compaction curve and soil initial state.

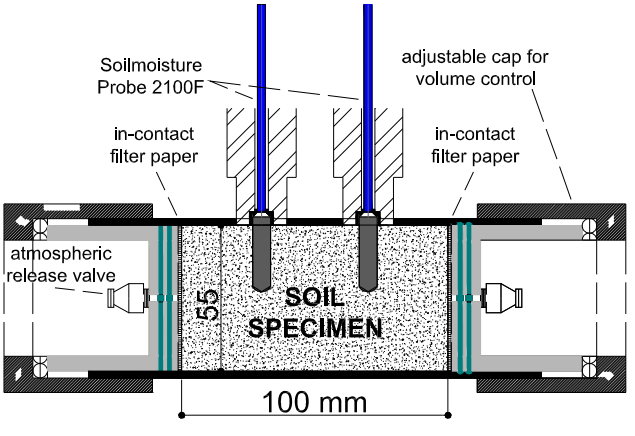

Fig. 3. Scheme of the measurement device: longitudinal section.

2 Testing Procedures

The investigation of the soil hydraulic properties has been carried out through two different strategies. One entails the monitoring of a real-scale seepage domain set

through the soil in a built on purpose physical model. Both the soil WRC and k(s) controlling seepage are then derived by means of an inverse numerical analysis of the seepage monitoring data. The second strategy entails the measurement of the evolving soil state during wetting-drying tests on soil specimens set in the device shown in Fig.3 (longitudinal section), and brings to the definition solely of the soil WRC; the *k(s)* can be then deduced according to the relation between *k(s)* and the WRC (Mualem 1976, van Genuchten 1980), once the saturated hydraulic conductivity k_s is known. A detailed description of the device shown in Figure 3 can be found in Bottiglieri (2009).

The used physical model has been shown in Cafaro et al. (2008); it consists of a stainless tank, one longitudinal side of which is made of perspex, hosting a soil layer of one cubic metre volume (base: 1*m* x 2 *m*; height: 0.5 *m*). The tank was inclined of 7% on the horizontal. Thin successive soil layers were pluviated in the tank. After pluviation, each layer was very mildly compacted just to yield a smooth top surface, before being buried and compressed under successive layers. At the end of process specimens were taken at different depths in the model to measure the model void ratio profile. As shown in Cafaro et al. (2008) the measured void ratios, e_0, were found to vary in the range 0.79÷0.83, giving evidence to a uniformity of the soil state across the layer. As a matter of fact, the increase in self-weight loading down the model (0.5 m maximum depth) appears to produce negligible effects. Table 1 reports the dry unit weight γ_d, gravimetric water content, w_0, void ratio, e_0, saturation degree, *Sr*, and volumetric water content, θ_i, characterizing the average soil initial state in the model.

Table 1. Initial soil state.

G_s	γ_d (kN/m^3)	w_0 (%)	e_0	*Sr*(%)	θ_i
2.649	14.3	1.44	0.81	4.7	0.021

The perspex side of the model tank was equipped with two pairs of 2100F Soilmoisture Probes(each provided with a suction transducer), each pair being mounted along one vertical. The tensiometers could measure matric suction in the range 0 – 100 kPa (Cassel & Klute, 1986; Stannard, 1992). After 24 hour equalization time since installation within the soil model, the tensiometers measured initial matric suctions in the range 60-63 kPa (Fig.4; point I, grey triangle). Thereafter, a controlled water infiltration test was started, through the generation of a controlled rainfall on the model surface (Cafaro et al. 2008), during which the progression of the water front and the soil matric suction at the four measuring points were monitored. Thereby, a two-dimensional finite element inverse analysis of the infiltration process has been developed by means of 2.102 Hydrus-2D (IGWMC, 1999), adopting the Mualem - van Genuchten formulation (Mualem 1976, van Genuchten 1980) of the hydraulic functions:

$$\begin{cases} \Theta = \dfrac{\theta - \theta_r}{\theta_0 - \theta_r} = \left[\dfrac{1}{1 + (\alpha s)^n} \right]^m \\ k(s) = k_s \Theta^l \left[1 - \left(1 - \Theta^{1/m} \right)^m \right]^2 \end{cases} ; \; s > 0; \; m = 1 - \frac{1}{n} \tag{1}$$

and assigning the soil initial conditions measured across the model as discussed previously: θ_i = 0.021 and s_i = 62 kPa. The analysis has been carried out by calibrating the fitting intervals of the different parameters (eq.1) according to ranges of values expected for the soil class the tested soil belongs to and searching for a solution of high coefficient of determination, R^2=0.976. Table 2 reports the shape factors vector of the primary wetting water retention function, *PW-WRC-i.a.*1*,* resulting from the inverse analysis, that is also shown in Figure 4. The inverse analysis has also assumed the saturate hydraulic conductivity k_s as unknown; the numerical solution has yielded k_s=1.58E-06 m/s, that is consistent with the k_s measured by means of permeameter testing on a soil sample of the same initial state as that of the soil in the physical model.

During the primary wetting, the soil has experienced an irreversible volumetric collapse of about Δe=0.16. Both this phenomenon and the well known air entrapment taking place upon wetting of sandy soils (Hopmans and Dane, 1986; Stauffer and Kinzelbach, 2001) are the causes of a volumetric water content at zero suction, θ_0 (Table 2), much lower than the initial porosity n_0=0.45 (Table 1).

Table 2. WRC parameters from inverse analysis.

	θ_r	θ_0	α (kPa^{-1})	n
PW-WRC-i.a.1	0.01	0.350	1.590	1.645
PW-WRC-e.v.1	0.01	0.353	0.396	1.622
PW-WRC-e.v.1	0.01	0.353	0.396	1.622
MD-WRC-e.v.1	0.01	0.352	0.104	1.668
PW-WRC-i.a.2	0.01	0.350	0.550	2.050
PW-WRC-e.v.2	0.01	0.353	0.389	1.669
MD-WRC-e.v.2	0.04	0.362	0.136	1.681

The device in Figure 3, used for the direct measurement of the WRC, is a perspex cylinder cell, hosting a specimen of 55 mm diameter and 100 mm length. The device has been implemented with two tensiometers of the same type as those installed in the physical model. As such it allows for measurements of the specimen volume and weight as well as of the suction across the specimen, during drying-wetting tests. Each specimen was made of air dried soil (at the same initial gravimetric water content as the model soil, w_0 Table 1) compacted in the cell at densities very close to that of the model soil (Fig.4, states in the black cross, Y). Following a step by step wetting path using distilled water, retention data were collected (series *e.v.(PW)* in Fig.4). Optimization of these data performed by RETC, a computer program developed by van Genuchten et al. (1991) to analyze

the soil water retention and hydraulic conductivity data of unsaturated soils, returns the parameters of the primary wetting retention function, *PW-WRC-e.v.*1*,* reported in Table 2 and Figure 4. Also during the element volume primary wetting, volumetric collapse was observed. After primary wetting, two specimens, *e.v.a(MD)* and *e.v.b(MD)* were subjected to free drying in the device, following a procedure illustrated in Bottiglieri (2009). The experimental data of both tests provide the *MD-WRC-e.v.*1 (Fig.4), whose van Genuchten parameters are reported in Table 2. As expected, the data are indicative of a parallelism between the drying-wetting transition branches and of a hysteretic loop, of magnitude consistent with that observed for similar soils (Fredlund 2006). Nevertheless, the suction data at $\theta_w < 0.1$, circled in Figure 4, are all at about s=60 kPa and plot quite far from the interpolation function (*MD-WRC-e.v.*1). Different explanations may be envisaged for this discrepancy: e.g. inadequacy of the van Genuchten model for the pore size distribution of the tested soil, or fault of the Soilmoisture Probe in the measurement of suctions higher than 60 kPa for the examined medium-grained soil. In order to investigate this discrepancy, assuming the validity of the van-Genuchten model, the residual branch of the soil drying curve has been explored by means of the filter paper technique, as discussed in the following.

3 Use of the Filter Paper Test Data and Conclusions

To overcome the errors rising from the limited measurement range of the tensiometers, the complete WRC has been deduced using a different suction measurement method at high suctions (Evangelista et al., 2006). To this aim, the cap closing both ends of the cell in Figure 2 has been designed to host a filter paper, set in contact with the base of the soil specimen. It was used Whatman N° 42 filter paper, according to the setup and weighing prescriptions from Lu & Likos (2004) and Marinho & Oliveira (2006) and adopting equalization times, calibration curves and data interpretation procedures from recent literature (Chandler 1992, Leong et al., 2002; Marinho & Oliveira, 2006;). It has been assumed that, as demonstrated by Marinho (1994), there is no difference between the calibration curves for total and matric suction and that with in-contact filter paper technique, the measured suction represents the matric suction, if below 1 *MPa*, and the total suction if higher. Since during wetting distilled water was used and considering that, for low clay fraction soils mixed with distilled water, such as the one under study, the osmotic suction may be expected to be negligible for w <0.1 (Sreedep & Singh, 2006), the suction measured by means of filter paper is likely to be the matric one. In Figure 4 for each filter paper measurement the suction values accounting for different calibration curves (Chandler et al. 1986; 1992; Leong et al. 2002) have been plotted.

The data denoted as "*PW-FP-e.v.*" correspond to the initial state of the soil if suction is measured by means of filter paper and corresponds to far higher suctions than that assessed by means of the tensiometers. The data denoted as "*MD-FP-e.v.*", instead, were logged at the end of the main drying test; each being the average of the top and bottom filter paper measurements. The high suctions being measured are consistent with those reported by Salager et al. (2010) for a

soil of similar composition and state as the tested one. The van Genuchten curve resulting from the fitting of the tensiometer measurements, up to s = 60 kPa, and the filter paper measurements, for 60 kPa < s < 10000 kPa, is denoted as *MD-WRC-e.v.*2 in Figure 4. It is characterized by a much higher correlation than that fitting solely the tensiometer data, *MD-WRC-e.v.*1. Therefore, if the van-Genuchten law applies to the soil, the filter paper technique is more appropriate to assess the medium-grained soil retention properties at suctions higher than 60 kPa.

As shown in Figure 4, the retention function resulting from an inverse analysis that accounts for the suction in the initial state measured by means of the filter paper technique, that is the *PW-WRC-i.a.*2 curve, results in an air entry value upon wetting (relating to α_w) that is far more consistent with that resulting from the element tests. It may be concluded that the hydraulic characterization of the self-weight compacted medium-grained soil under study can be achieved using the van-Genuchten model to regress soil state measurements acquired using different suction measurement techniques in the low and high suction ranges, that correspond to suction values below and above 60 kPa respectively for the type of tensiometer used in the present study.

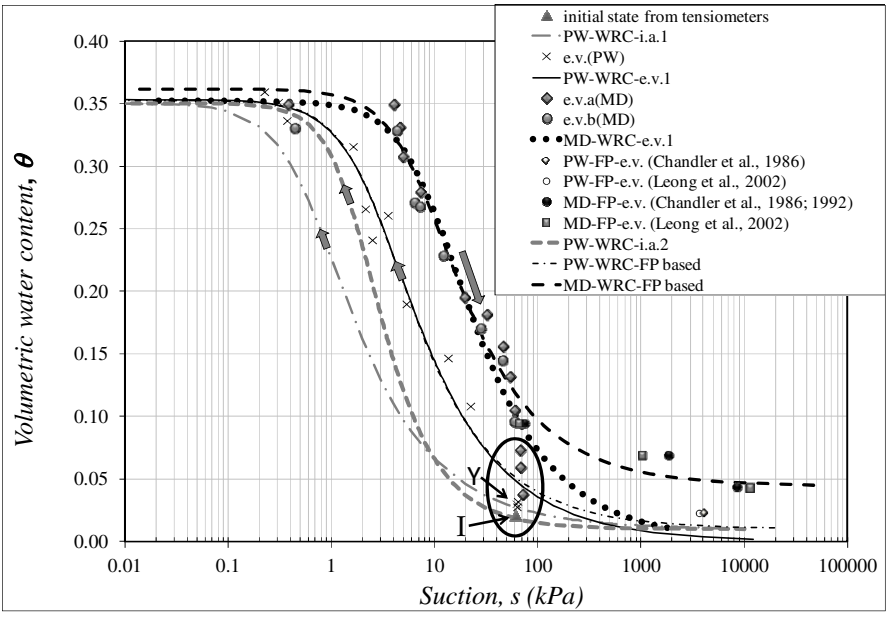

Fig. 4. Experimental data and water retention functions.

References

ASTM 2006 - Standard practice for classification of soil for engineering purposes (Unified Soil Classification System) ASTM standard D2487. ASTM, West Conshohocken, Pa (2006)

Bottiglieri, O., Cafaro, F., Cotecchia, F.: Modellazione fisica e numerica dell' infiltrazione in terreno a grana media non saturo. In: Incontro Annuale dei Ricercatori di Ingegneria Geotecnica, IARG, Catania, Italy (2008)

Bottiglieri, O.: Caratterizzazione idraulica di un terreno a grana media parzialmente saturi. PhD Thesis, Politecnico di Bari, Italy (2009)

Cafaro, F., Hoffmann, C., Cotecchia, F., Buscemi, A., Bottiglieri, O., Tarantino, A.: Modellazione del comportamento idraulico di terreni parzialmente saturi a grana media e grossa. Rivista Italiana di Geotecnica (2008)

Chandler, R.J., Gutierrez, C.I.: The filter paper method of suction measurement. Géotechnique 36(2), 265–268 (1986)

Chandler, R.J., Crilly, M.S., Montgomery-Smith, G.: A low-cost method of assessing clay desiccation for low-rise buildings. Proceedings of Institution of Civil Engineers 92, 82–89 (1992)

Cassel, D.K., Klute, A.: Water Potential: tensiometry. Methods of Soil Analysis, part 1, pp. 563–596 (1986)

Evangelista, A., Nicotera, M.V., Papa, R., Urciuoli, G.: Prove di evaporazione per la determinazione delle caratteristiche idrauliche di terreni piroclastici. In: Giornata di Studio Sulla Meccanica dei Terreni Non Saturi, December 4. Universita' di Cassino (2006)

Fredlund, D.C.: Unsaturated soil mechanics in Engineering Practice. Journal of Geotechnical and Geoenviromental Engineering (2006)

Hopmans, J.W., Dane, J.H.: Temperature dependence of soil water retention curves. Soil Science Society of America Journal 50, 562–567 (1986)

IGWMC, Hydrus 2D: Simulating Water flow, Heat and Solute Transport in variably Saturated media. U.S. Salinity Lab. Agricult. Research Service and U.S. Dept of Agriculture Riverside California (1999)

Kodesová, R.: Determination of hydraulic properties of unsaturated soil via inverse modeling. Lecture Given at the College on Soil Physics, Trieste (March 3-21, 2003)

Leong, E.C., He, L., Rahardjo, H.: Factors affecting the filter paper method for total and matric suction measurements. Geotech. Tech. Test. J. 25, 321–332 (2002)

Lu, N., Likos, W.J.: Unsaturated Soil Mechanics. John Wiley, Hoboken (2004)

Marinho, F.A.M.: Shrinkage Behaviour of Some Plastic Clays, Ph.D. Thesis, Imperial College. University of London, UK (1994)

Marinho, F.A.M., Oliveira, O.M.: The Filter Paper Method Revisited. Geotechnical Testing J. 29(3), 250–258 (2006)

Mualem, Y.: A new model predicting the hydraulic conductivity of unsaturated porous media. Water Resour. Res. 12, 513–522 (1976)

Salager, S., El Youssoufi, M.S., Saix, C.: Definition and experimental determination of a soil-water retention surface. Canadian Geotechnical Journal 47, 609–622 (2006)

Stannard David, I.: Tensiometers-Theory, Construction, and Use. Geotechnical Testing Journal 15(1), 48–58 (1992)

Stauffer, F., Kinzelbach, W.: Cyclic hysteretic flow in porous medium column: model, experiment, and simulations. Journal of Hydrology 240, 264–275 (2001)

Sreedep, S., Singh, D.N.: Methodology for determination of osmotic suction of soils. Geotech. Geol. Eng. 24, 1469–1479 (2006)

van Genuchten, M.T.: A closed form equation for predicting the hydraulic conductivity of unsaturated soils. Soil Science Society of America Journal 44, 892–898 (1980)

van Genuchten, M.T., Leij, F.J., Yates, S.R.: The RETC code for quantifying hydraulic functions of unsaturated soils. Technical Report IAG-DW 12933934, US Salinity Laboratory, US Department of Agriculture, Agricultural Research Service, Riverside, CA (1991)

Constructing Fast, Accurate Soil Water Characteristic Curves by Combining the Wind/Schindler and Vapor Pressure Techniques

Colin S. Campbell, Douglas R. Cobos, Leonardo D. Rivera, Kelsey M. Dunne, and Gaylon S. Campbell

Abstract. The measurement of suction in unsaturated soils is essential in many areas of geotechnical engineering like modeling hydraulic properties or analyzing shrink-swell characteristics from the soil water characteristic curve (SWCC). For many years, filter paper and axis translation made the majority of the SWCCs, but these techniques are time consuming and inaccurate. The vapor pressure method (VPM) overcomes these, but past instruments lacked the resolution in the critical 100 to 1000 kPa range. Recently, technological advances have made it possible to measure soil suction up to 50 kPa. In addition, a new, automated method (Wind/Schindler; WSM) provides the wet end of the SWCC. Several water retention curves were run for a variety of soil types. Characteristic curves crossed over each other smoothly. The VPM method combined with the WSM provide both speed and accuracy to the measurement of soil suction, construction of SWCC, and soil hydraulic properties evaluation.

Keywords: soil water characteristic curve, soil suction, chilled mirror dew point, vapor pressure technique.

Colin S. Campbell
Decagon Devices, Inc., Pullman, WA, USA
e-mail: colin@decagon.com

Douglas R. Cobos
Decagon Devices, Inc., Pullman, WA, USA
e-mail: doug@decagon.com

Leonardo D. Rivera
Decagon Devices, Inc., Pullman, WA, USA
e-mail: leo@decagon.com

Kelsey M. Dunne
Decagon Devices, Inc., Pullman, WA, USA
e-mail: kelsey@decagon.com

Gaylon S. Campbell
Decagon Devices, Inc., Pullman, WA, USA
e-mail: gsc@decagon.com

1 Introduction

Soil water characteristic curves (SWCC) are critical for analyzing the behavior of unsaturated soil in a variety of applications (Fredlund & Rahandjo 1993). SWCCs can provide valuable information about soil swelling potential, compressibility, hydraulic conductivity, and shear strength. Despite the critical need for this information, SWCCs are often estimated through parametric functions rather than measured (Imre et al. 2010), leading to poor understanding of soil behavior.

Relatively few techniques are available for measuring a SWCC in spite of its importance. Clearly, the main difficulty lies in measuring the soil suction, as soil water content is a relatively simple parameter to measure with good accuracy. There is no single solution that will give accurate suction measurements across the entire range of interest. Especially difficult is the 100 to 1000 kPa suction range where a critical portion of the curve is defined, but has been very difficult to characterize using standard techniques. However, recent developments in water potential measurement technology have simplified and improved SWCC analysis allowing for a more complete understanding of unsaturated soil behavior.

1.1 Techniques for Measuring Soil Suction

Filter paper equilibration has long been a popular technique for measuring soil suction in geotechnical engineering (McQueen & Miller 1968, Al-Khafaf & Hanks 1974, and Campbell & Gee 1986). Filter paper is a secondary measurement method that relates the measured water content of a piece of filter paper in suction equilibrium with a soil sample to soil suction through a SWCC of the filter paper itself. Although the filter paper technique is attractive from a cost perspective, measurement errors and time expenditure limit its usefulness.

Traditionally, axis translation methods (pressure plate extractors) have also been used to create SWCCs by equilibrating samples at preset matric suctions, and then determining the water content of the equilibrated samples by oven drying. However, questions about its performance at suctions drier than 200 to 300 kPa (Campbell, 1988, Gee et al. 2002, Bittelli & Flury, 2008) combined with whether the process of water loss from soil under pressure is similar to water loss under suction (Frydman & Baker 2009) highlight a need for alternative methods for suction analysis.

Tensiometers provide another popular method to measure matric suction. Most are limited to the range 0 to 80 kPa. (Lu & Likos, 2004). Though special designs and pretreatments allow some units to reach 1500 kPa (Ridley & Burland, 1993), they are not widely available. Installing tensiometers in an evaporating soil core, Schindler (1980) and Schindler & Muller (2006) were able to continuously measure both suction and gravimetric water content to produce an automated SWCC for wet soil (called the Wind/Schindler method, WSM).

Vapor pressure methods (VPM) are ideal from making suction measurements of samples that are drier than the tensiometer or axis translation range. These measurements are possible because lowering the potential energy (increasing suction) of water in the soil matrix (ψ_t) will also reduce the number of water molecules (and the equilibrium vapor pressure, p) in the headspace above the sample. This relationship is given by the Kelvin equation:

$$\psi_t = \frac{R(T+273.15)}{V_w} \ln\left(\frac{P}{P_0}\right) \quad (1)$$

Here, R is the gas constant (8.3143 J/mol), T is Celsius temperature, V_w is the molar volume of water (1.8 x 10^{-5} m^3 mol^{-1}), and p_o is the saturated vapor pressure at the sample temperature. The units of ψ_t are J m^{-3} or N m^{-2} or Pa. Thus, measuring the vapor pressure in the head space by wet bulb depression, as with the thermocouple psychrometer (Rawlins & Campbell 1986) or the dew point temperature as with the dew point potentiometer (Gee et al. 1992) will give a direct measurement of total soil suction, as long as the vapor gap between the sample and the sensor is a perfect semi-permeable membrane (which it is).

The objective of this work was to investigate the viability of combining the VPM for the dryer soil suctions with the WSM for the wet suctions to construct a rapid, accurate, and consistent SWCC. Of particular interest is the performance of the VPM in the critical 100 to 1000 kPa suction range.

2 Methods

Five different soil types were chosen to create SWCCs over a wide range of textures. They included Hanipoe Silt Loam (volcanic in origin) from two field plot locations, a Palouse silt loam (SL), a Kiona very fine sandy loam (FSL), and a Schawana loamy fine sand (LFS). Properties of each soil are shown in Table 1.

All samples tested using VPM (except SL) began air dry and were wetted to varying degrees using distilled water so as to obtain a wide range of suctions. The SL samples were collected as intact cores and were either wet up or dried down from the field water content. This is important to note because all samples besides the dry region of SL SWCC were measured on the wetting leg of the hysteresis loop while the dry region of the Palouse silt loam SWCC was measured on the drying leg of the hysteresis loop.

After wetting or drying, samples were sealed in airtight containers and equilibrated for > 24 h at room temperature. Next, the soil was placed in 15-ml stainless steel sample cups, inserted into a VPM chilled-mirror dew point instrument (WP4C, Decagon Devices, Inc, Pullman, WA, USA) and read on precision mode for 10 to 15 minutes (depending on sample wetness). Following the VPM measurements, we measured the gravimetric water content by weighing the sample in the stainless sample cup on a precision scale (0.1 mg), oven drying at 105° C for 24 h, and weighing again.

Table 1. Physical properties of test soils. Bulk density (ρb) for each soil is shown at a pressure of 1/3 bar along with the gravimetric water content (w) at permanent wilting point and the coefficient of linear extensibility (COLE).

	†Sand	†Clay	†Silt	†$\rho_{b\ (1/3\ bar)}$	*w* (-1500 kPa)	†COLE
	%	%	%	Mg m^{-3}	g g^{-1}	-
Kiona Very Fine Sandy Loam	64.4	10	25.6	1.59	0.05	1.5
Schawana Loamy Fine Sand	79.4	4	16.6	1.5	0.03	1.5
Palouse Silt Loam	67.7	21	11.3	1.2	0.07	1.5
Hanipoe Silt Loam B2	*	*	*	0.52	0.14	*
Hanipoe Silt Loam B4	*	*	*	0.61	0.21	*

* unavailable

† values from published NRCS soil surveys

For the two volcanic Hanipoe silt loam samples, tensiometers measured suction in the low (high water content) range. Tensiometers read only matric, not total suction like the VPM. However, because the soil electrical conductivity was low, we assumed a negligible osmotic suction and therefore the matric suction measured by the tensiometer should be equivalent to the total suction measured by the WP4C. Samples were prepared in a similar manner to that noted above. High-tension tensiometers (Model T5, UMS, GmbH, Munich, Germany) were inserted in soils prepared at several suctions between 0 and 100 kPa and allowed to equilibrate. Subsamples were collected in soil sampling tins and analyzed for water content using the method described above.

The low suction portion of the SWCCs of the remainder of the soils were measured using the WSM (HyProp, UMS, GmbH, Munich, Germany; Peters & Durner, 2008), where two tensiometers are installed, one at 1.5 and the other at 4.5 cm from the surface, in an intact (where possible) soil core (250 cm^3, height 6 cm) (Schindler, 1980; Schindler & Müller, 2006). Prior to installation the sample is saturated from the bottom for 24 to 48 hours then allowed to freely drained to release any free water. The sample is sealed at the bottom and placed on a balance where water is freely evaporated from the upper surface while suction and mass are recorded over time (for complete explanation, see Peters & Durner 2006).

3 Results and Discussion

Tensiometer measurements on the two Hanipoe volcanic soils matched well with suction values measured using VPM (Fig. 1). In the critical region of 100 to 1000 kPa, there is good agreement in the trend of the data, elucidated by fit of the unsaturated SWCC function given by Campbell & Shiozawa (1992).

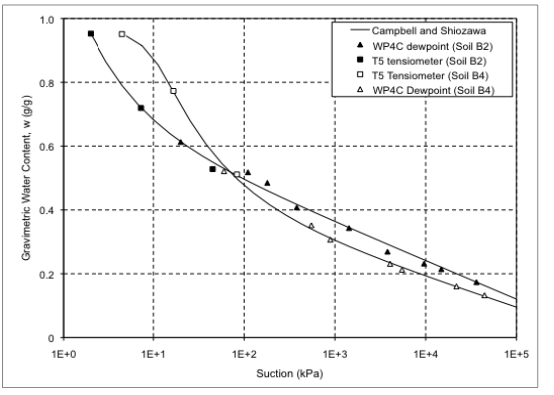

Fig. 1. SWCCs for Hanipoe silt loam samples from different plots. Data show good agreement between tensiometer and chilled mirror dew point measurements as well as acceptable fits from Campbell and Shiozawa model.

Soils tested using the combined WSM and VPM also showed the expected crossover between the two measurement techniques (Figs. 2, 3, and 4) and the van Genuchten Bimodal retention function (Durner, 1994) appeared to fit the data well. Still, there are several differences that illustrate some areas for improvement in the measurement method. The SWCC for the LFS shows an excellent transition between 10 and 1000 kPa (Fig. 2). This is particularly interesting because the VPM samples were wetted from air dry and the WSM sample was dried from saturation, raising the possibility of hysteresis.

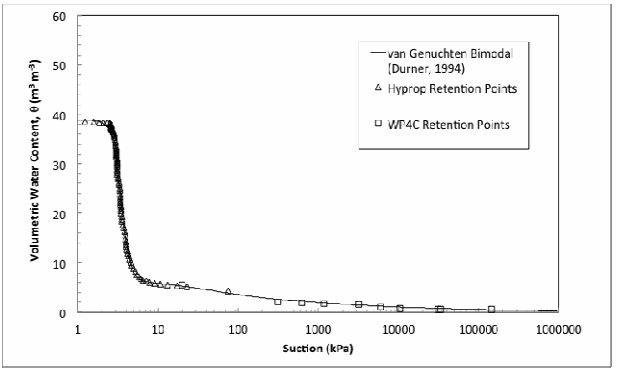

Fig. 2. SWCC for Schawana Loamy Fine Sand . Data show good agreement between VPM data taken at high suctions and WSM data at low suctions. Although water was added to the VPM samples and evaporated from the WSM sample, no hysteresis is seen in the measurements.

However, due to the low quantity of silt and clay size particles in the sample, we presume a low surface area for water binding and the associated similarity between wetting and drying processes. Although the FSL was prepared in a similar manner to the LFS, the SWCC shows a significant transition between 60 and 1000 kPa with the trend of the VPM SWCC far below that of the WSM (Fig. 3). Although fit well by the retention function, the failure to match these curves may be caused by hysteresis in the measurement. The FSL has considerably more fine particles whose wetting (for VPM samples) and drying (for WSL samples) will exhibit considerably different water content levels at the same level of suction.

The SL SWCC further supports this finding (Fig. 4). Here, two differences in methodology should be noted. First, samples collected from the field were left intact. Second, samples were either wet up or dried down from field suction values (~100 kPa). Figure 4 shows good agreement between WSM and VPM for samples drier than 100 kPa, which were dried from field conditions and therefore fall on the drying leg of the hysteresis loop similar to the WSM method. However, the VPM samples wetter than 100 kPa were wet up from field conditions placing them on the wetting leg of the hysteresis loop, possibly leading to their divergence.

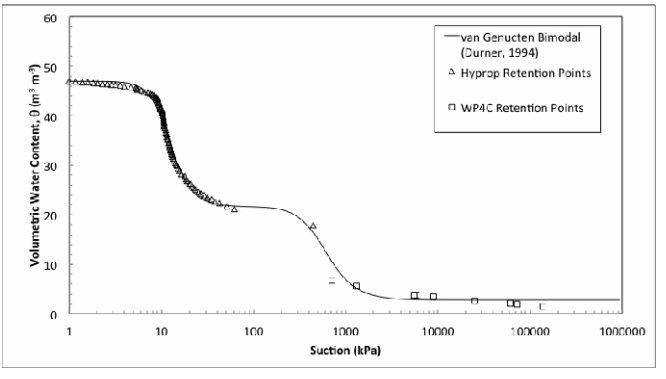

Fig. 3. SWCC of Kiona very fine sandy loam. This curve exhibits a distinct difference between the wetting leg measured using the VPM and drying leg using the WSM. Deviations from the expected trend appear to be caused by differences in sample preparation and bulk density.

It is interesting to note that this deviation is relatively small compared to that of the FSL (Fig. 3). We can speculate that using intact soil cores, for which we can maintain an accurate bulk density for all samples, may have lead to the improved correlation.

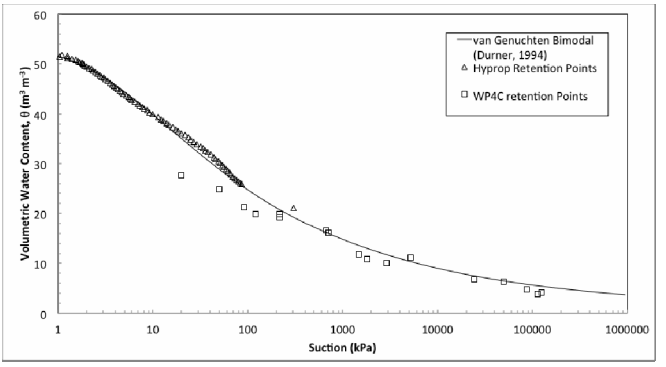

Fig. 4. SWCC for Palouse silt loam exhibits excellent agreement between VPM and WSM measurements. Deviations from the van Genuchten retention curve fit only occur in VPM samples below ~ 100 kPa suction. It appears that this deviation was caused hysteresis in the SL due to these samples being wet up from field conditions rather than dried down from field conditions.

4 Conclusion

Pairing the vapor equilibration method with the Wind/Schindler method for measuring suction and deriving soil water characteristic curves provided data that effectively crossed the 100 to 1000 kPa range and gave highly detailed SWCC. Using the two techniques in concert speeds the process of analysis and removes the difficulties inherent in past techniques that are diminished by long wait times and poor equilibration.

The authors are not aware of any previous work that has paired the VPM and WSM techniques and shown the match between the two very different techniques. These new methods provide an exciting opportunity to effectively measure the entire SWCC range including the under-characterized region between 100 and 1000 kPa. Still, with the extended region of measurement, additional care must be taken in sample preparation to ensure that confounding factors like soil bulk density and hysteresis do not affect the shape of the curve. *In situ* sampling, including intact cores for soils with larger surface areas may improve VPM and WSM agreement. In addition, starting all samples at a low suction and allowing them to evaporate will help to ensure all measurements are on the drying curve and align the two methods. More research is needed to further understand the hysterical features of the fine textured soils.

References

Al-Khafaf, S., Hanks, R.J.: Evaluation of the filter paper method for estimating soil water potential. Soil Sci. 117, 194–199 (1974)

Bittelli, M., Flury, M.: Errors in water retention curves determined with pressure plates. Soil Sci. Soc. Am. J. 73, 1453–1460 (2008)

Campbell, G.S., Gee, G.W.: Water Potential: Miscellaneous Methods. In Methods of Soil Analysis, Part 1. Physical and Mineralogical Methods. Agronomy Monograph no. 9:619-633. Madison, WI, USA (1986)

Campbell, G.S.: Soil water potential measurement: an overview. Irrig. Sci. 9, 265–273 (1988)

Campbell, G.S., Shozawa, S.: Prediction of hydraulic properties of soils using particl-size distribution and bulk density data. In: van Genuchten, M.T., Leij, R.J., Lund, L.J. (eds.) International Workshop on Indirect Methods for Estimating the Hydraulic Properties of Unsaturated Soils, pp. 317–328. Univ. of California, Riverside (1992)

Campbell, G.S., Smith, D.M., Teare, B.L.: Application of a Dew Point Method to Obtain the Soil Water Characteristic. In: Schanz, T. (ed.) Experimental Unsaturated Soil Mechanics, pp. 71–77. Springer, New York (2007)

Durner, W.: Hydraulic conductivity estimation 703 for soils with heterogeneous pore structure. Water Resour. Res. 30, 211–223 (1994); Fredlund, D.G., Rahardjo, H.: Soil mechanics for unsaturated soils. John Wiley and Sons, Inc., New York (1993)

Frydman, S., Baker, R.: Theoretical Soil-Water Characteristic Curves Based on Adsorption, Caivitation, and a Double Porocity Model. International Journal of Geomechanics 9(6), 250–257 (2009)

Gee, G.W., Campbell, M.D., Campbell, G.S., Campbell, J.H.: Rapid measurement of low soil water potentials using a water activity meter. Soil Sci. Soc. Am. J. 56, 1068–1070 (1992)

Gee, G.W., Ward, A.L., Zhang, Z.F., Campbell, G.S., Mathison, J.: The influence of hydraulic nonequilibrium on pressure plate data. Vadose Zone J. 1, 172–178 (2002)

Greenspan, L.: Humidity fixed points of binary saturated aqueous solutions. J. Res Nat. Bureau Stds. – A. Physics and Chemistry 81A, 89–96 (1977)

Imre, E., Rajkai, K., Genovese, R., Jommi, C.: A transfer function of a soil water characteristic curve model for sands. In: Alonso, E., Gens, A. (eds.) Unsaturated Soils, pp. 453–459. CRC Press (2010)

Leong, E.C., Tripathy, S., Rahardjo, H.: Total suction measurement of unsaturated soils with a device using the chilled-mirror dew-point technique. Geotechnique 53, 173–182 (2003)

Lu, N., Likos, W.J.: Unsaturated Soil Mechanics. Wiley, Hoboken (2004)

McQueen, I.S., Miller, R.R.: Calibration and evaluation of a wide-range gravimetric method for measuring moisture stress. Soil Sci. 105, 225–231 (1968)

Peters, A., Durner, W.: Improved estimation of soil water retentioin characteristics from hydrostatic colum experiments. Water Resour. Res. 42, W11401 (2006), doi:10.1029/2006WR004952

Peters, A., Durner, W.: Simplified Evaporation Method for Determining Soil Hydraulic Properties. J. Hydrology 356, 147–162 (2008)

Rawlins, S.L., Campbell, G.S.: Water potential: Thermocouple Psychrometry. In: Methods of Soil Analysis Part 1, Agron. Monogr. 9, 2nd edn., Madison, WI, pp. 597–618 (1986)

Ridley, A.M., Burland, J.B.: A new instrument for the measurement of soil moisture suction. Géotechnique 43, 321–324 (1993)

Robinson, R.A., Stokes, R.H.: Electrolyte Solutions: Second Revised Edition. Dover Publications, Mineola (2002)

Schindler, U.: EinSchnellverfahrenzurMessung der Wasserleitfähigkeiimteilgesättigten Boden an Stechzylinderproben. Arch. Acker- PflanzenbauBodenkd 24, 1–7 (1980)

Schindler, U., Müller, L.: Simplifying the evaporation method for quantifying soil hydraulic properties. J. Plant. Nutr. Soil Sci. 169, 623–629 (2006)

Schindler, U., Durner, W., von Unold, G., Müller, L., Wieland, R.: The evaporation method: Extending the measurement range of soil hydraulic properties using the air-entry pressure of the ceramic cup. J. Plant Nutr. Soil Sci. 173, 563–572 (2010)

Enhancement of a Commercial Pressure Plate Apparatus for Soil Water Retention Curves

Marco Caruso and Cristina Jommi

Abstract. Pressure plates are widely used to measure soil water retention properties of soils in the laboratory with axis-translation technique. Imperfect sealing of the pressure chamber, exchange of water vapour between the soil and the air in the chamber, lack of soil-plate contact, part of the porous plate directly in contact with air in the pressure chamber, and evaporation of water from the ballast tube may lead to incorrect estimation of the water volumes exchanged by the soil. An improved version of a commercial pressure plate apparatus is presented, which proved able to reduce the intrinsic drawbacks of the original design. The system was also equipped with an image-processing based data acquisition system for continuous measurement of exchanged water.

Keywords: axis translation, experimental techniques, matric suction, retention curve.

1 Introduction

Pressure plate apparatus has been widely used as a standard technique for the determination of soil water retention curve (SWRC) since Richards' (1948) proposal. In the original arrangement, pore water is kept at constant atmospheric pressure, allowing drainage, while the gas pressure (typically air pressure) is raised, to apply suction via the axis translation technique. Water retention data are obtained by increasing the suction and measuring the water content at equilibrium.

Marco Caruso
Politecnico di Milano, Milano, Italy
e-mail: caruso@stru.polimi.it

Cristina Jommi
Politecnico di Milano, Milano, Italy
e-mail: cristina.jommi@polimi.it

A body of literature is devoted to the assessment of the pressure plate data accuracy. Campbell (1988) showed that lack of sample suction equalisation with imposed external pressures is often due to poor contact between the sample and the porous plate. Even under ideal contact, low hydraulic conductivity of the soil can hinder full equalisation. Madsen et al. (1986) highlighted some problems related to equalisation issues at suctions higher than 500 kPa. Cresswell et al. (2008) investigated the accuracy of pressure plate measurements at 0.5 and 1.5 MPa, and stressed on the problems arising from contact loss due to soil shrinkage. Bittelli & Flury (2009) showed differences between the data obtained by a standard pressure plate apparatus, equipped with a 15 bars ceramic, and dew point meter measurements, suggesting the need for further investigation on the experimental techniques.

Gee et al. (2002) studied how sample equilibrium is affected by both soil and ceramic hydraulic conductivity, by means of numerical simulations. They concluded that for coarse grained soils (sands and gravels) long time lapses are necessary for equilibrium to be achieved (days to weeks) because of the very low soil water conductivity at low suctions. Equilibrium can be achieved in a reasonable time interval for finer soils, but only if ceramic plates having relatively high conductivities, greater than 10^{-10} m/s, are mounted in the apparatus. They showed experimental data on sand, silt, and clayey soils obtained with a high entry value (1.5 MPa) ceramic plate, and they concluded that neither loading the samples, nor the use of kaolinite slurry could allow the samples to equilibrate in times up to 10 days. These drawbacks are also shown to depend on samples height, and they can be reduced if thin samples, about 10 mm thick, are tested.

Wang & Benson (2004) put in evidence how pressure plate apparatuses suffer from a few problems due to their mechanical design. Imperfect sealing of the chamber, air leakage through the external part of the plate (especially at high pressures), diffusion of gas through the ceramic plate, air entrapment beneath the ceramic plate lead to poor control of the mass of water in the specimen. The authors tried to limit these drawbacks by means of a new design for the position of the porous plate and by improving the sealing system. Leong et al. (2004) paid attention to air diffusion in the water drainage system, and they suggested a modified apparatus equipped with a "flushing assembly" that enables flushing of air to be performed during the test without closing the air pressure line.

Notwithstanding its well-known drawbacks, pressure plate extractor is a cheap and generally appreciated equipment for the determination of water retention properites of unsaturated soils. A research effort has been made to suggest possible improvements to a commercial equipment, to increase data reliability. The suggested enhancements and experimental verification of the modified apparatus are described in the following.

2 The Modified Pressure Plate Apparatus

The reference apparatus is a commercial Soilmoisture® 1250 volumetric pressure plate extractor. It is claimed to be a high precision extractor, designed so that the outflow section of the instrument gives stable reading (Soilmoisture 2005). When used in conjunction with a "hysteresis attachment", it allows the measurement of the volume of water inflowing or outflowing from the sample at any pressure level. Following literature suggestions, the cell should be equipped with ceramic plates as permeable as possible, and with entry values (AEV) as low as possible, depending on the soil to be tested.

The experimental tests were run on silty sands, hence two ceramic plates with AEVs of 250 kPa and 500 kPa, having hydraulic conductivity of $6.3 \cdot 10^{-9}$ m/s and $1.7 \cdot 10^{-9}$ m/s, respectively, were mounted in two identical pressure plate extractors. A series of preliminary tests carried out with the original commercial testing apparatus showed many of the experimental issues affecting data reliability reported in the previous literature review.

Therefore, various enhancements were performed and tested. The ones which proved to be effective to improve data reliability are briefly described in the following. They consist in the design of a combined contact and counter-evaporation system, in improving hydraulic connections, in modifying the pressure control manifold, and in providing some modifications to the measurement system.

2.1 The Contact System

Preliminary tests run in the laboratory of the Politecnico di Milano (Caruso 2007) had confirmed the problems related to poor contact between the soil specimen and the ceramic plate to be the most influent negative factor affecting the pressure plate experimental success. Therefore, a contact device has been developed to ensure better contact between the soil specimen and the ceramic plate along all test duration.

The system (figure 2) is based on a cave variable-length stainless steel piston driven by a spring mounted inside the cave piston itself. The spring allows constantly pushing the specimen against the pressure plate, regardless any soil shrinkage or swelling. The vertical load, which can be calibrated by choosing the elastic constant of the spring, is transmitted to the specimen as uniformly as possible through to a plate with holes positioned on the top surface of the sample. A high number of holes in the plate are necessary to ensure continuity between pressurised air in the chamber and air in soil pores.

To prevent radial strain due to the even small vertical load applied to the specimen a stainless steel ring was designed to laterally confine the specimen. The stainless steel ring is equipped with a cutter on its top, in order to use it already for sampling tasks. If axial strain occurs, the top loading plate can slide inside the ring

without friction. The ring also prevents water outflow from the specimen lateral surface.

The contact system has been designed for testing of 80 mm or 75 mm diameter specimen. The diameter was chosen to allow testing of undisturbed samples from standard site probes. The sample thickness has been chosen to be 15 mm, following previous literature suggestions, and ensuring both reasonable testing times and the accuracy of the water volume measurement system to be sufficiently high compared to the amount of water volume expected to be exchanged by the soil.

2.2 Improving the Measurement Accuracy

The need for accurate measurement of water volume is mandatory, especially when trying to determine the SWRC by means of multi-stage test on a single specimen, consisting in applying a series of increasing pressure steps and waiting until the equilibrium condition are established (i.e. water flow lowers under a predefined tolerance). The specimen water content at the end of each step can be estimated only on the basis of exchanged water measurements, while check on the actual water content can be performed only at the end of the test.

The first hindering effect on measurement may be due to air leakage through the porous ceramic and, as a consequence, into the water measurement circuit. Air leakage can be identified only by visual inspection and, for this reason, all circuit bundle tubes have been replaced with transparent ones. Diffusion of air can be prevented mostly by careful saturation of the porous ceramic before the beginning of the test. It was observed that submerging it in a sealed box filled with de-aired water while applying vacuum can be effective to ensure full saturation of the porous stones chosen for the experimental tests on silty sands. Further details on similar procedures may be found, for instance, in Tarantino & Mongiovì (2002). Careful saturation ensures air diffusion reduction in the first steps of a multi-stage test. Nonetheless, air diffusion was noticed in tests lasting more than two weeks, even if the difference between air and water pressure was maintained below the air entry value of the porous stone. Diffused air can be removed by forcing it to move along the outlet circuit connecting the chamber to the air trap. Afterwards, the air can be eliminated with the aid of a vacuum pump, re-establishing the reference water level in the trap.

Water evaporation from the sample into the extractor cell, occurring until the air in the chamber becomes saturated, should be avoided as much as possible, as this volume exchange cannot be measured. To reduce evaporation in the chamber, an air saturator was placed along the air inlet into the chamber. A possible drawback of this procedure is that moisture may condense due to temperature differences on the free area of the porous stone, which has a diameter of about 120 mm larger than the 80 mm diameter of the specimens. To avoid free moisture flux through the porous plate, which would mix with the water extracted from the soil and hinder the reliability of soil moisture exchange measurement, a stainless steel isolation ring is placed around the specimen covering the free ceramic portion.

The measurement system (figure 2) was enhanced by graduating the horizontal ballast tube every 0.1cm^3, in order to avoid the need for sucking water in the burette to perform any reading. As a consequence, more frequent readings can be performed continuously, especially immediately after air pressure increments.

To allow for automatic reading of water volume exchanged by the soil sample, an image acquisition system was placed to track the ballast filling status as frequently as desired, with a minimum time interval of 10 s.

The image processing system permits accurate estimate of water fluxes, and allows for reliable determination of hydraulic conductivity as a function of water content by means of a backward analysis based on Richard's equation.

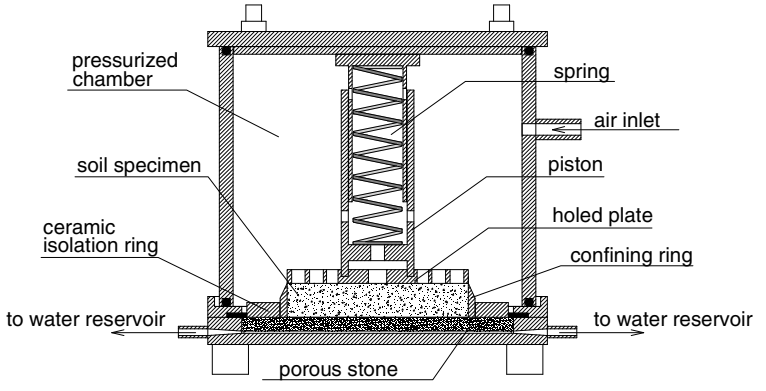

Fig. 1. Schematic representation of the contact and leakage reduction system into the pressurized chamber.

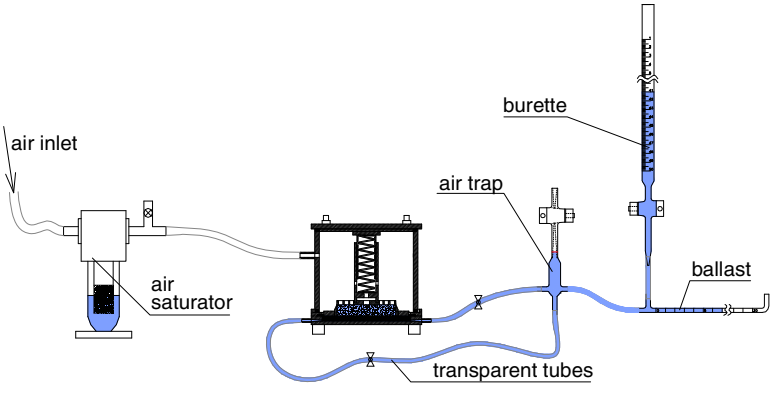

Fig. 2. Schematic representation of the hydraulic connections and water volume measurement system of the modified pressure plate apparatus.

3 Experimental Results

The image-based acquisition system and the hydraulic circuit improvements are permanently installed and used throughout any test. Two set of preliminary tests were conducted to evaluate effectiveness of the enhanced contact system on the SWRC data from a multi-step procedure. The soils used were a silty sand and a clayey silt.

The data (i.e. the exchanged water volumes) were post-processed to obtain the drying branch of the SWRC both following a forward and a backward procedure. In the forward procedure, the initial water content (estimated from direct measurements on the part of the sample discarded from the trimming procedure) is taken as reference value, and the current water volume is calculated by subtracting the observed volume outflow at equilibrium. On the contrary, in the backward procedure the water contents are estimated based on the water content measured at the end of the test by means of oven drying. If no errors occurred during the test, the two procedures should give the same values for the water retention results.

A comparison between the results obtained by means of the original equipment and those obtained in the enhanced apparatus are compared in figure 3 for the clayey silt (table 1). The air-dried soil sieved with a 2 mm sieve was prepared by moist-tamping into cylindrical 80x30 mm specimens at e = 0.63 and Sr = 0.9. Each specimen was then trimmed to the required size, saturated by constant-head flow, and mounted into the pressure plate.

Table 1. Soil properties (AASHTO standard)

%sand	%silt	%clay	Specific gravity	Liquid limit	Plastic limit
18	59	21	2.71	0.34	0.19

The results obtained by forward and backward processing the data coming from the enhanced apparatus tend to overlap, and they differ by an amount which can be disregarded for practical purposes. The same two elaborations of the data coming from the original equipment show differences of more than 30%.

The experimental data obtained with the enhanced apparatus correctly represent the water content exchanges of the soil. On the contrary, measurements which can be done with the original equipment suffer from relevant losses (among which evaporation in the chamber may be considered the most important), which hinder suction control, hence correct description of the soil hydraulic behaviour.

The data obtained with the pressure plate apparatus are also compared in the figure with experimental points previously obtained by means of direct suction measurement with tensiometers (Caruso, 2003). The two data sets are consistent, with tensiometers giving slightly higher suctions for the same water content, as often observed when data sets of the two types are compared one to the other.

In figure 4 the measured water outflows obtained by means of the two setups are compared with each other for the two soils investigated. The comparison confirms the importance of assuring optimal contact between the porous stone and the sample during the test to correctly estimate the water content at equilibrium, for both soils. Besides, the data presented in the figure allow appreciating the influence of contact loss on the time evolution of the results. The original setup does not allow evaluating correctly the flow rates, which limits to a great extent the possibility of deriving reliable information on the hydraulic conductivity of the soils.

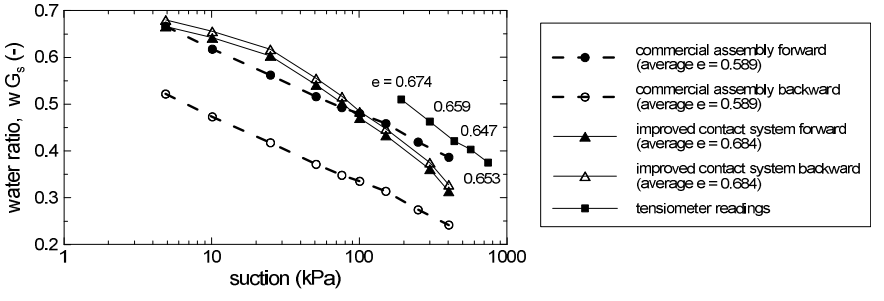

Fig. 3. Data obtained for the drying branch of the SWRC of the clayey silt.

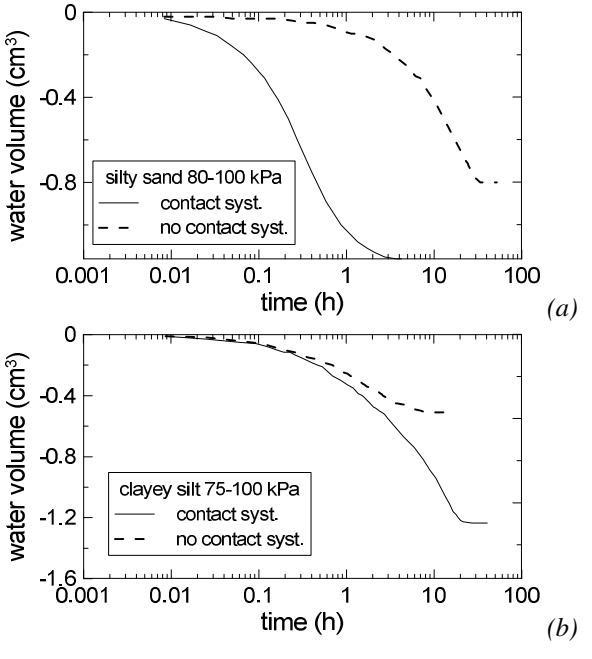

Fig. 4. Pressure increment step analysis (a) 80-100 kPa and (b) 75-100 kPa

4 Conclusions

The relevant effects on data elaboration of some drawbacks of the original design of commercial pressure plate extractors are discussed in the paper. The most important limitations come from air evaporation in the chamber, affecting suction control, air diffusion in the measuring system and imperfect contact between the sample and the porous AEV stone. Although the data obtained with the original equipment could be post-processed to obtain realistic water contents for practical applications relying mostly on the initial water content, the outflow rates exclusively due to soil-water exchanges during each step are lost, and no reliable information can be deduced on the hydraulic conductivity of the soil.

In the paper a few modifications are proposed to enhance the accuracy of the commercial equipment, providing improved contact, limited losses and more reliable data on water outflow and flow rates. The use of a contact spring allows partial control of axial stress, especially for soils having limited deformability.

Acknowledgements. The authors acknowledge the Italian Ministry of Education and Research (MIUR) for the financial support provided through the grant: Italian National Research Project PRIN 2008B5T829 004, "Durability of clays used in waste containment systems".

References

Bittelli, M., Flury, M.: Errors in water retention curves determined with pressure plates. Soil Sci. Soc. Am. J. 73, 1453–1460 (2009), doi:10.2136/sssaj2008.0082

Campbell, G.S.: Soil water potential measurement: an overview. Irrig. Sci. 9, 265–273 (1988)

Caruso, M.: Studio della resistenza di un limo costipato mediante prove di taglio diretto con misure di suzione. Graduate Thesis. Politecnico di Milano, Italy (2003)

Caruso, M.: Una metodologia teorica, sperimentale e numerica per la previsione del bilancio idrico nei terreni superficiali non saturi. PhD Thesis, Università degli Studi di Parma, Italy (2007)

Cresswell, H.P., Green, T.W., McKenzie, N.J.: The adequacy of pressure soil plate apparatus for determining soil water retention. Soil Sci. Soc. Am. J. 72, 41–49 (2008), doi:10.2136/sssaj2006.0182

Gee, G.W., Warda, A.L., Zhanga, Z.F., Campbell, G.S., Mathison, J.: The influence of hydraulic nonequilibrium on pressure plate data. Vadose Zone J. 1, 172–178 (2002)

Leong, E.C., Tripathy, S., Rahardjo, H.: A modified pressure plate apparatus. Geotechnical Test. J. 27, 322–331 (2004)

Madsen, H.B., Jensen, C.R., Boysen, T.: A comparison of the thermocouple psychrometer and the pressure plate methods for determination of soil water characteristic curves. Eur. J. Soil Sci. 37, 357–362 (1986), doi:10.1111/j.1365-2389.1986.tb00368.x

Richards, L.A.: A pressure membrane extraction apparatus for soil solution. Soil. Sci. 51, 377–386 (1948)

Tarantino, A., Mongiovì, L.: Design and construction of a tensiometer for direct measurement of matric suction. In: Proc. 3nd Int. Conf. on Unsaturated Soils, Recife, Brasil, vol. 1, pp. 319–324 (2002)

Wang, X., Benson, C.H.: Leak-free pressure plate extractor for measuring the soil water characteristic curve. Geotechnical Test. J. 27, 163–172 (2004)

Characterizing Liquid Phase Fabric of Unsaturated Specimens from X-Ray Computed Tomography Images

Kalehiwot N. Manahiloh and Balasingam Muhunthan

Abstract. Pore-water in the funicular and pendular saturation regimes of the SWCC (Sr < 90%) assumes a complex fabric consisting of saturated pockets of water under negative pressure and a network of liquid bridges formed from menisci at the contact points of particles. Measurement and characterization of this liquid fabric for unsaturated soil assemblies over a range of saturation, stress, and deformation plays a pivotal role in improving our fundamental understanding of unsaturated soil behavior. However, lack of microstructural visualization techniques has hindered the consideration of liquid fabric distribution and evolution in macroscale geotechnical formulations. In this study X-ray CT scanning was used to monitor the changes in the liquid fabric of unsaturated glass beads. Images showing the three distinct phases of unsaturated specimens were successfully obtained. A computer code that automatically analyzes multiple images to quantify the components of a second-order fabric tensor was developed and applied to CT images obtained along the drying and wetting paths of a SWCC determined by digital image processing. Principal values, principal directions and invariants are quantified and implications of the changes to better description of unsaturated soil behavior are discussed.

Keywords: unsaturated soils, X-ray CT, fabric tensor, granular geomaterials, SWCC.

Kalehiwot N. Manahiloh
Washington State University, Pullman, USA
e-mail: knega@wsu.edu

Balasingam Muhunthan
Washington State University, Pullman, USA
e-mail: muhuntha@wsu.edu

1 Introduction

Most flow, stress and deformation related problems are influenced by the engineering properties of unsaturated soils (Lu & Likos 2004). Even though, a considerable research has been conducted in the past (Matyas & Radhakrishna 1968, Likos & Lu 2004, Lu & Likos 2004) further studies are crucially important to fully incorporate unsaturated soil mechanics into engineering practice. In addition, investigations need to include microstructural considerations over ranges of saturation, stress and deformation so as to resolve fundamental issues in unsaturated soil behavior. In this study, funicular and pendular saturation regimes of unsaturated granular media (see Fig. 1) are investigated at a microstructural level and attempts are made to characterize their liquid fabric distribution.

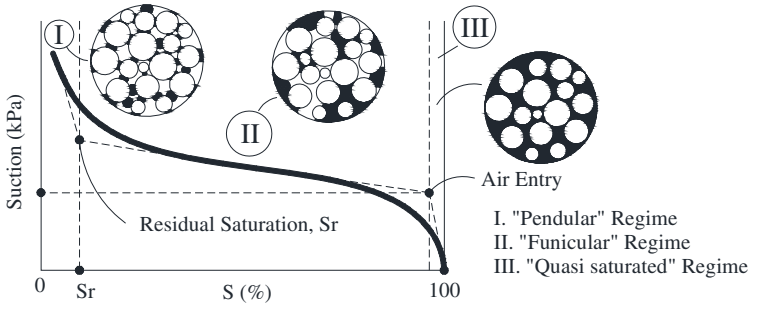

Fig. 1. Regimes of SWCC for partially saturated granular soil.

Nondestructive imaging techniques such as X-ray computed tomography (CT) have provided superior tools to quantitatively describe the 3-D microstructure of granular materials (Desrues et al. 1996, Wang et al. 2003, Gebrenegus et al. 2006). X-ray CT scanning combined with digital image processing can provide directional data and characterize microstructure of partially saturated specimens.

The objective of this study is to automate the handling of liquid phase fabric in X-ray CT images of unsaturated specimens and obtain their fabric tensor. Directional data gathered from X-ray CT scanning of 1mm glass beads at different suctions are digitally analyzed. The present interest is not to treat the complete theory covering unsaturated specimens, but rather to exemplify the use of image processing in quantifying directional data for phases of interest and combine the technique with statistical correlations to describe phase distribution.

2 Fabric Tensor of the Liquid Phase

Mathematically, *fabric* had been defined (Scott 1963, Mitchell 1976, Muhunthan 1991) in a number of ways and most researchers (e.g. Cowin & Satake 1978,

Nemat-Nasser & Mehrabadi 1983, Kanatani 1984, Kanatani 1985) studied fabric tensor for solid particles only. For two dimensional cases, Oda and Nakayama (1989) followed Kanatani's definition of fabric tensor and sought for measures by defining a vector along the longest chord of solid particles.

According to Muhunthan (1991), defining tensor parameters on the void phase have a potential of delivering a unified measure for all particulate media. Moreover, the advent of X-ray CT and its application to scanning of geomaterials has enabled to distinctly image the solid, liquid, and gas phases at a microstructural level. Therefore, in this study, fabric is accepted as a term referring to parameters like size, shape and arrangement of the solid particles, the organic inclusions and the associated voids. Also, statistical correlations applicable to solid particles are assumed to appropriately describe directional distributions on the liquid phase. Following the preceding discussion, this study will quantify higher measures of fabric on the liquid phase of a partially saturated specimen.

3 Mathematical Background for Fabric Tensor

Kanatani (1984) studied and gave mathematical expressions for quantities that characterize directional distribution of particles. The subsequent discussion revises the mathematical formulation of these quantities.

Assume directional data n that is observed for a material idealized as an assembly of solid spheres. Assume also, $f(n)$ is the *probability* distribution density satisfying $\int f(n)dn = 1$. Where, dn is the differential solid angle related to the spherical coordinates θ and ϕ as:

$$\int dn = \int_0^{\pi} \int_0^{2\pi} \sin\theta d\phi d\theta \quad \text{(For 3-D)} \quad (1) \qquad \int dn = \int_0^{2\pi} d\theta \quad \text{(For 2-D)} \quad (2)$$

To estimate the true distribution density, the singular distribution function, $f(n)$ is approximated by a smooth function $F(n)$. In this procedure a *parametric form* is first assumed and then a *measure of approximation* is introduced. Parameters are then chosen in such a way that the introduced measure of approximation is maximized. A polynomial parametric form of $F(n)$ (Kanatani 1984) can take the form given by equation (3) where the C terms represent coefficients.

$$F(n) = C + C_i n_i + C_{ij} n_i n_j + C_{ijk} n_i n_j n_k + \ldots \quad (3)$$

A measure of approximation, invariant to coordinate transformation, is given in equation (4) (Kanatani 1984) and is termed the *least square error approximation*. This approximation takes the polynomial parametric form to the spherical harmonics and the Fourier series expansions in the 3-D & 2-D cases respectively.

$$\int [F(n) - f(n)]^2 dn \rightarrow Minimum \quad (4)$$

Assuming a pair of unit vectors with opposite directions to be generated so that *f(n)*is a symmetric function (i.e. only even powers of *n* to be included), equations (3) and (4) can be combined such that the square error *E* is minimized, to obtain the following form.

$$E = \int [(C + C_{ij} n_i n_j + C_{ijkl} n_i n_j n_k n_k + ...) - f(n)]^2 dn \rightarrow Minimum \quad (5)$$

Kanatani (1984) approximated distribution functions for solid particles and gave expressions for fabric tensors of the *first*, *second* and *third* kind as expansions of relevant subspace. In three dimensional subspaces, for $n = 2$, the *second* (F_{ij}) and *third* (D_{ij}) kind reduce to equations (6) and (7) respectively. The corresponding tensor definitions in two dimensional subspaces are given by equations (8) and (9).

$$F_{ij} = \frac{15}{2}\left[N_{ij} - \frac{1}{5}\delta_{ij} \right] \quad (6) \qquad D_{ij} = \frac{15}{2}\left[N_{ij} - \frac{1}{3}\delta_{ij} \right] \quad (7)$$

$$F_{ij} = 4\left[N_{ij} - \frac{1}{4}\delta_{ij} \right] \quad (8) \qquad D_{ij} = 4\left[N_{ij} - \frac{1}{2}\delta_{ij} \right] \quad (9)$$

4 Experimental Setup

Spherical glass beads of 1mm were packed into a 10 mm diameter cylindrical plexiglass Tempe-cells that can maintain constant suction applied from a hanging water column. Samples were scanned with X-ray CT and digital image processing was applied on the resulting images. The liquid phase was systematically captured by doping the saturating fluid with 6% CsCl solution. The components of higher order fabric tensors and associated invariants are computed from image analysis. To illustrate the techniques applied, a two dimensional image shown in Fig. 2 is considered. In the figure, $n^{(k)}$ represents a unit vector aligned with the longest chord of the k^{th}-particle making an angle θ with respect to the horizontal axis.

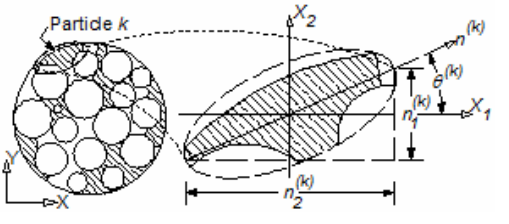

Fig. 2. Particle Orientation: (a) 2-D slice & global axes; (b) k^{th} particle, local axes, longest chord & fitting ellipsoid.

Decomposing the unit vector into its orthogonal components, one can obtain expressions for n_1 and n_2 as follows:

$$n_1 = \sin\theta^{(k)} \text{ and } \quad n_2 = \cos\theta^{(k)} \tag{10}$$

In each X-ray CT slice, the total number of data points (i.e. each liquid completely or partially surrounded by solid particles) for which directional data is sought is represented by M. Following Oda & Nakayama (1989) the components of the fabric tensor can be calculated as:

$$N_{11} = \frac{1}{M}\sum_{k=1}^{M}\sin^2\theta^{(k)} \tag{11}$$

$$N_{12} = \frac{1}{M}\sum_{k=1}^{M}\cos\theta^{(k)}\sin\theta^{(k)} \tag{12}$$

$$N_{22} = \frac{1}{M}\sum_{k=1}^{M}\cos^2\theta^{(k)} \tag{13}$$

Image Pro Plus platform is used to run a macro that handles the direction assignment, angle measurement and computations for components of the fabric tensor. A typical image from X-ray CT scanning is shown in Fig. 3a. AutoCAD simulation of the same image where the three independent phases (i.e. solid, liquid and gas) are distinctively represented is shown in Fig. 3b. In Fig. 3c the liquid phase is extracted and shown shaded. Fig. 3d shows the longest chords of each discretized liquid phase constituent. The samples considered for the analysis are summarized in Table 1 where each column has a heading that explains what is represented.

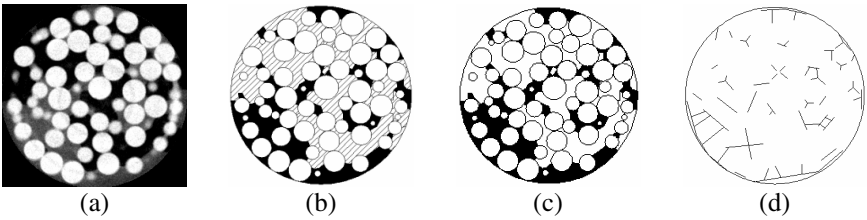

Fig. 3. Image from X-ray CT: (a) 1mm Glass Bead at suction of 0.6kPa (Drying); (b) All Phases: stripe = gas, black = liquid and white = solid; (c) Liquid Phase (black); (d) Longest chords of discretized liquid phases.

5 Results and Discussion

The distributions of N_{11}, N_{12} and N_{22} for sample 1 are shown in Figs. 4 through 6. These distributions were obtained by coding equations (11) to (13) into Image-Pro Plus platform and running on images. Average values for the distribution descriptors and their invariants are summarized in Table 2. From the results, the fundamental property of fabric tensors can be proven such that the first invariant, I_1, is always Unity. The invariants are plotted together (Fig. 7) to show their variation as a function of the sample preparation pressure.

Table 1. Sample details.

(1)	(2)	(3)		(4)	(5)	(6)	(7)
Sample	Suction (kPa)	Diameter		Height (mm)	Calibration mm/pixel	Cropping co-ordinates	Threshold for Liquid
		pixel	mm				
1	0.0	236	10	14.32	0.042	(0,0;236,236)	31-127
2	0.4	236	10	13.97	0.042	(0,0;236,236)	31-127
3	0.6	234	10	14.58	0.043	(0,0;234,234)	31-127
4	0.8	271	10	11.95	0.037	(0,0;271,271)	31-127
5	2.5	238	10	13.98	0.043	(0,0;238,238)	31-127

Table 2. Average values for N_{ij} and associated invariants.

Sample	Suction (kPa)	N_{11}	N_{12}	N_{22}	I_1	I_2
1	0	0.504	0	0.496	1.000	0.250
2	0.4	0.503	0	0.497	1.000	0.250
3	0.6	0.506	0	0.494	1.000	0.250
4	0.8	0.512	0	0.488	1.000	0.250
5	2.5	0.502	0	0.498	1.000	0.250

Following the previous assertion, N_{ij} is written in full as a symmetric second order tensor and the obtained values for sample 1 are indicated below.

$$\begin{bmatrix} N_{11} & N_{12} \\ N_{21} & N_{22} \end{bmatrix} = \begin{bmatrix} 0.504 & 0 \\ 0 & 0.496 \end{bmatrix} \tag{15}$$

Since N_{ij} is a symmetric second order tensor, the components can be converted to two principal values N_1 and N_2 in the corresponding principal directions. Their mathematical formulations and corresponding principal directions are given by equations (15) and (16).

$$\begin{bmatrix} N_1 \\ N_2 \end{bmatrix} = \frac{1}{2}[N_{11} + N_{22}] \pm \left[\frac{1}{4}(N_{11} - N_{22}) + N_{12}{}^2 \right]^{0.5} = \frac{1}{2}(1 \pm \Delta) \tag{15}$$

$$\begin{bmatrix} \theta_1 \\ \theta_2 \end{bmatrix} = \frac{1}{2} \arctan \frac{2N_{12}}{N_{22} - N_{11}} \tag{16}$$

Curray (1956) introduced an index measure that shows the intensity of a preferred orientation of particles. This measure, referred to as *the vector magnitude,* is given as equation (17).

$$\Delta = \frac{1}{M} \left[\sum_{k=1}^{M} \left(\cos 2\theta^{(k)} \right)^2 + \sum_{k=1}^{M} \left(\sin 2\theta^{(k)} \right)^2 \right]^{0.5} \tag{17}$$

The results for the principal values, principal directions and the vector magnitude values are summarized in Table 3.

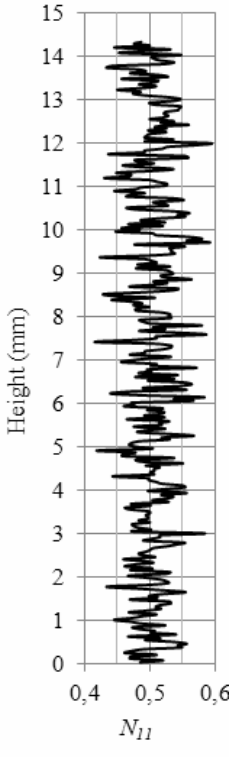

Fig. 4. N_{11} distribution over height.

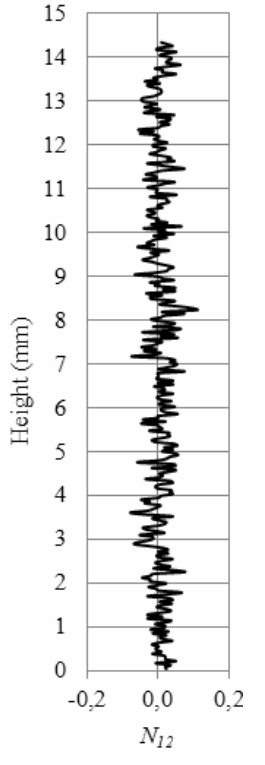

Fig. 5. N_{12} distribution over height.

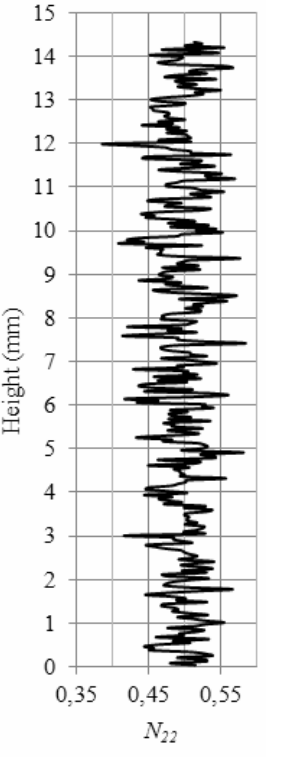

Fig. 6. N_{22} distribution over height.

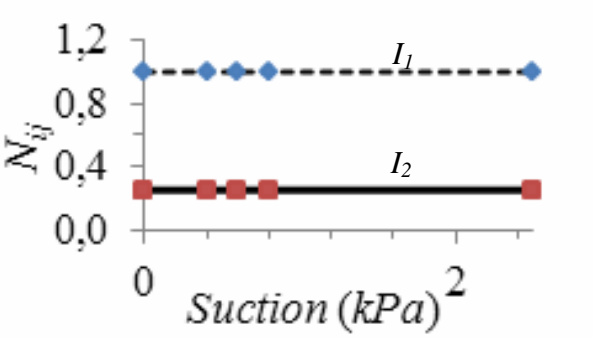

Fig. 7. Average N_{ij} values for all samples.

Table 3. Principal values, principal directions and vector magnitudes.

Sample	N_{11}	N_{12}	N_{22}	N_1	N_2	Δ	θ_1	θ_2
1	0.504	0	0.496	0.546	0.454	0.091	0	90
2	0.503	0	0.497	0.537	0.463	0.074	0	90
3	0.506	0	0.494	0.556	0.444	0.111	0	90
4	0.512	0	0.488	0.579	0.421	0.157	0	90
5	0.502	0	0.498	0.531	0.469	0.061	0	90

Table 4. Kanatani's fabric tensor of the *second* kind.

Sample	F_{11}	F_{12}	F_{22}	F_1	F_2	Δ
1	1.017	0	0.983	1.184	0.816	0.092
2	1.011	0	0.989	1.148	0.852	0.074
3	1.025	0	0.975	1.222	0.778	0.111
4	1.049	0	0.951	1.314	0.686	0.157
5	1.007	0	0.993	1.124	0.876	0.062

Table 5. Kanatani's fabric tensor of the *third* kind.

Sample	D_{11}	D_{12}	D_{22}	D_1	D_2	Δ
1	0.017	0	-0.017	0.184	-0.184	0.092
2	0.011	0	-0.011	0.148	-0.148	0.074
3	0.025	0	-0.025	0.222	-0.222	0.111
4	0.049	0	-0.049	0.314	-0.314	0.157
5	0.007	0	-0.007	0.124	-0.124	0.062

The relationship between F_{ij} and D_{ij} can be obtained from equations (8) and (9). The principal components of F_{ij} and D_{ij} can also be derived from these same equations and employing the representation indicated in equation (14), they can be written as equations (18) and (19). Tables 4 and 5 give their numerical values.

$$\begin{bmatrix} D_1 \\ D_2 \end{bmatrix} = \pm 2\Delta \quad (18) \qquad \begin{bmatrix} F_1 \\ F_2 \end{bmatrix} = 1 \pm 2\Delta = 1 + \begin{bmatrix} D_1 \\ D_2 \end{bmatrix} \quad (19)$$

6 Conclusions

This study presented an investigation on microstructural evolution of the anisotropic liquid fabric in unsaturated soils. Since void fabric and the liquid bridge vectors change dramatically with wetting and deformation, their characterization is important towards the development of effective stress formulations for unsaturated soils.

Second order fabric descriptors of the anisotropic liquid fabric are quantified from X-ray CT scanned images of unsaturated specimens. The results confirm that the liquid fabric is anisotropic and that the components satisfy the basic tensorial properties such as symmetry and equality of diagonal summation to unity. The results include principal values, principal directions, and vector magnitudes for the liquid fabric. These parameters can be used by researchers in developing advanced theories for modeling the behavior of unsaturated soils.

Acknowledgements. The study presented in this paper was sponsored by the National Science Foundation under the grant CMMI-0856793 to Washington State University.

References

Cowin, S.C., Satake, T.: Continuum mechanical and statistical approaches in the mechanics of granular materials, Tokyo, Japan, Gakujutsu Bunken Fukyu-Kai (1978)

Curray, J.R.: Analysis of two-dimensional orientation data. J. Geology. 64, 117–131 (1956)

Desrues, J., Chambon, R., Mokni, M., Mazerolle, F.: Void ratio evolution inside shear bands in triaxial sand specimen studied by computed tomography. Geotechnique 46(3), 529–546 (1996)

Gebrenegus, T., Tuller, M., Muhunthan, B.: The Application of X-ray computed tomography for characterization of surface crack networks in sand-bentonite mixtures. In: Proc. Advances in X-ray Tomography for Geomaterials, pp. 207–212. ISTE Publishing Company (2006)

Kanatani, K.I.: Distribution of Directional Data and Fabric Tensors. International Journal of Engineering Science 22, 149–164 (1984)

Kanatani, K.I.: Procedures for stereological estimation of structural anisotropy. International Journal of Engineering Science 23(5), 587–598 (1985)

Likos, W.J., Lu, N.: Hysteresis of capillary stress in unsaturated granular soil. Journal of Engineering Mechanics 130(6), 646–655 (2004)

Lu, N., Likos, W.J.: Unsaturated soil Mechanics. Wiley, New Jersey (2004)

Matyas, E.L., Radhakrishna, H.S.: Volume change characteristics of partially saturated soils. Geotechnique 18(4), 432–448 (1968)

Mitchell, J.K.: Fundamentals of soils behavior. John Wiley and sons, Inc., New York (1976)

Muhunthan, B.: Micromechanics of Steady State, Collapse and Stress-Strain Modeling of Soils. Ph.D. Thesis, 221 p. Perdue University, West Lafayette (1991)

Nemat-Nasser, S., Mehrabadi, M.M.: Stress and Fabric in Granular Masses. In: Jenkins, J.T., Satake, M. (eds.) Mechanics of Granular Materials: New Models and Constitutive Relations, pp. 1–8. Elsevier, Amsterdam (1983)

Oda, M., Nakayama, H.: Yield Function for soil with Anisotropic Fabric. Journal of Engineering Mechanics 115(1), 89–104 (1989)

Scott, R.F.: Principles of soil mechanics, pp. 267–275. Addison-Wesley Publishing Co. Inc., Massachusetts (1963)

Wang, L.B., Frost, J.D., Voyiadjis, G.Z., Harman, T.P.: Quantification of damage parameters using X-ray tomography images. Mechanics of Materials 35, 777–790 (2003)

Water Retention Behaviour Explored by X-Ray CT Analysis

Ismael Riedel, Edward Andò, Simon Salager, Pierre Bésuelle,
and Gioacchino Viggiani

Abstract. This study aims to experimentally characterise the link between partial water saturation and suction in a sand sample at the micro scale. The paper presents the first results of an experimental study in which high resolution (7.5µm/px) X-ray tomography has been performed on a small (10×10mm) cylindrical sample of Hostun HN31 sand at several different levels of imposed suction. A specialised cell allowing X-ray scanning as well as fine control of suction (imposed both by negative water pressure as well as by positive air pressure) has been developed for this study and is described herein. The 3D images resulting from X-ray tomography are treated in order to define each voxel in the image as either air, water or grain. From these "trinarised" 3D images, local and global values of porosity and degree of saturation are then measured. This method enables the study of water retention behaviour of sand at the grain scale, all the while allowing characterisation of water retention in the sample as a whole.

Keywords: water retention behaviour, X-ray CT, pore water, suction, saturation.

1 Introduction

The water retention behaviour of soils is usually characterised by the so-called water retention curve, which expresses the degree of saturation as a function of suction (*e.g.*, Fredlund & Xing, 1994). Many aspects of the water retention behaviour of soils have been investigated over the last few decades, including the effects of a number of variables (*e.g.*, porosity, temperature and stress path) as well as the hysteresis that typically characterises water retention behaviour, with

Ismael Riedel · Edward Andò · Simon Salager · Pierre Bésuelle · Gioacchino Viggiani
Grenoble-INP, UJF-Grenoble 1, CNRS UMR 5521, Laboratoire 3SR,
Grenoble F-38041, France
e-mail: simon.salager@hmg.inpg.fr

different responses upon drying and wetting. However, the large majority of experimental results on water retention have been interpreted at the macro level; notable exceptions are the recent studies by Kim *et al.* (2011) – who have used neutron imaging for visualising and quantifying water distribution in partially saturated sand – and Higo *et al.* (2011), who have analysed microstructural changes in partially saturated soil related to strain localisation, using X-ray tomography. From an experimental standpoint, it appears that the basic physics and mechanics of partially saturated granular materials are still to be explored at the grain scale. This is the main objective of the present study, in which X-ray micro tomography is suggested as an effective tool allowing unprecedented observations and new insights into the water retention behaviour of sand at the grain scale.

First, the experimental methods used in this work are described and detailed to some extent. In particular, a "micro" pressure plate apparatus suitable for high-resolution X-ray tomography is presented, which has been specially developed for this work. Also, a short description is given of the X-ray scanner used in this study. Then, a few preliminary results obtained on Hostun sand are presented, which show the potential of the technique for the experimental study of partially saturated sand.

2 Experimental Methods

A "micro" pressure plate apparatus suitable for high-resolution X-ray tomography has been specially developed for this work. The technique imposes limits on the design: the material selected for the cell is an acrylic fabric (PMMA), chosen for its low X-ray attenuation. The size of the sample is dictated by the spatial resolution desired from X-ray scanning to be a 10×10mm cylinder – considerably smaller than standard samples. The apparatus allows suction to be controlled in two different ways: tensiometry and axis translation, *i.e.*, negative water pressure and positive air pressure, respectively. The cell itself, as can be seen in Figure 1, has two main parts. These parts, once screwed together form an air- and watertight cell. The sand sample is located between a ceramic disk in the bottom (air entry value equal to 5 bar) and a porous stone in the top, where water continuity from the bottom and air continuity from the top are guaranteed. From the upper part of the cell, a pipe connected to a pump allows the control of positive air pressure. A water tank that can move vertically over a scaled rule is connected to the water reservoir in the bottom of the cell. The upper level of water in this tank is initially levelled to the zero value of the rule which is coincident with the middle level of the sand sample. In this condition the suction is equal to zero (at least at mid-height of the sample). Moving the tank down creates difference in hydraulic head and since there is continuity in the liquid phase, suction is thus applied in the sample. The maximum height difference applicable with this setup is 75 cm, corresponding to a suction of 7.5 kPa.

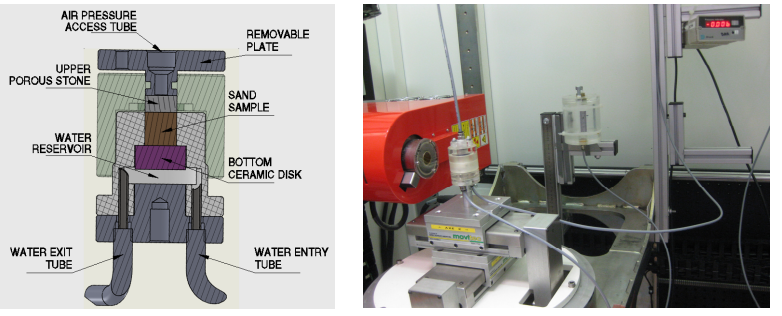

Fig. 1. Pressure plate apparatus: schematic view (left); photograph in place in the scanner (right).

The study presented is carried out on Hostun HN31 sand, an angular quartz sand successor to the RF varieties detailed in Flavigny *et al.*, (1990).

To ensure full saturation, all phases of sample preparation are carried out completely under water. Loose sand is deposited under water, and then static compaction in layers is applied to reach the target porosity; note that this method does not guarantee homogeneous porosity. Note furthermore that no contrast agent is added to the water, which is demineralised and de-aired as per standard.

The X-ray scanner used in this study is a specialised lab scanner in Laboratoire 3SR (Grenoble). It includes a Hamamatsu micro-focus X-ray source emitting a cone beam and a 1920 by 1536 pixel X-ray flat panel detector (measuring 195 by 244 mm). The sample to be scanned is placed between the source and the detector, on a translation and rotation stage, the latter being necessary for the specimen to be imaged at different angular positions. Translation (in the axis of the beam) allows control of the distance between the sample and the source, which in turn controls the size of the image of the sample on the detector (the zoom). The range of X-ray energy of the source is 40 to 150 keV, allowing a range of different sample sizes and densities to be imaged. The spatial resolution (expressed in terms of voxel size) depends on the "zoom" level (*i.e.*, the distance between the sample and the source); it cannot be smaller than the smallest spot size (5µm in low-power mode) and is limited upward by the physical size of the detector.

Scans are performed close to the highest zoom level for this apparatus: 7.5µm/px. In order to perform successful scans, the spot size must be carefully controlled, which means putting a limit on the total X-ray power (and therefore the flux); this implies a relatively long scanning time of three hours for a single tomography with 1200 angular positions. Such long scans are vulnerable to differential displacements (due to temperature change in the cabin) in the acquisition system, requiring corrections to the acquired images.

A set of 1200 images acquired in a given state of suction are reconstructed into a 3D volume measuring 1500^3px where each voxel (a pixel in 3D) measures 7.5^3µm and contains a value of X-ray attenuation. The reconstruction is performed on high-speed GPU software (Digisens' DigiCT 2.4.2) using a cone-beam

algorithm – reconstructions are post-processed for beam hardening. The reconstructed images give slices of the entire volume, that once stacked allows a 3D examination of the entire sample domain. Figure 2 presents the reconstructed images obtained for a suction of 1.2 kPa through a horizontal slice at mid-height of the sample, and a vertical slice containing the sample's axis. Due to the fact that the reconstructed X-ray attenuation coefficient depends mainly on the mass density, the three phases in the specimen can be distinguished in terms of their grey level. Grains are the most attenuating phase and appear lighter, air is the least attenuating and appears dark, water corresponds to an intermediate grey level. The completely white grains correspond to very dense grains that are found in a small proportion in Hostun sand. The repartition of the water menisci and air bubbles are clearly seen, together with the shape of grains.

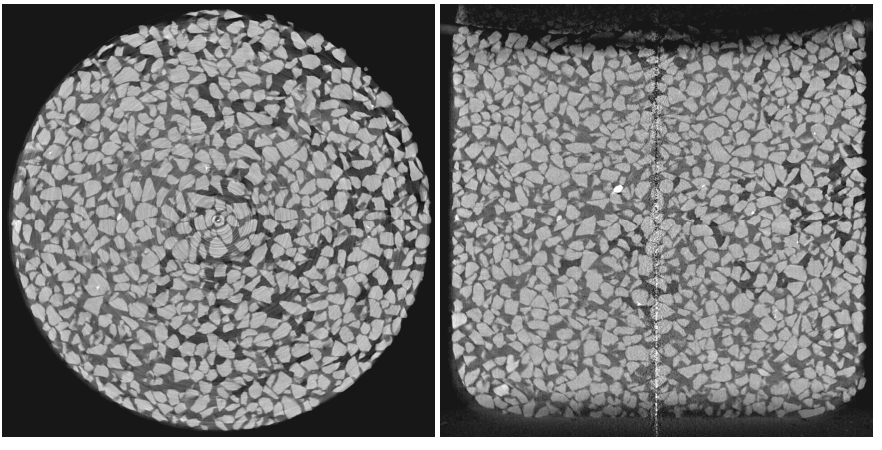

Fig. 2. Reconstructed images obtained for a suction of 1.2 kPA. Horizontal slice at half of the height (left) and vertical diametric slice (right).

Figure 3 shows the volume grey level distribution in the whole specimen for the state corresponding to 1.2 kPa. . To obtain the correct graph, only the sample space should be considered. Therefore, the volume is first processed to cut (assign a zero value) the parts of the upper and lower porous stones and of the cell that are present in the original total volume. The distribution shows three peaks corresponding to the three phases in the specimen. The darker values of grey correspond to the air, the intermediate to the water and the lighter to the grain voxels in accordance with their mass density. Because voxels outside the sample have been assigned to a zero value (black), the distribution presents also a fourth peak at the zero abscise, however this one is ignored because it has no physical meaning. The three other peaks present a spread grey distribution, especially for air and water. This spread for air and water can not be explained by a dispersion of the X-ray absorption because the properties in these phases are expected to be homogeneous (albeit a small heterogeneity is possible inside grains). This spreading is due to i)

image noise due to acquisition and reconstruction, ii) partial volume effect when several phases "share" the space inside one voxel, this causes the grey level of this voxel to be a result of the volume average of phase attenuation values and so is an intermediate value between peaks.

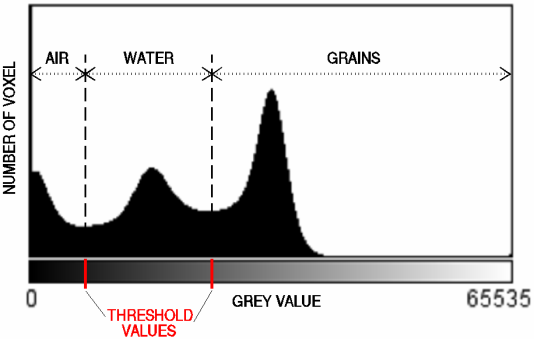

Fig. 3. Histogram for the state corresponding to 1.2 kPa, grey values correspond to a 16-bit integer range, to which the image is converted for treatment.

Measurements of the spatial distribution of grains, water and pores requires a separation of the three phases The challenge here is that the ranges are continuous and there is a certain degree of overlapping between {air, water} and {water, grain}. The volume has been "trinarised" using two thresholds, one between air and water peaks and the second one between water and grain peaks. This last one is chosen in such a way that volume of voxels identified as grain phase correspond to volume of grains that has been estimated from the weight of the sample (in a dry state). The threshold between air and water is chosen to correspond to the local minimum in the grey level distribution.

The principal source of error from such treatment stems from the fact that a voxel which in reality contains a grain-air interface may appear to have the averaged attenuation value of water, due to partial volume effect. This can be easily identified on trinarised volume as a one or two voxel-thick shell of "water" around grains which are dry. This in turn can be corrected simply by removing all small water-structures from the volume by running some cycles of an erosion algorithm (which strips the outmost layer of water voxels from every water structure in the image – with the hope that all small structures will disappear), and then dilating by the same number of cycles the water structures which remain, in order to help preserve the total water volume. This helps remove these water artefacts, but has some effect on the shape of the water structures that remain. More robust trinarisation options which rely less strongly on thresholds, such as anisotropic diffusion (Perona & Malik, 1990), are being investigated.

3 Results and Interpretations

Figure 4 shows horizontal slices from (trinarised) 3D images from X-ray tomography of Hostun sand at four different levels of imposed suction. The vertical location of the slices is chosen to best highlight different water retention states. The two slices on the top row show liquid phase continuity for both full saturation and at 1.2 kPa suction (the funicular domain). At higher suctions (1.8 kPa to 2.5 kPa), the pendular domain is reached in some parts of the sample, as shown in Figure 2 (bottom left); complete continuity of the liquid phase is lost, with liquid bridges between the grains. Finally, the hygroscopic domain, with only absorbed water at the surface of the grains, is apparent at 7.0 kPa suction (Figure 4, bottom right); note that the hygroscopic domain was observed in some regions of the sample already at 3 kPa suction.

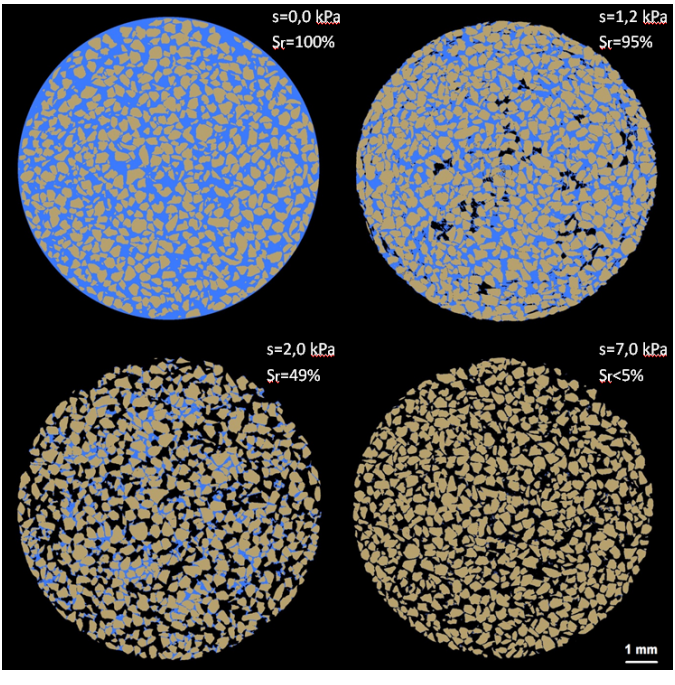

Fig. 4. Four different domains (fully saturated, funicular, pendular and hygroscopic) shown in slices from trinarised 3D images of Hostun sand; water in light blue, air in black and solid in light brown. The degrees of saturation noted are global.

Figure 5 shows a vertical and a horizontal slice from a trinarised image of the sample at 2.0 kPa suction. The global degree of saturation of the sample in this state is 49%. However, the trinarised image clearly shows a *patchy* pattern of saturation, with regions in the sample that are essentially fully water saturated, and regions where the local degree of saturation is well below the average value in the

sample. The non-homogeneous distribution of porosity in the sample (mean value is 43%, local values between 37 and 49%) can explain this non-homogeneous distribution of the liquid phase. However, other controlling parameters should be taken into account, such as the variability in the shape of the pores and that of the grains. Furthermore, the non-linear relation between degree of saturation and porosity at constant suction is such that small porosity heterogeneities can result in large heterogeneities of water distribution, and hence of the degree of saturation.

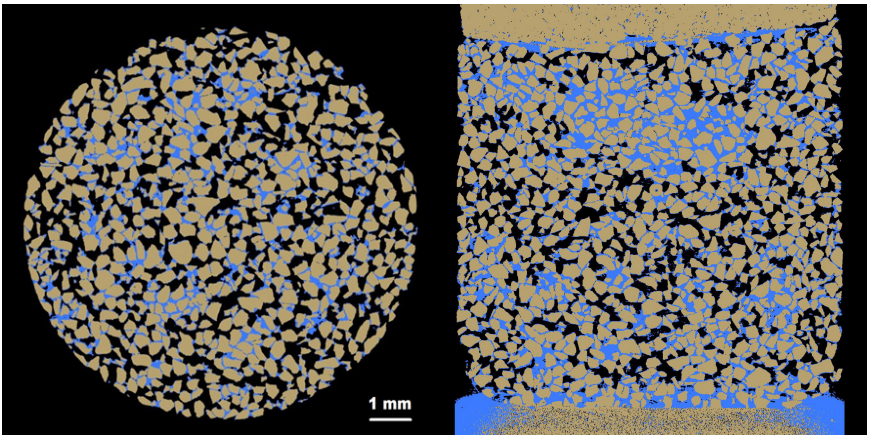

Fig. 5. Horizontal and vertical slices of a sample at 2.0 kPa suction; colours as in Figure 2.

4 Conclusion

X-ray tomography gives unprecedented, non-destructive, 3D access to the microscale of materials, at spatial resolutions that were simply unimaginable a few decades ago. In this work, X-ray tomography has been used to characterise a relatively small sample of Hostun sand at different suctions at a spatial resolution of 7.5μm/px. With some image processing it is possible to "trinarise" the 3D images for each level of suction, resulting in a map of air, water and grain. From these 3D maps for each level of imposed suction, the arrangement of the void space and water inside the sample can be explored. Small variations in the porosity of the sample prepared (43% ±6%) are observed, with large variations in the spatial water distribution – a distinctly *patchy* water content in some states of imposed suction. Such 3D observations are only really possible with X-ray tomography. Furthermore, since X-ray tomography scans are non-destructive, the evolution of water distribution can be followed for different suction levels in the same sample, which has potential to offer new experimental insights into the *real-world* meaning of partial saturation. Ongoing work aims to define a Representative Elementary Volume for both the grain skeleton – in order to access a local measure of porosity, as well as one for the water content – which is possibly more challenging due to the patchiness of its distribution.

Future work will include more systematic studies of initial arrangements of the solid skeleton, aiming for more homogeneous initial porosities. Further work will also explore the hysteresis in the 3D evolution of the water distribution between wetting and drying cycles.

References

Flavigny, E., Desrues, J., Palayer, B.: Le sable d'Hostun RF. Revue Francaise de Geotechnique 53, 67–69 (1990)

Perona, P., Malik, J.: Scale-space and edge detection using anisotropic diffusion. IEEE Transactions on Pattern Analysis and Machine Intelligence 12(7), 629–639 (1990)

Fredlund, D.G., Xing, A.: Equations for the soil-water characteristic curve. Canadian Geotechnical Journal 31(3), 521–532 (1994)

Higo, Y., Oka, F., Kimoto, S., Sanagawa, T., Matsushima, Y.: Study of strain localization and microstructural changes in partially saturated sand during triaxial tests using microfocus X-ray CT. Soils & Foundations 51(1), 95–111 (2011)

Kim, F., Penumadu, D., Hussey, D.: Water Distribution Variation in Partially Saturated Granular Materials Using Neutron Imaging. Journal of Geotechnical and Geoenvironmental Engineering (2011) (in press)

Detection of Fissures in Desiccated Soils Using Spectral Analysis of Rayleigh Waves

Bernardo Caicedo, Julián Tristancho, and Luc Thorel

Abstract. Retrospective analysis of surface waves is a non destructive method that is widely used nowadays. This paper focus on the application of surface waves as a tool to detect fissures in desiccated soils. As a first approach, this paper presents the results of tests carried out using compacted Speswhite kaolin in unsaturated state and artificial fissures.

Keywords: fissures detection, Rayleigh waves, physical modeling, SASW.

1 Introduction

Geophysical methods have been used to characterize soils since 1960. Among these methods, the analysis of surface waves has received considerable attention for example to study the deterioration of materials (Wardany et al 2003) the evaluation of the sub grades of pavements and to assess the dynamic properties of soils, (Bertel 2006). Mechanical waves propagate in an elastic half space following two main propagation patterns: body waves and surface waves.

Body waves propagate in all directions within the half space, and in the case of homogeneous materials the propagation front is spherical. These body waves are

Bernardo Caicedo
Universidad de los Andes, Bogota, Colombia
e-mail: bcaicedo@uniandes.edu.co

Julian Tristancho
Universidad Distrital Francisco Jose de Caldas, Bogota, Colombia
e-mail: jatristanchoo@udistrital.edu.co

Luc Thorel
LUNAM University, IFSTTAR, Department of Geotechnical Engineering & Risks, Physical Modelling in Geotechnics Group, F-44341 Bouguenais, France
e-mail: Luc.Thorel@lcpc.fr

classified in primary waves (P) which are compressive waves and secondary waves (S) which are shear waves.

On the other hand, surface waves propagate along surfaces having high contrast in stiffness (free surface or different layer in the soil profile). These waves propagate at lower velocity than shear waves, and their amplitude decreases with the distance (r) from the source with lower rate than body waves. In fact, surface waves amplitude decreases proportionally to $\lambda / \sqrt{r}$, although the so called far field terms of the body waves decreases proportionally to λ / r^2 - the near field ones attenuates even more rapidly with λ / r^3. There are two types of surface waves: Rayleigh and Love waves, Rayleigh waves propagate only at the free surface although Love waves propagate within the interface between materials of different stiffness.

This paper presents laboratory tests of surface waves propagation carried out on reduced scale models. The retrospective analysis of the Rayleigh waves gives some inputs to assess fisuration on soils. This paper describes the characteristics of Rayleigh waves, then the experimental setup is described and finally the results are presented. The main purpose of this study is identifying fissures on desiccated soils however as a first approximation this work focuses on artificial fissures.

2 Rayleigh Waves

Rayleigh waves have low velocity, low frequency and high amplitude. When a compression source is used to produce surface waves, around 2/3 of the energy is transformed in Rayleigh waves. Furthermore Rayleigh waves propagate in a half space following a dispersive pattern, it means that waves of higher wavelenghts and therefore lower frequency propagate affecting deeper soil layers than short wavelengths and high frequency waves.

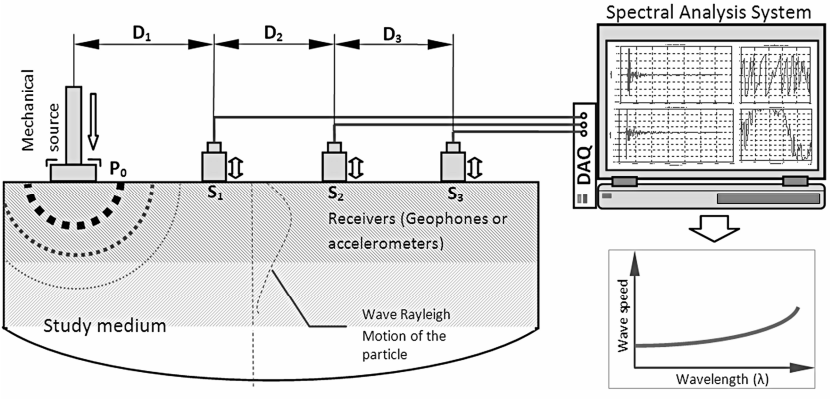

Fig. 1. Schematic configuration of the experimental setup to measure the propagation of surface waves.

The dispersive propagation characteristic of Rayleigh waves is at the base of the SASW method (Spectral Analysis of Surface Waves). This method was developed by Nazarian & Stokoe, 1983 in its early development stage it was used to characterize pavement structures but the possibilities of applications increase rapidly. Nowadays the SASW method is used widely to characterize the dynamic properties of soils in situ, to evaluate the liquefaction susceptibility, and others, Stokoe et al., 2004.

3 Experimental Setup

The experimental setup used in this research is presented in fig. 1. This figure shows the different components of the system, the mechanical input is created by a Piezoelectric actuator (P_0), this actuator have a piezoelectric load cell to measure the input compression wave. The system has a set of broad spectrum accelerometers (S_1, S_2, S_3, etc.), these accelerometers are located at different distances from the input source (D_1, D_2, D_3, etc.). The accelerometers and the load cell are linked to a data acquisition system allowing high frequency measurements.

The mechanical input produces P, S and Rayleigh waves that propagate from P_0, fig. 1. However body waves decrease at higher rate than surface waves, as a result after some distance the recorded signals are made mainly by surface waves. On the other hand for distances close to the source the recorded signal have both body and surface waves, this is the near field effect. It is important to note that to avoid the presence of body waves on the recorded signals the first accelerometer must be located at a distance that guarantee the dissipation of body waves, Murillo, 2006. The fig. 2 presents the wave lengths for different frequencies and for different shear wave velocities, showing the relation between frecuency, wavelength and stiffness.

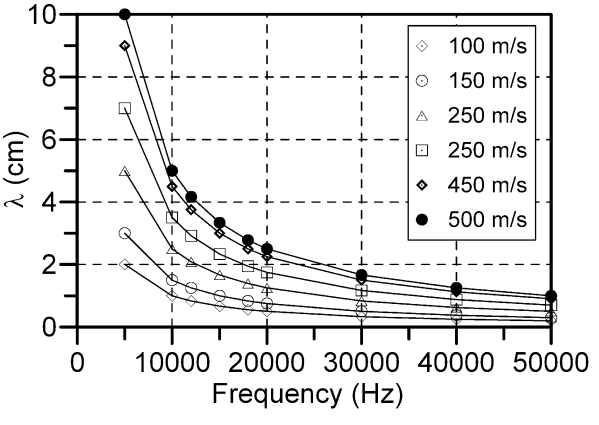

Fig. 2. Exploration wavelength values as a function of the shear wave velocities of soils and the frequency of the signal (Murillo, 2009).

3.1 Materials and Instrumentation

The soil tested was compacted kaolin Speswhite produced by Imerys. This soil was mixed with water to achieve the optimum water content of the Proctor Standard compaction tests (29.3%), then a vertical stress of 2 MPa was applied and the consolidation process was verified using the Asaoka method(Asaoka, 1978). Once compacted, the soil suction was 800 kPa, Murillo, 2006.

The mechanical source is a piezoelectric actuator type Cedrat PPA40M, with this actuator it is possible to impose sinusoidal or impact waves. This kind of actuator needs a high voltage level to achieve the required load and stroke (i.e. displacements up to 40 μm are achievable using -20 to 150V). The signal used to experimental procedure was an impulsive signal (type step). An example of the input signal used on piezoelectric actuator is show in fig. 3.

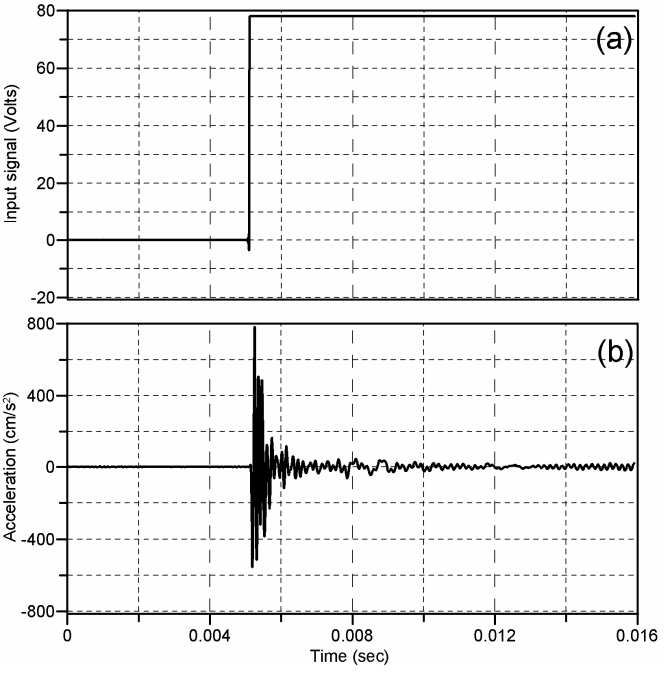

Fig. 3. Example of input signal for experimental tests. a) Input signal of piezoelectric actuator and b) Accelerometor signal to 0 cm from piezoelectric actuator.

The set of accelerometers used for the tests were PCB 352 A10. These accelerometers are uniaxial and have a broad frequency bandwidth (from 2Hz to 10 KHz), their acceleration range goes up to 500g and their weight is less than 1 gr. These accelerometers are located at the surface of the soil as shown in fig. 2.

The data acquisition system used for the tests was the system CAREMBA (Chaîne d'acquisition Rapide Embarquée) developed at the IFSSTAR in Nantes France. This system has three VME cards with 32 channels with independent amplification factors imposed by software, the A/D.

The sampling frequency is a key point to analyze the signals. According with the Nyquist theorem, (Smith, 1999), the frequency band available to carry out the analysis is limited to the half of the sampling frequency. Therefore to avoid any problem with the frequency analyses related to the aliasing, the sampling frequency used was higher than 50 kHz.

4 Experimental Procedure

To perform the tests, the soil was compacted applying a static compressive stress of 2 MPa in a cylindrical mould (30 cm in diameter). Then the set of accelerometers were placed at the surface of the mould. Four accelerometers were used: one placed over the plate that applies the load and three other accelerometers were placed with 50 mm of separation between them, fig. 3. Afterwards the fissures were created artificially at the middle distance between accelerometers, the depth of the fissures was increased progressively from 8 mm to 34 mm and measures were made for each depth.

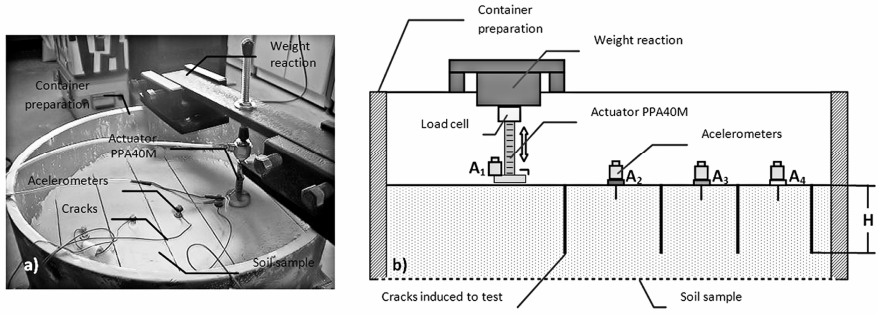

Fig. 4. (a) Experimental setup, (b) details of the location of fissures and accelerometers.

For each fissure a spectral analysis was carried out using the Fourier transform as shown in fig. 4. This figure presents the Fourier transform measured by the same accelerometer (accelerometer A_2 in fig. 3, located 10 cm from the piezoelectric actuator) for different depths of the artificial fissures. Depending on the depth of the fissures the surface waves are affected as follows: shallow fissures affect the propagation of the waves having shorter wavelength and higher frequencies; as the depth of the fissure increases the frequency band where the propagation is affected goes to lower frequencies. It is possible to calculate the frequency band where the propagation is affected, this is possible knowing the Rayleigh wave velocity and assuming that the penetration depth of the surface waves correspond

approximately to its wave length, these bands for each fissure depth are presented in fig. 5. These results show that the fissures act as a filter for surface waves; this could be a new possibility to identify fissures in desiccated soils.

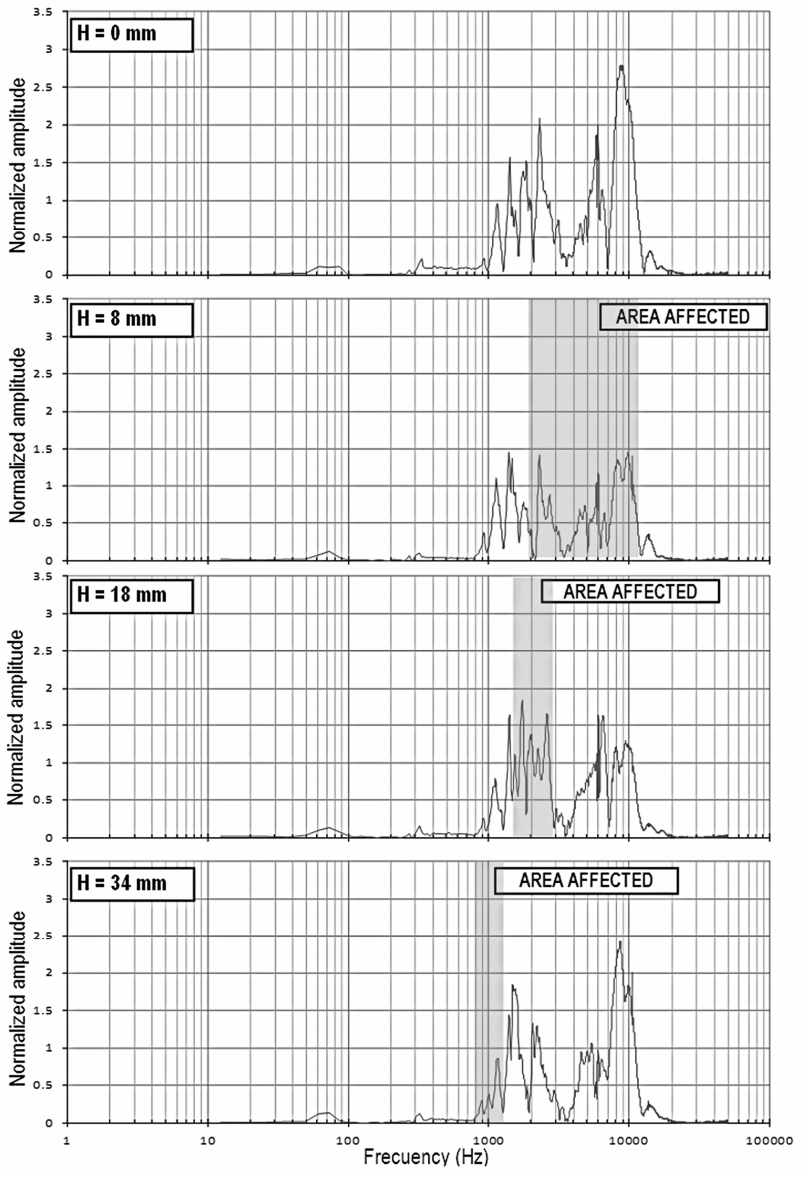

Fig. 5. Example Fourier spectrum for each depth of the fissures.

The table 1 is a summary of the results of the experimental tests. The first column is the fissure depth, the second column is the frequency associate with the wavelength equal to fissure depth and a wave velocity of 220 m/s (Mean Rayleigh wave velocity for material tested. Murillo, 2006) and the third column show the frequency band that was affect in the spectral analysis (fig. 5).

Table 1. Summary of the results of the experimental tests.

Crack depth (mm)	Frec. assoc (kHz)	Band affected(kHz)
8	27.5	2 – 12.0
18	12.2	1.7 – 3.0
34	6.5	0.8 - 1.1

5 Conclusions

The experimental study presented in this paper show the possibility of identifies fissures in soils using surface waves. The results show that the fissures act as a filter for the propagation of Rayleigh waves.

The results presented in this paper correspond to the first results concerning wave propagation in fissured soils; several points need further research to progress to an operational in situ method: the near field effect has an important influence on the quality of the measures, the effect of the suction and water content on the wave propagation on fissured soil, also improving the relationship signal/noise for long wavelength waves is necessary to identify deep fissures.

References

Asaoka, A.: Observational Procedure of Settlement Prediction. Soils and Foundations 18(4) (December 1978); Japanese Society of Soil Mechanics and Foundation Engineering

Bertel, J.: Analytical Study of the Spectral-Analysis-of-Surfacewaves Method at Complex Geotechnical Sites. Thesis Faculty of the Graduate School, pp. 1–43. University of Missouri-Columbia (December 2006)

Murillo, C.: Caracterización Geotecnica de Estructuras Multicapas en Centrifuga Empleando Ondas de Superficie. Thesis Doctoral Universidad de Los Andes, Bogotá Colombia, 2–18, 131–147 (Abril 2006)

Murillo, C., Thorel, L., Caicedo, B.: Spectral analysis of surface waves method to assess shear wave velocity within centrifuge models. Journal of Applied Geophysics 68, 135–145 (2009)

Nazarian, S., Stokoe, K.H., Hudson, W.R.: Use of spectral analysis of surface waves method for determination of moduli and thicknesses of pavement systems, Transportation Research Record, No. 930, Washington, USA, pp. 38–45 (1983)

Smith, S.: The Scientist and Engineer's Guide to Numérique Signal Processing, 2nd edn., pp. 141–161. California Technical Publishing, San Diego (1999)

Stokoe, K.H., Joh, S.H., Woods, R.D.: Some contributions of in situ geophysical measurements to solving geotechnical engineering problems. In: Da Fonseca, V., Mayne (eds.) Proceedings ISC-2 on Geotechnical and Geophysical Site Characterization, Porto, Portugal (September 2004)

Wardany, R.A.L., Rhazi, J., Ballivy, G., Gallias, J.L., Saleh, K.: Use of Rayleigh wave methods to detect near surface concrete damage, Research Group on NDT and Instrumentation, Université de Sherbrooke, Sherbrooke, Canada; Laboratoire de Modélisation, Matériaux et Structures, Université de Cergy Pontoise, Cergy-Pontoise, France, Research Institute of Hydro-Québec, Varennes (Québec), Canada (2003)

Field Scale Water Content Measurement by TDR Technique

Armando Carravetta, Nicola De Paolis, and Riccardo Martino

Abstract. The paper presents an extended version of TDR technique for distributed large scale measurement of water content. Long Distance Reflectometry (LDR) technique is based on the propagation of electromagnetic waves through a transmission line consisting of two rods inserted in the soil horizontally and on the interpretation of the reflected signal for the assessment of the water retention curve. The lack in precision determined by the signal attenuation as an effect cables length is well balanced by the economical advantage of obtaining a low cost field scale representation of water content. Experiments confirm LDR capability in revealing variations in soil water contents, even in presence of sharp water retention curves.

Keywords: TDR, soil moisture content, field scale, calibration.

1 Introduction

In civil and environmental engineering, as well as in agronomy, the measurement of soil moisture content is of major interest. Ground stability, surface runoff, infiltration processes, and crop stress all involve the assessment of water flow in the unsaturated region. In many cases, prediction models are based on remote controlling

Armando Carravetta
Università di Napoli Federico II, Napoli, Italy
e-mail: arcarrav@unina.it

Nicola De Paolis
Università di Napoli Federico II, Napoli, Italy
e-mail: nikdep@libero.it

Riccardo Martino
Università di Napoli Federico II, Napoli, Italy
e-mail: riccardo.martino@unina.it

by measurement water content measurement. The most popular measurement techniques are based on electric or electromagnetic properties of soils.

Time domain reflectometry (TDR) relies on the measurement of the velocity of electromagnetic waves propagating through the soil, which in turn depends on the soil water content (Topp et al. 1980, Topp et al. 1984, see Robinson et al 2003 for a review on TDR methods). This technique was firstly utilized for signal transmission line maintenance, because it allows localization of cable faults through remote testing. In a well-functioning transmission line, electromagnetic waves propagate along the line down to the load, which captures the whole energy of the wave. In contrast, faults along the line (e.g. shortcuts or interruptions) cause local mismatches that reflect a portion of the energy of the electromagnetic wave [Dasher 1996, AA.VV. 2000].

TDR systems are also widely used in soil science to detect the local distribution of the soil dielectric permittivity. Calibration test is used to relate such distribution measurement to the water content distribution. For the aforementioned applications different kind of probes can be used, but generally no longer than 0.20 m.

A TDR system for field water content measurements requires a wave generator, an auxiliary transmission system with multiplexer to connect single probes, a receiver, a wave analyzer, and, finally, a CPU with storage unit. However, the cost of this system, even for a small number of probes, is extremely high. Research is therefore focusing on the development of measurement systems having lower cost (Jones et al. 2006).

A new low cost TDR technique -LDR (Long Distance Reflectometry) technique- is described in the paper. The novelty with respect to traditional applications is that LDR is here exploited to detect water content profile using a long transmission line and the theory for the assessment of water retention curves by measurement in different soil humidity conditions. It can be anticipated that with respect to mismatches that directly affect the usual TDR probes, LDR has less detection capabilities in this case (Knight 1992, Miyamoto & Chikushi 2006). Anyway, it can be shown that LDR is still a viable approach to detect in an economic way hydro-geological shortcomings (Postiglione et al. 2000).

This paper presents the preliminary laboratory results obtained by using a prototype system for the measurement of water content profile. Data processing algorithms were developed to infer the water content profile from a set of LDR data.

2 Theoretical Background

In LDR technique the probe is a couple of transmission lines made up of conductors separated by the soil, which acts as a dielectric medium. The system is electrically characterized in terms of impedance Z_0, which is defined at any point of the line by the ratio between voltage and current phasors. Impedance depends on the physical geometrical and electromagnetic properties of both conductors and dielectric medium. It can be determined by assuming that the transmission line

consists of a continuous structure of series resistance R and inductance L, which represent the ohmic losses and inductance of the cables respectively, with shunt conductance G representing the ohmic losses of the dielectric, and a distributed capacitance C between the two conductors. In the case of infinitely long line, the former quantities are given per unit length, and the resulting expression for the characteristic impedance can be determined as follows:

$$Z_0 = \sqrt{\frac{R + j\omega L}{G + j\omega C}} \tag{1}$$

The expression of *R*, *L*, *G* and *C* depends on the specific type of transmission line. For a twin-lead (two-conductor ribbon cable) they are determined as follows:

$$R = \frac{R_s}{\pi a} \qquad G = \frac{\pi\sigma}{\cosh^{-1}\left(\frac{D}{2a}\right)} \qquad L = \frac{\mu}{\pi}\cosh^{-1}\left(\frac{D}{2a}\right) \qquad C = \frac{\pi\varepsilon}{\cosh^{-1}\left(\frac{D}{2a}\right)} \tag{2}$$

with

$$R_s = \sqrt{\frac{\pi \cdot f \cdot \mu_c}{\sigma_c}} \tag{3}$$

where *a* is the radius of the conductors, *D* the separation distance between the conductors, μ, ε and σ the magnetic permeability, dielectric permittivity and conductibility of the dielectric respectively, and μ_c and σ_c are the magnetic permeability and electrical conductivity of the conductors.

A voltage wave applied at an input section of a transmission line propagates at a velocity v that, for transmission lines with air dielectric, approaches the speed of light *c*. For other dielectrics, characterized by relative dielectric permittivity $\varepsilon_r = \varepsilon / \varepsilon_0$ (where ε_0 is the permittivity of vacuum) the velocity of propagation is lower, according to:

$$v = \frac{c}{\sqrt{\varepsilon_r}} \tag{4}$$

The attenuation of signals during propagation is related to the value of parameters R and G. LDR, as well as TDR, is a straightforward and intuitive measurement technique adopted to reveal impedance characteristics of transmission lines starting from the observation of the superposition of the incident and reflected wave. In practice, the line under test is stimulated at the input section with a step signal produced by a waveform generator. An oscilloscope is used to observe the signal at a particular point along the line, usually at the input section. For a lossless line terminated on a perfectly matched load, and without discontinuities along its path,

the recorded signal is identical to the one applied at the input because no reflection occurs.

When the line is matched, its finite length s, equally causes a mismatch and a time delay t between the rising or falling edge of the compound reflection waveform, and can be easily measured recalling that:

$$s = \frac{v \cdot t}{2} \tag{5}$$

where v is the velocity of propagation as in (4) and the division by 2 accounts for the fact that the path travelled during t is twice the length s.

Any impedance mismatch 'spoils' the signal observed by the oscilloscope. The amplitude of waves reflected at interfaces between media that are far from the measuring point (oscilloscope) can be less evident because of the multiple reflections and, hence, loss of energy that the reflected waves encounter when travelling backward to the oscilloscope. Additionally, in dissipative media the amplitude of the generated or reflected wave could reduce with travel distance as an effect of the different traveling speed of the components of the broadband signal input signal. Moreover, for dissipative medium, the permittivity appearing in equation 4 is a frequency-dependent permittivity and therefore the term ε_r in equation 4 is to be intended as an apparent dielectric permittivity to consider the effects of the dispersions upon the speed propagation both for dissipative and non dissipative media. It is evident that in a non dissipative medium, in which the factors of energy loss are very low, the apparent permittivity and the dielectric constant can be considered equivalent.

The proposed system for ground monitoring consists of a transmission line deployed in the ground, a function generator capable of producing steep voltage signals, a digital storage oscilloscope, and a control and processing unit.

The transmission line in the proposed LTR is made up of a pair of insulated metal conductors, positioned at constant depth and buried beneath the soil surface. For field installations, the transmission line can be positioned by cutting the surface with machine saws.

The instrumentation required for signal generation and monitoring is typically available in any test and measurement laboratory and can be easily miniaturized for in situ low cost acquisition.

In the original TDR technique, cable length is generally not over 20 cm. In order to overcome interpretation problems connected with the change in water content along the probe: soil water content has to be determined numerically by inverse profiling of TDR waveforms (Greco, 2006). In the new LDR technique the transmission line is inserted in the soil horizontally . Therefore any change in water content has the same effect on the dielectric constant along the whole cable length.

3 Experimental Setup

The first experiments have been set up and carried out in a laboratory site under controlled humidity conditions. The system consists in a waterway, characterized by a section equal to 0.20x0.30 m, and length equal to 3.3 m. The channel, placed on two plastic deformable rolls filled with water, is free to move vertically due to increases/decreases in weight caused by variations in water content. . The total weight of the open channel comes out by water pressure measurement in the rolls. Preliminary experiments were performed in order to assess the error in water content corresponding to the maximum error in pressure measurements: such error was estimate in 1.24%. The channel can be completely drained by two bottom discharge valves. Water table elevation was measured by a piezometer. The channel was filled in the following way:

- gravel for the first 3 cm (Fig. 1);
- a layer of geotextile material (Fig. 1);
- a PVC pipeline connecting 10 porous cups, 10 spacing, joined with a pressurization system;
- the transmission line, consisting of two isolated metal conductors 1.5 mm diameter, 5 cm spaced, positioned at a distance of 14,5 cm from the bottom of the channel;
- a 26 cm deep layer of homogeneous granular sand - 1.5 mm average diameter test granular material - (Fig. 1).

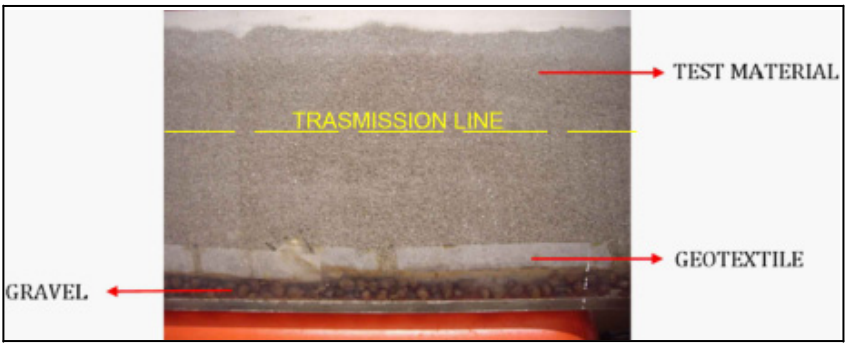

Fig. 1. Side view of the experimental channel.

The sand was not compacted during channel filling and, therefore, it is characterized by a very large value of porosity, n=42%. Experiments with this material were performed by completely saturating the soil and operating a progressive desaturation by opening the bottom discharge. The elevation of water table was assessed by a piezometer.

4 Experimental Results

Reflection waves measured for different water table elevations are plotted in Fig. 2. Waveform modification with soil water content change is evident. From each measured wave the propagation time was determined by the procedure introduced by Strickland (1970).

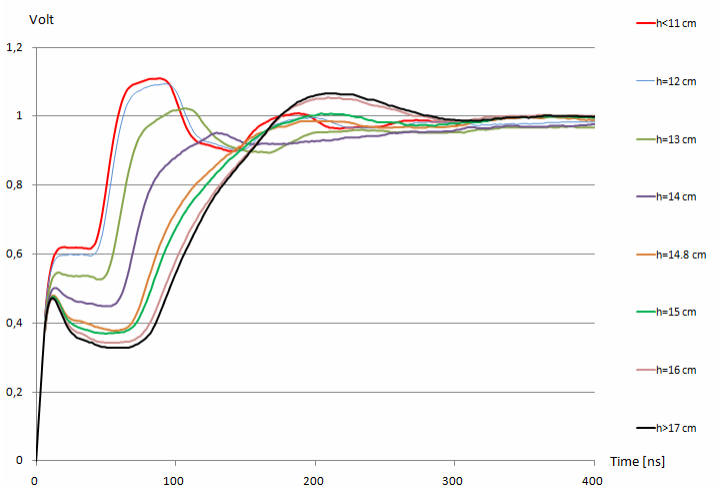

Fig. 2. LDR wave forms for different water table elevations.

The travel time T of the signal is calculated by identifying the departure time of the signal at the base of the first peak voltage corresponding to a first reflection, caused by the impedance mismatch between the cable in air and the cable in the ground, and a second reflection at the end of the probe (Fig. 3).

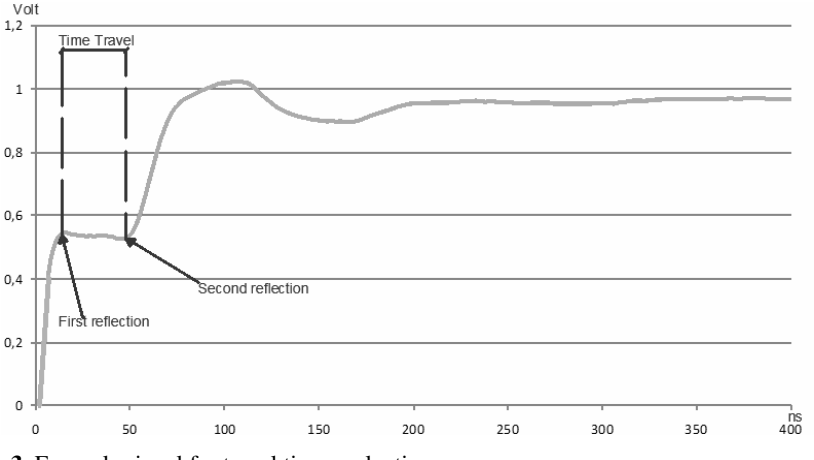

Fig. 3. Example signal for travel time evaluating

Then, the velocity of wave propagation was obtained by eq. (5), and the related value of the relative electric permittivity by eq. (4). The values of permittivity are plotted in Fig. 4 versus water table elevation.

Not only the $h(\varepsilon_r)$ relationships, but the parameters of the Brooks-Corey water retention curve (Brooks & Corey, 1964) can be assessed by a new calibration procedure set up for LDR.

A main difference between TDR and LDR is that in the latter the rods disposition is horizontal and the electromagnetic wave crosses different layers of the ground at different moisture elevation dependent. This effect is more evident in the more coarse-grained soils. Consequently the new technique parameters calibration can be done through the determination of the water retention curve.

In fact, only a small part of the porous media surrounding the transmission line contributes in a relevant way to wave propagation. This part is called the electromagnetic bulb. It is evident in Fig. 4 that the relative electric permittivity is variable in a limited range of water table elevations, as an effect of a variation of water content from the saturated value to the residual one. Therefore, the vertical dimension of the electromagnetic bulb can be estimated to be approximately 6 cm. The electromagnetic bulb, presenting in section an elliptic form, has been simplified in a prism having rectangular section, as shown in Fig. 5.

Within the bulb a variation of water content is present in the vertical direction, and, correspondingly, a variation of relative electric permittivity is present too.

In what follows we assume, that a Topp like relations is valid between the electric permittivity measured by LDR and the average value of water content in the electromagnetic bulb as expressed by Brooks-Corey formula (1964). Consequently, for each measurement the following relation exists:

$$a_1\overline{\varepsilon}^3 + a_2\overline{\varepsilon}^2 + a_3\overline{\varepsilon} + a_4 = \int\left(\frac{\psi}{\psi_b}\right)^{-\lambda} dz \tag{6}$$

where a_1, a_2, a_3 and a_4 are the coefficients of the Topp relation, ψ_b is the bubbling pressure and λ is a soil characteristic parameter.

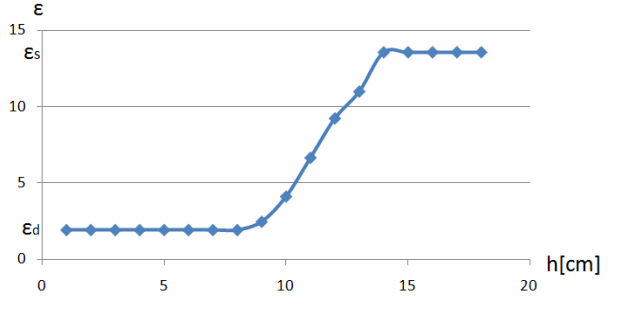

Fig. 4. Measured value of the relative electric permittivity for each elevations of the water table.

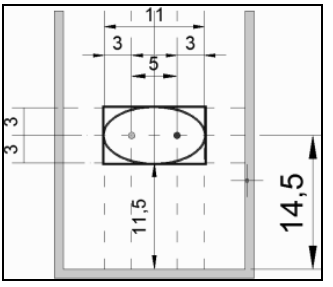

Fig. 5. Geometry of the electromagnetic bulb and its simplification.

In order to estimate the parameters, a system of six equation based on six tests has been solved. For each test, measured values of electric permittivity and elevation of the water table have been used. The results of the calibrations are listed in Table 1.

In Fig. 6, the re-calibrated Topp relation for LDR is plotted and compared with the original Topp relation for TDR. The LDR relation nicely fit the limiting values $\varepsilon(\varepsilon_d)$ and $\varepsilon(\varepsilon_s)$, corresponding to drained and saturated conditions of the soil in the electromagnetic bulb.

The soil water retention curve, based on calculated Brooks-Corey parameters is very steep because of the sediment size and the large value of porosity.

Table 1. Results of the calibrations

A_1	a_2	a_3	a_4	ψb	λ
0.000559	-0.23187	0.16244	-0.01606	4.55 cm	405.4

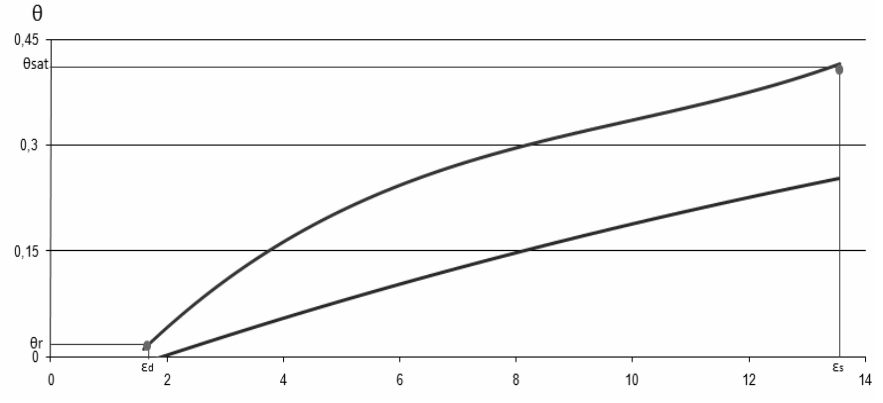

Fig. 6. Topp relation for LDR (blue curve) and for TDR (red curve).

5 Conclusions

The replacement of the traditional TDR probes with 3.3 meter conductor cables, allowed to overcome the main limitation of the TDR technology in measuring the water content: the installations of long horizontal probes , overcome the punctuality of the traditional TDR analysis , allowing the measurement of a mean value of moisture for large surfaces.

The output waveform of the new technological application TDR, provided encouraging results in term of interpretative possibilities of the signal: the expected attenuation related to the long probes, proved not to be compromising the analysis which yielded well identifiable tension profiles.

Subsequent studies will evaluate the maximum possible length for cables in relation to the intensity of the input signal.

References

AA.VV. Time domain reflectometry theory. Application Note 1304-2, Agilent Technologies, Lit. number 5966-4855E (2000)

Brooks, R.J., Corey, A.T.: Hydraulic properties of porous media. Hydrol. Pap. 3. Colo. State Univ., Fort Collins (1964)

Dascher, D.J.: Measuring parasitic capacitance and inductance using TDR. Hewlett-Packard Journal (April 1996)

Greco, R.: Soil water content inverse profiling from single TDR waveforms. Journal of Hydrology 317(3-4), 325–339 (2006)

Knight, J.H.: Sensitivity of time domain reflectometry measurements to lateral variations in soil water content. Water Resour. Res. 28, 2345–2352 (1992)

Jones, S.B., Robinson, D.A., Friedman, S.P.: A subsurface open-ended TDR probe for on-the-go mapping of water content. In: Proceedings of the 3rd International Symposium and Workshop on Time Domain Reflectometry for Innovative Soils Applications, September 17-20. Purdue University (2006)

Miyamoto, H., Chikushi, J.: Calibration of Column-Attaching TDR Probe Based on Dielectric Mixing Model. In: Proc. TDR 2006, Paper ID3, 7 p. Purdue University, West Lafayette (2006), https://engineering.purdue.edu/TDR/Papers

Postiglione, L., Santini, A., Fagnano, M.: Modelli di agricoltura sostenibile per la pianura meridionale: gestione delle risorse idriche nelle pianure irrigue. In: Postiglione, L., Santini, A., Fagnano, M. (eds.) Proceedings of Conference POM (B19), Salerno, November 6, pp. 76–90 (2000)

Robinson, D.A., Jones, S.B., Wraith, J.M., Or, D., Friedman, S.P.: A review of advances in dielectric and electrical conductivity measurement in soils using time domain reflectometry. Vadose Zone Journal 2, 444–475 (2003)

Strickland, J.A.: Time-domain reflectometry measurements, pp. 11–13. Tektronix Inc., Beaverton (1970)

Topp, G.C., Davis, J.L., Annan, A.P.: Electromagnetic determination of soil water content: measurements in coaxial transmission lines. Water Resour. Res. 16, 574–582 (1980)

Topp, G.C., Zebchuk, W.D., Davis, J.L., Bailey, W.G.: The measurement of soil water content using a portable TDR hand probe. Can. J. Soil Sci. 64, 313–321 (1984)

Use of TDR Probes to Measure Water Content in Pumiceous Soils

Raffaele Papa and Marco V. Nicotera

Abstract. The time domain reflectometry has become a technique commonly used in geotechnical engineering to determine soil water content of soil. The possibility to determine soil properties depends on the proper understanding of the parameters that affect the propagation of an electromagnetic pulse along the TDR wave guide. Dielectric permittivity measurements in coarse grained soils indicate that the determination of the apparent relative permittivity of this materials may be complicated by a non uniform water content distribution along the rods of the TDR probe. This problem is quite evident when pumiceous soils are of concern due to their water retention properties (very low air entry value and sharp transition from full saturation to residual saturation). In order to conceive an interpretation procedure apt to manage this complexity a specific laboratory testing programme was designed and carried out. During the tests the water content of a reconstituted pumiceous soil sample was changed by means of the negative water column technique along a number of wetting and drying cycles, and simultaneously the waveforms were registered. The soil utilized was collected from a trial field in the neighbourhood of Monteforte Irpino (Avellino, Italy).

Keywords: TDR probe, pumiceous soil, dielectric constant, soil-water content.

1 Introduction

In coarse-grained soils such as pumiceous ones, suction is difficult to measure in the field by means of tensiometers. However the complete understanding of the

Raffaele Papa
Università di Napoli Federico II, Napoli, Italy
e-mail: rafpapa@unina.it

Marco V. Nicotera
Università di Napoli Federico II, Napoli, Italy
e-mail: nicotera@unina.it

groundwater flow processes in a number of subsoil conditions, which can be encountered in geotechnical applications, may require monitoring at least the soil water content in coarse grained soil strata (NIcotera et al., 2010). Currently Time Domain Reflectometry (TDR) is prevalently used to measure the water content of fine to medium grained soils both in the laboratory and in the field. TDR is based on the measurement of the velocity of an electromagnetic wave travelling along a probe inserted in the soil. The velocity is related to dielectric permittivity of the soil, K_a, which is in turn related to volumetric water content through a suitable calibration curve. Nevertheless the correlation between the apparent relative permittivity and the soil water content may be confused by a non uniform distribution of the soil moisture along the rods of the TDR probe (Dobson et al., 1985; Regalado, 2004; Regalado et al., 2003; Tomer et al., 1999; Schneider & Fratta, 2009; Tarantino & Pozzato, 2008; Papa & Nicotera, 2011).

In this paper we will show the first results of a series of laboratory calibration tests finalised to the measurement of the water content in some pumiceous soil strata identified in the subsoil of the Monteforte trial field.

2 Material and Methods

The soil utilised was recovered from one of the pumiceous soil strata identified in the subsoil of the trial field of Monteforte Irpino; this strata was constituted of a quite uniform coarse-grained material produced by one of the main plinian eruption (Avellino eruption 3.7 ky b.p.) of the volcano *Somma-Vesuvius*. Each soil sample was reconstituted by dry pluviation inside a PVC cylindrical sampler (20cm diameter, 25cm height); the soil sample was reconstituted in four layers 50 mm thick achieving a mean value of the dry density γ_d equal to 4.70 kN/m^3 and a mean value of the porosity n equal to 0.799. A drainage grooves was machined in the base sealing acrylic cup to allow both saturation and drainage of the specimens. The drainage circuit was connected to a water reservoir and a levelling device was used to control the hydraulic head acting at the sample bottom end (see Figure 1.b); by varying the constant elevation imposed by the levelling device it was possible to vary the pore pressure applied ad the sample bottom in the range 0 to 2 kPa. A piezometric pipe was used to check the water level in the sample (Figure 1.b).

After the sample preparation a three-rod TDR probe (15 cm long) was inserted vertically into the soil sample and the total weight was recorded. The soil core was placed on an electronic balance and simultaneously a TDR reading was performed. The measurement of the electromagnetic wave velocity was carried out with TDR equipment consisting of a wave generator (Campbell Scientific TDR 100), a PDA with integrated software and a battery. The probe remained permanently inserted into the soil core during the calibration experiment.

The test began with a wetting phase during which the water level from the sample bottom *h* (see Figure 1.a), was raised in four 5 cm subsequent steps from 0 cm up to 20 cm. Each increment of the water level produced an equalization process during which the water flowed into the soil sample increasing the sample weight as depicted in Figure 2a. The end of the equalization process was clearly identified by observing the diagram of the sample weight as function of the logarithm of the elapsed time. At the end of each equalization process a TDR reading was performed (Figure 3a) and the derived value of the apparent electric permittivity was compared to the mean value of the volumetric water content (see Figure 4). The wetting phase was followed by a drying phase carried out with a similar procedure (see Figure 2b and 3b) but reducing the water level up to 0 cm. Four complete wetting-drying cycles were performed in total.

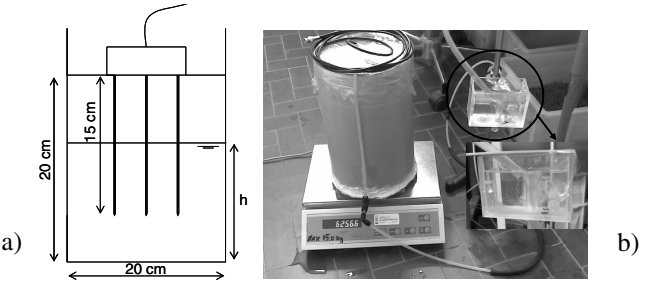

Fig. 1. a) TDR probe installation and water level h; b) test equipment.

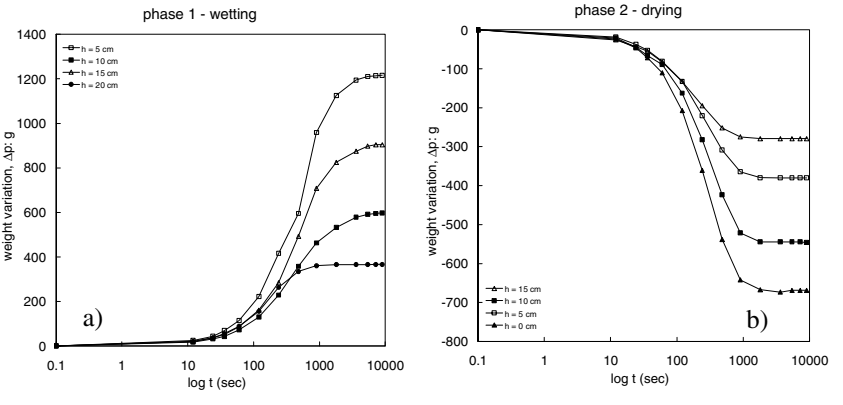

Fig. 2. Sample weight variation during equalization steps: a) wetting; b) drying.

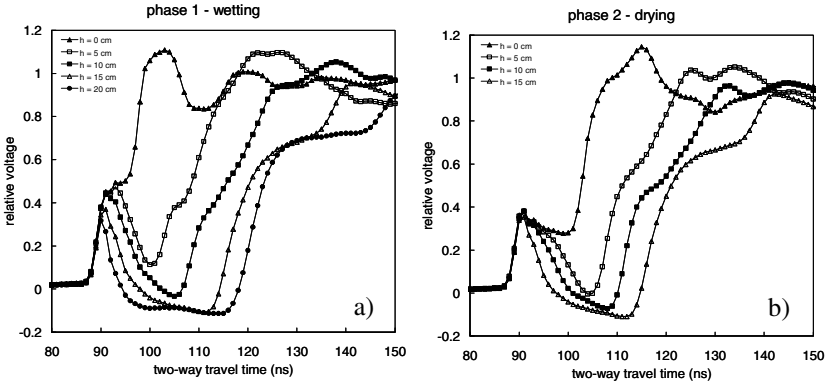

Fig. 3. Waveforms measured at the end of each equalization steps: a) wetting; b) drying.

3 Results and Discussion

The testing program was aimed to evaluate the possibility of using the TDR technique in the pumiceous soils under carefully controlled conditions.

The waveform collected along the first of four rounds of wetting-drying are shown in Figure 3. For a water level between the ends of the TDR probe (i.e. 5, 10, 15 and 20 cm), two distinct reflection were observed. The first arrival in the waveform was the signal reflection off the water level (i.e., a sudden drop in the signal amplitude) and the second arrival is the signal reflection from the tip of the TDR probe (i.e. a sudden increase in the signal amplitude). The time required for the step pulse to travel along the entire waveguide is used to measure a equivalent apparent dielectric permittivity K_a of the soil. The higher is the water level (h increases), the higher is the soil bulk permittivity and, hence the lower is the velocity at which the wave propagates into the guide (Robinson et al., 2003b).

The waveforms were collected and analysed to determine the equivalent value of the apparent relative dielectric permittivity and subsequently the experimental values of K_a were plotted as function of the corresponding imposed water level h (Figure 4a). The observed hysteresis shown by the relationship between the water level and the apparent relative dielectric permittivity (Figure 4a) could mainly be ascribed to the hysteretic feature of the pumices water retention behaviour; hydraulic hysteresis was indeed quite evident in the relationship between the water level (i.e. the applied matric suction) and the mean value of the volumetric water content (see Figure 4b). Nevertheless hysteresis persisted even in the experimental relationship between the apparent relative dielectric permittivity and the mean value of the volumetric water content. As a consequence it seemed that the mean value of the soil water content could be correlated to the mean value of the apparent dielectric permittivity only with a limited accuracy. This limitation was likely produced by the non uniform distribution of the water content along the TDR

probe; two different distributions of water content could indeed corresponds to the same travelling time of the step pulse along the rods. However a different interpretation procedure taking into account the complete waveform must be considered in order to achieve a higher accuracy.

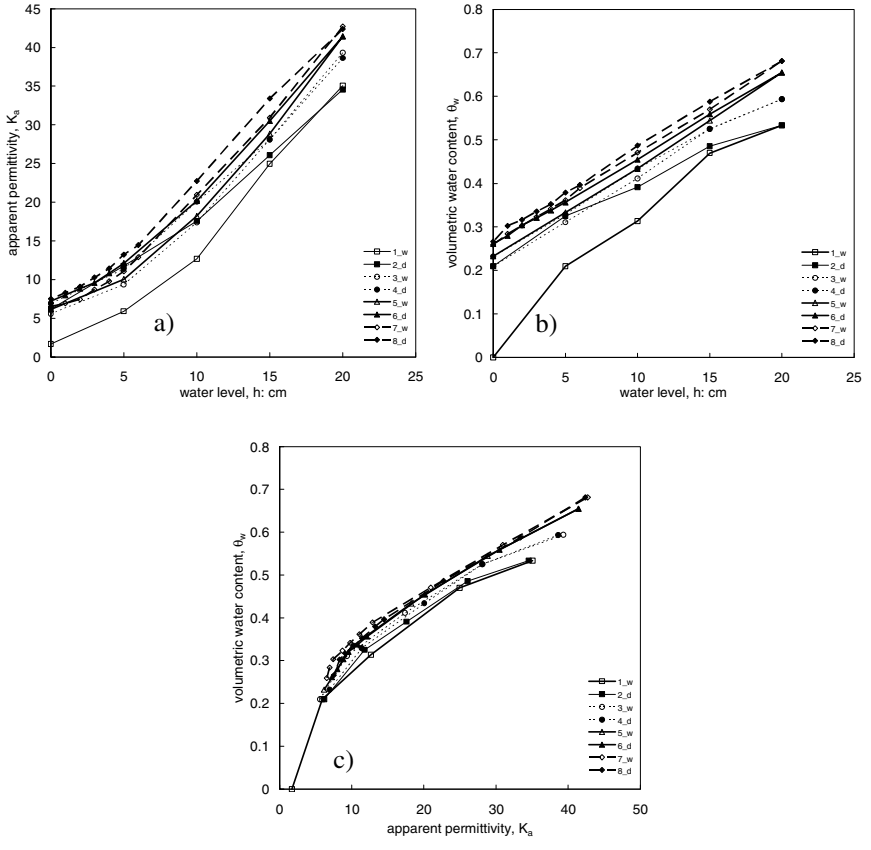

Fig. 4. Variation of apparent dielectric permittivity with water level. a) increasing value of K_a with increasing of wet-dry cycles; b) relationship between volumetric water content and water level variation for different cycles; c) relationship between volumetric water content and apparent dielectric permittivity for different cycles.

4 Concluding Remarks

In the paper the first results of a series of lab calibration tests finalised to the measurement of the water content in a pumiceous soil stratum by means of a TDR probe were presented. The observed hysteresis between the water level and the apparent relative dielectric permittivity could mainly be due to the hydraulic hysteretic behaviour of the pumices. This effect was quite evident in the relationship

between the water level and the mean value of the volumetric water content. Nevertheless a calibration curve correlating the mean value of the soil water content to the mean value of the apparent dielectric permittivity was identified. However the correlation was scattered due to the non uniform distribution of the soil moisture along the rods of the TDR probe and a different interpretation procedure taking into account the complete waveform must be considered in order to achieve a higher accuracy.

References

Dobson, M.C., Ulaby, F.T., Hallikainem, M.T., El-Rayes, M.A.: Microwave dielectric behaviour of wet soil. IEEE Trans. Geosci. Remote Sens. GE-23, 35–46 (1985)

Nicotera, M.V., Papa, R., Urciuoli, G.: An experimental technique for determining the hydraulic properties of unsaturated pyroclastic soils. Geotechnical Testing Journal 33(4), 263–285 (2010)

Regalado, C.M.: A physical interpretation of logarithmic TDR calibration equations of volcanic soils and their solid fraction permittivity based on Lichtenecker's mixing formulae. Geoderma 123, 41–50 (2004)

Regalado, C.M., Munoz-Carpena, R., Socorro, A.R., Hernandez-Moreno, J.M.: Time domain reflectometry models as a tool to understand the dielectric response of volcanic soils. Geoderma 117, 313–330 (2003)

Tomer, M.D., Clothier, B.E., Vogeler, I., Green, S.: A dielectric-water content relationship for sandy volcanic soils in New Zealand. Soil Sci. Soc. Am. J. 63, 777–781 (1999)

Robinson, D., Schaap, M., Jones, S., Friedman, S., Gardner, C.: Considerations for improving the accurancy of permittivity measurement using TDR: air/water calibration, effects of cable length. Soil Sci. Soc. Am. J. 67, 62–70 (2003b)

Schneider, J., Fratta, D.: Time domain reflectometry – parametric study for the evaluation of physical properties in soils. Canadian Geotechnical Journal 46, 753–767 (2009)

Tarantino, A., Pozzato, A.: Theoretical analysis of the effect of the temperature, cable length and double-impedance probe head on TDR water content measurement. In: First European Conference on Unsaturated Soils, Durham, July 2-4 (2008)

Papa, R., Nicotera, M.V.: Calibration of TDR probes to measure water content in pyroclastic soils. In: 5th Asia-Pacific Conference on Unsaturated Soils, Pattaya, Thailand (2011)

Observations from Borehole Shear Testing in Unsaturated Soil

Gerald A. Miller and Charbel N. Khoury

Abstract. The Iowa Borehole Shear Test (BST) is an in situ device to rapidly determine a Mohr-Coulomb failure envelope in a borehole. Under the right conditions in clayey soils, the failure envelope from the BST may yield a friction angle and cohesion intercept in agreement with effective stress strength parameters determined from laboratory tests. Generally, this occurs when the in situ soil is in a nearly saturated condition and where shear-induced excess pore pressures are minimal, such as for stiff clays. For unsaturated soils, the interpretation of BST results is complicated by the presence of, and unknown variations in, soil suction during the test. This paper presents and discusses the results of BSTs and corresponding suction determinations in unsaturated clayey soils at two test sites. Results indicate that soil suction, in addition to other test variables, has a strong influence on failure envelope. Range of normal stress used in the test was also observed to have a strong influence on the resulting Mohr-Coulomb failure envelopes.

Keywords: borehole shear test, shear strength, suction, unsaturated soil.

1 Introduction and Background

The Iowa Borehole Shear Test (BST) is a rapid and simple in situ test to obtain the Mohr-Coulomb shear strength parameters of soil. It simply involves expanding diametrically opposed, curved, serrated shearing plates to engage the sidewalls of a borehole as shown in Fig. 1. The normal force on the plates is applied in increments and the shearing resistance is determined by measuring the maximum force required to move the shearing plates vertically upward. Dividing the normal and shear forces by the area of the plates provides stresses that can be used to construct

Gerald A. Miller
University of Oklahoma, Norman, OK, USA
e-mail: gamiller@ou.edu

Charbel N. Khoury
KMA Consulting Engineers, Inc., Medford Medford, NJ, USA
e-mail: charbelk@kmapc.net

a failure envelope. The BST has been extensively used in many geotechnical engineering investigations such as slope stability analysis associated with landslides (Handy 1986) and prediction of uplift capacity of drilled shafts (Lutenegger & Miller 1994) among others. A preliminary laboratory study of the BST in unsaturated silty soil within a rigid wall calibration chamber was carried out by Miller et al. (1998). More recently, Khoury & Miller (2006) conducted BST field testing on clayey soil to study the influence of borehole flooding (FBST) on the BST results in unsaturated soil.

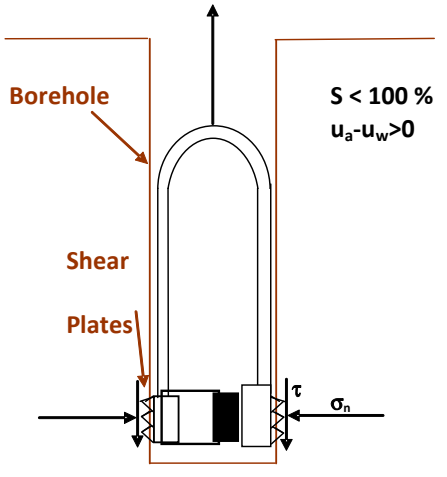

Fig. 1. Schematic of BST.

This paper discusses the effect of initial suction and range of normal stress on the shear strength parameters determined with the BST. In addition to the BSTs, laboratory testing including filter paper and multistage triaxial tests were conducted to determine soil suction and strength parameters, respectively. While this research effort is ongoing, the results presented in this paper have important implications regarding the use and interpretation of the BST strength parameters in stability analyses involving unsaturated soil.

2 Test Sites and Soil Description

Two test sites were chosen for the research located within 10 miles of the University of Oklahoma in the City of Norman; these are the I-35 Interstate Site (I-35), and Westheimer Airport Site (AP). These two sites are relatively close to one another and in the same soil formation. These sites were selected because: 1) they have CH and CL soil layers with relatively uniform composition that allowed for multiple BST tests in each layer, 2) moisture content and suction tends to vary

with depth in the profile allowing for BST tests under different conditions, and 3) they were close to campus and have been used in other studies. Characteristic properties of the soil at the I-35 and AP sites are presented in Table 1.

3 Borehole Shear Testing

BST multi-stage tests were conducted in hand-augered boreholes at several depths ranging from 0.46 m (1.5 ft) to 2.29 m (7.5 ft) at an interval of 0.305 m (1 ft). A multi-stage test consists of applying successively higher normal pressures while leaving the shear head in place. This method may produce less accurate strength envelopes if the shear plates are not in good contact with the soil as reported by Handy et al. (1985). However, a number of researchers have observed that the multi-stage BST procedure gives similar results to BST tests involving a "fresh" soil location for each increment of normal stress at a given depth (e.g. Lutenegger & Tierney 1986). Also, Miller et al. (1998) observed that fresh and multistage BST results in unsaturated soil were similar.

4 Results and Discussions

4.1 Suction-Water Content Relationship

In order to assess the BST results, it was first necessary to estimate soil suction present at the time of testing. To accomplish this, thin-walled tube samples were obtained for suction measurement. These tube samples were obtained from boreholes on the same day or within a few days of the borehole shear tests and within several feet of the BST test borings. Soil samples from depths corresponding to the BST test depths were subjected to filter paper testing. The idea was to establish a relationship between the water content of the tube samples and the suction, which could then be used to estimate suction corresponding to water contents of soil samples obtained during the BSTs. This was necessary because water contents in tube samples subjected to filter paper testing were sometimes different than water contents for similar depths during the BSTs.

Data from filter paper tests are presented in Table 1 along with soil properties. The relationship between matric suction and gravimetric water content determined from the filter paper tests showed significant scatter (Fig. 2a). Scatter is attributed to the variation in soil composition at each depth. Thus, a new relationship that incorporates consistency and grain size into the relationship was developed, in which water content values were divided by the Plasticity Index (PI) and the percent passing the number 200 sieve (75 μm openings). The normalized water content shows a strong relationship to matric suction (Fig. 2b). Water content of samples obtained from the borehole immediately prior to a BST were used in conjunction with the best fit equation shown in Fig. 2b to estimate the initial

matric suction prior to testing. Values of suction obtained in this way are discussed relative to the results of the BSTs in the following sections.

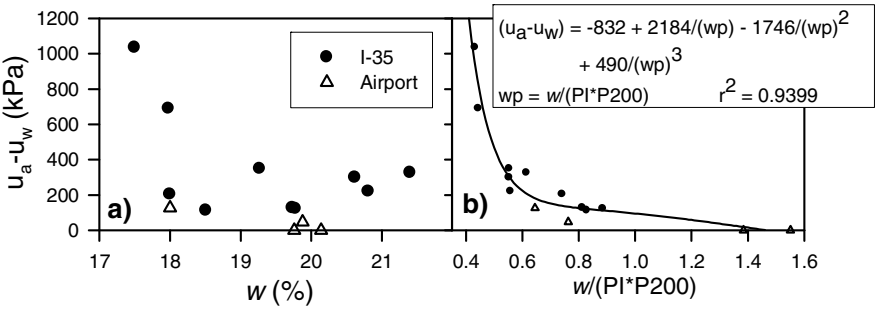

Fig. 2. Suction-water content relationship from Filter Paper Tests: a) Matric Suction versus Gravimetric Water Content and b) Matric Suction versus Water Content Normalized by Plasticity Index and Percent Passing #200 sieve.

Table 1. Filter paper (Suction) test results and soil properties.

Site	Depth (m)	LL (%)	PL (%)	PI (%)	%<2mm (%)	%<#200 P200 (%)	u_a-u_w (kPa)		w (%)	
							B3	B4	B3	B4
	0.76	62	19	43	37	94	1035	689	17.5	18.0
	1.07	56	19	37	38	94	326	348	21.4	19.3
	1.37	56	18	38	42	98	220	298	20.8	20.6
	1.68	40	16	24	41	93	112	121	18.5	19.8
I-35	1.98	41	16	25	47	97	203	126	18.0	19.7
	0.76	52	22	30	39	93	126		18.0	
	1.37	46	15	31	41	98	47		19.9	
	1.98	30	17	13	33	98	0		19.8	
AP	2.29	34	19	15	41	97	0		20.1	

4.2 BST Results for Lower Normal Stress Range

The BST results involving normal stresses in the range of 15 to 100 kPa are presented in Fig. 3. Friction angles (ϕ_{BST}) and cohesion intercepts (c_{BST}) are plotted in this figure against matric suction for both sites. Note that all of the BST tests were of high quality with coefficients of determination (r^2) for the strength envelope close to or greater than 0.99. Some important observations follow from Fig. 3:

1. BST friction angles can be quite high, and were in a range of 17 to 50° for the three sites. Some values are much higher than typical effective stress friction angles from laboratory tests; effective stress friction angles from backpressure saturated triaxial tests at these sites ranged from 17-30°. Some values of BST friction angles that were obtained for lower matric suction are more consistent with drained friction angles.
2. While there is scatter in these plots, there is a clear tendency for increasing BST friction angle with increasing matric suction. This is similar to previous observations by Miller et al. (1998).
3. As shown in Fig. 3, there is a tendency for the BST cohesion intercept to decrease with increasing suction at each site.

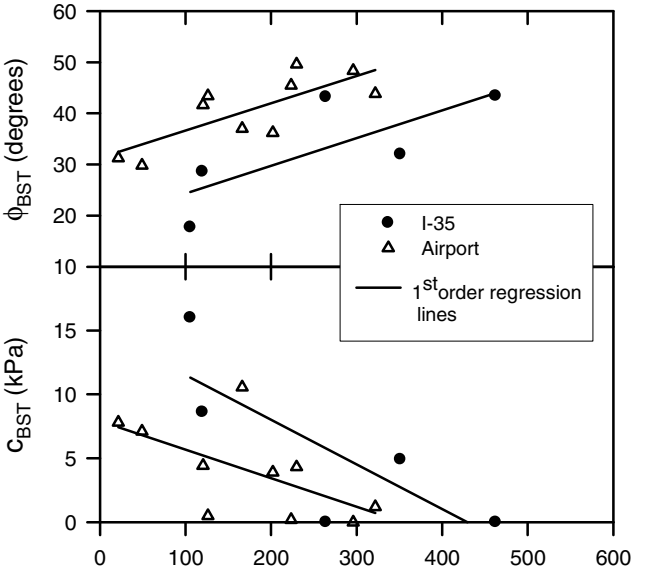

Fig. 3. Strength parameters from BSTs using with normal stresses in the range of 0-120 kPa.

The trend lines in Fig. 3 tend to be different for each site. Other than inaccuracies inherent with using the correlation in Fig. 2b, two factors that may contribute to these differences are the slight disparities in soil properties at each site and variations in suction due to natural wetting and drying cycles at the sites. Some questions naturally arose from the results observed in Fig. 2, which led to research into other factors that may be affecting the BST results from unsaturated soil. Of particular interest was why the BST friction angles were quite large in many cases. Furthermore, the BST results are generally not consistent with unsaturated strength behavior observed during laboratory testing. Laboratory observations from unsaturated strength testing under suction control often show that the friction

angle with respect to net normal stress tends to remain constant with increasing suction while the cohesion intercept increases (e.g. Fredlund and Rahardjo 1993). It is not clear why the BST strength parameters vary with suction in the manner observed; however, this may be partly attributed to the fact that suction is not controlled during testing and may actually change during application of net normal stress and shearing. This behavior is the subject of further study.

4.3 BST Results in for Higher Normal Stress Range

Two tests were conducted at the Airport Site (AP) using standard shearing plates with applied normal stresses in the range of 15 to 250 kPa. The standard plates are serrated and have a contact area with the soil of 32.3 cm^2 (5 in^2) per plate. Failure envelopes are presented in Fig. 4. Interestingly, the results obtained showed a nonlinear trend with the failure envelopes becoming flatter at normal stresses above about 75 to 100 kPa. The results were analyzed for the lower and higher stress range using a bilinear failure envelope. The equations are shown in Fig. 4 for the low and high normal stress range. The difference in failure envelopes is significant at lower and higher stress ranges. It may be possible that at higher normal stress levels, the soil in the shearing zone is compressed to such a degree that saturation markedly increases, resulting in a significant decrease in suction. Possibly, this may occur when the preconsolidation stress is exceeded, at which point substantial changes in void ratio and degree of saturation may occur with increasing net normal stress. For comparison, backpressure saturated triaxial compression tests on tube samples obtained at this site between depths of 0.8 and 2 m gave friction angles of 17, 22 and 27 degrees.

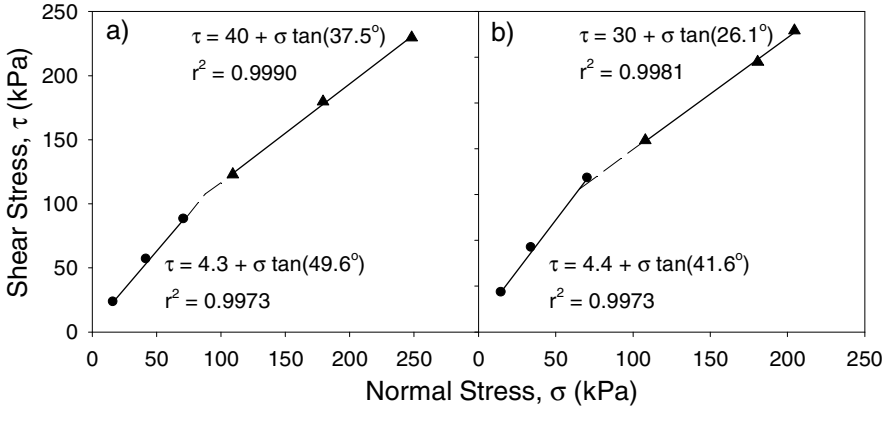

Fig. 4. Results of BSTs at Airport Site Showing Influence of Normal Stress Range at Two Test Depths: a) 0.76 m and b) 1.08 m.

5 Conclusions

The influence of initial suction and normal stress range on Borehole Shear Tests (BST) in unsaturated soil was investigated. Conclusions are summarized as follows:

1. Matric suction can have a significant influence on BST friction angles and cohesion intercepts in unsaturated soil. Generally, the BST friction angle was found to increase and BST cohesion to decrease with increase in suction.
2. For the soils tested in this study, the influence of suction on the BST friction angle was significant when the normal stress during the BST was below 100 kPa. For normal stresses above 100 kPa, the BST friction angles were closer to saturated effective stress strength friction angles determined from backpressure saturated multistage triaxial compression tests. This suggests that BSTs in unsaturated soil should be conducted using a larger range of normal stress in order to estimate effective stress friction angles.

References

Fredlund, D.G., Rahardjo, H.: Soil Mechanics for Unsaturated Soils. John Wiley and Sons, Inc., New York (1993)

Handy, R.L.: Borehole Shear Test and Slope Stability. In: Proceedings of In Situ 1986 ASCE Specialty Conference on Use of In-Situ Tests and Geotechnical Engineering, pp. 161–175. Virginia Tech, Blacksburg (1986)

Handy, R.L., Schmertmann, J.H., Lutenegger, A.J.: Borehole Shear Tests in a Shallow Marine Environment. In: Chaney, R.C., Demars, K.R. (eds.) Strength Testing of Marine Sediments: Laboratory and In-Situ Measurements, ASTM STP 883, Philadelphia, pp. 140–153 (1985)

Khoury, C.N., Miller, G.A.: Influence of Flooding on Borehole Shear Test (BST) Results in Unsaturated Soil. In: Proceedings of the 4th International Conference on Unsaturated Soils, In-Situ Testing in Unsaturated Soil, Carefree, Arizona, vol. 1, pp. 235–246 (2006)

Lutenegger, A.J., Miller, G.A.: Uplift Capacity of Small-Diameter Drilled Shafts from In-Situ Tests. Journal of the Geotechnical Engineering Division, ASCE 120(8), 1362–1379 (1994)

Lutenegger, A.J., Remmes, B.D., Handy, R.L.: Borehole Shear Test For Stiff Soil. Journal of the Geotechnical Engineering Division, ASCE 104(GT11), 1403–1407 (1978)

Lutenegger, A.J., Tierney, K.F.: Pore Pressure Effects in Borehole Shear Testing. In: Proceedings of In Situ 1986 ASCE Specialty Conference on Use of In Situ Tests in Geotechnical Engineering, pp. 752–764. Virginia Tech, Blacksburg (1986)

Miller, G.A., Azad, S., Hassell, C.E.: Iowa Borehole Shear Testing in Unsaturated Soil. In: The Proceedings of the 2nd International Conference on Unsaturated Soils, Geotechnical Site Characterization, vol. 1, pp. 1321–1326. International Academic Publishing House, Beijing (1998)

Microstructure and Hydraulic Behaviour

Microstructure Characteristics of Unsaturated Compacted Scaly Clay

Camillo Airò Farulla and Marco Rosone

Abstract. Microstructure characteristics of unsaturated compacted scaly clay are investigated by MIP tests on freeze dried samples and observation of SEM photomicrographs. Effects of scale microstructure and increasing compaction stresses, and microstructure changes induced by loading and unloading paths and clay saturation are analysed.

Keywords: microstructure, compacted clay, wetting, loading, MIP tests.

1 Introduction

Extensive experimental studies have demonstrated the strong dependence of mechanical behaviour of tectonised clays on their structural arrangement characterised by different sets of discontinuities which subdivide the clays in tightly interlocked hard clayey fragments (scales). A wide evidence has been also collected on the influence that scales which survive compaction have on the mechanical properties of compacted scaly clays. In this respect, a better interpretation of the evolution of stiffness and shear strength of unsaturated compacted scaly clays, when subjected to complex suction and loading paths, could be obtained by a systematic analysis of microstructure evolution in consequence of stress paths applied.

Previous investigations have shown that at a microscopic level as-compacted scaly clays present an aggregated structure determined by scales and assemblages made of scale fragments and clay particle aggregations with different elementary

Camillo Airò Farulla
Università degli Studi di Palermo, Palermo, Italy
e-mail: camillo.airofarulla@unipa.it

Marco Rosone
Università degli Studi di Palermo, Palermo, Italy
e-mail: marco.rosone@unipa.it

particle arrangements. Scales are composed by very dense aggregates of oriented elementary particle arrangements (Airò Farulla & Jommi, 2005). The microstructure is characterised by a clear double porosity network, in which two principal levels can be identified: micropores inside assemblages and clay particle aggregations, and macropores between them (Airò Farulla et al., 2010).

The paper presents further data on the effects on microstructure of unsaturated compacted scaly clay of such factors as: scale microstructure, compaction effort, loading and unloading at constant suction, clay saturation and successive loading and unloading paths.

Microstructure was investigated by mercury intrusion porosimetry (MIP) tests along with observation of photomicrographs obtained by Scanning Electronic Microscope (SEM) on freeze dried samples (Romero & Simms, 2008).

2 Tested Material

Two different sample groups, named AC and B, were prepared using a stiff and highly fissured clay outcropping near Palermo (Sicily). It is a silty clay, with plasticity index $PI = 28 \div 30\%$, mean specific gravity $G_s = 2.76$, and natural water content $w_n = 20\%$.

The air dried clay was disaggregated by a rubber pestle and the material passing through a No. 10 ASTM sieve (mesh aperture of 2 mm) was selected for preparing samples AC. The selected material (composed mainly by sand-size clay fragments) was moistened to reach water content $w = 15\%$, and after a curing time of 2 or 3 days it was statically compacted into a small rigid cylindrical mould (inner diameter of 9 mm and height of 9.3 mm).

Samples B, subjected to wetting and/or loading-unloading paths by means of two oedometers were prepared by statically compacting ($\sigma_{vmax} \cong 1$ MPa) material passing through a No. 4 ASTM sieve (mesh aperture of 4.75 mm) after moistening to $w = 15\%$ (Airò Farulla et al., 2010). At the end of compaction values of void ratio, saturation degree and total suction, ψ, were: $e = 0.556 \div 0.577$, $S_r = 0.70 \div 0.75$, $\psi \cong 2$ MPa. Specimens for MIP tests and SEM observations were recovered from B samples at the end of the oedometer tests by means of a small cylindrical sampler (inner diameter of 10 mm and height of 10 mm).

3 Testing Equipment

MIP tests were performed using a porosimeter (Pascal 140-240 series, Thermo Scientific Corp.) attaining a maximum intrusion pressure of 200 MPa, which corresponds to an entrance pore diameter of 7.5 nm. Macropores were detected at the beginning of the tests in the low pressure unit operating between 0 and 400 kPa. The advancing non-wetting contact angle between mercury and the clay minerals was assumed to be 140° (Romero & Simms, 2008). SEM observations were performed on FEI Quanta 200f (maximum magnification 1000000X). MIP tests and

SEM observations were carried out on samples dehydrated by means of a freeze-drying technique consisting in quick freezing the samples by dipping them in liquid nitrogen (boiling temperature -198°C) and sublimation with vacuum pump at -60°C for 24 hours.

4 Experimental Programme

The MIP tests referred to in the paper were carried out on an intact stiff clay fragment (scale), on a group of three as-compacted scaly clay samples prepared with different initial unit dry weight (AC), and on three compacted samples subjected to different stress paths by means of two oedometers (B).

The scale (SC), drawn from an air dried clay sample, was moistened to a water content of about 14% by exposing it for a few days to a confined vapour saturated atmosphere at constant temperature ($T = 20° \pm 1°C$).

In order to evaluate microstructure evolution of the as-compacted material at increasing density, samples AC1, AC2, and AC3 were statically compressed at increasing stresses to achieve initial dry unit weight, γ_d, equal to 14, 16 and 18 kN/m^3, respectively.

Effects of applied stress paths on microstructure were investigated by tests carried out on the specimens B1, B2, B3 all prepared with initial $\gamma_d = 18$ kN/m^3 (like sample AC3). Sample B1 was subjected to a loading-unloading cycle in a suction controlled oedometer to maximum vertical net stress $\sigma_{vnet} = 1.6$ MPa at constant matric suction $s = 0.6$ MPa. Sample B2, was let swell in a conventional oedometer under applied vertical stress $\sigma_v = 10$ kPa (free or unconfined swelling). Specimen B3, after the initial saturation phase likewise sample B2, was subjected to a loading-unloading cycle to maximum applied vertical stress $\sigma_v = 6$ MPa.

5 Results Analysis

Results of MIP tests carried out on SC and AC samples are represented in the diagrams of Fig. 1 as cumulative intrusion pore volume of mercury normalized by solid volume ("intruded void ratio" e_i) (Fig. 1a) and pore size density ($PSD = -\delta e_i/\delta(\log D)$) (Fig. 1b) against pore entrance diameter D. With reference to the initial physical properties of the samples it is important to report that moistened scale presented void ratio $e_0 = 0.386$ and saturation degree $S_r = 0.97$. At the end of compaction values of void ratio and saturation degree of AC samples were: AC1: $e_0 = 0.959$, $S_r = 0.43$; AC2: $e_0 = 0.691$, $S_r = 0.60$; AC3: $e_0 = 0.533$, $S_r = 0.78$; measured total suction values were in the range $\psi = 2 \div 2.5$ MPa. Values of intruded e_i and measured void ratio e_0 of SC and AC samples are collected in Table 1.

Intact stiff clay (SC) begins to intrude at mercury pressure in the order of 1.5 MPa corresponding to a pore entrance diameter of about 1 μm. The PSD function shows a single porosity mode at $D = 0.09$ μm. The overall intruded void ratio is 0.241 lower than the initially measured void ratio $e_0 = 0.386$ (Table 1), in

consequence of the limited capacity of the porosimeter to enter the smallest pores and the entrapped pores.

Overall intruded void ratio, e_i, of the as-compacted clay samples AC decreases significantly as material density increases (Fig. 1a and Table 1). However, assuming a pore entrance diameter D =1 μm to separate micropore from macropore domains, micropore intruded void ratios (e_{micro}) fall in the narrow range 0.226 ÷ 0.247, while macropore intruded void ratios (e_{macro}) sharply decrease (from 0.319 to 0.153) as material dry density increases (Table 1). It can be argued that intruded void ratio decrements are mainly due to macropore volume reduction. The difference ($e_0 - e_i$) between measured and overall intruded void ratio increases as sample dry unit weight decreases, mainly because the non-detected largest pores are filled by mercury in the low pressure unit before test starting (Koliji et al., 2010).

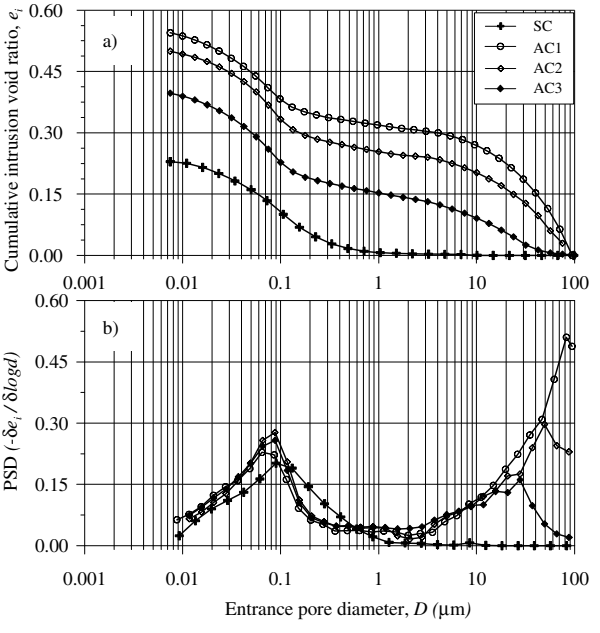

Fig. 1. Results of MIP tests on intact clay (SC) and as-compacted scaly clay (AC1-AC3, γ_d = 14 ÷ 18 kN/m^3).

The PSD functions (Fig. 1b) of the as-compacted scaly clay samples show a clear bimodal pore size distribution. The prevalent macropore entrance diameters decrease from 80 to 30 μm as γ_d increases from 14 to 18 kN/m^3, while the prevalent micropore diameters coincide with the prevalent diameter (0.09 μm) of the intact scale SC. It is evident from the diagrams in Fig.1 and the data collected in Table 1 that the scale and the as-compacted clay samples present only small differences as regarding to pore volume and PSD distributions for D < 1 μm.

It can be concluded that the fabric of aggregates is determined mainly by intact stiff clay (scale) microstructure.

The SEM photomicrograph of Fig. 3a highlights the structure of the as-compacted clay (sample AC3), characterised by large aggregates of particles and macrovoids between them. Micropores inside aggregates are not easily discernible at photomicrograph magnification.

Loading-unloading effects on microstructure characteristics of unsaturated compacted clay can be inferred by comparing results of MIP tests carried out on B1 and AC3 samples. Sample B1 was let equalize in a suction controlled oedometer to a net vertical stress σ_{vnet} = 50 kPa and matric suction s = 600 kPa, measuring a volumetric expansion strain ε_v = - 0.25%, and then subjected to a loading–unloading cycle (σ_{vnet} = 1.6 MPa). At the end of loading cycle a volumetric compression strain ε_v = 3.41% was measured and a final void ratio of 0.520 was calculated. Before freeze drying, void ratios, e_0, of AC3 and B1 samples are not very dissimilar: 0.533 and 0.520, respectively (Table 1). Compaction at constant matric suction induces only a small difference in the overall intruded void ratio, as e_i is 0.372 for B1 and 0.397 for AC3. However, macropore volume decreases significantly and e_{macro} reduces from 0.153 for AC3 to 0.090 for B1. Conversely, micropore volume for sample B1 increases as e_{micro} rises from 0.244 (AC3) to 0.283 (B1). Sample B1 retains a double porosity network, however its prevalent micropore diameter (D = 0.07 μm) is lower than the prevalent micropore diameter of sample AC3. Yet, in interpreting collected results it has to be considered that the stress path applied to sample B1 included a moderate matric suction reduction step before the loading cycle. In this respect, suction effects on pore size distribution may be considered as negligible because of the low intensity of applied suction reduction and induced material volumetric deformation (Monroy et al., 2007).

Table 1. Intruded (overall, e_i; macropore domain, e_{macro}; micropore domain, e_{micro}) and measured (e_0) void ratios.

Specimen	e_i	e_{macro}	e_{micro}	e_0	e_0 - e_i
SC	0.241	0.007	0.234	0.386	0.145
AC1	0.545	0.319	0.226	0.959	0.414
AC2	0.500	0.253	0.247	0.691	0.191
AC3	0.397	0.153	0.244	0.533	0.136
B1	0.372	0.090	0.283	0.520	0.148
B2	0.508	0.135	0.373	0.642	0.134
B3	0.357	0.027	0.330	0.520	0.163

On the contrary, saturation deeply modifies the microstructure of as-compacted scaly clay as shown by MIP test results relative to sample B2 (Fig. 2). Starting from the clear bimodal pore size distribution of the as-compacted clay samples (Fig.1), saturation leads to a prevalent monomodal pore size distribution with a sharp peak at D = 0.91 μm, even if a much more attenuate peak could be individuated at about D = 0.07 μm. Volume of macropores reduces significantly (e_{macro} = 0.135) and macropores with D > 10 μm almost disappear (Table 1; Fig. 2a).

On the contrary, micropore volume and PSD peak value of the prevalent diameter sharply increase (Table 1; Fig. 2b). The relevant increment of the overall intruded porosity in sample B2 is due to the micropore volume increment (Table 1).

Effects of saturation are well evident in the SEM photomicrograph of Fig. 3b: scale fragments and particle aggregations formed during compaction strongly expand invading macropores. Expanded aggregates are arranged in a very uniform pattern with very few macrovoids ($D = 5 \div 10$ μm) between them. Aggregates are still discernible as distinct units.

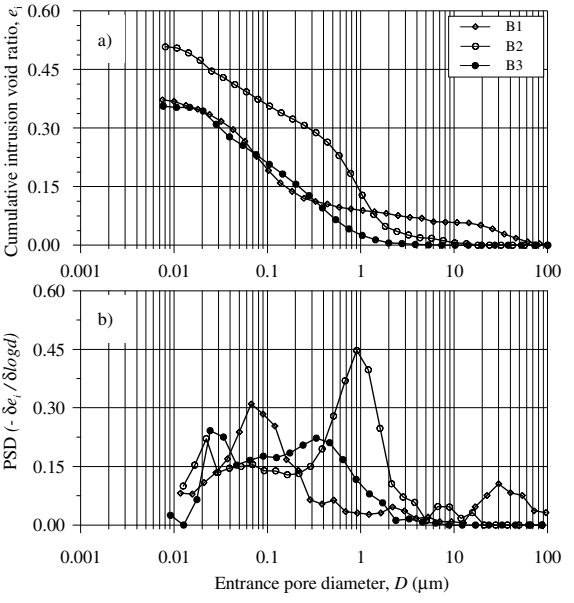

Fig. 2. Results of MIP tests on B1, B2 and B3 samples.

During saturation sample B2 swelled accumulating an overall volumetric expansion strain ε_v = - 4.1 % and increasing void ratio from 0.577 (as-compacted condition) to 0.642 (referred as e_0 in Table 1). Volumetric expansion induced by suction reduction is due to the high density of the as-compacted material (γ_d = 18 kN/m^3) and the low total vertical stress applied. At a microscopic level, material swelling is the consequence of the expansion of scales and clay particle aggregation. Indeed, MIP test results (Fig. 2a,b) and photomicrograph in Fig. 3b indicate that both volume and size of inter-aggregate macropores reduce significantly in consequence of saturation. It is also of interest to underline that at saturation the prevalent pore diameter D = 0.91 μm is very near to the diameter assumed to separate micro and macro pore domains (Della Vecchia, 2009; Cardoso & Alonso, 2010).

The effects of compaction on the microstructrure of saturated compacted scaly clay can be detected by comparing results of tests on B2 and B3 samples. During

unconfined saturation B3 experienced a volumetric swelling strain ε_v = - 6.0 %, achieving at equilibrium a void ratio of 0.669. The loading-unloading cycle (σ_{vmax} = 6 MPa) induced a total volumetric compression strain ε_v = 2.4% , with a corresponding void ratio e_0 = 0.520 (Table 1). The results of B3 test show that the loading-unloading cycle reduces intruded void ratio of the saturated material from 0.508 to 0.357 essentially as consequence of the reduction of macropore volume which almost disappears (e_{macro} = 0.027) (Table 1). The PSD function of sample B3 retains a monomodal distribution, but in comparison with PSD of B2 it is shifted to the left (micropore dominium) and both values of prevalent pore diameter and peak PSD reduce greatly (Fig. 2b). However, for D < 0.05 μm intruded void ratio and PSD function of saturated compacted clay before (B2) and after loading-unloading cycle (B3) are very similar.

The dependence of aggregated soil structure on stress paths applied can be illustrated by considering results of tests carried out on B1 and B3 samples. As evident from the data collected in Table 1, the samples have the same measured void ratio (e_0 = 0.520) and their overall intruded void ratios are not very different: 0.372 for B1 and 0.357 for B3 (Fig. 2a). However their PSD functions are characterised by some significant differences. Sample B1 retains some macropore volume (e_{macro} = 0.090) and presents a sharp PSD peak (0.30) for D = 0.07 μm. Sample B3 presents a greater intrude volume in the micropore domain and a more uniform micropore diameter distribution. As a matter of fact densities of pore entrance diameter in the range 0.03 ÷03 μm share very similar values (0.18÷0.21).

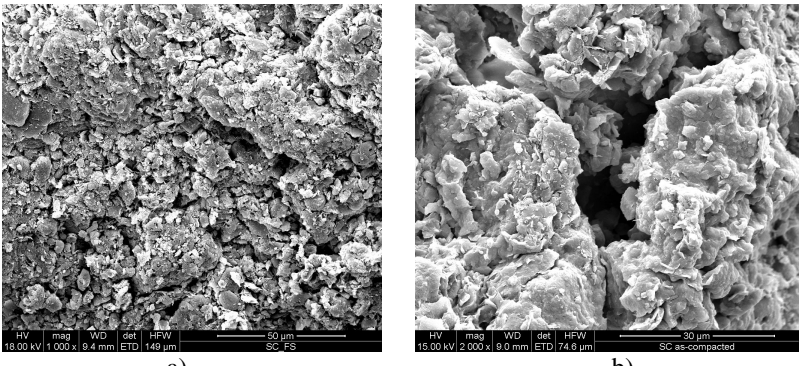

a) b)

Fig. 3. SEM photomicrographs on freeze-dried samples: a) as-compacted scaly clay (γ_d = 18.0 kN/m^3); b) compacted scaly clay saturated under free swelling conditions.

6 Conclusions

Analysis of the data presented in the paper enables to state that the microstructure of as-compacted scaly clay depends mainly on the microstructure of intact stiff clay fragments (scales) which survive compaction irrespective of the intensity of

compaction stress. Pore volume reduction induced by increasing material dry density derives from the inter-aggregate pore volume reduction, while intruded volume and PSD function of intra-aggregate pores remain constant even if compaction stress is strongly increased. Besides, they present only minor differences respect to intruded volume and PSD distribution in the micropore domain of intact stiff clay.

A loading and unloading cycle at constant suction of unsaturated as-compacted scaly clay reduces overall intruded void ratio mainly by a corresponding reduction of macropore volume.

Saturation is able to deeply change the microstructure of the compacted scaly clay modifying the double porosity network of the as-compacted material in a prevalent mono-modal pore diameter distribution. Suction reduction in oedometer under a low confinement stress induces a very high expansive volumetric strain as consequence of expansion of scale fragments and particle aggregations formed during compression. Aggregates expand invading macropore volume which strongly reduces. As a consequence, volume of micropores and their prevalent diameter density sharply increase.

The data presented in the paper contribute to give further evidence of some characteristic effects of stress paths applied, and suction reduction in particular, on the microstructure of clayey soils with an aggregated structure as well documented in previous research works. They also evidence the peculiar influence that the presence of stiff clay fragments exercises upon the behaviour of compacted scaly clays.

References

Airò Farulla, C., Ferrari, A., Romero, E.: Volume change behaviour of a compacted scaly clay during cyclic suction changes. Can. Geotech. J. 47, 688–703 (2010), doi:10.1139/T09-138

Airò Farulla, C., Jommi, C.: Suction controlled wetting drying cycles on a compacted scaly clay. In: Proc. of Int. Conf. on Problematic Soils, vol. 1, pp. 229–238 (2005)

Cardoso, R., Alonso, E.: Structural changes of compacted marls subjected to suction cycles. In: Buzzi, F., Sheng (eds.) Proc. South East Asiatic Conference on Unsaturated Soils, pp. 83–88 (2010)

Della Vecchia, G.: Hydro-mechanical coupled behaviour of compacted clayey soil. PhD thesis, Politecnico di Milano (2009)

Koliji, A., Vulliet, L., Laloui, L.: Structural characterization of unsaturated aggregated soil. Can. Geotech. J. 47, 297–311 (2010), doi:10.1139/T09-089

Monroy, R., Zdravkovic, L., Ridley, A.: Fabric changes in compacted London Clay due to variations in applied stress and suction. In: Schanz, T. (ed.) Experimental Unsaturated Soil Mechanics, pp. 41–47. Springer, Heildelberg (2007)

Romero, E., Simms, P.H.: Microstructure investigation in unsaturated soils: a review with special attention to contribution of mercury intrusion porosimetry and environmental scanning electron microscopy. Geotechnical and Geological Engineering 26, 705–727 (2008), doi:10.1007/s10706-008-9204-5

Soil Fabric of Compacted and Natural Swelling Soils Studied by Mercury Intrusion Porosimetry

Hossein Nowamooz and Farimah Masrouri

Abstract. This article compares the Pore Size Distribution (PSD) study of two different fine graded swelling soils, in natural state, and remoulded at the same initial state. The soil fabric of these clayey soils including the macropores, mesopores, and micropores was mainly studied by the mercury intrusion porosimetry (MIP) technique. For both soils, the results showed clearly that the soil fabric of the remoulded samples compacted in the laboratory are significantly different from the natural ones. Therefore, as the artificial compacted samples do not correctly represent the natural soil fabric, hydro-mechanical parameters measured on them would be different from those obtained on the intact natural samples.

Keywords: soil fabric, mercury intrusion porosimetry, clayey soils.

1 Introduction

Clay soils subjected to hydraulic solicitations can induce relative settlements that can affect the structures, including shallow foundations and drainage channels, as well as buffers in radioactive waste disposal sites. The complex hydromechanical behaviour of these expansive materials is connected to their fabric (Pusch, 1982; Gens & Alonso; 1992; Alonso et al., 1999), which have become the main subject of additional studies on their micro- and macrostructure (Delage & Lefevre 1984, Romero et al. 1999, Pusch & Yong, 2003; Lloret et al., 2003; Nowamooz 2007, Nowamooz & Masrouri 2008, 2009).

Hossein Nowamooz
INSA de Strasbourg
e-mail: Hossein.Nowamooz@insa-strasbourg.fr

Fariamh Masrouri
Nancy Université
e-mail: Farimah.Masrouri@ensg.inpl-nancy.fr

Based on the classification of IUPAC (1997), the pores with widths exceeding about 0.05 µm or 50 nm are called macropores; those with widths not exceeding about 0.002 µm or 2 nm are called micropores and the pores of intermediate size are called mesopores. We consider in this article that the macrostructure is equivalent to macropores, the mesostructure to the mesopores and the microstructure to the micropores. A pore diameter of 0.150 µm was also proposed as the pore boundary between the inter- and intra-aggregate of the compacted swelling soils (Lloret *et al.,* 2003; Delage *et al.,* 2006). We take this value as a diameter size limit between macro- and mesopore as a simplifying hypothesis however we believe that this diameter size limit which is not constant depends highly to the soil initial state (Nowamooz & Masrouri, 2009).

The pore size distribution (PSD) obtained by the mercury intrusion porosimetry (MIP) test has been used as an essential method in soil fabric studies. It has been observed that the double structural level is much more evident on the dry side of the optimum point of the compaction curve than on the wet side which shows a homogeneous structure (Barden & Sides, 1970; Sridrahan *et al.,* 1971; Collins & McGown, 1974). It has been observed that mechanical loading significantly influences the macropores without producing important modifications in the meso- and micropores for compacted tills (Simms & Yanful, 2004) and for compacted bentonite (Hoffman *et al.,* 2007).

Most investigations on the swelling soils were done on the compacted samples artificially prepared in the laboratory. The important question is whether the soil fabric of these artificial swelling soils represents correctly the fabric of the natural swelling soils or not. To address this question, this article compares the Pore Size Distribution (PSD) of the natural samples with the remoulded samples (prepared exactly at the same initial states of the natural ones).

2 Soil Fabric Tests

MIP tests were performed to evaluate the pore size distribution of the studied materials. MIP tests were conducted using a porosimeter, where the mercury pressure was continuously raised from 0.007 to 450 MPa and the device was able to detect pore diameters ranging from 3 nm to 300 µm. The MIP tests required dehydrated samples with volumes less than 3000 mm^3 (limited by the sample holder and the cell stem volume). Starting with a prepared and compacted sample, the MIP specimens were carefully trimmed into cubes and subsequently freeze-dried to remove the pore water, and then placed in a desiccator until testing. One assumption is that the larger pores can be intruded from the outside without the mercury having to penetrate through smaller pores. However, it is possible that large pores with a small access diameter are not intruded until high pressures are reached; as a result, their volume appears to be associated with much finer pores. Therefore, in this article we prefer to use the term “pore access diameter” rather than “pore diameter.”

3 Soil Fabric of Natural Swelling Soils

The experimental results in literature were more frequently reported on the compacted samples in the laboratories rather than the natural samples.

In this section, we studied natural swelling soils taken from an experimental site in the Mignaloux-Beauvoir region, near Le Deffend, about 4 km south-east of Poitiers (France). Two in-situ boreholes were performed in the same season to a depth of 7 meters for geological and geotechnical investigations within the framework of the ANR ARGIC project (Vincent et al., 2006), including one in the pasture (site E1) and the second in the forest (site E2). The studied clayey layer is located between 6.20 and 6.80 m depth in the E1 core. The second soil comes from between 5.20 and 5.70 m in the E2 core. We call the first soil E1 and the second one E2. The physical and geotechnical properties respectively for soils E1 and E2 are the liquid limit of 86% and 65%, the plasticity index of 32 and 25%, the specific gravity (Gs) of 2.60 and 2.62 and the clay size content of 72% and 52%. The mineralogical composition of both natural soils, as determined by X-ray diffraction, shows that smectite minerals are dominant.

In parallel, the samples were remoulded by static compaction to the initial states very close to natural states in the laboratory: a water content of 43% and 14%, an initial dry density of 1.21 and 1.84 Mg/m^3 corresponding to a void ratio of 1.15 and 0.42 respectively for soils E1 and E2. In other words, the soils were initially prepared at the indicated initial water contents and then compacted at the initial dry densities very close to their initial in-situ states.

To analyse the influence of the compaction process on the soil fabric of the studied samples, two series of MIP tests were performed on the natural soil and on the remoulded samples (compacted to their initial natural state) for both soils E1 and E2. Fig. 1 and 2 present the variation of Pore Size Distribution (PSD) function (= Δ void ratio / Δlog pore diameter) as well as the cumulative void ratio versus the pore access diameter.

The distributions showed two distinct structural levels for soil E1: meso- and macropore (Fig. 1-a). The dominant diameter of about 50 µm, corresponding to the macropores of this natural soil, decreased to 10 µm after compaction. However, the macropores were absent for soil E2 (Fig. 2-a). The compaction decreased the mesopores significantly without modifying their peak at 0.011 µm for soil E1 and 0.02 µm for soil E2.

A same boundary limit value of 0.150 µm was taken between the meso- and macropore for both soils E1 and E2. The void ratios corresponding to an average pore size of to 0.150 µm (Fig. 1-b) allowed the estimation of the macrostructural void ratio (e_M). The residual space starting from the e_M and ending at the final intruded void ratio (maximum void ratio obtained by the MIP test) can be considered as the meso-structural void ratio (e_m). This residual space corresponds also to the micropores not intruded by porosimeter. Tables 1 and 2 summarize these values for both samples compacted at the same initial total void ratio (e_T) for both soils E1 and E2.

Table 1. Soil fabric variation for the natural and compacted soil E1.

Soil E1	Natural	Compacted
Total void ratio (e_T)	1.15	1.15
Void ratio of macropore (e_M)	0.59	0.54
Void ratio of mesopore (e_m)	0.56	0.42
Void ratio of micropore (e_n)	---	0.19

Table 2. Soil fabric variation for the natural and compacted soil E2.

Soil E2	Natural	Compacted
Total void ratio (e_T)	0.42	0.42
Void ratio of macropore (e_M)	0.10	0.06
Void ratio of mesopore (e_m)	0.32	0.18
Void ratio of micropore (e_n)	---	0.18

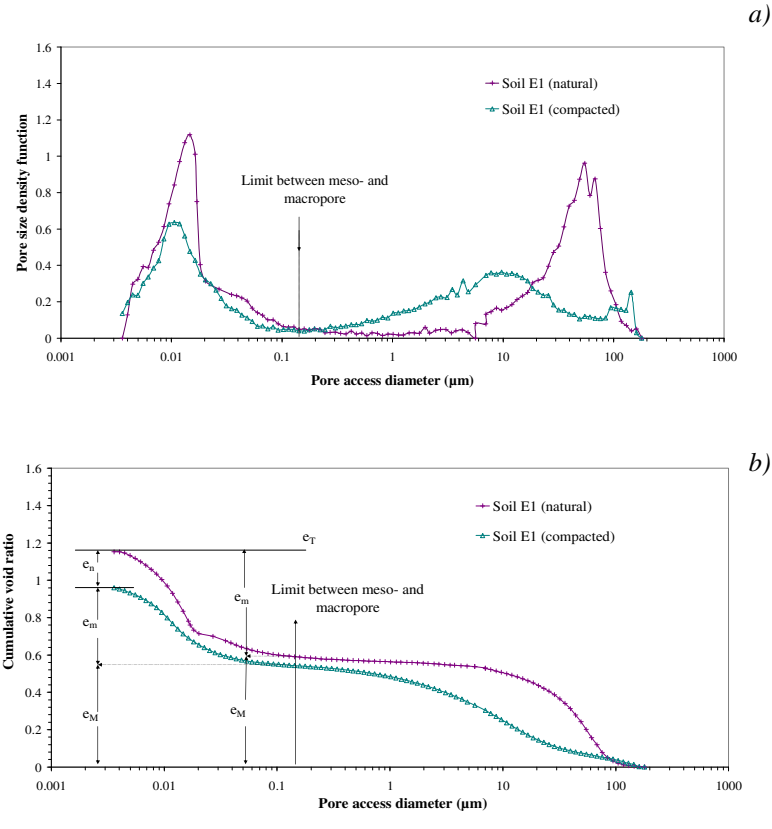

Fig. 1. Results of MIP tests on the natural and compacted soil E1, a) Pore size distribution function, b) Cumulative void ratio versus pore size.

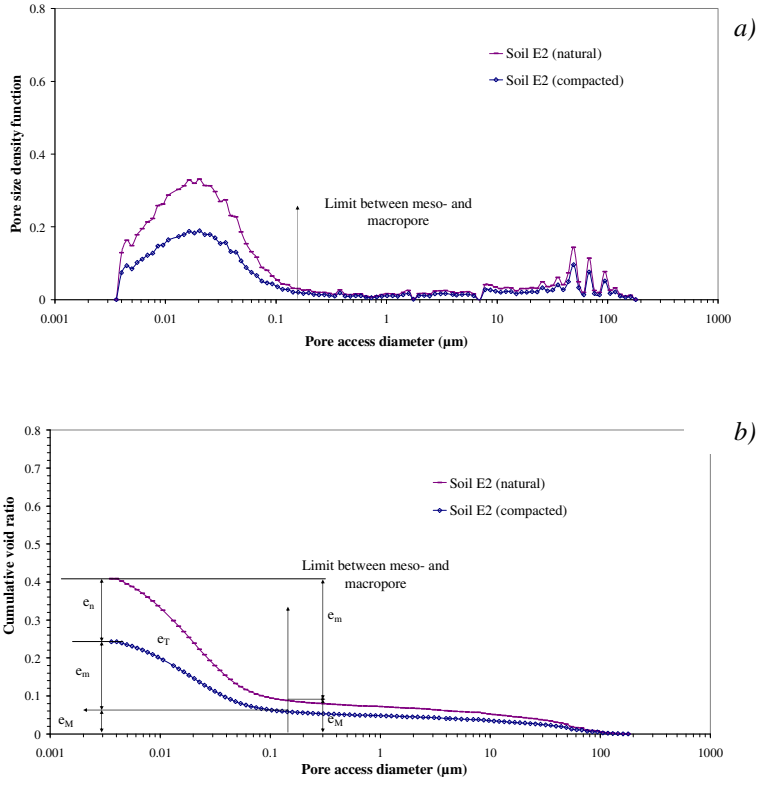

Fig. 2. Results of MIP tests on the natural and compacted soil E2, a) Pore size distribution function, b) Cumulative void ratio versus pore size.

The same boundary limit value of 0.150 µm was taken between the meso- and macropore for both soils E1 and E2. This diameter size limit which is not constant depends extremely to the soil initial state. For example, when the macropores are absent in the dense soil structure, a higher discriminating diameter can be taken between macro- and mesopores. The different limits modify the estimated void ratio of macro-, meso- and micropore.

4 Conclusion

The experimental study focused on the evolution of the soil fabric of the clayey soils including the macropore, mesopore, and micropore mainly studied by the mercury intrusion porosimetry (MIP) technique. We compared the Pore Size Distribution (PSD) of the natural samples with the remoulded samples (prepared exactly at the same initial states of the natural ones). The results showed that the soil fabric of the remoulded samples compacted in the laboratory can be significantly

different from the natural ones. This point would directly impact the hydro-mechanical parameters obtained in laboratory conditions on remoulded samples such as the Soil Water Retention Curve (SWRC), the compression curves at the constant imposed suctions and the swelling/shrinkage strain accumulation during the wetting and drying cycles.

References

Alonso, E.E., Vaunat, J., Gens, A.: Modelling the mechanical behaviour of expansive clays. Engineering Geology 54, 173–183 (1999)

Barden, L., Sides, G.R.: Engineering behavior and structure of compacted clays. Journal of Soil Mechanics and Foundation Analysis 96, 1171–1200 (1970)

Delage, P., Lefebvre, G.: Study of the structure of a sensitive Champlain clay and of its evolution during consolidation. Revue Canadienne de Géotechnique 21, 21–35 (1984)

Delage, P., Marcial, D., Cui, Y.J., Ruiz, X.: Ageing effects in a compacted bentonite: a microstructure approach. Géotechnique 56, 291–304 (2006)

Gens, A., Alonso, E.E.: A framework for the behaviour of unsaturated expansive clays. Revue Canadienne de Géotechnique 29, 1013–1032 (1992)

Hoffemann, C., Alonso, E.E., Romero, E.: Hydromechanical behavoiur of bentonite pellet mixtures. Physics and Chemistry of the Earth 32, 832–849 (2007)

IUPAC: IUPAC Compendium of Chemical Terminology (Gold Book) by A. D. McNaught and A. Wilkinson. Blackwell Science (1997) (1997)

Lloret, M., Villar, M., Sanchez, A., Gens, X., Pintado, E., Alonso, E.E.: Mechanical behaviour of heavily compacted bentonite under high suction changes. Géotechnique 53(1), 27–40 (2003)

Nowamooz, H., Masrouri, F.: Hydromechanical behaviour of an expansive bentonite/silt mixture in cyclic suction-controlled drying and wetting tests. Engineering Geology 101(3-4), 154–164 (2008)

Nowamooz, H., Masrouri, F.: Density-dependent hydromechanical behaviour of a compacted expansive soil: experimental and analytical aspects. Engineering Geology 106(3-4), 105–115 (2009)

Push, R.: Mineral-water interactions and their influence on the physical behaviour of highly compacted Na-bentonite. Revue Canadienne de Géotechnique 19, 381–387 (1982)

Pusch, R., Yong, R.N.(eds.): Special Issue, Clay microstructure. In: Proc. Workshop Lund, Sweden, October 15-17 (2002); Applied clay science, 23(1-4) (2003)

Romero, E., Lloret, A., Gens, A.: Water permeability, water retention and microstructure of unsaturated Boom clay. Engineering Geology 54, 117–127 (1999)

Simms, P.H., Yanful, E.K.: A discussion of the application of mercury intrusion porosimetry for the investigation of soils, including an evaluation of its use to estimate volume change in compacted clayey soils. Geotechnique 54(6), 421–426 (2004)

Sridharan, A., Altaschaeffl, A.G., Diamon, S.: Pore-size distribution studies. Journal of the Soil Mechanics and Foundation Division, ASCE 97, 771–787 (1971)

Vincent, M., Bouchut, J., Fleureau, J.M., Masrouri, F., Oppenheim, E., Heck, J.V., Ruaux, N., Le Roy, S., Dubus, I., Surdyk, N.: Étude des mécanismes de déclenchement du phénomène de retrait-gonflement des sols argileux et de ses interactions avec le bâti. BRGM/RP-54862-FR (Octobre 2006)

Porosity Changes due to Hydration of Compacted Bentonite

María Victoria Villar, Roberto Gómez-Espina, Rocío Campos, Icíar Barrios, and Luis Gutiérrez

Abstract. As a contribution to the understanding of bentonite hydration, the porosity of two different compacted bentonites with different degrees of saturation was analysed by mercury intrusion porosimetry and X-ray diffraction. The percentage of macropores, as well as the macropore mode, decreased with dry density both in wet and dry samples. Wet samples showed a predominance of microporosity. The basal spacing increased with water content. The porosity distribution for a given water content was not the same for samples hydrated before compaction than for samples saturated under constant volume. In the latter case it clearly evolved over time, the interlayer distance becoming higher.

Keywords: bentonite, hydration, porosity, interlayer, MIP.

1 Introduction

Deep geological repository concepts for high-level nuclear waste disposal often include a bentonite barrier around the waste containers. The bentonite is used with its hygroscopic water content, what means that initially the barrier is unsaturated. It will interact with the groundwater and eventually become saturated. The understanding of the hydration mechanism of compacted bentonite is key to assess the performance of engineered barriers, the time needed for their full saturation, their

María Victoria Villar
CIEMAT, Madrid, Spain
e-mail: mv.villar@ciemat.es

Roberto Gómez-Espina · Rocío Campos · Icíar Barrios · Luis Gutiérrez
CIEMAT, Madrid, Spain
e-mail: roberto.gomez@ciemat.es, rocio.campos@ciemat.es,
iciar.barrios@ciemat.es, l.gutierrez@ciemat.es

mechanical behaviour and their geochemical response. This work is a contribution to this understanding from a microstructural point of view.

Bentonites are mainly composed of clay minerals of the smectite type, which are made up of structural units known as laminae or layers that are piled one on top of the other, forming primary particles. The positions between these units are usually occupied by exchange cations and water may enter between them, causing the crystalline network to expand in the direction of *c*-axis. For this reason, this dimension of smectite –the basal spacing– is not fixed, but varies depending on the size of the molecule located between the units and on its hydration state.

The organisation of the laminae, particles and aggregates in any clay material gives rise to different types of porosity (Stepkowska 1990), as shown schematically in fig. 1:

- Interlaminar or interfoliar porosity, to which only polar molecules have access and whose spacing is usually up to 2 nm.
- Intra-aggregate porosity, inside the primary particles and between adjacent laminae piles. This is also known as microporosity, and includes pores having diameters of less than 0.002 μm.
- Inter-aggregate porosity (greater than 0.002 μm), which in turn may be classified as macroporosity or mesoporosity, depending on whether the diameter is above or below 0.05 μm.

There is experimental evidence that the microstructure of bentonite evolves during hydration (Villar & Lloret 2001). Thus, the proportion of external water (contained in macro and mesopores) in smectites decreases with increasing material density and decreasing water content (Pusch et al. 1990). Consequently, in highly compacted bentonite there is a predominance of interlayer water. Smectites typically show a stepwise hydration behaviour of the interlayer corresponding to the intercalation of discrete sheets of water molecules which are responsible for the crystalline swelling. It is considered that smectites display basal spacings of about 1.0, 1.25, 1.55 and 1.85 nm for the homogeneous 0, 1, 2 and 3 water layers hydration states, respectively (Cases et al., 1992; 1997).

Mercury intrusion porosimetry (MIP) has been used for long to study the microstructure of clays and its changes along mechanical and hydraulic paths (see Romero & Simms 2008 for a review). However, the adequacy of the PSD as measured by MIP is often questioned (Simms & Yanful 2004), in particular with respect to the representativity of the samples used (due to their size and way of preparation), the possible disruption of microstructure caused by the injection pressure, and the accessibility issues. The latter include the upper and lower pore entrance limits associated to the technique, and the bottle neck effect, which implies a difference between the pore entrance diameter and the actual diameter. In clay materials, and particularly compacted smectites in which the microporosity (pores of diameter smaller than 2 nm) may constitute most of the total porosity, the percentage of pores not intruded by mercury due to their small size can become predominant. Other techniques should then be applied to explore this range

of porosity, such as the adsorption of gases. Additionally, X-ray and neutron diffraction can be used to measure the interlayer spacings (through the *d*(001) reflection), what also helps describing the microporosity.

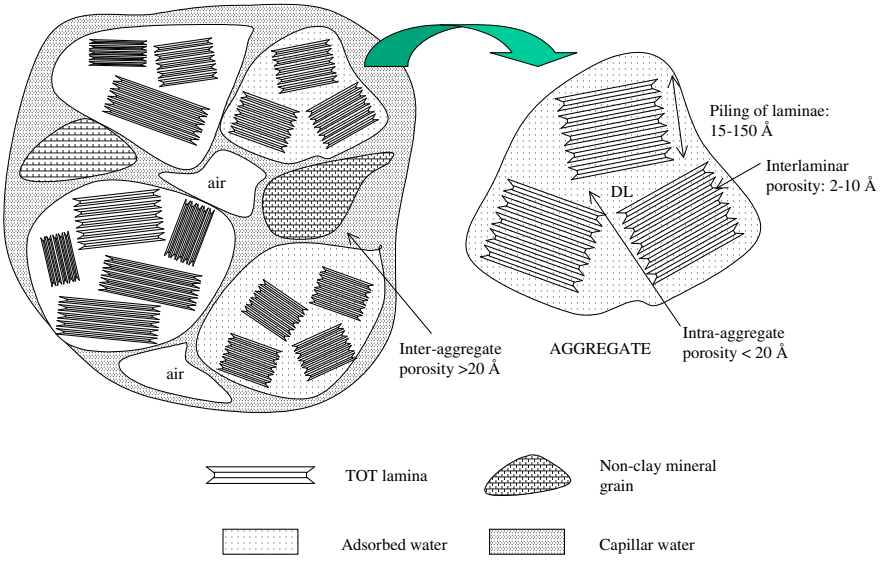

Fig. 1. Schematic diagram of the organisation of a clay material: types of porosity and water (Villar 2002).

2 Materials and Methods

The tests were performed with two untreated bentonites, the FEBEX and the MX-80.

The FEBEX bentonite was extracted from Almería (SE Spain). The montmorillonite content was above 90% (92±3 %) and it also contained variable quantities of quartz (2±1 %), plagioclase (2±1 %), K-felspar, calcite and opal-CT (cristobalite-trydimite, 2±1 %). The cation exchange capacity was 102±4 meq/100g, the main exchangeable cations being calcium, magnesium and sodium. The density of solid particles was 2.70 Mg/m^3 (ENRESA 2006).

The MX-80 bentonite was extracted from Wyoming (USA). The MX-80 batch used in this investigation was composed mainly of montmorillonite (83%) and it also contained quartz (4%), feldspars (7%), cristobalite (6%) and smaller quantities of calcite, gypsum, dolomite, halite and pyrite. The CEC was 65 meq/100g, and the major exchangeable cations were sodium, calcium and magnesium. The density of solid particles was 2.82 Mg/m^3.

All the results presented in this paper were obtained in compacted samples, although they were prepared in two different ways. In the first way the sample water content was fixed before compaction, whereas in the second one the sample water content changed after compaction, but in both cases under constant volume conditions:

- The bentonite was either mixed with deionised water to obtain a nominal water content of 30% (wet samples) or dried in a low relative humidity (4%) environment until reaching an equilibrium water content of 6% (FEBEX) and 2% (MX-80) (dry samples). Subsequently the bentonite, both wet and dry, was compacted to dry densities between 1.0 and 2.1 Mg/m^3 and the specimens were let stabilise for different periods of time wrapped in paraffined foil under no confinement at 20°C. At least two samples were compacted with the same dry density, water content and stabilisation time. The samples obtained through compaction of the bentonite with a water content of 30% are referred to in the rest of the paper as "wet samples", whereas those obtained through compaction of the desiccated bentonite are referred to as "dry samples".
- Other samples were manufactured by uniaxial compaction of the clay with its hygroscopic water content to dry densities between 1.1 and 1.8 Mg/m^3. They were flooded at room temperature with deionised water in oedometers, keeping their volume constant by adding the appropriate loads when tendency to swell was observed. Under a constant vertical load the vertical strain stabilised after about 4 days, but the tests were prolonged for much longer, up to durations of between 8 and 160 days. The samples reached full saturation at the end of the tests.

The pore size distribution of both kinds of samples was determined by mercury intrusion porosimetry (MIP). Samples smaller than 3 cm^3 were cut and lyophilised to eliminate the water in the pores. The porosimeter used was a Micromeritics AutoPore Series IV 9500, allowing the exploration of pore diameter sizes between 0.006 and 600 μm.

For the determination of the basal spacings of the smectite a sufficiently flat surface of the samples was X-rayed at room temperature without any previous treatment. An anticatode of Cu (CuK_α) radiation was used with a Philips model X'Pert-MPD diffractometer at 40 mA, 45 kV operating condition.

3 Results

The mercury intrusion method allows access only to the macroporosity (pores smaller than 600 μm) and to part of the mesopores (pores of diameter larger than 0.006 μm). An estimation of the percentage of pores actually intruded can be made by comparing the actual void ratio of the samples (computed from their dry density and density of solid particles) and the apparent void ratio calculated from mercury intrusion. Thus, the pore size distribution curves obtained by MIP were

corrected to take into account the percentage of pores not intruded (fig. 2). The percentage of pores intruded decreased with dry density and was higher for the dry samples than for the wet ones.

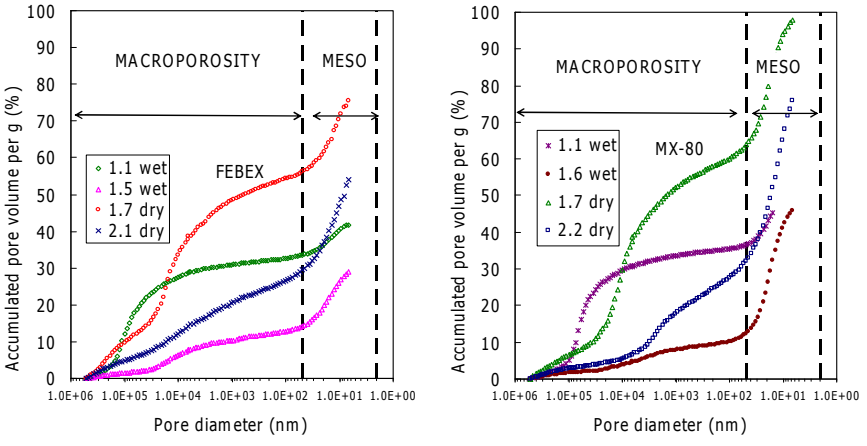

Fig. 2. Mercury intrusion curves of samples of FEBEX and MX-80 bentonites compacted at different dry densities (in Mg/m^3) and water contents and stabilised under no confinement for 150-230 days.

The percentage of pores not intruded by mercury included not only those whose sizes were below or above the technique limit, but also those whose entrance pore size was below the lower entrance limit of the equipment or those isolated, even if the pores themselves were larger. Nevertheless, assuming that the percentage of pores not intruded in a clay corresponds entirely to the micropore size, an estimation of the percentage of micropores can be inferred from the percentage of pores intruded. This was done for all the samples and the percentage of each pore size recalculated (fig. 3). The micropores were clearly predominant in the wet samples (30% water content). There was a clear trend both in the wet and the dry samples for the percentage of micropores and mesopores to increase as the dry density was higher, while the macropore percentage tended to decrease. Under no confinement, the maturation time did not seem to affect these pore size distributions. The comparison between both bentonites showed a higher percentage of micropores in the FEBEX than in the MX-80 bentonite.

Under no confinement, the macropore size mode of the two bentonites decreased as the dry density increased, both in the dry and the wet state (fig. 4). In fact, the macropore size was the less represented for the highest density (2.1 Mg/m^3). In the dry state the pore mode of the mesopores decreased also with dry density. The macropore size mode tended to be smaller for the MX-80 bentonite. However, in samples saturated under confinement (oedometer tests), the macro

and mesopore size mode was the same irrespective of the dry density and even of the bentonite, with average values of 25.9±9.2 μm and 16±3 nm, respectively (the effect of maturation time was not investigated).

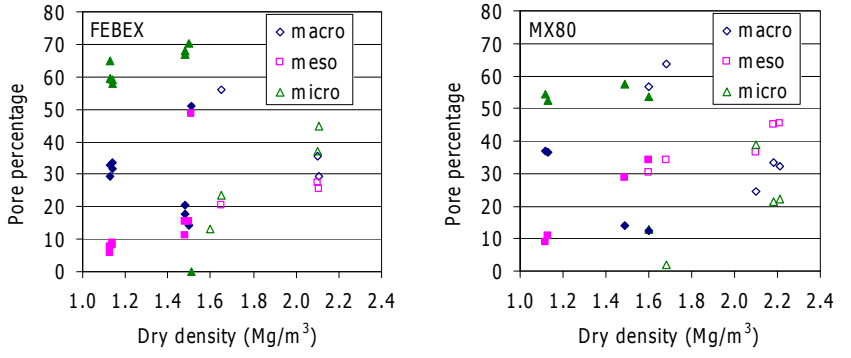

Fig. 3. Pore size distribution in bentonite samples compacted at different dry densities and stabilized for different periods of time under no confinement. Filled symbols: wet samples, open symbols: dry samples.

In each specimen stabilized under no confinement two X-ray measurements were performed on two perpendicular surfaces. Fig. 5 shows the average values for each pair of specimens (3 to 5 measurements). There was not a clear evolution of basal spacing over time either in the wet or in the dry samples, so in the figure the basal spacings shown correspond to different maturation times between 0 and 130 days. For all the densities and times of stabilisation, the average value of the *d*(001) reflection for the 30% water content samples indicated the predominance of the 2-layer hydrate state and the transition to the 3-layer hydrate state, with values slightly lower for the MX-80 bentonite. In the low water content samples the basal spacing corresponded to a 1-layer hydrate, although in the case of the FEBEX bentonite there must have been still a significant proportion of particles with a 2-layer hydrate. The effect of dry density on the basal spacing was not clear.

The basal spacings measured at the end of the oedometer tests are shown in fig. 6 as a function of the duration of the tests. For similar dry densities different basal spacings were measured at the end of the tests depending on their duration. Overall, longer tests gave place to higher final basal spacings, despite the fact that the final water content and swelling pressure values were quite independent on the duration of the tests. The dispersion of the results could be due to the slight differences in dry density, since the samples were grouped in dry density intervals of 0.1 Mg/m^3. Except for the shortest durations (especially if the density was high), the basal spacings corresponded to the 3-layer hydrate.

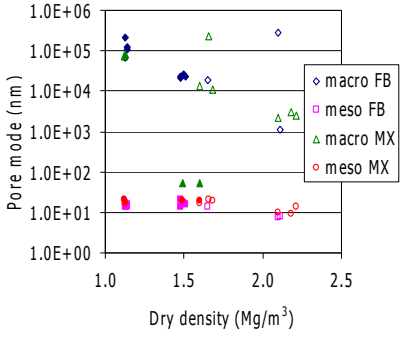

Fig. 4. Pore mode of macropores and mesopores of FEBEX (FB) and MX-80 (MX) compacted with different water contents and stabilised under no confinement (filled symbols: wet samples, open symbols: dry samples).

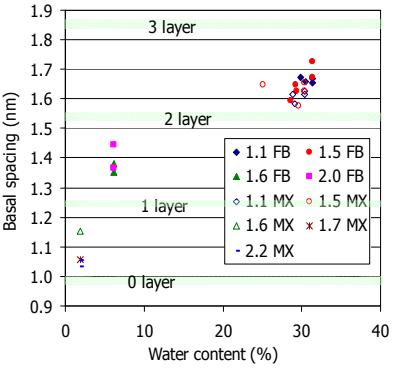

Fig. 5. Basal spacings of samples of FEBEX (FB) and MX-80 (MX) compacted at different dry densities (indicated in Mg/m^3) measured at different times after compaction.

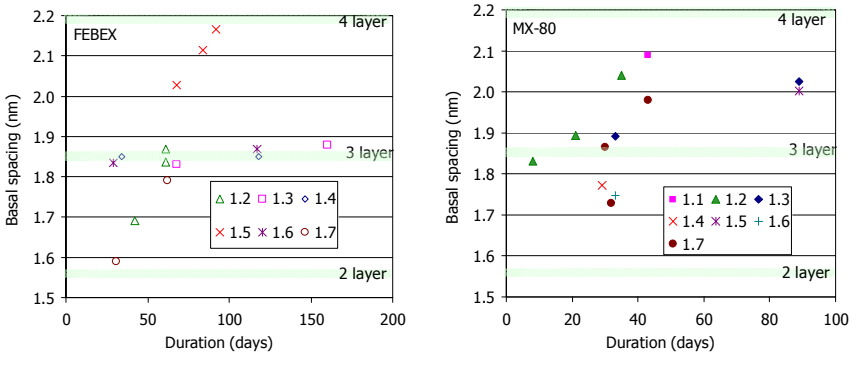

Fig. 6. Basal spacings measured at the end of the oedometer tests (dry densities in Mg/m^3).

4 Conclusions

Both the pore size distribution and the basal spacings of bentonite depended on the water content and the way of hydration. Samples hydrated prior to compaction showed a decrease of the percentage of macropores and their mode with dry density, while microporosity was higher in wet samples than in dry samples. The basal spacing increased with water content. The maturation time had no noticeable effect on the pore size distribution or basal spacing. However, in samples saturated at isochoric conditions, the interlayer distance increased with time, even for the

highest dry densities. This points to a redistribution of the water inside the clay microstructure over time with no impact on swelling pressure. In fact, samples with the same water content and dry density had higher basal spacings if they were saturated under constant volume than if they were hydrated before compaction.

Acknowledgements. The preparation and analyses of samples was carried out by Ramón Campos, Juan Aroz, Ana González and Francisco Javier Romero. Part of the research leading to these results has received funding from the European Atomic Energy Community's Seventh Framework Programme (FP7/2007-2011) under Grant Agreement no249681, the PEBS project.

References

Cases, J.M., Bérend, I., Besson, G., François, M., Uriot, J.P., Thomas, F., Poirier, J.E.: Mechanism of adsorption and desorption of water-vapor by homoionic montmorillonite. 1. The sodium-exchanged form. Langmuir 8(11), 2730–2739 (1992)

Cases, J.M., Bérend, I., François, M., Uriot, J.P., Michot, L.J., Thomas, F.: Mechanism of adsorption and desorption of water vapor by homoionic montmorillonite. 3. The Mg^{2+}, Ca^{2+}, Sr^{2+} and Ba^{2+} exchanged forms. Clays Clay Miner. 45(1), 8–22 (1997)

Enresa: FEBEX Full-scale Engineered Barriers Experiment. Updated Final Report 1994-2004. Publicación Técnica ENRESA 05-0/2006, Madrid, 590 p. (2006)

Pusch, R., Karnland, O., Hökmark, H.: GMM -A general microstructural model for qualitative and quantitative studies on smectite clays. SKB Technical Report TR 90-43. SKB, Stockholm (1990)

Romero, E., Simms, P.: Microstructure investigation in unsaturated soils: a review with special attention to contribution of mercury intrusion porosimetry and environmental scanning electron microscopy. Geotech. Geol. Eng. 26(6), 705–727 (2008)

Simms, P.H., Yanful, E.K.: A discussion on the application of mercury intrusion porosimetry for the investigation of soils, including an evaluation of its use to estimate volume change in compacted clay. Géotechnique 54(6), 421–426 (2004)

Stepkowska, E.T.: Aspects of the clay electrolyte water-system with special reference to the geotechnical properties of clays. Eng. Geol. 28(3-4), 249–267 (1990)

Villar, M.V.: Thermo-hydro-mechanical characterisation of a bentonite from Cabo de Gata. Publicación Técnica ENRESA 04/2002, 258 p. Enresa, Madrid (2002)

Villar, M.V., Lloret, A.: Variation of the intrinsic permeability of expansive clay upon saturation. In: Adachi, K., Fukue, M. (eds.) Clay Science for Engineering, pp. 259–266. Balkema, Rotterdam (2001)

Effect of Initial Water Content and Dry Density on the Pore Structure and the Soil-Water Retention Curve of Compacted Clay

Emanuel Birle

Abstract. An experimental study was carried out to investigate the influence of the initial water content and dry density on the structure and the SWRC of compacted clay. The soil structure was studied by MIP. For the determination of the soil-water retention curve suction-controlled oedometer cells and a chilled mirror dew-point hygrometer were used. The paper describes the changes of pore structure due to different initial water contents and dry densities and its influence on the soil-water retention curve.

Keywords: soil-water retention curve, compaction, suction, mercury intrusion porosimetry.

1 Introduction

Compacted clays are used for hydraulic barriers in many geotechnical structures, e.g. in surface sealing systems of landfills or embankments built of slightly contaminated soils. For the determination of the seepage flow through compacted clay the soil-water retention curve (SWRC) and the unsaturated hydraulic conductivity are of particular interest. Both depend on the soil structure, which in turn is strongly influenced by the initial water content and the dry density.

First investigations on the influence of the compaction conditions on the microstructure of compacted clays were carried out by Lambe (1954) and Seed & Chan (1959). They showed that the pore size distribution depends strongly on the initial water content. As later described by Delage et al. (1996), the pore size distribution (PSD) of clays compacted dry of Proctor optimum takes a bimodal

Emanuel Birle
Zentrum Geotechnik, Technische Universität München, Germany
e-mail: e.birle@bv.tum.de

shape consisting of pores within the aggregates (intra-aggregate pores) and larger pores between the aggregates (inter-aggregate pores). If the soil is compacted wet of Proctor optimum, the distinction between intra- and inter-aggregate pores usually is not possible. Besides, several investigations (Romero et al. 1999, Sivakumar et al. 2006, Thom et al. 2007, Li & Zhang 2008) show that samples compacted at the same water content but different dry densities differ only in the larger inter-aggregate pores. Investigations of Monroy et al. (2010) demonstrate that the originally aggregated fabric of compacted clay can change into to a unimodal shape, if the soil is wetted. However, according to results of Romero et al. (2011) the aggregation created by compaction dry of Proctor optimum is a permanent feature of the compacted soil fabric.

As matric suction arises mainly from capillary forces, the SWRC of compacted fine-grained soils reflects the pore size distribution. Hence, the SWRC is strongly influenced by the initial water content (Vanapalli et al. 1999, Tinjum et al. 1997, Tarantino & Tombolato 2005, Romero et al. 2011) as well as by the initial dry density (Tinjum et al. 1997, Romero et al. 1999, Miller et al. 2002, Sun et al. 2006, Miao et al. 2006, Romero et al. 2011). However, due to different testing methods and procedures the different investigations cannot be compared to each other. Furthermore, only few investigations focussed on the influence of the initial water content as well as the initial dry density on the SWRC.

In this paper the influence of the initial water content and dry density on the SWRC and the pore size distribution of compacted clay is described. In comparison to previous investigations (Birle et al. 2008) the present study uses suction-controlled oedometer cells as well as a chilled-mirror dew-point hygrometer for experimental tests.

2 Material and Sample Preparation

For the experimental investigations, a Lias-clay powder used as a raw material in the production of bricks was chosen. According to DIN 18196, the Lias-clay powder utilized is a clay of medium plasticity with a water content at the liquid limit LL of 46.5 % and at the plastic limit PL of 19.5 %. The grain density ρ_s of the material determined by capillary pycnometer is 2.78 g/cm^3.

The samples were prepared as described by Birle et al. (2008): At first, the dry clay powder was wetted to a water content w of approximately 27 %, thoroughly mixed and crushed in a cutter, and then stored in an airtight container for at least 1 week to allow homogenization to occur. Thereafter, at a temperature of 50 C°, the water content of the material was decreased to roughly 14 % and the material was once more placed in an airtight container for at least 1 week to allow for homogenization. A few days before the test sample preparation this material was wetted to the desired water content and then again thoroughly mixed and crushed in a

cutter. After homogenization over 24 h, the test samples were compacted statically to the desired dry density.

In order to select the initial dry densities as well as the initial water contents for the experiments, a standard Proctor test (W=0.6 MN/m^3), a modified Proctor test (W=2.7 MN/m^3), as well as a partially modified Proctor test (W=1.0 MN/m^3) were carried out. The results of the Proctor tests are shown in Figure 1. On the basis of the Proctor curves the eight test points presented in Figure 1 were selected.

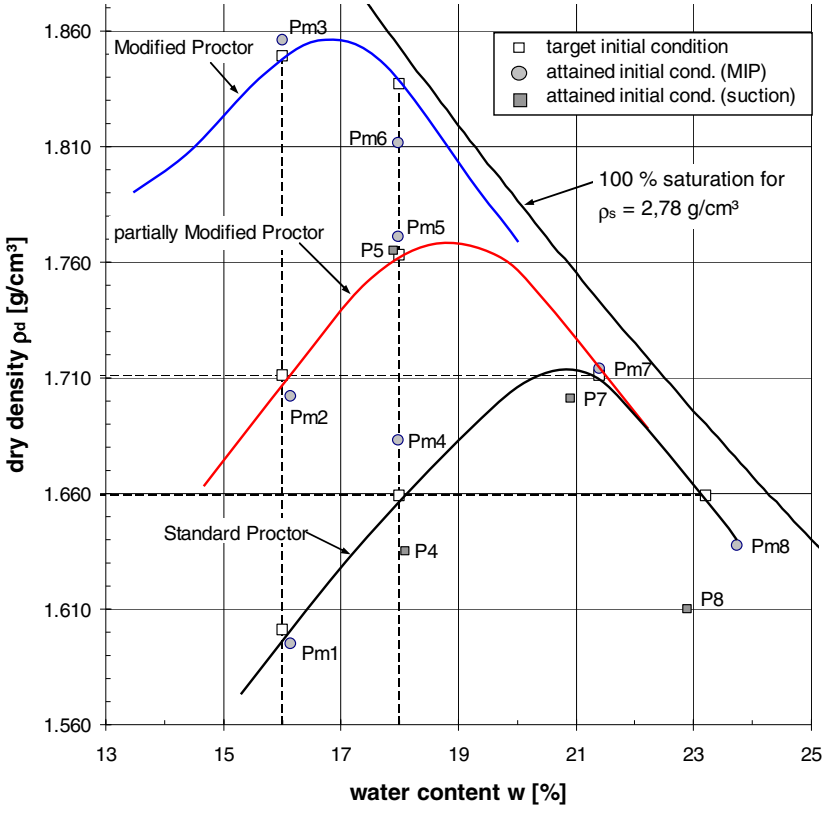

Fig. 1. Proctor tests and samples for the MIP and suction tests.

3 Equipment and Test Procedure

The PSD was determined by means of mercury intrusion porosimetry (MIP). To minimize the influence of the drying process on the soil structure, the freeze-drying technique was applied (Ahmed et al. 1974). Rapid freezing of the samples was achieved by immersing the samples in liquid nitrogen. After freezing the

samples were placed immediately in the freeze-drying apparatus Alpha 1-4 and dried by sublimation. The mercury intrusion porosimetry was conducted in the Grimm 4.700 apparatus with a maximum mercury pressure of 207 MPa. An intrusion followed by an extrusion was performed.

The SWRCs were experimentally determined by means of suction-controlled oedometer cells and a chilled-mirror dew-point hygrometer (WP4 Dew-point PotentiaMeter). The experimental set-up of the oedometer cells is explained in detail by Birle (2011).

In the suction-controlled oedometer cells suction was applied using the axis-translation-technique. In this process the water pressure was kept constant at 300 kPa, while the air pressure was increased. The statically compacted samples had a height of 1 cm and a diameter of 7 cm. Starting from the state after compaction, the samples first were wetted to a minimum matric suction of approx. 10 kPa and then dried by increasing the matric suction step by step to a maximum value of 1350 kPa. The vertical net stress was kept constant at 30 kPa during the tests. Air bubbles that accumulated due to diffusion beneath the high air-entry ceramic disc were expelled by flushing the water line every 6 hours during the tests. The equalisation stages lasted about 3 to 7 days until no more water content changes were recorded. After dismounting the samples part of the sample was taken for measuring the suction in the high suction range using the chilled-mirror dew-point hygrometer. The other part of the sample was used for determining the water content. The principle of operation of the hygrometer is based on the thermodynamic relationship between relative humidity, temperature and total soil suction according to Kelvin's equation (Fredlund and Rahardjo 1993). By these means the total soil suction can be determined from the measurements of relative humidity and temperature above a soil sample.

After measuring the total suction in the chilled-mirror dew-point hygrometer the specimens were weighed and air-dried to the next desired water content. The next measurement was done after a homogenization phase of at least 24 h. After the last measurement the specimens were oven-dried and the final water content was determined. The maximum suction measured by the hygrometer WP4 Dew-point PotentiaMeter used was 60 MPa.

4 Results and Discussion

Fig. 2 and Fig. 3 show the results of the MIP for the samples Pm4, Pm5, Pm7 and Pm8. The samples Pm4 and Pm5 were compacted at the same water content dry of Proctor optimum, but at different initial dry densities. The sample Pm7 was compacted approximately at Proctor optimum, while Pm8 lies on the wet side of Proctor optimum.

The cumulative intrusion porosities of the samples Pm4 and Pm5 compacted dry of Proctor optimum, show typical bimodal shapes. By the construction of two tangents to the intrusion curve the intra-aggregate pores and the inter-aggregate

pores can be distinguished. That way the inter-aggregate porosity of the sample Pm5 is much smaller than the inter-aggregate porosity of the sample Pm4. As the curve of the sample Pm5 is translated approximately parallel to the curve of the sample Pm4, it can be seen, that the higher compaction of the sample Pm5 leads mainly to a reduction of the pores with a size of 4 to 20 µm in contrast to the sample Pm4. Besides, the intra-aggregate porosity of the sample Pm5 is even a bit higher than that of the sample Pm4, as the sample Pm5 is denser and thus consists of more aggregates. This means that the compaction on the dry side of the Proctor optimum has nearly no influence on the intra-aggregate porosity and that a higher compaction results mainly in a reduction of the larger inter-aggregate pores.

With increasing water content the aggregates become softer and contribute to the deformation during compaction. Thereby the larger inter-aggregate pores diminish and the pore-size distribution takes on a more unimodal form. This can be seen especially for the cumulative porosity of sample Pm8 in Fig. 2, where a distinction between inter- and intra-aggregate pores is no longer possible.

Furthermore, the results of the MIP show that for small pore sizes (approx. < 0.1 µm) the shape of the cumulative intrusion porosity is similar for all samples and that they are only translated in a parallel manner.

A common way to distinguish between inter-aggregate and intra-aggregate pores is based on the analysis of the pore size density function (Romero et al. 2011). For the four samples the pore size density functions are given in Fig. 3. For the samples Pm4 and Pm5, which were compacted at the same water content but at different dry densities, the discriminating pore size between inter- and intra-aggregates can be assumed in the range of 0.5 to 1 µm. In comparison to the previous criterion based on the analysis of the cumulative intrusion curve this criterion gives a slightly higher discriminating pore size for the two samples.

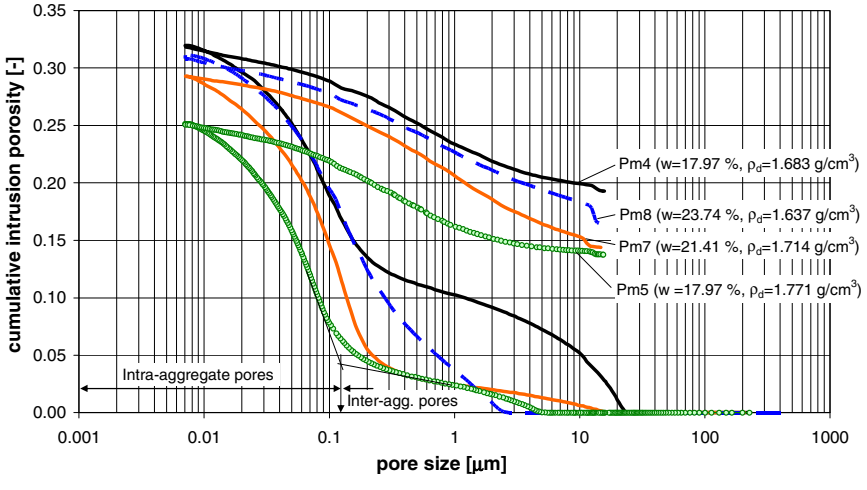

Fig. 2. Results of MIP for the samples Pm4, Pm5, Pm7 and Pm8 (intrusion and extrusion).

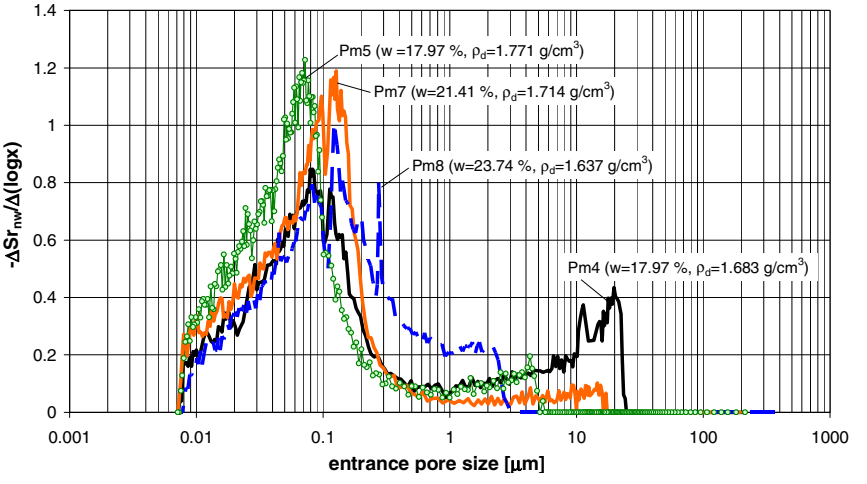

Fig. 3. Pore size density function of the samples Pm4, Pm5, Pm7 and Pm8.

Fig. 4 shows the retention curves of the samples P4, P5, P7 and P8 in terms of water content. The drying paths of the samples P4 and P5, which were compacted at the same initial water content, differ only in the low suction range at matric suctions smaller than 1500 kPa, while in the high suction range (> 1500 kPa) the drying paths are very similar. This agrees with the results of the MIP, that showed that the higher compaction of the sample Pm5 results only from the reduction of the larger inter-aggregate pores. Furthermore it can be seen that during the drying process, the curves P7 and P8 approach the curves P4 and P5 until they converge at a suction of 5.5 MPa. At suction values higher than 5.5 MPa the shape of all curves is very similar as already described by Birle et al. (2008).

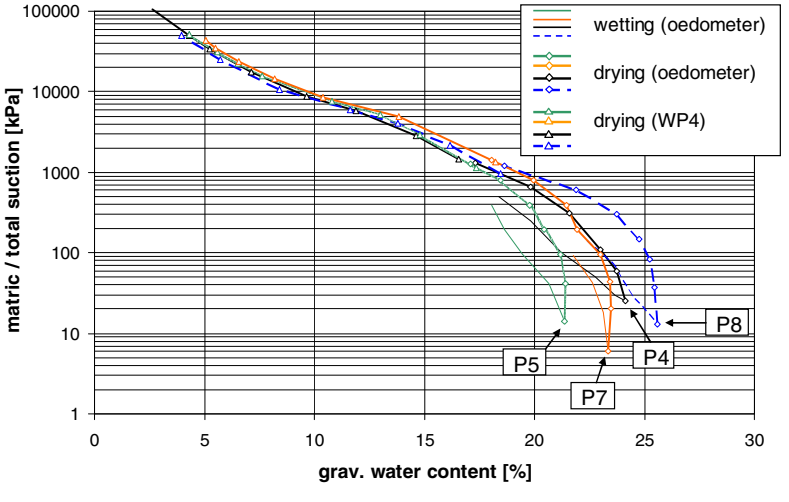

Fig. 4. SWRCs in terms of water content for the samples Pm4, Pm5, Pm7 and Pm8.

The SWRCs in terms of degree of saturation are presented in Fig. 5. Due to the higher dry density of the sample P5 its air entry value is much higher than that of the sample P4. Besides, in the high suction range the higher density of P5 results in higher suction at same degree of saturation in comparison to the sample P4.

Despite the low density of the sample P8, its air-entry value is much higher than that of the dry compacted sample P4. According to the results of the MIP this is caused by the smaller inter-aggregate porosity of the sample P8. In the high suction range the retention curves of the samples P4 und P8 are very similar, although the initial dry density of P4 was higher than that of P8. However, during the drying process the sample P8 exhibited a larger shrinkage than that of P4. Due to compaction at Proctor optimum the sample P7 has a small inter-aggregate porosity and hence a high air-entry value similar to that of the sample P5.

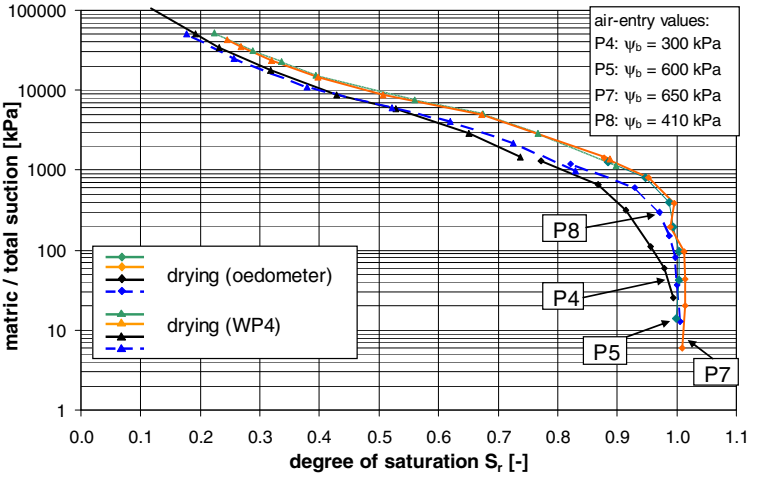

Fig. 5. SWRCs in terms of degree of saturation for the samples Pm4, Pm5, Pm7 and Pm8.

5 Conclusions

An experimental study was carried out to investigate the influence of the initial water content and dry density on the structure and the SWRC of a compacted clay. The soil structure was investigated by means of MIP. For the determination of the SWRC suction-controlled oedometer cells and a chilled mirror dew-point hygrometer were used. The following results, which agree with several publications cited above, were obtained:

- The SWRC in terms of gravimetric water content is independent of the initial dry density in the high suction range (> 1500 kPa). This is supported by the results of the MIP, which show that only the inter-aggregate porosity changes if the dry density increases at constant water content.
- At suction pressures higher than 5.5 MPa the SWRC is even independent of the initial water content. Correspondingly, the results of the MIP gave very similar results for all samples at small pore sizes (< 0.1 µm).

- For the SWRC in terms of degree of saturation it can be stated, that the air-entry value increases, if the dry density increases at constant water content or if the water content increases at constant dry density. Both effects are linked to a reduction of the inter-aggregate pores.

References

Ahmed, S., Lovell, C.W., Diamond, S.: Pore sizes and strength of compacted clay. J. Soil. Mech. Found. Div (ASCE) 100(GT4), 407–425 (1974)

Birle, E., Heyer, D., Vogt, N.: Influence of the initial water content and dry density on the soil-water retention curve and the shrinkage behaviour of a compacted clay. Acta Geotechnica 3(3), 191–200 (2008)

Birle, E.: Geohydraulische Eigenschaften verdichteter Tone unter besonderer Berücksichtigung des ungesättigten Zustandes, Doctoral thesis, TU München, München (2011)

Delage, P., Audiguier, M., Cui, Y.J., Howat, M.D.: Microstructure of a compacted silt. Canadian Geotechnical Journal 33, 150–159 (1996)

Fredlund, D.G., Rahardjo, H.: Soil mechanics for unsaturated soils. Wiley, New York (1993)

Lambe, T.W.: The permeability of compacted fine-grained soils. In: Symposium on Permeability of Soils, ASTM STP, vol. 163, pp. 56–67 (1954)

Li, X., Zhang, L.M.: Characterization of dual-structure pore-size distribution of soil. Canadian Geotechnical Journal 46, 129–141 (2009)

Miao, L., Jing, F., Houston, S.L.: Soil-water Characteristic Curve of Remolded Expansive Soils. In: Proc. of the 4th Int. Conf. on Unsat. Soils, Arizona 2006, ASCE, vol. 1, pp. 997–1004 (2006)

Miller, C.J., Yesiller, N., Yaldo, K., Merayyan, S.: Impact of soil type and compaction conditions on soil water characteristic. J. Geotech. Geoenviron. Eng. 128(9), 733–742 (2002)

Monroy, R., Zdravkovic, L., Ridley, A.: Evolution of microstructure in compacted London Clay during wetting and loading. Géotechnique 60(2), 105–119 (2010)

Romero, E., Gens, A., Lloret, A.: Water permeability, water retention and microstructure of unsaturated compacted Boom clay. Engineering Geology 54, 117–127 (1999)

Romero, E., Vecchia, G.D., Jommi, C.: An insight into the water retention properties of compacted clayey soils. Géotechnique 61(4), 313–328 (2011)

Seed, H.B., Chan, C.K.: Structure and strength characteristics of compacted clay. Journal of the Soil Mechanics and Foundations Division (ASCE) 85(SM 5), 87–128 (1959)

Sivakumar, V., Tan, W.C., Murray, E.J., McKinley, J.D.: Wetting, drying and compression characteristics of compacted clay. Géotechnique 56(1), 57–62 (2006)

Sun, D., Sheng, D.C., Cui, H.B., Li, J.: Effect of density on the soil-water-retention behaviour of compacted soil. In: Proc. of the 4th Int. Conf. on Unsat. Soils, 2006, ASCE, Arizona, vol. 2, pp. 1338–1347 (2006)

Tarantino, A., Tombolato, S.: Coupling of hydraulic and mechanical behaviour in unsaturated compacted clay. Géotechnique 55(4), 307–317 (2005)

Thom, R., Sivakumar, R., Sivakumar, V., Murray, E.J., Mackinnon, P.: Pore size distribution of unsaturated compacted kaolin: the initial states and final states following saturation. Géotechnique 57(5), 469–474 (2007)

Tinjum, J.M., Benson, C.H., Blotz, L.R.: Soil-water characteristic curves for compacted clays. ASCE J. Geotech. Geoenviron. Eng. 123(11), 1060–1069 (1997)

Vanapalli, S.K., Fredlund, D.G., Pufahl, D.E.: The influence of soil structure and stress history on the soil-water characteristics of a compacted till. Géotechnique 49(2), 143–159 (1999)

Water Retention Properties of a Compacted Clayey Silt Including Void Ratio Dependency and Microstructural Features

Rodrigo Gómez, Enrique Romero, Gabriele Della Vecchia, Cristina Jommi, Josep Suriol, and Antonio Lloret

Abstract. An experimental study focused on the water retention properties of a compacted clayey silt with dominant bimodal pore size distribution is reported. A water retention model accounting for soil microstructural features and void ratio is used to track the observed hydraulic behaviour. The model parameters were calibrated on the basis of drying and wetting data at a given dry density and the model predictions are verified along drying and wetting paths at different void ratios.

Keywords: water retention curve, laboratory tests, model, compacted soil.

Rodrigo Gómez
Universitat Politècnica de Catalunya, Barcelona, Spain
e-mail: rodrigo.gomez@upc.edu

Enrique Romero
Universitat Politècnica de Catalunya, Barcelona, Spain
e-mail: enrique.romero-morales@upc.edu

Gabriele Della Vecchia
Politecnico di Milano, Milano, Italy
e-mail: gabriele.dellavecchia@polimi.it

Cristina Jommi
Politecnico di Milano, Milano, Italy
e-mail: cristina.jommi@polimi.it

Josep Suriol
Universitat Politècnica de Catalunya, Barcelona, Spain
e-mail: jose.suriol@upc.edu

Antonio Lloret
Universitat Politècnica de Catalunya, Barcelona, Spain
e-mail: antonio.lloret@upc.edu

1 Introduction

In recent years, significant efforts in unsaturated soil mechanics have been dedicated to the development of constitutive models capable to describe the main aspects of soil-water retention behaviour. The model proposed by Della Vecchia (2009) and Romero et al. (2011), for instance, pursues this scope accounting for the dependency of the air-entry value on both the current void ratio and the intra-aggregate pore space by considering the volume changes of the aggregates on water content changes. To further explore the capabilities of this model of capturing the dependency of the hydraulic response on void ratio, data obtained using different experimental techniques on a compacted clayey silt are reported. The soil, characterised by an aggregated bimodal pore size distribution, was retrieved from an experimental embankment built to study the earth-structure response in areas liable to flooding (LCPC 2007). Experimental data come from controlled-suction oedometer tests, as well as measurements from tensiometer and psychrometer under unstressed conditions, and mercury intrusion porosimetry tests.

2 Characterisation of the Material and Water Retention Results

The clayey silt has a liquid limit of 33%, a plastic limit of 20%, a clay-size fraction (≤2 μm) of 29%, and density of solids of $\rho_s = 2.66$ Mg/m³. Intact samples were retrieved from the soaked zone of the experimental embankment having experienced collapse, which present a void ratio around 0.60. Other samples were prepared by static compaction to match *in-situ* conditions to obtain a poorly compacted soil, prone to collapse upon flooding (dry density $\rho_d = 1.40$ Mg/m^3 and $w = 17\%$ at void ratio $e = 0.90$ and degree of saturation $S_r = 50\%$).

The *in-situ* material was just placed and levelled out, and the maximum vertical stress applied corresponded to overburden depth. The low-stress static compaction process adopted in the laboratory is thus representative of these field conditions. Additional information on the material can be found in Gómez et al. (2009, 2010).

Besides controlled-suction oedometer results at constant vertical net stress of 100 kPa, retention curve data were also obtained under unstressed conditions using different techniques such as low-range tensiometer (Keller 2009), high-range tensiometer (Delage et al. 2008) and dew-point mirror psychrometer (Cardoso et al. 2007). Mercury intrusion porosimetry (MIP) results were also used to determine the water retention properties upon drying for matric suctions lower than 0.1 MPa, assuming that injection of non-wetting mercury were equivalent to removal of water (see, for instance, Romero & Simms 2008).

The water retention properties along drying and wetting paths at two distinct void ratios are shown in Fig. 1. 'SC' refers to static compaction data at $e = 0.90$, 'Blk' and 'Bh' to data coming from intact block and borehole samples, respectively, at approximately $e = 0.60$. Water ratio $e_w = S_r e$ (i.e., volume of water over volume of solids) is chosen to quantify the amount of water in the soil, which tends to e under fully saturated conditions.

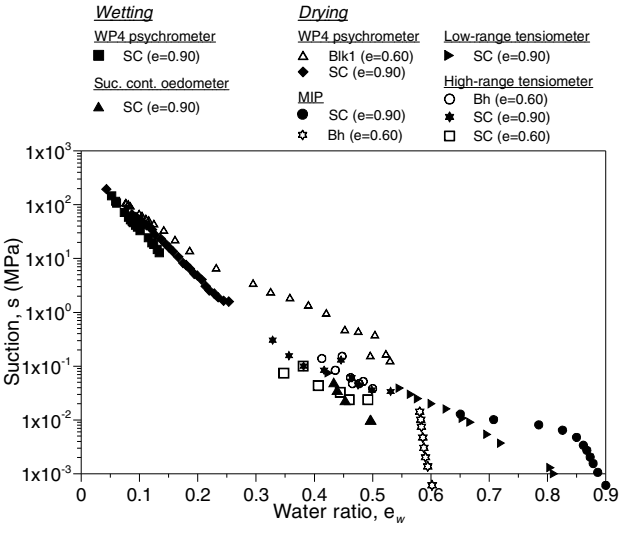

Fig. 1. Experimental data of retention curves upon drying and wetting at different void ratios.

Relevant void ratio effects on water retention properties are clearly observed from the data reported in the figure. This dependency on void ratio, more important in the low suction range, should be considered if accurate analyses of the embankment behaviour have to be performed (Della Vecchia et al. 2012).

3 Water Retention Model Accounting for Void Ratio and Fabric Changes: Model Capabilities

The water retention model for compacted clayey soils with intrinsic double structure proposed by Della Vecchia (2009) and Romero et al. (2011) was used to fit experimental data on drying at the as-compacted state $e = 0.90$. The model considers microstructural volume changes (swelling and shrinking aggregates), as well as global volume changes (changes in void ratio e), induced by water content changes. It is formulated in terms of water ratio e_w and matric suction s. A key point is the conceptual separation of the amount of water adsorbed in the micropore volume (microstructural void ratio, e_m) from that stored in the inter-aggregate void space (macrostructural void ratio; $e_M = e - e_m$).

The evolution of the microstructural void ratio e_m with water ratio is given by:

$$e_m = e_m^* + \beta \left\langle e_w - e_m^* \right\rangle \tag{1}$$

where $\langle\ \rangle$ designating the Macauly brackets and e^*_m and β are microstructural parameters.

For $e_w < e^*_m$, a constant $e_m = e^*_m$ results from Eq. (1); this corresponds to a microstructure with completely empty macropores and fully saturated micropores. The microstructural parameter e^*_m was estimated by the following expression (Romero *et al*. 2011), assuming a specific surface of $S_s = 5$ m^2/g that was obtained from MIP results (as a first approximation, $e^*_m = \beta$ was considered)

$$e^*_m = 0.088 \ln\left(\frac{S_s}{S_{sr}}\right) + 0.05 = 0.19; \text{ where } S_{sr} = 1 \text{ m}^2/\text{g} \tag{2}$$

An analytical expression for the dry end of the main wetting and drying branches, not dependent on void ratio e, may be assumed for e_w lower than e^*_m

$$e_w = \frac{b e^*_m}{\ln\left(\frac{s_{max}}{s^*_m}\right)} \left[\frac{b + \ln\left(\frac{s_{max}}{s^*_m}\right)}{b + \ln\left(\frac{s}{s^*_m}\right)} - 1 \right] \tag{3}$$

where s^*_m is the suction corresponding to e^*_m, s_{max} is the maximum suction attainable for $e_w = 0$ ($s_{max} = 1$ GPa corresponding to oven drying), and b is a parameter describing the average slope of the curve. The dependency of the macrostructural part of the water retention curve on e may be achieved by adopting a linear scaling or adding an appropriate dependency of the air entry value (associated with parameter α) on e and the evolving microstructure e_m (Della Vecchia *et al*. 2012). For e_w ranging between $e_m \leq e_w \leq e$, the water ratio reads

$$e_w = e_m + (e - e_m) \left(1 - \frac{\ln\left[1 + \frac{s}{s_m}\right]}{\ln 2} \right) \left(1 + (\alpha s)^n\right)^{\left(\frac{1}{n} - 1\right)} \tag{4}$$

where parameter $n > 1$ is equivalent to the one proposed by van Genuchten (1980).

In Fig. 2, experimental data of drying at constant $e = 0.90$ are fitted to the model. A similar procedure was followed with wetting data at a different void ratios (Gómez, in prep.). The set of fitted parameters further used in the model predictions are summarised in Table 1.

Table 1. Soil parameters used in the simulations.

e^*_m	β	n	wetting		drying	
			s^*_m (MPa)	b	s^*_m (MPa)	b
0.19	0.19	1.45	3	25	5	15

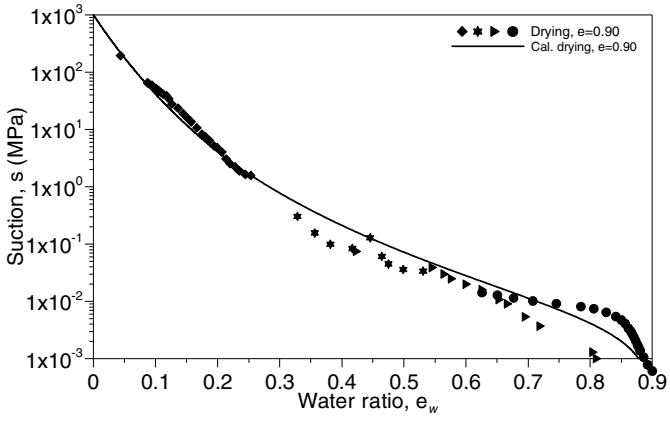

Fig. 2. Model fitted to experimental data on drying at e=0.90.

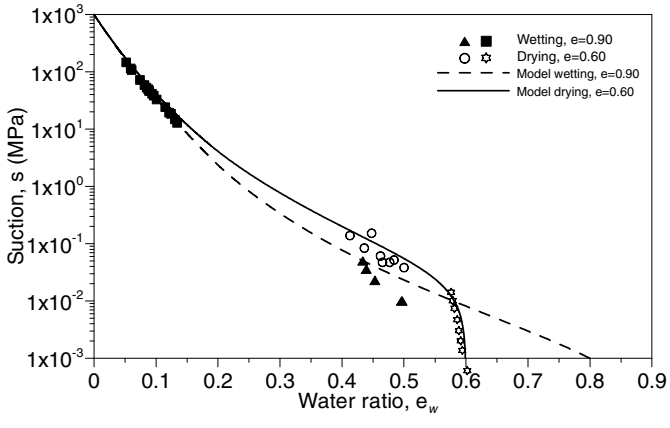

Fig. 3. Comparison between experimental data and model predictions at different void ratios and different hydraulic branches.

The capabilities of the model are illustrated in Fig. 3 for two different void ratios of the soil and different hydraulic branches of the soil-water retention curve. As observed, the experimental data referring to the two different void ratios look to be well reproduced by the model, despite the limited data on wetting at e = 0.90 in the low suction range. Further experiments are in progress to cover this range of suction, as relevant water content changes are expected at suctions below 10 kPa.

4 Summary and Concluding Remarks

The compacted clayey silt considered in this paper shows a strong influence of void ratio on its water retention behaviour, as demonstrated by the data obtained with different techniques and laboratory equipments. A water retention model

formulated in terms of water ratio and accounting for soil microstructural features and void ratio is used to track the observed water-retention behaviour. Model capabilities were illustrated by comparison between blind numerical predictions and experimental data at two different void ratios on both drying and wetting. The model seems to be able to capture the main features of wetting and drying branches at different void ratios, not only in terms of the water storage capacity but also in terms of the evolution of air-entry and air-occlusion values.

References

Cardoso, R., Romero, E., Lima, A., Ferrari, A.: A comparative study of soil suction measurement using two different high-range psychrometers. In: Schanz, T. (ed.) Proc. 2nd Int. Conf. Mechanics of Unsaturated Soils, Weimar, Germany, March 7-9. Springer Proceedings in Physics, vol. 112, pp. 79–93 (2007)

Delage, P., Romero, E., Tarantino, A.: Recent developments in the techniques of controlling and measuring suction. In: Toll, D.G., Augarde, C.E., Gallipoli, D., Wheeler, S.J. (eds.) Proc. 1st European Conf. on Unsaturated Soils, Durham, UK, July 2-4. Unsaturated Soils: Advances in Geo-Engineering, pp. 33–52. CRC Press (2008)

Della Vecchia, G.: Coupled hydro-mechanical behaviour of compacted clayey soils. PhD Thesis, Politecnico di Milano, Italy (2009)

Della Vecchia, G., Jommi, C., Romero, E.: A fully coupled elastic–plastic hydromechanical model for compacted soils accounting for clay activity. Int. J. Numer. Anal. Meth. Geomech (2012); Published online in Wiley Online Library, doi:10.1002/nag.1116

Gómez, R., Romero, E., Lloret, A., Suriol, J.: Characterising the collapsible response of an in-situ compacted silt. In: Buzzi, O., Fityus, S., Sheng, D. (eds.) Proc. 4th Asia-Pacific Conf. on Unsaturated Soils, Newcastle, Australia, November 23-25. Experimental Studies in Unsaturated Soils and Expansive Soils, pp. 371–376. CRC Press (2009)

Gómez, R., Romero, E., Lloret, A., Suriol, J., Jommi, C.: Parameter calibration for hydromechanical modelling using numerical simulations of test results. In: Alonso, E.E., Gens, A. (eds.) Proc. 5th Int. Conf. on Unsaturated Soils, Barcelona, Spain, September 6-8, vol. 2, pp. 823–828. CRC Press (2010)

Gómez, R.: Evaluación del comportamiento de explanadas y terraplenes a través de la mecánica del suelo no saturado. PhD Thesis, Universitat Politècnica de Catalunya, Spain (in prep.)

Keller, T.: UMS T5/T5x Pressure transducer tensiometer. Users manual. UMS GmbH, Germany (2009)

LCPC, Remblais en zones humides et inondables. Conséquences de l'inondation du remblai expérimental de Rouen et enseignements tirés pour la conception. Rapport final. Convention SNCF-LCPC-CETE Normandie Centre (2007)

Romero, E., Simms, P.: Microstructure investigation in unsaturated soils: A review with special attention to contribution of mercury intrusion porosimetry and environmental scanning electron microscopy. Geotech. Geol. Engng 26(6), 705–722 (2008)

Romero, E., Della Vecchia, G., Jommi, C.: An insight into the water retention properties of compacted clayey soils. Géotechnique 61(4), 313–328 (2011)

van Genuchten, M.T.: A closed-form equation for predicting the hydraulic conductivity of unsaturated soils. Soil Science Society of America Journal 44, 892–898 (1980)

Effect of Density in the Water Retention Curve of a Compacted Silt-Bentonite Mixture

Emad Jahangir, Hossein Nowamooz, and Farimah Masrouri

Abstract. In unsaturated swelling-shrinking soils, like clay soils, water content change results in significant volume change and drying is associated with high water content gradients.This work presents initially the soil water retention curve (SWRC) of a bentonite-silt mixture compacted at three different initial dry densities (1.27, 1.35 and 1.55 $Mg.m^{-3}$). The SWRCs were fitted by the van Genuchten (1980) and Brooks and Corey (1964) type functions. The estimated parameters were used to model the SWRC of the intermediate samples.

Keywords: SWRC, swelling soils, initial density, bimodal soil fabric.

1 Introduction

The soil water retention curve (SWRC) is one of the important hydraulic functions for modeling flow transport in porous media. It contains important information regarding the amount of water contained in the pores at a given soil suction and the pore size distribution corresponding to the stress state in the soil (Fredlund et al., 2002). Unsaturated soil parameters such as shear strength, volume change, diffusivity, and adsorption are related to the SWCR (Fredlund & Rahardjo, 1993). Various empirical equations have been suggested to describe the SWRC. Among these equations, the relationships proposed by Brooks & Corey (1964), van Genuchten (1980) and Fredlund & Xing (1994) have been used in geotechnical engineering. Due to

Emad Jahangir
Nancy Université
e-mail: Emad.Jahangir@ensg.inpl-nancy.fr

Hossein Nowamooz
INSA de Strasbourg
e-mail: Hossein.Nowamooz@insa-strasbourg.fr

Fariamh Masrouri
Nancy Université
e-mail: Farimah.Masrouri@ensg.inpl-nancy.fr

difficulties and labor costs when measuring SWRC, it has become necessary to develop methods to describe the function utilizing available data.

This work presents initially the SWRC of a bentonite-silt mixture compacted at three different initial dry densities (1.27, 1.35 and 1.55 $Mg.m^{-3}$). A three-parameter van Genuchten (1980) type function as well as a two-parameter bimodal Brooks and Corey (1964) were fitted to the obtain SWRC for loose and dense samples. The SWRC of the intermediate density samples were then estimated based on these models.

2 Experimental Program

The study was conducted on an artificially prepared mixture of 40% silt and 60% bentonite. The mineralogical composition of the compacted material was determined by X-Ray Diffraction (XRD). The silt contained 60% quartz, 20% montmorillonite, 11% feldspar, and the remaining part was made up of kaolinite and mica. The bentonite was composed of more than 90% of calcium montmorillonite. The main geotechnical properties of the materials and of the mixture are shown in Table 1. The size of the particles used to prepare the samples was less than 400 μm, and these particles were obtained via sieving. The initial dry densities (ρ_{di}) of the compacted soil were about 1.27, 1.35 and 1.55 Mg/m^3, respectively, under three vertical pressures of 1000, 1500 and 3000 kPa and an initial water content (w_i) of 15% in the dry side of optimum. In this paper, these samples are respectively called loose (L), Intermediate (I) and dense (D). The initial matric suction, measured by the contact filter paper method (ASTM 1995), was between 20 and 25 MPa for all compacted samples.

The variation of degree of saturation for all compacted samples was studied during a wide suction cycle ranging between 0 and 289.7 MPa using the osmotic method for suctions below 8.5 MPa (Delage et al. 1998, Cuisinier & Masrouri 2005) and the vapor equilibrium technique for suctions higher than 8.5 MPa (Lide, 2002). A wide range of suction comprised between 0 and 287.9 MPa was applied to the samples producing a wetting path between 20 and 0 MPa and a drying path between 20 and 287.9 MPa. At the end of this phase all the samples dried in the oven were saturated at the same time. Subsequently, a range of suction between 0 and 289.7 MPa was imposed to all saturated samples.

3 Modeling Results

Figures 1 and 2 present the SWRC of loosely and densely compacted samples (1.27 and 1.55 Mg/m^3). The SWRC results were fitted by Brook and Corey and van Gunechten functions generally used in unsaturated geotechnical engineering. The Brooks and Corey equation for the SWRC is written as follows:

$$\begin{cases} Sr = (\frac{\psi_b}{\psi})^{-\lambda} & \psi \geq \psi_b \\ Sr = 100 & \psi \leq \psi_b \end{cases} \quad (1)$$

in which Sr is the degree of saturation; ψ is the suction; λ is a fitting parameter, which represents the slope of the curve in a logarithmic space and ψ_b is the bubbling pressure (or air entry pressure). The relation of van Genuchten is written as follows:

$$S(\psi) = \left[\frac{1}{1+(\alpha\psi^n)}\right]^m \quad (2)$$

ψ is the suction, α, m et n are constant model parameters (Table 1). It can be noted that almost the same air entry value can be obtained in the SWRC (estimated by both models) for loose and dense states on the wetting and drying paths.

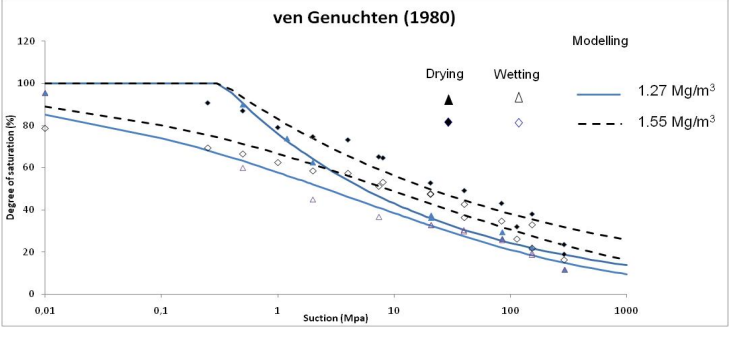

Fig. 1. SWRC for loosely and densely compacted samples estimated by van Gunechten (1980) equation.

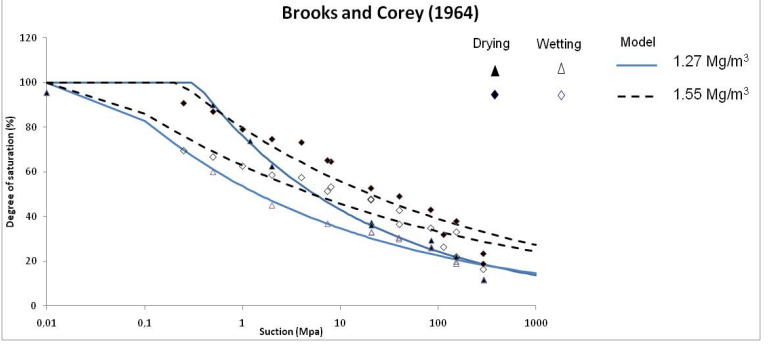

Fig. 2. SWRC for loosely and densely compacted samples estimated by Brooks and Corey equation.

Table 1 summarizes all the parameters of the van Genuchten model. It seems that the parameter n is affected directly by the density. This parameter increases with the increase of density for both wetting and drying paths. The parameter m is affected inversely by the density, so it decreases with the increase of the density. The parameter α remains almost constant in the loose and dense states and consequently the same air-entry value can be obtained from the different curves.

Table 1. Estimated parameters of van Gunechten equation.

van Genuchten model		α (1/MPa)	n	m
Loose state	Wetting path	3	24.19	0.01
	Drying path	0.03	0.29	1.79
Dense state	Wetting path	3	41.10	0.004
	Drying path	0.021	0.295	1.469

Table 2 presents all the parameters of the Brooks and Corey model. The parameter λ decreases with the increase of density for wetting and drying paths. The air entry value (s_e) decreases slightly from loose to dense states for both hydraulic paths.

Table 2. Estimated parameters of Brooks and Corey equation.

Brook and Corey model		λ	s_e (MPa)
Loose state	Wetting path	0.333	0.248
	Drying path	0.037	0.189
Dense state	Wetting path	0.232	0.155
	Drying path	0.034	0.137

Using the fitted parameters of these models at two different initial states, the SWRC of the intermediate sample (1.35 Mg/m^3) during several suction cycles was predicted. To estimate the parameters for the intermediate samples, a linear regression was performed between the loose and dense soils parameters.

The following points can be noted:

- In the van Genuchten model, the parameters n and especially m are affected by the soil initial state.
- In the Brooks and Corey model, the initial dry density increase influences more the parameter λ.
- The whole results showed a good capacity of the models to predict the hydric behaviour of the intermediate samples.

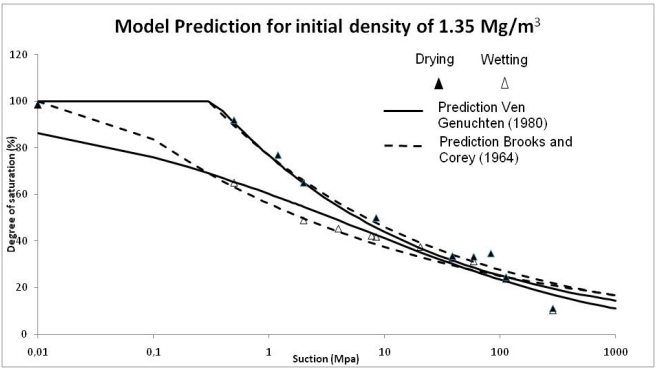

Fig. 3. Model prediction for the intermediate compacted samples based on Brooks and Corey and van Gunechten equations.

4 Conclusion

This work presents initially the SWRC of a bentonite-silt mixture compacted at three different initial dry densities (1.27, 1.35 and 1.55 $Mg.m^{-3}$). A van Genuchten and Brooks and Corey type functions were used to obtain SWRC at the dense and loose initial states. The proposed equations were then used to model the SWRC of the intermediate samples. It can be pointed out that the air entry value is less affected parameter in the both van Genuchten and Brooks and Corey model comparing to the fitted parameters (m, n and λ).

References

ASTM D5298-94, Measurement of soil potential (suction) using filter paper, Annual book of ASTM Standards, vol. 4.09, pp. 154–159 (1995)

Brooks, R.H., Corey, A.T.: Hydraulic properties of porous media. Hydrol. Pap. 3. Colorado State Univ., Fort Collins (1964)

Cuisinier, O., Masrouri, F.: Hydromechanical behavior of a compacted swelling soil over a wide suction range. Engineering Geology 81, 204–212 (2005)

Delage, P., Howat, M.D., Cui, Y.J.: The relationship between suction and the swelling properties in a heavily compacted swelling clay. Engineering Geology 50, 31–48 (1998)

Fredlund, D.G., Rahardjo, H.: Soil mechanics for unsaturatedsoils. Wiley, New York (1993)

Fredlund, M.D., Wilson, G.W., Fredlund, D.G.: Use of grain-size distribution for estimation of the soil water characteristic curve. Can. Geotech. J. 39(5), 1103–1117 (2002)

Fredlund, D.G., Xing, A., Huang, S.: Predicting of the permeability function for unsaturated soil using the Soil-water characteristic Curve. Canadian Geotechnical Journal 31, 533–546 (1994)

Lide, D.R. (ed.): Handbook of chemistry and physics, 82th edn., pp. 15.25 – 15.26. CRC Press (2002)

van Genuchten, M.T.: A closed-form equation for predicting the hydraulic conductivity of unsaturated soils. Soil Sci. Soc. Am. J. 44, 892–898 (1980)

Effect of Vertical Stress on the Soil Water Characteristic Curve of Highly Expansive Soils

Tamer Y. Elkady and Ahmed M. Al-Mahbashi

Abstract. This study investigates the effect of vertical loading and sample saturation procedure on the drying soil water characteristic curve (SWCC) of expansive clay from Al-Qatif area in Saudi Arabia. An experimental program is conducted on remolded samples using Fredlund SWCC device with simultaneous application of vertical stress and suction. Samples are tested under vertical stresses of 4, 300, and 600 kPa and over a range of suction up to 1400 kPa. During the test, volume changes experienced by tested samples are evaluated using image processing method for the determination of SWCC in terms of degree of saturation. Results indicate that sample saturation have a significant effect on the shape and air entry value of SWCC of expansive clay. Furthermore, at specific suction level, the combined application of vertical stress and suction cause a reduction in gravimetric water content and degree of saturation.

Keywords: expansive soils, soil water characteristic curves, image processing.

1 Introduction

Variation of soil suction with water content (whether gravimetric or volumetric) or degree of saturation is defined using the soil water characteristic curve (SWCC). In other words, SWCCs is a measure of the ability of soil to retain water under different suction levels. The ability of fine-grained soils to retain water is directly related to its fabric which includes macropores, minipores and micropores (Mitchell 1993).

Tamer Y.Elkady
King Saud University, Riyadh, Saudi Arabia
e-mail: tyelkady@yahoo.com

Ahmed M. Al-Mahbashi
King Saud University, Riyadh, Saudi Arabia
e-mail: ena_almahpashi@hotmail.com

Mitchell (1993) stated that the hydraulic properties of soil are mainly controlled by the macropores and minipores. The influence of stress state on the SWCC was recognized in research by Fredlund & Rahardjo (1993) and Vanapalli et al. (1998). Recently, several investigators (Simms & Yanful 2002, Nowamooz & Masrouri 2010) identified the influence of mechanical loading and suction application on soil fabric of fine-grained soils.

Determination of the SWCCs of expansive soils in terms of volumetric water content or degree of saturation requires estimation of sample volume change during the test. SWCCs are typically determined using standard tests methods (ASTM D6836) that do not account for vertical stress, sample saturation procedure and volume change measurements during the test. Some researchers adopted different techniques including caliper measurements and archimedes' principle for sample volume change measurements (Chao et al. 1998, 2008). Different researchers investigated the effect of vertical loading and sample saturation procedure on the SWCC of expansive soils. Miao et al. (2002), using pressure extraction device, investigated the effect of sample saturation procedures on the hysteresis of SWCC of expansive soils. Laboratory tests conducted by Li et al (2007) in suction controlled oedometer indicated that vertical stress has a significant effect on SWCCs of expansive soils.

This study investigates the effect of sample saturation procedure and vertical loading on the SWCCs of Al-Qatif expansive soils. Laboratory testing was performed using Fredlund SWCC device where suction was applied up to 1400 kPa. Vertical stresses applied ranged from 4 kPa to 600 kPa. Sample volume changes experienced during the test were evaluated using image processing techniques.

2 Experimental Program

2.1 Soil Used and Index Properties

The expansive clay considered in this study is from the city of Al-Qatif located on the western shoreline of the Arabian Gulf, in the eastern province of Saudi Arabia. Several researches conducted to investigate the swelling characteristics of Al-Qatif expansive clay revealed that the soil is highly expansive in nature due to the presence of smectite mineral content in the range of 25-30% (Abduljauwad & Al-Sulaimani 1993, Azam et al. 1998; Al-Shayea 2001, Azam 2003).

Disturbed samples of greenish brown clay were obtained from open pits excavated to a depth of 1.5 - 2.0 m below ground surface. Extensive laboratory tests were performed for the full characterization of soil and assessment of swelling characteristics of Al-Qatif soils. Based on characterization data, the soil is classified as clay of high plasticity (w_L = 137%, w_P = 60%, w_{sh}= 12%). Swelling pressure of was evaluated to be 550 – 600 kPa as per ASTM D4546-08- Method B.

2.2 Experimental Device

SWCCs for this study were evaluated using Fredlund SWCC device. Details of this device were provided by Pham et al. (2004). This device provides independent control of suction and vertical stress on tested samples. Suction was imposed on tested samples placed in the pressure cell with high air entry value ceramic disk embedded in its base. The ceramic disk used for this study has an air entry value of 15 bar (1500 kPa). The water in the compartment below the ceramic disk was connected to two graduated burettes to measure the flow of water in and out of the sample. Before commencement of each test, the ceramic disk was saturated by applying air pressure to a partially filled pressure cell and monitoring the rate of water flowing through the disk. Ceramic disk was considered saturated when the rate of water flow through the ceramic disk was constant. Vertical loading was applied on tested samples using compressed air piston with regulator. A dial gauge was connected to the loading rod to measure the vertical displacement of tested samples during the test.

2.3 Sample Preparation

Remolded samples were used in this study to minimize soil heterogeneity due to sampling. The soil was air dried, pulverized and sieved over sieve No. 40. Tested samples were prepared at maximum dry density and optimum moisture content using standard proctor compaction effort (γ_d =12 kN/m^3 and w = 32%). Samples were extruded from the compacted soil using test rings of 50 mm in diameter and 20 mm high. The final height of the samples was trimmed to be 4 mm below the top rim of ring to accommodate any swelling that may occur during sample saturation or suction application. Extruded samples including ring are stored in plastic bags and stored in humid environment for at least 24 hours before test.

2.4 Testing Procedure

In this study, the drying soil water characteristic curves of expansive clays were of interest. This entails that expansive clay samples be saturated at the beginning of each test. During saturation, the expansive clay samples are expected to undergo volume change. In this study, different saturation procedures of expansive clay were investigated; namely, free swell and preloading. Free swelling procedure involved saturation of the samples under low vertical stress of 10 kPa. The preloading procedure involved the same process as free swelling except, after saturation under low vertical stress, the vertical stress on the sample was increased to reconsolidate the sample back to its original height. This required increasing the vertical stress in increments to values in the neighborhood of the swelling pressure of tested soil (i.e., 550-600 kPa). At the end of each procedure, the initial weight and height of the sample was recorded.

After saturation, samples were transferred to the pressure cell and placed on the high air entry value ceramic disk in the pressure cell overlain with a filter paper and porous stone. Vertical stress was initially applied on the sample and dial gauge reading was monitored until no change in vertical displacement was observed. Vertical stress levels considered for this study include 4 kPa, 300 kPa, and 600 kPa representing different stress conditions; namely, low vertical stress, below swelling pressure and at swelling pressure. Suction was then applied in increments up to 1400 kPa and the amount of water leaving or entering the sample under each increment was recorded using graduated burettes. Each suction level was maintained until equilibrium was achieved. Equilibrium was assumed when no change in water level was observed within 24 hours.

During preliminary tests, it was observed that the expansive clay samples underwent lateral as well as vertical shrinkage as a result of suction application. Lateral shrinkage resulted in the development of circumferential cracks in tested samples as well as separation between the tested sample and the confining ring. Development of these cracks is bind to introduce errors during the evaluation of sample volume (Peron et al. 2007). Furthermore, cracks will change the hydraulic conductivity and water storage capacity of the soil samples which, in turn, affect the shape of SWCC (Abbaszadeh et al. 2010). To minimize sample cracking, the inner walls of the ring were initially coated with thin layer of oil to minimize friction between the samples and the inner ring walls. This resulted in the development of intact samples that simplified the evaluation of sample volume.

Measurements of sample lateral changes were performed using image processing techniques. After equilibrium was attained under each suction level, the pressure cell was disassembled and an image of the top surface of the tested samples was captured using a digital camera located at a fixed distance above the sample. The image was then transferred to an image manipulation program where the outer perimeter of the sample was traced and the area of the upper surface of the sample was computed as shown in Fig. 1. During suction applications, it was observed that bottom surface of the tested sample underwent little shrinkage as compared to the top surface due to friction between the bottom surface of the sample and the ceramic disk as illustrated in Fig. 2. As such, the sample volume was computed as the average surface area of the top and bottom faces of the sample multiplied by the height of the sample recorded at each suction level.

At the end of test, the sample was weighed and oven-dried for water content determination. The water contents at each suction level stage were back-calculated based on the final water content and the amount of the water change recorded after each suction level.

Fig. 1. Sample shrinkage after application of suction.

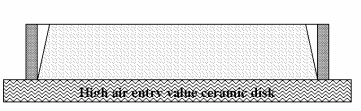

Fig. 2. Non-uniform shrinkage along sample height.

3 Results and Discussions

3.1 Effect of Sample Saturation Procedures

This section discusses the effect of sample saturation procedures described in section 2.4 on the SWCCs of expansive clay samples. Fig. 3 depict the SWCCs in terms of gravimetric water content (hereinafter referenced as SWCC(w)) of expansive clay samples initially saturated using proposed saturation procedures. From Fig. 3, it is observed that free swelling method resulted in higher initial water content in tested samples as compared to those saturated using preloading method.

SWCC(w) for samples saturated using free swell method (Fig. 3) shows a sharp decrease in gravimetric water content with increase in suction up to 400 kPa followed by slow reduction in gravimetric water content at suctions greater than 400 kPa. "Air entry value" evaluated from SWCC(w) for free swelling samples is in the range of 25-30 kPa. On the other hand, SWCC(w) of preloaded samples show a smooth transitional curve similar to a loading consolidation curve with air entry value of about 550-600 kPa. It is also observed from Fig. 3 that the rate of desaturation of samples with the application of suction is less for preloaded samples than that for free swelling samples.

The above observations can be attributed to fabric changes in samples during saturation and suction application. Variation of void ratio with suction presented in Fig. 4 is considered a simple indicator of sample's fabric change. From Fig. 4, it is observed that the response of free swell samples to suction increase is different than that for preloaded samples. This is because free swell samples initially underwent increase in void ratio as a result of swelling which is expected to obliterate the initial fabric of the sample. Free swell samples underwent minor decrease

in void ratio with suction increments up to 100 kPa followed by notable decrease in void ratio with increment increase in suction. On the other hand, preloaded samples underwent minor change in void ratio with increase in suction up to 800 kPa. Further increase in suction increment beyond 800 kPa resulted in greater decrease in void ratio. In the reminder of this paper, samples will be saturated using the preloading procedure to isolate structural change effects when studying the effect of vertical stress on the SWCC.

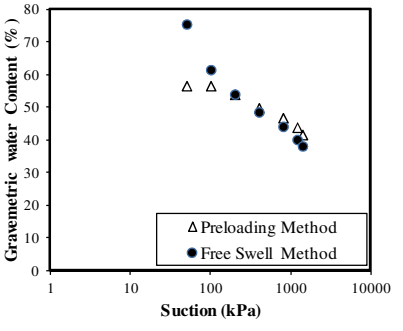

Fig. 3. Effect of saturation procedure on the SWCC(w) of expansive clay under vertical stress of 4 kPa.

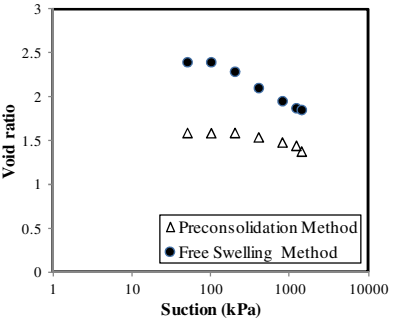

Fig. 4. Soil Variation of void ratio with suction for Al-Qatif soil under different saturation procedures.

3.2 Effect of Vertical Stress on SWCCs

SWCCs of expansive clay samples in terms of gravimetric water content and degree of saturation [hereinafter referenced as SWCC(S)] are presented in Fig. 5 and Fig. 6; respectively. From these figures, it is evident that the vertical stress has a notable effect on the SWCCs. At any specific suction, as vertical stress increases, gravimetric water content and degree of saturation decreases. This indicates that the combined application of vertical stress and suction result in the expulsion of more water than in the case of application of suction alone. It should be noted that the vertical stress effect is more pronounced in case of SWCC(w) than SWCC(S). One exception to the aforementioned observation is the SWCC(S) under low vertical stress (i.e., 4 kPa) where the shape of the SWCC(S) is different from that observed under vertical stress of 300 and 600 kPa. This is because, under suction 50 kPa, water was observed to enter the sample accompanied by sample swelling. This resulted in initial changes in void ratio which subsequently affected the shape of the SWCC.

The air entry value deduced from SWCCs(W) is less than that deduced from SWCCs(S). Air entry value deduced from SWCCs(w) is in the range 300 – 400 kPa. For SWCCs(S), the air entry value range between 800 and 1100 kPa. In case of soil samples with minimum volume change, these two values should be the

same. However for expansive soils that undergo considerable swelling and shrinkage, changes in water content under suction is also accompanied by volume (void ratio) change causing the samples to de-saturate under higher suction level.

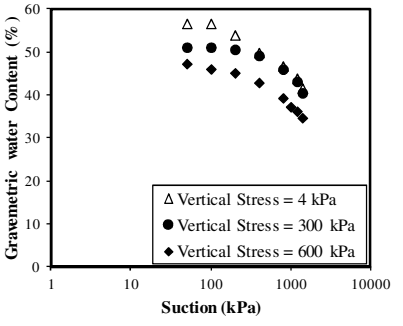

Fig. 5. SWCC(w) of expansive clay under different vertical stress.

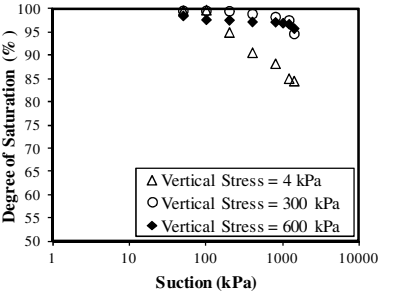

Fig. 6. SWCC(S) of expansive clay under different vertical stress.

4 Conclusions

Based on this study, the following conclusions can be derived:

- Measures should be considered for the reduction of soil adhesion to test ring to minimize the development of circumferential cracks and to produce intact samples for the proper determination of soil volume.
- Image processing can be used a simple technique to estimate the sample lateral changes due to application of suction.
- Air entry value deduced from SWCC(w) was less than that observed from SWCC(s). This is attributed to the expulsion of water from samples during the application of suction accompanied by reduction in sample volume (i.e., void ratio).
- Vertical stress has a notable effect on the SWCCs of expansive clay whether in terms of gravimetric water content or degree of saturation. However, the vertical stress effect is more pronounced for SWCCs(w).

Acknowledgements. This study was supported by Eng. Abdullah Bugshan Research Chair in Expansive Soils, Civil Engineering Department, King Saud University.

References

Abbaszadeh, M.M., Houston, S., Zapata, C., Houston, W., Welfert, B., Walsh, K.: Laboratory determination of soil-water characteristic curves for cracked soil. In: 5th International Conference on Unsaturated Soils, Barcelona, pp. 409–415. Taylor & Francis Group, London (2010)

Abduljuawad, S.N., Hameed, R.A., Al-Sulaimani, G.J., Basunbal, I.A., Safar, M.M.: Expansive soils in Eastern Province of Saudi Arabia. In: Proceedings of 7th International Conference on Expansive Soils, Dallas, TX, vol. 1, pp. 426–431 (1992)

Al-Shayea, N.: The combined effect of clay and moisture content on the behavior of remolded unsaturated soils. Engineering Geology 62, 319–342 (2001)

ASTM D4546, Standard Test Methods for One-Dimensional Swell or Settlement Potential of Cohesive Soils, West Conshohocken, PA (2008)

ASTM D6836-02, Standard Test Methods for Determination of the Soil Water Chararcteristic Curve for Desorption Using a Hanging Column, Pressure Extractor, Chilled Mirror Hygrometer, and/or Centrifuge, vol. 15.09, Annual book of ASTM Standards, West Conshohocken, PA (2008)

Azam, S.: Influence of mineralogy on swelling and consolidation of soils in eastern Saudi Arabia. Canadian Geotechnical Journal 40, 964–975 (2003)

Azam, S.: Large-scale oedometer for assessing swelling characteristics and consolidation behavior of Al-Qatif clay. In: Expansive Soils: Recent Advancement in Characterization and Treatment, pp. 85–99. Taylor and Francis Group, London (2006)

Azam, S., Abduljauwad, S.N., Al-Shayea, N.A., Al-Amoudi, O.S.B.: Expansive characteristics of gypsiferous/anhydritic formations. Engineering Geology 51, 89–107 (1998)

Chao, K.C., Durkee, D.B., Miller, D.J., Nelson, J.D.: Soil retention characteristics for expansive soils. In: Proceedings of the Thirteenth Southeast Asian Geotechnical Conference, Taipei, Taiwan (November 1998)

Chao, K.C., Nelson, J.D., Overton, D.D., Cumbers, J.M.: Soil water retention curves for remolded expansive soils. In: Toll, D.G., Augarde, C.E., Gallipoli, D., Wheeler, S.J. (eds.) Unsaturated Soils: Advances in Geo-Engineering, Proceedings of the 1st European Conference, E-UNSAT 2008, Durham, United Kingdom, July 2-4, pp. 243–248. Taylor & Francis (2008)

Fredlund, D.G., Raharjo, H.: Soil Mechanics for Unsaturated Soils. Wiley Interscience, New York (1993)

Li, L., Sun, D., Sheng, D., Sloan, S., Fredlund, D.: Preliminary study on soil water characteristics of Maryland clay. In: Proceedings of the 3rd Asian Conference on Unsaturated Soils, Nanjing, China, pp. 569–574 (2007)

Miao, L., Liu, S., Lai, Y.: Research of soil characteristics and shear features of Nanyang expansive soils. Engineering Geology 65, 261–267 (2002)

Mitchell, J.K.: Fundamentals of Soil Behavior. John Wiley & Sons (1993)

Nowamooz, H., Masrouri, F.: Relationship between soil fabric and suction cycles in compacted swelling soils. Engineering Geology 114, 444–455 (2010)

Peron, H., Hueckel, T., Lyesse, L.: An improved volume measurements for determining soil water retention curves. Geotechnical Testing Journal, ASTM 30(1), 1–8 (2006)

Pham, H.Q., Fredlund, D.G., Padilla, J.M.: Use of the GCTS apparatus for the measurement of soilwater characteristic curves. In: 57th Canadian Geotechincal conference, 5th Joint IAH-CNC/CGS Conference, Quebec, Canada, October 24-27, pp. 1–6 (2004)

Simms, P.H., Yanful, E.K.: Predicting soil water characteristic curves of compacted plastic soils frommeasured pore-size distributions. Geotechnique 52(4), 269–278 (2002)

Vanapalli, S.K., Pufahl, D.E., Fredlund, D.G.: The effect of stress on the soil-water characteristic behavior of a compacted sandy clay till. In: 51st Canadian Geotechnical Conference, Edmonton, pp. 81–86 (1998)

Role of the Soil Mineralogy on the Temperature Dependence of the Water Retention Curve

Bertrand François and Sana Ettahiri

Abstract. This paper presents experimental results of water retention curves of a compacted clay silt at different temperature. For limited suction values (up to 220 kPa), the results show a significant effect of the temperature variation (from 22°C to 50°C) on the water content at constant suction. This effect cannot be exclusively attributed to the thermal decrease of the surface tension of water. Through this study, the thermal decrease of the thickness of the diffuse double layer around the clay particles is assumed to be the most significant effect that explains the decrease of water retention capability when temperature increases. With this approach, the temperature effect on the water retention curve of any clayey soil can be estimated from the mineralogical composition of the soil. This theory is applied on five different clayey soils.

Keywords: degree of saturation, suction, temperature, diffuse double layer.

1 Introduction

The recent developments in the field of unsaturated soils have underlined the key role of the water retention curve on the mechanical behaviour of an unsaturated soil. So, it is essential to quantify the amount of water stored in an unsaturated soil as a function, not only of the suction, but also of additional environmental parameters (Gallipolli et al. 2003, Nuth & Laloui 2008, François & Laloui 2008).

Two main effects may significantly modify the water retention curve of a soil: the deformation and the temperature. The effect of soil deformation on the water

Bertrand François
Université Libre de Bruxelles, Brussels, Belgium
e-mail: bertrand.francois@ulb.ac.be

Sana Ettahiri
Université Libre de Bruxelles, Brussels, Belgium
e-mail: sana.ettahiri@ulb.ac.be

retention curve is mainly related, at the micro-scale, to the change in the dimensions of voids. The smaller the pores, the higher the suction that the capillary meniscus can sustain before air enters the pores. The effect of temperature on the water retention curve is more complex. It is the consequence of several physical mechanisms that act at the particle scale. These phenomena are related to the role of temperature on the capillary mechanisms, on the short-range solid-liquid interaction or on the phase change mechanisms (Romero et al. 2003). This paper focuses exclusively on this thermal influence on the water retention curve. It is suggested, and demonstrated, that the main thermal effect is probably related to the evolution of the thickness of the diffuse double layer with temperature.

2 Experimental Results

A series of water retention curves of a compacted clay silt have been obtained at three different temperatures (22°C, 35°C and 50°C) with pressure plate apparatus. The tested soil is a clayey silt (classification USCS: CL-ML) from the region of Namur in Belgium, called Marches-les-Dames (MLD). Its index properties are: w_L=28.4%, I_P= 8.8%. The clayey fraction represents 23%, the silty one 67% and the sandy one 10%. The samples have been compacted upon the optimum standard Proctor conditions $\gamma_{d,opt}$ = 18.4 kN/m^3 and w_{opt} = 14.8%. After resaturation with a low positive water pressure (10 kPa), the pressure plate apparatus have been placed in temperature-controlled chambers regulated at 22°C, 35°C and 50°C. Suction has been applied step by step until a suction of 400 kPa.

Fig. 1 represents the obtained water retention curve in terms of water content as a function of the applied suction. For the limited suction values applied in this experimental program, the results show a significant effect of the temperature variation on the degree of saturation at constant suction. The experimental points are fitted with the analytical expression of Van Genuchten (1980).

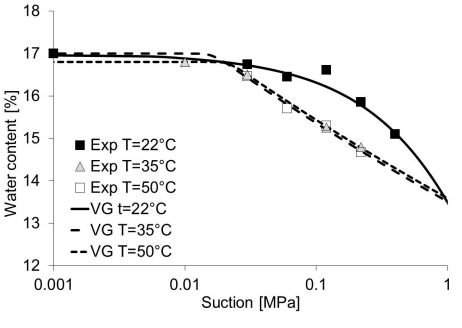

Fig. 1. Water retention curve of the compacted MLD clayey silt obtained at 22, 35 and 50°C. Fitting with the expression of Van Genuchten (1980) (VG).

3 Thermal Degradation of Water Retention Capacity

The retention capability of a soil, at a micro-scale, results from the equilibrium between stresses in fluid phases, capillary forces acting at the interface of each phase and attractive forces between water and particles. A change of temperature induces a modification of the properties of the different phases and also of their interfaces. Some thermal effects will dissipate with time by means of the diffusion of fluid phases (short term effects), while other effects directly affect the intrinsic properties of materials and are not dampened with time (long term effects), except if the temperature recovers its initial value (François 2008).

First, because water dilates more than the solid skeleton, water phase occupies proportionally more pore space when temperature increases. However, this effect is dampened with time when a new equilibrium is reached after diffusion of the excess of water in the voids. Also, during soil heating, the thermal decrease of the solubility of air in water produces the release of a quantity of air from water. Consequently, it may decrease the proportion of water in the voids. However, through air diffusion, this effect can also dissipate with time.

A well-known effect is related to the thermal decrease of the surface tension between air and water phases. Through the Young-Laplace equation, the decrease of surface water-air tension with temperature decreases the radius of the meniscus. As a consequence, some pores which were water-filled at ambient temperature can be drained at elevate temperature. It causes the degree of saturation to decrease.

Finally, in clayey soils, water can also be stored in the diffuse double layer of the clay platelets. In that zone, the cations of water are strongly attracted by the particle. The thickness of this diffuse double layer is affected by temperature. Mitchell (1976) defined a quantity that is a good approximation of the measure of the thickness of the double layer. This quantity is proportional to the square root of "the dielectric constant (D) of water multiplied by the temperature (T) in Kelvin". When temperature increases, the product $D \times T$ drops which induces a degradation of the diffuse double layer. So, the retention capability of water in the vicinity of the clay platelet decreases with temperature.

Table 1 summarize the quantification of the four main thermal effects in terms of the degree of saturation decrease for a temperature variation from 0°C to 60°C.

4 Applications

In this section, the focus is on the thermal degradation of the diffuse double layer. To do so, there are several uncertainties that need to be approximated. Indeed, the objective of this study is not to bring a rigorous quantitative approach, but rather to give a qualitative proof that the thermal degradation of the double layer is probably the most significant effect that explains the decrease of the retention capability of soils with temperature (as already suggested by Table 1). At that scale of the problem, the amount of water stored in the diffuse double layers depends on the

thickness of the diffuse layer and the specific surface of the soil. The thickness of the diffuse layer depends on many parameters of the solution and of the clay mineral (Mitchell 1976). At ambient temperature and for usual electrolyte concentration in water, a thickness of 60 Å is a good approximation. The specific surface of the soil particles can be obtained as a function of the mineralogy of the clay. Table 2 summarizes the specific surface of the main clay minerals.

Table 1. Quantification of the different thermal effects on the evolution of the degree of saturation at constant suction (François 2008).

Thermal effect	Variation of S_r for a ΔT from 0°C to 60°C
Thermal dilation (Short term)	$\Delta Sr = 2.16$ %
Air solubility in water (Short term)	$\Delta Sr = 1.24$ %
Surface tension of water (Long term)	$\Delta Sr = 1$ to 3 % depending on the pore size distribution of the material.
Diffuse double layer (Long term)	$\Delta Sr = 4$ % if all the water is included in the diffuse double layer

Table 2. External specific surface of the main clay minerals (Morel 1996).

Clay mineral	External specific surface [m^2/g]	
	Range of variation	Average value
Illite	80-120	100
Vermiculite	40-70	57.5
Kaolinite	10-30	20
Chlorite	100-175	137.5
Montmorillonite	80	80

The water content stored in the diffuse double layer is:

$$w_{DDL} = \left(\sum_i p_i SS_i \right) t_{DDL} \rho_w \tag{1}$$

where p_i and SS_i are, respectively, the mass proportion and the specific surface of the clay mineral i. t_{DDL} is the thickness of the diffuse double layer (assumed = 60 Å = 6.10^{-9} m) and ρ_w is the bulk density of water (=10^6 g/m^3).

The total variation of the water content dw with temperature changes dT can be considered by the sum of the effects of the variation of surface tension $d\sigma_s$ of air/water interface (as deduced analytically by Salager et al. 2010) and the evolution of the thickness of the double layer (linked to the square root of DxT), the second effect being the most significant in clay:

$$dw = dw_{\sigma_s} + dw_{DDL} = -\frac{s}{F_w \sigma_s} \frac{d\sigma_s}{dT} dT + \left(\sum_i p_i SS_i \right) \rho_w t_{DDL} \frac{d\left((DT)^{1/2} \right)}{dT} dT \tag{2}$$

Table 3. Clay mineralogy of the different soils addressed in the next part.

	Soil	Authors	Clay mineralogy
(a)	MLD (clayey silt)	This study	Illite: 12%; Vermiculite: 9%; Kaolinite: 4 %
(b)	Boom Clay	Romero et al. (2003)	Kaolinite: 29% ; Smectite: 22% ; Illite: 19%
(c)	FoCa Clay	Imbert et al. (2005)	Kaolinite: 42% ;Beidellite: 38% (≈ Smectite)
(d)	Clayey silty sand	Salager et al. (2010)	Smectite: 5% ; Chlorite: 5%
(e)	FEBEX Bentonite	Villar & Lloret (2004)	Smectite: 92%

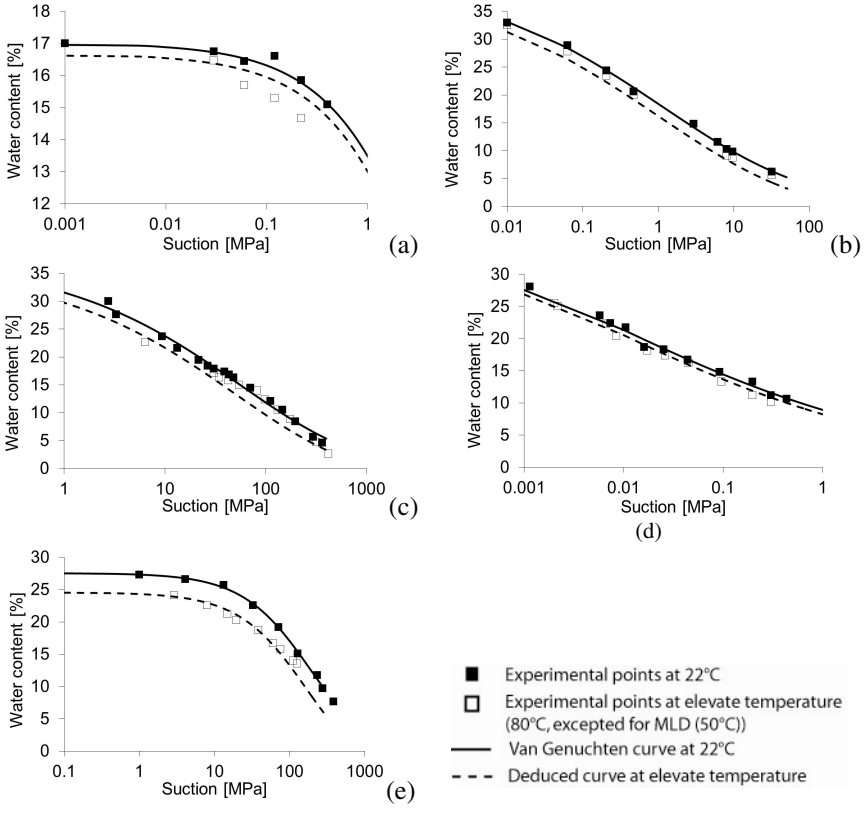

Fig. 2. Application of the proposed relation to deduce the effect of temperature on the water retention curve. The dashed line is deduced from the full line by equation (2). Experimental points: (a) MLD, (b) Boom Clay, (c) FoCa Clay, (d) Clayey silty sand, (e) FEBEX bentonite.

where F_w is the derivative of the matric suction as a function of w. In the following, Equation (2) is tested on five different soils, the mineralogical compositions of which are reported in Table 3.

In Fig. 2, the obtained results at ambient temperature have been fitted with the Van Genuchten analytical expression. Then, from equation (2), the curve at

elevate temperature has been obtained. It reveals the very good agreement between the theoretical development and the experimental observations. The soils having the larger specific surface exhibit a stronger thermal effect on their water retention curve. In particular, the FEBEX bentonite (Fig. 2e) shows a decrease of the water content of about 4% upon heating up to 80°C at constant suction. On the contrary, the clayey silty sand (Fig 2d), having a low specific surface; shows a limited effect of temperature on the water retention curve.

5 Conclusions

The thermal decrease of the water retention capacity of soils is usually explained by the temperature-dependence of the surface tension of water. However, in clayey soil, this is probably not the most significant effect. The role of the temperature on the thickness of the diffuse double layer surrounding the clayey platelets is probably predominant. This thickness decreases of about 4% when temperature increases from 20°C to 80°C. It may seem insignificant but when the most part of the pore water is included in the diffuse double layer (as it is the case in dense clay), this is the main mechanism that explains the loss of water upon heating at constant suction. This hypothesis has been verified by applying it on five different soils for which water retention curves at two temperatures were available. Also, a new series of experimental curves have been obtained on a compacted clayey silt at three temperatures that confirms the suspected phenomenon.

References

Gallipoli, D., Wheeler, S.J., Karstunen, M.: Modelling the variation of degree of saturation in a deformable unsaturated soil. Géotechnique 53(1), 105–112 (2003)

François, B.: Thermo-plasticity of fine-grained soils at various saturation states: Application to nuclear waste disposal. PhD Thesis No. 4188, EPFL, Lausanne (2008)

François, B., Laloui, L.: ACMEG-TS: A constitutive model for unsaturated soils under non-isothermal conditions. Int. J. Num. Anal. Meth. Geomech. 32, 1955–1988 (2008)

Imbert, C., Olchitzky, E., Lassabatère, T., Dangla, P., Courtois, A.: Evaluation of a thermal criterion for an engineered barrier system. Engineering Geology 81, 269–283 (2005)

Mitchell, J.: Fundamentals of Soil Behavior. Wiley (1976)

Morel, R.: Les sols cultivés. Lavoisier, Paris (1996)

Nuth, M., Laloui, L.: Advances in modelling hysteretic water retention curve in deformable soils. Computers and Geotechnics 35(6), 835–844 (2008)

Romero, E., Gens, A., Lloret, A.: Suction effects on a compacted clay under non-isothermal conditions. Géotechnique 53(1), 65–81 (2003)

Salager, S., El Youssoufi, M.S., Saix, C.: Effect of temperature on water retention phenomena in deformable soils: theoretical and experimental aspects. European J. Soil Sc. 61, 97–107 (2010)

van Genuchten, M.T.: A closed-form equation for predicting the hydraulic conductivity of unsaturated soils. Soil Science Society of America Journal 44, 892–898 (1980)

Villar, M., Lloret, A.: Influence of temperature on the hydro-mechanical behaviour of a compacted bentonite. Applied Clay Sciences 26, 337–350 (2004)

Water Retention Properties of Two Deep Belgian Clay Formations

Analice Lima, Enrique Romero, Yessenia Piña, Antonio Gens, and Xiangling Li

Abstract. Belgium investigates the design for disposal of its high-level radioactive waste in two deep clay formations: the Boom clay at Mol, considered the reference host formation, and Ypresian clay at Kallo that is the alternative one. High suctions develop as a consequence of sample retrieval, which affect the hydro-mechanical response of these materials. The water retention properties of both clays, covering a wide suction range and using different complementary techniques, are presented and discussed.

Keywords: deep clay formations, water retention properties, microstructure.

1 Introduction

Boom clay (located between 160 and 270 m deep) is considered the Belgian reference host formation for disposal of high-level radioactive wastes and the objective of extensive research programmes. Ypresian clay (located between 300 and 450 m

Analice Lima
Universitat Politècnica de Catalunya, Barcelona, Spain
e-mail: analicelima@hotmail.com

Enrique Romero
Universitat Politècnica de Catalunya, Barcelona, Spain
e-mail: enrique.romero-morales@upc.edu

Yessenia Piña
Universitat Politècnica de Catalunya, Barcelona, Spain
e-mail: p.yessenia@gmail.com

Antonio Gens
Universitat Politècnica de Catalunya, Barcelona, Spain
e-mail: antonio.gens@upc.edu

Xiangling Li
EIG EURIDICE, Mol, Belgium
e-mail: xli@sckcen.be

deep) has been also recently considered. Particular attention has been focused on the water retention properties of these deep low-porosity formations for two main reasons. On one hand, high suctions develop as a consequence of sample retrieval, which affect the hydro-mechanical response of these materials. On the other hand and from an operational viewpoint, water retention properties have also been studied to better assess possible desaturation effects due to venting of the disposal facility galleries.

2 Tested Materials and Experimental Programme

Boom clay (Rupelian stage) consists mainly of clay minerals dominated by illite (20-30%), kaolinite (20-30%) and smectite (10%). The non-clayey fraction is dominated by quartz (25%) and feldspar. The Ypresian clay is also constituted by marine sediments deposited during the Ypresian stage. It presents a clay fraction of 45%. Smectite is the dominant phase (25%), followed by illite (15%) and a small amount of kaolinite and chlorite. Non-clayey fraction is constituted predominantly by quartz (45%) and feldspar (5%). The studied block and borehole samples of Boom and Ypresian clays were retrieved at depths of 223 m (Mol) and 350 m (Kallo), respectively. Table 1 summarises the basic characterisation, the main volumetric and gravimetric properties of the intact materials, which are lightly overconsolidated, as well as the water permeability properties. Ypresian clay displays a larger liquid limit and void ratio (despite being formed at a larger depth), which is consistent with the important smectite content.

In the case of Boom clay, the *in situ* condition at the sampling depth is characterised by a vertical total stress σ_{vi}=4.50 MPa and a water pressure u_{wi}=2.25 MPa (vertical effective stress σ'_{vi}=2.25 MPa). Lima (2011) reported a preconsolidation vertical effective stress σ'_{vmax}=5.2 MPa at the end of the deposition process that includes diagenesis and creep effects, resulting in an overconsolidation ratio *OCR*=2.3. Based on a drained friction angle of the natural material ϕ'=20° (Lima, 2011), the earth pressure coefficient at rest can be estimated as $K_0^{SC} = (1-\sin\phi')\sqrt{OCR} \approx 1$ (Della Vecchia et al., 2010). The mean effective stress at *in situ* condition is

$$p'_i = \frac{1}{3}\left(1+2K_0^{SC}\right)\sigma'_{vi} = 2.25\,\text{MPa} \tag{1}$$

Assuming a constant mean effective stress on sample retrieval ($\Delta p'$=0), the pore water pressure change can be estimated in Δu_w=-4.5 MPa with a final pore water pressure u_{wf}=-2.25 MPa, which in principle should be similar to the initial suction measured under laboratory conditions.

For Ypresian clay, the vertical stress and pore water pressure under *in situ* conditions are σ_{vi}=7.8 MPa and u_{wi}=4 MPa (σ'_{vi}=3.8 MPa). A vertical effective preconsolidation stress σ'_{vmax}=5.50 MPa is reported in Piña (2011), which results in an overconsolidation ratio (yield stress ratio) *OCR*=1.4. An earth pressure coefficient at rest K_0^{SC}≈0.85 was estimated considering ϕ'=16º (Nguyen, 2011) that

allowed the determination of the mean effective stress at *in situ* condition p'_i=3.4 MPa. The final pore water pressure after sample retrieval can be estimated in u_{wf}=-3.4 MPa.

The final pore water pressures induced on stress relief should be compared with the initial suctions reported in Table 1. In the case of Boom clay, a similar initial total suction was measured under laboratory conditions using psychrometers. For Ypresian clay, despite being retrieved at a larger depth, the measured initial total suction was somewhat lower (1.9 MPa). This fact is a consequence of the lower air-entry value of this clay (the final water pressure that was calculated based on stress relief considerations cannot be sustained under saturated conditions), which will be discussed in the next section.

Table 1. Main properties of Boom and Ypresian clays.

Property	Boom clay	Ypresian clay
Density, ρ *(Mg/m^3)*	around 2.05	1.97 to 2.02
Dry density, ρ_d *(Mg/m^3)*	1.65 to 1.67	1.55 to 1.60
Gravimetric water content, *w (%)*	around 25	26 to 26.6
Initial total suction, Ψ *(MPa)*	2.0-2.5	1.9
Density of soil solids, ρ_s *(Mg/m^3)*	2.67	2.76
Void ratio, *e*	0.60 to 0.62	0.72 to 0.78
Degree of saturation, S_r *(%)*	around 100	94 to 98
Liquid limit, w_L *(%)*	56	142 to 158
Plastic limit, w_p *(%)*	29	26
Vertical water permeability, $k_{w\,v}$ *(m/s)*	2.4×10^{-12}	6.6×10^{-12}
Horizontal water permeability, $k_{w\,h}$ *(m/s)*	4.3×10^{-12}	7.9×10^{-12}

Mercury intrusion porosimetry tests were performed on intact freeze-dried samples to characterise the pore network. Figure 1 presents the pore size distribution (PSD) curves of both clays. In the case of Boom clay, the plot shows one dominant pore mode at around 90 nm. On the contrary, Ypresian clay presents two dominant pore modes, one at 700 nm and another at 80 nm. This structural feature that has been consistently observed at different depths (Piña, 2011) is not typical for a deep clay formation that has undergone a depositional sequence similar to Boom clay. Larger water permeability values are expected for Ypresian clay (Table 1) not only as a consequence of its higher void ratio but also due to these macroporosity features. Water retention properties of Ypresian clay will be also affected due to its lower air-entry value, as discussed in the next section.

Water retention properties under unstressed conditions were determined using chilled-mirror dew-point (WP4, Decagon Devices Inc, USA) and transistor (SMI, Australia) psychrometers. The tests using WP4 were carried out following a multi-stage procedure, in which the same sample was first subjected to drying followed by wetting. Boom clay results were complemented with vapour equilibrium tests on samples installed in hermetic jars containing saline solutions.

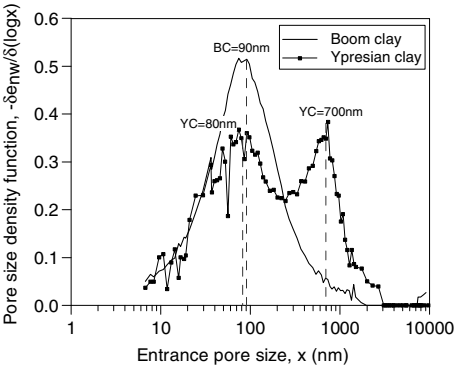

Fig. 1. Pore size distribution curves of Boom and Ypresian clays.

3 Experimental Results

Figure 2 summarises the water retention results obtained for Boom clay. Generally speaking, a good consistency in the results using different techniques is observed. Nevertheless, vapour equilibrium and transistor psychrometer results systematically lie below WP4 psychrometer readings. The systematic higher total suctions measured with WP4 psychrometer for a given water content can be explained in terms of the hydraulic paths undergone by the soil (drying) during the suction measurement process (Cardoso et al., 2007). Besides hydraulic hysteresis, volume change also affects the differences observed between drying and wetting paths. As observed in Figure 2a and with reference to SMI psychrometer readings on drying, important changes in water content occur when total suction is above 3-4 MPa, indicating some kind of air-entry value for Boom clay in terms of water content. For total suctions < 2.5 MPa, the material is under fully saturated conditions, since this value is the initial suction after sample retrieval (Table 1).

Figure 3 shows the water retention curve of Ypresian clay compared to Boom clay obtained with WP4 psychrometer readings. As indicated in Table 1, the initial water content of Ypresian clay is slightly larger, which is also reflected at the starting point –water storage capacity at saturation– of the drying curve (Fig. 3a). Ypresian clay also exhibits a larger water retention capacity in both wetting and drying paths, as a consequence of the smectite phase of the clay fraction. It also appears that Ypresian clay loses slightly larger water content (from the water storage capacity at saturation) when applying a total suction of 8 MPa (Fig. 3a). As also observed in Figure 3a, at a total suction around 3 MPa, an early desaturation process seems also to occur on Ypresian clay. This desaturation process is associated with the double porosity network detected on Ypresian clay and its effects on air-entry value (Fig. 1). To better interpret the consequences of this double porosity structure, Figure 4 plots the water retention curves estimated from mercury intrusion results in terms of water content (Romero & Simms, 2008). Boom clay displays an air-entry value consistent with the one estimated in terms of water content (Fig. 3a). Nevertheless, Ypresian clay presents a much lower air-entry value (around 0.4 MPa) associated with macropores, which affects the maximum total suction measured on the

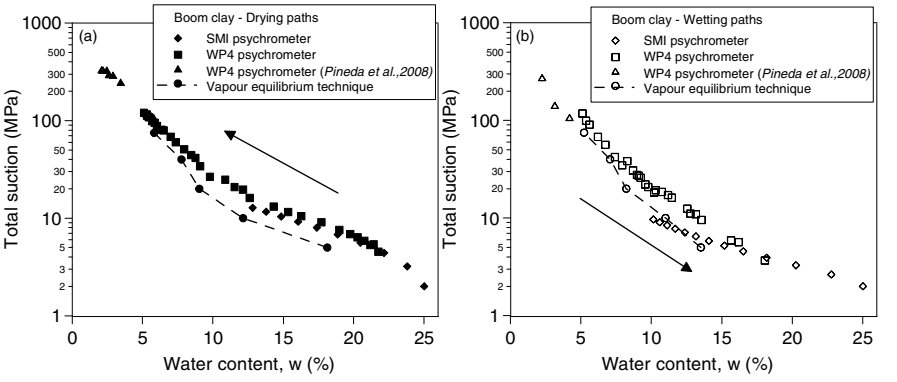

Fig. 2. Water retention curves of Boom clay. (a) Drying and (b) wetting paths.

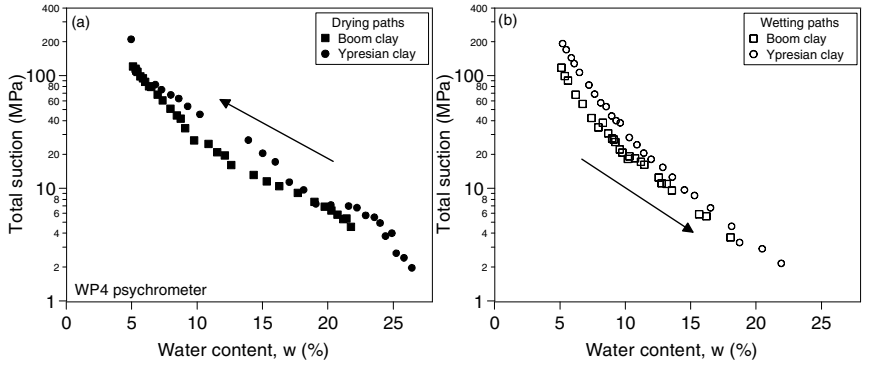

Fig. 3. Water retention curves of Ypresian and Boom clays. (a) Drying and (b) wetting paths.

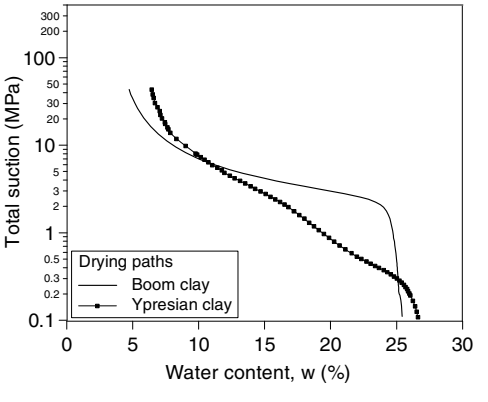

Fig. 4. Water retention curves estimated from MIP data.

retrieved material. The estimated pore water pressure of Ypresian clay after retrieval (-3.4 MPa) is higher (in suction terms) than the estimated air- entry value and cannot be sustained under saturated conditions. The estimated degree of saturation corresponding to a total suction of 3.4 MPa is around 90% (refer also to Table 1).

4 Conclusions

Two deep Belgian clay formations were studied from microstructural and water retention viewpoints. The clays, that share a common depositional sequence, display quite different microstructural features. Boom clay displays a dominant pore mode at 90 nm, whereas the deeper Ypresian clay presents two dominant ones (at 700 nm and 80 nm), which have important consequences on the hydraulic response of the material (slightly larger water permeability and lower air-entry value). The initial total suction is of importance when interpreting the state of these materials after retrieval. The estimated pore water pressure after Ypresian clay retrieval (-3.4 MPa) is higher (in suction terms) than the air-entry value and cannot be sustained under saturated conditions.

Acknowledgements. EIG EURIDICE and ONDRAF/NIRAS are gratefully acknowledged for funding the work presented in this paper.

References

Cardoso, R., Romero, E., Lima, A., Ferrari, A.: A comparative study of soil suction measurement using two different high-range psychrometers. In: Schanz, T. (ed.) Proc. 2nd Int. Conf. Mechanics of Unsaturated Soils, Weimar, Germany, pp. 79–93. Springer, Berlin (2007)

Della Vecchia, G., Lima, A., Jommi, C., Romero, E.: Some remarks on the hydro-mechanical constitutive modelling of natural and compacted Boom clay. In: Proc. 5th Int. Conf. on Unsaturated Soils, Barcelona, Spain, pp. 803–809. Taylor and Francis Group, London (2010)

Lima, A.: Thermo-hydro-mechanical behaviour of two deep Belgian clay formations: Boom and Ypresian clays. PhD Thesis. Universitat Politècnica de Catalunya, Spain (2011)

Nguyen, X.P., Cui, Y.J., Tang, A.M., Li, X.L.: THM behaviour of Ypresian clay. In: 3rd Ypresian Clay Meeting, Barcelona (December 2010)

Pineda, J., Lima, A., Romero, E.: Influence of hydraulic paths on the low-strain shear modulus of a stiff clay. In: Proc. 1st European Conf. Unsaturated Soils–Advances in Geo-engineering, Durham, United Kingdom, pp. 519–523. Taylor and Francis Group, London (2008)

Piña, Y.: Thermo-hydro-mechanical behaviour of Ypresian clay. MSc Thesis. Universitat Politècnica de Catalunya, Spain (2011)

Romero, E., Simms, P.H.: Microstructure investigation in unsaturated soils: A review with special attention to contribution of mercury intrusion porosimetry and environmental scanning electron microscopy. J. Geotechnical and Geological Engineering 26(6), 705–727 (2008)

Effect of Suction Changes on the Microstructure of Compacted Crushed Argillites under Constant-Volume Conditions

Qiong Wang, Chaosheng Tang, Anh-Minh Tang, and Yu-Jun Cui

Abstract. Crushed and compacted argillite extracted from Bure site (France) has been proposed as a possible sealing and backfilling material in the geological high-level radioactive waste disposal. In order to better understand its coupled hydro-mechanical behaviour in the real storage situation, changes in microstructure of two crushed argillites of different grain size distributions with decreasing suction under confined condition were investigated using mercury intrusion porosimetry (MIP). The results show that wetting under constant-volume condition reduces the size of macro-pores, without significantly affecting the micro-pores size. A clear effect of grain size distribution on the microstructure was also observed: two pore families were identified for the coarse soil; however, there was only one maro-pore family for fine soil (inter-aggregates pores).

Keywords: suction, microstructure, constant volume, MIP, pore size distribution.

1 Introduction

In most conceptual designs of the deep geological repository for high-level radioactive wastes, expansive clays are considered as engineering barrier materials,

Qiong Wang
Ecole des Ponts ParisTech, Paris, France
e-mail: wangq@cermes.enpc.fr

Chaosheng Tang
Nanjing University, Nangjing, China
e-mail: tangchaosheng@nju.edu.cn

Anh-Minh Tang
Ecole des Ponts ParisTech, Paris, France
e-mail: anhminh.tang@enpc.fr

Yu-Jun Cui
Ecole des Ponts ParisTech, Paris, France
e-mail: yujun.cui@enpc.fr

thanks to their low permeability, high swelling and high radionuclide retardation capacities (Pusch, 1979; Yong et al., 1986; Villar et al., 2008). In France, the crushed Callovo-Oxfordian (COx) argillite excavated from the Bure site of the ANDRA underground research laboratory - URL (-490 m, North-eastern France) was proposed as a possible sealing and backfill material, because of the following advantages: (i) it is more economical compared to the commercial bentonites to use local excavated argillite; (ii) the negative impacts on the environment is reduced by recycling the excavated material; (iii) there is better compatibility with host rock because of the same mineralogical and chemical compositions (Andra, 2005; Tang et al., 2011a; Tang et al., 2011b).

In the real repository, after the local groundwater redistribution the water in the host rock formation will move into the repository. Due to the restriction of the host formation, the clays cannot swell, resulting in the development of swelling pressure. The generated swelling pressure will then result in the soil microstructure changes. A good understanding of this micro-structure change is essential as it is directly related to the macroscopic engineering behaviour and physical properties of this material (Cui et al., 2002; Delage, 2007; Tang et al., 2011a).

This study focuses on the compacted crushed Callovo-Oxfordian (COx) argillite. Soils with two different grain size distributions were compacted, and then hydrated by different suctions (from 57 to 38 MPa) using the vapour equilibrium technique under constant volume conditions. After equilibrium, the microstructure was observed using mercury intrusion porosimetry (MIP), allowing the analysis of the effect of suction on the changes of micro-structure.

2 Materials and Experimental Methods

Callovo-Oxfordian (COx) argillite taken from the Bure site of the ANDRA URL was studied. It contains 40–45% clay minerals (mainly interstratified minerals illite–smectite), 20–30% carbonates and 20–30% quartz and feldspar (Hoteit et al., 2000; Lebon & Ghoreychi, 2000; Zhang et al., 2004). The in-situ water content is 2.8–8.7 %; the bulk density is 2.32–2.61 Mg/m3 and the specific gravity is 2.70 (Fouché et al., 2004; Tang et al., 2011a).

The excavated argillite was air-dried and crushed following two different procedures, leading to two soils: (1) the coarse soil with the maximum grain size of 8 mm; its air-dried water content was 2.8%; (2) the fine soil with the maximum grain size of 0.25 mm; its air-dried water content was 2.4%. The grain size distributions of the two soils determined by dry sieving are presented in Fig.1; the coarse soil contains 18% fine grains (0.08 mm) while the fine soil contains 70% fine grains. The grain size distribution determined by sedimentation is also presented in Fig.1, the two curves are similar, and it confirms that about 40% grains are clay particles (< 2 μm).

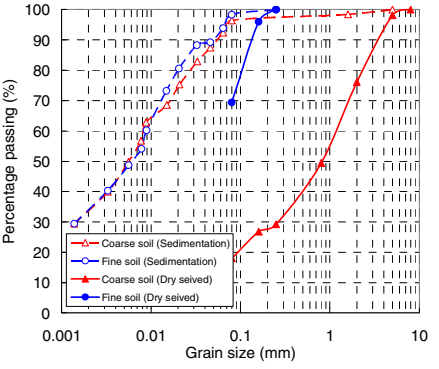

Fig. 1. Grain size distribution of crushed COx argillite.

MIP tests were performed on samples hydrated with different suctions under constant-volume conditions to analyse the soil microstructure changes with suction. The air dried soil was firstly statically compacted to a dry density of 2.0 Mg/m3 (e = 0.35), with an initial suction of about 150 MPa (measured by a relative humidity sensor). Then, the sample was hydrated under constant volume conditions at different suctions using the vapour equilibrium technique. After equilibrium, the sample was cut to small sticks and freeze-dried. Mercury intrusion was then performed by progressively increasing mercury pressure, and the volume of the pores penetrated during the increase in pressure is continuously monitored (see Delege & Lefevbre, 1984; Cui et al., 2002., Tang et al., 2011a for more details).

3 Results and Discussion

The results of the coarse soil at different suctions are presented in Fig. 2. It is observed that the final values of intruded mercury void ratio (e_m) are lower than the soil void ratio (e = 0.35). This is mainly attributed to the limited range that the MIP technique can cover. For the high-plasticity soils, there is a significant pore volume (entrance diameter smaller than 6 nm) that the mercury could not penetrate to (Delage et al., 2006). The same phenomenon was noted by Lloret et al. (2003) in the pore size distribution curve of compacted Almeria clay (Spain), due to an important amount of pores of very small entrance diameter; the total intra-aggregated void ratio appears to be much larger than the intruded one. Comparison of the curves at three suctions shows that with decreasing suction, (150 MPa, 57 MPa, and 38 MPa), the amount of accessible porosity decreases, indicting that during wetting (suction decrease) under constant-volume conditions, the macro-pore is filled by small clay particles (Cui et al., 2002).

Fig. 3 presents the pore size distribution curves, $de_m/dlog(d)$ versus log(d), of the coarse soil for different suctions. At the initial state (s = 150 MPa, ρ_d = 2.0 Mg/m^3, e = 0.35), two pore populations are observed, that are micro-pores (having a mean size of 0.03 μm) and macro-pores (having a mean size of 1.5 μm)

(Fig.3). The decrease of suction leads to a slight change in micro-pores size, but a significant change of the macro-pores family (Fig.3): the application of a suction of 57 MPa decreases the modal size of macro-pores to 1.0 µm; a subsequently decrease of suction to 38 MPa reduces the macro-pores size to 0.8 µm. Similar phenomenon was also observed by Cui et al. (2002) who investigated the microstructure changes of Kunigel/sand mixture with suction under constant-volume conditions. The results show the decrease in inter-aggregate pore size with decreasing suction. It confirms the conclusion that wetting under constant volume conditions leads to clay aggregate hydration, and exfoliation phenomenon occurs around the macro-pores leading to the clogging of macro-pores.

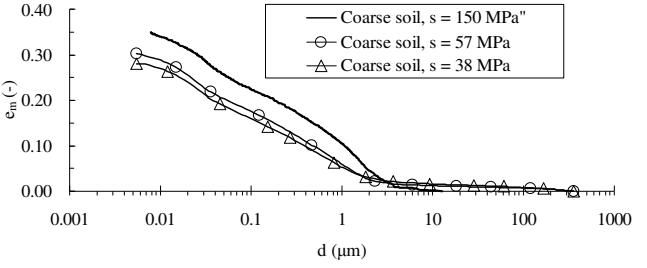

Fig. 2. Intruded mercury void ratio versus pore size for coarse soil.

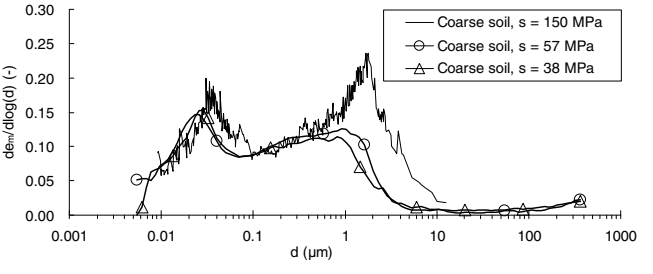

Fig. 3. Pore size distribution curves of coarse soil at different suction.

The results obtained on the fine soil are presented in Fig. 4 and Fig. 5. In the e_m - log (d) plot (Fig. 4), a lower value of e_m compared to the global void ratio of the soil (e = 0.35) was obtained due to the limited range of the MIP technique as for the coarse soil; with decreasing suction, the amount of accessible porosity decreases as the macro-pore is filled by small clay particles. However, in the $de_m/dlog(d)$ versus log(d) plot (Fig. 5), different phenomenon was observed for the fine soil: there is only one pore family with a mean size of 0.4 µm at the initial state (s = 150 MPa), that also corresponds to the macro-pores family (inter-aggregates pores), the micro-pores (intra-aggregates pores) are not clearly observed. It indicts the obvious effect of grain size distribution on the microstructure: for the finer soil, the intra-aggregate pores would be hidden by the inter-aggregate

pores having similar size because of the large amount of fine grains created during crushing (see Fig.1). With the subsequent decrease of suction, the macro-pores size reduces to 0.2 µm and 0.15 µm at suction of 57 MPa and 38 MPa (Fig.5) respectively, showing the clogging of macro-pores upon wetting.

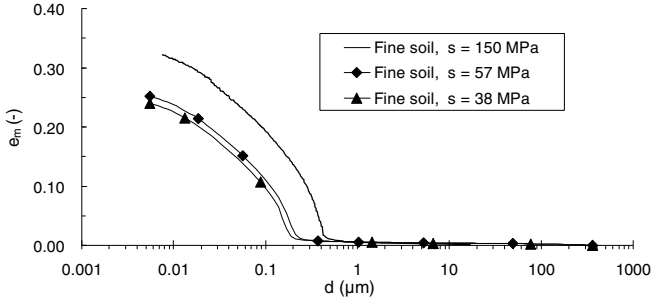

Fig. 4. Intruded mercury void ratio versus pore size for fine soil.

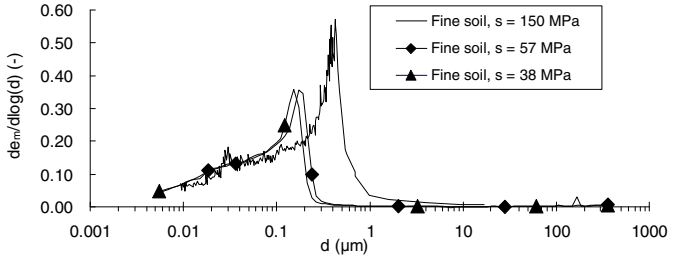

Fig. 5. Pore size distribution curves of fine soil at different suction.

4 Conclusion

In order to better understand the coupled hydro-mechanical behaviour of the compacted expansive soil used as sealing and backfill material in the deep geological repository for high level radio-active wastes, the microstructure changes of crushed COx argillites (having two different grain size distributions) with decreasing suction under confined conditions are investigated using mercury intrusion porosimetry (MIP). The results show that under constant-volume conditions, decreasing suction reduces the size of macro-pores, but the changes in micro-pores size being not significant. A clear effect of grain size distribution on the microstructure was also observed, two pore families (macro-pores and micro-pores) were identified for coarse soil. By contrast, there was only one pore family for the fine soil (macro-pores) because of the large amount of fine grains produced during crushing.

References

Andra: Référentiel des matériaux d'un stockage de déchets à haute activité et à vie longue – Tome 4: Les matériaux à base d'argilites excavées et remaniées. Rapport Andra No. CRPASCM040015B (2005)

Cui, Y.J., Loiseau, C., Delage, P.: Microstructure changes of a confined swelling soil due to suction controlled hydration. In: Unsaturated Soils: Proceedings of the Third International Conference on Unsaturated Soils, UNSAT 2002, Recife, Brazil, March 10-13, p. 593. Taylor & Francis (2002)

Delage, P., Marcial, D., Cui, Y.J., Ruiz, X.: Ageing effects in a compacted bentonite: a microstructure approach. Geotechnique 56(5), 291–304 (2006)

Delage, P.: Microstructure features in the behaviour of engineered barriers for nuclear waste disposal. In: Springer Proceedings in Physics, vol. 112, p. 11 (2007)

Fouché, O., Wright, H., Le Cléac'h, J.M., Pellenard, P.: Fabric control on strain and rupture of heterogeneous shale samples by using a non-conventional mechanical test. Applied Clay Science 26(1-4), 367–387 (2004)

Hoteit, N., Ozanam, O., Su, K.: Geological Radioactive Waste Disposal Project in France: Conceptual Model of a Deep Geological Formation and Underground Research Laboratory in Meuse/Haute-Marne Site. In: The 4th North American Rock Mechanics Symposium, Seattle, July 31-August 3 (2000)

Lebon, P., Ghoreychi, M.: French Underground Research Laboratory of Meuse/Haute-Marne: THM Aspects of Argillite Formation. In: EUROCK 2000, Aachen, pp. 27– 31 (2000)

Lloret, A., Villar, M.V., Sanchez, M., Gens, A., Pintado, X., Alonso, E.E.: Mechanical behaviour of heavily compacted bentonite under high suction changes. Géotechnique 53(1), 27–40 (2003)

Pusch, R.: Highly compacted sodium bentonite for isolating rock-deposited radioactive waste products. Nucl. Technol, United States 45(2), 153–157 (1979)

Tang, C.S., Tang, A.M., Cui, Y.J., Delage, P., Barnichon, J.D., Shi, B.: A study of the hydro-mechanical behaviour of compacted crushed argillite. Engineering Geology 118(3-4), 93–103 (2011a)

Tang, C.S., Tang, A.M., Cui, Y.J., Delage, P., Schroeder, C., De Laure, E.: Investigating the Swelling Pressure of Compacted Crushed-Callovo-Oxfordian Argillite. Physics and Chemistry of the Earth (special issue) (2011b) (in press)

Villar, M.V., Lloret, A.: Influence of dry density and water content on the swelling of a compacted bentonite. Applied Clay Science 39(1-2), 38–49 (2008)

Yong, R.N., Boonsinsuk, P., Wong, G.: Formulation of backfill material for a nuclear fuel waste disposal vault. Canadian Geotechnical Journal 23(2), 216–228 (1986)

Zhang, C.L., Rothfuchs, T.: Experimental study of the hydro-mechanical behaviour of the Callovo-Oxfordian argillite. Applied Clay Science 26, 325–336 (2004)

Water Retention Properties and Microstructure of Compacted Expanded Perlite

Marco Caruso and Donatella Sterpi

Abstract. A double porosity structure is recognized in compacted expanded perlite, a granular material made from crushed perlite rock subjected to heating treatment. Due to its generation process, each grain has a micro-scale porosity network and a series of closed pores (isolated holes), while particle size distribution is highly uniform. An experimental investigation combining water retention tests and mercury intrusion porosimetry is presented. The results allowed for a detailed description of the double porosity system and retention properties and may represent a basis for a future contribution on hydraulic and mechanical aspects of the behaviour of double porosity materials.

Keywords: perlite, double porosity, SWRC, axis translation, filter paper, MIP.

1 Introduction

Compacted soils have been largely recognized (Tarantino, 2010) to exhibit a double porosity structure, or aggregated structure, strongly affecting the hydraulic and mechanical behaviour in unsaturated condition (fig. 1*a*). The dimensions of aggregates and of inter- and intra-aggregate pores are strongly influenced by the compaction water content and the compactive effort (Birle et al. 2008).

A double porosity structure has also been observed in compacted expanded perlite. Perlite (Roulia et al. 2006) is a glass volcanic rock of rhyolitic composition containing 2-5 % of combined water. Expanded Perlite is the result of a rapid heating to a suitable point in softening range (800-1100°C) during which water recombines, vaporises and the steam expands the softened material thus creating a

Marco Caruso
Politecnico di Milano, Milano, Italy
e-mail: caruso@stru.polimi.it

Donatella Sterpi
Politecnico di Milano, Milano, Italy
e-mail: sterpi@stru.polimi.it

foamy structure and decreasing the original density and heat conductivity (Zhäringer et al. 2001). In the compacted material an intra-grain and inter-grain porosity system can be identified (fig 1*b*). The intra-grain pores can be interconnected each other and with the outside or can be in form of occluded pores inside the grain itself.

Besides the different industrial application (e.g. component of soilless growing mixes to provide better aeration and optimum moisture retention for superior plant growth, loose-fill insulation in masonry construction, filters for reducing suspended soil loads and concentration in urban runoff) Georgopoulos & Vardoulakis (2006) and Jamei et al (2011), among others, recognized expanded perlite as a model material to be used in geotechnical research, due to its porous, soft, and crushable grains. Georgopoulos & Vardoulakis (2006) adopted expanded perlite to highlight the importance of grain stiffness and strength on the overall macroscopic strength of saturated specimen; Jamei et al (2011), focusing on unsaturated hydraulic behaviour, take advantage of it to analyse the evolution of water retention characteristics with crushing in a double porosity system. Holding that expanded perlite could be considered a resource in geotechnical experimental investigations, a preliminary set of experimental results is presented, aimed at analysing its microstructure and retention properties.

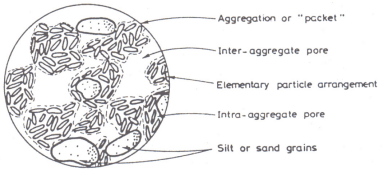

(a) after Alonso et al. (1987)

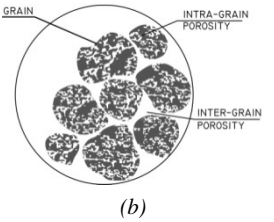

(b)

Fig. 1. Double porosity systems in compacted soil (a) and in compacted expanded perlite (b).

2 The Tested Perlite

The adopted perlite is a product by Perlite Italiana (Milano, Italy) named Peralit® 13. In commercial documentation, it is described to have a particle size distribution ranging between 0.1 and 1 mm in diameter. A first set of experimental investigation has been devoted to its classification following procedures customarily adopted for sandy soils.

The attempt to evaluate grain density with standard ASTM D854 picnometer method revealed some experimental problems due to grain floatation, the density of perlite grain being much lower than the density of distilled water.

Even so, according to Jamei et al. (2011) who indicated in a few seconds the time necessary for water to be absorbed by the grains, a procedure has been developed to provide a continuous mixing of water and floating perlite in order to allow penetration of water inside all pores exposed to the surface. This has led to an

estimation of $\gamma_s = 0.61$ g/cm^3. A further determination has been carried out considering the sole fraction passing ASTM 80 sieve (0.177 mm) of perlite crushed in a mortar, and leaving into the picnometer only the submerged solids by sucking up the remaining (small) floating portion. The grain density γ_s is now estimated to be 2.47 g/cm^3, very close to the undisturbed perlite rock density. This result seems to confirm the presence of unconnected voids inside the grain that the crushing procedure had almost cancelled. Therefore the total porosity of a compacted sample may be seen as a sum of two components. The first, n_o, groups all the occluded voids expected to belong to intra-grain level. The second, n_c, represents the connected ones which may be filled by a fluid flowing through the sample.

The grain size distribution curve has been evaluated by sieving, since the tendency to floatation does not permit to adopt the conventional procedure of sedimentation. The results presented in fig. 2 have been obtained for two different samples in order to identify possible grain crushing due to manipulation. The experimental particle size distribution lies within the range provided by the manufacturer. The grain size distribution is also compared with the one by Jamei et al. (2011) obtained from sieving and X-diffraction techniques on a perlite sample having 1 mm as maximum grain size. The comparison confirms that by the sieving procedure it is possible to describe a large part of the curve.

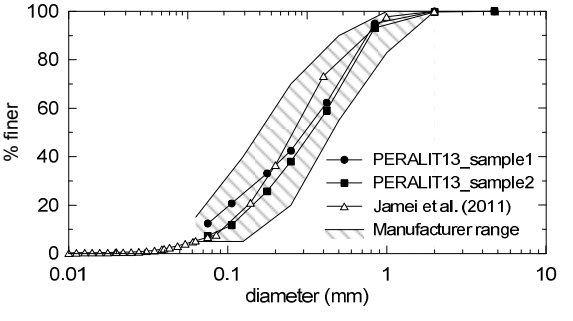

Fig. 2. Grain size distribution of Peralit 13.

3 Water Retention Curve

The drying soil water retention curve of perlite has been determined on compacted samples combining two techniques, axis translation and filter paper.

A modified pressure plate extractor (Caruso & Jommi 2012) equipped with a 500 kPa porous stone has been adopted to get SWRC points within the range 0-400 kPa. Calibrated Whatman no. 42 filter paper has been considered reliable for suction greater than 300 kPa. The results are presented in figure 3, where the bulk densities of each sample are also reported, evaluated considering only the connected portion n_c as total sample porosity and assuming it as the only one influencing the retention of water into soil. This assumption seems reasonable as far as

no crushing occurs during the SWRC test. A reasonable correlation can be observed between the values obtained from axis translation technique and filter paper, and a bimodal behaviour can be clearly recognized. A first rapid desaturation occurs in large pores followed by a desaturation of smaller voids when their air entry value is reached. An interpretation of the observed behaviour is given by way of Van Genuchten model as modified by Burger & Shackelford (2001):

$$w = \begin{cases} w_j + (w_s - w_j)\left[\dfrac{1}{1+(\alpha_M\, s)^{\lambda_M}}\right]^{(1-1/\lambda_M)} & s < s_j \\ w_r + (w_j - w_r)\left[\dfrac{1}{1+(\alpha_m\, s)^{\lambda_m}}\right]^{(1-1/\lambda_m)} & s \geq s_j \end{cases} \quad (1)$$

where subscript *M* and *m* identifies the parameters (α and λ) respectively describing the inter-grain and intra-grain region, w_s and w_r are the saturated and residual water content. At suction s_j, corresponding to a water content w_j complete desaturation of intra-grain voids occurs. Estimated parameters are reported in table 1.

A comparison between experimental data and some data from the literature, obtained for similar compacted perlite samples (but at different porosity) is shown in fig. 4. The experimental data confirm the already noticed bimodal behaviour and point out that the air entry suction for small pores appears to depend on density. This may be due to the grain limited stiffness, owing to a modification in intra-grain structure at the high compaction efforts necessary to obtain denser samples.

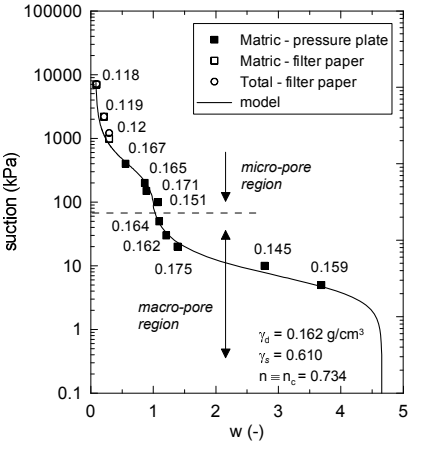

Fig. 3. SWRC for compacted perlite.

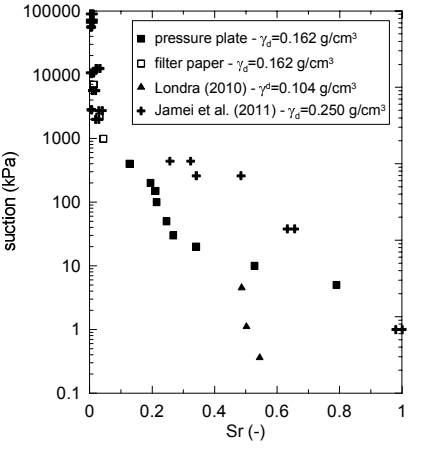

Fig. 4. SWRC of compacted perlite: comparison with literature data.

Table 1. Parameters (equation 1) associated with the model by Burger & Shackelford, 2001.

w_s	5.78	α_M	0.179 kPa^{-1}	α_m	0.0032 kPa^{-1}
w_r	0.075	λ_M	2.46	λ_m	2.5
w_j	1.03				

4 Microstructure

For the evaluation of pore size distribution of an "as compacted" oven dried sample (Romero & Simms 2008 for further references), a mercury intrusion porosimetry test (MIP) has been performed on 'Micromeritics-AutoPore IV' equipment, attaining maximum intrusion pressures of 220 MPa. Some experimental difficulties also arose, due the high brittleness of dry perlite samples. The pore size density function (PSD) is reported in figure 5. For consistency with previous analyses, the sole connected porosity network has been considered, thus assuming a solid density $\gamma_s = 0.61$ g/cm^3. The result clearly highlights the double porosity structure of the compacted perlite, characterized by inter-grain macropores ranging between 8 μm and 100 μm in diameter and intra-grain micropores whose diameter size is about 3.5 μm.

In the same figure 5 a comparison is also proposed with MIP data obtained by Jamei et al., 2011 (fig. 2). They considered a compacted sample whose grain size distribution is similar to the one of Peralit® 13 and reported a PSD obtained from MIP data assuming a porosity system formed by both n_o and n_c voids. Their experimental information is now reassessed following the approach herein proposed to assume only n_c as porosity and the consequent γ_s. The macropore dimension range appears to be the same for both samples, while the higher density seems to correspond to both a reduction in the number of large pores and a shrinkage of grain micropores whose average dimension decreases to about 2 μm.

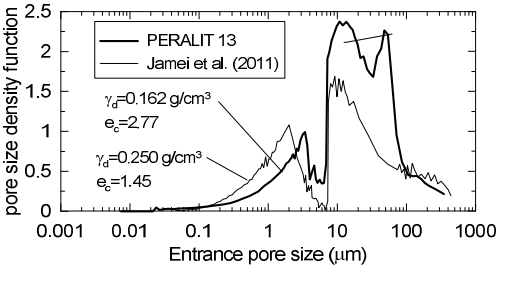

Fig. 5. Pore size density as a function of pore size (MIP results).

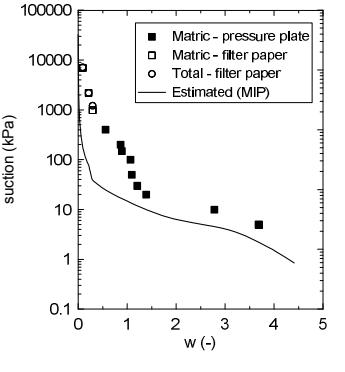

Fig. 6. SWRC obtained from MIP tests.

MIP data have been used to predict the matric suction-water content relationship at constant void ratio (Romero 1999) reported in figure 6. A qualitative agreement in trend between predicted and experimental curves can be observed in the macropore region. A better quantitative agreement could probably be obtained with a more accurate quantification of the intra-grain occluded porosity by improving the procedure of grain destructuration for γ_s determination. The behavior in the micropore region seems to be not correctly predicted. As for soils, further analyses may confirm also for perlite a negative effect due to oven drying in MIP specimen preparation.

5 Conclusions

Some experimental results and their comparison with literature data are discussed for water retention curve and microstructure of compacted expanded perlite samples. The results confirm the presence of a double porosity system and gives insights into some aspects that could be further investigated in order to correctly assume expanded perlite as a model material for soil.

References

Alonso, E.E., Gens, A., Wight, D.: General report of IX Europ. Conf. of International Society for Soil Mechanics and Foundation Engineering. In: Proc. IX ICSMFE, Dublino, pp. 1087–1146 (1987)

Birle, E., Heyer, D., Vogt, N.: Influence of the initial water content and dry density on the soil–water retention curve and the shrinkage behaviour of a compacted clay. Acta Geotech. 3, 191–200 (2008)

Burger, C.A., Shackelford, C.D.: Evaluating dual porosity of pelletized diatomaceous earth using bimodal soil–water characteristic curve functions. Can. Geotech. J. 38, 53–66 (2001)

Caruso, M., Jommi, C.: A modified pressure plate apparatus for determining soil water retention curves. In: Proc. of II E-UNSAT Europ. Conf. on Unsat. Soils, Napoli, June 20-22 (2012)

Georgopoulos, I.-O., Vardoulakis, I.: Expanded perlite as a model material to study the role of grain stiffness and strength in granular media. In: Proc. 15th U.S. National Congress on Theoretical and Applied Mechanics, Boulder, Colorado, USA, June 25-30, pp. 25–30 (2006)

Jamei, M., Guiras, H., Chtourou, Y., Kallel, A., Romero, E., Georgopoulos, I.: Water retention properties of perlite as a material with crushable soft particles. Eng. Geol. 122, 261–271 (2011)

Londra, A.P.: Simultaneous determination of water retention curve and unsaturated hydraulic conductivity of substrates using a steady-state laboratory method. Hort. Sci. 45, 1106–1112 (2010)

Romero, E.: Thermo-hydro-mechanical behaviour of unsaturated Boom clay: an experimental study. PhD thesis, Universidad Politècnica de Catalunya, Barcelona, Spain (1999)

Romero, E., Simms, P.H.: Microstructure investigation in unsaturated soil: a review with special attention to contribution of mercury intrusion porosimetry and environmental scanning electron microscopy. Geotech. Geol. Eng. 26, 705–727 (2008)

Roulia, M., Chassapis, K., Kapoutsis, J.A., Kamitsos, E.I., Savvidis, T.: Influence of thermal treatment on the water release and the glassy structure of perlite. J. Mater. Sci. 41, 5870–5881 (2006)

Tarantino, A.: Unsaturated soils: compacted versus reconstituted states. In: Proc. 5th Int. Conf. Unsat. Soil, Barcelona, September 6-8, pp. 113–136 (2010)

Zähringer, K., Martin, J.-P., Petit, J.-P.: Numerical simulation of bubble growth in expanding perlite. J. Mater. Sci. 36, 2691–2705 (2001)

Water Retention Characteristics of Non-plastic Granular Materials

Gilbert J. Kasangaki, Gabriela M. Medero, and Jin Y. Ooi

Abstract. This paper presents experimentally determined water retention curve (WRC) for glass beads. Due to its usefulness in the determination of other unsaturated properties of particulate media, WRC has become pivotal to the implementation of the mechanics of unsaturated soil and other particulate materials. In the work reported herein tests were carried out on spherical glass beads using a pressure plate. Digital microscopic images were also taken at different matric suctions to observe water bridges between the particles as the sample dried out. Results indicate a marked difference, called the hysteresis, between the primary drying and wetting paths of the water retention curve. Within the pendular bridges zone, however, the hysteresis disappeared. It is also shown that as matric suction increases water menisci and distribution of water changes.

Keywords: water retention curve, matric suction, liquid bridges, glass beads.

1 Introduction

The relationship between matric suction and water content in a material at given conditions, termed the water retention curve (WRC) is pivotal to the implementation of unsaturated soil mechanics (Fredlund & Houston 2009). Water content is

Gilbert J. Kasangaki
Heriot-Watt University, Edinburgh, UK
e-mail: gjk4@hw.ac.uk

Gabriela M. Medero
Heriot-Watt University, Edinburgh, UK
e-mail: G.Medero@hw.ac.uk

Jin Y. Ooi
University of Edinburgh, Edinburgh, UK
e-mail: J.Ooi@ed.ac.uk

commonly expressed as gravimetric water content. Alternatively it can be expressed in terms of degree of saturation or volumetric water content.

The usefulness of WRC in determining unsaturated parameters has been demonstrated by many authors (e.g. Fredlund et al. 1995). It is particularly instrumental in the estimation of unsaturated soil permeability, shear strength, transient flow and modulus of elasticity. Though simple and less costly to determine than the direct measurement of other unsaturated properties in the laboratory, WRC can be time consuming. The desire to reduce experimental efforts to obtain WRC and to implement the data in numerical modelling has motivated the need to determine WRCs empirically (van Genuchten 1980). A comprehensive review of WRC empirical models has been presented elsewhere (Leong & Rahardjo 1997).

To date several attempts have been made to correlate soil physical properties with the fitting parameters of empirical models for WRC (Arya & Paris 1981). The scatter exhibited by such correlations (Yang et al. 2004) is evidence that more experimental data is necessary before the fitting parameters can be directly determined from physical properties. The fitting parameters are usually obtained through least squares (regression) methods. As such, WRC experimental data continues to be a pre-requisite for the application of most empirical models. Moreover for cohesionless materials, the experimental data for wetting path is scanty though the hysteretic behaviour of WRC is widely recognised.

In this study pressure plate tests were carried out to determine the WRC for spherical glass beads of different size range. Spherical particles are usually assumed when numerically modelling capillary pressure in granular materials. Matric suction has also been related to the liquid bridges which were observed using a digital microscope. It is shown that matric suction within pendular bridges zone is not insignificant.

2 Material Characteristics and Sample Preparation

The glass beads were purchased from Sigmund Lindner and used as supplied. The spherical beads had the following physical properties: specific gravity: 2.5; particle size range: 0.25-0.50mm; D_{10}: 0.29mm; D_{30}: 0.33mm; D_{50}: 0.35; D_{60}: 0.36mm (D_X denote particle size for which X% are finer); maximum density: 1.630 Mg/m^3; and minimum density: 1.471Mg/m^3. The glass beads are thus comparable to medium sand in terms of particle size range. Samples were prepared directly on a saturated 1500kPa air-entry ceramic disk in 38.6mm diameter and 10.5mm height moulds. All the samples were prepared using oven dried material. Careful tamping was made to achieve the desired initial void ratio of 0.55 corresponding to 88% relative density. The dry mass, measured using a digital balance accurate to 0.01g, was the variable used to ensure that the desired initial sample void ratio was achieved. The samples were then saturated prior to starting the determination of the drying WRC.

3 Experimental Programme

3.1 Water Retention Curve

The WRCs for the glass beads were studied. Tests were carried out using the pressure plate equipment (Fig. 1) manufactured by Soilmoisture Equipment Corporation. The pressure plate was fitted with 1500kPa air-entry ceramic plate. Both the drying and wetting curves were determined using the axis translation technique (Hilf 1956). The imposed air pressure, u_a, and water pressure, u_w, were measured using transducers accurate to 1.0kPa. Water pressures less than 1.0kPa were controlled taking advantage of the hydrostatic pressure head, h_s, in the connecting water tube (Fig. 1).

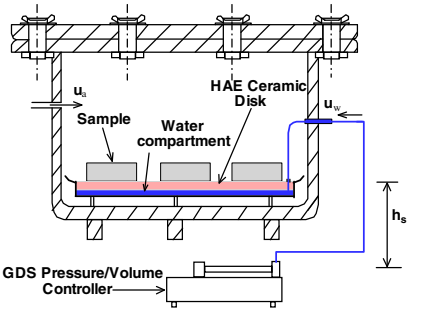

Fig. 1. Schematic of the pressure plate setup.

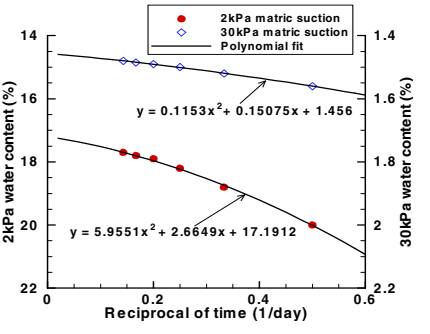

Fig. 2. The dependence of equilibrium on matric suction.

After equilibrium, water content was determined by oven drying one of the samples at 105°C until no further change in mass was recorded. Equilibrium was investigated for the 2kPa and 30kPa matric suctions on the drying path of the curve in separate but identical tests. The process involved measuring daily water content in the sample and plotting it against the reciprocal of time (Fig. 2). The equilibrium time for the points along the wetting curve was not as rigorously investigated. From Fig. 2 it can be seen that equilibrium is a function of matric suction. Unlike at the start of funicular bridge zone where the samples took about 7 days to approach equilibrium, only about 4 days was necessary in the residual zone. In this study, equilibrium was assumed when water flow out of the sample resulted in gravimetric water content change of not more than 0.1% in 24hours. The dependence of equilibrium on matric suction notwithstanding, equilibrium was considered at 7 days in all the tests.

If however, the samples were allowed more time to equilibrate further change in water content was possible (Fig. 2). Based on the equations used to best-fit the measured data, extending the equilibrium time to 14days and 56days, the respective

additional loss in water content would be about 0.3% and 0.5% for the 2kPa matric suction and about 0.1% and 0.2% for the 30kPa matric suction.

3.2 Liquid Bridge Observation

Besides measuring equilibrium water content at different matric suctions, microscopic observations were made at a magnification of 205±5 using Dino-Lite digital microscope to see if liquid bridges under matric suction can be observed. Images were taken at the time of measuring the water content. Not to lose significant moisture due to evaporation, the time spent taking out the sample for water content and images was kept very short, typically 3-5minutes. Images were taken with microscopic light on to minimise the influence of variation in light intensity on the observations. The shortfall of making two-dimensional surface observations notwithstanding, the observations are indicative of liquid bridges necessary to maintain particular matric suction.

4 Results and Discussion

4.1 Water Retention Characteristics

Figure 3 shows the water retention characteristics for the glass beads. In the drying path, increasing the matric suction up to 2kPa (about the air-entry value) was not accompanied by any significant change in water content. Within this saturated capillary regime, the surface tension of water prevents air from entering into the sample voids (Fredlund and Rahardjo 1993). This is corroborated by the microscopic observations. However, between the air-entry value and 7.3kPa (the residue matric suction), water content changed by about 3.7% per unit change in matric suction. The steep slope of the curve in this funicular bridge zone implies a considerable increase in drainage of water from the sample. Microscopic image (Fig. 4) shows that both air and water remained continuous at this stage. Further increase in matric suction beyond the residual value was then followed by small changes in water content (0.003% per unit change in matric suction). Finally at the matric suction of about 300kPa, no measurable water content change was observed in the sample. Within this part of the pendular bridge regime, the remaining liquid water is discontinuous and localised at inter-particle contacts. Matric suction is thus only due to the menisci water and higher energy is necessary to remove any further liquid from the void.

When matric suction for the previously dried sample (through increasing the matric suction to ~300kPa) was decreased the sample rewetted. Matric suction was decreased in stages with equilibrium being allowed at each stage until the wetting path was observed (Fig. 3). Until about 2.9kPa, the water-entry value, water content increased at a rate of 0.003% for every 1kPa, similar to the drying path. Thereafter the change of water content per unit suction change increased to about 9%. The resultant wetting path was different from the drying path, giving rise to a hysteresis that has been observed in previous studies (e.g. Staple 1962). For

instance at 15% water content matric suction is about 3.3kPa and 0.9kPa on the drying and wetting path respectively. The hysteresis reduces as matric suction increases subsequently disappearing at the matric suction of about 10kPa. At 5% water content the drying and wetting matric suctions are 6kPa and 2kPa respectively. The van Genuchten (1980) empirical model (Eq. 1) was found to provide a satisfactory fit to the hysteretic drying-wetting experimental data, as shown in Fig. 3. The least squares curve fitting parameters are $\alpha = 0.278$ and $n = 3.868$ on the drying path while they are 0.754 and 3.847 respectively on the wetting path. $m = 1\text{-}1/n$.

$$\theta = \theta_r + \frac{(\theta_s - \theta_r)}{\left(1 + (\alpha\psi)^n\right)^m} \tag{1}$$

where θ is the volumetric water content at a given matric suction, ψ and θ_r and θ_s are the residual and saturated volumetric water contents. In this study however, water content is presented as gravimetric water content.

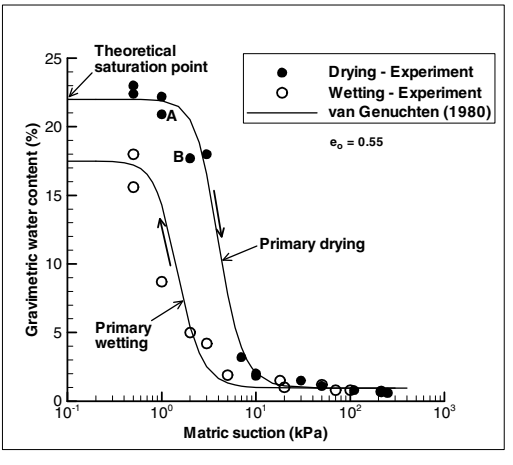

Fig. 3. Water retention curves for the tested glass beads.

4.2 Liquid Bridges

As mentioned in section 3.2, besides measuring equilibrium water content, microscopic images were taken of the samples in the pressure plate. The purpose was to observe the liquid bridges if any and to relate to the matric suction. Two such images are shown in Fig. 4. They were all taken at a magnification of 205±5 and on the same sample. The initial sample conditions have been presented in section 2. Shown also on the scaled figure is the matric suction value for which each of the images was taken.

From the images (not all are shown here due to space constraint) it was observed that when the samples were saturated the glass beads were virtually unidentifiable. As air started entering into the samples, the shape of the beads became apparent. About 20µm thick water films surrounded most of the particles at 1kPa matric suction (Fig. 4a taken on sample at condition A in Fig. 3). The glass beads became even clearer and the water films decreased to about 10µm thick as matric suction was increased to 2kPa, somewhat the start of the funicular bridges zone (Fig. 4b taken on sample at condition B in Fig. 3). As mentioned in section 4.1, within this zone both pore air and pore water are continuous. It is therefore probable that within the funicular bridges zone matric suction is due to both the adsorbed and menisci water. Within the residual zone (100kPa), no water films existed at the sample surface (not shown). It was however noted that when the mould containing the beads was lifted, the beads did not fall apart from the gravitational forces suggesting that the liquid bridges induced adhesive forces were holding the sample together. In the images, all the glass beads present with a regular pattern of white spots. These are a result of reflection of light.

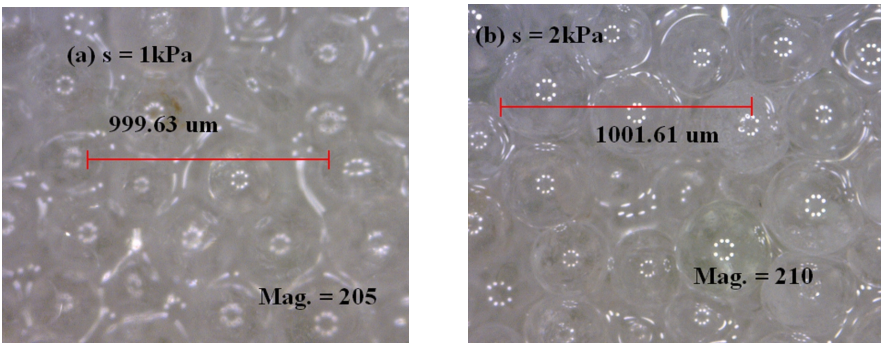

Fig. 4. Microscopic images of the formation of liquid bridges at different matric suctions on the drying path: (a) at 1.0kPa and (b) at 2.0kPa.

5 Conclusions

The water retention curves for 0.25-0.50mm glass beads have been presented. Starting from a saturated sample, the hysteretic drying and wetting paths have been carefully measured and was found to be well described by the van Genuchten empirical model through least squares curve fitting procedure. The microscopic observations of the liquid bridges seem promising in visualising and relating to the different stages of matric suction. More work on this aspect is underway.

Acknowledgements. This study is part of a research project funded by the Civil & Environmental Engineering Joint Research Institute, Edinburgh, UK.

References

Arya, L.M., Paris, J.F.: A physicoempirical model to predict the soil moisture characteristic from particle-size distribution and bulk density data. Soil Sci. Soc. Am. J. 45, 1023–1030 (1981)

Fredlund, D.G., Houston, S.L.: Protocol for the assessment of unsaturated soil properties in geotechnical engineering practice. Can. Geotech. J. 46, 694–707 (2009), doi:10.1139/T09-010

Fredlund, D.G., Rahardjo, H.: Soil Mechanics for Unsaturated Soils. John Wiley and Sons Inc., New York (1993)

Fredlund, D.G., Xing, A., Fredlund, M.D., Barbour, S.L.: The Relationship of the unsaturated shear strength to the soil-water characteristic curve. Can. Geotech. J. 32, 440–448 (1995)

Leong, E.C., Rahardjo, H.: Review of Soil-Water Characteristic Curve Equations. J. Goetech. Geoenv. Eng., ASCE 123(12), 1106–1117 (1997)

Staple, W.J.: Hysteresis effects in soil moisture movement. Can. J. Soil Sci. 42, 247–253 (1962), doi:10.4141/cjss62-033

van Genuchten, M.T.: A closed-form equation for predicting the hydraulic conductivity of unsaturated soils. Soil Sci. Soc. Am. J. 44, 892–898 (1980)

Yang, H., Rahadjo, H., Leong, E.C., Fredlund, D.G.: Factors affecting drying and wetting soil-water characteristic curves of sandy soils. Can. Geotech. J. 41, 908–920 (2004), doi:10.1139/T04-042

Experimental Investigation of Hydraulic Conductivity in Unsaturated Compressible Soils

Ali Mirzaii, Seyyed Shahaboddin Yasrobi, and Nasser Khalili

Abstract. The paper represents data of an elaborate laboratory test program on the water flow behaviour in two different compressible soils. The experimental tests were carried out with a flexible wall permeameter. The hydraulic conductivity of statically compacted samples was evaluated in different net confining stress and saturation conditions. The results showed that the increment of net stress and reduction of pore volumes at a given soil suction followed a different pattern than the trend associated to the effect of void ratio on water permeability of saturated soils. The increment of degree of saturation within the reduction of pore spaces was utilized to qualify the opposite detected response.

Keywords: unsaturated compressible soils, matrix suction, degree of saturation, water flow, net stress.

1 Introduction

The water coefficient of permeability, k_w, is a measure of soil resistance to the flow of water and is majorly a function of soil water content and pore spaces (Lloret & Alonso 1980).

For saturated soils, the extensive amount of research in the past century shows a decrease of water permeability when soil voids are confined.

Ali Mirzaii
Tarbiat Modares University, Tehran, Iran
e-mail: al.mirzaii@gmail.com

Seyyed Shahaboddin Yasrobi
Tarbiat Modares University, Tehran, Iran
e-mail: yasrobis@modares.ac.ir

Nasser Khalili
University of New South Wales, Sydney, Australia
e-mail: n.khalili@unsw.edu.au

Many experimental attempts have been previously made to examine the effect of soil water content on hydraulic conductivity of unsaturated soils (e.g. Burdine 1953, Klute 1965, Fleureau & Taibi 1994, Samingan et al. 2003, or Simmens & Blatz 2007). All the experimental results show the increase of water permeability with increment of soil water content.

Relatively few amount of information is available on void ratio dependency of water permeability in unsaturated deformable soils. Barden & Pavlakis (1971) studied the hydraulic conductivity of a clay in constant water content in different confining stress and observed increasing water permeability values when soil was compressed and matrix suction reduced. Nimmo & Akstin (1988) determined the water permeability of a sand in different void ratios with centrifugal testing and observed that k_w is void ratio dependent. The results of Huang et al. (1998) on a sand showed that the effect of void ratio on unsaturated water permeability is different than the effect of void ratio on hydraulic conductivity of saturated soils. Romero (1999) examined the hydraulic conductivity of a clay in two compaction states and determined that for a constant degree of saturation, k_w is increased with increment of pore spaces. Pereira et al. (2005) showed increasing and decreasing water permeability values within compression of a sand in unsaturated and saturated conditions respectively.

This paper presents the results of an elaborate experimental testing program aimed to investigate the different effects of void ratio on hydraulic conductivity of saturated and unsaturated soils. Saturated and unsaturated water permeability test results are presented and the trends observed are described. The different effect of net confining stress on water permeability of unsaturated soils is then discussed with accordance to the displacement of soil-water characteristic curve.

2 Materials and Laboratory Equipment

Firouzkouh clay and a mixture of 60 % sand- 40 % kaolin were used in tests. The index properties of test soils are summarized in Table 1.

Permeability tests were performed with the flexible wall permeameter apparatus configuration as shown in fig. 1, designed and built in Tarbiat Modares University, which was consisted of a flexible wall permeameter cell and pressure and volume change controlling devices. Water flow thorough the soil was controlled with two 5 bar high air entry ceramic disks installed in top and bottom pedestals of the permeameter cell. Soil matrix suction was controlled using axis translation technique. Pressurized air was entered to the soil through the porous stones located in top and bottom pedestals of permeameter cell. The top and bottom water flow rates were measured with two automatic pressure/volume change controllers of the Imperial college type. The metallic wall of the cell was thick enough to measure sample (total) volume change in accordance to the volume of de aired water exchanged by the cell. For current study, the mechanical twin burettes type total volume change measuring system of the former configuration of permeameter apparatus in Adelian et al. (2011) was replaced with an automatic pressure/volume change controller.

Table 1. Index properties of investigated soils.

	Sand- kaolin mixture	Firouzkouh clay
Liquid limit, %	23.5	30
Plastic index, %	9.5	9
Specific gravity	2.66	2.75
Percentage < 75 µm	40	88.7
Optimum water content[a], %	9.6	14.1
Maximum dry density[a], kN/m^3	19.71	18.06
Sample dry density, kN/m^3	17.16	15.77

[a] attained from Standard Proctor compaction test.

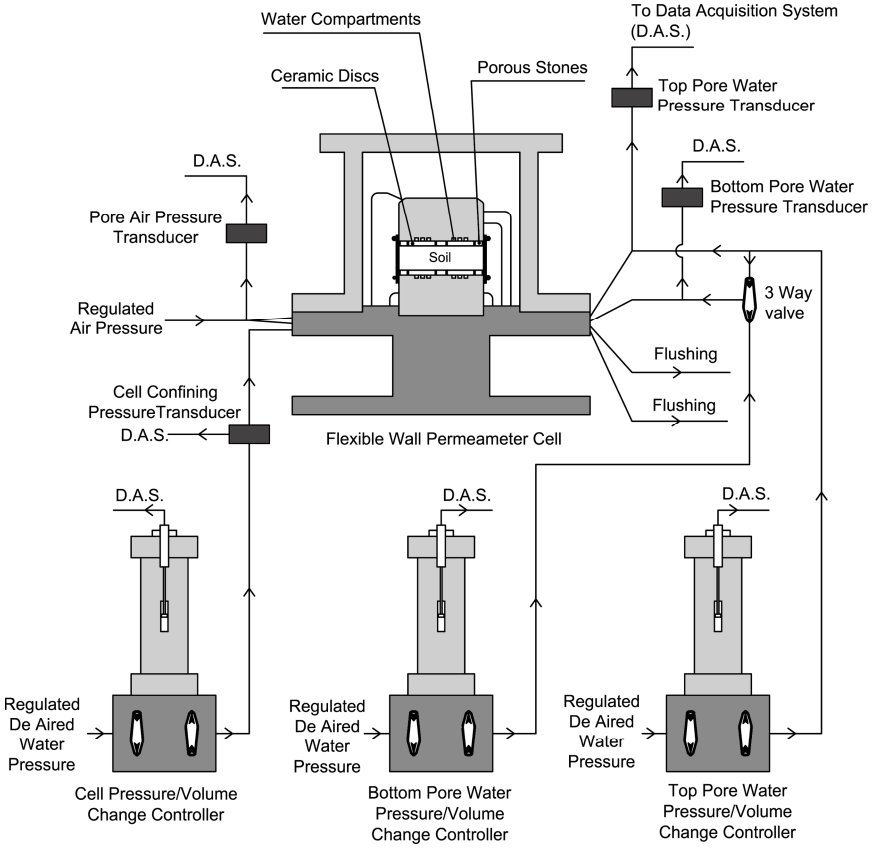

Fig. 1. Schematic of permeameter apparatus configuration used in tests.

3 Test Procedure

Soil samples were statically compacted in the dry densities listed in Table 1 in Standard Proctor optimum water content, and their water coefficient of permeability was measured in matrix suctions of 30, 100, and 180 kPa in net confining stresses of 20, 150, and 300 kPa. Additionally, a series of saturated water permeability tests was carried out on identical compacted samples and analogous effective lateral stress.

Soil samples were compacted inside a load frame by statically compression of a known mass of soil to a mold with internal diameter of 7 cm and height of 1 cm with the loading speed of 1 mm/min. Samples were then carefully extruded from the mold and were appropriately installed inside the apparatus.

Hence, the water permeability was measured in different combinations of net confining stress and soil matrix suction. The change of soil matrix suction and consolidation took placed simultaneously. To achieve this, pore air pressure was set to 300 kPa and pore water and net confining pressures were set to desired values. An equilibrium condition was reached between 18-24 hours.

The water permeability of samples was measured within a steady state flow of water with the flow head of 40 kPa. Similar to Barden & Pavlakis (1971), the average matrix suction of specimens remained unchanged by 20 kPa increment of sample bottom pore water pressure and 20 kPa decrement of sample top pore water pressure. The rates of inflow and outflow of water reached to analogous constant values in a steady state condition within 30 to 50 hours. The flow of water may slightly change the soil fabric; therefore the above steps were repeated on a new specimen for each combination of matrix suction and net confining stress.

Additionally, a series of saturated water permeability tests were performed as the above procedure was not practical for accurate water permeability measurement in saturated or near saturation condition because the bottom pore water pressure would exceed the pore air pressure and water flow to the pore air pressure conduits. Therefore, suitable pedestals for conventional saturated hydraulic conductivity tests were installed inside the permeameter cell, and soil samples were saturated with a water backpressure of 300 kPa. Soil samples were then consolidated in the similar confining stresses that were used in unsaturated tests. Water permeability measurements were then carried out by utilizing a similar approach that was used in unsaturated tests.

The validity of Darcy's law was just verified in saturated condition by additional permeability tests in the flow heads of 10, 20 and 30 kPa only in the lateral pressure of 20 kPa where samples had larger pore spaces and water flow rate was higher. The plot of the results in fig. 2 postulates that, for the level of applied flow head in two test soils, Darcy's law applies. For the validity of Darcy's law in unsaturated tests, the soil can be treated as a saturated soil having a reduced void ratio as water can only flow thorough the pore spaces filled with water and the air filled pores behave similarly to the solid phase. Therefore, the validity of Darcy's law is also applied for the flow of water in unsaturated tests.

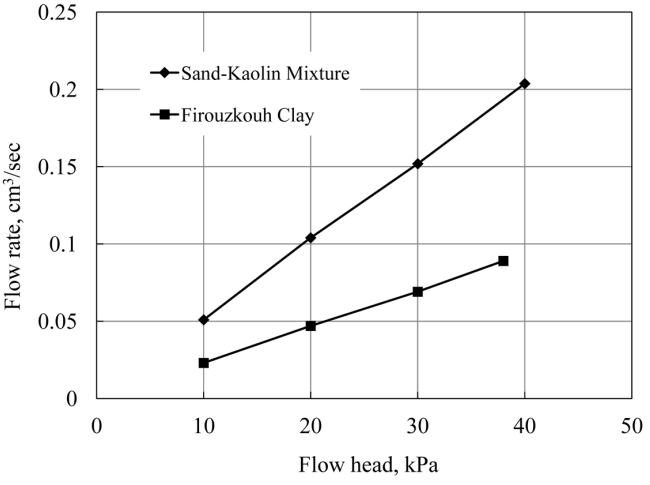

Fig. 2. Saturated water flow rate versus flow head for samples consolidated in lateral pressure of 20 kPa.

4 Results

Fig. 3 illustrates the results of saturated tests in terms of the water coefficient of permeability versus void ratio. The values of k_w were calculated using Darcy's law. The net confining stress corresponding to each void ratio is also indicated in the text boxes. For two different investigated soils, an increment of net confining stress has reduced the void ratio and has resulted to a reduction in the volume of water flow channels and caused to lower water permeability.

Figs. 4.a and 5.a demonstrate the results of measured unsaturated k_w versus matrix suction in different net confining stress. In a similar approach to Samingan et al. (2003), a three layer system of ceramic disk-soil-ceramic disk was assumed for calculation of the coefficient of permeability of unsaturated tests. The water permeability of ceramic disks in the flow head of 40 kPa was measured for several times, and the average value of 1.62×10^{-8} cm/sec was utilized in calculations.

The trend in figs. 4.a and 5.a shows that for a given net stress the water coefficient of permeability of both soils is decreased with increment of matrix suction. Further investigation of the results also state that for a given soil suction the increment of net stress and reduction of pore voids has increased the value of k_w. This behaviour is observed in all tests and is peculiar with the decrement of water coefficient of permeability of saturated soils when their voids are confined.

When the value of net stress increases, the dimensions of air filled voids and their connecting passageways would be expected to decrease, so that for a given matrix suction a higher degree of saturation is produced, resulting an upward movement of the soil- water characteristic curve. This behaviour is illustrated in

figs. 4.b and 5.b by plotting the variation of degree of saturation versus matrix suction in different net stress. To this, data of samples at the end of wetting and consolidation stage are utilized. The upward displacement of soil-water characteristic curve with reduction of void spaces has increased the degree of saturation and continuity of water filled pores in the soil, and in spite of the compression of void spaces, the hydraulic conductivity of test soils are increased.

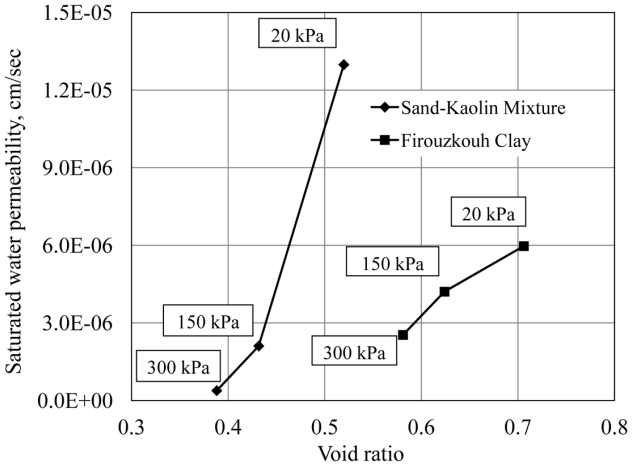

Fig. 3. Saturated water permeability versus void ratio in test soils.

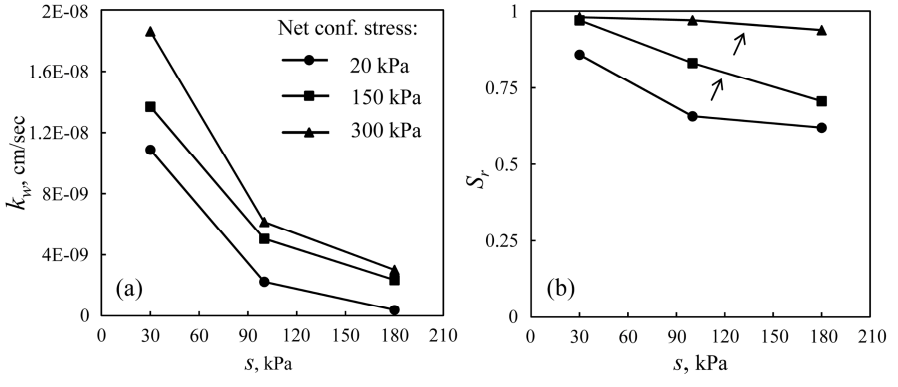

Fig. 4. Variation of a) water permeability; and b) degree of saturation, S_r; versus matrix suction, s in sand-kaolin mixture.

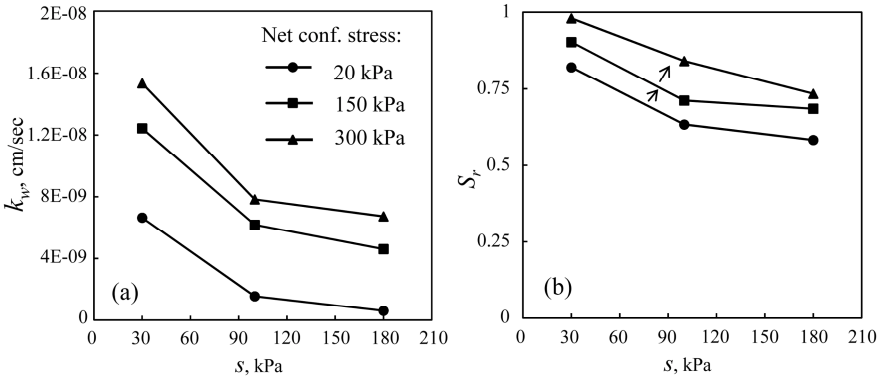

Fig. 5. Variation of a) water permeability; and b) degree of saturation; versus matrix suction in Firouzkouh clay.

5 Conclusion

Permeability test results on two different compressible soils showed that a reduction of pore volumes can in fact increase the hydraulic conductivity of unsaturated soils. The different observed pattern to the response of saturated soils is due to the reduction of air filled voids and their connecting passageways that resulted a higher degree of saturations during the increment of net stress.

References

Adelian, G., Mirzaii, A., Yasrobi, S.S.: Infiltration of water thorough a clayey sand in wetting and drying portions of SWCC. In: Proceedings 5th Asian Pacific Conference on Unsaturated Soil, Pattaya, Thailand, pp. 779–784 (2011)

Barden, L., Pavlakis, G.: Air and water permeability of compacted unsaturated cohesive soils. J. Soil Sci. 22, 302–318 (1971)

Burdine, N.T.: Relative permeability calculation from pore-size distribution data. Petroleum Transactions, American Institute of Mining, Metall. Pet. Eng. 198, 71–78 (1953)

Fleureau, J.M., Taibi, S.: A new apparatus for the measurement of polyphasics permeabilities. In: Proceedings of the 1st International Conference on Environmental Geotechnics (ICEG), Edited by the Technical Program Committee of the 1st ICEG, July 11-14, pp. 227–232. BiTech Publishers, Edmonton. Alta (1994)

Huang, S., Fredlund, D.G., Barbour, S.L.: Measurement of the coefficient of permeability for a deformable unsaturated soil using a triaxial permeameter. Can. Geotech. J. 35, 426–432 (1998)

Klute, A.: Laboratory measurement of hydraulic conductivity of unsaturated soil. In: Black, C.A., Evans, D.D., White, J.L., Ensminger, L.E., Clark, F.E. (eds.) Methods of Soil Analysis. Mono, vol. 9, Part 1, pp. 253–261. American Society of Agronomy, Madison (1965)

Lloret, A., Alonso, E.E.: Consolidation of unsaturated soils including swelling and collapse behavior. Geotechnique 30, 449–477 (1980)

Nimmo, J.R., Akstin, K.C.: Hydraulic conductivity of a sandy soil at low water content after compaction by various Methods. Soil Sci. Soc. Am. J. 52, 303–310 (1988)

Pereira, J.H.F., Fredlund, D.G., Cardao Neto, M.P., Gitirana, G.F.N.: Hydraulic behavior of collapsible compacted gneiss soil. J. Geotech. Geoenv. Eng. 131, 1264–1273 (2005)

Romero, E.: Characterisation and thermo-mechanical behaviour of unsaturated Boom clay: An experimental study. Ph.D. thesis, UPC Barcelona (1999)

Samingan, A.S., Leong, E., Rahardjo, H.: A flexible wall permeameter for measurements of water and air coefficients of permeability of residual soils. Can. Geotech. J. 40, 559–574 (2003)

Siemens, G., Blatz, J.A.: Development of a hydraulic conductivity apparatus for bentonite soils. Can. Geotech. J. 44, 997–1005 (2007)

Examination of Unsaturated Conductivity Curves Using Transparent Soil

Greg Siemens, Andy Take, and Stephen Peters

Abstract. Numerical simulations of unsaturated flow require the retention curve and unsaturated conductivity curve as inputs. Except in research or in the case of large projects these material properties are estimated to some degree. This manuscript examines the accuracy of unsaturated conductivity estimations for an unsaturated transparent soil. Using transparent soil allows accurate measurement of degree of saturation along the soil profile as well as the spatial measurements of conductivity. The estimations show the correct trend and are found to be within one order of magnitude compared with the experimental data.

Keywords: unsaturated flow, material property estimation, transparent soil.

1 Outline

Numerical and physical modeling of flow in unsaturated soils requires either measurement or estimates of the water retention curve and the unsaturated hydraulic conductivity curves. In research the water retention curve is often measured however, at times estimations are still used in practice. In both research and practice the unsaturated hydraulic conductivity curve is very rarely measured. Therefore questions remain as to the accuracy of fitted curves.

Greg Siemens
GeoEngineering Centre at Queen's-RMC, Royal Military College, Canada
e-mail: siemens@rmc.ca

Andy Take
GeoEngineering Centre at Queen's-RMC, Queen's University, Canada
e-mail: andy.take@civil.queensu.ca

Stephen Peters
Thurber Engineering, Canada
e-mail: speters@thurber.ca

One of the potential challenges associated with measuring the unsaturated hydraulic conductivity curve is accurate measurement of the degree of saturation. The authors have recently developed a transparent soil for use in unsaturated applications (Peters et al. 2011). The soil is transparent at Sr=1.0 and white when dry. Between the two extremes the color intensity of the transparent soil varies non-linearly. Fig. 1 displays the trend of change in pixel intensity using close-up photographs of the transparent soil at selected saturation levels (0.99, 0.9, 0.7 and 0.6). From the photographs the change in pixel intensity from dark to light is clear even over this range of saturation. The soil was placed in a column apparatus constructed of acrylic and digital images taken of experiments. A relationship between digital pixel intensity and degree of saturation was calibrated and validated using full-column tests as well as hanging column tests. Interpreting the digital photographs of experiments allows measurement of the degree of saturation at approximately 1 mm resolution. This level of resolution provides new insights to be gained in unsaturated applications.

In this paper a grain-size analysis estimation is used to predict the retention curve and unsaturated conductivity curve of the coarse gradation transparent soil. Using the transparent soil allows measurement of the complete degree of saturation profile. Saturated hydraulic conductivity is measured using a drawdown test and unsaturated conductivity is measured using constant flow tests. Results show the estimations capture the correct trend for the unsaturated conductivity curve within one order of magnitude.

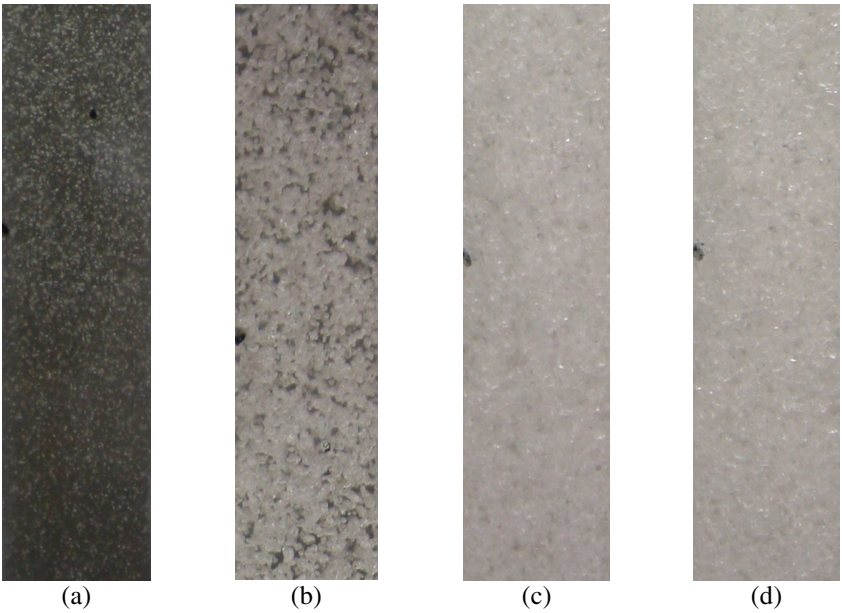

Fig. 1. Close-up photographs of transparent soil displaying change in pixel intensity: (a) Sr~1, (b) Sr~0.9, (c) Sr~0.7, (d) Sr~0.6.

2 Materials and Methods

The coarse gradation of transparent soil is described in detail in Peters et al. (2011) and material characterization is also given in Ezzein & Bathurst (2011). Transparent soil is composed of solid and liquid with matching refractive indices. The soil is fused quartz while the liquid is formed by a combination of mineral oils. The coarse gradation soil is a poorly graded sand according to the Unified Soil Classification System. Relevant properties of the oil include its density (0.845 g/cm^3), refractive index (1.459) and dynamic viscosity at 25 ^{o}C (10.1 cP).

The soil is placed in a 1450 mm tall column apparatus composed of 19 mm thick Perspex with an inside cross-sectional dimensions of 45.6 mm x 45.6 mm. The apparatus allows application of boundary conditions at the surface and base of constant head as well as constant flow. Ports along the side of the apparatus allow instrumentation or lateral drainage if desired. Three (3) digital cameras are located along the length of the apparatus to capture digital images during experiments.

In this manuscript a drawdown test and three (3) constant flow tests are presented to measure points on the unsaturated conductivity curve of the transparent soil. Using these test results the conductivity value at specific saturation levels can be interpreted and compared with grain-size estimations. The procedure and method of interpreting drawdown and constant flow tests generally followed ASTM D 5084. For completing drawdown tests the valve connected to the bottom of the apparatus was opened and oil allowed to exit through the constant head boundary overflow. During the test the only required measurement is the elevation of the oil surface with time. For unsaturated conductivity testing, constant flow boundary conditions were applied at the top of the column using a Mariotte bottle. The flow rate was set to a value lower than the saturated conductivity of the soil. As such the soil remained unsaturated throughout the test. Measurements taken during the test included mass of oil exiting the apparatus. Tests were continued until the outflow rate remained stable.

3 Test Results

The test results from one drawdown test and three constant flow tests are presented in this section. The soil conductivity with respect to degree of saturation is interpreted to compare with the Fredlund et al. (1994) and van Genuchten (1980) estimations that were based on retention curves estimated from grain-size data (Aubertin et al. 2003). Estimations were performed using Seep/W (Geostudio 2007). The drawdown test results are shown in Fig 2 including elevation of drying front with time, outflow versus time and interpreted conductivity. The profile of saturation is also shown in Fig 3. Initially the soil is at Sr=1 (Fig 1a and Fig 3). The drawdown test is initiated at time t=0 and the flow rate quickly equilibrates. The interpreted conductivity value of 1.2×10^{-3} m/s is in-line with similar sand materials. As the drying front

enters the soil column the soil de-saturates. Siemens et al. (2010) reported a method for interpreting the conductivity during the drainage test by taking the length of soil as the vertical distance from the drying front to the bottom of the soil column in Eq. 1. A similar methodology is employed here to give a consistent measurement of conductivity throughout the soil profile. As the drying front approaches the elevation of the overflow its rate of descent reduces coinciding with a reduction in outflow. The drying front approaches the constant outflow elevation asymptotically.

Three constant flow tests were completed on the same column setup. Flow rates were selected to represent values less than the saturated conductivity to ensure the soil column remained unsaturated during the test. Flow from the Mariotte bottle was applied to the surface of the soil. Tests were continued until the outflow rate equilibrated with the inflow rate. Digital images were taken throughout the experiments at 5 s intervals. The saturation profiles plotted in Fig. 3 were taken after equilibration had occurred. The Sr=1 profile is taken from the falling head test and shows consistent measurements with depth. The Sr=0.93 profile shows some variation with depth but the saturation profile remains relatively vertical across the profile. The two tests with lower overall saturation levels show more variation across the profile. Looking at the close-up photos in Fig. 1 shows little variation visible to the naked eye however, image analysis allows local variations to be detected. Given the constant flow conditions across the soil specimen the variations in saturation are due to local variations in the soil grain-size distribution. This would lead to more or less oil retention. The applied test conditions of constant flow at the surface and constant head at the base allow for the average conductivity of the column to be interpreted. Therefore the average saturation over the elevation of interest within the pressure transducer measurements (El. 400-1200 mm) was used for interpretation.

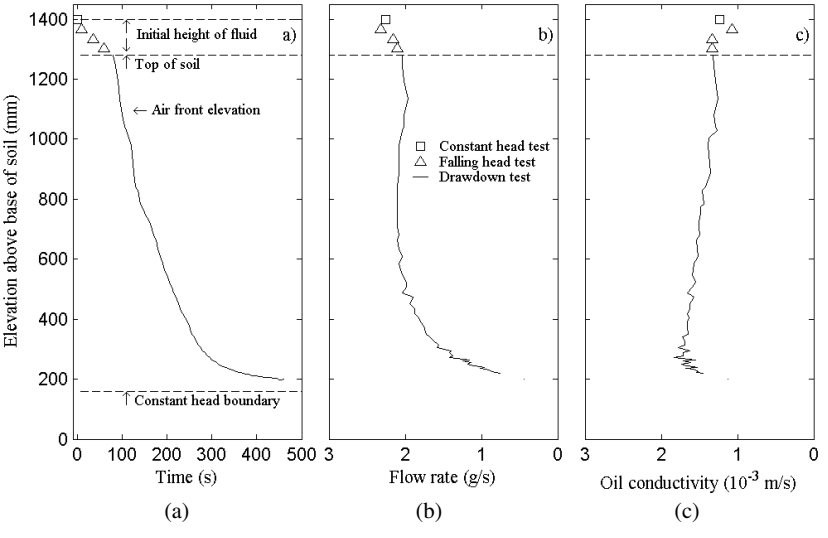

Fig. 2. Drawdown test: elevation of drying front versus (a) time, (b) outflow (c) conductivity.

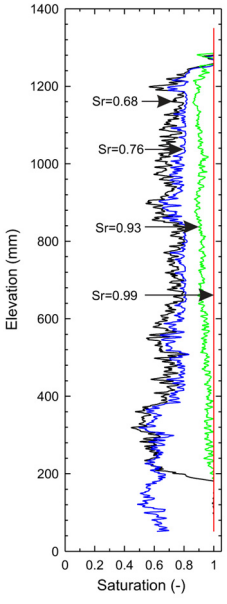

Fig. 3. Saturation profiles or drawdown and constant flow tests.

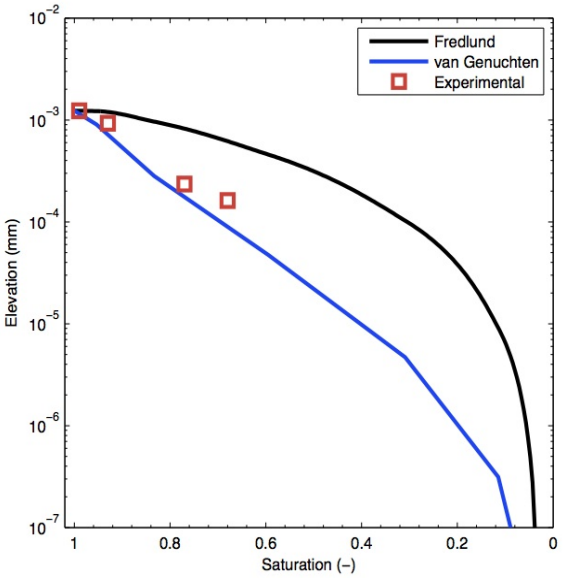

Fig. 4. Unsaturated conductivity curve versus degree of saturation.

4 Discussion

Conductivity values interpreted from the falling head and constant flow tests versus degree of saturation are plotted in Fig. 4. Also included are the Fredlund et al. (1994) and van Genuchten (1980) estimations over the applied range. As expected the overall trend in the experimental data and fitted curves is decreasing conductivity with decreasing saturation levels. Overall the Fredlund et al. fit overestimates the unsaturated curve over the range examined while the van Genuchten slightly underestimates the experimental data. Although conductivity varies over orders of magnitude due to de-saturation the range tested is relatively narrow (Sr=0.68-1.0). Higher accuracy in the unsaturated curve would be desirable in order to obtain acceptable unsaturated flow models. Improvements to the estimations would be possible by measuring the retention curve of the transparent soil as well as measuring more points on the unsaturated conductivity curve.

In engineering practice and in some research projects the unsaturated functions are estimated for various economic and efficiency related issues. The cost of such a decision is the additional risk from unknown errors in the estimations compared with the true values. In flow applications the required inputs are the water retention curve and the unsaturated conductivity curve. The data in Fig. 4 shows a one order of magnitude differential between the Fredlund et al. and van Genuchten fitted curves. Use of either of these curves would either overestimate or underestimate the true flow rate. Engineers are often required to make decisions with a number of unknowns and associated

risk. However, in flow applications the saturated conductivity can vary over orders of magnitude. In addition, the unsaturated conductivity function can vary orders of magnitude even at low suction values. Therefore use of estimations in these applications should be made with the utmost caution.

5 Conclusions

Numerical simulations of unsaturated applications as well as interpretation of physical modelling experiments benefit from accurate unsaturated functions. In practice these functions are only measured for large projects. This paper investigated the accuracy of unsaturated conductivity estimations based on a water retention curve estimated using a grain-size analysis. The results were compared with experimental data generated testing transparent soil. Comparing the experimental data to the estimations shows they are within an order of magnitude. In order to accurately model unsaturated flow applications a greater magnitude of accuracy is required which would entail measuring the unsaturated conductivity and retention curves.

References

ASTM D 5084, Standard Test Method for Measurement of Hydraulic Conductivity of Saturated Porous Materials Using a Flexible Wall Permeameter, American Society for Testing and Ma-terials, West Conshohocken, Pennsylvania, USA

Aubertin, M., Mbonimpa, M., Bussière, B., Chapuis, R.P.: A model to predict the water reten-tion curve from basic geotechnical properties. Can. Geotech. J. 40, 1104–1122 (2003)

Ezzein, F.M., Bathurst, R.J.: A Transparent Sand for Geotechnical Laboratory Modeling. Geotech. Test. J. 34(6), 1–6 (2011), doi:10.1520/GTJ103808

Fredlund, D.G., Xing, A.Q., Huang, S.Y.: Predicting the permeability function for unsaturated soils using the soil-water characteristic curve. Can. Geotech. J. 31, 533–546 (1994)

Geo-Slope International Ltd. 2007. Seepage modeling with SEEP/W, An Engineering Methodology, 2nd edn., 307 p. (2007)

Peters, S., Siemens, G., Take, W.A.: Characterization of transparent soil for unsaturated appli-cations. ASTM Geotechnical Testing Journal Special Issue on Innovations in Characterizing the Mechanical and Hydrological Properties of Unsaturated Soil 34(5), 445–456 (2011), doi:10.1520/GTJ103580

Siemens, G.A., Peters, S., Take, W.A.: Analysis of a drawdown test displaying the use of transparent soil in unsaturated flow applications. In: Proceedings of the 5th International Conference on Unsaturated Soils, Barcelona, Spain, September 6-8, pp. 733–738 (2010)

van Genuchten, M.T.: A closed-form equation for predicting the hydraulic conductivity of unsaturated soils. Soil Science Society of America Journal 44, 892–898 (1980)

Stress-Strain and Strength Characteristics

SWRC Modelling Framework for Evaluating Volume Change Behavior of Expansive Soils

Aravind Pedarla, Anand J. Puppala, Laureano R. Hoyos, Sai K. Vanapalli, and Claudia Zapata

Abstract. The soil-water Retention curve (SWRC) has been used as a tool by geotechnical researchers and practitioners to determine the properties such as the shear strength, coefficient of permeability, bearing capacity and the modulus of elasticity of unsaturated soils. Such studies are valuable to the practicing engineers as they alleviate the use of time consuming and elaborate testing techniques required for determining the unsaturated soil properties. In this paper, an attempt is made to study the relationship between the SWRC and the swelling pressure including the one dimensional swell behavior for two different expansive soils using statically compacted specimens. Test results were analyzed to evaluate the clay mineralogy and influence of initial compaction moisture content or matric suction on both swell strain and swell pressure properties in one-dimensional test conditions. Comparisons of swell pressures and swell strain potentials and related SWRC properties of these soils are also made.

Keywords: soil water retention curve, swell potential, mineralogy.

Aravind Pedarla
PhD student, University of Texas at Arlington, Tx, USA
e-mail: aravindcivil@gmail.com

Anand J. Puppala
Distinguished Professor, University of Texas at Arlington, Tx, USA
e-mail: anand@uta.edu

Laureano R. Hoyos
Associate Professor, University of Texas at Arlington, Tx, USA
e-mail: lhoyos@uta.edu

Sai K. Vanapalli
Professor & Chair, University of Ottawa, Canada
e-mail: sai.vanapalli@uottawa.ca

Claudia Zapata
Assistant Professor, Arizona State University, Tempe, AZ, USA
e-mail: claudia.zapata@asu.edu

1 Introduction

Expansive soils are widely distributed in many arid and semi-arid regions of the world. These soils pose a serious threat to the lightly loaded structures constructed above them. The alternate swell and shrink behavior caused by moisture fluctuations in the ground leads to foundation failures of the structures built on these soils. In the United States alone the damages associated with expansive soils problems cause a greater economic loss annually in comparison to the damages associated with the natural disasters such as the floods, hurricanes, tornadoes and earthquakes (Nelson & Miller, 1992). The swelling behavior of expansive clays is mainly caused due to the strong soil-water interaction in the shallow soil layers when they are subjected to seasonal wetting-drying cycles. Previous studies show that the soil-water interaction induced by the climatic changes is very complex and involves the coupled effects of the changes in water content, suction, stress, deformation and shear strength (Ng et al., 2003; Zhan, 2006).

Studies by several investigators show the prediction procedures that use soil suction as a tool to provide more reliable estimates of anticipated volume change behavior in the field behavior in comparison to other empirical methods (Snethen, 1980; Puppala et al. 2006; Vanapalli et al. 2011, Vanapalli and Lu 2012). Kassif and Ben Shalom (1971) conducted swell pressure–soil suction studies using modified oedometer cells. They found out that the swell pressures reach 95% of its ultimate value after a moisture intake of only one third that is required for sample saturation. In addition, these studies also suggest that the swell pressure developed upon wetting is approximately equal to the difference between the soil suction of a sample in constant volume test at its final water content and the freshly prepared sample under the same water content with no confining pressure.

Alonso et al. (2005) conducted studies on sand-bentonite mixtures and predicted the swelling behavior using an elasto plastic constitutive model, which uses a double structure approach. There is a reasonably good agreement between the model predictions and the volumetric deformations measured during the application of different suction cycles.

To investigate the behavior of soil suction and swell pressure, Erzin & Erol (2007) performed experiments on statically compacted samples of different clay mixtures which include Bentonite-Kaolinite clay mixtures. A linear relationship was found between logarithm soil suction and the swell pressure and initial soil suction and the swell pressure of the soil. Erzin (2007) used artificial neural networks (ANN) approach and investigated the influence of soil suction on the swell pressure of expansive soils along with other basic soil properties that include initial dry density, and plasticity index. The results of the study suggest that the initial soil suction and mineralogy of the clay are the governing parameters for the swell behavior.

The focus of the present research was directed to better understand the relationship between the matric suction and swelling potential of clayey soils with different

dominant clay minerals. Also, a SWRC variation along with both swell pressures and swell strain potentials are presented for both expansive clays.

2 Soil Selection and Basic Soil Properties

The main objective of the research is to investigate the key parameters that influence the swelling behavior of expansive clays. Two expansive clays, one from Texas and the other from Oklahoma were selected as test soils. These two soils were selected due to their different mineralogical characteristics. Clay mineralogical properties are determined as per the procedures outlined in Chittoori and Puppala (2011). Table 1 summarizes the mineralogy of the clays along with the other basic properties. The optimum moisture content and the dry density properties were determined using Standard Proctor Test and these results are summarized in Table 1.

Table 1. Basic Soil Characterization.

Property	Texas soil	Oklahoma soil
Liquid limit, w_L (%)	55	41
Plasticity index, w_P (%)	37	21
USCS classification	*CH*	*CL*
% of soil passing through U.S. Sieve No. 200	92	90
Specific gravity, G_s	2.72	2.83
% of Montmorillonite in clay fraction	40	20
% of Kaolinite in clay fraction	40	20
% of Illite in clay fraction	20	60
Maximum dry density (Mg/m^3)	1.64	1.59
Optimum moisture content (%)	17	24

The soil from Texas is fat clay with equal amounts of Montmorillonite and Kaolinite in its clay fraction. As Kaolinite is a non expansive mineral, the swelling characteristics in this clay are attributed to high Montmorillonite content and traces of Illite present in the soil. The soil from Oklahoma is low compressible lean clay with Illite being its dominant mineral.

3 Specimen Preparation and Saturation

Soils used in the present research were pulverized after oven drying and allowed to pass through U.S. No 40 sieve. The prepared soil was then mixed with desired amount of water and then transferred to the compaction mould as shown in Fig. 1(a). Soil specimens of 25 mm height and 62.5 mm in diameter were compacted at their maximum dry density (MDD) condition. The specimens were compacted

statically at a strain rate of 2.27 mm/min. The compacted clay specimens were then extracted and transferred into metallic moulds and these moulds clamped on both ends with the help of porous disks as shown in Fig. 1(b). Two metallic plates were used on top and bottom of the metallic moulds and then tightly held together throughout the saturation process.

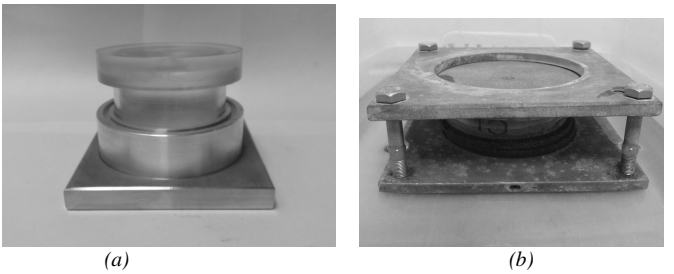

(a) *(b)*

Fig. 1. Showing *(a)* Compaction mould and *(b)* Saturation apparatus.

The apparatus was placed in a container and water was filled up to the bottom porous disk. The specimen was allowed to imbibe moisture for a period of 12 hours and then water was filled up to the top of the apparatus. Trial studies have shown that the immersed soil specimen was saturated in a period of 24 hours following this technique. The degree of saturation was ensured from mass-volume relationships. The above technique was used such that specimens were saturated under constant volume (CV) conditions. The specimen after saturation was transferred to the pressure plate apparatus to determine the soil-water retention curve (SWRC) by performing drying or de-saturating at different pressures.

4 Soil-Suction Testing

The soil-water retention curve (SWRC) was measured using a pressure cell apparatus at low matric suction range and filter paper technique at high matric suction range. The pressure cell apparatus with a 500 kPa ceramic plate was used for measuring the SWRC following the drying path in the suction range of 0 to 500 kPa (ASTM D6836-02). The filter paper technique (ASTM D5298-10) was then used for measuring the matric suction for a range of 500 to 10,000 kPa. For this technique, Whatman No.42 filter paper was used in the present experimental program. Fig. 2 shows the SWRCs measured for the suction range of 0 to 10,000 kPa. At select suction cycles, the specimen dimensions were measured. The volumetric change measured was then estimated and applied to the calculations of volumetric water contents corresponding to the respective values of suction pressures.

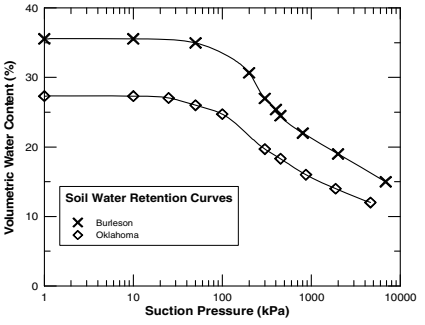

Fig. 2. Soil water retention curves for Texas and Oklahoma soils.

The change in volume is predominant in expansive clays during application of suction conditions which alters the volumetric water content in the compacted soil specimens. Hence forth, care is taken to measure the volumetric changes during suction cycles.

For swell studies, clay specimens were first subjected to different suction pressures of 100, 300 and 450 kPa via pressure cell testing. The specimens after reaching equilibrium conditions were then taken out and transferred to the oedometer cells for swell studies. It is likely that there will be a small increase in the volume of soil specimen during the transfer process which may contribute to a slight increase in the soil suction. This increase in soil suction was however kept to minimum by performing the test immediately.

4.1 Relationship between Initial Suction and Free Swelling Strain

The extracted specimen was transferred to oedometer for the determination of 1-D swell. The unsaturated specimen housed in a steel ring was first wetted under a small token load of 1 kPa and the vertical swelling was monitored. The test was conducted for a period of 48 hours or until the secondary swelling of the clay was approached.

The expansive clay specimens subjected to higher suction levels have shown higher percentage of free swell. The slopes of the one dimensional swell curves for Texas clay are steep when compared to Oklahoma clay. The presence of mineral Montmorillonite could be the key factor governing the slopes and the vertical heave. A swell strain of 9.5% is obtained for Texas soil specimen at OMC-MDD where as a swell strain of 5.2% is measured for Oklahoma soil specimen at OMC-MDD as shown in Fig. 3. Variations in swell strains are attributed to the dominant clay minerals and their percents in the clay fraction. Fig. 4 shows the variation of maximum 1D vertical swell with change in matric suction in the soil. Swell strains are determined for both soils at full saturation conditions (i.e matric suction of 0 kPa). Swell strains were obtained since both soil specimens were restrained during the saturation process. However, when they were taken out from the moulds and

then subjected to free vertical swell movements, they experienced same magnitudes of swell strains. These samples were tested for several days and hence full saturation conditions were recorded in the soil specimens. Overall, these tests indicate that both soils experienced similar swell strains due to swelling of different clay minerals in them. However this trend is not noted when the same soils were compacted and tested at other matric suction states. Higher swell strains were recorded in soils containing high Montmorillonite minerals. It can be stated that the matric suctions in soils are related to the pore size distribution in clays, which in turn depends on the fines distribution in particular with fine clay fraction, Montmorillonite. Also, it is possible that clay mineral swelling will be higher at desaturation conditions as clay particles at this state will have more affinity towards holding water molecules.

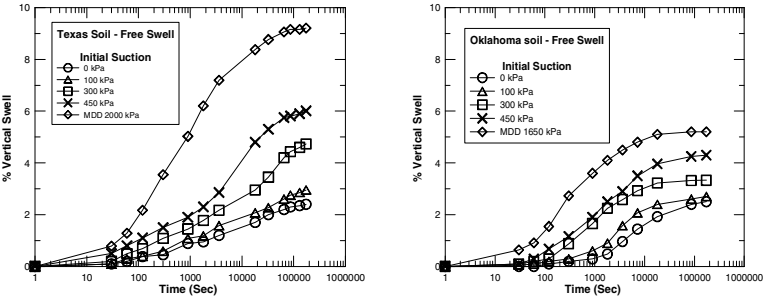

Fig. 3. Relationship between the percentage 1 Dimensional vertical swell and time for the two compacted expansive soil specimens tested at different initial suctions.

4.2 Relationship between the Initial Suction of the Soil Specimen and the Constant Volume (CV) Swelling Pressure

The clay specimens after subjecting them to the desired matric suction pressures (100, 300 & 450 kPa) were also transferred to the standard oedometer cell for swell pressure tests. The oedometer assembly was then fixed to a light frame consolidometer and tested for Constant Volume (CV) swelling pressure test in accordance with ASTM D4546 (2000). Fig. 5 shows the plot of swelling pressure versus logarithmic of soil initial suction (ψ_i) for the two expansive clays.

Test results summarized in Fig. 5 show that the swelling pressure increased with an increase in matric suction and this relationship shows a non-linear trend. The maximum bend in the swelling pressure curve occurs at an air entry pressure (ψ_a) value. The slope of the swelling pressure curve corresponding to the Texas clay is relatively high when compared to the same measured on Oklahoma clay.

The Montmorillonite dominant Texas soil as expected showed significantly higher swelling pressures with respect to matric suction in comparison to the Oklahoma soil which predominantly had Illite. Also, the swelling pressure curve appears to have a same pattern as that of the SWRC plots. The maximum change in

swelling pressure occurs at the air entry pressure of the SWRC. The intersection of the two tangents drawn from the initial portion of the swelling pressure curve and final portion is approximately same as the air entry pressure (ψ_a) of the SWRC.

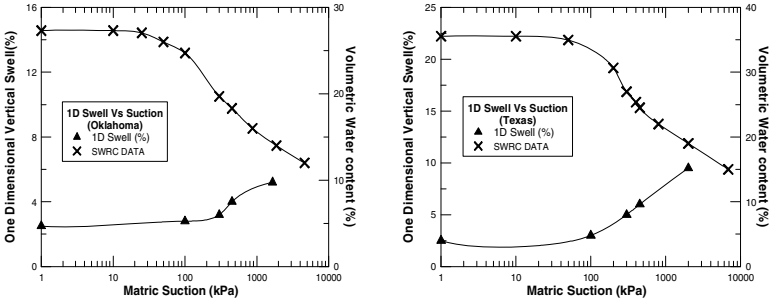

Fig. 4. Showing the soil water retention curves and maximum one dimensional vertical swell (%) plotted against matric suction.

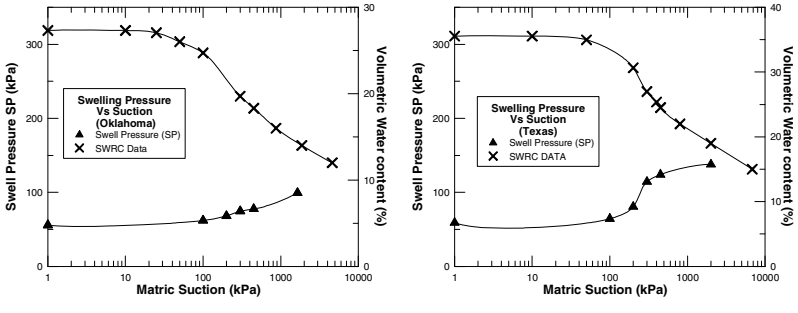

Fig. 5. Showing the soil water retention curves and Swelling pressure plotted against matric suction.

5 Conclusions

In the present study two expansive clays were studied for their swell and matric suction behaviors. The SWRC for Texas soil exhibits a higher water retention capacity and a steeper slope when compared to the same of Oklahoma soil. Also, the air entry value is higher for the Texas soil. Texas soil showed the maximum swelling behavior which is mainly attributed to the presence of mineral Montmorillonite. Specimens with higher suction have exhibited higher percentage of free swell. The slopes of the best fit line for the swell test for Montmorillonitic clay are steep when compared to Illitic dominant soils. There exists a similarity in the curves of swelling pressure and SWRCs. The matric suctions in soils is related to the pore size distribution in clays, which in turn depends on the clay minerals. Current on-going studies are exploring these swellings in clays as functions of

clay mineralogy and compaction state by studying several soils with distinct clay minerals.

Acknowledgement. The authors would like to acknowledge the National Science Foundation (Program Director: Dr. Richard J. Fragaszy) for supporting this research under NSF Grant No.1031214.

References

Alonso, E.E., Romero, E., Hoffmann, C., García-Escudero, E.: Expansive bentonite–sand mixtures in cyclic controlled-suction drying and wetting. Engineering Geology 81, 213–226 (2005)

ASTM D4546 – 08. Standard Test Methods for One-Dimensional Swell or Settlement Potential of Cohesive Soils, American Society for Testing and Materials

ASTM D5298 – 10, Standard Test Method for Measurement of Soil Potential (Suction) Using Filter Paper, American Society for Testing and Materials (2010)

ASTM D6836 – 02, e1. Standard Test Methods for Determination of the Soil Water Chararcteristic Curve for Desorption Using a Hanging Column, Pressure Extractor, Chilled Mirror Hygrometer, and/or Centrifuge, American Society for Testing and Materials (2008)

Chittoori, B.S., Puppala, A.J.: Quantification of Clay Mineralogy. ASCE, Journal of Geotechnical and Geoenvironmental Engineering (2011) (in press)

Erzin, Y., Erol, O.: Swell pressure prediction by suction methods. Engineering Geology 92, 133–145 (2007)

Erzin, Y.: Artificial neural networks approach for swell pressure versus soil suction behavior. Canadian Geotechnical Journal 44, 1215–1223 (2007)

Kassif, G., BenShalom, A.: Experimental Relationship between Swell Pressure and Suction. Geotechnique 21(3), 245–255 (1971)

Nelson, D.J., Miller, D.J.: Expansive Soils, Problems and Practice in Foundation and Pavement Engineering. John Wiley and Sons Inc., New York (1992)

Ng, C.W.W., Zhan, L.T., Bao, C.G., Fredlund, D.G., Gong, B.W.: Performance of an unsaturated expansive soil slope subjected to artificial rainfall infiltration. Géotechnique 53(2), 143–157 (2003)

Puppala, A.J., Punthutaecha, K., Vanapalli, S.K.: Soil-Water Characteristic Curves of Stabilized Expansive Soils. Journal of Geotechnical and Geoenvironmental Engineering 132(6), 736–751 (2006)

Snethen, D.R.: Characterization of expansive soils using soil suction data. In: Proceedings of the 4th International Conference on Expansive Soils, Boulder, Colorado, pp. 18–23 (1980)

Vanapalli, S.K., Lu, L., Oh, W.T.: Comparison between the measured and estimated 1-D heave of several case studies from various regions of the world. In: GEOMAT 2011, Keynote address, First International Conference on Geotechnique, Construction Materials and Environment, Tsu City, Mie, Japan, November 21-23 (2011)

Vanapalli, S.K., Lu, L.: 1-D heave prediction methods for expansive clays: State-of-the-Art. Accepted for Publication in the International Journal of Geotechnical Engineering (2012)

Zhan, L.T., Ng, C.W.W.: Shear strength characteristics of an unsaturated expansive clay. Canadian Geotechnical Journal 43(7), 751–763 (2006)

Zhan, L.T., Chen, P., Ng, C.W.W.: Effect of suction change on water content and total volume of an expansive clay. Journal of Zhejiang University Science Academy 8(5), 699–706 (2007)

Wetting Characteristics of Compacted Bentonites at Large Applied Suctions

Claire L. Bennett, Snehasis Tripathy, and Hywel R. Thomas

Abstract. The wetting suction-water content soil-water characteristic curves of two bentonites (MX80 and Yellow) were experimentally established using vapour equilibrium technique for a suction range of 3.0 to 300.0 MPa. Compacted bentonites specimens were prepared by statically compacting bentonite powder at targeted densities of 1.2, 1.3, and 1.4 Mg/m^3. The bentonite specimens still within the specimen rings were equilibrated at several relative humidities in test desiccators at zero applied stress. The test results clearly showed that the influence of compaction dry density on the wetting characteristics of the bentonites was insignificant for the entire range of suction considered. On the other hand, the chemical properties of the bentonites influenced the equilibrium water contents.

Keywords: suction, soil-water characteristic, bentonite, swelling.

1 Introduction

Bentonites have numerous industrial uses (Alther 2004, Lagaly & Ziesmer 2004), but have attracted particular interest in specific fields of application, such as landfill cover lining systems and underground toxic waste disposal repositories. The low permeability and high swelling ability of bentonites prevent pollutants and leachate from permeating through the engineered barrier systems into the surrounding environment.

Claire L. Bennett
Geoenvironmental Research Centre, Cardiff University, UK
e-mail: BennettCL@cardiff.ac.uk

Snehasis Tripathy
Geoenvironmental Research Centre, Cardiff University, UK
e-mail: TripathyS@cardiff.ac.uk

Hywel R. Thomas
Geoenvironmental Research Centre, Cardiff University, UK
e-mail: ThomasHR@cardiff.ac.uk

A detailed understating of the hydration processes and the water uptake capacities of compacted bentonites are required in order to assess their behaviour in placement conditions.

The wetting suction-water content soil-water characteristic curves of two bentonites were experimentally determined for laterally confined condition and at zero applied stress. The effects of compaction dry density and the exchangeable cation type on the equilibrium water contents of the bentonites were studied.

2 Background

Bentonites are clays that are composed of mineral crystals of montmorillonite commonly arranged in stacks of several unit layers. Swelling of bentonites occurs in two stages; crystalline swelling and osmotic swelling (van Olphen 1963). Crystalline swelling is a step-wise process of the adsorption of discrete water layers between dry clay platelets (Grim 1968). Hydration of the exchangeable cations and of the exposed clay surfaces occurs at low water contents, whereas osmotic phenomenon is more effective at high water contents (Schanz & Tripathy 2009).

Water vapour transfer within compacted soils generally occurs under thermal, thermo-hydraulic, and hydraulic gradients. Under an applied thermal or thermo-hydraulic gradient, an equilibrium is attained in which the water content of soil increases with an increasing distance from the drying front, whereas it decreases with an increasing distance from the wetting front. Swelling upon adsorption of water vapour is significant in the case of bentonites. Studies on the water adsorption characteristics of homo-ionised bentonites equilibrated at various relative humidities have been well researched in the past (Grim 1968, Likos & Lu 2006). However, studies on the influence of compaction conditions on the water adsorption behaviour of bentonites containing mixture of various exchangeable cations are scarce in the literature.

Keren & Shainberg (1975) stated that at low water contents or high suctions, the adsorption energy of the water is the main driving force responsible for the crystalline swelling in bentonites. An increase in the interlayer space in bentonites occurs while overcoming two attractive forces, such as an electrostatic attraction between the negatively charged clay platelets and the exchangeable cations and van der Waals forces of attraction between the clay platelets. The net effect of the hydration energy and the attraction energies along with the changes in the water phase, lattice geometry and position of the cations influence the amount of water adsorbed by a bentonite.

The amount of water vapour adsorbed by Ca-bentonite has been shown to be greater than Na-bentonites within a relative humidity range of 0 to 85.0% (Grim 1968, Keren & Shainberg 1975, Likos & Lu 2006). Keren & Shainberg (1975) stated that in Ca-bentonites, the energy of interaction between the negatively charged surfaces of clay platelets and first mono-layer of water molecules adsorbed is greater than the energy of condensation of the subsequent layers, whereas in Na-bentonite, the difference between these two energy terms is less, indicating that the hydration forces in Na-bentonite are less than those in Ca-bentonite.

Meleshyn & Bunnenberg (2005) stated that a demixing of divalent and sodium cations occurs in the interlayer spaces of a sodium-rich/magnesium-poor montmorillonite, and such a demixing strongly changes the swelling behaviour of bentonites. Likos & Lu (2006) showed that for a range of void ratio of 0.65 and 1.35, Ca-bentonite exhibited greater axial deformations as compared to Na-bentonite at a relative humidity of 93.0%.

3 Materials and Methods

Two commercially available bentonites were selected for the current study: MX80 bentonite, from Wyoming, and Yellow bentonite, from Greece. The total and fractional cation exchange capacities of the bentonites were determined. The exchangeable cations present in MX80 bentonite were found to be sodium (51.24 meq/100g), calcium (28.24 meq/100g), and magnesium (9.43 meq/100g). A majority of exchangeable cations in Yellow bentonite were found to be calcium and magnesium (63.42 and 12.97 meq/100g) with a small fraction of sodium ions (7.66 meq/100 g). The properties of the bentonites used are presented in Table 1.

Table 1. Properties of the bentonites.

Properties	MX80 bentonite	Yellow Bentonite
Specific gravity of soil solids, G_s	2.80	2.84
Liquid limit, w_L (%)	437.0	135.0
Plastic limit, w_P (%)	63.0	58.0
Shrinkage limit, w_S (%)	12.2	13.6
Specific surface area, S (m^2/g)	676.0	797.0
Cation exchange capacity, B (meq/100g)	90.31	84.91
Weighted average valency, v	1.42	1.90

The initial water content of Yellow bentonite (17.6%) was found to be greater than that of MX80 bentonite (9.8%). The wetting suction-water content soil-water characteristic curves of the bentonites were established using vapour equilibrium technique. In total six saturated salt solutions were considered (ASTM E 104-85, 1998). The saturated salt solutions generated relative humidities between 11.0 and 98.0% (Table 2). The total suction is related to the relative humidity by Kelvin's law. The applied suction varied between 3.3 and 294.8 MPa.

Compacted bentonite specimens were prepared by statically compacting bentonites powder at hygroscopic water contents in thick-walled stainless steel specimen rings in a single lift to targeted dry densities of 1.2, 1.3, and 1.4 Mg/m^3. The diameter and height of the specimens were 45.0 mm and 8.0 mm, respectively. The bentonite specimens, still within the specimen rings, were equilibrated at several relative humidities in the test desiccators at zero applied stress. Additionally,

powder specimens of the bentonites were also tested for comparison. The laboratory tests were carried out in a temperature controlled laboratory at 20 ^{0}C.

Table 2. Details of the saturated salt solutions used in this study.

Salt	Relative humidity (%), at 20^{0}C	Suction (MPa)
Potassium Sulphate (K_2SO_4)	97.6 ± 0.5	3.3
Potassium Nitrate (KNO_3)	94.6 ± 0.7	7.5
Potassium Chloride (KCl)	85.1 ± 0.3	21.8
Sodium Chloride (NaCl)	75.5 ± 0.1	38.0
Potassium Carbonate (K_2CO_3)	43.2 ± 0.3	113.3
Lithium Chloride (LiCl)	11.3 ± 0.3	294.8

The equilibration time was found to be less than two months in all tests. In general, the equilibration time reduced with a decrease in the relative humidity. Typical elapsed time versus water content test results for Yellow bentonite specimens are shown in Fig. 1. The test results are for a dry density of 1.4 Mg/m^3.

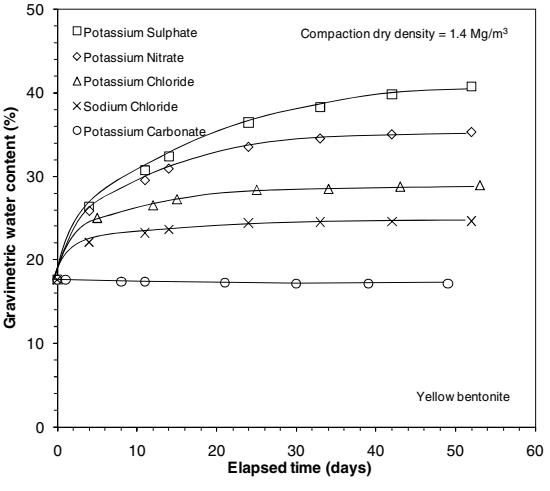

Fig. 1. Typical vapour equilibrium test results for Yellow bentonite specimens.

4 Results and Discussion

The wetting suction-water content soil-water characteristic curves for MX80 and Yellow bentonites are presented in Fig. 2. Fig. 3 presents the test results in a semi-*log* plot. The test results clearly showed that the gravimetric water contents for

Yellow bentonite were considerably greater than that of MX80 bentonite at all suctions considered in this study. This occurred primarily due to greater fractions of divalent cations present in Yellow bentonite as compared to MX80 bentonite. Additionally, the influence of compaction dry density on the equilibrium water contents of the bentonites was found to be negligible. Some minor differences were noted between the test results of the powder specimens and the compacted specimens, particularly at smaller applied suctions (< 21 MPa) and can be attributed to microstructural differences between the powder and compacted specimens.

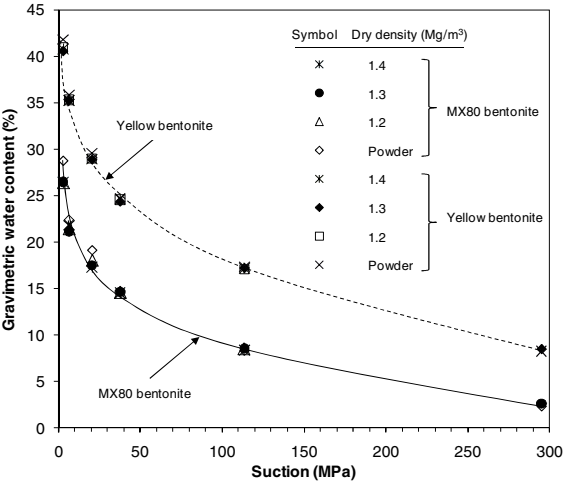

Fig. 2. Wetting suction-water content soil-water characteristic curves of the bentonites.

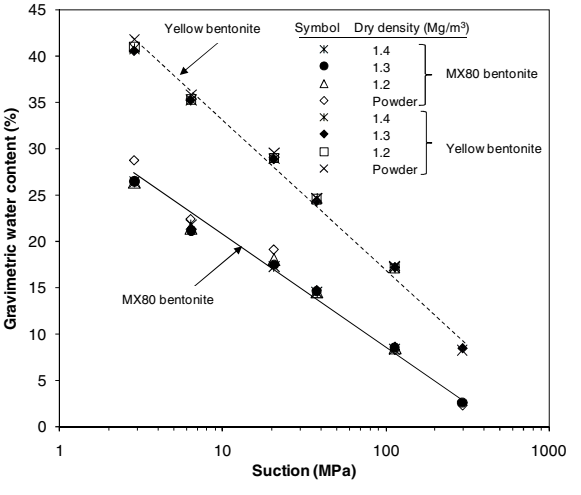

Fig. 3. Wetting soil-water characteristic curves of the bentonites (semi-*log* plot).

The suction-water content soil-water characteristic curves of the bentonites (Fig. 2) were found to be concave upward, similar to that which has been observed for Ca-bentonite (Keren & Shainberg, 1975). This indicates that the energy of interaction between the first mono-layer of water molecules adsorbed and the negatively charged surfaces in both cases were similar, with only difference being the magnitude of hydration force. In a semi-*log* plot the wetting suction-water content soil-water characteristics exhibited near-linear relationships (Fig. 3).

5 Conclusions

The water adsorption characteristics of two bentonites were investigated for a range of suction of 3.0 to 300.0 MPa. Compacted bentonites specimens with dry densities of 1.2, 1.3, and 1.4 Mg/m^3 and powder specimens of the bentonites were allowed to equilibrate at several relative humidities in vapour equilibrium tests. The test results showed that the effect of dry density had negligible impact on the water uptake behaviour of the bentonites. The divalent-rich Yellow bentonite demonstrated greater water uptake capacity than the Na-rich MX80 bentonite. The difference in the water adsorption behaviour of the bentonites is primarily due to the difference in the adsorption energy.

References

Alther, G.: Some Practical Observations on the Use of Bentonite. Environmental and Engineering Geoscience X(4), 347–359 (2004)

ASTM E 104-85, Standard Practice for Maintaining Constant Relative Humidity by means of Aqueous Solutions, Annual book of ASTM standards (11.03), pp. 781–783 (1998)

Grim, R.E.: Applied Clay Mineralogy. McGraw-Hill, New York (1968)

Keren, R., Shainberg, I.: Water vapour isotherms and heat of immersion of Na/Ca-montmorillonite systems I: homo-ionic clay. Clays and Clay Minerals 23, 193–200 (1975)

Lagaly, G., Ziesmer, S.: Colloid chemistry of clay minerals: the coagulation of montmorillonite dispersions. Advances in Colloid and Interface Science 100-102, 105–128 (2004)

Likos, W.J., Lu, N.: Pore-Scale Analysis of Bulk Volume Change from Crystalline Interlayer swelling in Na- and Ca- Smectite. Clays and Clay Minerals 54(4), 516–529 (2006)

Meleshyn, A., Bunnenberg, C.: Swelling of Na/Mg-montmorillonites and hydration of interlayer cations: A Monte Carlo study. The Journal of Chemical Physics 123, 074706 (2005)

Schanz, T., Tripathy, S.: Swelling pressure of a divalent-rich bentonite: Diffuse double-layer theory revisited. Water Resources Research 45, W00C12 (2009), doi:10.1029/2007WR006495

Van Olphen, H.: An Introduction to Clay Colloid Chemistry. Wiley, New York (1963)

Measurement of Swelling Pressure for Bentonite under Relative Humidity Control

Tomoyoshi Nishimura, Junich Koseki, and Masafumi Matsumoto

Abstract. Several experimental producers including using suction control to interpret swelling pressure for compacted bentonite have become generally accepted in geo-environmental engineering. This study focuses on both soil-water characteristic curve and swelling pressure of compacted bentonite. Soil-water characteristic curve was measured using vapour pressure technique. Compacted bentonite having two different soil suctions were prepared for swelling pressure tests. This new swelling pressure testing apparatus was developed in order to measure swelling pressure in a constant relative humidity environment. The apparatus was mainly consisted of the triaxial chamber and relative humidity control circulation system. The total volume of compacted bentonite was maintained constant during absorption process. This study demonstrates the influence of soil suction on swelling pressure under permitted adsorbed water into the compacted bentonite. Change of soil suction influenced the maximum swelling pressure of compacted bentonite.

Keywords: soil suction, bentonite, soil-water characteristic curve, swelling pressure, relative humidity.

Tomoyoshi Nishimura
Ashikaga Institute of Technology, Tochigi, Japan
e-mail: tomo@ashitech.ac.jp

Junich Koseki
University of Tokyo, Tokyo, Japan
e-mail: koseki@iis.u-tokyo.ac.jp

Masafumi Matsumoto
Geotechnical Engineering General Institute, Tochigh, Japan
e-mail: mmand3e@nifty.com

1 Introduction

Several experimental procedures to interpret shear strength, volume change and seepage hydraulic conductivity for unsaturated soils have become generally accepted in geotechnical and geo-environmental engineering. Soil suction or total suction corresponds to the free energy of the soil water and is comprised of two components identified as matric suction and osmotic suction (Krahn & Fredlund 1972). Delage et al. (1987) successfully used the osmotic technique to investigate unsaturated soil behaviour. The vapour pressure technique is used in the triaxial test apparatus for determining the unsaturated soil parameters. Several papers have reported modified shear testing devices to determine the shear strength of unsaturated soils over the last several decades (Blatz & Graham 2000, Nishimura & Fredlund 2001).

This study focuses on both soil-water characteristic curve and swelling pressure of compacted bentonite with high soil suctions. A new swelling pressure testing apparatus was developed to determine swelling pressure in a constant relative humidity environment. The apparatus consists of a triaxial chamber and relative humidity control circulation system. This study demonstrates the influence of soil suction on the swelling pressure under permitted absorbed water into the compacted bentonite. Soil suction used in this paper means total suction.

2 Test Procedure

2.1 Soil Material

Sodium bentonite was in for this test program. Silica sand was mixed with bentonite at a ratio of 30 % by dry weight. The specimen was statically compacted in rigid steel mold at an initial water content of 5.9 %. The compacted bentonite specimen had a dry density of 1.6 g/cm^3 as target value. The height of specimen was 25.5 mm. Also the diameter of specimen was 60.0 mm. Soil suctions of both compacted bentonite and salt solutions were measured directly using a chilled mirror dew point potentiometer (WP4-T of DECAGON DEVICES).

2.2 Modified Swelling Pressure Apparatus

The modified swelling pressure testing apparatus consisted mainly of a triaxial chamber, a pedestal, a steel mold, a double glass burette, a differential pressure transducer, a difference displacement sensor, load cell sensor and relative humidity control circulation system. The relative humidity control circulation system is established using a conventional pump, along with a small chamber with salt solution. The air flow maintained a constant relative humidity surrounding the compacted bentonite.

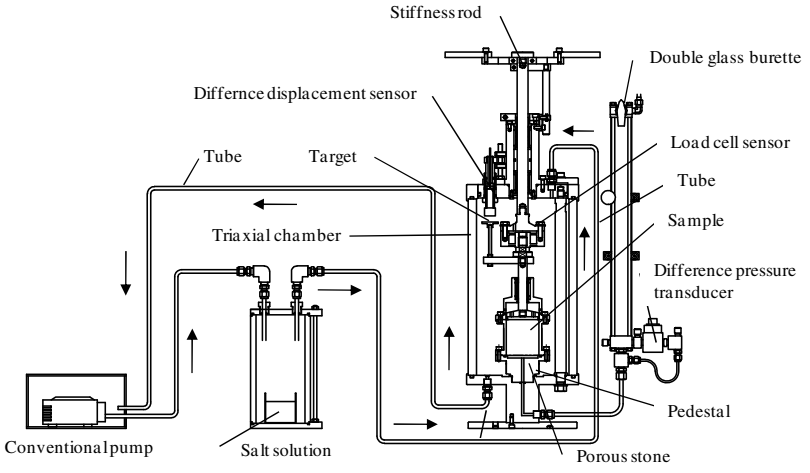

Fig. 1. Newly modified swelling pressure apparatus.

Fig. 1 shows the modified swelling pressure testing apparatus. All compacted bentonite specimens were placed into steel mold. Inflow from the double glass burette due to absorption was allowed from the low portion of specimen. Absorption water volume change in the double burette was measured using the differential pressure transducer. Initial total volume was maintained constant for all compacted bentonite specimens.

2.3 Testing Program

The soil-water characteristic curve is measured in this testing program. The small samples were put on glass contains that were placed in the glass desiccators with salt solutions for at least one month. The initial sample had a diameter of 2.0 cm and a height of 1.0 cm, respectively. The salt solution created the equilibrium relative humidity. After all samples have achieved equilibrium condition, both the gravimetric water content and volume deformation were measured.

Compacted bentonite specimens with two different soil suctions were prepared for swelling pressure tests. Initial compacted bentonite had a soil suction of 105 MPa. Soil suction of 2.8 MPa was imposed using vapour pressure technique. Soil suction of 2.8 MPa corresponds to relative humidity of 98 %. The gravimetric water content changed due to effect of relative humidity. The gravimetric water content of the compacted bentonite sample subjected to relative humidity of 98 % increased to 9.7 % from 5.9 %. Also, expansive deformation was induced when soil suction was decreased resulting in a vertical strain of 9.5 %. The dry density of the sample having soil suction of 2.8 MPa decreased to 1.427 g/cm^3.

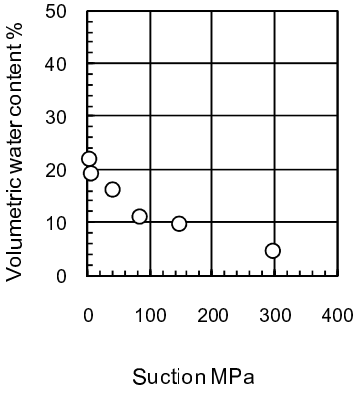

Fig. 2. Soil-water characteristic curve of compacted bentonite.

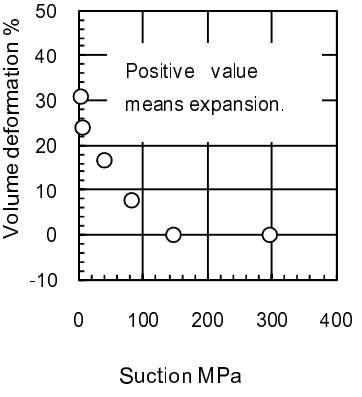

Fig. 3. Relationship between volume change and soil suction of compacted bentonite.

3 Test Results

3.1 Soil-Water Characteristic Curve

Relationship between gravimetric water content and suction of the compacted bentonite is shown in Fig. 2 as a soil-water characteristic curve. The bentonite had a gravimetric water content of 2 % at a suction value of 296 MPa. The soil suction at 105 MPa corresponds to initial gravimetric water content of 5.9%. Volume deformation with soil suctions are shown in Fig.3. The expansions increased with decreasing of soil suction.

3.2 Swelling Behaviour

Swelling pressure tests under constant volume were conducted on compacted bentonite specimens. Fig. 4 shows the swelling behaviour of compacted bentonite at initial water content of 5.9 % with an initial soil suction of 105 MPa. The swelling pressure increased rapidly at the beginning of the absorption phase. The swelling pressure remained increasing till elapsed time was 75 hours and reached swelling pressure of 353 kPa. Subsequently, the compacted bentonite decreased in swelling pressure. The swelling pressure indicated minimum value near elapsed time of 350 hours. The swelling pressure increased smoothly after the swelling pressure achieved a minimum value.

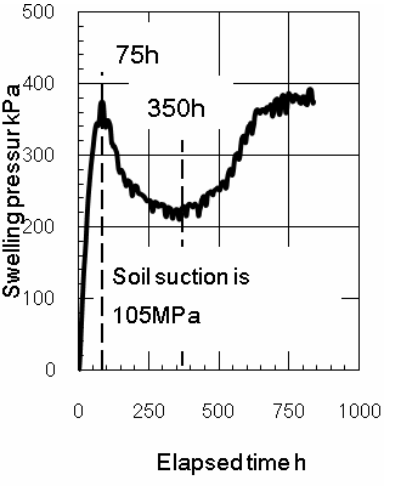

Fig. 4. Variation of swelling pressure for soil suction of 105 MPa.

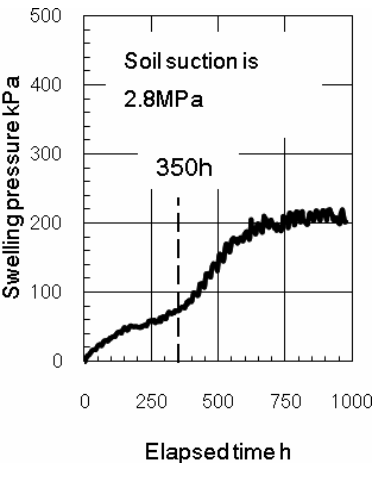

Fig. 5. Variation of swelling pressure for soil suction of 2.8 MPa.

Table 1. Summary of swelling pressure tests.

Sample	Initial	1
Soil suction before swelling test MPa	105	2.8
Maximum swelling pressure kPa	376.3	206.9
Total absorption water cc	31.4	35.6
Gravimetric water content after swelling test %	31.1	38.7

It is observed that swelling pressure become steady condition at 750 hours. Swelling pressure of 376.3 kPa was measured at end of test. The compacted bentonite with soil suction of 2.8 MPa shows smoothly increasing swelling pressure at beginning of test to the elapsed time of 350 hours. This behaviour is shown in Fig. 5. Subsequently, inclination of swelling pressure becomes to be large. The swelling pressure approached steady state similar to the characteristic observed in the compacted bentonite with soil suction of 105 MPa as previously mentioned. The variation of swelling pressure was influenced by soil suction of compacted bentonite before swelling. Particularly, the compacted bentonite having soil suction of 2.8 MPa showed smoothly increasing swelling pressure compare to initial soil suction.

Maximum swelling pressure and total absorption water obtained from swelling pressure tests are summarized in Table 1. In case of initial compacted bentonite specimen maximum swelling pressures are larger than bentonite with soil suction of 2.8 MPa. Due to decreasing soil suction maximum swelling pressure decreased. There is a reduction of 169.4 kPa between initial compacted bentonite and

bentonite with soil suction of 2.8 MPa, and reduced to 45 % in maximum swelling pressure according to decreasing of soil suction. The gravimetric water contents at end of swelling tests were presented in Table 1. Measured gravimetric water contents ranged from 31.1 % to 38.7 %. All samples approached to saturation.

4 Conclusions

The soil-water characteristic curve of compacted bentonite was determined as relationship between volumetric water content and soil suction. Volume expansions increased with decreasing of soil suctions. Before swelling pressure test, dry density of compacted bentonite decreased with decreasing soil suction. The maximum swelling pressure is less than that of bentonite with initial soil suction. This shows the influence of soil suction on the swelling pressure. The compacted bentonite approached saturation regardless of soil suction before swelling.

Acknowledgements. Ashikaga Institute of Technology supported this research. The first author acknowledges the discussion with Dr. Julian Gan MDH Engineering Solutions, Saskatoon, Canada.

References

Blatz, J.A., Graham, J.: A system for controlled suction in triaxial tests. Geotechnique 50(4), 465–469 (2000)

Delage, P., Suraji De Silva, G.P.R., De Laure, E.: Un novel appareil triaxial por les sols non-satures. In: Proceedings of 9th ECMFE, Dublin, vol. 1, pp. 25–28 (1987)

Krahn, J., Fredlund, D.G.: On total matric suction and osmotic suction. Journal of Soil Science 114(5), 339–348 (1972)

Nishimura, T., Fredlund, D.G.: Failure envelope of a desiccated, unsaturated silty soil. In: Proceedings of the 15th International Conference on Soil Mechanics and Geotechnical Engineering, Istanbul, August 27-31, vol. 1, pp. 615–618 (2001)

Swelling of Highly Compacted Bentonite-Sand Mixtures Used as Sealing Materials in Radioactive Waste Disposal

Simona Saba, Anh-Minh Tang, Yu-Jun Cui, and Jean-Dominique Barnichon

Abstract. In the radioactive waste disposal concepts, highly pre-compacted bentonite-sand mixtures are considered as appropriate sealing materials to fill the galleries. Compacted elements of bentonite-sand mixtures are placed adjacent to each others, forming a plug that should limit the transfer of radionuclide. The bentonite has proven to have the capability of retaining radionuclides and the capability of swelling when getting in contact with water and then closing all the voids in the system especially the radial technological void being the gap between the bentonite-sand elements and the host rock. Indeed, when the bentonite-sand elements is emplaced in the gallery, they are first in an unsaturated state and they will start being saturated by the host-rock pore water. They will then start swelling, forming a gel that will close the gap. In this work, such hydration process is experimentally analysed on a small scale. The swelling is analysed by time-lapse photography, its kinetic is also studied by image processing. We can see that the swelling of this material is fast and large, and we can distinguish different states of the material during swelling, starting from the dry centre to the outer boundary. On the other

Simona Saba
Institut de Radioprotection et de Sûreté Nucléaire (IRSN), Fontenay Aux Roses, France
Ecole des Ponts ParisTech, Laboratoire Navier, Marne-La-Vallée, France
e-mail: simona.saba@enpc.fr

Anh-Minh Tang
Ecole des Ponts ParisTech, Laboratoire Navier, Marne-la-Vallée, France
e-mail: anhminh.tang@enpc.fr

Yu-Jun Cui
Ecole des Ponts ParisTech, Laboratoire Navier, Marne-la-Vallée, France
e-mail: cui@cermes.enpc.fr

Jean-Dominique Barnichon
Institut de Radioprotection et de Sûreté Nucléaire (IRSN), Fontenay Aux Roses, France
e-mail: jean-dominique.barnichon@irsn.fr

hand, the presence and behaviour of sand grains in the gel formation is evidenced by images as well. The sand grains are found to be covered by bentonite particles and being carried with the bentonite swelling.

Keywords: radioactive waste disposal, bentonite-sand mixture, swelling, digital image analysis.

1 Introduction

In the high-level radioactive waste repository concepts, pre-compacted elements of bentonite-sand mixture could be used as sealing material thanks to its low permeability, high swelling and high radionuclide retardation capacities (Pusch, 1979; Yong et al., 1986). When emplaced in the gallery, such bentonite-based seals are first in an unsaturated state. Once the repository is closed and local groundwater conditions are re-established, water in the host rock formation will flow towards the repository and start saturating the seals from their extremity. When absorbing water, bentonite swells and forms a gel which should fill the radial technological void as the gap between the seal and the host rock. After filling all the technological voids, the gel will be consolidates between the host rock and the swelling core.

In this study, the radial swelling and gel formation are investigated. Small compacted bentonite-sand disks were immerged in distilled water and time-lapse photography coupled with digital image analysis was performed to study their swelling kinetics for different dry densities. Swelling was defined as the variation of the disk surface with time. The growth of the total surface and the reduction of the dry central surface were monitored. The movement of sand grains was also investigated. It was found that the sand grains were firstly pushed radially by the swelling of the bentonite aggregates until the surrounding material becomes too loose to support them: the grains finally dropped down by gravity.

2 Materials and Methods

2.1 Materials

The soil studied is a mixture of MX-80 bentonite (Gelclay WH2) and quartz sand with a bentonite content of 70% in dry mass. The bentonite has a montmorillonite content of 92%; it has an average specific gravity of 2.76, a liquid limit of 520%, and a plastic limit of 42%. The grain size distribution curve determined by sedimentation shows that 84% grains are smaller than 2 μm (clay fraction).

2.2 Methods

The prepared disks have been compacted statically using a mechanical press, they have a diameter of 35 mm and a thickness of 10 mm. Several disks were prepared by compaction at different dry densities. They were then placed between two transparent Plexiglas plates to avoid the axial swelling of the disk when the whole frame was immerged in distilled water. A computer controlled camera was fixed on a special holder above the container at a defined height and was able to take photos automatically at a given time interval. Artificial lighting was used and the system was covered with a black fabric to isolate it from external lights in order to avoid the changing in lights between day and night (see fig. 1).

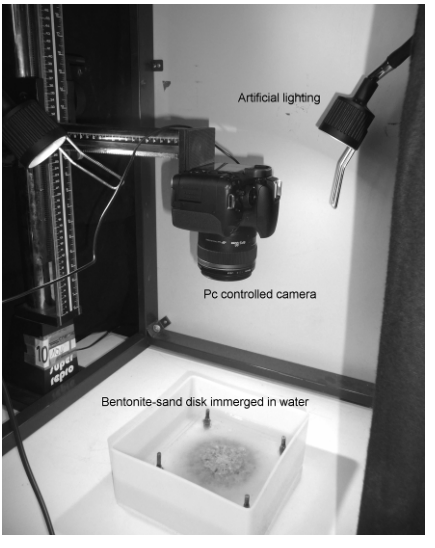

Fig. 1. The experimental system: A computer controlled camera is fixed above a bentonite-sand sample immerged in distilled water to follow its swelling with time.

Photos were then analysed using an image processing program (*Fiji of ImageJ*) to help estimate surface and tracking object movements. For the estimation of surface, an automatic method can be used: photos were first treated (contrast enhancing, illumination, background removal), then a threshold value was applied to isolate the surface of interest. This is a delicate action especially as the interface gel/water is not sharp since the bentonite gel is transparent. Therefore, for the estimation of the surface evolution with time, a manual selection of the surface was used. Finally, to avoid confusion in units, photos are calibrated with the original object units (in mm).

3 Results and Discussion

3.1 General Observation

The swelling of bentonite-sand disks was studied using time lapse photography coupled with digital image analysis. The swelling of the disk is due to the swelling of bentonite present in the mixture.

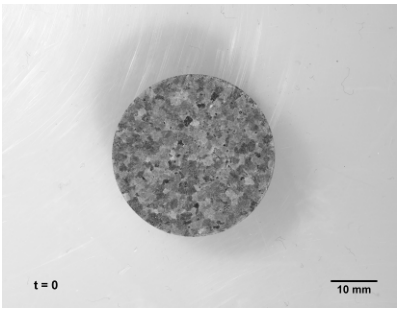

Fig. 2. Initial state of a bentonite-sand disk with a dry density of 1.97 Mg/m^3.

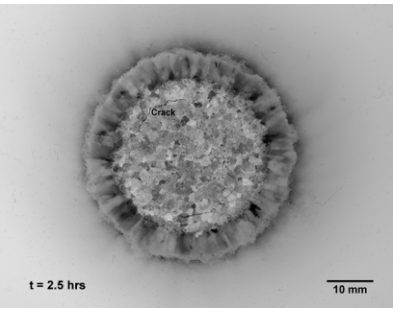

Fig. 3. Same disk after 2.5 hours (swelling = 60%).

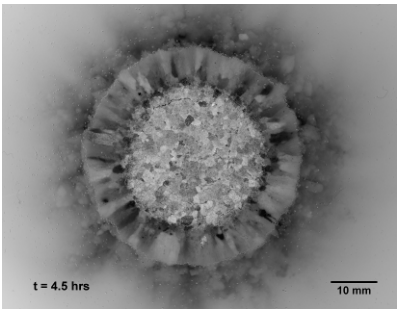

Fig. 4. Same disk after 4.5 hours (swelling = 70%).

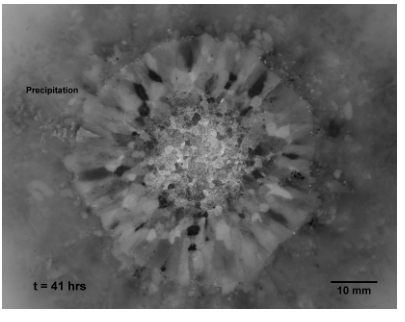

Fig. 5. Same disk after 41 hours (swelling = 125%).

Figs. 2, 3, 4 and 5 show a bentonite-sand disk compacted to a dry density of 1.97 Mg/m^3 at different times during swelling starting from its initial state (Fig. 2). In Fig. 3, it is noted that there are some cracks in the dry centre during the first hours of swelling, and they are closing with time (see Fig. 4) to disappear at the end. This is explained by the rearrangement of the aggregates. The last three

figures show three different states of the material in the disk viewed from its upper face: an external ring of loose gel, a ring of saturated material not turned into gel yet and a dry centre. In fact, water was absorbed by the disk starting from its boundary; the bentonite aggregates on the boundary started swelling first as they have enough free space to produce a gel. Actually, knowing the microstructure of the bentonite aggregates we understand the way they swell when in contact with water (Mitchell, 1993). As water continued infiltrating to the disk, internal bentonite aggregates did not have enough space to swell freely and then did not turn into a gel, while in the dry centre water still did not arrive. With time, the gel on the extremity became very loose due to the exfoliation of the bentonite aggregates and their precipitation to form a bentonite suspension (see Fig. 5). This phenomenon of water over-saturation of aggregates was also evidenced by Montes (2002). It is explained by the existence of a certain amount of water causing the exfoliation of aggregates into small particles (Ye et al. 2009). Consequently, the internal bentonite started swelling freely following the same mechanism. As an overall result, the gel surface became larger and the dry surface became smaller due to water infiltration.

3.2 Swelling Kinetics

Experimental results on the swelling of bentonite-sand disks are obtained after digital image analysis (i.e. a two-dimensional analysis). In Fig. 6, three curves are illustrated: one for the variation of the external total surface of the disk, one for the variation of the dry central surface and the difference between the two curves that represents the surface of the gel ring.

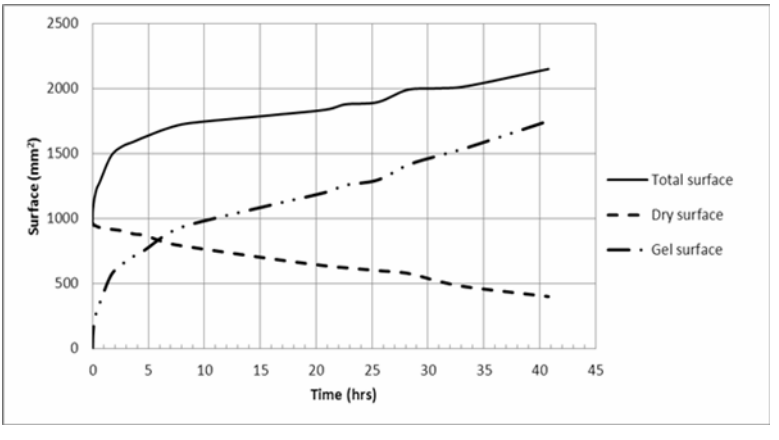

Fig. 6. Variation of the total surface, dry surface and gel surface with time for a bentonite-sand disk having a density of 1.97 Mg/m^3.

The shape of the total surface curve shows a rapid swelling for the first three hours, after that it becomes slightly slower and exhibits a constant rate. The test was stopped after 2 days when the swelling reached 300%. The variation of the dry surface is almost linear, which makes the shape of the gel surface curve similar to that of total surface but with a sharper slope. The gel surface curve is moving towards the total surface curve, which indicates that at a certain time the curves will superimpose and this corresponds to the state where the disk becomes saturated and the maximum swelling is reached.

3.3 Presence of Sand Grains

Fig. 7 shows the trajectory of a sand grain during the disk swelling; the grain apparently disappears after six and a half hours (Fig. 8). In fact, when the disk was in contact with water and the bentonite aggregates started to swell radially, the sand grains were covered by swelled bentonite and were pushed outwards by the pressure from the radial swelling. When the swelled bentonite around the sand grain exfoliated and became loose (similar to a bentonite suspension), the sand grains fell down.

From another point of view, the proportion of sand in the compacted disk is about 30% in dry mass. When the swelled bentonite formed an external ring containing transported sand grains, the volume fraction of sand grains became lower. The concentration in sand grains was lower on the outer boundary of the disk and is mainly located at the bottom.

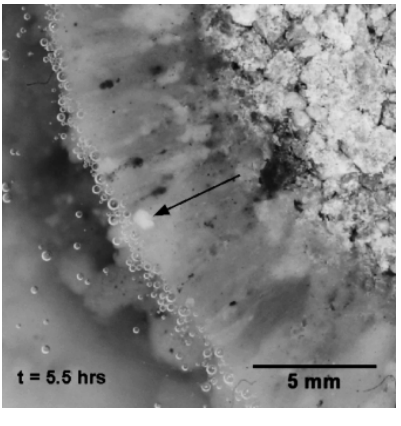

Fig. 7. A sand grain pushed radially in the gel formation.

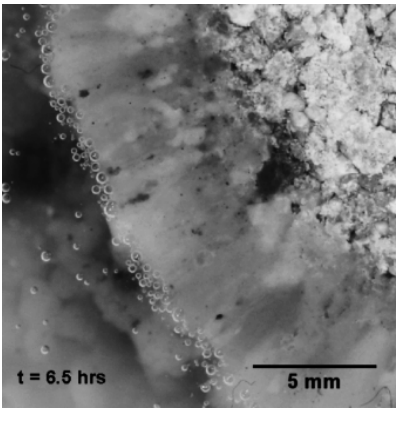

Fig. 8. Precipitation of the sand grain (not visible anymore).

4 Conclusion

The swelling of a compacted bentonite-sand disk is experimentally studied using time-lapse photography coupled with digital image processing. The main advantage

of this method is the rapidity for obtaining qualitative and quantitative results. However, it was difficult to analyse the images automatically due to lack of contrast.

Thanks to the observations of the photos it was possible to identify different states of the material during swelling: the dry centre, the gel extremity and a saturated un-swelled surface in between.

The image analysis allows drawing swelling kinetic curves and tracking the trajectory of a sand grain during swelling. It was found that the swelling started rapidly and then became slower. The sand grains were found to be covered with swelled bentonite and pushed outward until they dropped down and precipitated under gravity when the swelled bentonite became very loose similar to a bentonite suspension.

References

Mitchell, J.K.: Fundamentals of soil behaviour. John Wiley and Sons, Inc., New York (1993) ISBN: 0-471-85640-1

Montes-Hernandez, G.: Etude expérimentale de la sorption d'eau et du gonflement des argiles par microscopie électronique à balayage environnementale (ESEM) et analyse digitale d'images. PhD thesis, Louis Pasteur University, Strasbourg I, France (2002)

Pusch, R.: Highly compacted sodium bentonite for isolating rock-deposited radioactive waste products. Nucl. Technol. 45(2), 153–157 (1979)

Ye, W.M., Cui, Y.J., Qian, L.X., Chen, B.: An experimental study of the water transfer through compacted GMZ bentonite. Engineering Geology 108, 169–176 (2009)

Yong, R.N., Boonsinsuk, P., Wong, G.: Formulation of backfill material for a nuclear fuel waste disposal vault. Canadian Geotechnical Journal 23(2), 216–228 (1986)

Soil-Water Characteristic Curves and Evolution of the Tensile and Unconfined Compression Strength of Drying Slurried Soils

Michail Bardanis and Sofia Grifiza

Abstract. The experimental work presented in the paper explores the soil-water characteristic curve and the evolution of tensile and unconfined compression strength of drying slurried soils. The axis translation technique and the saturated salt solutions method were employed for matric and total suction control respectively. Tensile strength was determined using the splitting tensile (brazilian) test.

Keywords: soil-water characteristic curve, drying, tensile strength, unconfined compression strength, slurries.

1 Introduction

The motivation for studying the drying of slurried soils was the on-going research in the field of constitutive modelling of unsaturated soils, in this particular case of reconstituted soils in the form of slurries drying without any loading prior to the beginning of drying. In this paper fundamental properties of unsaturated slurried soils measured on four fine-grained soils from Greece such as the soil-water characteristic curve (SWCC), the unconfined compression and splitting tensile strength are presented. The tests performed are part of a larger programme on the particular subject and the properties mentioned will eventually be used for constitutive modelling of these soils during drying along with other properties measured.

Michail Bardanis
Edafos Consultant Engineers, Athens, Greece
e-mail: lab@edafos.gr

Sofia Grifiza
Edafos Consultant Engineers, Athens, Greece
e-mail: sgrifiza@edafos.gr

2 The Soils Tested

The soils tested by this stage of the ongoing research are the Corinth and Chalkoutsi Marls, the Parnitha weathered siltstone and the Maroussi Clay. The index properties of the soils are summarised in table 1. The Corinth Marls are a very well-studied formation (Kavvadas et al. 2002) through which the Corinth Canal was excavated until put in operation in 1893. Various experimental investigation programmes have been undertaken in order to investigate the properties of this material including the SWCC of the undisturbed marl and its recomposed counterpart (Bardanis & Kavvadas 2008), where recomposed is the material consolidated from a slurry condition to a desired value of void ratio (preferably that of the undisturbed soil) and then unloaded to zero stress. In this paper the results on reconstituted low plasticity Corinth Marl are presented for the first time. The Chalkoutsi Marl is a formation found 35km north of Athens. High, steep slopes are formed in the formation by sea erosion of their toe with occasional landslides occurring along the 5km coast that the formation outcrops in the highest slopes. The SWCC of the undisturbed material and its recomposed counterpart have been reported by Bardanis & Grifiza (2011). Parnitha weathered siltstone is found in mount Parnitha 30km north of Athens close to the ground surface. Finally, samples of Maroussi Clay came from boreholes drilled as part of a site investigation in the suburb of Maroussi in Athens close to the 2004 Olympic Games complex.

3 Experimental Method

Two methods were employed for suction control; the axis translation technique as applied in a SoilMoisture pressure extractor with 1500 kPa air-entry value porous ceramic disks for matric suction control and the salt solutions method for total suction control. Saturated solutions of the salts presented in table 2 were used. The saturation molalities were measured experimentally. This involves gradual addition of salt increasing the concentration by one m at a time until salt appears as sediment at the bottom of the jar holding the solution. This appearance of sediment is not the definite factor as sediment may appear during and after stirring but finally dissolve after a certain time. The solution prepared at each concentration therefore must be left for the time necessary for chemical equilibrium (typically 48h) and if the sediment at the bottom of the jar has not dissolved it is then recorded that this particular concentration leads to the appearance of sediment. Molalities of the solutions prepared for actual use for total suction control were increased by 1 m relative to the threshold values that sediment appeared for the first time, in order to ensure the ability of the solutions to remain saturated after applying the required suction value to the soil samples. Total weight of the solution was monitored and the required amount of salt was added in order to maintain the concentration constant. This was necessary as the samples placed in the solution chambers were saturated slurries. Water vapour from their drying therefore adds to

Table 1. Index properties of the soils examined.

Soil Name	Abr.	Grain Size Distr. (%)			Atterberg Limits (%)			G_s	USCS Clas.
		Sand	Silt	Clay	w_L	w_P	I_P		
Corinth Marl	CM	8.8	84.7	6.5	30.5	25.0	5.5	2.67	ML
Parnitha Weathered Siltstone	PWS	21.3	47.1	27.5	33.0	16.5	16.5	2.69	CL
Maroussi Clay	MC	18.0	41.9	40.1	47.0	19.0	28.0	2.66	CL
Chalkoutsi Marl	CHM	15.0	64.2	20.5	51.0	21.0	30.0	2.69	CH

Table 2. Characteristics of salt solutions used for total suction control.

Salt	K_2SO_4	$BaCl_2$	KCl	NaCl	$Mg(NO_3)_2$	$MgCl_2$
Total suction measured	4.10	14.1	23.6	39.0	85.5	151.7
Salt saturation molality	1	2	5	6	9	15

the amount of water in the solution as with any sample, but in this case much more as much more water evaporates from the slurries, given their very high initial water content. Therefore by knowing the initial amounts of water and salt in the solution and monitoring the weight of the samples in the chambers one could add the salt necessary to keep the solution saturated as drying of the slurries continued. Saturation molalities are presented in table 2 along with the total suction corresponding to the equilibrium relative humidity of the salt solutions that was measured in a Decagon Devices chilled-mirror hygrometer. Similarly, rather than relying on temperature measurements and Kelvin's law, the total weight of the soil samples placed in solution chambers was monitored until stabilisation and then the samples were taken out and cut in three pieces; one for total suction measurement using the chilled-mirror hygrometer, one for water content measurement and one for immersion in molten paraffin wax for total volume measurement and therefore calculation of void ratio.

All slurries were prepared at an initial water content of $1.5 \times w_L$ using deaired, deionised water, left for hydration for two days in a humidity chamber with occasional stirring in order to avoid sedimentation of coarser particles in the slurry and then placed for at least half an hour under vacuum for removal of air. Samples were placed in lubricated plastic tubes taped on the porous stone of the pressure extractor or tin holders for placement in the salt solutions chambers. Given that samples were slurries in their initial condition, volume decrease during their drying was large. Careful lubrication of the inner surfaces of the tubes was crucial so as to avoid cracking of the samples during shrinkage as any inhibition of the diameter decrease by adhesion to the inner surface of the tubes resulted in cracking.

4 Soil-Water Characteristic Curves

The soil-water characteristic curves measured for all soils are shown in fig. 1 expressed in terms of degree of saturation vs suction. Maroussi clay practically did

not desaturate up to 1500 kPa while all other three soils had already desaturated at 100 kPa of suction (at lower values immersion in molten paraffin wax was impractical as the samples were still very soft to handle). Regarding the second inflection point corresponding to residual water content, it appeared only on the curve of the Corinth Marl close to 800 kPa. Finally, regarding the capability of the samples to hold water in their pores this was found to be the lowest for Corinth Marl, becoming higher for Chalkoutsi Marl, even higher for Parnitha weathered siltstone and the highest for Maroussi clay. Another interesting observation is that curves for both Chalkoutsi Marl and Parnitha weathered siltstone appeared quite flat which will make their modelling very interesting. Modelling of the curves at this stage of the research was avoided until all the curves for reconstituted soils in the research programme are measured and a study of the evolution of their curve-fitting parameters by correlation with the index properties of the soils can be performed.

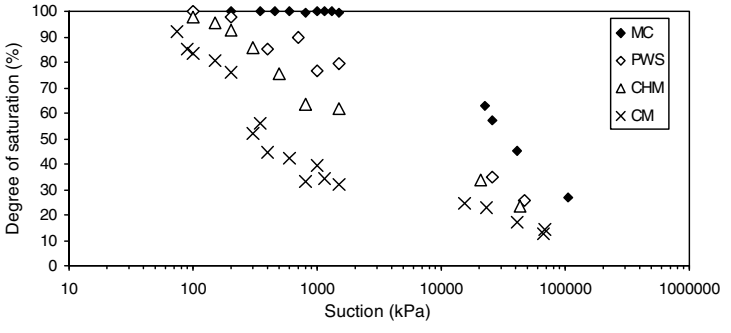

Fig. 1. Soil-water characteristic curves of the four soils dried from an initial condition of slurry.

5 Unconfined Compression Strength and Tensile Strength

Samples for measuring the unconfined compression strength and the tensile strength were prepared in the same manner as already described but were large enough at the beginning of drying in order to provide samples of sufficient size after suction was applied. Plastic tubes used for preparing samples for unconfined compression tests had an internal diameter of 46mm and 110mm height and tubes used for preparing samples for splitting tensile (brazilian) test had an internal diameter of 72mm and 60mm height. These dimensions were selected after several tests were performed as samples placed in them ended up with the required length over diameter ratio at the end of drying. A limited control over the height could be applied by filling the tube up to a certain point in the tubes. Fig. 2a depicts empty tubes taped on the porous stone, fig. 2b the same tubes filled with slurry of

Corinth Marl, and fig. 2c tubes with slurries of Corinth Marl and Maroussi Clay after applying suction. Short 46mm diameter tubes were used only for water content and total volume measurement (by immersion in paraffin wax) –fig. 2a and 2b- while short 72mm diameter tubes were used for splitting tensile (brazilian) tests samples and long 46mm diameter tubes for uniaxial compression test samples –fig. 2c. Occasional leaks observed through the tape at the bottom of the tubes were sealed with plasticine like that indicated by the arrow on fig. 2c. After application of the required suction in the pressure extractor for a minimum of 72h the samples were taken out, weighed immediately and then subjected to loading. After failure the samples were retrieved from the loading frame, carefully enough to collect all small pieces that may have fallen during loading, and weighed again for comparison with their weight before loading. The difference between the initial and the final total weight of the samples was considered a measure of the suction change between removal from the pressure extractor and finishing the loading stage as there was no suction control during this stage.

The tensile strength of unsaturated soils has been thoroughly researched as it gives insight into the modelling of the shear strength of unsaturated soils, whether that is limited to simple models like the extended Mohr-Coulomb failure criterion (linear on non-linear) or more complex constitutive models based on critical state theory extensions for unsaturated soils. Most researchers however have performed tensile strength tests of some sort on compacted soils (e.g. Tang & Graham 2000, Nahlawi et al. 2004) or reconstituted soils which were not undergoing drying (Nahlawi et al. 2004), or soils having undergone combined compression and drying paths (Vesga 2009). The series of tests presented in this paper have been performed on samples of slurry soils subjected to drying without any loading prior to the beginning of drying.

A review of research efforts into the measurement of unconfined strength of unsaturated soils is out of the scope of this paper given the very large number of researchers having studied the subject. For the purpose of completeness the results of Kato et al. (2002) and Pineda & Colmenares (2006) are reported.

Also a clarification of the various types of 'tensile' strength is considered useful. If a sample of soil is isotropically loaded in tension (fig. 3a) then the isotropic tensile strength is obtained, denoted σ_{ti}. To the authors' knowledge no experimental array set up to measure this property has ever been reported. If a sample of soils is uniaxially loaded in tension (fig. 3b) then the uniaxial tensile strength is obtained, denoted σ_{tu}. Another type of tensile strength is the splitting tensile (brazilian) test. In this case a disk-shaped sample is loaded by a linear load on its periphery and the stress condition corresponding to the centre of the sample at failure involves tension in the direction vertical to the external linear load, combined however with a compressive stress in the direction of the external linear load. The stress condition at the centre of the disk-shaped sample is plotted in fig. 3c and the tensile stress at failure is denoted $\sigma_{tb} = -2F/\pi dh$, where F is the external linear load, d and h the diameter and the height of the sample. Except for the tests described already, the stress state corresponding to the uniaxial compression strength is

plotted in fig. 3d. Vesga (2009) reported a new type of test combining the ability to apply direct shear under tensile loading of a specimen (called the direct tensile-shear test). Any combination of two of the stress state conditions shown in fig. 3 and described in this section can yield the cohesion intercept, the angle of friction and the isotropic tensile strength on the assumption of a model for the failure envelope. More combinations of these stress state conditions can offer insight into the appropriate model of the failure envelope to be selected for each soil.

The unconfined compression strength and splitting tensile strength were measured for all soils up to a suction of 1500 kPa applied using the axis translation technique. In fig. 4a the unconfined compression strength is plotted against suction for all four soils, while in fig. 4b the splitting tensile strength. Conventional equipment was used. There was no suction control during the actual loading of the samples. Still the change in their total weight was less than 0.1% before and after loading indicating a minimum change of suction. An important observation on fig. 4 is that both the unconfined compression and the splitting tensile strength obtain finite values after a certain value of suction. This is a critical observation as it indicates that reconstituted soils obtain strength after a value of suction that seems to be a function of the air-entry pressure (AEP) of the slurries. Also although the trend of the tensile strength is dubious, still it seems that the unconfined compression strength tends to stabilise for all soils after 900 kPa of suction.

Sheng et al (2008) reported on a new approach into constitutive modelling of unsaturated soils. They formulated their new model by examining the mechanical

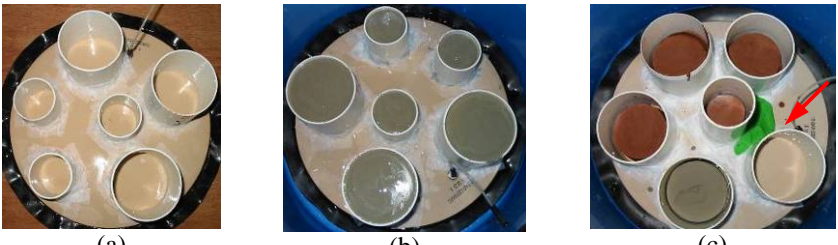

Fig. 2. a) Empty plastic tubes taped on the surface of the porous plate, b) tubes filled with slurried Corinth Marl, and c) tubes and slurried Corinth Marl and Maroussi Clay after drying.

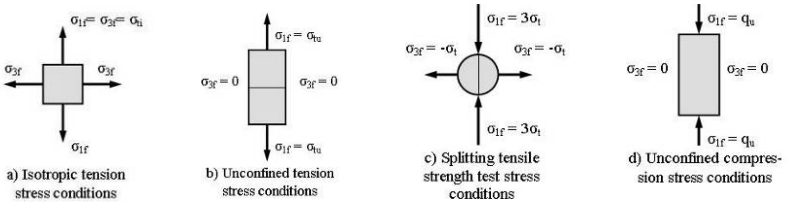

Fig. 3. Stress conditions during various types of tension applied in samples of soils and rock.

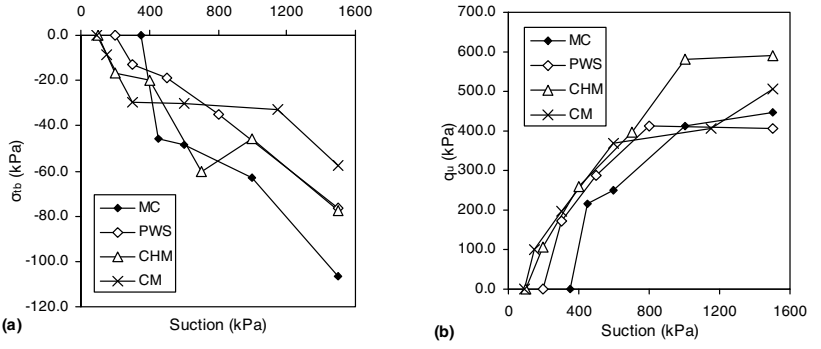

Fig. 4. a) Splitting tensile strength vs suction, & b) unconfined compression strength vs suction.

behaviour of a reconstituted soil that had been consolidated to a finite value of stress, it was then unloaded and started drying. This particular case examined by Sheng et al (2008) corresponds to a soil that when it undergoes drying lies at a distance from the yield locus. The focus of the ongoing research, part of which have been the tests presented in this paper, is to try and model the behaviour of a soil that lies on the yield locus since the beginning of each drying. A typical example of that is a reconstituted clay undergoing drying. This material has not developed any sort of structure, such as that developed due to loading and unloading, and since the beginning of its drying without any stress being applied on it, it undergoes plastic yielding since it obeys the principle of effective stress up to the suction corresponding to the air-entry value of the slurry. Up to that value of suction therefore it undergoes volumetric deformations corresponding to its compression index, therefore plastic volumetric deformation. As an indication of that two samples of Corinth Marl are shown in fig. 5. Both of them were dried and then splitting tensile strength tests were performed. A suction of 50 kPa was applied on the sample shown on the left in fig.5 and a suction of 400 kPa was applied on the

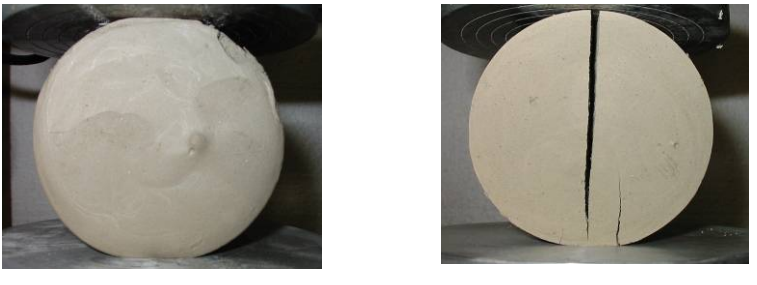

Fig. 5. Splitting tensile (brazilian) strength tests on reconstituted Corinth Marl subjected to 50 kPa of suction (left) and 400 kPa of suction (right).

sample shown on the right. 50 kPa of suction was a value lower than the AEP of the reconstituted Corinth Marl and 400 kPa a value higher than the AEP. The sample subjected to 50 kPa of suction deformed plastically as shown in fig. 5 without cracking or showing any resistance during loading. On the other hand the sample subjected to 400 kPa of suction failed after a minimum of strain was applied. The sample dried to a suction lower than the AEP therefore deforms plastically right from the beginning of loading without exhibiting the development of any strength due to drying. Similar observations were made for the samples of all the other soils dried to suction values below their AEP.

6 Conclusions

The soil-water characteristic curves, the unconfined compression strength and the splitting tensile strength were measured on four soils from Greece reconstituted to an initial water content of 1.5 times their liquid limit. The results presented constitute interim work part of a larger research programme on the properties of reconstituted soils drying without any loading prior to the beginning of drying. The most significant observation so far is that both the unconfined compression strength and the splitting tensile strength obtain finite values after a certain value of suction that seems to be a function of the AEP of the slurries.

References

Bardanis, M., Grifiza, S.: Measuring the soil-water characteristic curve of structured and recomposed soils. In: Anagnostopoulos, A., et al. (eds.) Proceedings of the 15th European Conference on Soil Mechanics and Geotechnical Engineering, Athens, September 12-15, pp. 609–614 (2011)

Bardanis, M.E., Kavvadas, M.J.: Soil-water characteristic curves and void ratio changes relative to suction for soils from Greece. In: Proceedings of the 1st European Conference on Unsaturated Soils, Durham, July 2-4, pp. 263–269 (2008)

Kato, S., Kawai, K., Yoshimura, Y., Sunden, W.: Effect of suction on unconfined compressive strength and undrained shear strength of a compacted silty clay. In: Juca, et al. (eds.) Proceedings of the 3rd International Conference on Unsaturated Soils, pp. 513–519 (2002)

Kavvadas, M.J., Anagnostopoulos, A.G., Georgiannou, V.N., Bardanis, M.E.: Characterisation and engineering properties of the Corinth Marl. In: Tan, et al. (eds.) Proceedings of International Workshop 'Characterisation and Engineering Properties of Natural Soils', Singapore, pp. 1435–1459 (2002)

Nahlawi, H., Chakrabarti, S., Kodikara, J.: A direct tensile strength testing method for unsaturated geomaterials. GTJ. 27, Paper ID GTJ11767 (2004)

Pineda, J.A., Colmenares, J.E.: Stress-strain-suction behaviour of two clayey materials under unconfined conditions. In: Miller, et al. (eds.) Proceedings of the 4th International Conference on Unsaturated Soils, Carefree, Arizona, April 2-5, pp. 1109–1120 (2006)

Sheng, D., Fredlund, D.G., Gens, A.: A new modelling approach for unsaturated soils using independent stress variables. Can. Geotech. J. 45, 511–534 (2008)

Tang, G.X., Graham, J.: A method for testing tensile strength in unsaturated soils. GTJ. 23, 377–382 (2000)

Vesga, L.F.: Direct tensile-shear test (DTS) on unsaturated kaolinite clay. GTJ. 32, Paper ID GTJ101563 (2009)

Shear Strength of a Compacted Scaly Clay from Suction-Controlled Triaxial Tests

Camillo Airò Farulla and Marco Rosone

Abstract. The paper presents the results of an experimental research aimed at investigating the shear strength characteristics of an unsaturated compacted scaly clay. Shear strength was investigated by suction-controlled triaxial compression tests on dynamically compacted samples. Collected results point out that suction effects on stiffness and shear strength can be very different for suction values applied lower or greater than air entry value (AEV), corresponding to the material void ratio.

Keywords: scaly clay, unsaturated soil, suction, shear strength.

1 Introduction

Scaly clays are stiff tectonised clays widespread in Sicily and South Italy. Due to their complex geological history, they are heavily over-consolidated and highly fissured. A thick network of discontinuities subdivides the clays in tightly interlocked small stiff clayey fragments (scales), almost always sharp cornered, whose size ranges from a few millimetres to a centimetre.

Because of their structural characteristics scaly clays may be compacted at natural water content to obtain a material with low permeability and appreciable stiffness and shear strength, suitable for construction material in many Civil and Environmental Engineering applications. The compaction of scaly clay does not eliminate scales which survive as distinct units; however it obliterates their initial geometrical pattern which becomes random (Airò Farulla & Valore 1993).

Camillo Airò Farulla
Università degli Studi di Palermo, Palermo, Italy
e-mail: camillo.airofarulla@unipa.it

Marco Rosone
Università degli Studi di Palermo, Palermo, Italy
e-mail: marco.rosone@unipa.it

Due to their technical properties as construction materials, extensive field and laboratory geotechnical investigations have been carried out at the Università di Palermo during the last forty years, to characterize the mechanical behaviour of unsaturated and saturated compacted scaly clays. With reference to this research work, the paper presents the results from an experimental programme aimed at investigating matric suction effects on the shear strength of an unsaturated compacted scaly clay.

2 Tested Material

Test samples were prepared using a stiff and highly fissured clay outcropping near Palermo (Sicily). It is a silty clay having liquid and plastic limits within the range of w_l = 60 - 64 %, w_p =20 - 26%, mean specific gravity G_s = 2.76, and natural water content w_n = 20%. The air-dried clay having a hygroscopic water content w_h = 5% was disaggregated by means of a rubber pestle, and the fraction passing through a No. 4 ASTM sieve (mesh aperture of 4 mm) was selected. The selected material was moistened to the water content w = 15% and dynamically compacted to the target dry density γ_d = 17.4 kN/m^3. The compaction was carried out by means of a modified Harvard apparatus with a cylindrical mould measuring 76 mm in height and having 38 mm inner diameter. The adopted procedure made use of 5 layers, 14 tamps per layer, and a tamping force of 275 N, giving optimum values: w_{opt} = 17%, $\gamma_{d\text{-}max}$ = 17.5 kN/m^3. Initial conditions of the tested samples were on the left of optimum (Table 1) (Rosone, 2011). Initial total suction of the as-compacted material was approximately 2 MPa (Airò Farulla et al., 2010a). Compacted clay is characterised by a double porosity network (Airò Farulla et al. 2010b).

Table 1. Initial characteristics of tested samples.

Sample	Dry unit weight (kN/m^3)	Water content (%)	Saturation degree (-)
A1	17.46	15.2	0.77
A2	17.30	14.6	0.71
A3	17.26	14.9	0.72
A4	17.48	15.0	0.75
A5	17.26	15.0	0.72
A6	17.55	14.8	0.74
A7bis	17.46	15.4	0.78
S16	17.55	15.0	0.77
S18	17.46	14.7	0.73
S19	17.26	15.4	0,75
S20	17.06	15.2	0.72

3 Testing Apparatus

Tests were carried out using a triaxial apparatus for testing unsaturated soil samples under controlled suction and stress-path conditions. The suction was controlled by means of the axis-translation technique according to the overpressure air method (Romero, 2001). The required suction value was applied by setting constant pore-air pressure (u_a) at the top base of the sample and varying water pressure (u_w) at the bottom of the sample through a high air entry value porous disk (HAEV = 5 bar).

Sample axial strains were calculated on the base of the piston axial displacements measured by means of a LVDT outside the cell. Radial strain values were obtained by monitoring water level variations in an inner cell coaxial to the sample (Rampino et al., 1999). A differential pressure transducer was used to measure the difference in water pressure between the base of the inner cell and that of a reference burette, with a resolution of ± 1 Pa (± 0.1 mm of water level). A similar system connected to the water drainage line allowed to measure water content variations.

4 Experimental Programme

The shear strength of the unsaturated compacted scaly clay was investigated by isotropic consolidated drained suction-controlled triaxial compression tests in the range of matric suction 50 - 200 kPa and confining net stress 50 - 200 kPa.

The applied stress-paths are represented in Fig. 1.

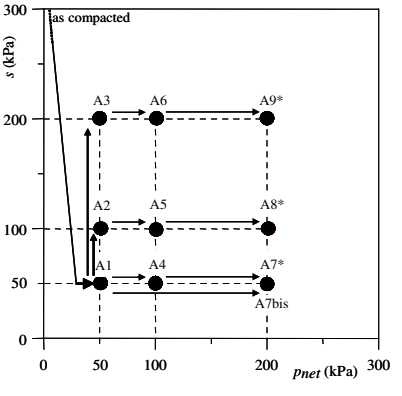

Fig. 1. Stress paths of triaxial compression tests (* multistage tests).

In the first step, specimens were equalized at p_{net} = 50 kPa and s = 50 kPa. The equalization stage was considered accomplished when sample water content variations lower than 0.02% per day were measured. Required time was in the range of

about 700-800 hours. Then, some of the samples were dried at constant confining stress (p_{net} = 50 kPa) by increasing suction to s = 100 - 200 kPa. Isotropic compression to p_{net} = 100 - 200 kPa was carried out at constant suction. Because of the long time required by equalization in the wetting and drying stages, some tests (A7*, A8* and A9*) were carried out with a multistage technique, increasing confining net stress (from 100 to 200 kPa) at constant suction after a first deviatoric step. Test A7bis (p_{net} = 200 kPa and s = 50 kPa) was carried out with the standard technique in order to evaluate reliability of multistage test results. Failure was achieved at constant suction in drained conditions (applied axial strain rate v = 0.028 mm/h). Tests were performed at a constant temperature of 20 ± 1 C°.

Four complementary isotropic consolidated drained triaxial compression tests were carried out on saturated (back pressure $u_{w,0}$ = 400 kPa) compacted scaly clay at confining effective stress σ'_3 = 50 - 300 kPa.

5 Results Analysis

In the initial equalization step specimens swelled, taking in water and increasing saturation degree to S = 0.83 - 0.89.

In the successive drying step, when s was increased to 100 kPa and 200 kPa, void ratio and saturation degree retained almost constant values. Similarly, isotropic compression to p_{net} = 100 kPa did not induce any appreciable volumetric deformation or S variations for all applied suction values. However, in the A7bis test, isotropic compression to p_{net} = 200 kPa (s = 50 kPa) produced a significant volumetric deformation ($\Delta\varepsilon_v \cong 3$ %) at almost constant water content, increasing S to 0.99.

The diagrams in Fig. 2, Fig. 3, and Fig. 4 show deviatoric stress q, volumetric deformation ε_v and saturation degree S as function of axial deformation ε_a for s equal to 50 kPa, 100 kPa and 200 kPa, respectively. The stress-strain behaviour (q-ε_a) can be represented by an elastic-perfectly plastic law. A maximum deviatoric stress is reached for axial deformation between 10% and 12 %.

A very high initial stiffness characterized samples tested with the multistage procedure (A8* and A9*), because of the unloading-reloading cycle of deviatoric stress as consequence of increasing confining net stress, σ_{3net}, from 100 to 200 kPa.

In the failure stage, volumetric deformation was in the range of 1 - 2.5 % for s equal to 50 kPa and 100 kPa, while lower values (ε_v close to 1 %) were measured for s = 200 kPa. Suction effects were also evident on the saturation degree evolution during the failure stage: S always increased for s = 50 and 100 kPa achieving values greater than 0.90 - 0.95, while it retained constant values (near 0.85) for s = 200 kPa. In the case of sample A7bis full saturation induced by the isotropic compression was maintained in the failure stage.

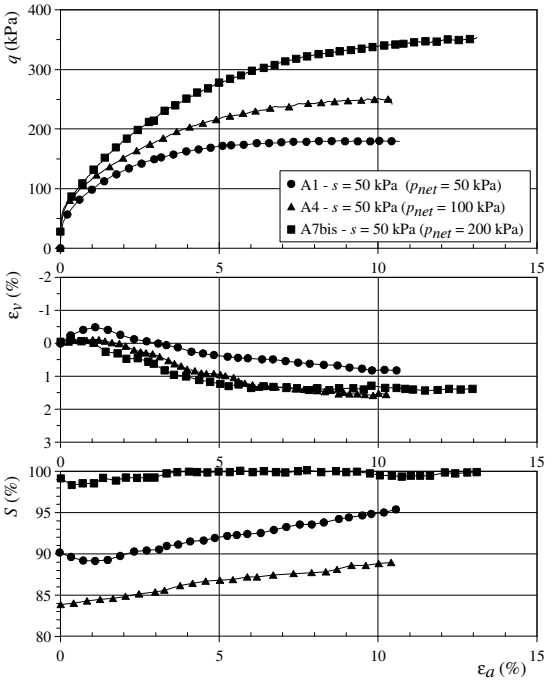

Fig. 2. Results of triaxial compression tests for s = 50 kPa.

Mohr circles at failure are shown in Fig. 5 as suction function, together with the circles related to saturated samples. The best fitting lines of each set of circles (least squares method) are characterised by shear strength angles φ′ in the range of 20°-22° and intercept cohesions increasing as suction increases. Complementary test programmes on the shear strength of saturated samples repeatedly give φ′ values very close to 22°.

According to the collected data, shear strength of the compacted scaly clay can be characterised by a shear strength angle φ′, which as first approximation can be considered constant and equal to 22°, and by an intercept cohesion *c*, which depends on applied suction, according to the Mohr-Coulomb criterion:

$$\tau = c + \sigma_{vnet} \tan \varphi'$$

The intercept cohesion values *c*, recovered from the diagrams in Fig. 5, are represented in Fig. 6 as function of suction. The diagram in Fig. 6 shows that for suction values lower or equal to 100 kPa intercept cohesion values increase according to tan φ′, indicating that suction increments are equivalent to effective normal stress increments as in saturated soils. However, for $s = 200$ kPa the increment of shear strength attenuates considerably. In order to interpret these results it is important to recall that air entry values of compacted scaly clay samples with void ratio $e = 0.55$ - 0.65 are in the range of 100 - 200 kPa (Airò Farulla et al., 2010a).

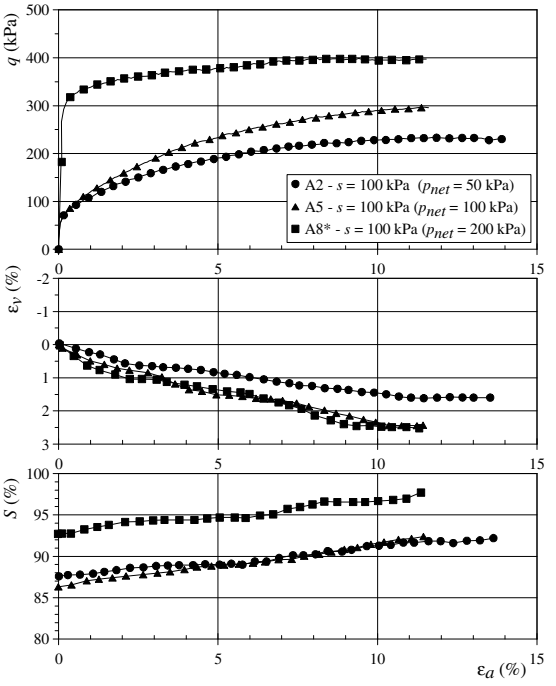

Fig. 3. Results of triaxial compression tests for s = 100 kPa.

Assuming for the shear strength a plane envelope in the space τ, σ_{vnet}, s, according to the equation (Fredlund & Rahardjo, 1993):

$$\tau = c' + (u_a - u_w) \tan \varphi^b + \sigma_{vnet} \tan \varphi' \tag{1}$$

the diagram in Fig. 6 enables to recover a φ^b value slightly higher than 15°.

However, c - s diagram in Fig. 6 shows that experimental data can be better fitted by an hyperbolic envelope, having equation:

$$c = s \,/\, (\cot \varphi' + s/c^*)$$

The best fit (least squares method) of data in Fig. 6 gives $c^* = 227$ kPa. As consequence, the shear strength of the compacted scaly clay can be represented by the following equation:

$$\tau = c' + (\sigma_n - u_a) \tan \varphi' + \frac{s}{\cot \varphi' + \dfrac{s}{c^*}} \tag{2}$$

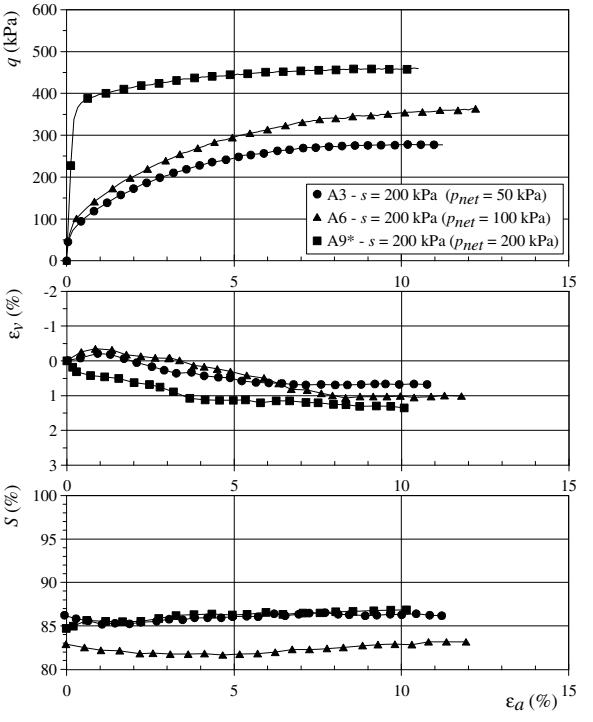

Fig. 4. Results of triaxial compression tests for s = 200 kPa.

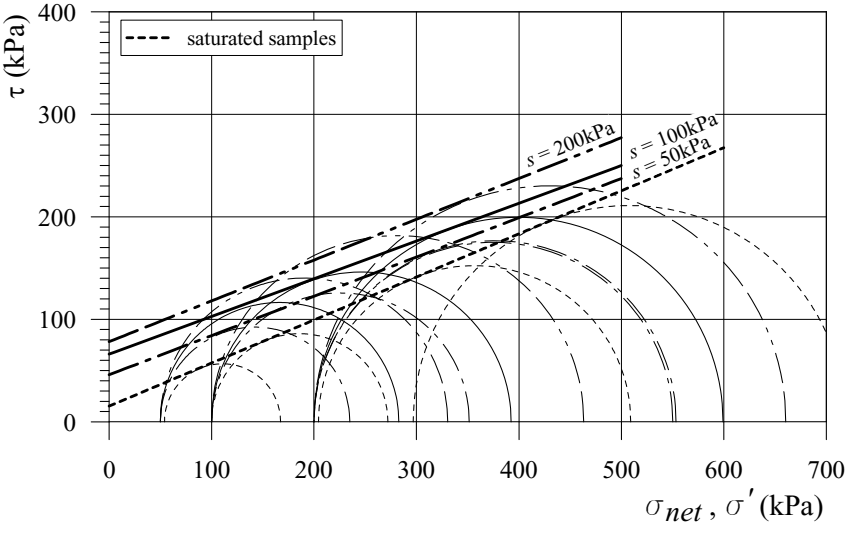

Fig. 5. Shear strength envelopes as suction function.

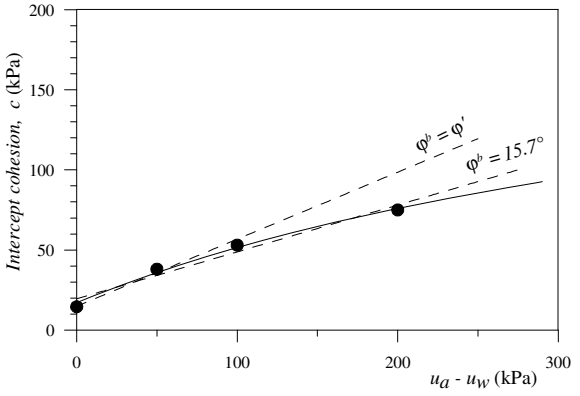

Fig. 6. Intercept cohesion values as suction function.

6 Conclusions

Characterization of shear strength behaviour of unsaturated compacted scaly clays is a fundamental topic in order to analyse stability of earthworks made of these materials. The results presented in the paper enable to make some interesting considerations about suction effects on the stiffness and shear strength of the tested samples. However, further research work is necessary in order to better understand the effects of suction variations on compacted scaly clay shear strength, as in the case of wetting and drying cycles deriving from climatic or earthworks operation conditions.

References

Airò Farulla, C., Battiato, A., Ferrari, A.: The void ratio dependency of the retention behaviour for a compacted clay. In: Alonso, E., Gens, A. (eds.) Proc. 5th Int. Conf. on Unsaturated Soils, Barcelona, Spain, vol. 1, pp. 417–422 (2010a)

Airò Farulla, C., Ferrari, A., Romero, E.: Volume change behaviour of a compacted scaly clay during cyclic suction changes. Can. Geotech. J. 47, 688–703 (2010b)

Airò Farulla, C., Valore, C.: Some aspects of the mechanical behaviour of compacted tectonized clays. In: Proc. Int. Symp. on Geotechnical Engineering of Hard Soil – Soft Rocks, Athens, vol. 1, pp. 335–342 (1993)

Fredlund, D.G., Rahardjo, H.: Soil mechanics for unsaturated soils. J. Wiley, New York (1993)

Rosone, M.: Resistenza a taglio di un'argilla a scaglie compattata non satura. Doctoral thesis - Università Mediterranea di Reggio Calabria – Università degli Studi di Palermo (2011)

Romero, E.: Controlled suction techniques. In: Gehling, W.Y.Y., Schnaid, F. (eds.) 4° Simposio Brasileiro de Solos Nao Saturados, Porto Alegre, Brasil, pp. 535–542 (2001)

Rampino, C., Mancuso, C., Vinale, F.: Laboratory testing on an unsaturated soil: equipment, procedures, and first experimental results. Can. Geotech. J. 36, 1–12 (1999)

Yielding Behaviour of an Alluvial Compacted Soil in Saturated and Unsaturated Conditions

Anastasia Capotosto and Giacomo Russo

Abstract. In this paper some results of an experimental work on the yielding of compacted soils are reported. The yielding behaviour has been investigated by means of triaxial tests on saturated and unsaturated samples. As observed for natural samples, saturated and unsaturated compacted samples showed a nearly elliptical and inclined shape of the yield curve in the effective stress space. Two different analytical expressions for the yield surface were used to fit the experimental data.

Keywords: compaction, triaxial test, partial saturation, yield surface.

1 Introduction

Over the years a significant development has been made with regard to the understanding of stress-strain behaviour of unsaturated compacted soils (Alonso et al. 1990, Toll 1990, Alonso et al. 1995, Wheeler & Sivakumar 1995, Sivakumar & Wheeler 2000) within the general framework of the hardening plasticity, capable of describing from a unified viewpoint the behaviour of saturated and unsaturated soils (Gens & Alonso 1992). In this respect, the fundamental aspect of the framework is the existence of a suction induced (SI) yield locus determined by the maximum previous suction that the soil experienced and a loading-collapse (LC) yield locus determined by the compaction effort.

Anastasia Capotosto
Università degli Studi di Cassino, Cassino, Italy
e-mail: a.capotosto@unicas.it

Giacomo Russo
Università degli Studi di Cassino, Cassino, Italy
e-mail: giarusso@unicas.it

An extensive triaxial testing program (Cantasale & Russo 2008, Capotosto & Russo 2011) has been developed on a compacted alluvial silt used for the construction of the impervious core of the Locone Earth Dam (Croce & Catini 1986). The research is mainly focused on the yield behaviour and the critical state of the compacted soil in both saturated and unsaturated states. In the present work some of the experimental results are presented, highlighting the effects of compaction and matric suction on shape and extension of the yield locus. Two analytical functions fitting the experimental yield envelopes are then critically analysed.

2 Experimental Procedures and Results

A selected passing of an alluvial sandy silt soil of low plasticity was used for the experimental work (Tedesco, 2007). The reconstituted triaxial samples were dynamically compacted following the Proctor Standard procedure (ASTM D 698-91ε1) at optimum water content (w_{opt} = 14.5%, γ_{dmax} = 17.8 kN/m^3). Triaxial tests were performed on saturated specimens (saturation degree S_r at least of S_r = 97%) and unsaturated specimens respectively by means of a controlled stress-path triaxial cell (Aversa & Vinale, 1995) and a stress-path and suction controlled triaxial cell (Aversa & Nicotera, 2002), the latter based on the axis translation technique.

Table 1. Triaxial tests on saturated samples (LSN data set).

Data Set	ID	e_0	w_0 [%]	H
LSN	EV	0.48	14.68	Variable
	E10	0.54	15.13	10
	E3	0.49	14.52	3
	E2	0.53	14.57	2
	E1.8	0.51	14.89	1.8
	E1-EV	0.50	15.06	1-variable
	E0.67	0.50	14.41	0.67
	E0.2-EV	0.47	14.21	0.2-variable

Table 2. Triaxial test on unsaturated samples (LUN data set).

Data Set	ID	e_0	w_0 [%]	η	s_0 [kPa]	S_{r0} [%]
LUN	EV	0.51	14.63	variable	29	78.48
	E10	0.53	13.93	10	55	72.7
	E3	0.48	14.47	3	35	82.2
	E2.5	0.49	14.98	2.5	59	84.41
	E1.5	0.50	14.55	1.5	28	80.09
	E1.2	0.49	14.41	1.2	40	81.2
	E1	0.51	14.64	1	50	78.5
	E0.5	0.56	14.54	0.5	53	71.7

The initial matric suction of unsaturated samples after compaction ranged from 28 to 53 kPa. Initial void ratio e_0 , initial water content w_0, saturation degree S_{r0}, initial suction s_0 of the unsaturated samples and the stress ratio $\eta = \Delta q/\Delta p'$ applied during the deviatoric stage of the tests are reported in Tab. 1 (saturated samples) and Tab. 2 (unsaturated samples).

In Fig. 1 the stress paths followed during saturated and unsaturated tests are represented. Saturated samples were isotropically compressed up to a mean effective stress of p' = 100 kPa, an then deviator stresses were applied at different stress ratios $\eta = \Delta q/\Delta p'$ up to failure. A first stage of suction increase was performed up to 80 kPa for the unsaturated samples, and then an isotropic compression was applied up to a mean net stress of $p\text{-}u_a$ = 100 kPa at constant suction. Then deviator stress at selected $\eta = \Delta q/\Delta(p\text{-}u_a)$ and constant suction was increased up to failure of the sample.

In order to determine the yield surface of saturated and unsaturated samples during shear, a strain energy criterion (Graham, 1974, Crooks & Graham 1976, Tavenas et al. 1979, Houlsby 1979, Houlsby 1997) was applied. The strain energy was then represented as a function of the scalar quantity length of the stress path LSP (Graham et al. 1983) in order to avoid the dependence of the strain energy on the direction of the stress path. Further details of the method can be found in Capotosto & Russo (2011). The graphical procedure for the identification of the yield point in the LSP – W plane is illustrated in Fig. 2a for the isotropic compression stage and in Fig. 2b for the deviatoric stage of the test.

Yield surfaces for natural saturated and unsaturated alluvial soil are reported in Fig. 3. The surfaces are nearly elliptical in shape with major axis inclined in the stress invariants plane, as a result of anisotropy induced by compaction.

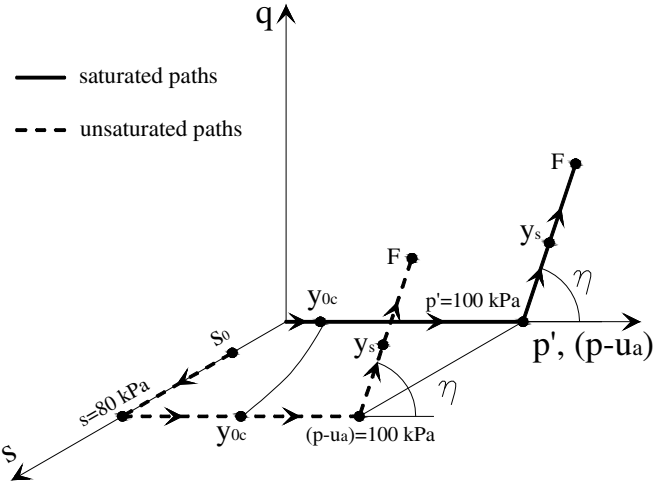

Fig. 1. Stress paths followed during triaxial tests on saturated and unsaturated samples.

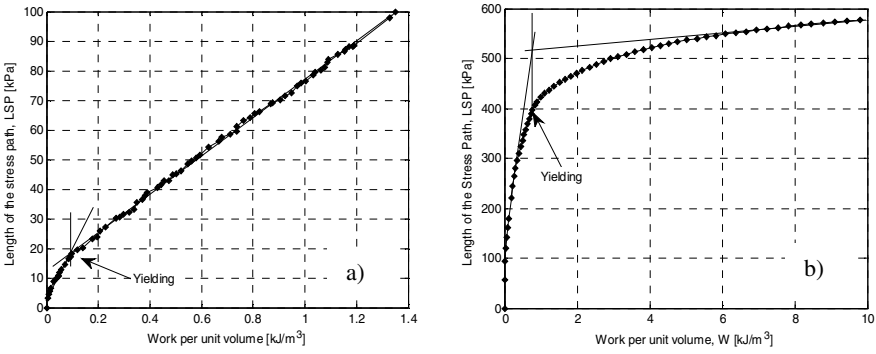

Fig. 2. Yield identification: (a) isotropic compression, (b) deviatoric stage.

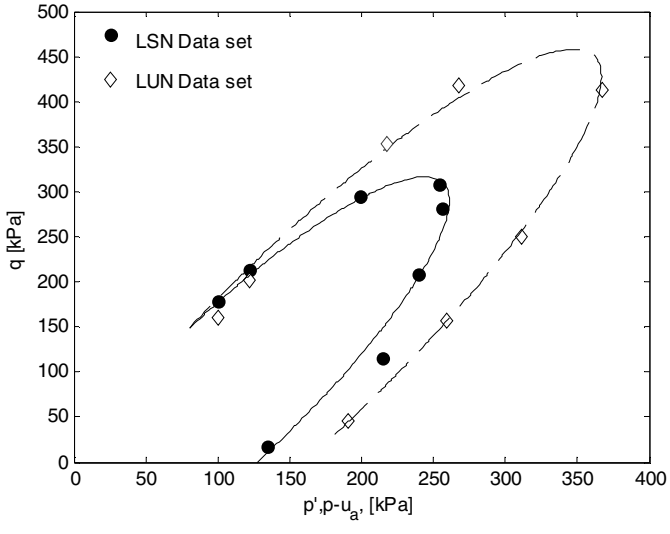

Fig. 3. Yield envelopes of saturated (LSN) and unsaturated (LUN) samples.

The evolution of the yield envelope with increasing suction corresponds to an expansion along the major axes with no significant changes in shape and inclination. As noted by Cui & Delage (1996), this effect can be compared with the stress - hardening effect observed by Graham et al. (1983) for natural soils sampled at various depths.

3 Interpretation of Yielding Behaviour

In order to determine an analytical function interpolating the experimental results, the ellipse function proposed by Taiebat & Dafalias (2010) was firstly considered.

The Authors proposed an analytical relation, very similar to the original yield surface of the modified Cam-clay model proposed by Roscoe & Burland (1968), whose expression in the triaxial space is the following

$$f = \frac{(q - p\alpha)^2}{N^2} + p(p - p_0) = 0 \tag{1}$$

where (Fig.4a) p_0 is the projection of the tip along the p axis (p-u_a for unsaturated conditions), α is a dimensionless variable accounting for anisotropy of the material, N is a factor controlling the shape of the surface. The point at which zero volumetric plastic strains occurs (i.e. $\partial f/\partial p = 0$) is characterised by the top stress ratio η_{top}, which is linked to N and α through the expression

$$\eta_{top} = N^2 + \alpha^2 \tag{2}$$

A best fit of the relevant parameters η_{top}, α, and p_0 of the ellipse functions was then performed on both saturated and unsaturated yield data; the values are summarised in Table 3.

Table 3. Best fit parameters of the Taiebat & Dafalias (2010) ellipse function model.

	α [rad]	η_{top}	p_0 [kPa]
Saturated	1.10	1.5	255.6
Unsaturated	1.10	1.5	367.0

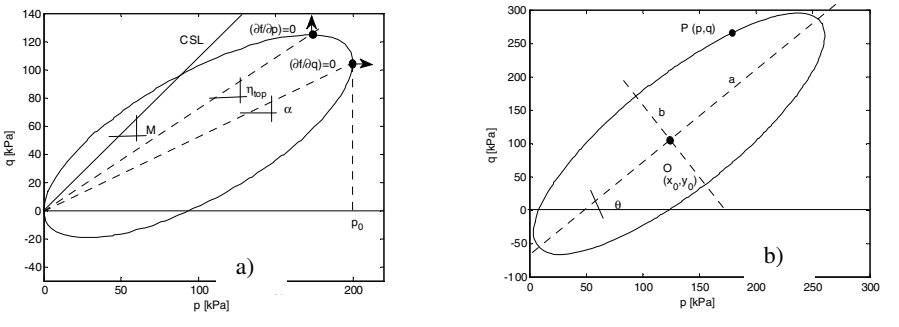

Fig. 4. Analytical yield envelopes: a) Taiebat & Dafalias (2010), b) adopted function.

A different analytical expression of the ellipse was adopted, taking account the possibility of a translation of the ellipse along both the horizontal and vertical axes of the triaxial stress space, differently from the Taiebat & Dafalias ellipse whose translation is allowed only along the horizontal axis. The ellipse function is:

$$\begin{aligned} f = b^2\left[(p-x_0)\cos\theta+(q-y_0)\sin\theta\right]^2 + \\ +a^2\left[-(p-x_0)\sin\theta+(p-x_0)\cos\theta\right]^2 - a^2b^2 = 0 \end{aligned} \tag{3}$$

Table 4. Best fit parameters of the adopted ellipse function.

	a (kPa)	b (kPa)	θ [°]	x_0 (kPa)	y_0 (kPa)
Saturated	212.6	63.1	33.4	132.1	114.4
Unsaturated	462.2	69.2	30.7	141.3	93.7

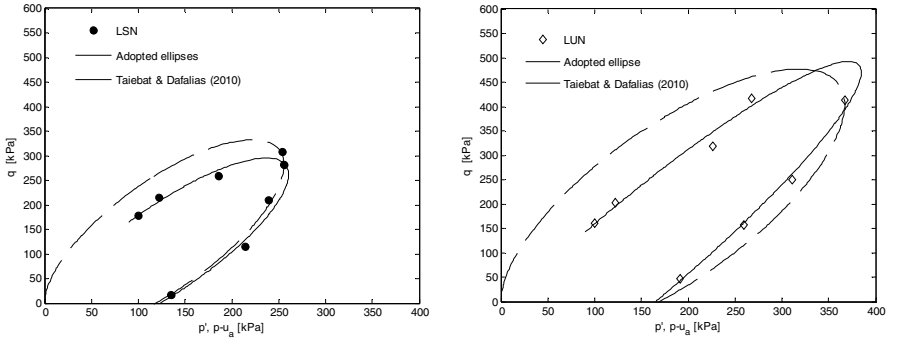

Fig. 5. Fitting of experimental yield data: a) saturated samples, b) unsaturated samples.

where (Fig.3b) x_0 and y_0 are the coordinates of the ellipse centre point, *a* and *b* the semi-axis lengths and θ the inclination angle of the major axis on the horizontal. The best fit of the five parameters was performed by using a procedure proposed by Bookstein (1979); the values are reported in Table 4.

Fig. 5a and 5b show the results of data fitting by means of the two considered models with respect of saturated and unsaturated conditions of the alluvial soil.

The Taiebat & Dafalias ellipse function well fits the saturated yield points (Fig. 5a) for stress ratios less than 3, while overestimates the yielding stresses corresponding to higher stress ratios. The same function doesn't fit with the same accuracy the unsaturated yield stresses, as evidenced in Fig.5b. The adopted ellipse function is capable to closely fit yielding points of the soil at any considered stress ratio, for both the saturated and unsaturated states of the compacted alluvial soil.

4 Conclusions

The study focused the yielding behaviour of a compacted alluvial soil in saturated and unsaturated conditions. The experimental yield stresses were determined by means of an extensive triaxial testing program, applying the strain energy criterion

along the deviatoric paths at different stress ratios. The yielding envelopes were nearly elliptical in shape for both saturated and unsaturated samples.

Two different analytical functions were used to fit the experimental yielding data, taking account of anisotropy of the material: the first was a function proposed by Taiebat & Dafalias, the second was a function adopted in this paper. The adopted function, differently from the Taiebat & Dafalias function, allowed a translational shift on both the horizontal and vertical axes, improving relevantly the fitting of experimental yield points for both the saturated and unsaturated samples. Further investigations are needed to verify the capability of the fitting ellipse function, with reference to yielding occurring at different suction levels and for different stress paths.

References

Alonso, E.E., Gens, A., Josa, A.: A constitutive model for partially saturated soils. Géotechnique 40(3), 405–430 (1990)

Alonso, E.E., Lloret, A., Gens, A., Yang, D.Q.: Experimental behaviour of highly expansive double-structure clay. In: Proc. 1st Int. Conf. Unsaturated Soil, vol. 1, pp. 11–16. Balkema, Paris (1995)

ASTM D 698-91e1. Standard Test Method for Laboratory Compaction Characteristic of Soil Using Standard Effort, ASTM, Annual Book of ASTM standard, Section 4: Construction, vol. 04.08: Soil and rock (I): D420-D4914., Am. Soc. Testing and Materials, Philadelphia (1998)

Aversa, S., Nicotera, M.V.: A Triaxial and Oedometer Apparatus for Testing Unsaturated Soils. Geotech. Testing J. 25(1), 3–15 (2002)

Aversa, S., Vinale, F.: Improvements to a Stress-Path Triaxial Cell. Geotech. Testing J. 18(1), 116–120 (1995)

Bookstein, F.L.: Fitting conic sections to scattered data. Comp. Graph. Image Process. 9, 56–71 (1979)

Cantasale, M., Russo, G.: Yielding and critical state behaviour of a compacted alluvial silt. In: Proc. 4th Int. Symp. Deform. Charact. Geomater., Atlanta, pp. 978–988 (2008) ISBN 978-88-6342-025-8

Capotosto, A., Russo, G.: Yielding and critical state behaviour of a lime stabilized compacted alluvial soil. In: Proc. 5th Int. Symp. Deform. Charact. Geomater., Seoul, pp. 738–745 (2011)

Croce, A., Catini, M.: La diga del Locone, Editori Romani Associati, Roma (1986)

Crooks, J.H.A., Graham, J.: Geotechnical properties of the Belfast estuarine deposits. Géotechnique 26(2), 293–315 (1976)

Cui, Y.J., Delage, P.: Yielding and plastic behaviour of an unsaturated compacted silt. Géotechnique 46(2), 291–311 (1996)

Gens, A., Alonso, E.E.: A framework for the behaviour of unsaturated expansive clays. Can. Geotech. J. 33, 11–22 (1992)

Graham, J.: Laboratory testing of sensitive clay from Lyndhurst. Ontario. Civil Eng. Research Report 74 (2) (1974)

Graham, J., Noonan, M.L., Lew, K.V.: Yield states and stress-strain relationships in a natural plastic clay. Can. Geotech. J. 20(3), 502–516 (1983)

Houlsby, G.T.: The work input to a granular material. Géotechnique 29(3), 354–358 (1979)

Houlsby, G.T.: The work input to an unsaturated granular material. Géotechnique 47(1), 193–196 (1997)

Roscoe, K.H., Burland, J.B.: On the generalized stress-strain behaviour of wet clay Engineering plasticity, pp. 553–609. Cambridge University Press, Cambridge (1968)

Sivakumar, V., Wheeler, S.J.: Influence of compaction procedure on the mechanical behaviour of an unsaturated compacted clay. Géotechnique 50(4), 369–376 (2000)

Taiebat, M., Dafalias, Y.: Simple yield surface expressions appropriate for soil plasticity. Int. J. Geomech. 10(4), 161–169 (2010)

Tavenas, F., Des Rosiers, J.-P., Leroueil, S., La Rochelle, P., Roy, M.: The use of strain energy as a yield and creep criterion for lightly overconsolidated clays. Géotechnique 29(3), 285–303 (1979)

Tedesco, D.V.: Hydro-mechanical behaviour of lime-stabilised soils. PhD Thesis, University of Cassino, Italy (2007)

Toll, D.G.: A framework for unsaturated soil behaviour. Géotechnique 40(1), 31–44 (1990)

Wheeler, S.J., Sivakumar, V.: An elasto-plastic critical state framework for unsaturated soil. Géotechnique 45(1), 35–53 (1995)

Effect of Compaction Water Content on the Drained and Undrained Behaviour of an Unsaturated Kaolin

Roberto Vassallo

Abstract. This paper reports the results of suction controlled and constant water content triaxial tests on a kaolin dynamically compacted at several water contents. Suction controlled tests, together with some tests on the material saturated in the triaxial cell, were meant to estimate the effects of partial saturation on shear strength. Constant water content tests were carried out to evaluate, in a faster but approximated way, the effects of the degree of saturation on shear strength. Results of the former type of tests are here used to calibrate an elasto-plastic model which is then used to simulate and interpret the results of the latter type of tests.

Keywords: compacted, drained, undrained, shear strength, triaxial cell.

1 Introduction

A commercial kaolin, of medium plasticity, was mixed with distilled water at several moulding contents (w_{mould}) and then dynamically compacted. A series of suction controlled triaxial tests was carried out on the material compacted at w = 21%, slightly wet than optimum, while a series of constant water content triaxial tests was performed on the material compacted in the range w = 10% - 25%. Such experimental program made it possible to compare the drained and undrained behaviour of the material. While the interpretation of drained tests is quite straightforward by using well-known elasto-plastic models (e.g. Alonso et al. 1990), the interpretation of the performed undrained tests is of course complicated by the need for taking into account the effect of w_{mould} on structure and the changes in

Roberto Vassallo
Università della Basilicata, Italy
e-mail: roberto.vassallo@unibas.it

pore air pressure and pore water pressure induced by volume changes during both the isotropic and the deviatoric stages. This paper proposes a first approximation approach to the problem by using a model with parameters independent of w_{mould}, thus neglecting the effect on structure.

2 Tested Material, Experimental Program and Procedures

The tested kaolin is a silt with about 30% clay which in the Casagrande chart is in the range of medium plasticity, with w_L=46% and PI=17%.

The specimens to be tested in the triaxial cell were obtained by standard Proctor compaction (ASTM 2005). The resulting compaction curve is reported in fig. 1 and shows that optimum is about at w=20%. A single water content of 21% was used both for specimens to be tested under suction controlled conditions and for those to be tested in the triaxial cell after a preliminary saturation. As mentioned above, constant water content tests were carried out on specimens with w ranging from 10% to 25%.

The testing program consisted of: 4 triaxial consolidated undrained (CIU) tests plus one isotropic test on the material saturated in the cell; 3 suction controlled isotropic tests plus 5 suction controlled triaxial tests on the unsaturated soil; 18 constant water content triaxial tests on the unsaturated soil.

CIU tests were carried out by a standard procedure. Saturation was obtained by seepage from the bottom to the top and then verified by B-test.

Suction controlled triaxial tests were carried out by a cell using the axis translation technique. After an equalization stage, drained isotropic compression stages were performed at 100, 150, 200 and 400 kPa of suction by increasing the mean net stress at a 4 kPa/h rate. For 150 and 400 kPa of suction a subsequent drained deviatoric stage was carried out by applying 0.1%/h axial strain rate.

For constant water content tests, traditional triaxial cells and the standard procedure for UU triaxial tests on saturated soils were used. This included using impervious disks at the specimen ends, so that pressure build-up was expected for both air and water phases. Volume changes were estimated by monitoring the cell liquid. A cell pressure equal to 100 kPa was applied for about 4 hours, which resulted sufficient for the specimen volume to stabilize. Then the shear stage was carried out by applying 2.5%/h axial strain rate.

3 Experimental Results

3.1 Saturated Soil

A permeability of about $5 \cdot 10^{-8}$ cm/s was estimated by interpreting the results of the preliminary stage of seepage induced – saturation.

From the isotropic compression test results, an overconsolidation pressure of about 35 kPa was estimated. Isotropic stages preceding shear stages consisted of a

single step to p' between 300 and 850 kPa, leading to normal consolidated conditions. Failure is representd in the $q:p'$ plane by a straight line $q=Mp'+\mu$ with negligible intercept μ on the q axis. A slope M=1.05, i.e. φ'=26.5°, is obtained by imposing the passage through the origin of axes.

3.2 Unsaturated Soil, Suction Controlled Drained Tests

The results of equalization stages provided some first information on the retention relationship. Fig. 2 shows final degree of saturation versus porosity multiplied by suction, together with the theoretical curve used for simulations in the following.

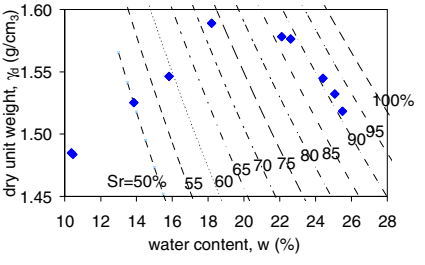

Fig. 1. Compaction curve.

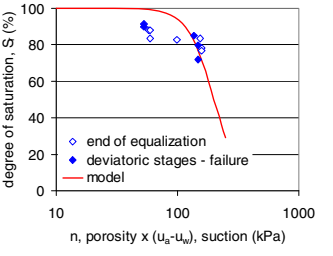

Fig. 2. Water retention relationship.

Isotropic stages showed a negligible suction effect, in the investigated range (100-400 kPa), on the slope of virgin compression lines in the plane $e:(p-u_a)$.

Fig. 3a reports the results of the deviatoric stages. Points at failure are fitted by straight lines $q=Mp'+\mu$ parallel to that relative to saturated conditions. Thus, suction effects on shear strength are described by the intercept μ, which increases with suction as shown by fig. 3b.

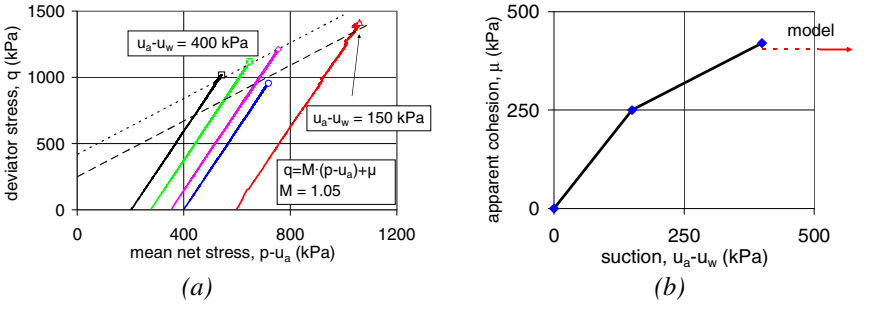

Fig. 3. Results of the deviatoric stages of suction controlled triaxial tests: deviator stress versus mean net stress at failure *(a)*; apparent cohesion versus suction *(b)*.

3.3 Unsaturated Soil, Undrained Tests

Constant water content triaxial tests were carried to obtain in a faster, even though approximated way, information of the influence of the degree of saturation on the shear strength in the range w=10%-25%. It is worth noting that such range could not have been investigated in suction controlled conditions on the material compacted at w=21%, given the limits in the suction values which can be applied in the triaxial cell (from 0 to 500 kPa).

At least two specimens were prepared at each chosen water content. A general decrease in undrained stiffness, along with undrained strength, was observed with w increasing. Fig.s 4a and 4b report the deviator at failure versus the degree of saturation S_r at failure and the moulding water content w_{mould}, respectively. Clearly, in the investigated range, both variables strongly influence the undrained strength. Strictly speaking, these plots do not allow to distinguish the effects of compaction induced structure from those of current water content and suction. However, from a qualitative point of view, it is possible to highlight the negligible variation in the range of S_r from 35% to 75%, with an average deviator at failure of 600 kPa. For greater S_r, a strong decrease of undrained strength is observed.

Part of such reduction is reasonably linked to the suction decrease and the air pressure increase induced by volume decrease during isotropic and deviatoric stages. There is some uncertainty in the evaluation of such air overpressure linked to the fact that the membrane and the impervious disks do not probably guarantee totally undrained conditions during triaxial tests.

4 Interpretation of Experimental Results

In order to interpret the results obtained for w_{mould} different from 21%, in the lack of information other than the measured strength versus the water content, some "strong" assumptions were necessary. It is well known (e.g. Wheeler & Sivakumar 2000 a,b) that different w_{mould} can induce structural effects, besides effects on the initial state. This, substantially, can give rise to different materials to be characterized by different constitutive parameters. In this work, a first approximation calculation is performed by neglecting the structure effect and characterizing the tested soil by parameters independent of moulding water content. So, based on the results of fig. 3, the variation of apparent cohesion μ with suction is considered representative for every other case, and the same constant slope M of the *CSL* in q:p-u_a plane is assumed. Of course, further suction-controlled test results would be needed to confirm these assumptions: while M could actually be not much influenced by the structure, the effect on other parameters could be significant.

Equations of the Alonso et al. (1990) model are used to compute: a) elastic strains due to mean net stress and suction variations; b) plastic volumetric strains due to mean net stress variations; c) yield stresses in the q:p-u_a plane.

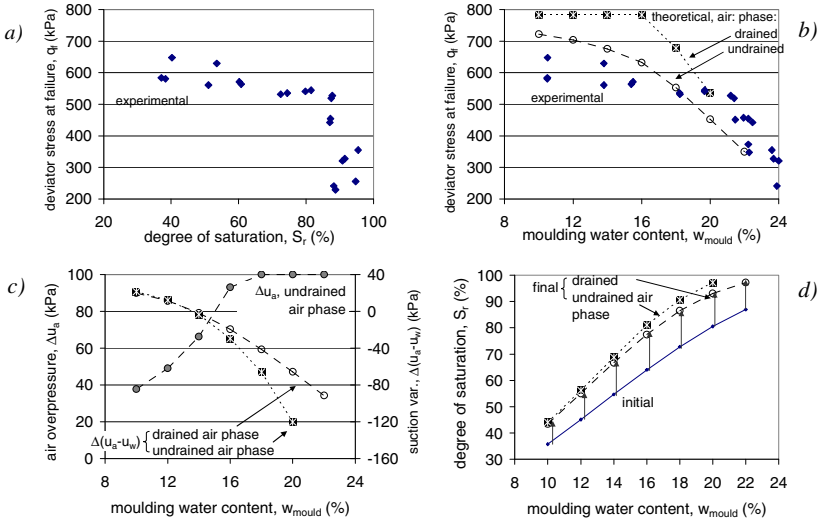

Fig. 4. Deviator stress at failure under undrained conditions: data from constant water content tests and modelling results (a-b). Computed increments of air pressure and suction (c) and of degree of saturation (d) versus moulding water content.

Based on experimental results on the material compacted at w=22%, minor modifications are made for:

- the *LC* yield locus: initial yield stress $(p\text{-}u_a)_0$ is assumed to vary linearly between 35 and 200 kPa for $(u_a\text{-}u_w)$ increasing from 0 to 100 kPa and then to be constant for greater suction;
- the slope of normal compression lines, λ, assumed independent of u_a-u_w;
- suction effect on apparent cohesion μ: for suction greater than 400 kPa, μ is assumed constant (fig. 3b).

To simulate undrained tests, the model was coupled to an equation of the water retention curve dependent on porosity n:

$$S_r = \frac{1}{1+\left[\frac{n\cdot(u_a-u_w)}{t}\right]^u} \tag{1}$$

with t=200 kPa and u=4, represented in fig. 2.

All the assumed parameters are reported in table 1.

As for the air phase, two different and "extreme" possibilities are considered.

As a first case study, assuming that the tests were effective to keep the air phase in undrained conditions, u_a variations are estimated based on the computed volume changes and on Boyle's law. A trial and error procedure was developed to take into account the equations for the soil skeleton, water and air phases simultaneously. Air overpressure is limited to a maximum value of 100 kPa, that is the value of the applied cell pressure.

Table 1. Parameter values assumed for modelling.

Alonso et al. (1990) model		Water retention	
λ	0.07	t (kPa)	200
κ	0.004	u	4
κ_s	0.004		
M	1.05		
k	0.962		

As a second case study, the same calculations are carried out by assuming that, notwithstanding the undrained condition, u_a kept the atmospheric value.

The results of calculations are reported in fig. 4. The model proves able to predict a strong decrease of shear strength with increasing w_{mould}. Such decrease is more abrupt under the hypothesis of drained air phase, but this is also a consequence of the assumed variation of apparent cohesion with suction (in test starting with the lowest w, suction does not drop below 400 kPa, so shear strength keeps constant). Both simulations do not succeed in reproducing with a very good approximation the experimental values of deviator at failure. In particular, values higher than the experimental ones are predicted for the lower water contents, notwithstanding the constancy of μ assumed for suction greater than 400 kPa, and values sensibly lower cannot be obtained in all probability by adjusting the assumed parameters without invoking structure effects. Further suction controlled tests are now scheduled to directly investigate the effect of w_{mould} and will hopefully be useful to improve the model performance.

5 Concluding Remarks

The described experimentation allowed to have a preliminary insight of the drained and undrained behaviour of a compacted kaolin. A negligible variation in undrained strength was observed for S_r from 35% to 75%, while a strong reduction was observed for higher S_r. Given the current availability of suction controlled test results just for one moulding water content value, the proposed interpretation had necessarily to be simplified. However, the results of modelling will be useful in guiding the complementary experimentation which is now scheduled.

References

Alonso, E.E., Gens, A., Josa, A.: A constitutive model for partially saturated soils. Géotechnique 40(3), 405–430 (1990)

ASTM, D698-91. Test method for laboratory compaction characteristics of soil using standard effort. ASTM Book of Standards, Philadelphia, USA (2005)

Wheeler, S.J., Sivakumar, V.: Influence of compaction procedure on the mechanical behaviour of an unsaturated compacted clay. Part 1: wetting and isotropic compression. Géotechnique 50(4), 359–368 (2000a); Part 2: shearing and constitutive modelling. Géotechnique 50(4), 369–376 (2000b)

Shear Strength and Volume Change of Unsaturated Collapsible Soil by CW Test

Seyed Mohammad Ali Zomorodian and Ahmad Faghihi

Abstract. Collapsible soil exhibited significant changes in volume upon addition of water content. This process causes serious damage to foundations built on such soil. Critical state theory has been extensively used to establish models for simulating elastic-plastic behavior of unsaturated soils. But, experimental works is relatively limited especially for collapsible clays. Based on this background, it is of extremely importance to experimentally investigate the shear strength characteristics and shearing induced volume change of these materials in unsaturated conditions. In this paper the shear strength and volume change behavior of a collapsible soil is studied using a series of Constant Water (CW) triaxial test at different matric suctions and net confining stress. The results indicate that the initial suction value and net confining stress have a great influence on the shear strength, pore-water pressure, and volume change behavior of the soil during shearing under the constant water content condition.

Keywords: collapsible soil, triaxial test, matric suction, volume change, shear strength.

1 Introduction

The shear strength of unsaturated soil as proposed by Fredlund et al. (1978) is expressed in terms of two independent stress state variables, net normal stress (σ-u_a) and matric suction (u_a-u_w) by the following equation

$$\tau_f = c' + (\sigma - u_a)\tan\phi' + (ua - uw)\tan\phi^b , \quad (1)$$

Seyed Mohammad Ali Zomorodian
Shiraz University, Shiraz, Iran
e-mail: mzomorod@shirazu.ac.ir

Ahmad Faghihi
Islamic Azad University-Estahban branch, Estahban, Iran
e-mail: ahmadrf60@gmail.com

where τ_f is the shear strength of an unsaturated soil, c' the effective cohesion of the soil, ϕ' the effective angle of shearing resistance for a saturated soil, σ the total stress, u_a the pore air pressure, u_w the pore water pressure, ϕ^b the angle of internal friction with respect to matric suction, $(u_a - u_w)$ matric suction and $(\sigma - u_a)$ the net normal stress.

The deformation of unsaturated soil is increased with the rise of water content. This deformation may be in form of decreasing or increasing volume changed or dispersive. Collapsible soils consist of loose, dry, low-density materials that collapse and compact under the addition of water or excessive loading. Collapsible soils are moisture sensitive in that increasing the moisture content is the primary triggering mechanism for the volume reduction of these soils. One of the major consequences of urbanization in arid regions is an increase in soil moisture content. Therefore, the impact of development-induced changes in surface and groundwater regimes on the engineering performance of moisture sensitive arid soils, including collapsible soils, becomes a critical issue for continued sustainable population expansion into arid regions. Thus, collapsible soil may appear as a fill or a foundation of many soil structures, such as earth dams, retaining walls, pavements, soil liners, and soil covers are in the state of unsaturated conditions. In cases where water penetrates the soil, the suction is reduced and collapsible soil can become unstable. Hence, large volume reduction can suddenly take place causing disruption and damage to structures. The effects of wetting include loss of apparent cementation, volume change, and loss of shear strength. The volume change upon wetting is either swell (if the material is plastic, initially dry, and lightly confined) or collapse (if the material is non-plastic or slightly plastic, initially dry, and heavily confined).Thus, shear strength and volume change of an unsaturated soil is required in the design of geotechnical and geo-environmental structures. Shear strength parameters of unsaturated soils which are used in geotechnical designs, are commonly obtained from a consolidated drained (CD) triaxial test. However in many field situations, fill materials are compacted where the excess pore-air pressure developed during compaction will dissipate instantaneously, but the excess pore-water pressure will dissipate with time. This condition can be simulated in a constant water content (CW) triaxial test. Only a limit experimental data on the mechanical behavior of unsaturated collapsible soil especially under total stress was available, due to difficulty of methods and time consuming in measuring suction and deformations. The main objective of this paper is to present the characteristics of the shear strength, volume change, and pore-water pressure of a compacted collapsible soil (CL) with in situ density during shearing under the constant water content condition.

2 Soil Properties and Sample Preparation

The soil used in this study was a collapsible taken from Sivand zone located northwest of Shiraz, Iran. The soil is classified as low plasticity clay (CL) on the

basis of the unified soil classification system. The index properties of the collapsible soil are given in Table 1.

Table 1. Index properties of the collapsible soil.

Type of soil	$\omega_{optimum}$	$\gamma_d(kN/m^3)$	LL(%)	PL(%)	PI(%)	Gs
CL	14.8	17.9	26.62	17.57	9.05	2.56

The soil used in this study with at water content of 10.5 % and dry density of 1.6 Mg/m^3 can classifieds as a high collapsible soil. The specimens were dynamically compacted in 5 layers of 20 mm prepared for triaxial tests. Fig. 1 shows the results from the standard saturated triaxial shearing tests under different confining stress. An effective angle of internal friction $\phi' = 26.9^{\circ}$ and effective cohesion $c' = 6(kPa)$ can be obtained from Fig. 1.

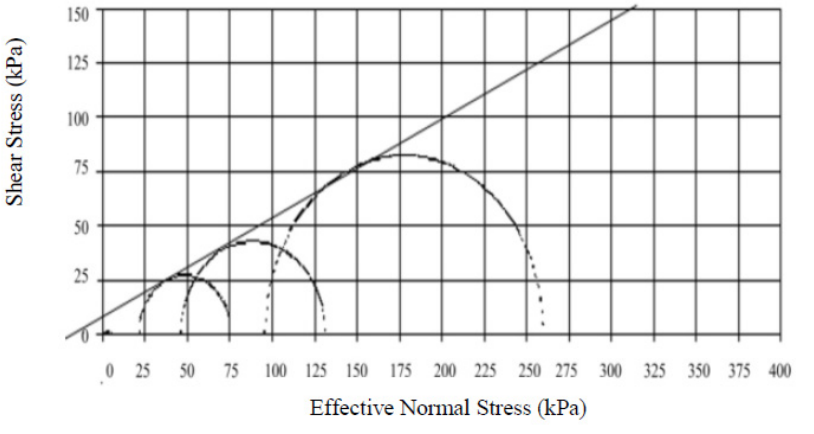

Fig. 1. Mohr-Coulomb failure envelope for saturated collapsible soil (CL).

The modified triaxial apparatus used in this study for the CW triaxial was similar to the modified triaxial apparatus described by Fredlund & Rahardjo (1933). The test set up consists of a dual cylinder cell, volume change indicator, pressure application system, pressure transducers and pressure gauges (Fig. 2). The results of the test were monitored and recorded by a data logger connected to a personal computer. During wetting process matric suction was decreased by increasing the pore-water pressure at the base plate. Using a porous stone air pressure applies on top of specimen and then to achieve especial matric suction simultaneously pore water pressure applies to base plate. As suggest by Sivakumar (1993), the equalization was assumed to have been achieved when the excess pore-water pressure

had fully dissipated and water volume change had decreased to 0.04 % per day. Each specimen required about 12 to 25 days. Fig. 3 shows wetting process in equalization stage for three matric suction of 50, 100 and 200 kPa.

Fig. 2. The test set up for unsaturated soil.

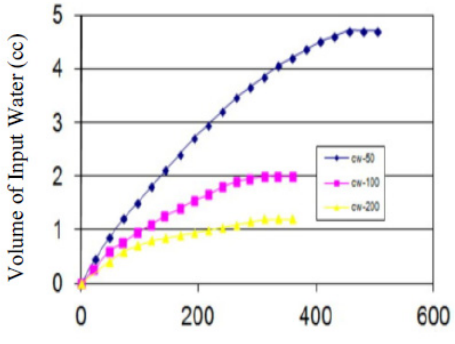

Fig. 3. Wetting process at equalization stage.

After equalization, the soil specimen was isotropically consolidated to the desired net confining stress (σ_3-u_w). Since in this study triaxial tests are done at constant water content (CW) the pore-air of the specimen was allowed to flow out (drained) and pore-water was undrained. In shearing stage, the pore-air pressure, u_a, was maintained at same magnitude as that obtained at the end of the equalization stage. In this study, the strain rate of 0.0009 mm/min as suggested by Ong (1999) and Rahardjo et al. (2004) for CW triaxial tests on the compacted residual soil was adopted. The maximum axial strain was set to 15 %. Each test specimen required about one to two days for shearing stage to be completed.

3 Test Results and Discussion

A series of CW triaxial test was carried out on dynamically compacted collapsible soil specimens of CL. For the CW test a designation Of CW_{x-y} was adopted. The

term x-y in CW_{x-y} means that the test was conducted under initial matric suction of x kPa and at net confining pressure of y kPa. Fig. 4 shows the results from CW triaxial shearing tests under net confining stress but at initial matric suction of 50kpa. The sign of volumetric change is negative when specimen under contraction and under dilation is positive. Contractive volumetric behavior of specimens is observed at the first stage of shearing then dilative behavior is observed. The specimen at constant matric suction with increasing confining pressure show highly reduction in volume. In general specimen with high matric suction undergo low contraction but high dilatancy.

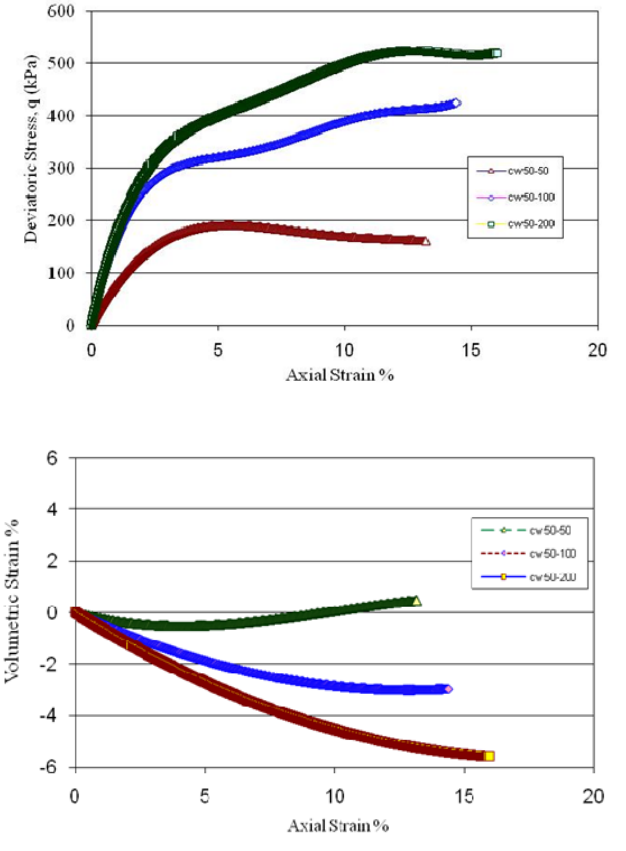

Fig. 4. Result of CW tests under initial matric suction of 50 kPa.

It is apparent that at low net confining pressure the specimen to exhibit dilatancy with increasing matric suction, but at high net confining pressure the specimen to exhibit contraction with decreasing matric suction. It can be seen that at constant net confining pressure as matric suction increases the specimen show more

dilatancy which show in Fig. 5. The shear stress at failure for the specimens used in the construction of Mohr circles for CW tests was determined using the peak deviatoric stresses obtained from stress-strain curves. At CW triaxial test the effective cohesion were determined by drawing the Mohr Columb failure envelope tangentially to the Mohr circles developed from each CW triaxial test using a constant angle of internal friction of 26.9˚. The typical result of Mohr Columb failure criteria at different matric suction and constant confining stress of 50kPa are shown in Fig. 6.

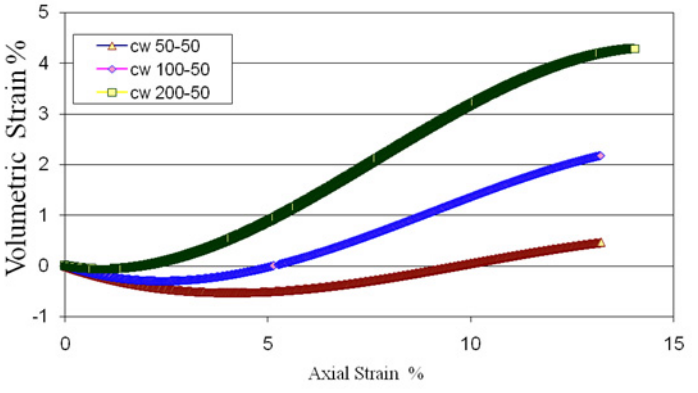

Fig. 5. Results of CW tests under different initial matric suction but with the same net confining stresses of 50 kPa.

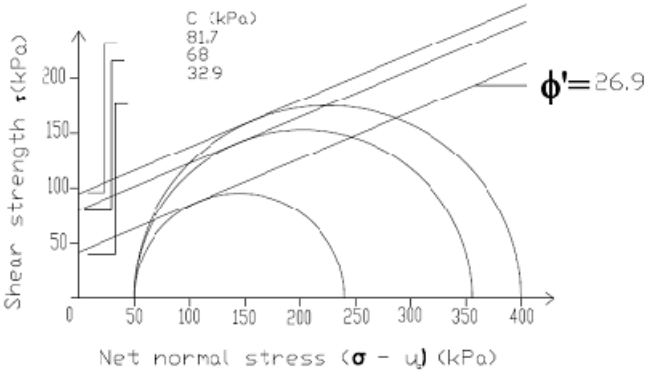

Fig. 6. Typical result of Mohr Columb failure criteria at different matric suction and constant confining stress.

It can be seen that at same net confining stress with increasing matric suction apparent cohesion increases too. Fig.7 shows shear stress versus matric suction at failure for CW test. These curves for CW test at different confining pressure are

nonlinear. Fig.7 shows that ϕ^b with matric suction at saturated soil equals to ϕ' and with increasing matric suction ϕ^b decreases significantly. Also, Fig.8 shows the nonlinearity behavior of ϕ^b with to matric suction for collapsible soli CL which in agreement of study of Satija (1987), Fredlund et al. (1978), Gan et al. (1988) and Thu et al. (2006).

Fig. 7. Intersection line between failure envelope and shear strength versus matric suction.

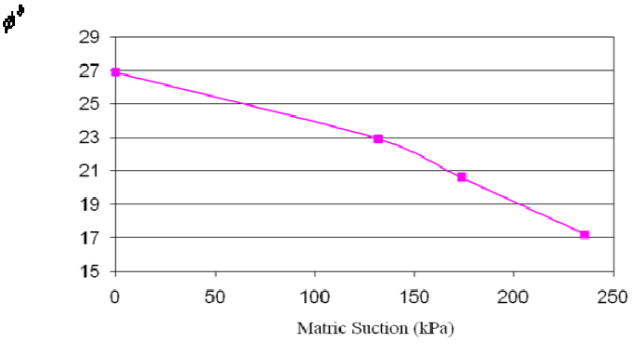

Fig. 8. Variation of ϕ^b versus matric suction at failure of CW triaxial tests.

4 Conclusion

The experimental of CW test on collapsible soil of CL show that at the same net confining pressure shear strength of unsaturated specimen is higher than saturated. At low confining pressure with increasing matric suction soil behaves like preconsolidated soil. The results show at same net confining pressure with increase matric suction the apparent cohesion is increase too. Also the result of this study show that shear strength with increasing matric suction is nonlinear when the range in suction is large. It is evidence that with increasing axial strain matric

suction increases too and failure strain become constant and with increasing initial matric suction change in failure matric suction also reduces.

References

Fredlund, D.G., Morgenstern, N.R., Widger, R.S.: The shear strength of unsaturated soil. Can. Geotech. J. 15(3), 313–321 (1978)

Fredlund, D.G., Rahardjo, H.: Soil Mechanics for unsaturated soils. John Wiley & Sons (1993)

Gan, J., Fredlund, D.G., Rahardjo, H.: Determination of the shear strength parameters of an saturated soil using the direct shear test. Can. Geotech. J. 25(3), 277–283 (1988)

Momeni, M., Shafiee, A.: Kerman Collapsible Soil. In: Identification Proceeding of GEOPROB 2005, Kibris (2005)

Ong, B.H.: Shear strength and volume change of unsaturated residual soil. ME thesis, Nanyang Technological Univ., Singapore (1999)

Rahardjo, H., Heng, O.B., Leong, E.C.: Shear strength of a compacted residual soil from consolidated drained and the constant water content triaxial tests. Can. Geotech. J. 41, 1–16 (2004)

Satija, B.S.: Shear behaviour of partly saturated soil. PhD thesis, Indian Institute of Technology, Delhi, India (1978)

Sivakumar, V.: A critical state framework for unsaturated soil, PhD thesis, Univ. of Sheffield, Sheffield, U.K (1993)

Thu, T.M., Rahardjo, H., Leong, E.C.: Shear strength and pore-water pressure characteristics during constant water content triaxial tests. Geotechnical & Geoenvironmental J. 132(3), 411–419 (2006)

The Effect of Relative Humidity and Temperature on the Unconfined Compressive Strength of Rammed Earth

Christopher Beckett and Charles Augarde

Abstract. Rammed earth (RE) is an ancient construction technique now being considered for construction in a wide range of climatic conditions. As such, a new range of scientific investigations treating it as a highly unsaturated soil are being undertaken by several institutions in order to fully understand its properties and behaviour. This paper introduces laboratory work determining the effect of changing climatic conditions on the unconfined compressive strength of RE and offers comments on preliminary results; full results and their interpretations shall be discussed in a forthcoming paper.

Keywords: Rammed earth, suction, climate change.

1 Introduction

"Rammed earth" (RE) is a construction technique in which moist sandy-loam subsoil is compacted in layers between removable formwork, forming free-standing, monolithic structures. RE is still widely used in arid and semi-arid regions around the world and it is in such areas that surviving examples of ancient structures can be found. RE techniques were first developed by pre-Iron Age cultures in order to remain comfortable in otherwise hostile climates and the longevity of the RE technique is thanks to this comfort, its use of readily-available raw materials and the durability of resulting structures (Fitch and Branch, 1960; Taylor and Luther, 2004). As a result of these qualities, RE is now being considered for construction in remote areas in order to reduce the environmental impact of the transportation of materials

Christopher Beckett
School of Civil & Resource Engineering, University of Western Australia, Perth WA
e-mail: christopher.beckett@uwa.edu.au

Charles Augarde
School of Engineering & Computing Sciences, Durham University, Durham, UK
e-mail: charles.augarde@durham.ac.uk

over large distances, as well as becoming a topic for investigation to improve structural design in arid regions. Furthermore, RE's natural appearance has also made it architecturally attractive, so that RE structures can also be found in affluent regions where other construction techniques, for example fired brick or concrete, are also common.

Despite its heritage, RE has only recently been identified and investigated as a highly unsaturated soil (Jaquin et al., 2008, 2009). RE derives its considerable strength through drying; as the walls are free-standing, a significant proportion of their surface is exposed to the air so that the material achieves very low water contents, often around 1%, corresponding to very high internal suctions (>100 MPa) (Nowamooz and Chazallon, 2011).

In an unstabilised state ("stabilisation" is the inclusion of cementitious materials for example cement or lime which will not be discussed in this paper), RE walls will absorb and release moisture depending on external conditions. As a result, the relative humidity within the structure remains roughly constant throughout the day (Allinson and Hall, 2010). However, prolonged exposure to high humidities, for example as might occur due to climate change, might subsequently cause a change in the material properties of RE due to a change in the internal water regime. Furthermore, the proliferation of the RE technique to regions not historically associated with RE construction might prove to be hazardous, as the use of techniques developed in a given region might not be suitable in another. Figure 1 shows the locations of RE structures built pre– and post the turn of the 19th century, clearly showing the significant increase in the range of climates in which RE is now expected to function; historically, most RE structures are confined to categories B and C ("arid" and "temperate" respectively), whereas structures built after this date are found across categories A ("tropical") to D ("cold") (Peel et al., 2007) (the reader is referred to this work for a more detailed explanation and derivation of the different climate categories). Therefore, it is necessary to determine the extent to which RE interacts with its environment and how that interaction affects the material properties if RE is to be successfully used in these new locations. Such knowledge would not only benefit the design of new structures but would also indicate how best to conserve heritage RE structures threatened by climate change.

The aim of this paper is to introduce work investigating the effect of climate change, in terms of temperatures and humidities selected to be representative of those climates identified in Figure 1, on the unconfined compressive strengths (UCSs) of RE samples, as part of a larger investigation (encompassing several institutions) into the properties and behaviour of RE. This paper will be supported by a forthcoming paper in which laboratory results will be presented and discussed.

2 Experimental Procedure

Figure 2 shows the principal experimental stages to be used during this investigation, where OWC refers to the material optimum water content and EC to the use of an environmental chamber.

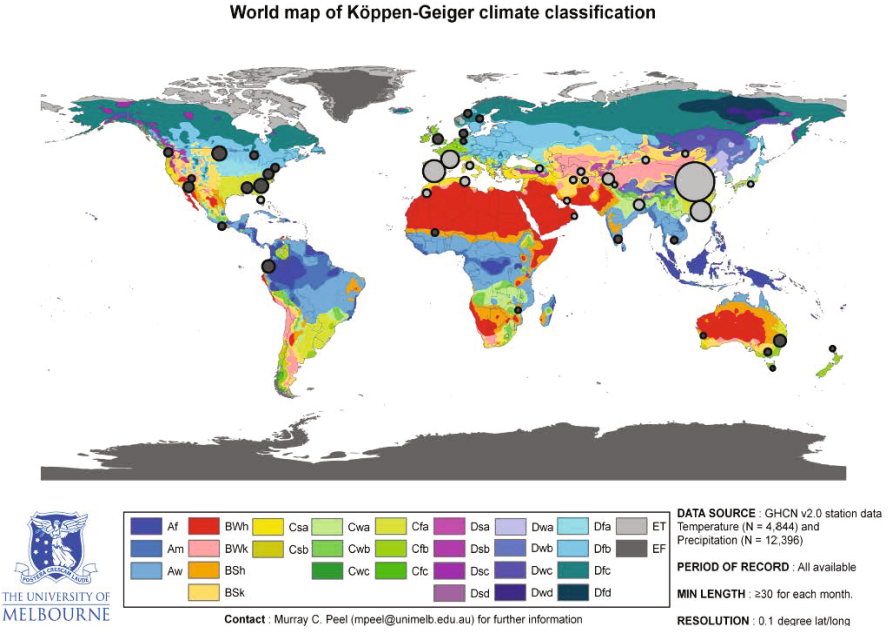

Fig. 1. Locations of RE sites compared to KGCC categories (after Peel et al. (2007)). Pre-19th century sites are shown as light markers and post-19th century are shown as dark markers. Larger markers represent a greater number of RE sites within a given area.

Material used to produce RE samples is manufactured from known quantities of sand, gravel and silty-clay, following work conducted by Hall and Djerbib (2004), and is referred to as a "soil mix", rather than a soil, as the latter suggests a natural material. This method allows for the careful control over the material particle grading, an important factor in RE construction due to the need to ensure adequate clay and "aggregate" (a term borrowed from concrete construction) contents (King, 1996; Walker et al., 2005; Easton, 2007). Soil mixes are referred to by their relative mix proportions; for example, mix "5-1-4" contains 50% sand, 10%gravel and 40% silty-clay by mass. Two soil mixes, namely 5-1-4 and 7-1-2, are to be used in this investigation in order to determine the effect of the presence of clay on the change in the material's water content on changes in temperature and relative humidity.

Dry silty-clay ('Birtley Clay', liquid limit 58.8%, plastic limit 25.7%, plasticity index 33.1%, predominantly kaolinite) is prepared by pulverising lumps of material which have been dried at 105°C for 48 hours. Pulverised material is then passed through a 2.36 mm sieve in order to produce sufficiently small particles to mix uniformly with the remaining mix fractions. The sand fraction is sieved to pass 2.36 mm to remove gravel-sized particles. Gravel is sieved to pass 10 mm in order to prevent large particles interfering with the compressive strength testing (Hall and Djerbib, 2004). To improve the particle grading, sieved gravel is mixed in a 1:1 ratio by mass with those sand particles which did not pass 2.36 mm but which also all pass 10 mm.

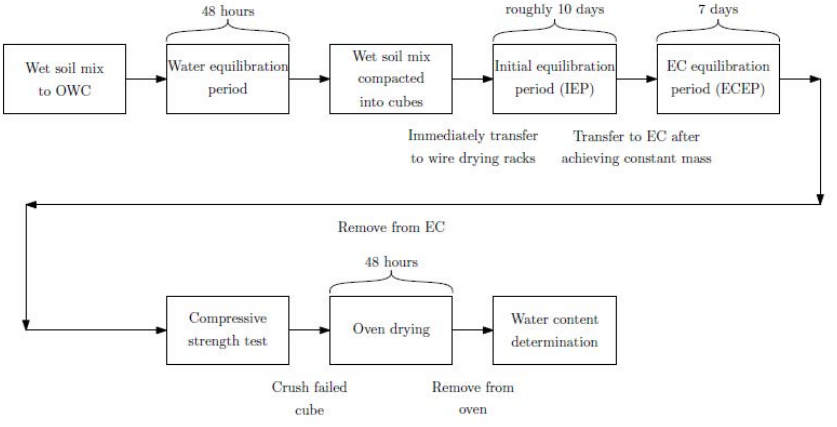

Fig. 2. Flow chart showing principal testing procedure stages and stage durations.

Soil mix OWC is determined via the light Proctor test following the work of Hall and Djerbib (2004). Wet soil mixes are prepared in sealable containers which are sealed and left to stand for 48 hours to allow for water equilibration.

100 mm cube samples are to be used for testing, as opposed to the traditional 200 mm $\times$ 100 mm diameter cylindrical samples, in order to produce a larger number of samples per amount of raw material and to be in keeping with current RE literature (Lilley and Robinson, 1995; Hall and Djerbib, 2004). The use of 100 mm cube samples is deemed acceptable given the use of particles $\leq$10 mm. Samples are manufactured in three layers, each compacted to the optimum density (as determined via the Proctor test) using an adjustable rammer. The sides of the mould are treated with form release oil in order to prevent the sample from being damaged on removal. A screed of mix material passing 1.18 mm is applied to the uppermost surface of the sample in order to provide a smooth surface for compressive testing; unlike in concrete testing, samples cannot be rotated to present a smooth surface due to material anisotropy (Bui and Morel, 2009).

Samples are left to dry naturally on wire racks until achieving a constant mass (the Initial Equilibration Period (IEP) water content). They are then transferred to an EC to be held at a given temperature and relative humidity for 7 days, judged to be sufficient to ensure equilibration with the selected conditions (determined during previous testing). Temperatures and humidities used for testing, selected given climate data obtained for those sites shown in Figure 1 and the operational limits of the EC, are shown in Table 1. The equivalent suction for a given combination of temperature and relative humidity can be determined using Eqn 1 where ψ is the total suction, R_u is the universal gas constant (8.314 J/molK), T is the absolute temperature, RH is the relative humidity and V_m is the molar volume of water (18.016×10^{-6} m^3/mol); example suction values are shown in Table 1. Samples are then removed and their UCSs determined. The UCS is chosen to characterise the performance of the two RE mixes to remain in keeping with existing RE

Table 1. Tested relative humidity and temperature values and equivalent suctions (at subscripted relative humidity and temperature values respectively using Eqn 1).

Humidity (%)	90	70	50	30
Temperature (°C)	15	20	30	40
Equivalent suction (MPa)	$\psi_{90,15} = 14.0$	$\psi_{70,20} = 48.2$	$\psi_{50,30} = 96.9$	$\psi_{30,40} = 173.9$

literature (Middleton and Schneider, 1992; Hall and Djerbib, 2004; Walker et al., 2005; Nowamooz and Chazallon, 2011). Sample material is then crushed and dried at 105°C for 48 hours in order to determine the final sample water content (the ECEP water content), which can be compared to the IEP water content in order to determine any changes in the internal water (and so suction) regimes.

$$\psi = -\frac{R_u T}{V_m} \ln(\mathrm{RH}) \tag{1}$$

3 Preliminary Results and Observations

Although full results are not yet available, several properties of the material are becoming apparent:

- The UCS of RE is greatly affected by changes in the humidity and temperature, and so suction;
- Results suggest that there are only very slight differences between wetting and drying suctions, due to the very low water contents present;
- Results suggest that pore water remains in the capillary (bulk) regime despite equivalent pore diameters of roughly 2 nm, determined via $d_{pore} = -\frac{4\gamma}{\psi}$, where d_{pore} is the pore diameter and γ is the air-water surface tension, estimated via $\gamma = 0.1171 - 0.0001516T$ (Edlefsen and Anderson, 1943). This is very close to the limit of capillarity of 1.4 nm given by Butt and Kappl (2009), further suggesting that the limit of capillarity is different for different clay types;
- The water contents and relative adsorbed water contents of samples of mix 5-1-4 for a given applied suction are higher than those of 7-1-2 for the same applied suction due to the former's higher clay content;
- For a given applied suction, samples of mix 7-1-2 achieve greater UCSs than those of mix 5-1-4, suggestibly due to the former's lower relative adsorbed water content (more water is available to contribute to capillarity).

It is clear that further work is required in order to fully understand the processes present in those RE samples tested, however it is also clear that the suction regime under which RE is found greatly affects its strength. Therefore, a reduction in the

suction present, say through the development of a cooler, wetter climate, is of significant concern to RE construction as structures could become in danger of collapse.

Acknowledgements. This work was carried out whilst the first author was a PhD student at Durham University and was supported by a studentship awarded by the School of Engineering and Computing Sciences, Durham University.

References

Allinson, D., Hall, M.: Hygrothermal analysis of a stabilised rammed earth test building in the uk. Energy and Buildings 42, 845–852 (2010)

Bui, Q.-B., Morel, J.-C.: Assessing the anisotropy of rammed earth. Construction and Building Materials 23(9), 3005–3011 (2009)

Butt, H.-J., Kappl, M.: Normal capillary forces. Advances in Colloid and Interface Science 146(1-2), 48–60 (2009)

Easton, D.: The Rammed Earth House (Completely Revised ed.). Chelsea Green Publication Company, Vermont (2007)

Edlefsen, N.E., Anderson, A.B.C.: The thermodynamics of soil moisture. Hilgardia 16, 31–299 (1943)

Fitch, J.M., Branch, D.P.: Primitive architecture and climate. Scientific American 203, 134–145 (1960)

Hall, M., Djerbib, Y.: Rammed earth sample production: context, recommendations and consistency. Construction and Building Materials 18(4), 281–286 (2004)

Jaquin, P.A., Augarde, C.E., Gallipoli, D., Toll, D.G.: The strength of unstabilised rammed earth materials. Géotechnique 59(5), 487–490 (2009)

Jaquin, P.A., Augarde, C.E., Legrand, L.: Unsaturated characteristics of rammed earth. In: Toll, D.G. (ed.) First European Conference on Unsaturated Soils, Durham, England, pp. 417–422. Durham Univeristy (2008)

King, B.: Buildings of Earth and Straw: Structural Design for Rammed Earth and Straw-Bale Architecture. Ecological Design Press, Sausalito (1996)

Lilley, D.M., Robinson, J.: Ultimate strength of rammed earth walls with openings. Proceedings of the Institution of Civil Engineers-Structures and Buildings 110(3), 278–287 (1995)

Middleton, G.F., Schneider, L.M.: Earth-wall construction, 4th edn. CSIRO Division of Building, Construction and Engineering. North Ryde, Australia (1992)

Nowamooz, H., Chazallon, C.: Finite element modelling of a rammed earth wall. Construction and Building Materials 25(4), 2112–2121 (2011)

Peel, M.C., Finlayson, B.L., McMahon, T.A.: Updated world map of the Köppen-Geiger climate classification. Hydrology and Earth System Sciences 11, 1633–1644 (2007)

Taylor, P., Luther, M.B.: Evaluating rammed earth walls: A case study. Solar Energy 76(1-3), 79–84 (2004)

Walker, P., Keable, R., Martin, J., Maniatidis, V.: Rammed Earth: Design and Construction Guidelines. BRE Bookshop, Watford (2005)

The Variation of Total Volume Change, Water Volume Change, Yielding Net Confining Stress and Shear Strength of Undisturbed Unsaturated Loess under Isotropic Compression

S. Mohsen Haeri and A. Akbari Garakani

Abstract. Catastrophic failures in residential building foundations due to wetting collapse is a very serious problem in loessial arid zones. In this research, the variation of total volume change, water volume change, yielding net confining pressure and shear strength of undisturbed unsaturated loessial soil samples obtained from an arid zone in Golestan province in Iran, is studied by manipulating a full stress path controlled unsaturated triaxial apparatus at Sharif University of Technology. For this purpose, isotropic compression tests were performed on the specimens for five different values of constant matric suction while raising the net confining pressures in wetting path. Also at the end of isotropic compression tests, deviator stress was applied to obtain the shear strength parameters of the soil. Results show that for different values of matric suctions the values of total volume changes, water volume changes and yielding net confining pressures vary significantly and the shear failure envelope supports the extended Mohr-Coulomb theory for unsaturated soils.

Keywords: loess, isotropic compression, total volume, water volume, yielding stress, shear strength.

S. Mohsen Haeri
Sharif University of Technology, Iran, Tehran
e-mail: smhaeri@sharif.edu

A. Akbari Garakani
Sharif University of Technology, Iran, Tehran
e-mail: Akbari_amir@civil.sharif.edu

1 Introduction

North eastern parts of Iran are widely covered by loessial soils which possess high apparent strength at their natural moisture content but are susceptible to large reduction in void ratio upon wetting. However the aforementioned subject and related governing parameters have not been surveyed on undisturbed loessial specimens perfectly, so far. Fredlund & Morgenstern (1977) used independent stress state variables for the study of the volume change behaviour of unsaturated soils. Chen et.al (1999) studied the overall volume change, water volume change, and yield associated with an unsaturated, compacted, low-plasticity loess from China by conducting two types of isotropic compression and triaxial shrinkage tests. Also the measurement of shear strength of unsaturated soils has gained increasing attention during the past several decades (Fredlund et.al 1978). In this research, the variation of total volume change, water volume change, yielding net confining pressure and shear strength of unsaturated loessial soil samples obtained from an arid zone in Golestan province in Iran, is studied under consolidated drained (CD) condition by manipulating a full stress path controlled unsaturated triaxial apparatus at Sharif University of Technology, Iran, and results are presented.

2 Stress and Volume-Mass Variables

In this paper the following notations are used to denote the stress state variables:

$$p = \frac{\sigma_1 + \sigma_2 + \sigma_3}{3} - u_a \tag{1}$$

$$s = u_a - u_w \tag{2}$$

$$q = \sigma_1 - \sigma_3 \tag{3}$$

In which, σ_1, σ_2, and σ_3 are the principal stresses; u_w and, u_a are the pore water pressure and the pore air pressure respectively; and p, s and q are the net mean stress, the matric suction and the deviator stress, respectively. Volume change associated with the soil structure is denoted using the variable, ε_v in which ΔV, and V_0 are the total volume change and initial volume of the specimen.

$$\varepsilon_v = -\frac{\Delta V}{V_0} \tag{4}$$

3 Testing Equipments and Procedures

3.1 Equipments

The modified triaxial apparatus used in this research (Fig. l) was designed and developed at Sharif University of Technology, Iran. A 500 kPa high air entry ceramic disk was installed, using epoxy around the perimeter, into the especially designed and made base plate of the triaxial apparatus. A digital volume change device was connected to the single-walled cell to measure the total volume change of the sample and another digital volume change device was connected to the base of the pedestal, just beneath the high air entry ceramic disk, to evaluate the water volume changes of the sample. The volume variations of the cell body and connecting pipes were evaluated and correlated with respect to the different pressure levels to correct the volume change assessments. To control the air pressure, water pressure and confining pressure independently, 3 accurate electronic pressure regulators adjoined with 3 pressure sensors were used, which made it possible to apply any stress paths to the sample.

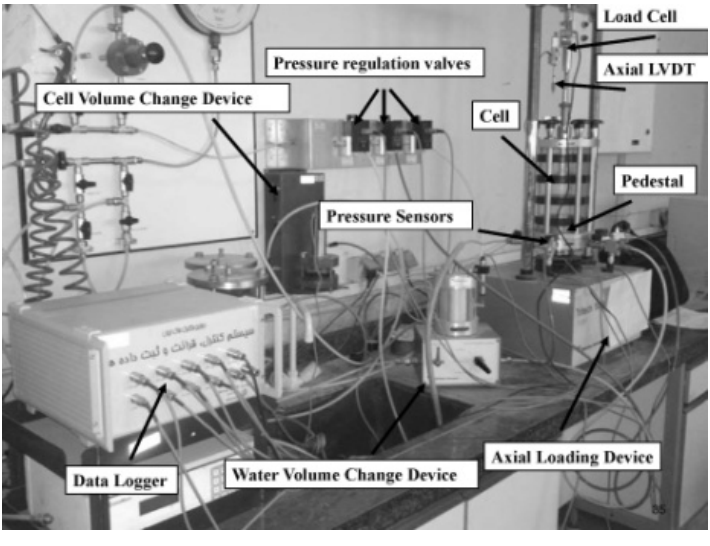

Fig. 1. Modified triaxial device used in the research program.

3.2 Triaxial Testing Procedure

The soil used in the study was undisturbed loess taken in waxed monolithic boxes from the city of Gorgan in Golestan province in North of Iran. Cylindrical specimens with 50mm in diameter and 100mm in height were then extracted from the

monolithic samples in laboratory. The initial conditions of the undisturbed specimens are listed in Table l. A total of five isotropic compression triaxial tests, followed by applying deviator stresses, were performed under CD conditions. Each test was performed by applying constant matric suction using the axis translation technique and rising the net confining pressure in steps. At the end of the last step, the deviator stress was applied to the sample. The values of net mean stress, matric suction and other information related to each test are listed in Table 2. Each test took from 20 to 35 days to complete. At the end of each test, the specimen was divided into three parts. The water content was measured for each part and in every case the water contents were found to be approximately equal and matched values computed from the recorded volume change data.

Table 1. Initial Physical Properties of the Undisturbed Loess from Gorgan.

Specific Gravity G_s	Dry Density ρ_d (kN/m3)	Void Ratio e_0	Initial water content w(%)	Degree of Saturation Sr (%)	USCS classification
2.72	16.4	0.66	3	12.4	ML (Silt with clay)

Table 2. Triaxial testing conditions.

Test No.	Initial water content of the sample (%)	Initial matric suction (kPa)	Target constant matric suction (kPa)	Net Confining pressure levels (kPa)
1	20	20	10	0, 50, 100, 150, 200, 250, 300, 400
2	8	600	50	0, 50, 150, 200, 400
3	8	600	100	0, 50, 150, 200, 250, 400
4	8	600	200	0, 50, 150, 200, 250, 300
5	6.8	2000	400	0, 50, 100, 150

4 Test Results

4.1 Total Volume Change and Yielding Net Confining Stress in Isotropic Compression Test under Constant Matric Suction

Figure 2 shows the ε_v - log p relationship. Each curve in Fig. 2 can be defined by two intersecting linear lines. The net mean stress corresponding to the intersection point is referred to as the yield stress, $p_0(s)$ (Chen et.al 1999). The results show that the higher the suction values, the larger the yield stress. If the yield points are plotted on the p-s plane shown in Fig. 2, a yield curve can be drawn through these points (Fig. 3). The yield curve is called the loading-collapse yield curve or the LC

curve (Alonso et al. 1990). The shape of the yield curve obtained appears to support the concept of the loading-collapse yield curve or the LC model. Values of the yielding net confining stress for the case in which the matric suction was 400 kPa could not be attained because the maximum net confining pressure applied to the sample was just 150 kPa due to the service pressure limits of the pneumatic compressor. Of course it could be estimated by the LC curve as being around 275kPa as depicted in Fig.3.

4.2 Water Volume Change of the Soil in Isotropic Compression under Constant Matric Suction

Figure 4 shows the variation of the water content of the samples for different values of constant matric suction during the isotropic compression tests. As depicted in Fig.4, for the cases when the matric suctions equal to 50, 100, 200 and 400kPa, the water content of the samples rise by increasing the net mean pressure. That is because the decrease in the porous volume inside the samples due to the raise of the net mean stress implies in increase of water inflow to keep the matric suction constant inside the sample. On the other hand, at low values of the matric suction (in test with matric suction equal to 10kPa) in which the soil voids are almost filled with water, by raising the net confining stress the sample loses water as shown in Fig.4. By making comparison between the diagrams depicted in Fig. 4, it could be concluded that the higher the value of the applied matric suction, the lower the soil water content would be attained, regardless of the value of the applied net mean stress.

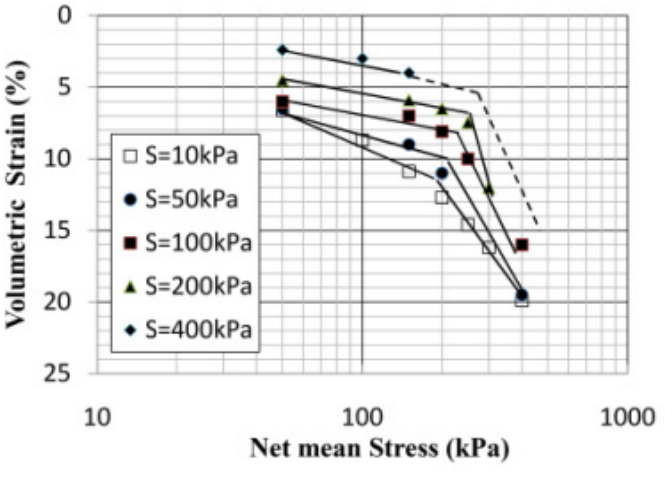

Fig. 2. Volumetric strains versus net mean stress.

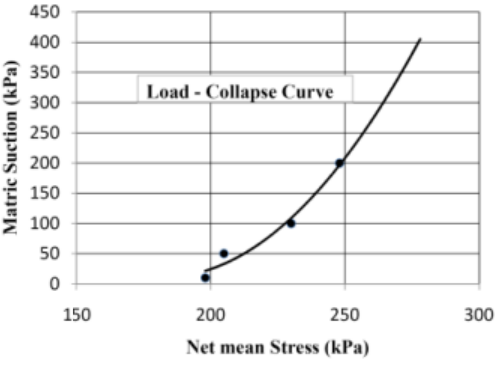

Fig. 3. Load-collapse curve of the Gorgan loess.

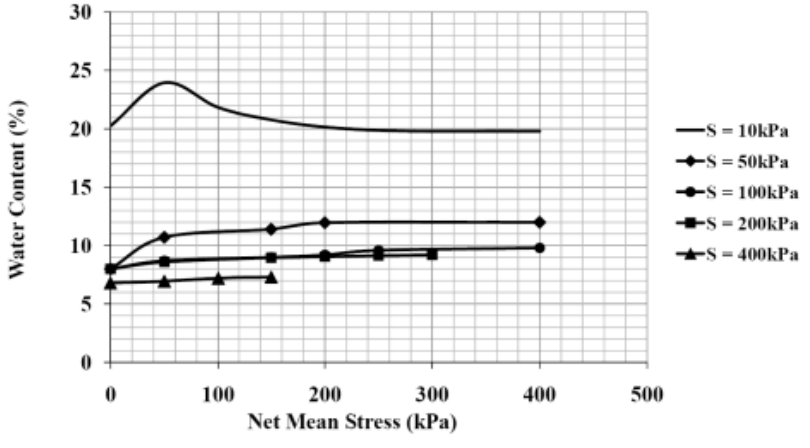

Fig. 4. Water content versus net mean stress.

4.3 Shear Strength Parameters

At the end of the last part of isotropic compression, the deviator stress is applied to the sample by using a fully strain controlled jack. The shear strength equation for an unsaturated soil can be written in terms of effective cohesion (c'), net normal stress at failure on failure plane, angle of internal friction (ϕ') and angle indicating the rate of change in shear strength relative to a change in matric suction (ϕ^b) as shown in Equation 5 (Fredlund et al. 1978). It defines a planar surface which is called extended Mohr-Coulomb failure envelope.

$$\tau_{ff} = c' + (\sigma_f - u_a)_f \tan\phi' + (u_a - u_w)_f \tan\phi^b \quad (5)$$

In Fig. 5 the aforementioned planar surface is illustrated based on the obtained results, as well as the Mohr circles for each test. The variation of the deviator stress versus axial strain for the loessial samples is presented in Figure 6. In accordance with the test results and using least square method, for the tested loess the values of c', ϕ', and ϕ^b are evaluated as 20.2 kPa, 26.2^0 and 12.5^0 respectively and the failure envelope is close to the shape of a plane. Of course it seems that more supplementary tests should be conducted on this soil to draw the shear failure envelope for wider ranges of net mean stress and matric suction. The supplementary tests are underway and the results will be reported in near future.

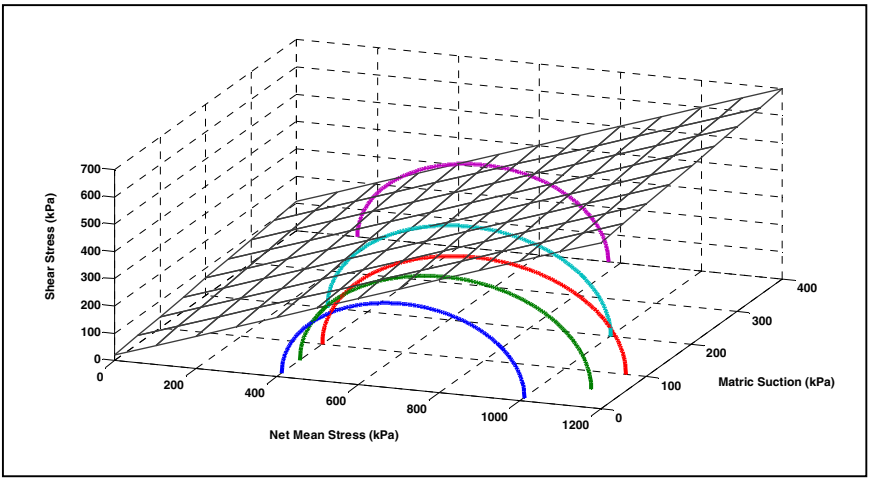

Fig. 5. Mohr circles and Mohr – Coulomb planar envelope for Gorgan loess.

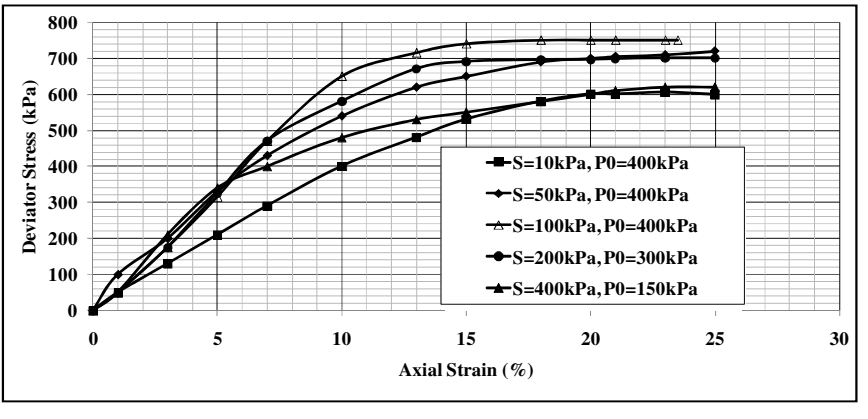

Fig. 6. Deviator stress versus axial strain.

5 Summary

A total of five isotropic compression triaxial tests followed by applying deviator stresses were performed under CD condition and constant matric suction on collapsible loess. In this regard, the variation of total volume strains and water content of the samples are presented as well as the values of yielding net mean confining pressures, loading collapse curve and shear strength parameters. Results show that the value of matric suction significantly affect the values of yielding net mean pressure and water content of the soil in isotropic compression tests. Also it was shown that the shear failure envelope supports the extended Mohr-Coulomb theory for unsaturated soils.

References

Alonso, E., Gens, A., Josa, A.: A constitutive model for partially saturated soils. Geotechnique 40(3), 405–430 (1990)

Fredlund, D.G., Morgenstern, N.R.: Stress state variables for unsaturated soils. Journal of the Soil Mechanics and Foundations Division, ASCE 103(GT5), 447–466 (1977)

Fredlund, D.G., Morgenstern, N.R., Widger, R.A.: The shear strength of unsaturated soils. Canadian Geotechnical Journal 15, 313–321 (1978)

Chen, Z.H., Fredlund, D.G., Gan, J.K.: Overall volume change, water volume change, and yield associated with an unsaturated compacted loess. Canadian Geotechnical Journal 36, 321–329 (1999)

Collapse Potential and Permeability of Undisturbed and Remolded Loessial Soil Samples

S. Mohsen Haeri, Atefeh Zamani, and A. Akbari Garakani

Abstract. Loessial collapsible soils are in the group of problematic soils and have been encountered in many parts of the world such as some regions in Iran. In these soils, sudden and large volume changes occur while the water content, overburden stress or both are passed a threshold limit. In this paper the collapse potential of a loessial soil taken from Gorgan; a city in Golestan province in North of Iran; has been investigated on both undisturbed and remolded specimens by using oedometer tests. For both types of samples, the effect of initial moisture content and also inundation stress have been investigated on the collapse potential and permeability behavior of the aforementioned soil. The results show that the type of specimen, initial water content, initial dry density and inundation stress have strong affect on collapse potential and permeability coefficient of the studied loess.

Keywords: collapse potential, loess, permeability, oedometer test, undisturbed samples, remolded samples.

1 Introduction

Loess is one of the major problematic soils in the world. There are similar features that are typical to most of collapsible soils. These features are: open structure,

S. Mohsen Haeri
Sharif University of Technology, Iran, Tehran
e-mail: smhaeri@sharif.edu

Atefeh Zamani
Civil Eng. Dept, Sharif University of Technology, Tehran
e-mail:zamani_atefeh@yahoo.com

A. Akbari Garakani
Sharif University of Technology, Iran, Tehran
e-mail: Akbari_amir@civil.sharif.edu

high void ratio, low dry density and geologically young or recently altered deposits. The behaviour of collapsible soils is highly affected by the change of water content and effective stresses (Rogers 1995).

Several researchers studied the effect of initial water content, dry density and overburden pressure on the magnitude of collapse such as Alawaji (2001), Fredlund (1996), Phien-wej et al. (1995) and Lawton et al. (1992). To summarize the major results of these studies, the following general conclusions can be reached:

1. For a given set of conditions, the amount of collapse decreases with increase in initial moisture content and increase in dry density.
2. For a given set of initial conditions, there is a critical pressure at which the amount of collapse is the greatest.
3. For any soil, there are specific combinations of initial water content, initial dry density and overburden pressure at which no volume change will occur when the soil is inundated.

In this study, the effects of initial moisture content and inundation stress on collapse potential are investigated. In addition, the permeability of Gorgan loess soil is studied. Tests have been conducted on specimens with different initial moisture contents and inundation stresses.

2 Test Program

In this study, a number of collapse potential tests were performed on remolded and undisturbed loess samples. Undisturbed samples of the soil for tests were taken from Gorgan, a city in Iran, by means of block sampling. The samples were carefully trimmed and waxed. When sampling the soil, its natural water content was about 3%. Undisturbed specimens were directly taken from mentioned boxes. After determining the water content of each specimen, sufficient water was gradually introduced to the specimen through spraying and waiting to get to the target water content of the test program.

In order to prepare remolded samples, loess soil was passed through a No. 100 sieve and oven dried. Having the volume of the ring, initial dry density and initial water content, the required volume of water and dry soil needed for making the remolded specimen could be calculated. The water was added to dry soil and thoroughly blended and the wet soil was compacted in odeometer rings to get to the preplanned density.

Undisturbed samples were prepared and tested in three groups of initial water content: 3-4% (natural water content), 8-9% and 13-15%. Remolded samples were prepared at four initial moisture contents: 3, 7, 11 and 15% with an initial dry density of 1.6 kg/cm^3.

3 Physical Characteristics

Index properties of the loess soil are summarized in Table 1 and Fig. 1, representing the particle size distribution of the soil.

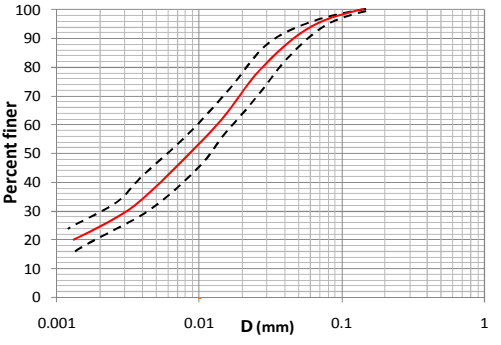

Fig. 1. Soil particle size distribution.

Table 1. Physical properties of soil tested in this study.

Property	
Specific gravity	2.72
Natural void ratio	0.67-0.77
Natural dry density (gr/cm3)	1.57-1.64
Natural water content (%)	2.9-3.6
Liquid limit (%)	33
Plastic limit (%)	24
Plasticity index (%)	9
Soil classification (USCS)	ML

4 Collapse Potential

The results of the tests conducted on undisturbed and remolded specimens with water contents of about 3-4% and 3%, respectively, and subjected to wetting at different levels of inundation stresses are presented in Figs. 2 and 3. The results indicate that the higher the inundation stresses the higher amount of collapse at that stress. However, if after inundation the loading continues, to say 16 kg/cm^2, the final volume change increases with decrease in inundation stress. This is clearly shown in Figs. 2 and 3 even during unloading.

Fig. 4 and Fig. 5 represent the best fits for both pre-wetted and wetted states of undisturbed and remolded samples. Test results showed that initial water content has a considerable effect on the final void ratio of specimen during collapse phenomenon due to wetting. The final void ratio of specimens with higher initial water content was higher in comparison with specimens with lower initial water content meaning that the amount of collapse increases as the initial water content decreases.

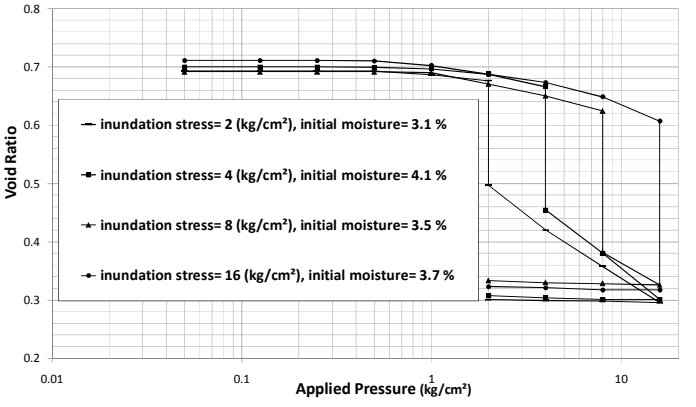

Fig. 2. Single oedometer collapse test for undisturbed loess specimens.

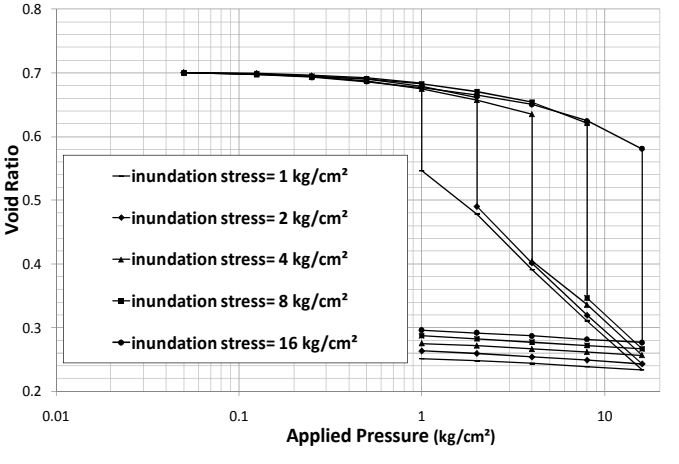

Fig. 3. Single oedometer collapse test for remolded loess samples.

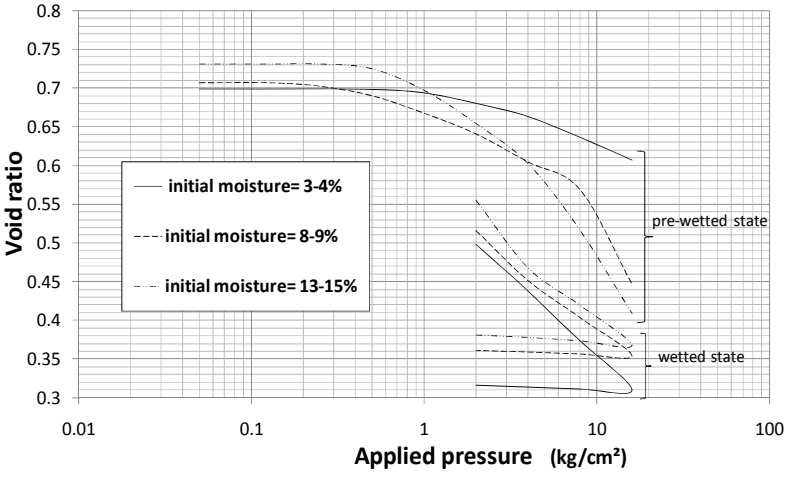

Fig. 4. Changes of the void ratio of undisturbed samples in pre-wetted and wetted state.

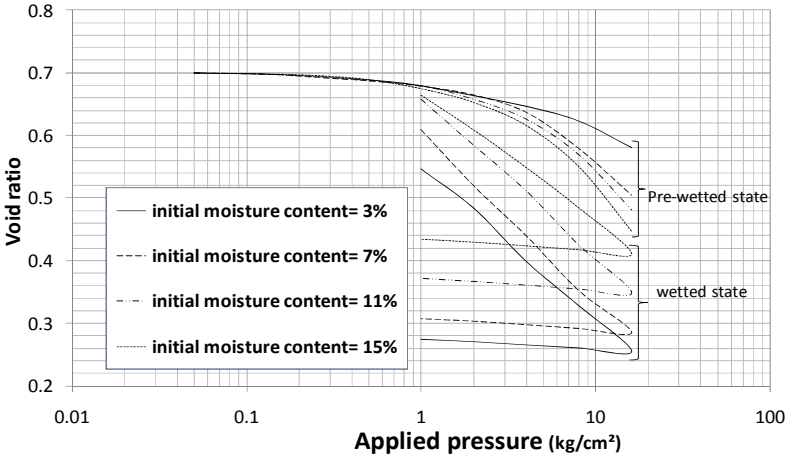

Fig. 5. Changes of void ratio of remolded samples in pre-wetted and wetted states.

Fig. 6 represents the variations of collapse potential (I_c), and applied pressure for undisturbed and remolded samples. I_c could be defined as expressed by Equation 1. In which ΔH and H_0 stand for the variation of the sample height due to inundation and the sample height just before inundation, respectively. For both types of specimens, at the same inundation stress, collapse potential increased with a decrease in initial water content. For the same initial water content, an increase in stress below critical pressure led to a greater collapse potential. However beyond the critical pressure at which the effect of stress alone caused significant soil collapses, the collapse potential decreased with a further increase in stress.

$$I_c = \frac{\Delta H}{H_0} \tag{1}$$

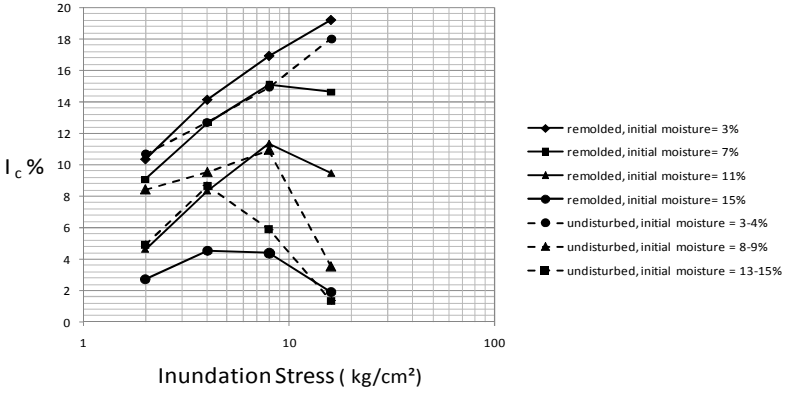

Fig. 6. Relationship between collapse potential and inundation stress of loess.

Critical pressure is the pressure at which the dry loess changes from a low compressibility response to a high compressibility response. The critical pressure is strongly influenced by initial water content. Increase in initial water content reduces the strength of the bond between loess particles and finally decreases the critical pressure. Table 2 represents the critical pressure of remolded and undisturbed samples with different initial water content.

Table 2. Critical pressure of undisturbed and remolded samples.

Initial moisture of undisturbed loess	Initial moisture of remolded loess	Critical Pressure (kg/cm^2)
3-4%	3%	>16
8-9%	7%	8
N.A	11%	4
13-15%	15%	4

5 Permeability

After inundating and collapse of the specimen and increase in stress level, the permeability coefficients of the collapsed specimens are measured in every stage of increasing stress and the result are illustrated in Fig.7. As it is presented in Fig.7, permeability of the collapsed loess increases with increase in initial water content of the specimen. As it is illustrated in Fig. 4, the specimens with higher

initial moisture content end in a higher void ratio after collapse. Void ratio is a factor that influences the permeability of soil and increase of void ratio results in an increase in permeability of the soil.

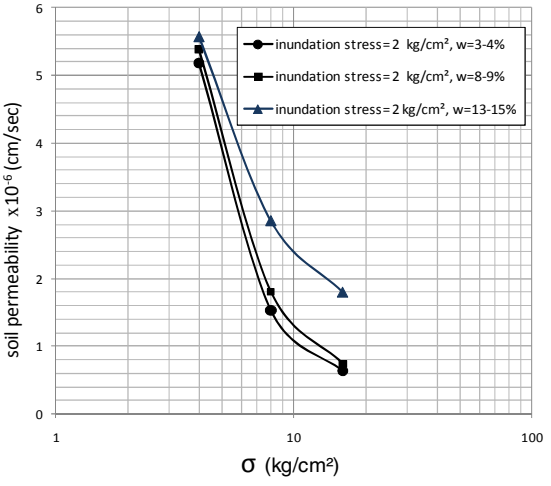

Fig. 7. The influence of initial moisture content and stress level after inundation on the soil permeability of collapsed soil (Undisturbed specimens).

6 Conclusions

1. The results indicate that the higher the inundation stresses the higher amount of collapse at that stress. However, if after inundation the loading continues, the final volume change increases with decrease in inundation stress.
2. In both remolded and undisturbed specimens, initial water content influences the amount of collapse potential. Collapse potential increases as initial water content decreases.
3. In both remolded and undisturbed specimens, critical pressure increases as the initial water content decreases.
4. Specimens with higher initial water content, in contrast with the specimens with lower initial moisture content, have a higher void ratio after collapse.
5. As the initial moisture content of the soil before collapse increases, the permeability of the soil after collapse increases.

References

Alawaji, H.A.: Settlement and bearing capacity of geogrid-reinforced sand over collapsible soils. Geotextiles and Geomembranes 19, 75–88 (2001)

Fredlund, D.G.: The emergence of unsaturated soil mechanics. In: The 4th Spencer J. Buchanan Lecture, College Station, Texas, 39 p. A&M University Press (1996)

Lawton, E.C., Fragazy, R., Hetherington, M.D.: Review of wetting-induced collapse in compacted soil. Journal of Geotechnical Engineering, ASCE 118, 1377–1394 (1992)

Phien-wej, N., Pientong, T., Balasubramaniam, A.S.: Collapse and strength characteristics of loess in Thailand. Engineering Geology 32, 59–72 (1992)

Rogers, C.D.F.: Types and distribution of collapsible soils. In: Derbyshire, E., et al. (eds.) Genesis and Properties of Collapsible Soils, pp. 1–17. Kluwer Academic Publishers (1995)

Geotechnical Behaviour of Unsaturated Tropical Clay Soils of Dhaka, Bangladesh

A.T.M.S. Hossain and David G. Toll

Abstract. Experimental testing has been carried out on samples collected from a borehole in the Curzon Hall area of Dhaka to investigate the geotechnical behaviour of some unsaturated tropical clay soils from Dhaka, Bangladesh. The soil was tested in its natural (undisturbed) state and also after destructuration in order to assess the influence of the natural iron oxide cementing on the strength and stiffness. Natural specimens consolidated at effective stresses below 500 kPa show a change in stiffness that can be interpreted as bond yield. The tests also show a difference in failure envelope between the natural and destructured specimens, confirming the influence of the iron oxide bonding on both stiffness and strength. Values of the Critical State stress ratio M were found to be 0.95-0.96.

Keywords: fabric, strength, stiffness, bond, yield.

1 Introduction

Dhaka is the capital of Bangladesh, which is expanding rapidly. Rapid urbanization in the city area has led to an increased interest in the geotechnical behaviour of the soils that are present within the city area. The soils within the city area are formed under warm to hot and humid to subtropical climatic conditions and derived from a residual soil horizon. They are invariably unsaturated. Monsur (1995) noted that the reddish brown colour of the Madhupur formation is clearly related to iron compounds. Monsur (1995) also mentioned that these are insitu

A.T.M.S. Hossain
Jahangirnagar University, Savar, Dhaka, Bangladesh
e-mail: shakhawathos2004@yahoo.com

David G. Toll
Durham University, Durham, UK
e-mail: d.g.toll@durham.ac.uk

developed soils and do not represent transported or re-deposited soil materials. He also noted that these soils have undergone intensive weathering processes that have released Fe ions in a free state and that appear in the form of nodules or in association with clay. They are mainly composed of illite, kaolinite, chlorite and some non-clay minerals, mainly quartz & feldspar (Hossain, 2001) and of intermediate to high plasticity inorganic clay (CI to CH). In addition, these red clay soils are bonded and are of a different nature to the other sedimentary soils of Bangladesh. The red colours of these soils indicate the presence of iron oxide that is common in well-oxidized soils. Therefore the present research was performed with a view to evaluate the microfabric, bonding and geotechnical behaviour of some of the tropical clay soils of Dhaka to assess the influence of the cementing on the strength and stiffness. Leroueil & Vaughan (1991), Jardine (1992) and Malandraki & Toll (1996; 2000; 2001) studied the natural & artificially bonded soil behaviour and noted that their behaviour is similar in terms of strength and stiffness.

2 Experimental Details

Undisturbed natural samples were very carefully trimmed by hand from 100 mm diameter samples (U100), using a soil lathe to obtain cylindrical test specimens of 38mm diameter and 76mm high. Destructured samples were prepared using the trimmings from the natural samples to match the void ratios measured in equivalent natural soils. Details of specimen preparation are discussed in Hossain, 2001. A series of undrained triaxial compression tests with pore water pressure measurements were carried out on undisturbed natural and destructured soils. The specimens were initially saturated for 4-5 days by a back pressure in order to achieve a B value of 0.98. Samples were consolidated at a range of effective confining stresses from 50-800 kPa before shearing. Sample mounted strain measuring devices capable of resolving axial strains to 0.001% (Burland and Symes, 1982) were used to measure the strains. A miniature pore water pressure probe (Hight, 1982) was used to measure pore water pressure at the mid height of the sample. Specimen details of the natural soils are listed in Table 1.

3 Test Results

3.1 Fabric of the Soils

A scanning electron microscope image of a soil sample (1SEM1) is shown in Fig. 1. It can be seen from Fig. 1 that the micrograph showed a random open microfabric of silt and clay. The randomly oriented clay platelets are intermixed

with large silt size grains. Most of the silt grains are coated with clay and iron (confirmed by EDX spectra). Intra and inter granular spaces are common throughout the fabric.

Table 1. Specimen details of natural soils (Location: Curzon Hall).

Test name	Specific gravity *Gs*	Bulk density ρ ($Mg/m^{3)}$	Dry density ρ_d ($Mg/m^{3)}$	Initial void ratio *e*
us50	2.59	2.176	1.846	0.403
us100	2.62	2.171	1.859	0.410
us200	2.64	2.150	1.883	0.402
us300	2.62	2.016	1.749	0.498
us400	2.60	2.062	1.806	0.440
us500	2.59	1.972	1.720	0.505
us600	2.63	2.060	1.773	0.482
us800	2.61	2.049	1.748	0.493

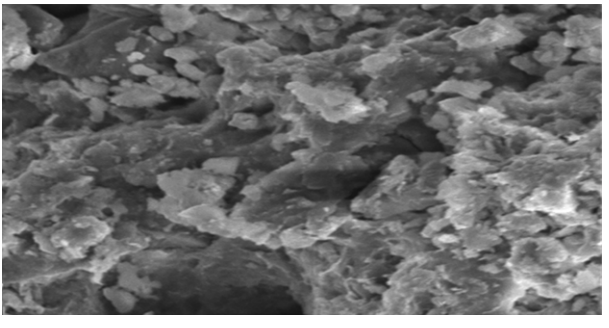

Fig. 1. Scanning electron micrograph of sample 1SEM1 (magnification x1000).

A large inter granular pore space can be observed at the left bottom side of the micrograph. EDX firing on the intra and inter granular spaces showed peaks of Fe, Si and Al from the material behind or the surrounding material. The clay cluster also showed the presence of Si, Al, K and Fe between them.

3.2 Stress-Strain and Pore Water Pressure Response

The stress-strain and pore water pressure responses of natural soils are shown in Fig. 2 and Fig. 3. Fig. 2 also shows the responses of destructured materials. The stress-strain curves of the natural soils show initially stiff behaviour with a smooth peak in stress-strain response (Fig. 2). It can be observed that the destructured samples in each case showed lower maximum deviator stresses, lower stiffness and larger strains to reach maximum deviator stress than the natural samples due

to the breakdown of bonds. This is clear evidence that the natural samples do demonstrate the existence of structure (bonding).

Tests at low confining pressures (50 to 200 kPa) initially showed low values of positive pore water pressures, followed by negative pore pressures at higher axial strains, which is indicative of a tendency to dilate (Fig. 3). No negative pore pressure was observed at higher confining pressures (300 to 800 kPa), although these samples show a fall-off in pore water pressure after an initially higher value, indicating dilative tendencies towards the end of the test. At low confining pressures (50-200 kPa), dilation during shearing occurred. This tendency to dilation caused a decrease in pore water pressure and ultimately showed negative values (Atkinson and Bransby, 1978). Only some samples at low confining pressures reached the critical state at very large strains approximately in excess of 20%. High confining pressure samples may not have reached the critical state due to the formation of distinct shear surfaces. It was found difficult to construct a single critical state line for the volumetric responses of these soils (Fig. 4).

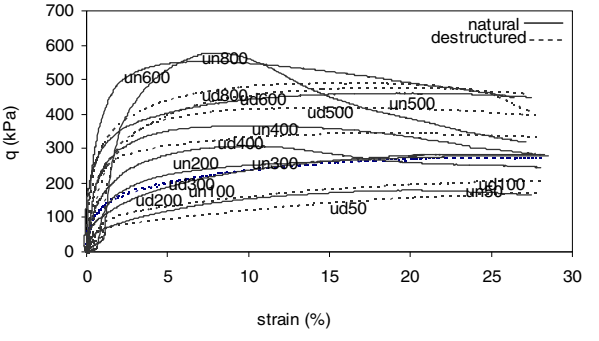

Fig. 2. Comparison of deviator stress versus axial strain curves for natural and destructured soils of Curzon Hall area.

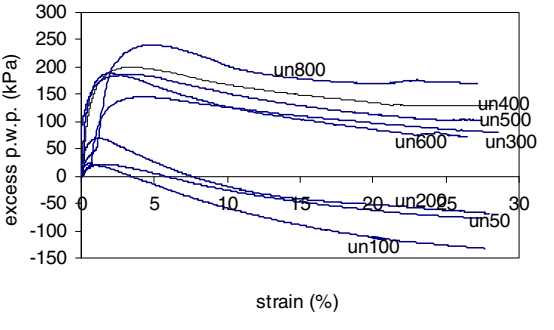

Fig. 3. Excess pore water pressure vs. axial strain curves of natural soils of Curzon Hall.

The samples showed a wide range of variations in ultimate stress ratio values. Few samples showed a common stress ratio value for different tests. Nevertheless values of the critical state stress ratio M (Fig. 5) were estimated to be 0.95- 0.96 for these samples.

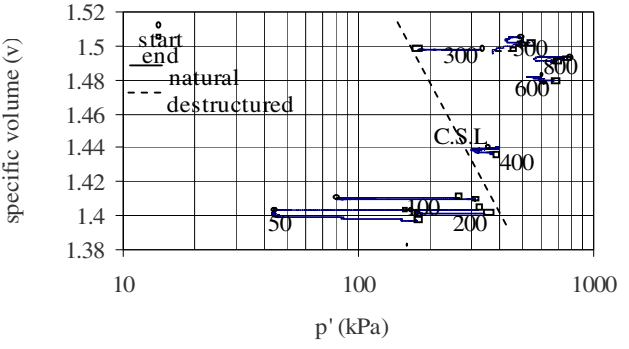

Fig. 4. Comparison between specific volume (v) vs. p´ for natural and destructured soils of Curzon Hall area.

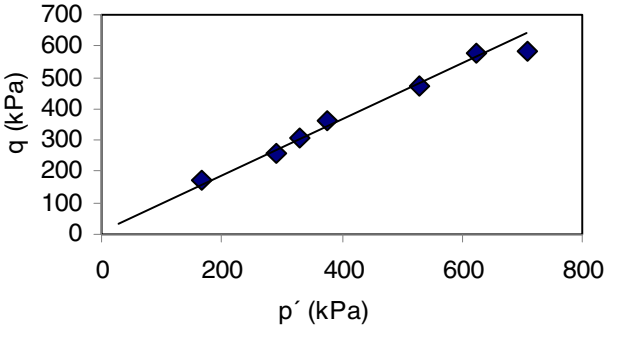

Fig. 5. Derivation of M at the critical state for natural soils of Curzon Hall area.

3.3 Stress Paths

The derived stress paths (Fig. 6) for natural soils always showed higher stress level in the q-p' space than the destructured samples. This variation in the stress paths indicates the destructuring of the clay. The stress paths show initial movement to the left but then curve to the right near failure. The stress path pattern of behaviour reflects the pore water pressure response.

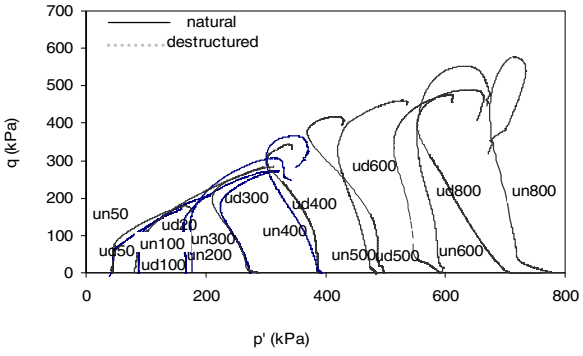

Fig. 6. Stress paths derived from a series of triaxial tests on natural and destructured samples of Curzon Hall area.

3.4 Stiffness and Yield

Undrained tangential stiffnesses were measured and yield of the natural soils has been investigated by plotting tangent values of shear stiffness (G) versus axial strain curves. A drop of stiffness values with increasing strain was observed. Two yield points were found to occur for the natural tropical clay soils of Dhaka before the final yield. The first yield point represents the end of the initial linear behaviour (almost constant G). A bond yield point was identified where a significant change in stiffness occurred (Fig. 7). Samples consolidated to above 500 kPa did not show a bond yield. The yield points are plotted in the q-p' space as shown in Fig. 8. Two yield surfaces were found to occur for natural tropical clay soils of Dhaka below the final yield surface under undrained shearing (Fig. 8). It was found that the bond yield surface occurs well below the failure surface.

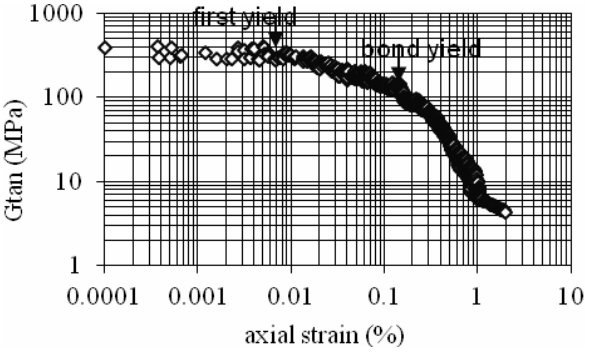

Fig. 7. First yield and bond yield for test un300.

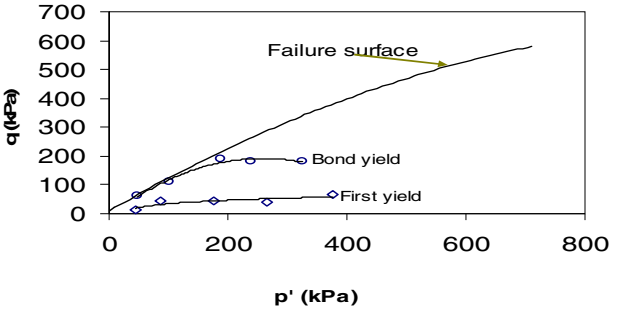

Fig. 8. Failure surface, first & bond yield surfaces for natural soils.

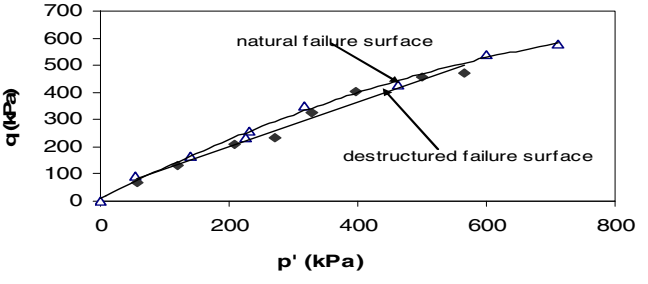

Fig. 9. Comparison of failure surfaces for natural and destructured soils.

The bond yield surface at very low confining pressure runs very close to the failure surface and then diverges at higher stresses. When the soil reaches the final yield surface, it loses almost all of its stiffness due to bonding (Fig 8).

3.5 Failure Surface

The failure surface for natural soils is positioned at higher stress level in the q-p' space than the destructured failure surface (Fig. 9). The variations of the shape of the two failure surfaces justify the presence of bonding in natural samples. The natural failure surface initially showed a curvature with the increase of p' up to approximately p' = 400-450 kPa and after that the slope of the natural failure surface moved towards the destructured failure surface. The natural and destructured failure surfaces coincided at higher stresses due to complete destruction of bonds. At higher stresses both the natural and destructured soils showed similar stress ratios.

4 Conclusions

Tropical clay soils of Dhaka showed a random open microfabric of silt and clay. The randomly oriented clay platelets are intermixed with large silt size grains.

Most of the silt grains are coated with clay and iron. Intra- and inter- granular spaces are common throughout the fabric. The stress strain curves and stress paths showed clear differences between the natural (undisturbed) state and after destructuration. This is clear evidence of the existence of structure (bonding) in the natural samples due to the influence of the natural iron oxide cementing. Low confining pressure (50-200 kPa) samples showed dilation during shearing. High confining pressure samples did not show any dilation, although there was a fall of pore water pressure at the end of the test. Only some samples at low confining pressures reached the critical state at very large strains approximately in excess of 20%. Values of the critical state stress ratio M were estimated to be 0.95- 0.96 for these soils.

Samples consolidated at effective stresses below 500 kPa show a clear change in stiffness that can be interpreted as a 'bond yield'. The natural failure surface initially showed a curvature with the increase of p' up to approximately p' = 400-450 kPa and after that the slope of the natural failure surface moved towards the destructured failure surface. The tests also show a clear difference in failure envelope between the natural and destructured samples, confirming the influence of the iron oxide bonding on both stiffness and strength. The natural and destructured failure surfaces coincided at higher stresses due to complete destruction of bonds.

References

Atkinson, J.H., Bransby, P.L.: The mechanics of soils. McGraw Hill, London (1978)

Burland, J.B., Symes, M.: A simple axial displacement gauge for use in the triaxial apparatus. Geotechnique 32(1), 62–65 (1982)

Hight, D.W.: A simple piezometer probe for the routine measurement of pore pressure in triaxial tests on saturated soils. Geotechnique 32, 397–401 (1982)

Hossain, A.T.M.S.: The engineering behaviour of the tropical clay soils of Dhaka, Bangladesh, PhD thesis, University of Durham (2001)

Jardine, R.J.: Some observations on the Kinematic nature of soil stiffness. Soils & Foundations 32(2), 111–124 (1992)

Leroueil, S., Vaughan, P.R.: The general and congruent effects of structure in natural soils and weak rocks. Geotechnique 40(3), 467–488 (1990)

Malandraki, V., Toll, D.G.: The definition of yield for bonded materials. Geotechnical and Geological Engineering 14(1), 67–82 (1996)

Malandraki, V., Toll, D.G.: Drained probing triaxial tests tests on a weakly bonded artificial soil. Geotechnique 50(2), 141–151 (2000)

Malandraki, V., Toll, D.G.: Triaxial tests on a weakly bonded soil with changes in stress path. Journal of Geotechnical and Geoenvironmental Engineering, America Society of Civil Engineers 127(2), 282–291 (2001)

Monsur, M.H.: An introduction to The Quaternary Geology of Bangladesh. City Press and Publications, Dhaka (1995)

Shrinkage Characterization of Some Italian Clay Soils

Claudia Meisina

Abstract. A study was conducted to investigate the shrinkage behaviour of clay soils of Oltrepo Pavese (Northern Apennines – Italy), which has experienced, in the last decades, many drought periods. The shrinkage characteristics were studied in laboratory with different methods. A quantitative description of the crack patterns at the soil surface was done in a site corresponding to a natural soil, which was used in the laboratory tests.

Keywords: shrinkage, clay soils, Oltrepo Pavese.

1 Introduction

The shrinkage of clay soils, due to drought periods, causes damage to foundations, road embankments, buildings and other infrastructures. Better characterization of shrinkage potential will help to evaluate the potential movements to include in the swelling/shrinking hazard assessment. Nevertheless, a limited number of methods have been developed for the measure and the prediction of the shrinkage of clays (Puppala et al. 2006).

The aim of the paper is to investigate the shrinkage behaviour of some clay soils of Oltrepo Pavese (Northern Apennines – Italy) using different methods.

2 Materials

Shrinking soils are frequent throughout the Oltrepo Pavese and they result in many geotechnical problems, in particular, damage to buildings. The material forming

Claudia Meisina
Università di Pavia, Pavia, Italy
e-mail: claudia.meisina@unipv.it

these soils comes from the weathering of the sedimentary rocks and of the alluvial deposits.

For this study remoulded and undisturbed soils belonging to different types (Meisina et al. 2006) were collected: the eluvial–colluvial soils (I) are distributed on the hilly areas with gentle slopes; the soils of the subtype IIa are located on the oldest alluvial terraces; the soils of the subtype IIb correspond to recent heterogeneous alluvial deposits.

On the basis of grain-size distribution, the soils were classified as silty clay (1, 2, 4, 5, 6, and 7) and clay silt (3, 8 and 9) (Table 1). According to the Unified Soil Classification System the soils can be classified as CH; the sample n°3 belongs to a low plasticity soil (CL). The values of blue determined with the methylene blue adsorption are very high for alluvial and colluvial soils and indicate that expansive lattice-type minerals are the most likely clay minerals present. According to the Williams & Donaldson (1980) classification chart all the soils have very high and high swelling potential.

Table 1. Geotechnical parameters of the study soils. C: clay content (%<2μm); Wl: liquid limit; PI: plasticity index; VB: value of blue; w: natural water; γd: dry density; Sr: degree of saturation; u: negative pore water pressure.

Sample	Type	Depth (m)	C (%)	Wl (%)	PI	VB (g/100g of soil)	w (%)	γ_d (kN/m^3)	Sr (%)	u (kPa)
1	IIa	1.25	50	72.1	52.2	8.2	21.1	16.9	93.3	1950
2	IIa	2.35	57	76.4	54.8	10.8	22.5	16.6	90.9	1230
3	IIa	1.5	30	45.7	28.5	3.7	19.4	17.7	91.8	620
4	IIa	6.7	75	104.4	81.2	10.8	33.6	14.3	100	1950
5	IIa	4.7	54	68.2	47.3	7.9	25.4	15.8	94	3890
6	IIa	8.2	60	74.5	55.9	8.99	25.8	15.9	97.5	780
7	IIa	1.30	72	81.2	61.9	16.99	27.9	15.0	91.9	310
8	IIb	0.4	46	59.4	38.2	4.9	21.8	16.6	94	100
9	I	0.4	48	67.9	46.0	7.75	30.1	15.0	100	30

The soils are saturated or quasi-saturated (saturation degree Sr>=85%) for most of the year. Only in exceptionally dry periods the soils become unsaturated and the water content drops near or below the shrinkage limit. The samples, except n° 4, 5 and 6, were collected in the active zone (zone of seasonal moisture content variation), which has a maximum depth from about 0.8 to 2.8 m.

3 Methods

Atterberg limit test method, following the standard ASTM D427, was firstly used to measure the shrinkage of soils. The natural soils were air-dried and crushed into powders with a grain size less than 0.425 mm. The soil powder was mixed with distilled water at a water content equal to the liquid limit in order to prepare oversaturated slurry specimens. The resulting slurries were mixed by hand, put onto plates with desired volume and were vibrated for 5 minutes in order to remove entrapped air bubbles. Finally, the specimens were exposed at room temperature to dry, than the soil material was oven dried and the final volume was measured.

A linear shrinkage test method was applied following the french AFNOR standard (NF P 94-060-2). Cylindrical undisturbed soil specimens of 50 mm diameter and 20 mm height were used in the tests. The samples were left at room temperature to limit the amount of soil cracking that could occur if the drying rate was too fast. During drying, the specimens were weighted with an accuracy of 0.001 g to record the water loss at varying intervals. The two (lateral and vertical) dimensions of the soil samples were then recorded manually using vernier calipers. The tests were carried out until there was no significant change in the mass of the specimens for 24 h. The specimens were then dried at 105 °C.

Digital imaging is a relatively new tool for analyzing digital images (Puppala et al. 2006; Tang et al. 2011). The main focus is to obtain accurate shrinkage strain measurements by capturing and analyzing digital images of desiccated soil specimens. The procedure for the sample preparation was the same described for the linear shrinkage test. A digital camera was fixed above the specimens to monitor lateral variations. Another camera was fixed at the side of the specimens to monitor the thickness changes of the clay during drying. The two cameras were fixed on a tripod and were so adjusted that the specimen was centred. The position of the specimen with respect to the camera was checked using a scaled paper placed on the background and on the lateral side of the specimen. The photographs were taken with a Canon Power Shot SX10IS, with a 10-Megapixel resolution, and the manual focus option was preferred to get the same focus adjustment for each image. A calibration object, at nearly the same dimensions of the specimens, was used to perform the transformation of the pixel values into millimetres. The digital images were taken at the same intervals of the manual linear shrinkage test. The software Image 1.44 was used to analyze the digital images and to calculate the diameter and height of the specimen at each measurement. Image J is a public domain Java image processing and analysis program. It runs, either as an online applet or as a downloadable application, on any computer with a Java 1.5 or later virtual machine. It can display, edit, analyze, process, save images, it can calculate area and pixel value statistics of user-defined selections, it can measure distances and angles and it supports standard image processing functions such as contrast manipulation, sharpening, smoothing, edge detection and median filtering.

The geometrical characteristics of cracks network are of great interest and were investigated in the field during the very severe drought period August–September 2003. The horizontal shrinkage SLo was calculated as follows:

$$SLo = \frac{Sv}{St} * 100 \quad (1)$$

where: Sv is the surface area of cracks; St is the surface area of the soil before the shrinkage.

4 Results

The Atterberg shrinkage limit (Ws) ranges from 6.3 to 15% in relationship with the soil plasticity and clay content (Table 2).

The results of linear shrinkage test are shown in Fig. 1. Different water loss stages can be identified during drying: upon drying, water content decreased linearly at the initial drying stage (normal shrinkage where the soil was kept quasi-saturated, Tang et al. 2011), than the decrease of water content slowed down gradually and finally stabilized at a residual water content. The effective linear shrinkage limit (SL) was estimated as the intersection of two lines: a) the regression line where the water content decreases linearly; b) the regression line where the water content reaches stabilisation. The values of effective linear shrinkage are in the range of 9.3-13.5 %, the higher values are reported for soils n°4, 7 and 6, which are characterized by high plasticity, clay and swelling mineral content.

Table 2. Shrinkage limits of studied soils. Ws: shrinkage limit determined with the ASTM D427 method; SLv: effective vertical linear shrinkage limit determined with the AFNOR standard, SLh: effective horizontal linear shrinkage limit determined with the AFNOR standard.

Sample	Type	Ws (%)	SLv(%)	SLh(%)
1	IIb	9.8	11	11
2	IIb	9.4	10	10.5
3	IIb	15.0	9.3	9.5
4	IIb	6.3	12.1	13
5	IIb	12.3	11.3	11.5
6	IIb	14.1	13.1	11.8
7	IIb	10.5	13	13
8	IIa	14	11	13.5
9	I	16.7	13.4	

Specimens 1, 2, 3, 4, 5, 6 took from 27 to 21 days to stabilise, for specimens 7 and 8 the stabilisation time was less than 10 days (Fig.2). This is mainly because the room temperature and the initial saturation degree significantly influence the water evaporation rate of specimens (Krisdani et al. 2008). No cracks occurred in specimens during drying. Significant (less than 1%) differences were not found between lateral and vertical shrinkage (Table 2).

The specimens of soil 9 break up prior to oven drying, then for the sample n° 9 another method was adopted: small soil clods were taken from the specimens at different drying intervals to determine their water contents and density. The clod volume used for the density determination was measured by immersing the clod in a non-wetting hydrocarbon liquid. According to the obtained water content, density and specific gravity, the void ratio and the corresponding degree of saturation of specimens was calculated. From the shrinkage curve (Fig.3), it can be seen that the void ratio decreases linearly with decreasing water content till the water content is approximately 16 %. Once the water content reaches this value (the air entry value), the specimens were no longer saturated and with further drying, the volume shrinkage slows down and the void ratio almost reaches stabilization when the water content is lower than about 13.4 %, this water content value being the shrinkage limit (SL).

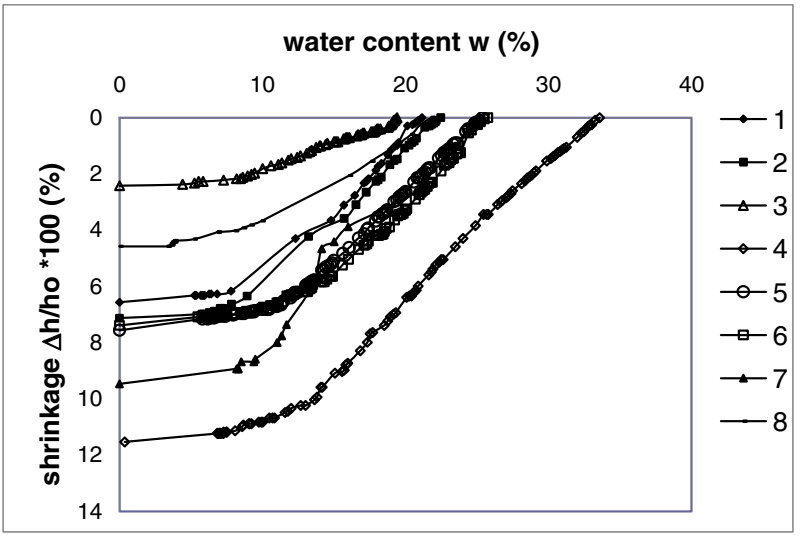

Fig. 1. Vertical linear shrinkage.

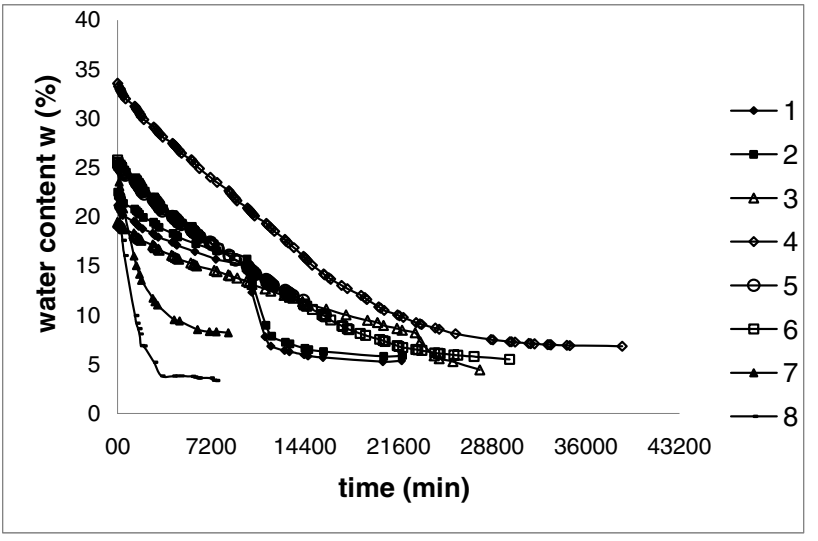

Fig. 2. Change in water content of specimens with drying time.

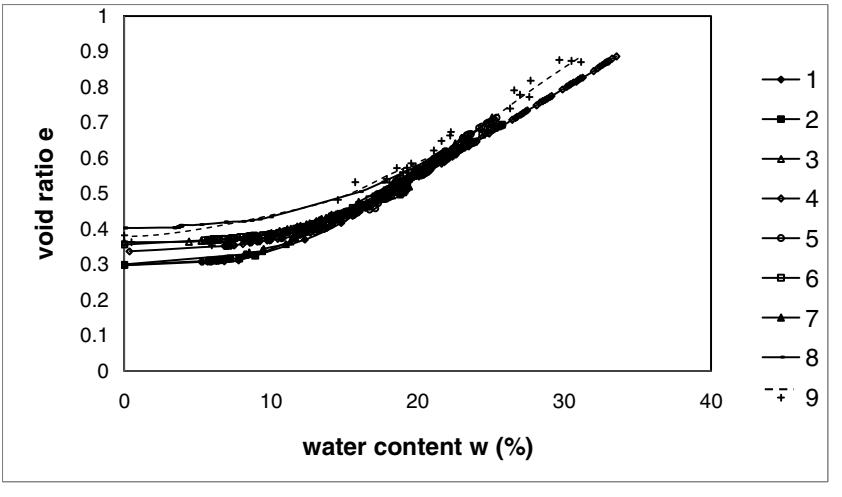

Fig. 3. The changes of void ratio with water content during shrinkage.

For samples n°8 manual measurement using vernier calipers and digital image technique were performed to determine the linear shrinkage. The results obtained from digital analysis were different from those obtained manually: 18% lateral and 17% vertical linear shrinkage. Such large variations were attributed to several factors including manual errors in measurements due to small grain decompositions (e.g. irregular surfaces were taken into account with the digital imaging).

Finally in situ conditions of soil n°9 were examined. Shrinkage cracks were near-vertical; they extended almost to the depth of seasonal moisture change in the ground (1.4 and 1.9m). The fissures are wide open till a depth of 0.5–0.8 m, where the soils are unsaturated and the water content is below the shrinkage limit. The horizontal shrinkage ranges from 3.4 to 18% (Fig. 4), strongly in relationship with the land use and the drainage conditions. The lowest value (3.4%) (Fig. 5a) corresponds to a soil with grass and a good drainage. The highest values (10.8 and 18%) (Fig. 4b) are associated to soil ploughed in the spring of the year 2003, and a poor drainage. The negative pore water pression associated with the onset of cracking is approximately $1x10^3$–$3x10^3$ kPa.

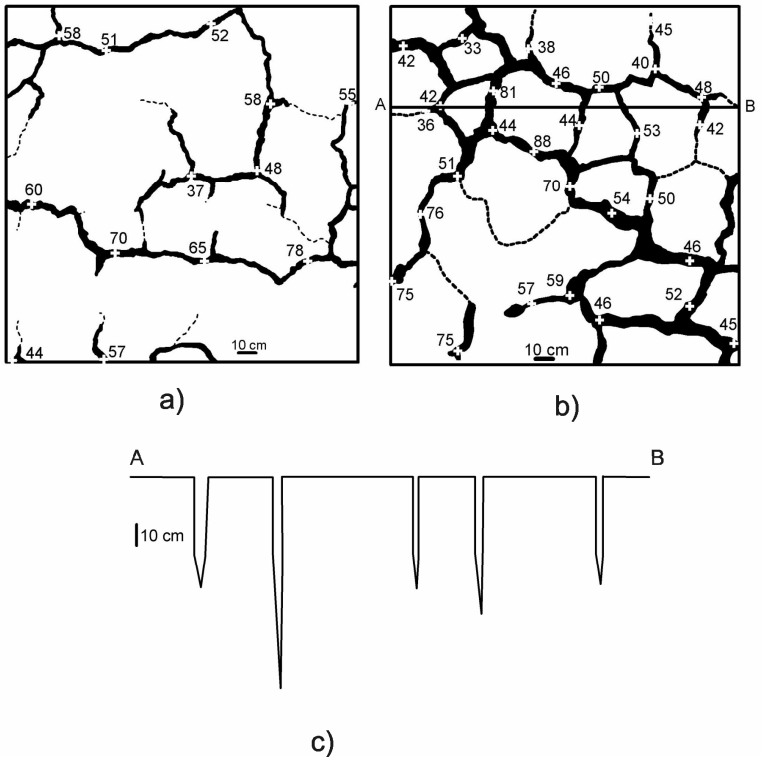

Fig. 4. Crack pattern at the soil surface of soil n°9. (a) soil with grass; (b) soil ploughed in spring; (c) cross-section showing the crack depth.

5 Conclusions

The preliminary results of a study concerning the shrinkage of Oltrepo Pavese clay soils highlight that the values of effective linear shrinkage are in a small range of 9.3-13.5 % in relationship firstly to the initial saturation degree of the samples and secondary to the clay type and content. In laboratory the volume shrinkage behaviour

in the vertical and lateral directions is homogeneous. In the field the shrinkage tests conducted on in-situ soils are influenced by different factors (e.g. land use, drainage conditions, stress state, soil structure, interactions with the atmosphere), but they are more realistic for engineering applications.

The Atterberg shrinkage test is easy to perform but it requires remoulded samples and it takes not into account the in situ soil conditions. The linear shrinkage of undisturbed soils represents shrinkage experienced by soils in real field conditions; nevertheless, the results depends on the initial condition of the specimen (dry or wet period) and the manual method is also limited by the manual measurement difficulties in non-homogeneous soils. Digital imaging is a simple and promising approach, since it offers steady, repeatable and continuous data.

References

Krisdani, H., Rahardjo, H., Leong, E.C.: Effects of different drying rates on shrinkage characteristics of a residual soil and soil mixtures. Engineering Geology 102, 31–37 (2008)

Meisina, C., Zucca, F., Fossati, D., Ceriani, M., Allievi, J.: Ground deformations monitoring by using the Permanent Scatterers Technique: the example of the Oltrepo Pavese (Lombardia, Italy). Engineering Geology 88, 240–259 (2006)

Puppala, A.J., Pathivada, S., Bhadriraju, V., Hoyos, L.R.: Shrinkage strain characterization of expansive soils using digital imaging technology. In: Al-Rawas, A.A., Goosen, M.F.A. (eds.) Expansive Soils: Recent Advances in Characterization and Treatment, Balkema, London (2006)

Tang, C.S.T., Shi, B., Liu, C., Suo, W.B., Gao, L.: Experimental characterization of shrinkage and desiccation cracking in thin clay layer. Applied Clay Science 52, 69–77 (2011)

Williams, A.B., Donaldson, G.W.: Developments relating to Building on expansive soils in South Africa: 1973-1980. In: Proc. of the 4th Int. Conf. on Exp. Soils, Denver, vol. 2, pp. 834–844 (1980)

Classification of Shrinkage and Swelling Potential of a Subgrade Soil in Central Thailand

Auckpath Sawangsuriya, Apiniti Jotisankasa, and Sekchai Anuvechsirikiat

Abstract. This paper presents the classification of shrinkage and swelling potential of soils based on total suction measurement. Undisturbed subgrade samples were collected from highway route no. 357 located in the central region of Thailand, which encountered severe longitudinal cracking along asphalt pavement shoulder prior to trafficking. Results suggested that the proposed method based on Atterberg limits and total suction measurement provided a more reliable means of classifying shrinkage and swelling potential than that based on the swelling oedometer test.

Keywords: total suction, shrinkage, swelling, expansion index.

1 Introduction

Recently, the Department of Highways, Thailand has conducted a detailed investigation on several highways constructed in the central region. The preliminary results indicated that most highways constructed on clay subgrades were subjected to pavement shoulder cracking and frequent routine maintenance. A national highway route no. 357 (Suparnburi Bypass) was investigated in this study. This highway encountered severe longitudinal cracking along asphalt pavement shoulder prior to trafficking as illustrated in Fig. 1. The construction was therefore de-

Auckpath Sawangsuriya
Department of Highways, Bangkok, Thailand
e-mail: sawangsuriya@gmail.com

Apiniti Jotisankasa
Kasetsart University, Bangkok, Thailand
e-mail: fengatj@ku.ac.th

Sekchai Anuvechsirikiat
Department of Highways, Bangkok, Thailand
e-mail: sekchai.doh@hotmail.com

layed for the rehabilitation and repair works, which resulted in an increase in construction cost.

Classification of shrinkage and swelling potential of soils provides an important step towards the engineering design and remedial measures of pavement structures in regions underlain by shrink-swell soils. The objective of this paper is to classify a shrink-swell subgrade soil that causes longitudinal cracks along pavement shoulder on highway route no. 357. A new method for assessing shrink-swell potential based on total suction measurement was proposed and compared with a conventional test method (e.g. a swelling oedometer test).

Fig. 1. Longitudinal cracking along pavement shoulder.

2 Shrink-Swell Soils in Thailand

According to the soil report by Department of Land Development, Thailand, there exist some shrink-swell soils, also known as Vertisols (shown in red region in Fig. 1), in the northern part of the central region of Thailand. Based on the soil taxonomy, such soils are high plasticity clays rich with Montmorillonite clay minerals, which exhibit large volumetric change due to soil moisture variations.

Past studies (e.g. Jotisankasa et al., 2011) revealed that the wetting and drying cycles of shrink-swell soils often induce large shrinkage and swelling strains, which result in volumetric change and corresponding failures in form of cracking and heaving. Those cracks developed in the pavements can further allow intrusion of moisture to subsoils, which results in weakening of subsoils and loss of foundation

support to pavements. Maintenance and repairs can be costly and often result in excessive capitol costs.

As indicated by Nelson & Miller (1992), there was no standard identification and classification of shrinkage and swelling potential of soils. Different classification schemes have been developed in different locations. Many classification schemes provide a potential shrink-swell rating for qualitative assessment of the degree of expansion such as "low", "medium", "high", or "very high" and are evaluated according to the conventional tests including Atterberg limits, linear shrinkage, free swell, colloid content, swelling pressure, etc. Some of these shrink-swell soil classification schemes are provided in Tables 1-3.

Table 1. Holtz and Gibbs (1956) shrink-swell soil classification.

Plasticity index	Expansion index	Degree of expansion
>35	> 30	Very high
25-41	20-30	High
15-28	10-20	Medium
<18	<10	Low

Table 2. Chen (1988) shrink-swell soil classification.

Plasticity index	Expansion index	Degree of expansion
>35	>10	Very high
20-55	3-10	High
10-35	1-5	Medium
<15	<1	Low

Table 3. Day (1999) shrink-swell soil classification.

Plasticity index	Expansion index	%Swell @ 2.8 kPa	%Swell @ 6.9 kPa	%Swell @ 31 kPa	Degree of expansion
>35	>130	>15	>12	>6	Very high
25-35	91-130	10-15	7-12	4-6	High
15-25	51-90	5-10	4-7	1-4	Medium
10-15	21-50	3-5	2-4	0-1	Low
<10	<20	<3	<2	0	Very low

McKeen (1992) also proposed a shrink-swell soil classification methodology based on total suction measurement. McKeen's methodology relies on a parameter "total suction-water content index", which is defined as the slope of the relationship between total suction and water content on a semilog plot (i.e., the soil-water characteristic curve, SWCC) as shown in Table 4.

Table 4. McKeen (1992) shrink-swell soil classification.

Total suction-water content index	Degree of expansion
>-6	Very high
-6 to -10	High
-10 to -13	Moderate
-13 to -20	Low
<-20	Nonexpansive

3 Test Method and Material

Several undisturbed subgrade samples were collected from highway route no. 357 at varied depths. The physical properties and classification of these samples are summarized in Table 5.

Table 5. Properties of subgrade samples.

Sample ID	Depth (m)	USCS	AASHTO	LL	PI	% Fines	% Clay
A	0.6	CL-CH	A-7-6	49	30	79.1	41.2
B	1.5	CL-CH	A-7-6	49	30	79.1	41.2
C-1	3.0	CH	A-7-6	66	38	97.4	61.9
C-2	3.0	CH	A-7-6	66	38	97.4	61.9

By incrementally allowing the samples to air dry, the total suction of undisturbed samples was measured with a relative humidity (RH) sensor at different equilibrated moisture contents. Fig. 2 illustrates a RH sensor used in this study. A device consists of the Honeywell polymer capacitive RH sensor encased in an open-end transparent tube. It was calibrated using salt solution in a temperature controlled chamber (20±0.5°C) (Jotisankasa et al., 2010). The total suction is related to the RH of the ambient air close to the soil by the following relationship:

$$\psi = -\left[\frac{RT}{V_{mol}}\right] \cdot \ln(R_h) \tag{1}$$

where R_h is the relative humidity, R is the universal gas constant (8.314 J.mol^{-1}.K^{-1}), V_{mol} is the molecular volume of water vapor (0.01802 m^3), and T the absolute temperature (K).

At least four total suction measurements were made for each specimen (Fig. 3a). It is important to note that during the RH measurement, the RH within the space between the sensor and the soil air must be at equilibrium. In this study, the RH sensor took at least three to four days to achieve the total suction equilibration. In addition, the swelling oedometer tests based on ASTM D4546-03: Standard Test Methods for One-Dimensional Swell Potential of Cohesive Soils – Method B were performed on two additional undisturbed samples (Fig. 3b). Although the

initial suction measurement prior to loading and soaking were not performed in the swelling oedometer test, the water content for the swelling oedometer test sample was about 19%. It can be inferred that the sample with a relatively high water content and low initial suction would exhibit low swelling potential.

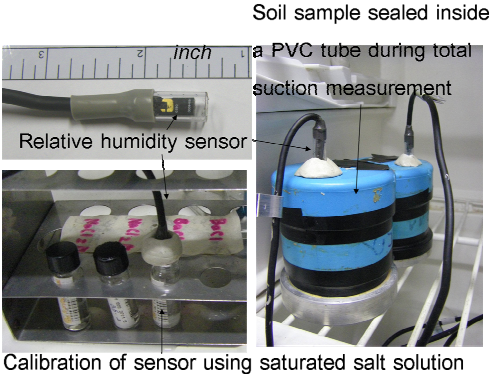

Fig. 2. Relative humidity (RH) sensor.

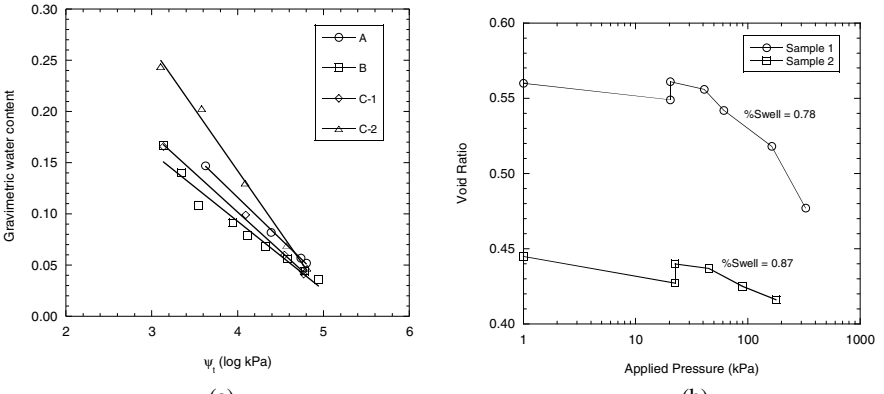

Fig. 3. Results from drying SWCC tests (a) and swelling oedometer tests (b).

4 Results and Discussion

Table 6 summarizes the shrink-swell soil classification results based on various tests, i.e., Atterberg limits, SWCC (total suction measurements) and swelling oedometer tests, according to Holtz & Gibbs (1956), Seed et al. (1962), Chen (1988), McKeen (1992) and Day (1999). As shown in Table 5, those classification methodologies based on Atterberg limits and total suction measurement suggested that the subgrade soil was classified as medium-to-high shrink-swell potential. However,

the classification based on swelling oedometer tests suggested that such soil was classified as low swelling potential, despite clear evidence that the highway shoulder suffered severely from shrink-swell cracks. Though, this swelling oedometer test result was believed to be true (provided that the initial soil suction was low), it would be giving a wrong impression to practitioners without understanding of unsaturated soil mechanics.

Although a simple Atterberg limits test and/or other index property can provide a similar prediction of swell potential, the total suction measurements are found to be useful. It seems if the volume change of the samples could also be measured during the total suction measurements, some additional value would be added to the test. Sawangsuriya et al. (2012) proposed a new method for the identification of potentially expansive soils based on the total suction-water content-volume change measurements.

Table 6. Classification of shrink-swell soils.

Sample ID	Degree of shrink-swell potential				
	Atterberg limits test;			SWCC test; McKeen (1992)	Swelling oedometer test; Day (1999)
	Holtz & Gibbs (1956)	Seed et al. (1962)	Chen (1988)		
A	High	Medium to high	Medium to high	Moderate (-12)[a]	Low (0.78-0.87)[b]
B	High	Medium to high	Medium to high	Low (-14)	
C-1	High to very high	High	High to very high	Moderate (-13)	
C-2	High to very high	High	High to very high	High (-8)	

[a] total suction-water content index, [b] %swell values.

5 Conclusion and Recommendation

In order to classify the shrink-swell potential of subgrade soils in central Thailand, various tests were carried out namely, Atterberg limits, SWCC (total suction measurement) and swelling oedometer tests. The shrink-swell classifications were evaluated based on various criteria. It was found that most classification systems based on the Atterberg limits and SWCCs results agreed reasonably well for most cases. However, it was found that the swelling oedometer test results can be misleading if the initial water content is high and suction is low. It would be also typical to have other index property measurements that could be used to support or refute the swelling oedometer results. The swelling oedometer is most useful in the prediction of the magnitude of volume change for given initial moisture content. Furthermore, one could always bring the samples to a lower moisture condition before testing.

Acknowledgements. Invaluable comments and suggestions from the reviewers are gratefully acknowledged.

References

Chen, F.H.: Foundations on expansive soils. Elsevier, NY (1988)

Holtz, W.G., Gibbs, H.J.: Engineering properties of expansive clays. Trans. Am. Soc. Civ. Eng. 121, 641–677 (1956)

Jotisankasa, A., Tapparnich, J., Booncharoenpanich, P., Hunsachainan, N., Soralump, S.: Unsaturated soil testing for slope studies. In: Proc. Int. Conf. on Slope. Thailand 2010: Geotechnique and Geosynthetics for Slopes, Chiangmai, Thailand (2010)

Jotisankasa, A., Vadhanabhuti, B., Lousuphap, K., Sawangsuriya, A.: Mechanisms of longitudinal cracks along highway shoulder in central Thailand. In: Proc. 5th Asia-Pacific Conf. on Unsaturated Soils, Pattaya, Thailand (2012)

McKeen, R.G.: A model for predicting expansive soil behavior. In: Proc. 7th Int. Conf. on Expansive Soils, Dallas, vol. 1, pp. 1–6 (1992)

Nelson, J.D., Miller, D.J.: Expansive soils problems and practice in foundation and pavement engineering. John Wiley and Sons, NY (1992)

Sawangsuriya, A., Jotisankasa, A., Vadhanabhuti, B., Lousuphap, K.: Identification of potentially expansive soils causing longitudinal cracks along pavement shoulder in central Thailand. In: Proc. 5th Asia-Pacific Conf. on Unsaturated Soils, Pattaya, Thailand (2012)

Seed, H.B., Woodard, R.J., Lundgren, R.: Prediction of swelling potential for compacted clays. J. Soil Mech. Found. Div., Am. Soc. Civ. Eng. 88(SM3), 53–87 (1962)

Experimental Characterization of Shrinkage Behaviour of Australian Expansive Soils

Xianfeng Liu and Olivier Buzzi

Abstract. This paper presents some preliminary results of the study of the shrinkage behaviour of Australian expansive soils under air-drying condition. A new coating product has been tested to allow for the measurement of bulk volume of soils having irregular shapes. The effect of the new coating has been first assessed before applying the method to three Australian soils, two being highly expansive. The effects of mineral compositions and structure of tested soils on shrinkage behaviour were discussed.

Keywords: expansive soil, bulk volume, air entry point, shrinkage, swelling.

1 Introduction

The shrinkage of soils is one of fundamental and problematic issues in geotechnical engineering. Upon drying, the evaporation of soil water results in soil shrinkage and cracks opening, the magnitude of which depends on clay minerals and soil microstructure. The hydraulic and mechanical properties of soils can be significantly affected by shrinkage, which can result in damage to geotechnical infrastructures (Tang et al. 2011). Over the last several decades, shrinkage behaviour of soils has been widely investigated by means of different experimental methods. One key aspect is to be able to accurately measure the bulk volume of soil specimens. This can be done by measuring specimen dimensions: by vernier caliper (Krisdani et al. 2008), digital camera imaging (Tang et al. 2011, Rojas et al. 2011),

Xianfeng Liu
Centre for Geotechnical and Materials Modelling, The University of Newcastle, NSW, Australia
e-mail: xianfeng.liu@newcastle.edu.au

Olivier Buzzi
Centre for Geotechnical and Materials Modelling, The University of Newcastle, NSW, Australia
e-mail: olivier.buzzi@newcastle.edu.au

or Environmental Scanning Electron Microscopy (ESEM) coupled with a digital image analysis (DIA) (Montes-H et al. 2003). A much simpler solution is to immerse the specimens in a fluid (e.g. kerosene, toluene or mercury) (Fleureau et al. 1993). In case of a wetting fluid, different coating techniques have been proposed using paraffin or saran resin (see review by Cornelis et al. 2006). Not coating the specimen poses a number of issues such as fluid retention possibly from the onset of shrinkage cracking, smearing of the soil surface because of specimen handling, possible high water adsorption rate (during swelling) resulting in high suction gradient and cracking. The coating materials usually employed tend to be quite impervious. This means that the coating has to be removed for the soil to adsorb or loose extra water, which does not always prove to be trivial and specimens can be damaged.

In this study, a new and efficient coating material has been tested. It consists of some spray band aid, referred to as Hand Spray Plaster, or HSP, commercialised by Hansaplast. This medical product is meant to waterproof wounds while letting them "breathe". Consequently, it allows slow adsorption or loss of water in a soil specimen while preventing fluid retention when the soil is immersed for volume measurement. The first part of the paper presents some results about the effect of the HSP coating on the shrinkage and swelling curve of an expansive Australian Soil while the second part presents some preliminary results on two other soils with some insight into the effect of mineralogy and soil preparation.

2 Materials Tested

Three Australian soils were used for this study: Maryland Clay (from New South Wales), Redbank and Wilsonton (from Queensland). For each soil, the proportion of dominant clay mineral, obtained by thermal gravimetric analysis, is presented in Table 1. Maryland (ML) and Redbank (RB) clays are smectite dominant while Wilsonton (WIL) clay is mainly made of kaolinite. Nonetheless, the WIL clay presents some features of expansive soils as shown in Table 1, which also presents some geotechnical properties.

The specimens tested were either intact (crumbs taken from the ground) or consolidated from a slurry under 50 kPa and their volume ranged from about 1 to 3 cm^3.

Table 1. Summary of some geotechnical properties. LL: liquid limit, PI: Plasticity Index, I_{ss}: Shrink swell index (remoulded), Gs: specific gravity.

Soil	Dominant mineral	G_s	LL (%)	PI (%)	I_{ss} (%)
Maryland (ML)	Smectite (78%)	2.65	69.8	45.7	5.5
Redbank (RB)	Smectite (87%)	2.60	73.2	45.6	5.3
Wilsonton (WIL)	Kaolinite (59%)	2.79	71.3	41.0	3.0

3 Testing Program and Methods

In this study, some swelling and shrinkage curves were firstly obtained on four intact specimens of Maryland clay to assess the effect of the HSP coating. Two specimens were coated and two were left uncoated. Then, the evolution of void ratio and saturation degree with diminishing water content (upon air drying) was followed for remoulded and intact specimens of Redbank and Wilsonton. Each time, two specimens of each were tested. These specimens were all coated with HSP.

The specific gravity was determined using an automated gas pycnometer (Autopyc) with an accuracy of 0.05%. The mass of soil was monitored using precision scale to the 1/1000 gram. The bulk volume was determined from immersion of the coated and uncoated specimens in silicone oil (referred to as SO) by using the same 1/1000 gram scale and a specifically designed hanger and basket. Based on Archimedes' principle, the bulk volume can be correlated to the mass of displaced oil. A comparison of the specimen mass before and after immersion was made to check for possible oil retention. The specimens were preserved in air-conditioned room with controlled temperature of 20 °C for the shrinkage tests and in a fog room with controlled relative humidity of 100% for the swelling tests. Because of the slow rate of water gain/loss and the relatively small dimensions of the coated specimen, it has been assumed that the water content was quite uniform within the specimen. Consequently, not much time was given between water content changes for redistributing moisture inside the specimen until equilibration.

4 Experimental Results

4.1 Effect of the Coating

The results of swelling and shrinkage tests on coated and uncoated specimens can be seen in Fig. 1(a)-(b) and (c), respectively. First, in Fig. 1(a), it can be noticed that the coating significantly reduces the water adsorption rate; the consequence being lower suction gradients within the specimen and no cracking. In fact, cracks have developed in the uncoated specimen until it fell apart after 10,000 minutes.

Then, Fig. 1(b) suggests that the coatings has little restraining effect on the specimen since the deformation curves, with or without coating, are similar. In fact, the coating film is very thin and can be stretched easily.

Finally, Fig. 1(c) highlights the benefit of using the coating: the shrinkage curve for the coated material is clear and can be followed down to about 12% water content. On the contrary, oil retention occurs in absence of coating, which impedes accurate measurement of water content. Indeed, the evolution of the specimen mass is highly scattered and depends on the amount of oil kept in the specimen. This phenomenon is exacerbated as shrinkage cracks develop. No conclusions can be drawn for water content lower than about 25%. Another benefit of the coating is that it preserves the natural surface of the specimen: almost no smearing occurs as a result of specimen handling.

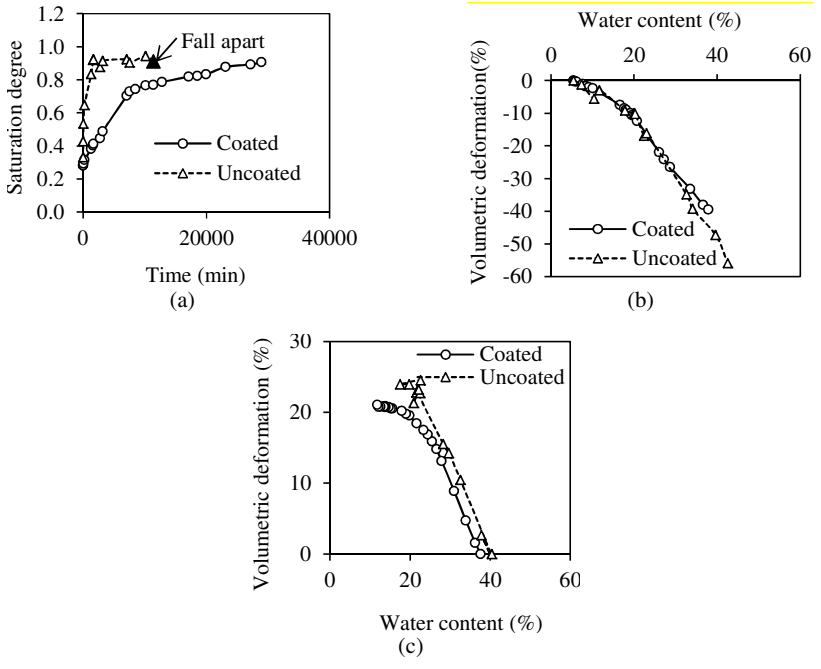

Fig. 1. Shrinkage and swelling behaviour of intact Maryland Clay (a): Evolution of saturation degree in time for a swelling test; (b): Volumetric deformation vs. water content for a swelling test; (c): Volumetric deformation vs. water content for a shrinkage test. Coated and Uncoated specimens were used.

4.2 Effect of Clay Minerals on the Shrinkage of Soils

The comparisons of saturation degree and volumetric deformation evolution with decreasing water content (during shrinkage tests) for reconstituted RB and WIL clay specimens are shown in Fig.2. As expected, the soil containing smectite. i.e. RB, remains saturated over a larger range of water content. Indeed, it desaturates at water content lower than 20% against 25% for the kaolinite soil (WIL) (Fig. 2(a)). However, the difference is not very significant and should be assessed in terms of suction to characterise the air entry value (AEV). This work is currently ongoing. The behaviour exhibited by WIL clay is however consistent with the properties shown in Table 1 suggesting that the soil displays swelling and shrinkage features of an expansive soil. This could be due to weathering of the clay resulting in absence of hydrogen bonding as it happens in some Illite Australian clays. The smectitic clay (RB) also shows a larger volumetric deformation (Fig. 2(b)). These curves were obtained by progressive drying of only one coated specimen. Compared to uncoated technique, the new coating technique does not require testing several specimens on a drying path, since it enables slow adsorption/loss of water while preventing oil retention when the soil specimen is immersed in the SO oil for short time. However, in case of uncoated specimens, high quantity of oil can be retained possibly from the onset of shrinkage cracking, resulting in poor accuracy of water content determination.

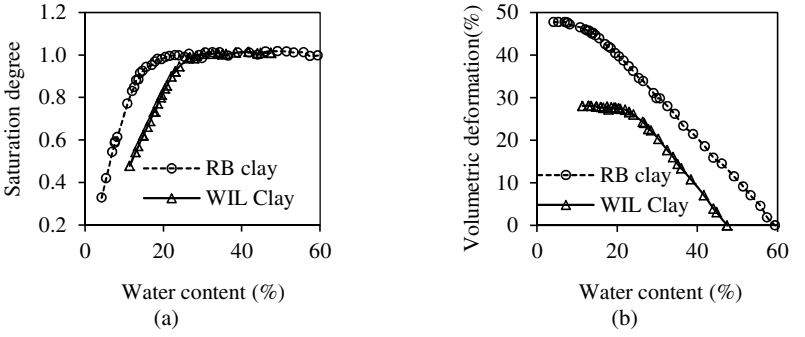

Fig. 2. (a): Saturation degree vs. water content upon drying for Redbank (RB) and Wilsonton (WIL) remoulded clays. (b): Volumetric deformation vs. water content upon drying for Redbank (RB) and Wilsonton (WIL) remoulded clays. Coated specimens were used.

4.3 Effect of Soil Structure on Shrinkage of Soils

Fig. 3 compares the evolution of saturation degree with water content for intact and remoulded specimens of Redbank (RB) and Wilsonton (WIL) clays. The difference between intact and remoulded specimens lies within the pore size distribution, which is not yet quantified. Mercury Intrusion Porosimetry (MIP) will be conducted on uncoated specimens. It is expected that the intact soil will exhibit several peaks in the pore size distribution while the remoulded one should be limited to one to two characteristic pore sizes of much smaller dimensions. This is somehow confirmed for WIL (Fig. 3(b)) since air enters the soil quite rapidly (from about 40% water content) but it is not quite the case for RB (Fig. 3(a)). The difference in air entry is not significant. Again, this should and will later be assessed in terms of suction. Extreme care has been taken to not smear the surface of Redbank (RB) clay when initially manipulating it. The coating itself does not produce any smearing effect as shown by Fig. 3(b). The MIP will help to draw conclusions on the structure of these specimens and on the effect on the air entry value.

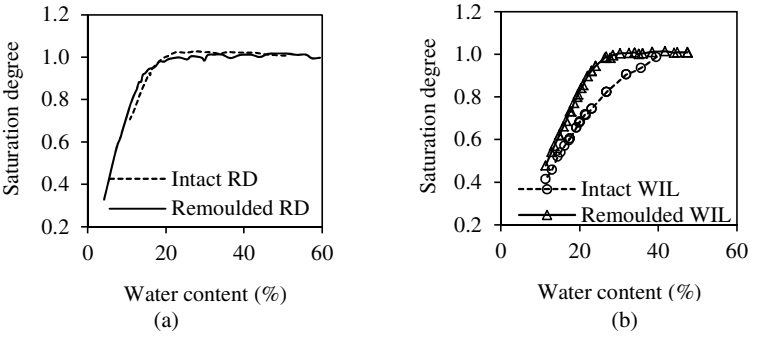

Fig. 3. Evolution of saturation degree vs. water content upon drying intact and remoulded RD (a) and WIL (b) specimens. Coated specimens were used. For the sake of clarity, the data points have not been shown in Fig. 3(a).

5 Concluding Remarks and Future Work

A new coating method using Hand Spray Plaster (HSP) for determining bulk volume of soils by oil immersion has been introduced. The validation of the method shows that the coating can significantly reduce swelling rate of soil specimen, which also limits suction gradients in the soil and cracking. The coating does not have any restraining effect on the specimens upon swelling. It has been found that this technique improves the accuracy of bulk volume measurement and allows measuring shrinkage over a wider range of water content as it prevents oil retention. Using this new method, the shrinkage behaviour of three Australian Expansive Soils (both intact and remoulded) has been investigated. The results are so far in accordance with the literature and the research is on-going to further characterize the shrinkage behaviour and the factors influencing the air entry value. In particular, mercury intrusion porosimetry will be conducted to quantify the structure of these soils.

References

Cornelis, W.M., Corluy, J., Medina, H., Díaz, J., Hartmann, R., Van Meirvenne, R., Ruiz, M.E.: Measuring and modelling the soil shrinkage characteristic curve. Geoderma 137(1-2), 179–191 (2006)

Fleureau, J.M., Kheirbek-Saoud, S., Soemitro, R., Taibi, S.: Behavior of clayey soils on drying–wetting paths. Can. Geotech. J. 30(2), 287–296 (1993)

Krisdani, H., Rahardjo, H., Leong, E.C.: Effects of different drying rates on shrinkage characteristics of a residual soil and soil mixtures. Eng. Geol. 102(1-2), 31–37 (2008)

Montes, H.G., Duplay, J., Martinez, L., Mendoza, C.: Swelling–shrinkage kinetics of MX80 bentonite. Appl. Clay Sci. 22(6), 279–293 (2003)

Tang, C.S., Shi, B., Liu, C., Suo, W.B., Gao, L.: Experimental characterization of shrinkage and desiccation cracking in thin clay layer. Appl. Clay Sci. 52(1-2), 69–77 (2011)

Rojas, J.C., Gallipoli, D., Wheeler, S.J.: Image analysis of strains in soils subjected to wetting and drying. Geotech. Test. J. 35(1) (2011), http://dx.doi.org/10.1520/GTJ103708

Nonisothermal Shear Strength of Compacted Silt under High Suction Magnitudes

Nahed A. Alsherif and John S. McCartney

Abstract. This study focuses on a preliminary evaluation of the peak shear strength of compacted silt under high suction magnitudes and temperatures, which are relevant conditions encountered when using heat exchangers to improve the mechanical response of compacted soil layers. Specifically, a series of constant water content triaxial tests were performed on specimens which had reached equilibrium with saturated salt solutions in insulated desiccators having controlled temperatures ranging from 24 to 65 °C. Results from these tests indicate that increased temperature leads to a slight increase in the peak shear strength of soils having a given initial total suction. The total suction has a greater impact on the peak shear strength of soils than temperature, which indicates that heat exchangers may be a suitable tool to increase the strength of compacted soils.

Keywords: shear strength, triaxial testing, temperature effects, high suction.

1 Introduction

The shear strength and volume change of unsaturated soils under nonisothermal conditions has recently been evaluated by Uchaipichat & Khalili (2009), who performed a comprehensive evaluation of compacted silt for suction magnitudes less than 300 kPa. For a given suction magnitude, they observed a decrease in peak shear strength with increasing temperature, although the strength at critical state conditions was unaffected by temperature. They found that the peak and critical state shear strength were more sensitive to matric suction than temperature.

Nahed A. Alsherif, M.S.
University of Colorado Boulder, Boulder, CO USA
e-mail: nahed.alsherif@colorado.edu

John S. McCartney, Ph.D., P.E.
University of Colorado Boulder, Boulder, CO USA
e-mail: john.mccartney@colorado.edu

Although interesting lessons were learned from these tests performed under relatively low matric suction magnitudes, there has not been a thorough study on the impact of temperature on the shear strength of unsaturated soils under higher total suction magnitudes. Most research on the impact of high suction magnitudes has focused on the impact of suction on the shear strength of soils, although the impact of temperature has not been thoroughly investigated. Nishimura & Fredlund (2000) conducted triaxial compression tests on silty soil under high suction magnitudes. They found constant values of shear strength with increasing suction after the soil reached residual saturation, and that the rate of increase in peak shear strength with net normal stress was similar to the effective internal friction angle for saturated conditions. Blatz (2002) examined the effects of high total suction and high confining pressure on the behavior of a compacted sand-bentonite by performing a series of undrained triaxial tests. Their test results show a nonlinear increase in the strength and stiffness with increasing suction. A ring shear apparatus adapted with suction control using the vapor equilibrium technique was used by Vaunant et al. (2007) and Merchan et al. (2008) to investigate the effect of high magnitudes of total suction on the residual shear strength of low plasticity clay, and an increase in strength was noted with increasing suction.

Other studies have evaluated the combined effects of high suction and temperature on the volume change and the soil-water retention curve (SWRC). An oedometer apparatus for high suction magnitudes was developed by Lloret et al. (2003) to study the yielding behavior of compacted bentonite, which was also used by Romero et al. (2003) to study the impacts of temperature on the SWRC and volume change of unsaturated bentonite. Tang & Cui (2005) also investigated the impact of temperature on the SWRC of compacted bentonite. The objective of this paper is to build upon the work described in this section to assess the roles of high suction magnitudes and temperature on the effective stress and peak shear strength of compacted silt.

2 Test Procedure

A ML silt obtained from the Bonny Dam on the Colorado-Kansas border was used in this experimental study. Specimens of soil, having a specific gravity of 2.62, were statically compacted using a static press to a dry unit weight of 16.8 kN/m3 (void ratio of 0.53) at a compaction water content of 14.5%. The testing procedures involved bringing the specimens to equilibrium to high total suction magnitudes using the vapor equilibrium technique at various temperatures (Delage et al. 2008), then measuring the shear strength of the soil specimens using constant water content triaxial tests. This is a preliminary testing program as the suction and temperature were not controlled within the triaxial setup itself.

Saturated salt solutions were prepared in glass desiccators by dissolving the salt in distilled water until precipitated salt remains visible. The specimens were suspended above the salt solution on a porous disc to allow a water exchange between the liquid and vapor phases in the container headspace. The desiccator was placed within a temperature controlled chamber as shown in Fig. 1. A strip heater and a temperature controller were used to maintain a target temperature.

The relative humidity and temperature were recorded hourly using a combined sensor-datalogger from Lascar Electronics. This sensor can measure temperatures ranging from -35 to +80 °C with an accuracy of ±0.5°C and relative humidity values ranging from 0 to 100% with an accuracy of ±3%. The change in gravimetric water content of the soil with increasing soil suction was measured by weighing the specimen every three days until it reaches a constant mass. This step was performed in less than 15 seconds after taking the specimen out of the desiccators. This duration was found to be short enough so that water evaporation during the weighing process was negligible. Different target total suction values, corresponding to different relative humidity values, were implemented using five different salt solutions at temperatures of 24, 45 and 65 °C, as shown in Fig. 2.

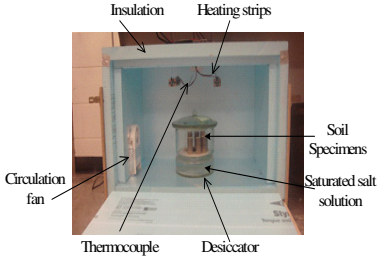

Fig. 1. Desiccator and temperature control chamber showing different soil specimens.

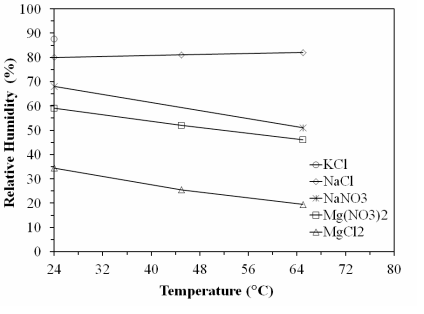

Fig. 2. Temperature effects on relative humidity for different saturated salt solutions.

The equilibration times required when imposing different total suction magnitudes using different salt solutions are shown in Fig. 3(a). A shorter time is needed to reach equilibrium at a room temperature of 24 °C with increasing total suction. Similar trends were noted for higher temperature tests in Fig. 3(b). The soil specimens at high temperatures reach equilibrium faster than specimens at room temperature for the suction values induced by the same salt solution.

3 Results

The SWRC for Bonny silt was defined by converting the equilibrium relative humidity to total suction using Kelvin's equation (Fredlund & Rahardjo 1993):

$$\psi = \frac{\rho_w RT}{M_w} \ln\left(\frac{R_h}{100}\right) \quad (1)$$

where ψ is the total soil suction (kPa), R is the universal (molar) gas constant, equal to 8.31432 J/molK, T is the absolute temperature in Kelvin, MW is the molecular mass of water vapor equal to 18.016 g/mol, ρw is the density of water (kg/m3), and Rh is the relative humidity of the pore air in percent. The effect of temperature on the water density was considered. The SWRC of the silt is shown in Fig. 4(a), obtained using the axis translation technique to evaluate the air entry suction and the vapor equilibrium technique to define the tail of the SWRC.

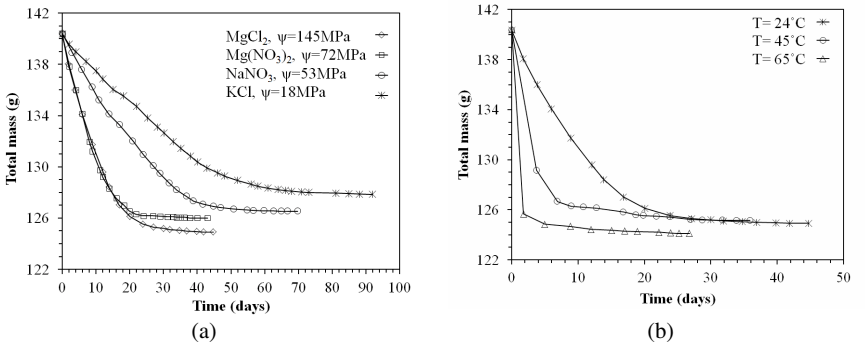

Fig. 3. Change in mass of the soil over time for: (a) Different suction values imposed using different salt solutions at T = 24 °C, (b) Different temperatures applied to an $MgCl_2$ salt solution.

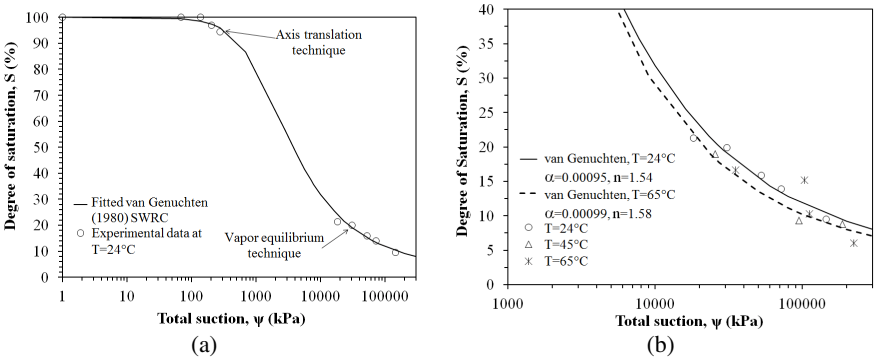

Fig. 4. SWRCs defined for soil specimens (a) for the entire range of suction under isothermal condition, (b) at high suction range under isothermal and non-isothermal conditions.

The impact of temperature on the SWRC at high suctions is shown in Fig. 4(b). The van Genuchten (1980) SWRC model was fit to each set of data, with the fitting parameters α and n reported in the figure. The fitted SWRCs indicate that temperature leads to a slight shift in the SWRC to the left, which is consistent with results from Romero et al. (2003) and Uchaipichat & Khalili (2009).

At equilibrium under the applied values of suction and temperature, the soil specimens were placed in the triaxial cell and an isotropic net confining pressure value ranging from 0 to 200 kPa was applied. Atmospheric air pressure was maintained at the top and bottom of the specimen while increasing the cell pressure and during shearing, and no access to water was permitted. The compacted specimens were relatively stiff so little volume change was noted during this process. Placement of the specimen in the triaxial cell was performed in less than 2 minutes to minimize changes in water content and temperature of the specimen. The specimens were then sheared until reaching a peak value of principal stress difference (occurring at a strain of 1.5 to 3%) at a rate of 0.127 mm/min. After shearing the specimen to failure, the final water content was measured.

The failure envelopes for specimens sheared under room temperature are shown in Fig. 5. The results show an increase in the shear strength of the soil with increasing suction and increasing net confining pressure. Because the excess pore water pressure generation in the unsaturated soil is expected to be negligible due to the low degrees of saturation, the total stress envelopes from constant water content triaxial tests should be close to the effective stress envelopes for these suction conditions. The friction angle for the silt specimens under high suction is larger (ϕ'=43°) than that from tests on saturated soil (ϕ'=36°). The difference may be attributed to the differences in consolidation of the unsaturated specimens from that of the saturated specimens tested in the consolidated undrained triaxial test. The total suction has similar effects on the failure envelopes to the trends observed by Nishimura & Fredlund (2000) for high suction magnitudes.

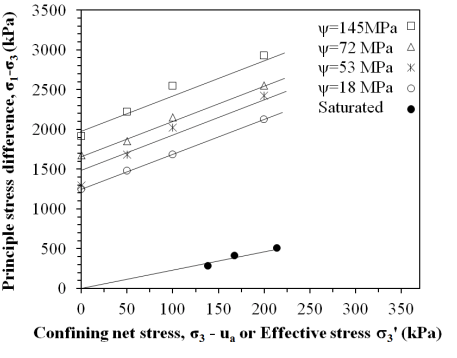

Fig. 5. Effective stress failure envelope for saturated silt along with total stress failure envelopes for unsaturated silt at constant room temperature of 24 °C (not to scale).

The failure envelopes defined for different salt solutions and temperatures are shown in Fig. 6. Similar to the isothermal failure envelopes in Fig. 5, the slope of the failure envelopes does not change with either increasing suction or temperature. Due to the use of saturated salt solutions, it was not possible to maintain constant suction values and increase the temperature, so the differences in the intercept values between the failure envelopes in Figure 6 can be attributed to both temperature and suction.

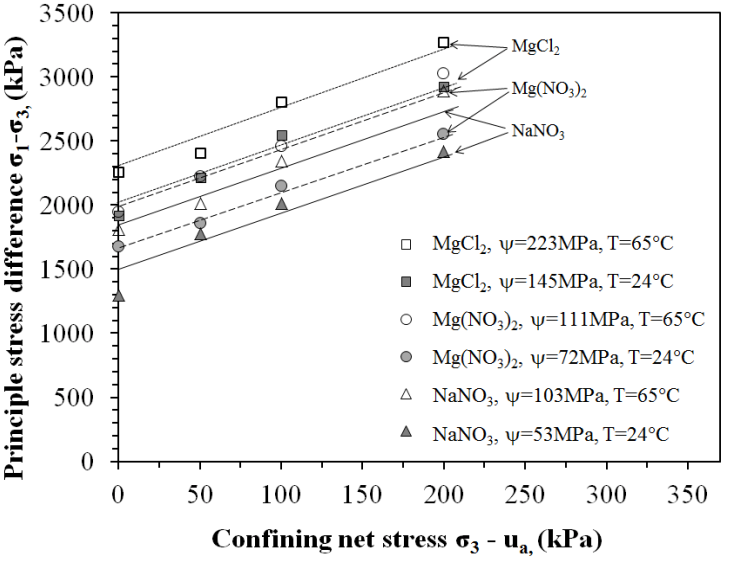

Fig. 6. Failure envelopes for silt in equilibrium with different suction values and temperatures.

4 Analysis and Discussion

The results in Figure 6 show a combined effect of temperature and suction on the shear strength. Accordingly, to better interpret the results shown in Fig. 6 the concept of the suction stress characteristic curve (SSCC) may be used to separate the effects of suction and temperature on the constant water shear strength. First, the slope of the failure envelope along with the apparent cohesion values for unsaturated silt specimens in Figs. 5 and 6 were used to back-calculate the suction stress σs of the soil at temperatures of 24 °C and 65 °C, as follows (Lu and Likos 2006):

$$\sigma_s = \frac{c'}{\tan\phi'} \tag{2}$$

The SSCC defined using Eq. 2 for different temperatures is shown in Fig. 7. The experimental results indicate a nonlinear increase in suction stress by up to approximately 30 kPa as the total suction increases up to 223 MPa. This interpretation of the results in Figs. 5 and 6 reflects that the peak shear strength increases slightly for compacted silt under high suction magnitudes with increasing temperature, which is contradictory to the observations of Uchaipichat & Khalili (2009) for low suction magnitudes. This may be due to the impact of temperature on the magnitude of excess pore water pressure generation during shearing in low and high suction ranges.

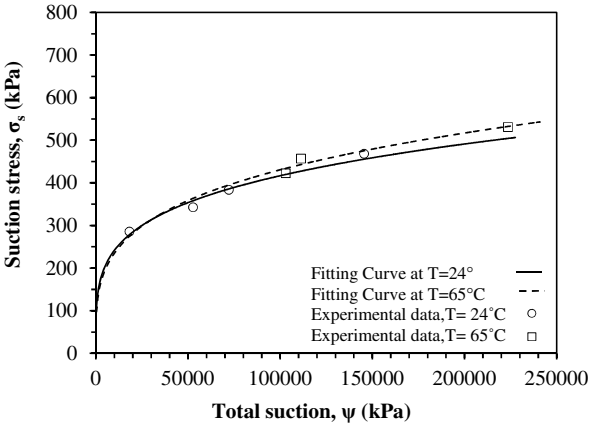

Fig. 7. SSCCs defined for compacted silt at temperatures of 24 °C and 65 °C.

In this preliminary set of tests, the specimens were brought to equilibrium outside of the triaxial cell, and then were quickly transported to the triaxial setup for shearing. Further, volume was not tracked during compression of the air voids during application of the cell pressure, or during shearing. Accordingly, these tests only provide an approximation of the effects of coupling between temperature, suction, net stress, and void ratio. In addition, the issues noted with the use of saturated salt solutions to independently control the temperature and suction in soils indicates that an alternative approach involving vapour control may be more appropriate.

Further research is needed to develop a triaxial cell which incorporates suction control and temperature control to understand the nonisothermal shear strength and deformation behavior of unsaturated silt under high suction magnitudes. The suction control system proposed by Likos & Lu (2003) is particularly suited for this application. They developed a system to control the relative humidity of pore air flowing through a soil specimen by using mass flow controllers to mix water-saturated and dry air to a known proportion. Further, the triaxial system developed by Uchaipichat & Khalili (2009), which incorporated a resistance heater, cell fluid circulation, a glass cell (to avoid thermal degradation encountered in acrylic cells), and digital image analysis to track changes in volume of specimens under various temperature and suction ranges.

5 Conclusion

The results in this study indicate that the total suction has a greater impact on the peak shear strength of soils than temperature. However, increased temperature was found to lead to a slight increase in the peak shear strength of unsaturated soils under high suction magnitudes, which is contradictory to the observed impact of temperature for low suctions. This emphasizes the importance of further investigation into the impacts of temperature on the shear strength of compacted silts under high suction magnitudes using more advanced testing approaches.

Acknowledgements. The writers would like to thank Kent Polkinghorne for his valuable assistance. The first author would like to thank the new Libyan government for their continued support of her research efforts. Support from CMMI 1054190 is greatly appreciated. The views in the paper are those of the authors alone.

References

Blatz, J., Graham, J., Chandler, N.A.: Influence of Suction on the Strength and Stiffness of Compacted Sand-Bentonite. Canadian Geotechnical Journal 39, 1005–1015 (2002)

Delage, P., Romero, E., Tarantino, A.: Recent Developments of Controlling and Measuring Suction in Unsaturated Soils. In: Proceedings of the 1st European Conference on Unsaturated Soils, Durham, pp. 33–52 (2008)

Fredlund, D., Rahardjo, H.: Soil mechanics for Unsaturated Soils. John Wiley and Sons (1993)

Lloret, A., Villar, M.V., Sanchez, M., Gens, A., Pintado, X., Alonso, E.E.: Mechanical Behaviour of Heavily Compacted Bentonite under High Suction Changes. Geotechnique 53(1), 27–40 (2003)

Lu, N., Likos, W.: Suction Stress Characteristic Curve for Unsaturated Soil. J. Geotechnical and Geoenvironmental Engineering 132(2), 131–142 (2006)

Merchan, V., Vaunat, J., Romero, E., Meca, T.: Experimental Study of the Influence of Drying on the Residual Friction Angle of Clays. In: Proceedings of the 1st European Conference on Unsaturated Soils, Durham, pp. 423–428 (2008)

Nishimura, T., Fredlund, D.G.: Relationship Between Sear Strength and Matric Suction in an Unsaturated Silty Soil. In: UNSAT ASIA 2000, Singapore, May 18-19, pp. 563–568 (2000)

Romero, E., Gens, A., Lloret, A.: Suction effects on a compacted clay under non-isothermal conditions. Geotechnique 53(1), 65–81 (2003)

Tang, A.M., Cui, Y.J.: Controlling Suction by the Vapour Equilibrium Technique at Different Temperatures and its Application in Determining the Water Retention Properties of MX80 Clay. Canadian Geotechnical Journal 42(1), 287–296 (2005)

Uchaipichat, A., Khalili, N.: Experimental investigation of thermo-hydro-mechanical behaviour of unsaturated silt. Geotechnique 59(4), 339–353 (2009)

van Genuchten, M.T.: A Closed-Form Equation for Predicting the Hydraulic Conductivity of Unsaturated Soils. Soil Science Society of America Journal 44, 892–898 (1980)

Vaunat, J., Merchan, V., Romero, E., Pineda, J.: Residual strength of clays at high suctions. In: Proc. of the 2nd Int. Conf. on Mech. of Unsat. Soils, Weimar, Germany, vol. 2, pp. 151–162 (2007)

Matric Suction and Deformation Behavior of Unbound Granular Base (UGB) Materials under Constant and Variable Cell Pressure

M. Ohiduzzaman, S.C.R. Lo, and Ovidiu Craciun

Abstract. In the laboratory, generally cyclic triaxial tests are performed either with a constant confining pressure (CCP) or with a variable confining pressure (VCP). CCP and VCP tests are commonly assumed to deliver similar test results as long as the average cell pressure is the same. However, this assumption is based on the limited number of test data in the literature. Therefore, this study is designed to evaluate the effect of stress paths (i.e. CCP & VCP) on the matric suction and deformation behavior of unbound granular base (UGB) materials. A series of cyclic triaxial tests with different stress path are performed to isolate the effect of stress path on the deformation behavior of UGB materials. The evaluation of matric suction and the mechanical behavior of the UGB materials under different stress path are systematically studied.

Keywords: stress path, matric suction, granular materials, triaxial test.

1 Background

A flexible pavement foundation system generally consists of two layers of geo-materials i.e. base or sub base layer which built on natural subgrade soil. The base or sub base layers are generally unbound granular materials but sometimes small

M. Ohiduzzaman
UNSW@ADFA, Canberra, Australia
e-mail: Ohiduzzaman.Md@student.adfa.edu.au

S.C.R. Lo
UNSW@ADFA, Canberra, Australia
e-mail: r.lo@adfa.edu.au

Ovidiu Craciun
Transport Group, SMEC Pty. Ltd, Sidney, Australia
e-mail: craiunovidiu11@yahoo.com

amount of binding materials are also added to augment the performance of these materials. This study is only constrained within the unbound granular base (UGB) materials which generally consist of silty sandy gravel with prescribed amount of fines content. Due to their geometric location, UGB materials are generally remained unsaturated state during construction and operation period. Therefore, their mechanical behavior should be analyzed in terms of unsaturated soil mechanics. However, analyzing the mechanical behavior in context of unsaturated soil mechanics required proper measurement of matric suction.

The UGB materials experienced a large number of load repetitions due to traffic movement throughout its service life. Each load repetition produces stresses on the pavement elements which consist of horizontal, vertical and shear stress component (Brown 1996). Therefore, for better understanding of the mechanical behaviour of these materials, the in-situ stress condition needs to be simulated in the laboratory. The cyclic triaxial test is probably the most suitable instrument that can simulate the in-situ field condition in the laboratory. Generally, constant confining pressure (CCP) and varying confining pressure (VCP) triaxial tests are performed in the laboratory. VCP tests can produce more realistic in situ stress condition comparing to the CCP test because the confining pressure in the field is also varied during the application of cyclic loading.

Most of the pavement design code is usually based on the simpler CCP test because it often considered that both types of test will deliver the similar result as long as the average stress is same. However, this assumption is based on the limited number of test results because fewer studies have been performed with VCP stress path test. Highly sensitive triaxial equipment is required for controlling the cyclic confining pressure which is one of the reasons for fewer studies with VCP test and this testing facility is not wide spread throughout the world. Therefore, many researchers (Allen & Thompson 1974, Brown & Hyde 1975, Nataamazda 1989, Rondon et al. 2009) tried to link the test results of both types of stress path. Of them, Allen and Thompson (1974) used the peak value of cell pressure of the VCP tests as the constant value of CCP tests. They concluded that lower resilient modulus (M_R) obtained for VCP tests comparing to the CCP tests at low bulk stress but the behaviour was reversed at higher bulk stress. Poisson's ratio was observed clearly higher for CCP tests at any level of bulk stress. Brown & Hyde (1975) used mean value of variable cell pressure as the constant value of CCP tests. They demonstrated that the similar values of M_R and permanent strain (ε_a^p) was observed for both types of tests but much higher Poisson's ratio was obtained for CCP tests. However, their interpretation was based on the single value of deviatoric stress (q^{max}=200 kPa) and multistage testing was adopted for M_R test. Nataatmajda (1989) also performed triaxial tests on the crushed rock and used mean value of cyclic confining pressure as constant cell pressure. They observed that higher values of M_R were obtained from CCP tests compared to the VCP tests. Recently, Rondon et al. (2009) compared the both types of stress path tests and registered that axial permanent strain was higher for VCP tests compared to the corresponding CCP test at low to medium level of deviatoric stress whereas, at

high deviatoric stress level, both types of stress path tests produced similar values of axial permanent strain.

The influence of stress path on the UGB behaviour is not quite clear yet as suggested from the above literature. Moreover, all these studies did not consider the matric suction though all the tests were done in unsaturated state. However, many researches showed that matric suction plays an important role on the deformation properties of unsaturated soil. However, measurement of matric suction of UGB materials under cyclic loading is a difficult task to perform as reported by limited literature. Recently, Craciun & Lo (2010) developed a method for measuring the matric suction under cyclic load. For this study, the same technique is applied for measuring the matric suction. The present study examines the matric suction and deformation behaviour of UGB materials under CCP and VCP stress paths tests. The test results were also analysed in context of matric suction under cyclic loading.

2 Materials Tested

A well graded high quality UGB materials is used for this study which have 15% fines content. The grading curve is shown in fig.1 whereas index properties are presented in table 1.

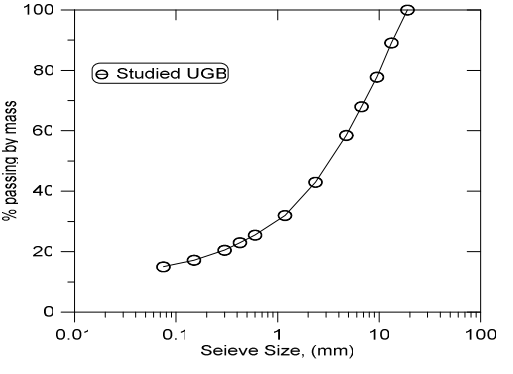

Fig. 1. Grading curve of the tested materials.

Table 1. Index properties of the studied materials.

Materials	FC	Atterberg Limit test			OMC	MDD	Gs
	(%)	LL (%)	PL (%)	PI (%)	(%)	(gm/cm^3)	
UGB-15%	15	28	26	2	5.70	2.428	2.966

[a]FC= Fines Content; LL= Liquid Limit; PL= Plastic Limit; PI= Plasticity Index; OMC= Optimum moisture content; MDD= Maximum dry density; Gs=Specific Gravity.

3 Testing Methodology

A modified triaxial testing apparatus is used for testing of unsaturated UGB materials under cyclic loading. This apparatus has been recently developed at the Geotechnical Laboratory of the University of New South Wales at Australian Defence Force Academy. The details description of this triaxial equipment and matric sution initialization process and verification of matric suction within the specimens can be found elsewhere (Craciun & Lo 2010). However, some of the key features are discussed briefly here.

The equipment uses an internal load cell for applying axial stress and this eliminates error due to ram friction which is more pronounced in case of cyclic loading. Radial stress was applied by pressurized water via servo-control actuator. For measuring axial deformation, a pair of internal Linear Variable Differential Transformers (LVDTs) was used. Both LVDTs were placed at the quarter distance from the top platen in order to eliminate any bedding error. A Hall Effect transducer was also used for measuring the radial strain. The transducer was attached onto the specimen with a pair of mounting pad which have curvature matching that of specimen.

Negative pore water pressure was controlled by high air entry ceramic disc incorporated at the bottom platen. The ceramic disk allows only the water phase to pass through as long as it is below the air entry value (AEV). The air entry value of ceramic disc was chosen 1 bar. Because, Raimbault (1986) showed that the matric suction of base materials is generally less than 100 kPa in field condition. A low compliance pore water pressure transducer was placed outside the triaxial cell in order to measure pressure transmitted through the ceramic disc. The pore air pressure line connected at the top platen was open to atmospheric pressure at all times. Any moisture loss through the air pressure line was detected via a “U” trap. However, no moisture loss was detected during the whole testing program.

Cylindrical soil specimens of 100 mm diameter x 200 mm height were prepared in a specially designed split compaction mould (Chen, 1997) which incorporated bottom platen at the time of compaction. The specimens were compacted in 7 layers by drop hammer compaction method where 25 blows were applied to each layer. After compaction, split mould was removed and a triaxial membrane was placed around the specimen. This process eliminated any sample disturbance during transferring of specimen from the mould to the triaxial base.

A layer of liquid rubber was also smeared on to the internal surface of triaxial membrane for avoiding any puncture of the membrane during cyclic loading. The use of liquid rubber in triaxial membrane and its application in cyclic triaxial test can be found in Lo et al. (1989). The specimen was transferred from compaction mould to triaxial base by using two steel rods inserted at the bottom platen only.

After transferring the specimen on the triaxial base, specimens were instrumented with on specimen LVDTs and radial caliper. The triaxial cell was filled with water and left overnight under a confining pressure of about 10 kPa which allowed drying of liquid rubber. At this time, 10 kPa vacuum pressure was also

applied. In the next day, the vacuum regulator was increased gradually to the desired initial matric suction. The cell pressure was then increased to an isotropic pressure of 25 kPa. After about two days, the 'no flow' condition was achieved which was an indicator for the completion of initialization of matric suction. The drainage valve between burette and pore water pressure (PWP) transducer was then kept closed to ensure constant water content condition testing. The cell pressure was then increased to the desired confining pressure.

4 Materials and Testing Program

The cyclic triaxial testing program is given in table 2. The three level of deviatoric stress is chosen for simulating the actual field loading condition. The confining pressure (70 kPa) used in the CCP tests is the mean value of cyclic confining pressure (25~115 kPa) used in the VCP tests. The initial matric suction (s_i) for both types of testing specimens is selected ~62 kPa (~70% of OMC) which was obtained via soil water characteristic curve (SWCC) which can be found elsewhere (Ohiduzzaman et al. 2011). However, s_i decreases and become stable (s_o) after few hours waiting period when confining pressure brought up to the testing cell pressure in case of CCP testing.

Table 2. Triaxial testing program.

Test Name	Stress Path	Δq (kPa)	σ_r (kPa)	s_i (kPa)	s_o (kPa)	MC_i (%)	RC (%)	DOS_i (%)
C15-360	CCP	360	70	62	53.84	3.92	98.73	50.33
C15-450	CCP	450	70	62	51.62	3.94	99.457	51.45
C15-540	CCP	540	70	62	52.65	3.89	99.53	50.75
V15-360	VCP	360	25/115	62	62	3.89	99.42	50.82
V15-450	VCP	450	25/115	62	62	3.92	98.95	49.54
V15-540	VCP	540	25/115	62	62	3.90	99.24	50.78

[a] σ_r= cell pressure; Δq= magnitude of cyclic deviator stress; s_i= initial matric suction; s_o= matric suction at the start of cyclic loading; MC_i= initial moisture content; RC= relative compaction to MDD; DOS_i= initial degree of saturation.

5 Test Results

The accumulation of permanent strain (ε_a^p) with the load cycles for both types of stress path is presented in fig.2. In general, at any particular deviatoric stress level, the rate of accumulation of permanent strain in the VCP tests is lower compared to the CCP tests. This is probably due to the combination of two factors i.e., higher mean stress at the peak of the cycle and higher matric suction at the start of cyclic loading in case of VCP tests. Although, octahedral shear stress is equal for both types of stress path but the mean stress is higher in case of VCP stress path test

which contribute the better performance in terms of axial strain which is shown in fig. 3. This is consistence with published literature. The higher matric suction at the start of cyclic loading in case of VCP tests will discuss in the following paragraph.

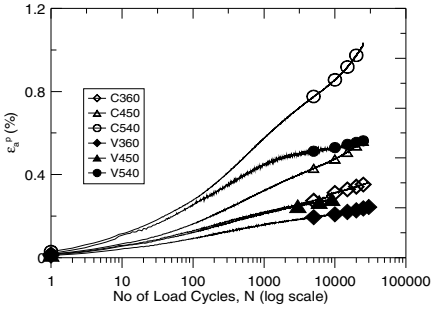

Fig. 2. Accumulation of axial permanent strain with the load cycles.

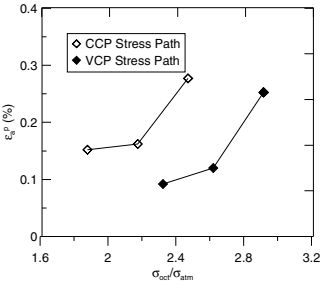

Fig. 3. Axial permanent strain with normalized mean stress at 100th cycle.

The evolution of volumetric strain (ε_v^p) with load cycles is presented in fig. 4 for the compared pairs of CCP and VCP tests. The trends of CCP tests plots appeared to be linear and showed only compressive (ε_v^p) behaviour whereas for VCP tests, the curve is quite noisy and turns towards the dilative side after few thousands of loading cycles.

The evolution of matric suction with load cycles for both types of tests is shown in fig. 5. However, at the start of cyclic loading, the matric suction for VCP tests was higher than CCP tests although both types of test specimens initialized at same value of matric suction. This is because the initialization process for both types of tests was completed at isotropic net pressure σ_r=25 kPa but matric suction decreases when cell pressure increased to the testing cell pressure (70 kPa) for CCP test. Nevertheless, matric suction reached a stable value after few hours and then cyclic axial load started. It is noteworthy that the effect of increased σ_r on s was quite significant as it decreased the initial value of s_i=62 kPa to s_o~52 kPa. However, for VCP tests, both axial and cyclic load starts when the initialization process was completed therefore no reduction of matric suction at the start of cyclic loading. Generally, the matric suction decreases with increasing load cycles and reached an asymptote value after few thousands of cycle. The decrease of matric suction is due to the excitation of the pore water pressure under undrained pore-water condition while the pore-air pressure is maintained constant. The number of load cycles is required to reach the asymptote value depends on the stress path and applied deviator stress. The residual matric suction for both types of stress path is almost similar though VCP test specimens have higher matric suction at the start of cyclic loading. However, for first few thousands cycles, the matric suction is generally higher for VCP tests specimen comparing to the CCP test specimens. The matric suction at 100th cycle is plotted against the normalized

mean stress in fig. 6. This higher matric suction along with higher mean stress (as described in the above paragraph) can be correlated to the improved performance in terms of axial strain for VCP test specimens compared to the CCP specimens.

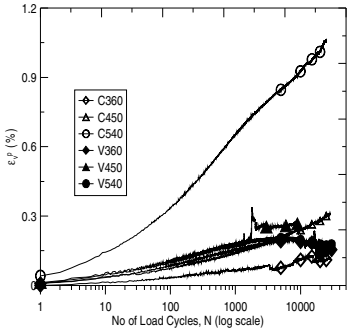

Fig. 4. Accumulation of volumetric strain with the load cycles.

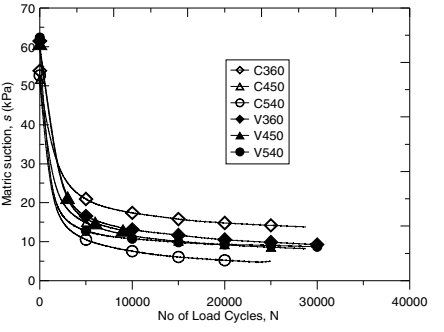

Fig. 5. Evolution of matric suction with the load cycles.

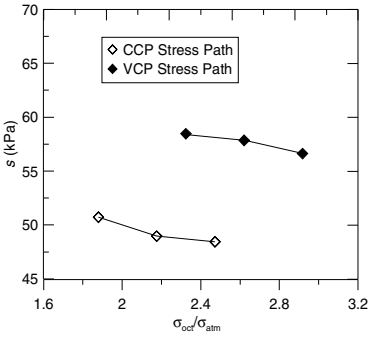

Fig. 6. Matric suction with normalized mean stress at 100th cycle.

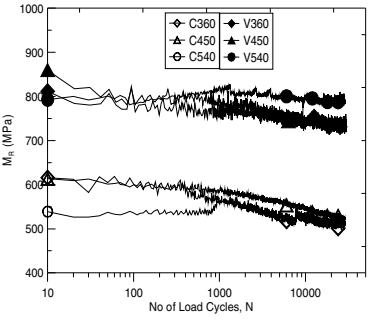

Fig. 7. Evolution of resilient modulus with load cycle.

The development of resilient modulus (M_R) with the load cycles is shown in fig. 7. The M_R value for VCP test is generally higher in comparison to the CCP test. This is consistence with the lower axial strain accumulations of these VCP specimens. All the specimens showed slightly stiffness degradation with load cycles which gives the indication that large number of load cycles is required for the M_R test.

6 Summary

The effect of stress path on the deformation behaviour of UGB materials is investigated under cyclic triaxial test. The mean value of the cell pressure in the VCP

tests is considered the cell pressure used in the CCP tests. For isolating the influence of stress path, triaxial tests were done on two sets of identical specimens. From the test results it was observed that the axial strain for CCP stress path tests is higher compared to the VCP stress path tests. This is probably due to the combined effect of higher mean stress and higher matric suction at the start of cyclic loading. The matric suction at the start of the cyclic load is higher for VCP stress path tests in comparison to the CCP stress path tests. However, matric suction decreases with increasing the load cycles and reached similar asymptote value for both types of stress path. The resilient modulus is higher for VCP stress path tests though both types of stress path tests showed degradation of the resilient modulus.

References

Allen, J.J., Thompson, M.R.: Resilient Response of Granular Materials Subjected to Time Dependent Lateral Stresses. Transportation Res. Rec. Transporation Research Board 510, 1–13 (1974)

Brown, S.F.: Soil Mechanics in Pavement Engineering. Geotechnique 46(3), 382–426 (1996)

Brown, S.F., Hyde, A.F.L.: Significance of Cyclic Confining Stress in Repeated Load Triaxial Testing of Granular Material. Transportation Res. Rec. Transporation Research Board, 537 (1975)

Chen, K.: Behaviour of pavement materials under cyclic loading. PhD Thesis, University of New South Wales at Australia Defence Force Academy, Australia (1997)

Craciun, O., Lo, S.-C.R.: Matric Suction Measurement of Stress Path Triaxial Cyclic Testing of Unbound Granular Base Materials. Geotechnical Testing Journal 33(1), 12 (2010)

Lo, S.-C.R., Chu, J., Lee, I.K.: A technique for reducing membrane penetration and bedding errors. Geotechnical Testing J. 12(4), 159–161 (1989)

Nataatmajda, A.: Variability of Pavement Material Parameter under Repeated Loading, PhD Thesis, Monash University, Australia (1989)

Ohiduzzaman, M., Lo, S.C.R., Craciun, O.: Influence of Initial Matric Suction on the Deformation behavior of Unbound Granular Base Materials (UGB). In: Proceedings of 13th International Conference of the International Association for Computer Methods and Advances in Geomechanics, Melbourne, Australia, May 9-11 (2011)

Raimbault, G.: Cycles annuels d'humidite dans une chaussee souple et son support. Bulletin de Liaison des Laboratoires des Ponts et Chaussée 145, 79–84 (1986)

Rondon, H.A., Wichtman, T., Triantafyllidis, T., Lizcano, A.: Comparison of Cyclic Triaxial Behaviour on Unbound Granular Material under Constant and Variable Confining Pressure. Journal of Transportation Engineering, ASCE 135(7), 467–478 (2009)

Wave Velocity Change and Small-Strain Stiffness in Unsaturated Soils: Experimental Investigation

Milad Asslan and Frank Wuttke

Abstract. Dynamic properties for unsaturated soil are of significant importance for analysing unsaturated soil behaviour for variety of geotechnical design applications. This paper presents an experimental investigation of the small-strain stiffness of unsaturated soil. Bender elements were used to excite and receive shear waves in controlled unsaturated conditions to determine shear wave velocity and corresponding small-strain stiffness. A special cell was designed and produced to control two stress state variables, the net confining pressure and the matric suction and with installed bender elements. The specimen starts at full saturation then it dries gradually while matric suction increases. In each test, the net stress was kept constant whereas the matric suction increases. In the meanwhile, time histories of shear waves were saved for each matric suction step. The objective of all measurements is the identification of the velocity/small-strain-stiffness dependency of the matric suction and saturation level.

Keywords: unsaturated soils, small-strain stiffness, shear wave velocity, bender elements, matric suction.

1 Introduction

The small-strain shear modulus G_{max} of soil is an important parameter for a variety of geotechnical applications. The bender elements technique provides a simple

Milad Asslan
Bauhaus-University Weimar, Weimar, Germany
e-mail: milad.asslan@uni-weimar.de

Frank Wuttke
Bauhaus-University Weimar, Weimar, Germany
e-mail: frank.wuttke@uni-weimar.de

way to obtain the small-strain shear stiffness of soil, G_{max}, by measuring the velocity of propagation of shear wave through a sample.

While many studies were done to establish a model to describe G_{max} in one-phase case, no consistent model was established for unsaturated soil. Most studies in the literature do not concern with small strain range. For this range, very few models have been proposed to quantify G_{max} in unsaturated soil.

Sawangsuriya et al. (2009) investigated the behaviour of cohesive soil at small strain with changing suction for five compacted subgrade soils under net confining pressure of 35 kPa. They experimentally investigated the dependence of G_{max} on matric suction, water content and dry unit weight. They confirmed that matric suction has a major effect on stiffness of soil since it represents the combined effects of the forces holding the water in soil. In their tests, shear modulus increases as matric suction increases. They observed no trend between shear modulus and dry unit weight. Furthermore, the maximum shear modulus did not correspond to the maximum dry unit weight.

Mancuso et al. (2002) studied small strain behaviour of a silty sand in controlled suction resonant column and torsional shear tests. The tests were carried out in the suction range from 0 to 400 kPa and mean net stresses of 100, 200, and 400 kPa. Most of the change in modulus is detected for suctions ranging from 0 to about 200 kPa, while for higher values, G_{max} tends toward a threshold that depends on the net stress level.

Increment of G_{max} with matric suction was also confirmed by other researchers (Alramahi et al. 2008, Hoyos et al. 2008, Picornell & Nazarian 1998). However, there is no consensus regarding the continuous increase of G_{max} with soil suction. Many researchers found that maximum value of G_{max} does not correspond with maximum matric suction. Marinho et al. (1995) indicated that G_{max} increased initially with increasing suction, and then G_{max} keeps constant or slightly decreases with suction. This findings were supported by several researchers (Marinho et al. 1995, Yesiller et al. 2000, Senthilmurugan & Ilamparuthi 2005, Nazarian & Yuan 2008, Weidinger et al. 2009).

In summery, it is evident that the results in the literature are controversial and researchers used different apparatuses range from wave propagation techniques to resonant column. Relationship between shear velocity/shear modulus and matric suction/saturation level is not clear.

2 Experimental Setup and Material Properties

A special cell was designed and produced to control two stress state variables, the net confining pressure and the matric suction and with installed bender elements. A triaxial cell was modified in order to allow water pressure and air pressure to be controlled separately. Two pairs of ceramic disks were installed in the top cap and the bottom base to control water pressure. Another pair of porous stone was installed to control air pressure. The confining pressure in the cell can be controlled

and measured. All previous pressures are connected to manometers through burettes to ensure controlling and measuring. A pair of bender elements was inserted in the top cap and bottom base of the cell to excite and receive shear waves. The input and output signals are commanded by LabVIEW software, a visual programming language, through a data logger and an amplifier (Asslan & Wuttke 2010).

The material used in this research is Hostun sand with d_{50}=0.33 mm, CU=1.81, e_{min}=0.647, e_{max}=0.947, G_s=2.65, and artificial material glass beads d=1.5 mm, G_s=2.5. The artificial material has no volume change during the test and the beads are perfectly round with no angularity. This can be used as a reference for other natural material and for modeling. The initial void ratio was 0.629 for the 100-kPa-net-stress test and 0.679 for the 50-kPa-net-stress test.

A cylindrical mould with height of 110 mm and diameter of 100 mm was used to give the right shape to the specimen. A thin latex membrane is placed inside the mould and fixed at the cell base using at least two o-rings. The o-rings prevent water from getting inside the specimen. A vacuum is applied between the latex membrane and the metal mould, hence the former stretches and this ensures perfect cylindrical shape. A filter paper is placed on the bottom porous stone to prevent soil from getting inside the pores of the porous stone. Then, the oven-dried soil is pluviated into the mould and compacted in layers where specific volume and weight are controlled. The top cap is then set on top of the mould with filter paper and the membrane is pulled around it then fixed with o-rings. The cell frame is then installed and fixed tightened by screws and filled with fresh de-aired water. Afterwards, de-aired water is allowed to run through the specimen in the saturation phase. Saturation was reached by increments of back pressure. In this procedure, pore water pressure was increased simultaneously with confining pressure. A difference of 20 kPa was held to support the specimen.

The axis translation technique was used to determine the relationship between the suction and the degree of saturation. The apparatus utilized was a modified pressure plate apparatus (Lins et al., 2009). In this apparatus, air pressure is applied through porous stone from the top of the cell while water flows outside through a ceramic disk. The drying curve of the suction-saturation relationship was considered in this paper and in this way the unsaturated tests were conducted.

In each test, the net stress (σ_0–u_a) was kept constant, while matric suction (u_a-u_w) increased following the drying path of the SWCC. For sand specimens, two net stress values were applied, 50 kPa and 100 kPa. The test starts with saturated specimen, then water pressure was decreased gradually, thus matric suction increased from 0 to 20 kPa. At each suction step shear wave measurement was taken. These steps were at 1, 2, 4, 6, 8, 10, 20 kPa. For Glass beads specimen, the SWCC is much shorter and only three suction steps, 1, 2 and 3 kPa, were enough to reach the residual water content. After applying each suction step, a period of time passed before equilibrium was reached. Equilibrium took a few days for most steps. In the meanwhile, wave measurements were recorded everyday.

3 Analysis Procedure and Experimental Results

Fig. 1 shows the SWCC of sand and the increment of shear wave velocity with matric suction, i.e. velocity gradient. The shear wave velocity is normalised to its initial value $V_{s,i}$. This small increment could be determined using a sensitive technique called the *coda wave interferometry*. The method is used to detect the wave velocities change related to small soil perturbations. Waves in soil encounter scattering due to heterogeneity (porosity or stiffness heterogeneity) in the medium. This phenomenon results in wave trains which come after the main part of the wave, called coda wave, which means the tail of the wave. This part of the wave, the coda, travels through different paths in the medium and, when the medium is limited, also back and forth stacking more information. This interfered wave paths result in a very sensitive time history which can detect minor change in the travel path due to changes in the medium. Details about this method can be found in (Wuttke et al. 2012, Dai et al. 2012, Wuttke et al. 2010). It is interesting to note that in fig. 1 both curves, SWCC and velocity gradient, have similar distinguished features. One can notice that at the air-entry value the velocity starts to rise for both specimens. As the degree of saturation rapidly decreases, the velocity has its highest increment. For example, between 2 and 4 kPa where saturation drops from 92% to 15%, shear wave velocity increases 4-6%, i.e. shear modulus increases 8-12%. This increase is for pure sand specimen, while for mixtures containing some percentage of fine content, the difference would be much larger. After this phase, saturation level and shear wave velocity are relatively stable. This demonstrates the importance of matric suction in determining shear wave velocity and shear modulus in soil. It can be also concluded that shear wave velocity increases with matric suction until residual water content and it does not have a peak point at optimum water content. The optimum water content for the sand is 10% that corresponds to about 40% saturation level. It is evident in fig. 1 that shear wave velocity increases further while saturation level decreases during the test. This agrees well with many researches from the literature (e.g. Alramahi et al. 2008, Hoyos et al. 2008, Picornell & Nazarian 1998).

This finding is verified in the glass beads specimen. Fig. 2 shows SWCC of glass beads and velocity gradient during the test. The SWCC is very short since the beads are coarse with diameter of 1.5 mm. Suction steps less than 1 kPa are experimentally difficult and not considered in this study. Same observation can be made for this case. The most increment in velocity is in the range between air-entry value and reaching residual water content. For this range, which is less than 1 kPa, shear wave velocity increased 6%, which corresponds to 12% increase in shear modulus.

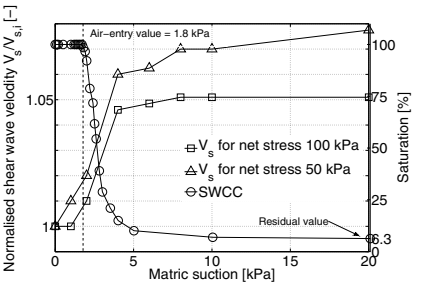

Fig. 1. Velocity gradient versus matric suction and SWCC of sand at two net stress values.

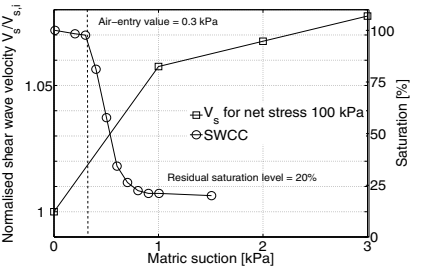

Fig. 2. Velocity gradient versus matric suction and SWCC of glass beads 1.5 mm at net stress 100 kPa.

Fig. 4 shows shear wave velocity versus saturation. Interestingly, velocity decreases almost linearly with saturation for the saturation range considered in this study. This suggests a linear relationship between both. Fitting curves are plotted in fig. 4 for both specimens. There are not enough velocity values to establish a relationship for the glass specimen. Cho & Santamarina (2001) proposed an empirical solution to calculate the capillary force in unsaturated soil but this solution is limited to low water content and cannot be applied for the whole range for saturation:

$$[V_s]_S = [V_s]_{S=1}[1+\frac{2\sigma'_{eq}}{(1+K_0)\sigma'_v}]^{\beta}\sqrt{\frac{e+G_s}{eS+G_s}} \quad (1)$$

where $[V_s]_S$ is shear wave velocity at a specific saturation level, σ'_{eq} is equivalent effective stress due to capillarity at a given degree of saturation S, e is void ratio, G_s is specific gravity of the grain particle, and K_0 is coefficient of lateral earth pressure at rest, σ'_v is vertical effective stress, and β is empirical parameter. σ'_{eq} is given for simple cubic packing SC as (Cho & Santamarina 2001):

$$\sigma'_{eq} = \frac{\pi T_s}{4R}[2-(\frac{8}{9}G_s w)^{1/4}] \quad (2)$$

where T_s is water surface tension (0.0727 N/m), R is radius of particle, and w is water content. For such large particles, σ'_{eq} obtains negligible values. For example, at w=1% and d_{50}=0.33 mm, σ'_{eq}=0.56 kPa. Thus, velocity in equation 1 depends only on saturation in our case. It is clear in fig. 4 that equation 1 overestimates values of velocity. By adding the effect of σ'_{eq}, this overestimation would be larger. On the other hand, the assumption of an easy linear relationship fits the data well:

$$V_S = 205-0.1\mathrm{S} \quad \text{and} \quad V_S = 214-0.12\mathrm{S} \quad (3)$$

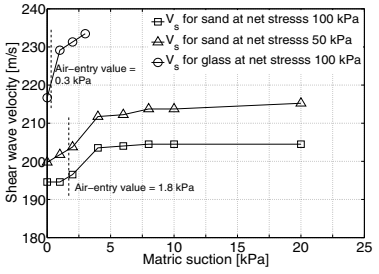

Fig. 3. Shear wave velocity versus matric suction for two sand specimens and one glass specimen.

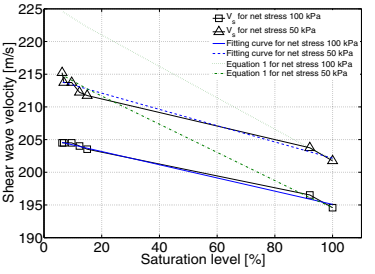

Fig. 4. Shear wave velocity versus saturation level for two sand specimens.

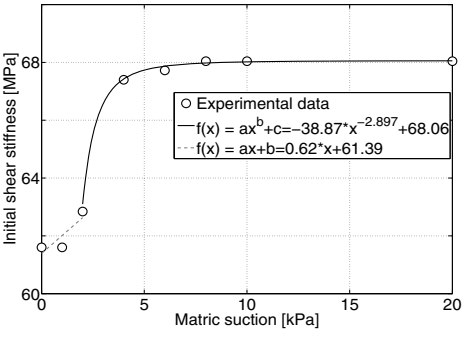

Fig. 5. Fitting models for initial shear stiffness with matric suction for net stress 100 kPa.

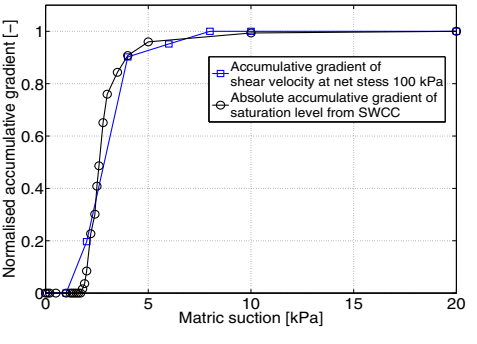

Fig. 6. Normalised accumulative gradient of shear velocity at 50 and 100 kPa net stress and normalised accumulative absolute change of saturation.

The experimental relation between shear wave velocity or respectively the small-strain shear modulus and the matric suction for net stress of 100 kPa is shown in fig. 5. As explained above, the most rapid increase of shear modulus/shear velocity occurs in the range between 2 and 4 kPa, i.e. shortly after the air-entry value. The experimental data could be fitted with two fitting models, one for low suction values before the air-entry value and the other one fits the data for values higher than the air-entry value. The first model is a linear one:

$$f(x) = ax + b \tag{4}$$

where a=0.62, b=61.39. The second model is a power model:

$$f(x) = ax^b + c \tag{5}$$

where a=-38.87, b=-2.897, c=68.06, which gives R-square=99.8%. Furthermore, it is visible that the gradients of the SWCC and shear modulus functions present large similarities.

Fig. 6 shows accumulative change in shear velocity, ($\Delta V_{s,acc}/V_{s,residual}$), for net stress values 100 kPa. In order to compare its shape with the SWCC, it was normalised to its last value at 20 kPa matric suction. Additionally, absolute change in saturation level was derived from SWCC, then accumulated and normalised to its residual value ($\Delta S_{acc}/S_{residual}$). Both shapes compare very well. This similarity suggests that saturation level changes with the same rate as same as shear velocity does for a given change of matric suction. This also means that saturation level can be directly related to shear velocity as their accumulative changes with suction are similar as done in fig. 4.

4 Summary

The objective of this paper was to analyse the relationship between shear wave velocity/initial shear modulus and matric suction/saturation level in soil. A new tool was used to determine the velocity gradients due to a small change in the structure or pressure. Shear wave velocity was found to increase with increasing matric suction and decreasing saturation. It was shown that the gradients of the velocity change and the SWCC change compare quite well, which indicates that both are directly linked. A linear relationship between velocity and saturation level was proposed. Additionally, linear and power models were proposed to relate data of initial shear modulus to matric suction.

Acknowledgments. The authors would like to thank the support of the German Research Foundation for funding the Research Training Group 1462, the support of the Free State of Thuringia as well as the European Regional Development Fund for funding of experimental devices with grand no. FKZ B 715-09010 and the support of the R&D-Program GEOTECHNOLOGIEN funded by the German Ministry of Education and Research (BMBF) and German Research Foundation (DFG), Grant 03G0636B. The Post Graduate Funding Programme from the Free State of Thuringia is also very much appreciated for its support of this research.

References

Alramahi, B., Alshibli, K.A., Fratta, D., Trautwein, S.: A suction control apparatus for the measurement of p and s-wave velocity in soils. Geotechnical Testing Journal 31(1), 12–23 (2008)

Asslan, M., Wuttke, F.: An experimental study on the initial shear stiffness in granular dry and saturated material using bender elements test. In: Proceedings of 14th European Conference of Earthquake Engineering (2010)

Cho, G., Santamarina, J.: Unsaturated particulate materials—particle-level studies. Journal of Geotechnical and Geoenvironmental Engineering, ASCE 127(1), 84–96 (2001)

Dai, S., Wuttke, F., Santamarina, J.C.: Coda wave analysis to monitor processes in soils. Journal of Geotechnical and Geoenvironmental Engineering, ASCE (submitted, 2012)

Hoyos, L.R., Takkabutr, P., Puppala, A., Hosain, M.: Dynamic Response of Unsaturated Soils Using Resonant Column and Bender Elements Testing Techniques. In: Proceedings of Geotechnical Earthquake Engineering and Soil Dynamics IV, pp. 485–492 (2008)

Lins, Y., Schanz, T., Fredlund, D.G.: Modified Pressure Plate Apparatus and Column Testing Device for Measuring SWCC of Sand. ASTM Geotechnical Testing Journal 32(5), 1–15 (2009)

Mancuso, C., Vassallo, R., D'Onofrio, A.: Small strain behavior of a silty sand in controlled-suction resonant column–torsional shear tests. Canadian Geotechnical Journal 39(1), 22–31 (2002)

Marinho, F., Chandler, R., Crilly, M.: Stiffness measurements on an unsaturated high plasticity clay using bender elements. In: Alonzo, E., Delage, P. (eds.) Proceeding of the first International Conference on Unsaturated Soils, UNSAT 1995, vol. 2, pp. 535–539. Balkema, Paris (1995)

Nazarian, S., Yuan, D.: Variation in moduli of base and subgrade with moisture. In: Proceedings of GeoCongress: Geosustainability and Geohazard Mitigation, pp. 570–577 (2008)

Picornell, M., Nazarian, S.: Effect of soil suction on the low-strain shear modulus of soils. In: Proceedings of 2nd International Conference on Unsaturated Soils, Beijing, pp. 102–107 (1998)

Sawangsuriya, A., Edil, T.B., Bosscher, P.J.: Modulus-Suction-Moisture Relationship for Compacted Soils in Postcompaction State. Journal of Geotechnical and Geoenvironmental Engineering 135(10), 1390–1403 (2009)

Senthilmurugan, T., Ilamparuthi, K.: Study of compaction characteristics and strength through ultrasonic methods. In: Proceeding of Geo-Frontiers Conference, Austin, ASCE, Geotechnical Special Publication no. 130, pp.1–12 (2005)

Weidinger, D.M., Ge, L., Stephenson, R.W.: Ultrasonic pulse velocity tests on compacted soil. In: Characterization, Modeling, and Performance of Geomaterials, Hunan, ASCE, Geotechnical Special Publication, no. 189, pp.150–155 (2009)

Wuttke, F., Asslan, M., Schanz, M.: Wave velocity analysis of state parameter changes in multi-phase granular materials. In: Proceedings of 5th International Conference of Unsaturated Soils, UNSAT, Barcelona, pp. 745–750 (2010)

Wuttke, F., Asslan, M., Schanz, T.: Time-lapse monitoring of fabric changes in granular materials by coda wave interferometry. ASTM Geotechnical Testing Journal 35(2) (2012)

Yesiller, N., Inci, G., Miller, C.J.: Ultrasonic testing for compacted clayey soils. In: Proceedings of Advances in Unsaturated Geotechnics, Denver, ASCE, Geotechnical special publication, no. 99, pp. 54–68 (2000)

Seismic Ground Response Analysis of Unsaturated Soil Deposits Using Suction Dependent Shear Modulus and Damping Ratio

Mahnoosh Biglari and Iman Ashayeri

Abstract. Seismic ground motion is profoundly affected by geometrical and mechanical properties of soil deposits overlaying bedrock. Local seismic ground response of saturated soil deposits was studied in literature by applying the effects of soil stress state and index properties on the strain-dependent normalized shear modulus reduction, G/G_0, and damping ratio, D, curves in an equivalent linear analysis. However, experimental investigations revealed that, G_0, G/G_0, and D of unsaturated soils are influenced by stress state as well as suction. This study presents the results of linear and equivalent linear seismic ground response analysis of unsaturated soil deposits with considering suction effects on G/G_0 and D curves. Seismic ground response analysis was done with the computer program EERA for two sets of soil profiles, which include in saturated, constant and linearly variable suction unsaturated soil deposits. Results show that natural frequency of the soil profile increases as the suction increases.

Keywords: unsaturated soil, soil dynamics, equivalent-linear, seismic ground response analysis, EERA.

1 Introduction

The local soil conditions have a profound influence on the ground response during earthquakes, which is modelled through direct non-linear elasto-plastic (Hashash & Park 2001) or equivalent-linear elastic ground response analysis (Idriss & Seed 1968,

Mahnoosh Biglari
Razi University, Kermanshah, Iran
e-mail: m.biglari@razi.ac.ir, mahnooshbiglari@yahoo.com

Iman Ashayeri
Razi University, Kermanshah, Iran
e-mail: i.ashayeri@razi.ac.ir

Bardet et al. 2000). In spite of its theoretical shortcomings, the latter has become the major tool in practical engineering applications due to its simplicity. The equivalent-linear analysis consists of modifying normalized shear modulus G/G_0, and damping ratio D, of a visco-elastic soil model with shear strain level, γ. Usually the strain-dependent normalized shear modulus reduction (G/G_0-γ), damping ratio (D-γ) curves are obtained by laboratory tests. However, mathematical functions were presented for (G/G_0-γ) and (D-γ) in terms of stress state and index properties of saturated soils based on enormous experiments by various investigators (Seed et al 1986, Vucetic and Dobry 1991, Ishibashi and Zhang 1993).

Experimental investigations revealed that initial shear modulus, G_0, of unsaturated soils is influenced by stress state as well as suction (Mancuso et al. 2002, Vassallo et al. 2007a,b, Ng & Yung 2008, Biglari et al. 2012, Biglari et al 2011b). Furthermore, recent investigation on the measurements of shear modulus of an unsaturated soil at wider shear strain range by suction-controlled cyclic triaxial apparatus show that G-γ and D-γ curves are influenced by the suction levels too (Biglari et al. 2011a). On the basis of this experimental evidence, Biglari & Ashayeri (2012) modified the empirical equation proposed by Ishibashi & Zhang (1993) for G/G_0-γ and D-γ to take into the account the influence of the suction level as well as stress state and index properties for unsaturated soils. D'Onza et al. (2008) investigated the effects of unsaturated soil suction on the seismic ground response by means of linear analysis which takes into the account the influence of suction on the shear wave velocity or initial shear modulus of the unsaturated soil deposits. They have presented the results in terms of amplification ratio of surface motion in the frequency domain and concluded that the natural frequency of soil deposit significantly increases with suction increase and the maximum amplification ratio is substantially reduced.

This study presents the results of linear and one dimensional equivalent linear seismic ground response analysis of unsaturated soil deposit not only considering the effects of suction variation on the shear wave velocity (or G_0), but also taking into the account the dependency of G/G_0-γ and D-γ on the suction level based on the developed empirical model for G-γ and D-γ (Biglari & Ashayeri 2012). Seismic ground response analysis was done with the computer program "Equivalent-linear Earthquake site Response Analyses" (EERA), (Bardet et al. 2000) for five soil suction profiles and three time histories of acceleration. The results are discussed in terms of comparison between the acceleration time history at surface and bedrock, the amplification ratio and natural frequency of soil deposits as well as spectral acceleration of the ground motion at surface and bedrock.

2 Soil Profiles

Five soil profiles were considered in this study within two sets of analysis. The first set compares two soil profiles P1 and P2 of lean clay deposit 24 meters deep overlaying the bedrock. Table 1 presents the variation of suction, shear wave

velocity, and total unit weight of different layers of the soil profiles P1 and P2. Soil profile P1 is formed of a two meters of saturated soil layer over the bedrock that is overlaid by 22 meters of unsaturated soil with variable suctions. The unsaturated soil deposit of P1 was divided into 6 layers of constant suction varying from zero to 250 kPa. On the other hand, soil profile P2 is formed of 24 meters of the saturated soil deposit overlaying the bedrock that is divided into 7 layers of variable shear wave velocity and unit weight.

Table 1. Description of soil profiles of the first set of analysis.

Layer	Thickness (m)	Profile					
		P1			P2		
		s[a] (kPa)	Vs[b] (m/sec)	γ[c] (kN/m^3)	s (kPa)	Vs (m/sec)	γ (kN/m^3)
1	4	250	159	13.43	0	125	19.30
2	4	200	159	13.63	0	125	19.30
3	4	150	170	14.18	0	130	19.38
4	4	100	187	15.15	0	142	19.57
5	4	50	201	16.19	0	154	19.61
6	2	0	195	19.86	0	164	19.65
7	2	0	200	19.95	0	172	19.77
8	Bed Rock		1219.2	22.02		1219.2	22.02

[a] s: suction, [b] Vs: shear wave velocity, [c] γ: unit weight

The second set of analysis compares three soil profiles P3, P4, and P5 of the same deposit 24 meters deep overlaying the bedrock. Table 2 presents the variation of suction, shear wave velocity, and total unit weight of the different layers of the soil profiles P3, P4, and P5. Soil profile P3 is formed of 24 meters of the saturated soil deposit overlaying the bedrock that is divided into 6 layers with variable shear wave velocity and unit weight. Soil profile P4 is formed of 24 meters of the unsaturated soil deposit with constant suction of 150 kPa overlaying the bedrock and is divided into 6 layers with variable shear wave velocity and unit weight. Soil profile P5 is formed of 24 meters of the unsaturated soil deposit with constant suction of 300 kPa overlaying the bedrock and again is divided into 6 layers with variable shear wave velocity and unit weight.

The shear wave velocities of the soil layers of all the five profiles were calculated from the model for initial shear modulus of unsaturated soils calibrated for the current material, which was presented by Biglari et al. (2011b and 2012).

3 Modulus Reduction and Damping Curves

In order to generate the modulus reduction and damping curves, the empirical models presented by Biglari & Ashayeri (2012) were used with considering the soil plasticity index (PI = 12%), and appropriate suction and confining pressure of

each layer of the soil profiles. Figs. 1 to 5 present the generated G/G_0-γ and D-γ for layers of soil profiles P1 to P5, respectively.

Table 2. Description of soil profiles of the second set of analysis.

Layer	Thickness (m)	Profile								
		P3			P4			P5		
		s (kPa)	Vs (m/sec)	γ (kN/m^3)	s (kPa)	Vs (m/sec)	γ (kN/m^3)	s (kPa)	Vs (m/sec)	γ (kN/m^3)
1	4	0	125	19.30	150	159	13.70	300	176	13.50
2	4	0	125	19.30	150	159	13.70	300	176	13.50
3	4	0	130	19.38	150	170	14.20	300	185	13.80
4	4	0	142	19.57	150	188	14.60	300	203	14.30
5	4	0	154	19.61	150	203	15.10	300	219	14.50
6	4	0	168	19.71	150	219	15.30	300	233	14.70
7		Bed rock	1219.2	22.02		1219.2	22.02		1219.2	22.02

4 Ground Response Analysis

Seismic ground response analysis was done with the computer program EERA (Bardet et al. 2000) for the five soil profiles P1 to P5. EERA is a modern implementation of the well-known concepts of equivalent linear earthquake site response analysis applied in SHAKE (Schnabel et al., 1972). The soil profiles are subjected to the input ground motion from the bedrock that is specified as an outcrop motion. To avoid dependency of the ground response to the input motion, three earthquakes were used in the analysis. These three input motions are the acceleration time history of Loma Prieta 1989, Kobe 1995, and Chichi 1999 earthquakes (Records P0782, P1043 & P1116 at http://peer.berkeley.edu/smcat/). The ground motions are normalized to a target peak acceleration of 0.1g.

The comparisons between Peak Ground Acceleration (PGA) at surface, amplification factor, and first natural frequency of each soil profile are presented in Table 3 for the three ground motions. The first natural frequency increases from 0.8 Hz for P2 to 1.4 Hz for P1 and it varies from 0.8 Hz for P3 to 1.6 Hz for P5 by increasing suction. The PGA of the motion at surface of the all profiles is larger than the bedrock motion and this is more significant at the unsaturated profiles.

Fig. 6 shows amplification between the surface motion and the base motion at varying frequencies for P1 and P2 for Loma Prieta earthquake. The increase in the natural frequency with suction increase reasonably can be assigned to the increase of shear modulus by suction. However, the variation of amplification factor is related to the admittance ratio between the soil and the bedrock, which resulted into increasing amplification factor by increasing suction. To provide comparison of

the effects of non-linearity, series of linear analyses were performed for P3 to P5 which, the results are presented in Figs. 7 to 9. It is clear that non-linearity has influenced the results significantly in terms of both amplification factor and natural frequency.

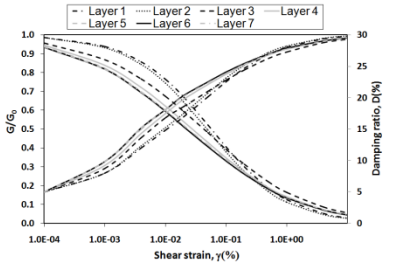

Fig. 1. G/G_0-γ and D-γ curves of layers of P1.

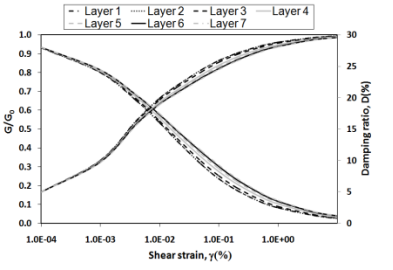

Fig. 2. G/G0-γ and D-γ curves of layers of P2.

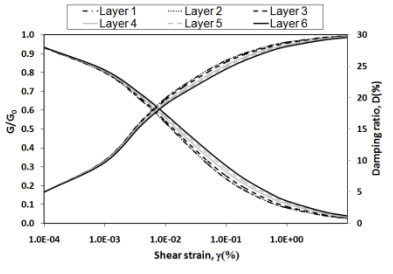

Fig. 3. G/G_0-γ and D-γ curves of layers of P3.

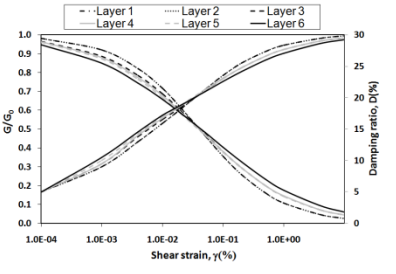

Fig. 4. G/G_0-γ and D-γ curves of layers of P4.

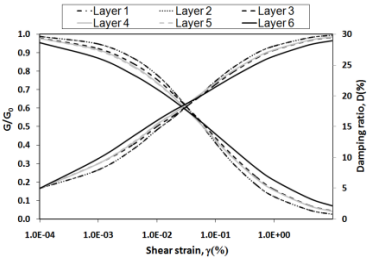

Fig. 5. G/G_0-γ and D-γ curves of layers of P5.

Table 3. Comparison between PGA values of bed rock and surface of the all profiles.

Profile	PGA (g), Amplification Factor, 1st natural frequency (Hz)		
	Loma Prieta	Kobe	Chichi
P1	0.146, 2.50, 1.4		
P2	0.113, 2.29, 0.8		
P3	0.113, 2.29, 0.8	0.117, 2.30, 0.8	0.104, 2.19, 0.8
P4	0.148, 2.61, 1.4	0.155, 2.56, 1.4	0.154, 2.59, 1.4
P5	0.146, 2.71, 1.6	0.154, 2.69, 1.6	0.175, 2.69, 1.6

Another index to seismic hazard of buildings and structures is response spectral acceleration curve. Spectral acceleration S_a, is the maximum acceleration of a single degree of freedom oscillator with different natural frequencies but unique damping. Figs. 10 to 13 compare the S_a with 5% damping ratio at the ground surface of the profiles with the one at bedrock for the two sets of analysis.

Shift of S_a to the lower frequencies (higher periods) at the surface of the saturated profiles (P2 and P3) is observed. However, S_a of the surface ground motion of unsaturated profiles (P1, P4, and P5) is considerably different with the ones of saturated profiles (P2 and P3) and the bed rock. The results show that the S_a increases by suction increase for high frequencies (periods less than 1 sec). This is very important and should be noticed in seismic design of structures on the unsaturated soil deposits particularly for short buildings with high natural frequency.

5 Summary and Conclusions

The aim of this study was to perform 1D equivalent linear site response analysis by considering the influence of suction on the shear wave velocity, shear modulus reduction and damping ratio curves. Two sets of analysis compare the response of three unsaturated soil profiles with the saturated ones due to three earthquakes. It came out with the following conclusions for the selected soil profiles.

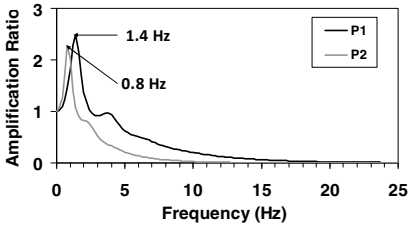

Fig. 6. Amplification functions of P1 and P2.

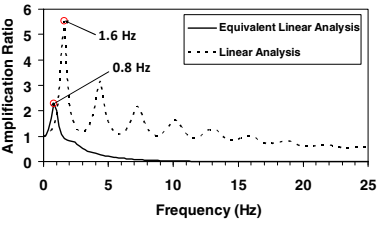

Fig. 7. Amp. functions of P3 in different analysis.

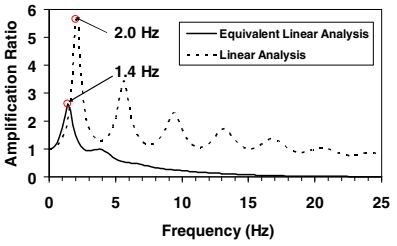

Fig. 8. Amp. functions of P4 in different analysis.

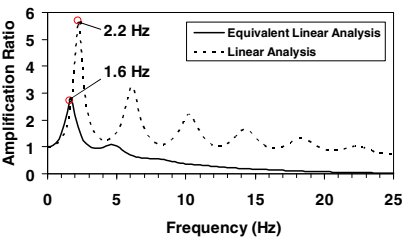

Fig. 9. Amp. functions of P5 in different analysis.

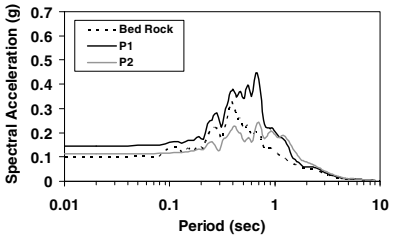

Fig. 10. S_a of P1 and P2 for Loma Prieta.

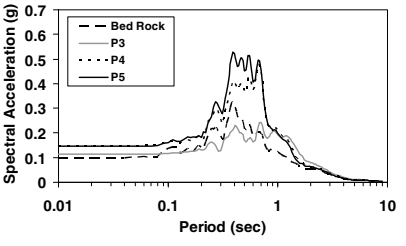

Fig. 11. S_a of P3, P4, and P5 for Loma Prieta.

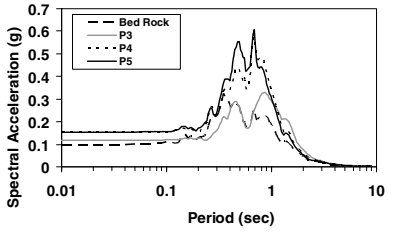

Fig. 12. S_a of P3, P4, and P5 for Kobe.

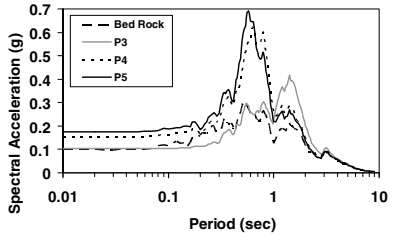

Fig. 13. S_a of P3, P4, and P5 for Chichi.

- The natural frequency of the soil profile increases as the suction increases. This will attract the attentions to the suitable natural frequency of the buildings on the unsaturated soil deposits.
- The ground motions were amplified at the surface for all of the saturated (P2 and P3) and unsaturated profiles (P1, P4 & P5). However, the combined conditions considered in the soil profiles showed that the amplification ratio is slightly larger at unsaturated soils that may not to be a general behaviour.
- Response spectral accelerations calculated for damping of 5%, show that the response of the structures on the unsaturated soil profiles are more severe than saturated ones, particularly at higher frequencies.

References

Bardet, J.P., Ichii, K., Lin, C.H.: EERA, A computer program for Equivalent linear Earthquake site Response Analysis of layered soils deposits. Software Manual. University of Southern California, Los Angeles (2000)

Biglari, M., Ashayeri, I.: An empirical model for shear modulus and damping ratio of unsaturated soils. In: Proc. 5th Asia-Pacific Conf. on Unsaturated Soils, Pataya, Thailand (2012)

Biglari, M., d'Onofrio, A., Claudio, M., Jafari, M.K., Shafiee, A.: Small strain stiffness of Zenoz kaolin in unsaturated conditions. Canadian Geotechnical Journal (2012) (accepted in press)

Biglari, M., Jafari, M.K., Shafiee, A., Mancuso, C., d'Onofrio, A.: Shear Modulus and Damping Ratio of Unsaturated Kaolin Measured by New Suction-Controlled Cyclic Triaxial Device. Geotechnical Testing Journal, ASTM 34(5) (2011a)

Biglari, M., Mancuso, C., d'Onofrio, A., Jafari, M.K., Shafiee, A.: Modelling the initial shear stiffness of unsaturated soils as a function of the coupled effects of the void ratio and the degree of saturation. Computers and Geotechnics 36, 709–720 (2011b)

d'Onza, F., d'Onofrio, A., Mancuso, C.: Effects of unsaturated soil state on the local seismic response of soil deposits. In: Proc. 1st European Conf. on Unsaturated Soils, Durham, UK, pp. 531–536 (2008)

Hashash, Y.M.A., Park, D.: Non-linear one-dimensional seismic ground motion propagation in the Mississippi embayment. Engineering Geology 62(1-3), 185–206 (2001)

Idriss, I.M., Seed, H.B.: Seismic Response of Horizontal Soil Layers. Journal of the Soil Mechanics and Foundations Division, ASCE 94(4), 1003–1031 (1968)

Ishibashi, I., Zhang, X.: Unified dynamic shear moduli and damping ratios of sands and clays. Soils and Foundations 33(1), 182–191 (1993)

Mancuso, C., Vassallo, R., d'Onofrio, A.: Small strain behavior of a silty sand in controlled-suction resonant column – torsional shear tests. Canadian Geotechnical Journal 39, 22–31 (2002)

Ng, C.W.W., Yung, S.Y.: Determination of the anisotropic shear stiffness of an unsaturated decomposed soil. Géotechnique 58(1), 23–35 (2008)

Schnabel, P.B., Lysmer, J., Seed, H.B.: SHAKE: A Computer Program for Earthquake Response Analysis of Horizontally Layered Sites, Report No. UCB/EERC-72/12, p. 102. Earthquake Engineering Research Center, University of California, Berkeley (December 1972)

Seed, H.B., Wong, R.T., Idriss, I.M., Tokimatsu, K.: Moduli and damping factors for dynamic analyses of cohesionless soils. Journal of Geotechnical Engineering, ASCE 112(11), 1016–1032 (1986)

Vassallo, R., Mancuso, C., Vinale, F.: Effects of net stress and suction history on the small strain stiffness of a compacted clayey silt. Canadian Geotechnical Journal 44, 447–462 (2007a)

Vassallo, R., Mancuso, C., Vinale, F.: Modelling the influence of stress–strain history on the initial shear stiffness of an unsaturated compacted silt. Canadian Geotechnical Journal 44, 463–472 (2007b)

Vucetic, M., Dobry, R.: Effect of soil plasticity on cyclic response. Journal of Geotech. Eng., ASCE 117(1), 89–107 (1991)

Ageing Effects on the Stiffness Behaviour of a Microbiologically Treated and Compacted Soil

Laura Morales, Enrique Romero, Jubert A. Pineda, Eduardo Garzón, and Antonio Giménez

Abstract. The paper describes an experimental study aimed at evaluating the evolution of some mechanical properties, specifically small-strain stiffness and unconfined compressive strength, induced by ageing after a microbiological treatment on a compacted soil. Bacillaceae microorganisms were used to induce microbial calcium carbonate precipitation and improve the mechanical properties of a compacted clayey silt. After compaction, samples were left to age and soil stiffness tracked every 24 hours using shear wave velocity measurements (bender elements). Parallel tests were run to determine the unconfined compressive strength at different elapsed times (just after compaction, 2, 4 and 7 days).

Keywords: biological treatment, compacted soil, ageing, small-strain stiffness, unconfined compressive strength.

1 Introduction

The use of bacteria and different microorganisms to improve the mechanical behaviour of soils has been recently recognized as an innovative and sustainable development tool to be applied in several engineering fields (Gray & Sorti 1996, Weiner & Addadi 1997). One of these biological treatments uses urea-degrading bacteria that produce ammonia via hydrolysis and create the alkaline conditions needed to precipitate calcium carbonate (Morales et al. 2011). One of the benefits of this kind of treatments is the increase in soil stiffness due to $CaCO_3$ generation

Laura Morales · Eduardo Garzón · Antonio Giménez
Universidad de Almería, Almería, Spain
e-mail: mhl274@ual.es, egarzon@ual.es, agimfer@ual.es

Jubert Andrés Pineda · Enrique Romero
Universitat Politècnica de Catalunya, Barcelona
e-mail: jubert.pineda@upc.edu, enrique.romero-morales@upc.edu

acting as cementing material (biocementation) or filling material (bioclogging) (DeJong et al. 2006, Ivanov & Chu 2008).

This paper describes the ageing effects of a microbiological treatment carried out on compacted clayey silt and their consequences on the small-strain stiffness and unconfined compressive strength of the soil. Soil stiffness was daily tracked during ageing by bender elements measurements.

2 Material Tested and Experimental Program

A microorganism of the Bacillaceae family was used for the precipitation of carbonated minerals, as previously reported by Morales et al. (2010). The microorganisms were added to the moulding water that was prepared to compact a clayey silt from South-East Spain, whose main properties are indicated in Table 1. The same target void ratio e=0.49 was used for the natural (B5) and treated (BT5) soils, which corresponded to the optimum dry density of B5 at standard Proctor energy (ρ_d=1.84 Mg/m^3). Two different initial water contents were used: (a) w_0=15% at a degree of saturation S_{r0}=0.84 that corresponds to the optimum water content and, (b) w_0=7% at S_{r0}=0.39 on the dry side. The initial total suctions were around 1 MPa and 20 MPa for states (a) and (b), respectively, according to the water retention curves plotted in fig. 1 that were determined on drying by dew-point psychrometer readings and starting from water contents lower than 15%. The data reported for the treated material included the determination of the water retention properties at different ageing periods, identified as BT5_d0 just after preparation, and BT5_d4 and BT5_d7 for four and seven days ageing, respectively. These drying curves corresponded to approximately constant void ratio conditions, since the clayey silt did not undergo important shrinkage on suction increase (void ratios were maintained between 0.45 and 0.50). As observed in the figure, a slightly lower water retention capacity is detected on the treated sample at high suctions (higher than 10 MPa), which may be a consequence of some loss of the activity of the clayey fraction and that is consistent with the small reduction of the specific surface –determined by nitrogen adsorption– reported in Table 1. In addition, no important effects on the water retention capacity were observed on ageing, as indicated by the consistent total suctions measured at different curing periods.

After compaction, both treated and natural samples were left ageing up to seven days inside desiccators at controlled relative humidity (consistent with their initial total suctions) and placed in an oven at 30°C to promote the growth of microorganisms (incubation process). Differences between natural and treated samples are captured since natural samples underwent the same curing process. It is worth remarking that during this process some small water content reduction occurred due to evaporation, especially in the wetter samples. This was systematically observed, since the samples were previously weighed before performing the tests. This progressive evaporation induced some small additional stiffening effect due to suction increase, which was assumed to affect in the same way both natural and treated samples.

Table 1. Main geotechnical properties of the tested soils (natural and treated).

Ref.	Liquid limit (%)	Plasticity index (%)	$CaCO_3$ content (%)	Solid density (Mg/m^3)	% < 75 μm	Specific surface (m^2/g)
B5	48	30	4.5	2.73	50	33-46
BT5	49	29	6.4	2.74	<50 (due to aggregation)	31-43

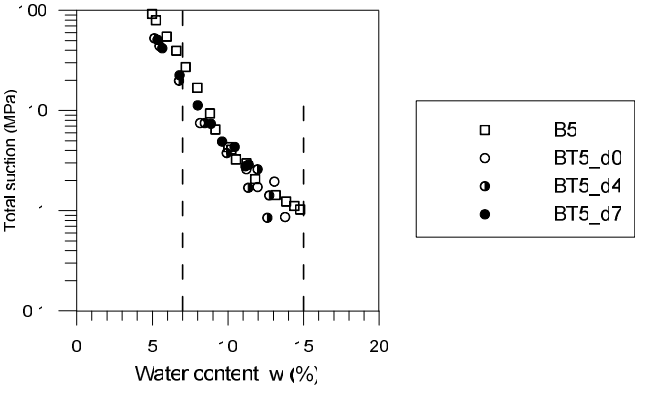

Fig. 1. Water retention properties of B5 and BT5 samples. BT5 at different curing periods.

The effects of the microbiological treatment on small-strain stiffness were evaluated using bender elements. The technique allows continuously tracking the low-strain shear modulus G_0 (along the vertical direction) through the measurements of the shear wave velocity, V_S. The shear modulus is calculated as $G_0=\rho_t V^2_S$, where ρ_t is the total density, and $V_S=l_{eff}/t_S$. The wave travel distance l_{eff} is taken as the distance between transducer tips. Arrival time t_S is determined by inspection of the received trace, looking for the first significant amplitude excursion. Regarding the experimental setup, input signals are generated and emitted using a programmable function generator, while both input and output signals are acquired through a digital oscilloscope. A sine pulse V_{pp}=20V with apparent input frequency ranging between 15-20 kHz was used as input signal. Additional details are given in Arroyo et al. (2010) and Pineda (2012). Bender elements measurements were performed every 24 hours during the ageing period.

The experimental program was complemented with unconfined compressive strength tests performed on treated samples to evaluate the influence of the incubation process on this mechanical response. Treated samples were compacted at the same initial conditions and subjected to compression after 2, 4 and 7 days of ageing. A constant displacement rate of 0.3mm/min was used.

3 Effects on Small-Strain Stiffness and Compressive Strength

Fig. 2(a) shows the evolution of the shear wave velocity *Vs* for different ageing periods and initial water contents. Just after static compaction, *Vs* ranged between

600 m/s (BT5) and 630 m/s (B5) for samples prepared at optimum water content (w_0=15%). For w_0=7%, *Vs* varied between 800 m/s (BT5) and 835 m/s (B5). The higher initial values on the drier samples are a consequence of the stiffening effect of suction. As ageing progressed in the treated soils, *Vs* increased as observed in the time evolution plots presented in Fig. 2(a) –*Vs* reached 715 m/s and 890 m/s for wet and dry states, respectively, at 7 days–. In the case of natural samples that underwent the same curing process, some reduction in water content during ageing also induced an increase in *Vs* that was smaller than the corresponding one of the treated samples. These reductions were mainly induced by some drying (evaporation) of the samples inside the sealed container. Nevertheless, reduction in water content for treated samples was also partially due to the microbiological treatment that required water uptake (avidity for water of the microorganisms to precipitate $CaCO_3$ minerals) that was not fully compensated for by the controlled relative humidity.

With regard to the small-strain stiffness, the microbiological treatment induced an important increase in the normalised shear modulus $G_{0\,aged}/G_0$ –ratio between the actual value and the initial one– as observed in Fig. 2(b). The stiffness increased around 40% and 20% for wet and dry treated samples, respectively, after 7 days of incubation, which was higher than the corresponding increase detected for the natural samples that underwent some drying. This higher increase in shear stiffness of the treated samples –that is clearly more important at higher water content– is consistent with the expected microbiological reactions of bacteria and with the precipitation of $CaCO_3$ minerals, which reach their maximum capacity after two or three days of ageing. The mechanism behind this stiffness increase is expected to be mainly associated with bioclogging, since precipitation minerals develop in the larger pore spaces between soil grains and aggregations (see for instance, Morales et al. 2011). The jump in stiffness observed in Fig. 2a between the 3rd and 4th days and detected in the soils compacted at the higher water contents (both on natural and treated samples) appear to be a consequence of some evaporation effects –both tests were carried out simultaneously following the same protocols, and probably the relative humidity prevailing at laboratory conditions affected the total suction applied in the desiccators–.

Fig. 3(a) shows the stress-strain curves during unconfined compression tests performed on treated samples at dry (w_o=7%) and wet (w_o=15%) conditions. Drier samples display larger deviatoric stress peaks, consistent with the higher initial suction. In addition, ageing effects during incubation process are clearly increasing the peak strength, as observed in the time evolution plot shown in Fig. 3(b). Nevertheless, suction effects may mask this ageing effect. The high peak stress observed after 4 days of curing in the driest state and associated with some drying undergone by the material is clearly enhancing the peak value and masking the ageing incubation effect. After 7 days and at the driest state, the peak stress reduces as a consequence of the increase in water content. Fig. 3 also shows that the peak strength at w_o=15% and t=0 for the treated material is somewhat higher when compared to the natural material, presumably as a consequence of the change in microstructure (aggregation) induced by the addition of microorganism to the moulding water. It is important to remark that these are preliminary results, which are being currently improved to minimise the important overlapping with suction that is masking the ageing results induced by biological action.

4 Summary and Concluding Remarks

The evolution of the small-strain stiffness and unconfined compressive strength during the incubation process (that lasted 7 days) of microbiologically treated and compacted clayey silt has been presented. Bacillaceae microorganisms were used to induce microbial calcium carbonate precipitation and improve the mechanical properties of the compacted soil at two different initial water contents (near optimum conditions of standard Proctor and on the dry side).The experimental results showed a larger increase in the normalised soil stiffness ($G_{0\ aged}/G_0$) with incubation time for the wet and treated samples (up to 1.4 times), which is consistent with the humid environment required for the precipitation of $CaCO_3$ by bacteria. Some water content reduction was observed in the natural samples induced by some evaporation when the same ageing protocol was followed on these samples.

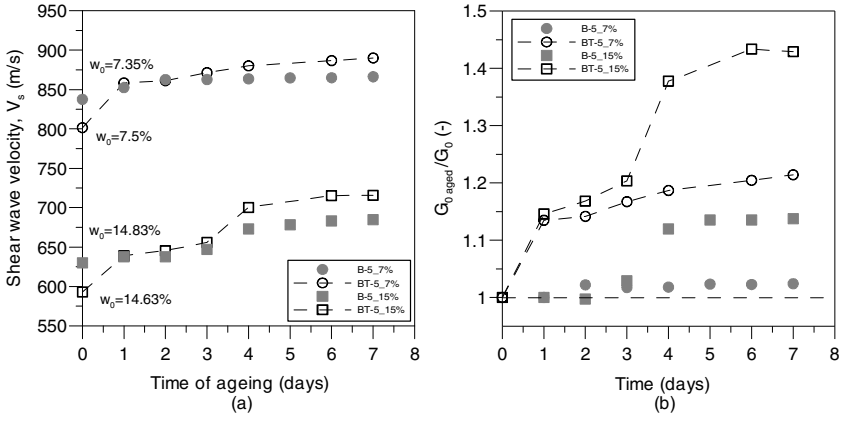

Fig. 2. (a) Time evolution of shear wave velocity during ageing. (b) Variation of normalised shear stiffness during ageing for natural and treated samples.

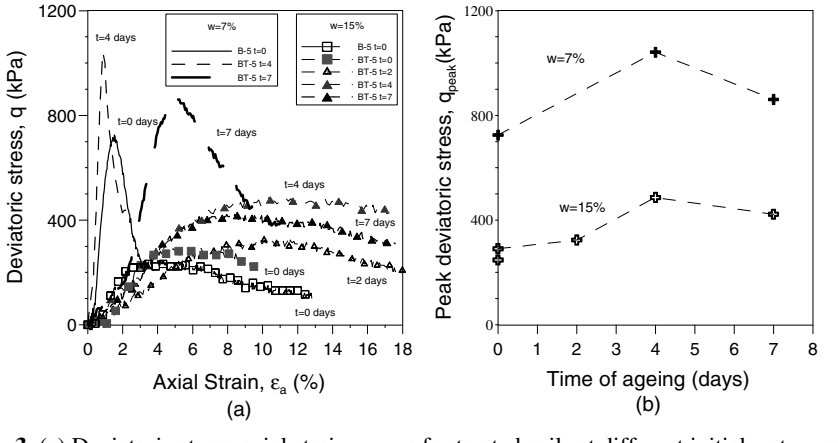

Fig. 3. (a) Deviatoric stress-axial strain curves for treated soils at different initial water contents and ageing periods. (b) Time evolution of peak strength during the incubation process.

Despite these water content losses that induced soil stiffening by suction increase, it was possible to detect the progressive increase in the small-strain stiffness during incubation. On regarding unconfined compression tests, a similar progressive increase in terms of peak compressive strength during incubation was observed. However, in these tests suction increase due to some water content loss is partially masking the ageing results induced by biological action. New protocols are currently being performed to overcome this experimental limitation.

References

Arroyo, M., Pineda, J., Romero, E.: Shear wave measurements using bender elements in argillaceous rocks. Geotechnical Testing Journal 33(6), 488–498 (2010)

DeJong, J.T., Fritzges, M.B., Nüsslein, K.: Microbial Induced Cementation to Control Sand Response to Undrained Shear. ASCE Journal of Geotechnical and Geoenvironmental Engineering 132(11), 1381–1392 (2006)

Gray, D., Sorti, R.: Biothechnical and soil bioengineering slope stabilization. A practical Guide for Erosion control. John Wiley & Sons, Inc. (1996)

Ivanov, V., Chu, J.: Applications of microorganisms to geotechnical engineering for bioclogging and biocementation of soil in situ. Reviews in Environ. Sci. Biotechnol. 7, 139–153 (2008)

Morales, L., Garzón, E., Romero, E., Jommi, C.: Effects of a microbiological compound for the stabilisation of compacted soils on their microstructure and hydro-mechanical behaviour. In: Alonso, Gens (eds.) Proc. 5th Int. Conf. Unsaturated Soils, Barcelona, September 6-8, vol. 1, pp. 573–578. Taylor & Francis Group (2010)

Morales, L., López-González, J.A., Garzón, E., Giménez, A., Romero, E.: Crecimiento de cristales de $Caco_3$ como resultado de la actividad microbiológica en suelos. In: Proc. XXXI Reunión de la Sociedad Española de Mineralogía, Barcelona, September 7-10, vol. 15, pp. 141–142. Revista de la Sociedad Española de Mineralogía, Macla (2011)

Pineda, J.A.: Swelling and degradation of argillaceous rocks induced by relative humidity effects: an experimental study. PhD Thesis, Universitat Politècnica de Catalunya, Barcelona (2012)

Weiner, S., Addadi, L.: Design strategies in mineralized biological materials. Journal of Materials Chemistry 7(5), 689–702 (1997)

The Effect of Treatment with Fly Ash and Cement upon the Characteristic Curve of a Collapsing Soil

Percy Durand, Manuel Vázquez, and José L. Justo

Abstract. The soil-water characteristic curve (SWCC) of collapsing silty clay is studied, both with and without addition of cement and fly ash from coal combustion. Collapse (decrease in volume upon wetting) is a major cause of damage to buildings and routes of communication founded on low-density soils. The material analysed is a mixture of sand, silt and clay, collected from the Guadalquivir basin in the province of Seville (Spain). In this paper, the characteristic curves of the collapsing silty clay with 2% by weight of cement or fly ash are studied through pressure membrane and vacuum desiccator techniques. The results are analysed with the model developed by Fredlund & Xing (1994).

Keywords: SWCC, partially saturated soil, suction, fly ash, cement.

1 Introduction

In power plants, 70% to 75% of ashes present in the coal are collected in the form of fly ash. In Spain, for instance, in the year 2009 alone, 11.359 MW of thermoelectric power was generated by coal combustion, which generated some 8 million Mg of waste in the form of ash, together with the corresponding associated environmental problem (Red Eléctrica Española 2010).

Percy Durand
University of Seville, Seville, Spain
e-mail: percy@us.es

Manuel Vázquez
University of Seville, Seville, Spain
e-mail: mboza@us.es

José L. Justo
University of Seville, Seville, Spain
e-mail: jlj@us.es

The mechanical properties and morphological characteristics of fly ashes obtained from coal combustion are analysed by several authors (Han bing et al. 2009, Xue & Lu 2008). These wastes are used in the stabilization of problematic areas such as expansive soils (Rao et al. 2008).

2 Material Used in the Research

The material analysed is a mixture of sand (30%), silt (32%), and clay (38%) collected from the Guadalquivir basin in the province of Seville (Spain). The X-ray diffraction analysis carried out on the mixture indicates that it is composed of quartz, calcite, dolomite and vermiculite.

In order to obtain an open structure and collapsible behaviour, the soil mixture was compacted at constant static pressure with dry density and at a moisture content corresponding to 90% on the dry side of the optimum moisture content of the Standard Proctor test. Since the moisture content corresponding to this density (w = 8.8%) did not allow acceptable handling conditions (the specimen fell apart when the ring of compaction was removed), the moisture content was increased to 11.3% with a corresponding dry density of ρ_d = 1580 kg/m^3.

Table 1 provides the results obtained from grain size tests (% T200) and Standard Proctor compaction of the soil mixture (w_o and ρ_{max}), the density of the solid particles (ρ_s) and the initial values of the void ratio (e), the degree of saturation (S_{r0}), and matrix suction (Ψ_o) obtained with a UMS T5 tensiometer, and Atterberg Limits (w_L and I_P).

Table 1. Properties of the mixture of sand, silt and clay.

% T 200 ASTM	w_o (%)	ρ_{max} (kg/m^3)	ρ_s (kg/m^3)	e_0	S_{r0} %	Ψ_o (kPa)	w_L	I_P
73.5	14.5	1760	2650	0.68	45	94.5	31	13.6

Class F fly ash, according to standard ASTM C618-92, used during the experiment, directly proceeds from the first cyclonic separation from the boiler of a combustion power station with anthracite. Cement added to the mixture of sand, silt and clay is type CEM II/BL 32.5 N (UNE EN 197-1:2000).

3 Experiment Methodology

Compacted samples were prepared at constant static pressure with w = 11.3% and ρ_d = 1611 kg/m^3, whereby collapsing silty clay was combined with fly ash and cement in accordance with the Table 2.

Table 2. Composition of the samples tested.

Sample	Treatment	% Weight
IN	Untreated	100% Initial Mixture
IN-CEM	Treated with cement	98% Initial Mixture + 2% cement
IN-ASH	Treated with fly ash	98% Initial Mixture + 2% fly ash

The treatment of collapsing soil consists of mixing silty clay, compacted at constant static pressure, with 2% by weight of cement or fly ash.

The techniques used for the implementation and control of suction in different samples are grouped by range as follows: pressure membrane equipment for suction below 500 kPa; vapour-equilibrium technique in a vacuum desiccator with saline solutions (NaCl, $CaCl_2$) for suctions between 500 kPa and 150 MPa; vapour-equilibrium technique in a vacuum desiccator with acid solution (H_2SO_4) for suctions greater than 150 MPa.

4 Experimental Results

4.1 SWCC Curves

SWCC curves of drying and wetting paths for samples type IN, IN-CEM and IN-ASH are shown in fig. 1, fig. 2, and fig. 3. To the naked eye and for ranges of suction between 40 kPa and 1 GPa, an acceptable fit between experimental and calculated data stands out, in accordance with equation 1 proposed by Fredlund & Xing´s (1994).

$$\theta = \left[1 - \frac{\left(1 + \frac{\psi}{\psi_r} \right)}{1 + \frac{10^6}{\psi_r}} \right] \frac{\theta_s}{\ln\left[e + \left(\frac{\psi}{a} \right)^n \right]^m} \tag{1}$$

Where θ is the volumetric water content, θ_s is the volumetric water content at saturation, ψ is the suction and ψ_r is the suction associated with residual moisture. The three parameters of the model are *a*, *m* and *n*.

The parameters of the model that best fit the experimental results for samples type IN, IN-CEM and IN-ASH are shown in Table 3. In equation 1, the parameters *a* and *m* are associated with the input values of air and residual water content in the sample, respectively. A high value of *a,* implies a high air entry value and a high value of *m* means a lower value of residual moisture.

As for the parameter *n*, a high value of this parameter implies a uniform distribution of the pore size (Puppala et al. 2006), and SWCC curves with steep slopes in areas of point of air entry and of residual moisture (Hoyos et al. 2007, Fredlund & Xing 1994).

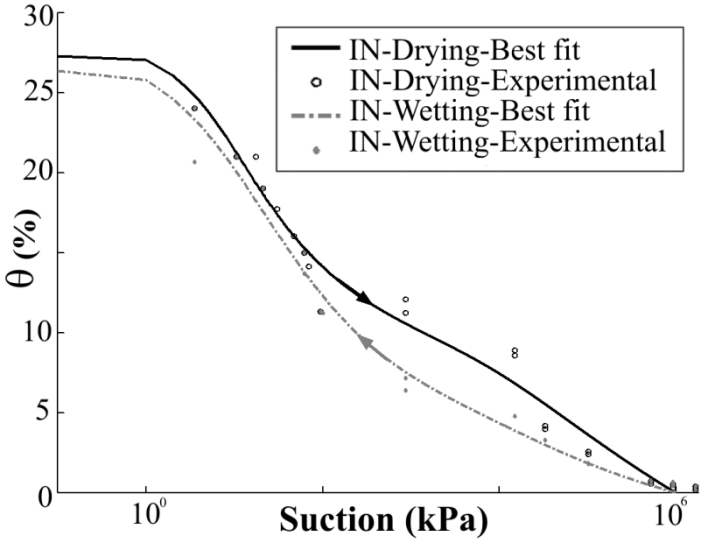

Fig. 1. SWCC for IN sample.

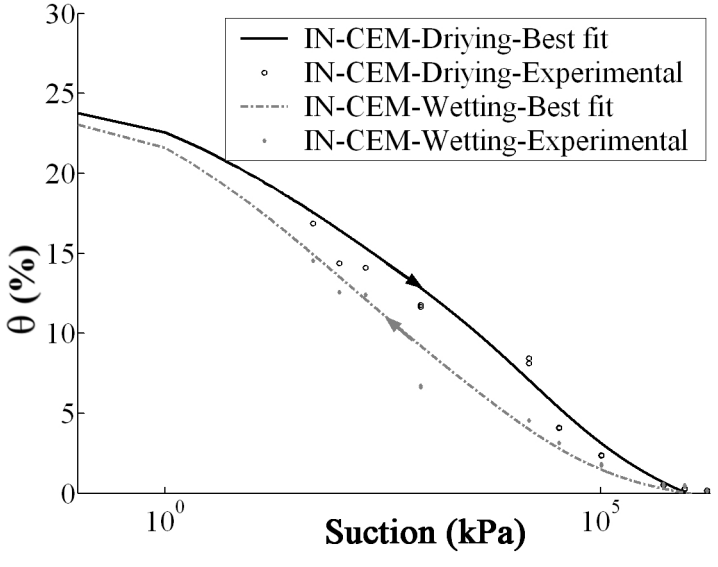

Fig. 2. SWCC for the IN-CEM sample.

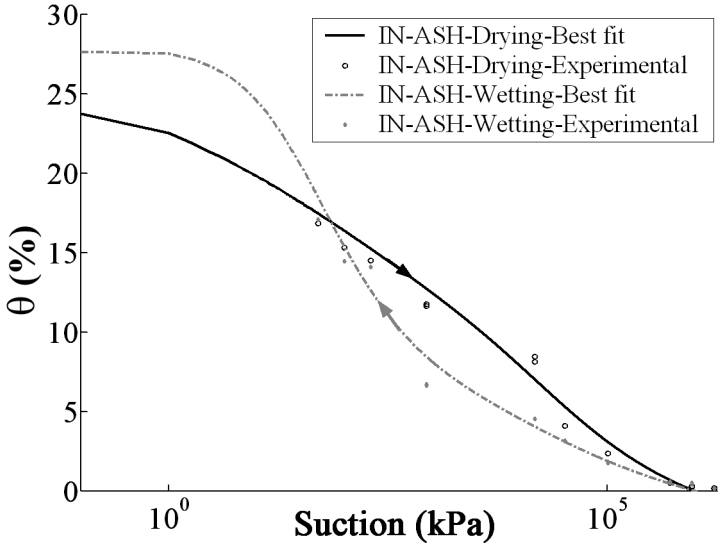

Fig. 3. SWCC for the IN-ASH sample.

Table 3. Parameters for the model of Fredlund & Xing´s (1994).

Parameters	IN Drying	IN Wetting	IN-CEM Drying	IN-CEM Wetting	IN-ASH Drying	IN-ASH Wetting
a	4.45	7.49	200.02	200.01	200.00	24.31
m	0.54	1.03	2.19	3.05	2.21	0.95
n	1.11	0.72	0.23	0.26	0.23	0.94
ψ_r	10010	10000	10000	10000	10000	10003

4.2 Influence of Different Treatments on the SWCC

The combination of collapsing soil with cement or fly ash reduces the saturation humidity of samples in the lowest range of suction (< 40 kPa) (fig. 1, fig. 2, and fig. 3). This loss of saturation humidity in the case of cement has been described by other authors in their research (Hoyos et al. 2007) and is attributed to the contribution of finer particles that are added to the original sample for both fly ash and cement. The fact that the finer particles of cement and ash occupy the interstitial spaces of the collapsing sample causes the air entry value of the treated samples to be much higher than in untreated samples, as reflected in the increase in the parameter *a* in the model of Fredlund & Xing´s (Table 3).

The largest air entry value of the treated samples compared to samples without treatment (fig. 1, fig. 2 and fig. 3) implies that the number of pores is reduced and that the distribution of the pore size is not as uniform as is reflected in the table for the lowest value of parameter *n*.

The samples were subjected to suctions of the order of 1 GPa, in order to carry out a more reliable study of the parameter *m* associated with residual moisture. In both treatments, this parameter increases with respect to its value associated with the initial condition. An increase in the value of *m* indicates a decrease in the residual moisture of the sample tested (Fredlund & Xing´s 1994).

It is observed that the saturation humidity is lower in the latter two samples than the first one at the end of the wetting process (fig. 1, fig. 2 and fig. 3). This behaviour is explained by the existence of a small percentage of vermiculite, with laminar microstructure similar to montmorillonite, in the composition of the collapsing silty clay.

Comparing samples IN-ASH and IN-CEM, it is observed that the saturation humidity is much lower in the latter, mainly due to the hydration and hardening of the particles that cause the closure of many pores (fig. 1, fig. 2 and fig. 3), which in turn reduces the interstitial space that can otherwise be occupied by water during the saturation process. Class-F fly ash is not a cementing agent and this effect is not visible in the samples treated in this way.

Hydration and hardening of the cement cause the air entry value of IN-CEM samples to be much greater than that of untreated samples, as is indicated by the increase in parameter *a* (see Table 3).

Sample IN-ASH has a slightly higher air entry value than the initial sample. The parameter *m* increases slightly while the value *n* decreases in the sample IN-CEM, in comparison with the sample without treatment (see Table 3). This indicates that the cement, in the wetting path, generates less residual moisture and a less uniform distribution of pore size. In the case of IN-ASH, the values of *m* and *n* are similar to those obtained with untreated samples.

5 Conclusions

This paper presents the characteristic curves (SWCC) of collapsing silty clay subject to two separate treatments: the addition of 2% by weight of either cement or fly ash. The results of the experiments are analysed with the model developed by Fredlund & Xing´s (1994).

In the course of drying, the two treated samples display very similar behaviour: they reduce saturation humidity, increase the air entry value, lower residual moisture, and do not generate a uniform distribution of pore size. In the wetting paths, cement and fly ash treatments reduce the soil saturation humidity, with cement leading to an even greater loss of moisture in the hydration and setting processes. The air entry value of the samples IN-CEM is much greater than that of samples IN-ASH. The behaviour of this sample differs very little from the behaviour of the sample without treatment.

For both wetting and the drying paths, treatment with cement has proved itself to provide the greatest reduction in the size and number of free pores, a fact that is borne out by the increase in the air entry value in the sample IN-CEM when compared with samples IN and IN-ASH. A reduction of the pore volume is associated with a greater rigidity and a reduced deformability of collapsing silty clay.

References

ASTM C618-92a, Standard specification for fly ash or raw or calcinate natural pozzoland for use as a mineral admixture in portland cement concrete. American Society for Testing and Materials, Annual Book of ASTM Standards, Pennsylvania, vol. 04(02) (2005)

Fredlund, D.G., Xing, A.: Equations for the soil-water characteristic curve. Can. Geotech. J. 31, 521–532 (1994)

Hang Bing, L., Chang, Y., Hai Bin, W.: Experimental research on the mechanical parameter of fly ash soil. In: Proceedings of the 9th International Conference of Chinese Transportation Professionals, ICCTP 2009: Critical Issues in Transportation System Planning, Development, and Management, vol. 358, pp. 41–48 (2009)

Hoyos, L.R., Thudi, H.R., Puppala, A.J.: Soil-Water retention properties of cement treated clay. In: Proceedings of Sessions of Geo-Denver 2007. Congress: Problematic Soils and Rocks and In Situ Characterization, vol. 162, pp. 4–11. Geotechnical Special Publication (2007)

Puppala, A.J., Konnamas, P., Vanapalli, S.K.: Soil-water characteristic curves of stabilized expansive soils. Journal of Geotechnical and Geoenvironmental Engineering 132, 736–751 (2006)

Rao, M.R., Rao, A.S., Babu, R.D.: Efficacy of lime-stabilised fly ash in expansive soils. Proceedings of the Institution of Civil Engineers: Ground Improvement 161, 23–29 (2008)

Red Eléctrica Española, Informe del sistema eléctrico español en. In: Editorial Red Eléctrica Española, Madrid (2010), ISBN M-31202-2010

Asociación Española de Normalización y Certificación. UNE EN 197-1-2000. Parte 1: Composición, especificaciones y criterios de conformidad de los cementos comunes, Madrid (2000)

Xue, Q., Lu, S.: Microstructure of ferrospheres in fly ashes: SEM, EDX and ESEM analysis. Journal of Zhejiang University: Science A 9, 1595–1600 (2008)

Influence of Kaolin Mixture on Unsaturated Shear Strength of Decomposed Granitic Silty Sand

Apiniti Jotisankasa, Auckpath Sawangsuriya, Patipat Booncharoenpanich, and Suttisak Soralump

Abstract. The paper reports on the influence of kaolin content on shear strength of a decomposed granitic silty sand. The granitic soil was mixed with kaolin, with the purpose of erosion protection and slope stabilization. Shear strength and water retention behaviour of the decomposed granitic silty sand, mixed with different proportions of kaolin (from zero up to 20% by weight) were tested. A tensiometer was also incorporated in a direct shear box to investigate unsaturated properties. The silty sand mixed with 10% kaolin possesses the highest saturated shear strength. The effective cohesion increases with increasing kaolin content, while the effective friction angle reaches the maximum value at the 10% kaolin. In the unsaturated condition, the angle of shear resistance with respect to suction increases with kaolin content. Based on the test results and field observation, the silty sand mixed with 10% kaolin appears to be most erosion-resistant.

Keywords: suction, shear strength, erosion protection, decomposed granite.

Apiniti Jotisankasa
Kasetsart University, Bangkok, Thailand
e-mail: fengatj@ku.ac.th

Auckpath Sawangsuriya
Department of Highways, Bangkok, Thailand
e-mail: sawangsuriya@gmail.com

Patipat Booncharoenpanich
formerly Kasetsart University, Bangkok, Thailand
e-mail: dasen24@hotmail.com

Suttisak Soralump
Kasetsart University, Bangkok, Thailand
e-mail: soralump_s@yahoo.com

1 Background

Shallow slope failure and surface erosion frequently occur in cut/fill granitic soil slopes causing damages to numerous infrastructures in Thailand. The residual granitic soil is one of the most commonly found and used as fill materials, consisting of predominantly sand and silt, which are very susceptible to erosion, and is of relatively low shear strength. In fact, there are several erosion control techniques commonly employed in engineering practices namely the utilization of vetiver grass, geotextile, geocell, jute net, soil-blanket, etc. One of the simplest protection methods in Thailand is to cover the slope or replace the granitic soil at shallow depth with a more plasticity soil (preferably with PI of less than 15%) which tends to minimize the infiltration into the soil slope as well as increasing the shear strength and the corresponding erosion resistance.

There was however still a limited number of studies (e.g. Kyu-Hyun et al., 2007) that investigated the influence of fine/clay contents on strength improvement of silty sand. Especially those considered unsaturated shear strength were still relatively rare. This paper thus reported on both saturated and unsaturated strength of granitic residual soil mixed with various proportions of kaolin. Some application of the test findings on erosion and slope protection will be presented. Finally, a field observation will be briefly reported to support the conclusion made based on the laboratory results.

2 Granitic Silt and Kaolin Mixture

The materials used in this study are decomposed granitic silty sand mixed with different amounts of kaolin. The sample was collected from a site near Wat Sukim Pagoda in Chantaburi province, Eastern Thailand. It is classified as silty sand (SM) based on the Unified Soil Classification System (USCS). The kaolin used was obtained from an industrial quarry in Uttradit province, North Thailand. Two materials were mixed thoroughly to form new mixtures with percentage (by weight) of Kaolin varying from zero to 20%. Basic properties of these different mixtures are shown in Table 1. Fig. 1 shows compaction curves of the mixtures based on the standard Proctor test. Variations of optimum moisture content and maximum dry density with kaolin contents are shown in Figs. 2 and 3. For the shear strength and soil-water retention curve, the samples used were compacted using the static method (i.e., compressing the soil mixture in one layer in a rigid mould using a loading frame) to initial properties as shown in Figs. 2 and 3. The standard Proctor dry densities and optimum water contents are the reference values for the static compaction of samples. Table 2 shows the initial properties of the as-compacted specimens. Even though the values of as-compacted suction were not measured during the tests, they were estimated based on the SWRC as shown in Table 2. The accuracy of these estimated as-compacted suctions is around $\pm$ 5kPa.

The soil-water retention curves (SWRC) of the compacted samples were determined using a miniature tensiometer for both drying and wetting paths. Each

sample was gradually either wetted or dried in companion with suction monitored incrementally during each stage. For drying, each sample's top surface was left exposed to air for a few hours (thereby reducing moisture content by 1-2%) before rewrapped and carefully sealed in a container. For wetting, some mist or spray water was applied directly to the sample surface until the desired increase of water content was reached. A minimum curing period of several days between each increment was allowed for suction equilibration throughout the sample. The values of suction both at the upper and lower surface were measured to ensure the uniformity of suction. Figs. 4 and 5 show the grain size distribution and SWRC curves during drying path.

Table 1. Basic properties of the materials.

Soil Symbol	Soil Type	Liquid Limit	Plastic Limit	Plasticity Index	G_s
SM	SM	-	-	-	2.63
SM+k 10%	SM	36.0	28.3	7.7	2.64
SM+k 15%	SM	33.6	25.1	8.5	2.64
SM+k 20%	SC	35.6	22.6	13.0	2.66

3 Shear Strength of Kaolin-Residual Soil Mixtures

3.1 Fully Saturated Strength

Conventional consolidated drained direct shear tests were carried out on the samples (63 mm in diameter) of different percentage of kaolin contents (at a shearing rate of 0.05 mm/min). Fig. 6 shows the failure envelopes of different mixtures. It can be clearly seen that a soil mixture with 10% kaolin (PI of 7.7%) exhibited the highest saturated shear strength, while a 20% kaolin mixture (PI of 13%) exhibited the lowest. Both mixtures however had a similar maximum dry density (~1.71 T/m^3) as shown in Fig. 2. Obviously, the clay fraction had a significant influence on the saturated shear strength.

3.2 Unsaturated Strength

A suction-monitored direct shear box, which incorporated a miniature tensiometer through its top cap (Jotisankasa et al., 2010), was used to determine unsaturated shear strength of the compacted samples. Samples were either wetted or dried to obtain the desired suction (ranging from zero to 45 kPa) outside the shear box prior to shearing (at the rate of 0.05 mm/min). This range of initial suction prior to shearing (as shown in Figs 7 and 8) was chosen because it encompassed the suction values commonly found in slopes in Thailand during rainy season. Figs 7 and 8 show variation of shear strength and suction with displacement for the SM+K10% samples, tested at a normal stress of 15.5 kPa. The values of initial suction indicated in Figs 7 and 8 are the suction value prior to shearing and not the

value of as-compacted suction. The failure envelope plotted between peak strength and suction is shown in Fig. 9. Again, the samples with 10% kaolin have the highest unsaturated strength.

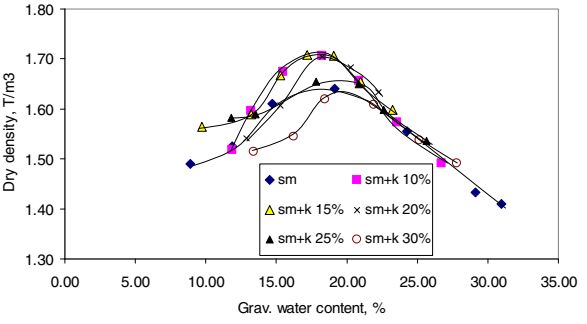

Fig. 1. Compaction curves for different mixtures.

Table 2. Initial state of the as-compacted specimen.

Soil Symbol	γ_d (T/m^3)	w, %	S_r, %	Void ratio, e	Estimated as-compacted suction, kPa
SM	1.65	17.5	77.5	0.594	25
SM+k 10%	1.71	17.8	86.4	0.544	30
SM+k 15%	1.72	18.0	88.8	0.535	30
SM+k 20%	1.71	18.5	88.6	0.556	40

4 Field Application

To validate the influence of kaolin content on strength of granitic soil, the desired mixture was consequently applied in a test fill slope near Doi Intanon, Chiangmai Province, North of Thailand. The slope consisted of residual silty sand (classified as SM) that previously suffered from severe surface erosion due to heavy rainfall. Several soil cover systems, e.g. natural geotextile (locally known as natural blanket), geocell, and erosion control mat, were later applied to different parts of slope to investigate their performance. Fig. 10 shows two sections that were covered by: (a) natural blanket alone (left); (b) natural blanket overlying plasticity soil (with PI of 8 to 12% specification and 10-15 cm in thickness) (right). The slope (b), covered by both natural blanket and soil cover layer, showed less surface erosion than the slope (a) which was covered with only natural blanket. Another slope (not shown here), used only soil cover without natural blanket, however suffered more severe erosion. It was believed that the natural blanket was necessary to maintain adequate suction in the soil cover and thus resulting in the erosion-resistance.

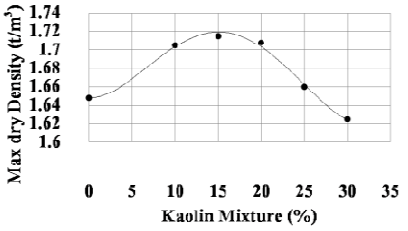

Fig. 2. Variation of maximum dry density with kaolin mixture percentage.

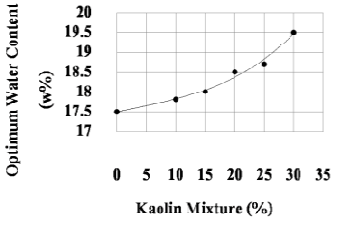

Fig. 3. Variation of optimum water content with kaolin mixture percentage.

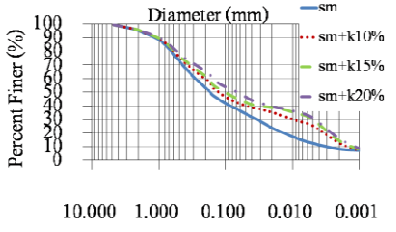

Fig. 4. Grain size distribution curve for different mixtures.

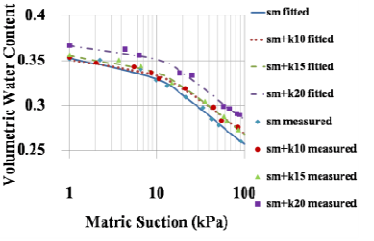

Fig. 5. Soil-Water Characteristic of the mixtures (drying path).

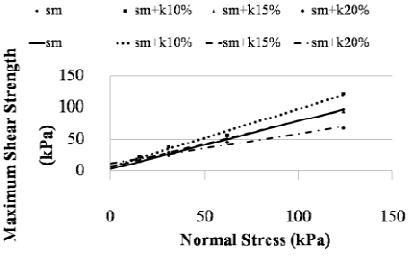

Fig. 6. Fully saturated failure envelopes of different mixtures.

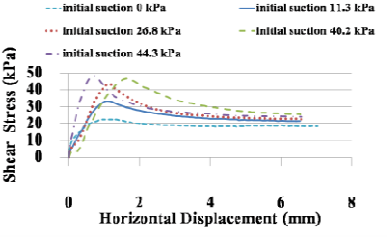

Fig. 7. Shear strength – horizontal displacement for SM+K10% samples.

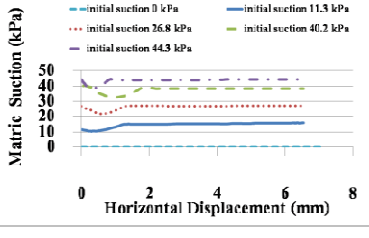

Fig. 8. Suction– horizontal displacement for SM+K10% samples.

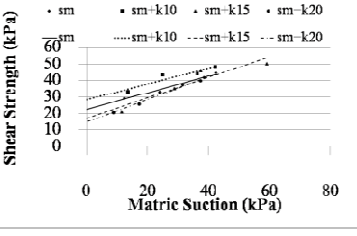

Fig. 9. Failure envelopes between strength and suction**.**

Fig. 10. Test slope with a section (left) covered with natural blanket, and another section (right) covered with natural blanket and plasticity soil.

5 Conclusion

The decomposed granitic silty sand in Thailand normally suffered from surface erosion due to rainfall. Based on direct shear test results, mixing the silty sand with a clayey material to obtain a new mixture with plasticity index of about 8% helps improve the shear strength of the material both in saturated and unsaturated conditions. Field observation in a test fill slope was illustrated to support this.

Acknowledgements. National Research Council of Thailand (NRCT), Kasetsart University Research and Development Institute (KURDI) and Department of Highways (DOH) are gratefully acknowledged for their financial supports.

References

Jotisankasa, A., Mairaing, W.: Suction-monitored direct shear testing of residual soils from landslide-prone areas. J.Geotechnical and Geoenvironmental Engineering, ASCE 136(3), 533–537 (2010)

Kyu-Hyun, L., Sang-Seom, J., Tae-Hyung, K.: Effect of Fines on the Stability of Unsaturated Soil Slope. Journal of the KGS 23(3), 101–109 (2007)

Mechanical Behaviour of Unsaturated Lime-Treated Clays: Experiments and Modelling

Maria Mavroulidou, Xiwei Zhang, Roberto Tamagnini, Michael J. Gunn, Worku Seyoum, and Robert Hiley

Abstract. This paper gives a brief account of ongoing research on the mechanical behaviour of lime-treated clays. First indicative results of a series of suction-controlled triaxial tests using the axis translation technique are presented based on which the effect of cementation is assessed. The results showed the overall beneficial effect of the lime on the compressibility behaviour of the soil as well as the dramatic increase in strength gained for ranges of strain relevant to engineering applications. A constitutive model for the behaviour of lime-treated soils is then introduced to account for the combined effects of suction and cementation.

Keywords: lime treatment, triaxial testing, constitutive modelling.

1 Introduction

Chemical soil improvement using additives such as lime is a technique that has been used extensively in construction, most commonly for pavement applications. With this application in mind, most international literature on lime treated soils focuses on simple tests such as CBR or unconfined compression tests. With an increasing use of the technique in a wider range of applications, the need has emerged for more thorough experimental evidence. This could provide the basis for constitutive models able to describe the behaviour of lime-treated soils for a

Maria Mavroulidou · Xiwei Zhang · Michael Gunn · Worku Seyoum · Robert Hiley
London South Bank University, London, UK
e-mail: mavroum@lsbu.ac.uk, zhangxw@lsbu.ac.uk, gunnm@lsbu.ac.uk, seyoumw@lsbu.ac.uk, hileyr@lsbu.ac.uk

Roberto Tamagnini
Formerly: London South Bank University, London, UK
e-mail: rob.tamag@gmail.com

variety of problems under saturated and unsaturated conditions. The latter aspect is particularly relevant, as lime-treated soils are typically compacted after treatment, and hence, by definition unsaturated. This paper presents indicative suction-controlled testing results of untreated and lime-treated London Clay. A constitutive model based on the extension of Tamagnini (2004) is then introduced to simulate the behaviour of the cemented lime-treated soil. It consists of a simple generalisation of the Modified Cam-Clay model with multiple isotropic hardening mechanisms and uses an appropriate generalised effective stress variable.

2 Experiments on the Mechanical Behaviour of Lime-Treated Soil

Suction-controlled triaxial tests using the axis translation technique were performed using pulverised bulk London Clay samples of which the portion passing through a BS 425 μm sieve was retained. The clay powder was thoroughly mixed with water to achieve a water content of 25.5% (the Proctor optimum) and left to hydrate in sealed bags for 72 h. The minimum required lime percentage of 4% for this soil was determined through the initial consumption of lime (ICL) test as well as the lime fixation point test (LFP). For consistence in the comparisons between the results of the two different soils, it was decided to compact statically all specimens at the same target dry density of 1.43 g/cm^3, corresponding to the maximum standard Proctor dry density of the London Clay soil and not to each soil's Proctor optimum characteristics (although this resulted in a higher compactive effort for the lime-treated soil). However for the lime treated specimens (which were thus prepared dry of the Proctor optimum of the lime treated soil) an additional 2% of water was added. This small additional amount of water was used for lime-treated specimens to ensure that enough water was available in view of the chemical reactions. The lime treated specimens were left to cure for a week wrapped in several layers of cling film and stored in controlled environmental conditions. The necessary curing time was determined based on prior Unconsolidated Undrained (UU) triaxial testing, which showed that for this amount of lime and curing method, for six different curing periods between 1 day and 166 days did not result in any further improvement of the shear strength of the soil beyond that already achieved after 7 days of curing. This was also confirmed by swelling test results showing that for samples cured at times beyond seven days, the swelling of the lime-treated soil was not further reduced compared to that of the untreated soil. The specimens were isotropically consolidated and then subject to constant suction shearing following a $q/(p-u_a)=3$ path with the exception of a few specimens that were sheared as compacted (unconsolidated undrained shearing). Fig. 1 presents isotropic compression results. These showed that, overall, lime treatment had a favourable effect on the compressibility of the material, which was drastically reduced both before and after yield. The yield stress of the lime-treated soil was also higher than that of the untreated soil, which is consistent with the behaviour of cemented geomaterials. However for the confining stresses involved in this study the compressibility

line of the cemented lime-treated soil did not eventually converge to that of the untreated soil (i.e. the range of pressures applied only captured perhaps some initial yield linked to the start of destructuration of the cementation bonds but not that corresponding to the full breakage of cementation bonds). Note that although the two soils were initially compacted at the same dry densities the London Clay underwent swelling during saturation so that the void ratio of the soil before isotropic compression had increased compared to that of the lime-treated soil. Conversely, very little swelling was noted for the lime-treated specimens. This shows the beneficial effect of the lime on the volumetric stability of the London Clay when subject to water content variations. Fig. 2 presents isotropic compression results of the lime-treated soil for different levels of suction. These do not give a clear indication that suction allows the Normal Compression Line (NCL) to cross into meta-stable states above the zero suction NCL (as is the case for uncemented partially saturated soils). The findings are consistent with those obtained from suction-controlled K_0 compression testing, not shown here for the sake of brevity. This could possibly indicate that the behaviour of the lime-treated soil in isotropic compression was largely controlled by the chemical reactions due to lime rather than suction. However for this statement to be conclusive the data needs to be extrapolated to higher pressures. Fig. 3 shows indicative comparative stress-strain relationships of untreated London Clay and lime-treated London Clay specimens tested under various conditions. All London Clay specimens show a strain hardening behaviour without any apparent peak in the stress irrespective of the suction level although there is an increase in strength with increasing suction as expected. Conversely the lime-treated soil shows a very pronounced peak in the strength within relatively low strain levels, followed by strain softening irrespective of the testing conditions, with the stress decreasing dramatically after only 4% of axial strain. This is consistent with the breakage of the cementation bonds. Whereas there is an increase in the peak strength for higher suction values from the relative difference between the strength of the treated and respective untreated specimens strengths it can be inferred that the predominant effect controlling strength is cementation bonding while this is not damaged.

3 Constitutive Modelling

The suggested elastoplastic model to describe the behaviour of unsaturated lime-treated soils is based on the extended Modified Cam Clay (MCC) constitutive model for unsaturated soils by Tamagnini (2004). The latter model is further extended to include the effect of cementation using a multiple-hardening mechanism accounting for the effects of changes in both the degree of saturation and cementation. Although in the representation of the experimental results the mean net stress was used as a more familiar representation, the model adopts a Bishop's-type effective stress, as a more appropriate stress variable, written as:

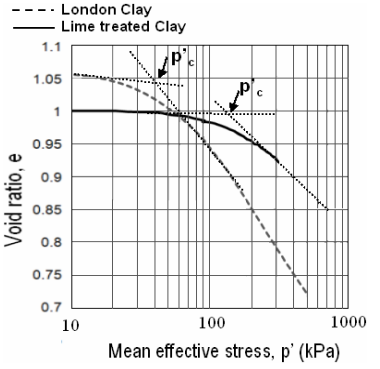

Fig. 1. Effect of lime on yield stress (indicative results from saturated samples)

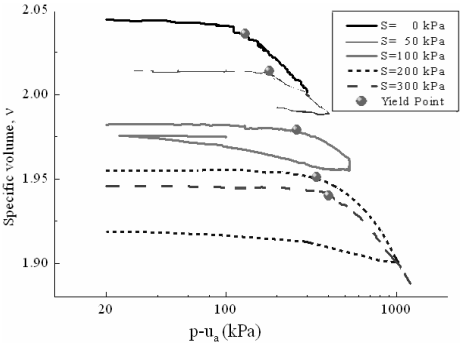

Fig. 2. Results of suction-controlled isotropic compression tests

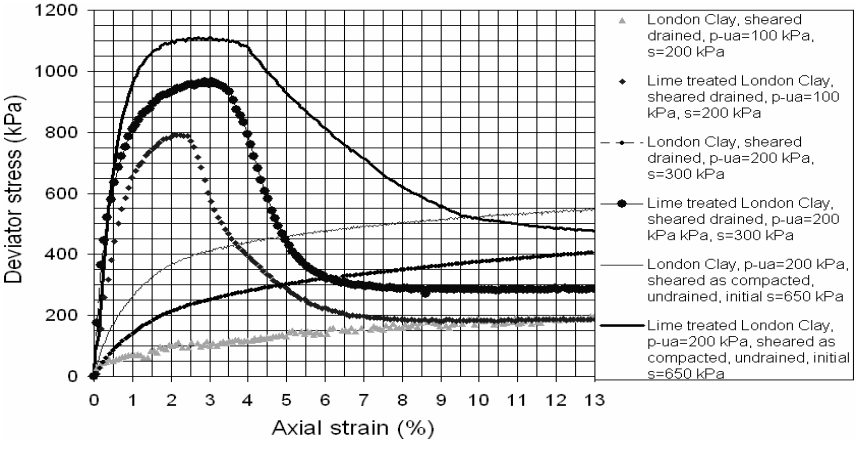

Fig. 3. Triaxial testing: indicative comparative q:ε_a results

$$\sigma'_{ij} = \sigma_{ij} - u_a \delta_{ij} + S_r \left(u_a - u_w\right) \delta_{ij} \tag{1}$$

where σ_{ij} are total stresses u_a and u_w = the air pressure and the water pressure respectively; δ_{ij} is the Kronecker delta and S_r = the degree of saturation of the wetting fluid. As in the MCC model, the elastic response within the yield locus is described by the shear modulus G (or Poisson's ratio μ) and the bulk modulus K through the elastic parameter κ (the slope of the unloading-reloading line). The bulk modulus is not a constant but depends on the mean effective stress, p', specific volume, v, and swelling line slope κ. At any point in the soil it is calculated as $K = vp'/\kappa$. Volumetric and deviatoric elastic strains are written respectively as $d\varepsilon_v^e = dp'/K = dp'\kappa/vp'$ and $d\varepsilon_q^e = dq/(3G)$; (where dq is the change in deviator stress q). Assuming an associated flow rule, we obtain:

$$d\sigma'_{ij} = D^{e}_{ijkl}\left[d\varepsilon_{kl} - d\lambda \frac{\partial f}{\partial \sigma'_{kl}} \right] \tag{2}$$

where $d\lambda$ is the plastic multiplier and f is the loading surface of the MCC model, which is a volumetric hardening model expressed as:

$$f = q^2 + M^2 p'(p' - p'_c) = 0 \tag{3}$$

where M is the slope of the critical state line in the p':q plane, and the pre-consolidation pressure p'_c is the internal variable describing the evolution of the ellipse dimension (i.e. the yield loci expanding at constant shape) and hence isotropic hardening. In the MCC model the change in p'_c (here denoted as $p'_{c(MCC)}$), and hence the evolution of the yield function, is controlled by the plastic volumetric strain ε_v^p:

$$dp'_{c(MCC)} = (vp'_c / (\lambda - \kappa))d\varepsilon^p \tag{4}$$

where λ is the slope of the normal compression line, i.e. $v = N - \lambda \ln p'_c$ in which N is a soil constant specifying the position of the normal compression line in the compression plane p':v). In the present extended model, the change in p'_c also accounts for effects of bonding/debonding and changes in S_r as follows:

$$dp'_c = dp'_{c(MCC)} + dp'_{c(BOND)} + dp'_{c(UNS)} \tag{5}$$

where: $dp'_{c(BOND)} = \omega p'_c dm$ and $dp'_{c(UNS)} = -bp'_c dS_r$ (6)

$dp'_{c(BOND)}$ describes the evolution of the yield surface linked to changes in the amount of bonding mass m produced by lime: an increase of the bonding mass $dm>0$ causes an expansion of the elastic domain; loading-induced destructuration causes a decrease in the bonding mass $dm < 0$ and the shrinking of the elastic domain; ω, a parameter controlling the rate of change in p'_c caused by changes in the cementation bonding mass m, is the only additional constitutive parameter of the suggested extended MCC model to account for bonding due to cementation. Similarly, $dp'_{c(UNS)}$ describes the evolution of the yield surface produced by changes in the degree of saturation S_r which may occur even if the current stress lies in the elastic domain; b, a parameter controlling the rate of change in p'_c caused by changes in the degree of saturation S_r, is the only additional constitutive parameter of the suggested extended MCC model to account for bonding due to partial saturation. The suggested model was implemented into the commercial software Abaqus. Implicit integration was performed enhancing the return-mapping scheme proposed Simo & Hughes (1998) as described in Tamagnini et al. (2010).

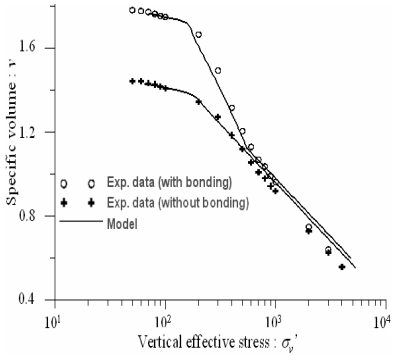

Fig. 4. Destructuration in isotropic compression

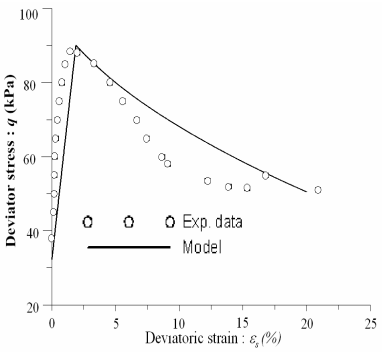

Fig. 5. Destructuration in shearing

The model, which was developed in parallel with the testing programme, was initially validated using closed form solutions and experimental results from a number of bonded geomaterials (see e.g. fig. 4 and 5 simulating destructuration during isotropic compression and triaxial testing using Abaqus and Tamagnini et al 2010). The curve fitting of the recently obtained lime-treated soil triaxial results using this model is currently underway.

4 Conclusions

The research addressed a problem of considerable practical importance, the study of the effects of lime treatment on natural soils. This concerned suction-controlled triaxial testing of a lime-treated clay and a constitutive model, implemented into the commercial software Abaqus. This can provide a predictive tool for engineers to quantify the response of the lime-treated soil in a wide range of applications. The experimental analyses results showed the beneficial effect of the lime on the soil properties and behaviour. These were shown to be mostly controlled by the effects of lime rather than suction.

Acknowledgements. The financial support received by the UK Engineering and Physical Sciences Research Council (EPSRC) through grant EP/E037305/1 is gratefully acknowledged. The authors would like to thank Z.Kichou for his help with specimen preparation.

References

Simo, J.C., Hughes, T.J.R.: Computational Inelasticity (Interdisciplinary Applied Mathematics). Springer, Berlin (1998)

Tamagnini, R.: An extended Cam-clay model for unsaturated soils with hydraulic hysteresis. Géotechnique 54(3), 223–228 (2004)

Tamagnini, R., Mavroulidou, M., Gunn, M.J.: Implicit integration of a constitutive model for partly saturated structured porous materials. In: Alonso, E., Gens, A. (eds.) Unsaturated Soils, pp. 1087–1092. Taylor and Francis, London (2010)

Collapse upon Wetting of Lime Stabilised Pyroclastic Soils

Manuela Cecconi, Andrea Ferretti, Elisabetta Cattoni, Giacomo Russo, and Anastasia Capotosto

Abstract. Compacted soils are commonly used in the construction of geotechnical works such as road embankments and earth dams. Several investigators have highlighted the wetting-induced behaviour of compacted soils resulting in collapse of the soil skeleton with increase of volume strains. The addition of lime, with the subsequent physic-chemical reactions, generally reduces the collapse potential of the stabilised soil if compared to the not treated one. In the paper, soil collapse has been investigated by means of soaking tests under constant stress on reconstituted not treated and lime stabilised pyroclastic soils. The soil collapse has been analysed for stress levels corresponding to pre-yield, yield and post-yield condition. The experimental results show the relevant dependency of the collapsible behaviour on the initial state of the compacted samples (void ratio, water content), the treatment parameters (curing time) and the reference stress level.

Keywords: pyroclastic soils, lime stabilisation, soil collapse, soaking tests, curing time.

Manuela Cecconi
Università di Perugia, Perugia, Italy
e-mail: ceccon@unipg.it

Andrea Ferretti
Università di Perugia, Perugia, Italy
e-mail: andreaferretti84@gmail.com

Elisabetta Cattoni
Università e-Campus, Novedrate (CO), Italy
e-mail: elisabetta.cattoni@uniecampus.it

Giacomo Russo
Università di Cassino, Cassino, Italy
e-mail: giarusso@unicas.it

Anastasia Capotosto
Università di Cassino, Cassino, Italy
e-mail: a.capotosto@unicas.it

1 Introduction

In some areas of the Central and Southern Italy pyroclastic soils are widespread. Since they are generally considered as problematic soils due to their nature, heterogeneity, microstructure features, and their complex unsaturated hydro-mechanical behaviour (e.g. structural collapse upon wetting), pyroclastic soils are not commonly used for earthwork construction. Their reuse by means of an improvement technique such as lime stabilisation is then an important perspective towards the sustainability for the construction of large infrastructures.

Even though it is well known that natural pozzolanas are very reactive with calcium oxide (CaO), there is a lack of systematic studies on the mechanical behaviour of lime stabilised pyroclastic soils. This circumstance has motivated the present research, aimed at assessing the improvement of physical and mechanical properties of different pyroclastic soils induced by addition of lime. Cecconi et al. (2010a) showed the suitability to lime treatment of two pyroclastic soils. Cecconi et al. (2011a) and Russo et al. (2011) highlighted the effects of treatment parameters (type and percent by weight of lime, compaction energy, initial water content, curing time) on the engineering properties of the stabilised pyroclastic soils. In this paper some results on the collapse behaviour upon wetting of reconstituted not treated and lime stabilised pyroclastic soils are reported.

2 Materials and Procedures

Two pyroclastic soils have been considered in this study; these are representative units of two wide volcanic regions, the volcanic complex of Colli Albani involving the south-east area of the city of Roma and the Campania region with the Somma-Vesuvius volcano. The Monteforte (MF) pyroclastic soil is a weathered and humified ashy soil belonging to the stratigraphic succession of Somma-Vesuvius eruptions products (fallout deposits). The MF soil characterizes the upper layers (stratum n.2) of the succession in the test site of Monte Faggeto, about 40 km northwest of the volcano Somma-Vesuvius, where an ongoing experimental research project on mudflows in pyroclastic soils is actually carried on (Evangelista et al., 2008). The relevant hydro-mechanical properties of MF soil are discussed in Papa (2007), Papa et al. (2008) and Nicotera et al. (2008). The second pyroclastic soil herein investigated is a coarse-grained pyroclastic weak rock originated from pyroclastic flows. The main outcomes of the study of the mechanical and hydraulic properties of such deposit (Pozzolana Nera, PN) in saturated and unsaturated conditions are described in detail in Cecconi & Viggiani (2001), Cattoni et al. (2007) and Cecconi et al. (2010b).

Reconstituted tested samples were prepared using a selected passing percentage (1 mm for PN soil, 2 mm for MF soil). Lime treated samples were prepared by hand mixing the soil with a fixed amount of quicklime powder and distilled water, allowing the quicklime to hydrate for 24 h. pH measurements were carried on stabilized samples prepared with different amounts of CaO varying in the range 0.07 – 15%, repeating the measurement at increasing curing time. Also, grain size

distribution, specific gravity, plastic limit, liquid limit of the treated soils were determined at various curing time (see Cecconi et al., 2010a for details). Grain size distributions were determined for both not-treated and stabilised MF and PN soils, at increasing curing times of 24h (referred to as 0 days), 7, 14, 28, 42 days and 24h (referred to as 0 days), 7, 14, 28, 48, 56, 84 days for MF and PN soils respectively. Figs. 1a and 1b show that significant effects of lime addition occur in the short term, leading to the reduction of the fine fraction and the increase of the coarser fraction. The formation of larger aggregates is mainly due to the flocculation of grains induced by ionic exchange on the short term, and this behavior still persists for longer curing times.

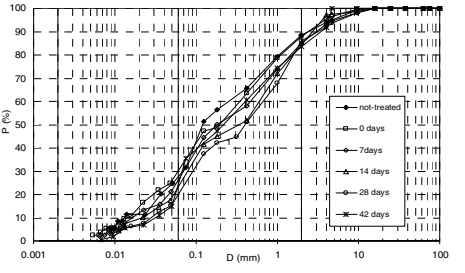

Fig. 1a. Grain size distribution curves obtained for not-treated and stabilized MF.

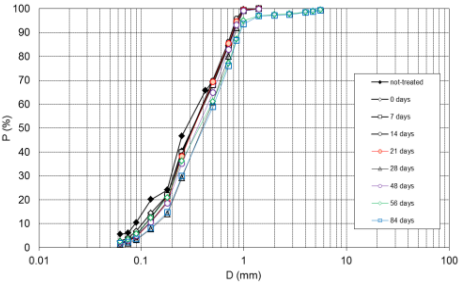

Fig. 1b. Grain size distribution curves obtained for not-treated and stabilized PN.

Soaking tests were performed upon one-dimensional loading; the adopted equipment consisted of standard oedometer cells. Vertical stress was conventionally applied in successive steps ($\Delta\sigma_v/\sigma_v = 1$). However, stress increments were applied every hour, in view of the fact that the 90% of settlement systematically took place very quickly, in less than 10 min. Micrometer dial gauges with an accuracy of 0.001 mm were used to measure vertical displacements.

Lime treated unsaturated samples for oedometer tests were prepared following this procedure: the soil was hand mixed with a weight-percentage of quicklime at fixed water content (MF soil: $w_0 = 30\%$, lime content = 7%; PN soil: $w_0 = 20\%$,

lime content = 10%). The mixture was then hand compacted inside the oedometer mould. Samples of MF soil were prepared at initial voids ratio e_0 ranging between 1.28 and 1.33. Two distinct sets of reconstituted samples of PN were obtained, the former characterized by relatively "low" values of e_0 (= 1.0÷1.1), the latter by relatively large void ratios (e_0 = 1.4÷1.6). It is noted that even if much care was given in the sample-preparation technique, it was not possible to achieve through dynamic compaction the initial voids ratio of the natural parent material; this, in fact, is about 0.8 ÷ 0.9, i.e. rather low if compared to the typical values estimated for other pyroclastic soils (Cecconi et al., 2011b).

3 Experimental Results

The one dimensional compressibility curves of saturated and unsaturated samples of the Monteforte ashy soil are reported in Fig. 2. The experimental curves highlight the combined effect of partial saturation and compaction-induced structure in the investigated stress range. The unsaturated samples prepared at similar void ratio were characterized by initial saturation degrees respectively of 62% and 68%. The reduced volumetric strain observed for lower value of degree of saturation is consistent with the higher suction developed during compaction.

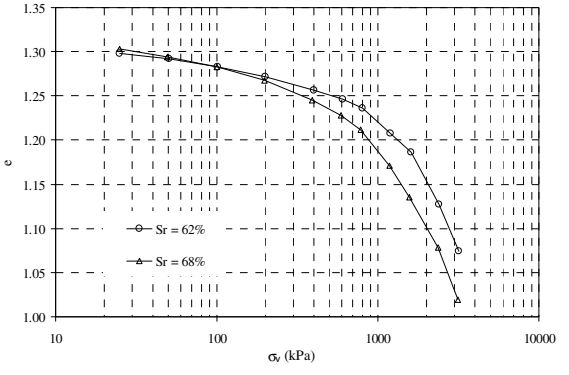

Fig. 2. Not-treated MF soil: compressibility curves of unsaturated samples.

The collapse behaviour of the MF soil has been analysed for three reference stress levels, namely 200 kPa, 600 kPa and 1200 kPa, corresponding to pre-yield, yield and post-yield behavior. In particular, samples were incrementally loaded to the desired pressure and then inundated with water after the initial stage of consolidation due to the applied load increment took place. As shown in Fig. 3, the collapse was detected for each stress level, with larger settlements being for the specimen wetted at the yield stress level of 600 kPa (see also, Russo et al., 2011).

The final observed settlement of soaked samples was used to calculate the collapse potential, I_c, which is defined as follows:

$$I_c(\%) = \frac{-\Delta e}{1+e_0} x100 \tag{1}$$

whereas Δe represents the reduction of voids ratio on wetting upon constant loading and e_0 is the initial voids ratio of the not-wetted specimen (ASTM D 5333-92). I_c assumes a positive sign when the sample collapses.

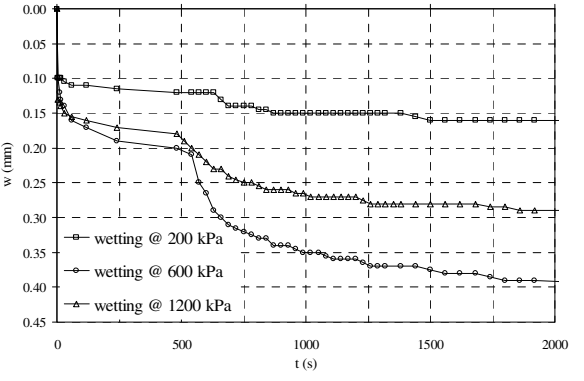

Fig. 3. Not-treated MF soil: collapse upon wetting at different stress levels.

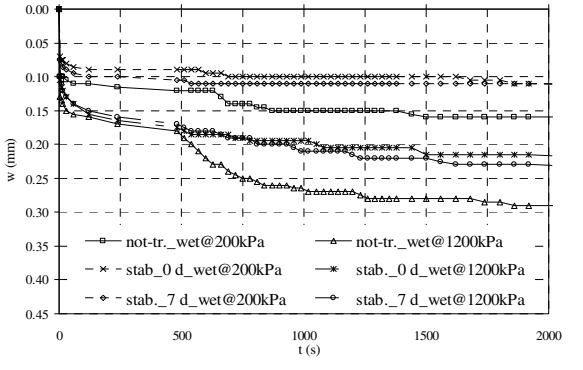

Fig. 4. Stabilised MF soil: collapse upon wetting at different stress levels.

The lime addition induces a relevant modification of the observed phenomenon. In Fig. 4 the comparison between load induced settlements for two treated specimens cured for 24h (0 days sample) and 7 days is reported. The wetting path was performed at 200 kPa and 1200 kPa stress levels, corresponding to the pre-yield and post-yield stress levels of treated MF soil. The increase of the saturation degree does not trigger collapse of the specimen, differently from the observed

behavior of the natural material. Considering the reduced curing time of the tested specimen, the cementitious products of pozzolanic reactions are probably far to be effective on the mechanical response of the treated soil. The improvement observed is then connected to the short time effects of lime on the fabric of the soil, mainly depending on the ionic exchange induced by lime and characterised by the flocculation of soil grains. In Fig. 5 the collapse potentials I_c of not treated and stabilized samples are reported for comparison. The not treated samples exhibit the largest value of I_c around the yield stress and a consistent reduction of collapse potential for pre-yield and post yield stress levels. A further validation of the effectiveness of the improvement is given by the reduced values of the collapse potentials of the stabilized and 7 days cured samples, for the tested stress levels of 200 kPa and 1200 kPa.

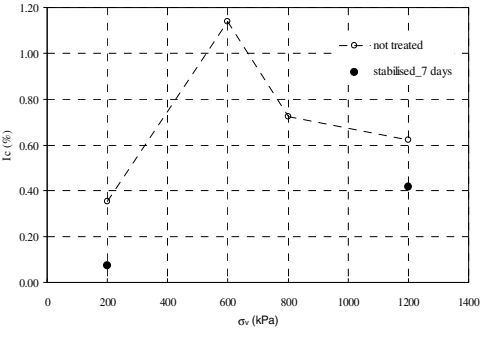

Fig. 5. MF soil: Collapse potential I_c *vs.* vertical stress σ_v upon wetting for not treated and stabilised samples.

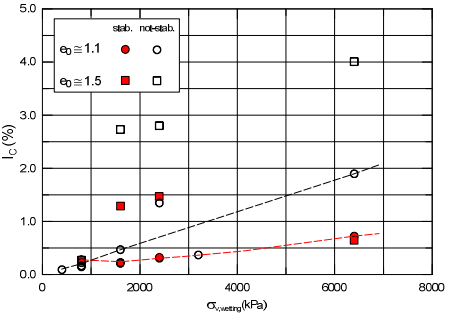

Fig. 6. Not-treated and stabilised samples of PN after 7 days of curing time. Collapse potential I_c *vs.* vertical stress σ_v upon wetting.

A similar investigation was also performed on not-treated and stabilized oedometer samples of reconstituted Rome pozzolana (PN), through wetting paths following the application of vertical stress. The soaking tests were performed at stress levels of 800 kPa, 1600, 2400 and 6400 kPa. The majority of the not treated

samples exhibited a "collapsible" behaviour, whose amount obviously depends on initial voids ratio, degree of saturation and stress level. In particular, for both values of initial voids ratio ($e_0 \cong 1.1$ and $e_0 \cong 1.5$), the collapsible behaviour clearly depends on vertical stress, as shown in Fig. 6, which shows the collapse potential *vs*. applied vertical stress: the larger is the vertical stress, the larger is the volume strain due to sample saturation. For not-treated samples, the collapse potential, I_c, is lower than 2% for samples with lower e_0 while it attains the 4% approximately for looser samples. However, no significant collapse-strains are observed for stress smaller than σ_v = 1600 kPa. On the other hand, the lime addition induces a discernible modification of the collapsible behaviour of Rome pozzolana, since in this case, the collapse potential I_c is lower than 0.75% for denser samples and it does not exceed 1.5% for looser samples (see Fig. 6).

4 Conclusions

At this stage, the on-going research activity on lime stabilisation of pyroclastic soils has been focused on the effects of lime addition on the collapse behaviour upon wetting exhibited before the treatment. It has been found that lime stabilization reduces the collapsible behaviour of the unsaturated soil. This result has been observed already for treated samples cured for 24 hours, when it is likely that cementitious bonds between aggregates are far to be effective. This means that the reorganisation of the pore space for the treated soil, mainly due to flocculation of grains, yields an increased stability of the soil skeleton, independently from the stability induced by matric suction. The results have been interpreted by means of collapse potential. The stabilised samples of both pyroclastic soils showed a systematic decrease of the potential after lime addition, for each initial voids ratio and curing time.

Acknowledgements. This research is part of the Italian PRIN Research Project, 2008, "Miglioramento dei terreni con calce/cemento". The Authors are grateful to Giacomo Tancetti, France-sca Fassiotti and Arcadio Capotosto for their support during the experimental work performed at Universities of Perugia and Cassino.

References

ASTM D 5333-92, Standard Test Method for measurement of collapse potential of soils (1996)

Cattoni, E., Cecconi, M., Pane, V.: Geotechnical properties of an unsaturated pyroclastic soil from Roma. Bull. Eng. Geol. Environ. 66, 403–414 (2007)

Cecconi, M., Viggiani, G.M.B.: Structural features and mechanical behaviour of a pyroclastic weak rock. Int. J. Numer. Anal. Meth. Geomech. 25, 1525–1557 (2001)

Cecconi, M., Pane, V., Marmottini, F., Russo, G., Croce, P., dal Vecchio, S.: Lime stabilisation of pyroclastic soils. In: Proc. Vth Int. Conf. on Unsaturated Soils, Barcelona, September 6-8, vol. I, pp. 537–541. Balkema Editors (2010a)

Cecconi, M., Scarapazzi, M., Viggiani, G.M.: On the geology and the geotechnical properties of pyroclastic flow deposits of the Colli Albani. Bull. Eng. Geol. Environ. 66, 403–414 (2010b)

Cecconi, M., Ferretti, A., Russo, G., Capotosto, A.: Mechanical properties of two lime stabilised pyroclastic soils. In: International Symposium on Deformation Characteristics of Geomaterials, Seoul, Korea, September 1-3, vol. II, pp. 772–778 (2011a)

Cecconi, M., Rotonda, T., Tommasi, P., Viggiani, G.M.B.: Microstructural features and compressibility of volcanic deposits from Central Italy. In: International Symposium on Deformation Characteristics of Geomaterials, Seoul, Korea, September 1-3, vol. II, pp. 884–891 (2011b)

Evangelista, A., Nicotera, M.V., Papa, R., Urciuoli, G.: Field investigations on triggering mechanisms of fast landslides in unsaturated pyroclastic soils. In: Toll, et al. (eds.) Unsaturated Soils: Advances in Geo-Engineering, pp. 909–915. Taylor & Francis Group, London (2008)

Nicotera, M.V., Papa, R., Urciuoli, G., Russo, G.: Caratterizzazione in condizioni di parziale saturazione di una serie stratigrafica di terreni suscettibili di colata di fango. In: Incontro Annuale dei Ricercatori di Geotecnica (IARG), Catania (2008)

Papa, R.: Indagine sperimentale sulla coltre piroclastica di un versante della Campania. PhD Thesis, University of Napoli Federico II, Napoli, Italy (2007)

Papa, R., Evangelista, A., Nicotera, M.V., Urciuoli, G.: Mechanical properties of pyroclastic soils affected by landslide phenomena. In: Toll, et al. (eds.) Unsaturated Soils: Advances in Geo-Engineering, pp. 917–923. Taylor & Francis Group, London (2008)

Russo, G., Croce, P., Cecconi, M., Pane, V.: Proprietà fisiche e meccaniche di terreni piroclastici stabilizzati a calce. In: XXIV Convegno Nazionale di Geotecnica, Napoli, giugno 22-24, vol. 2, pp. 557–564. Edizioni AGI (2011)

Fabric Alteration of a Compacted Lime-Treated Expansive Soil upon Drying and Wetting

Guillaume Stoltz, Olivier Cuisinier, and Farimah Masrouri

Abstract. The main purpose of this study is to examine both at micro- and macro scales the effects of wetting / drying on swelling / shrinkage behaviour of a compacted expansive clayey soil treated with lime. The results showed that lime treatment was efficient to prevent the swelling, but the shrinkage remained unchanged, regardless of the added lime content. Even if no significant volumetric variation was observed upon wetting, a reorganisation of the lime-treated soil microstructure was evidenced. Moreover, an alteration of both micro- and macro-porosity of the lime-treated materials was observed upon drying.

Keywords: expansive soil, lime treatment, fabric, swelling / shrinkage behaviour.

1 Introduction

Among the potential techniques likely to improve the behaviour of expansive soils and to reduce the potential damages associated with large volume changes, lime treatment may be worthwhile and practical in preventing expansive soils from swelling/shrinkage. Indeed, some authors have shown that lime treatment may reduce the swelling potential of expansive upon wetting (e.g. Basma & Tuncer, 1991).

Whilst the effects of lime treatment on the swelling of expansive soils are well characterised, less is known about the impact of lime on shrinkage upon drying. Some studies have indicated that lime addition increases the shrinkage limit (Christensen 1969) but very few studies have examined the volumetric shrinkage ability of compacted lime-treated samples.

Guillaume Stoltz · Olivier Cuisinier · Farimah Masrouri
Université de Lorraine, Nancy, France
e-mail: olivier.cuisinier@univ-lorraine.fr

The volume changes induced by the variations of water content and suction are closely linked to the soil fabric. Several studies have shown that variations of suction may induce dramatic alterations of the soil fabric (Simms & Yanful, 2002). Moreover, even if no swelling is observed when a lime-treated expansive clayey soil is subjected to saturation, the soil fabric may change (e.g. Cuisinier & Laloui, 2004). Some studies that have focused on the effects of lime treatment at the micro-scale have shown that quicklime addition induces modifications in the soil fabric, and these modifications depend on the soil nature, compaction conditions (i.e., soil moisture content, compaction energy), lime content and curing time (Choquette et al., 1987; Russo et al., 2007).

In this context, the objective of this study was to investigate the evolution of the fabric of lime-treated soils subjected to wetting or drying paths. At the macro-scale, the soil water retention curves (SWRCs) of the compacted lime-treated materials (0%, 2% and 5% lime content) were determined after three curing times (i.e., 0, 28 and 180 days). At microscopic level, the impact of suction variations on the lime-treated materials fabric was assessed by mercury intrusion porosimetry (MIP) tests.

2 Material and Methods

2.1 Tested Materials

The studied soil was an expansive clayey soil sampled in the Eastern part of France. Its plasticity index was 42% and the smectite content was 50%. Quicklime (CaO) was used in this study and the dosages 2 and 5% (% CaO by dry weight) were considered.

For the sample preparation, the water content of the clayey soil was adjusted to the optimum water content of compaction (Table 1). The soil and lime were mixed together and the mixture was stored one hour in an airtight container before compaction. Then, the mixture was statically compacted in a mould to the maximum dry density (Table 1). When a curing period prior to testing was required, the compacted samples were wrapped in plastic sheets to prevent any water loss and kept at 20°C.

The initial suctions of the compacted untreated and lime-treated materials were determined as a function of the curing period (0, 28 and 180 days) using the Filter Paper Method (ASTM D 5298 - 94, 1995) (Table 2).

Table 1. Compaction characteristics under normal Proctor energy of the lime-treated samples.

Lime content (% CaO dry weight)	0%	2%	5%
Maximum dry density ρ_{di} ($Mg.m^{-3}$)	1.45	1.34	1.20
Optimum water content w_i (%)	26.5	32.0	37.0

Table 2. Suctions of the untreated and lime-treated specimens after different curing periods.

Curing period (days)	0	28	180
0% lime content	0.4 MPa	-	-
2% lime content	0.5 MPa	1.0 MPa	1.1 MPa
5% lime content	0.5 MPa	0.9 MPa	2.1 MPa

2.2 Experimental Techniques

The SWRC were determined between 0 and 292 MPa of suction by combining two methods, the osmotic method to impose a suction between 0 and 8 MPa and the vapour equilibrium method to impose a suction between 8 and 292 MPa (Stoltz et al. 2012). In both suction control methods, the temperature was maintained at 20 ± 1.5°C. The compacted samples were cut into several small cubes (1.5 cm in size). The cubes were either wetted or dried during 7 days to reach the equilibrium suction. Then, the water content of the cubes was determined.

The mercury intrusion porosimetry (MIP) was selected to investigate the fabric of the samples because this method allows the measurement of a wide pore-size range (intruding pore radius from 90 µm to 0.0018 µm). The MIP tests were conducted on completely dried soil samples. In this study, freeze-drying was applied to limit the effects of shrinkage from water on drying.

3 SWRC Alteration with Lime Content and Curing Time

SWRC was altered by the lime treatment and the lime content (Fig. 1). However, no significant impact of the curing time was observed. Therefore, the major impact of lime treatment could be associated to immediate reactions and compaction process, while the long-term reactions have not led to significant alterations of the SWRC.

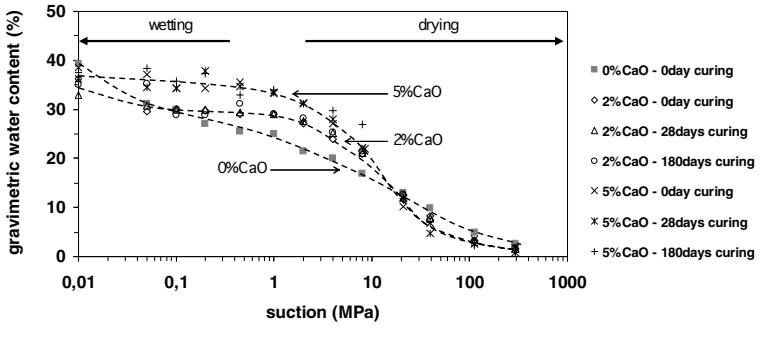

Fig. 1. SWRC of the untreated and lime-treated expansive clayey soils obtained from different curing periods.

The wetting and drying parts of each SWRC were then separately analysed and compared for all of the tested configurations. Along the wetting path, the effect of lime treatment was assessed by determining the amount of water uptake during the saturation of the samples. In the case of the untreated material, the water content increased by +13%, while an increase of only +3% (for 2% lime) and +1% (for 5% lime) was observed in the case of the lime-treated materials. Therefore, the water uptake of the soil was dramatically reduced by the lime treatment. Along the drying path below 20 MPa, the retention capacity was higher for the treated samples. However, no treatment effect was found for the suctions above 20 MPa.

4 Fabric Alteration Upon Wetting / Drying

The MIP tests were first performed to determine the fabrics of the untreated material and of the two lime-treated materials after a curing period of 28 days. Other MIP tests were conducted on four untreated and lime-treated samples for which the suction was modified using the osmotic or salt solution (vapour equilibrium) method. The target suctions were 0, 2.8, 8 and 113 MPa.

The fabric of the untreated material (Fig. 2b) consisted of two classes of pores. This type of structure is usually observed on compacted clayey soils (dry side of optimum). The smallest pores (micro-pores) correspond to the pores inside the aggregates, while the largest pores (macro-pores) are the spaces between these aggregates. The fabrics of the two lime-treated materials (Fig. 2d and 2f) presented a similar type of structure. Lime addition to the expansive clayey soil resulted in an increase in the amount of micro-pores, and the higher the lime content, the higher the amount of micro-pores.

To further interpret the MIP data, the void ratio of the materials were evaluated from the injected mercury volume (Table 3), which allowed the assessment of volumetric swelling / shrinkage ($\Delta V/V_{ref} = \Delta e/(1+e_{ref})$) from the reference state corresponding to the compacted materials without suction modification.

The fabrics were analysed in comparison with the reference state. Concerning the untreated material, saturation led to a strong volumetric swelling (+31%), corresponding to an increase in the amount of macropores (Fig. 2b). In the case of the two lime-treated materials, no volumetric swelling was observed upon saturation (Table 3). This showed that the lime treatment prevented effectively the swelling. However, the material treated with 2% lime exhibited a modification of the distribution of the macro-pores (with an increasing mean radius), while the distribution of the micro-pores was almost unchanged (Fig. 2d). The material treated with 5% lime exhibited slight modifications in both the distribution of the macro-pores and micro-pores after saturation (Fig. 2f).

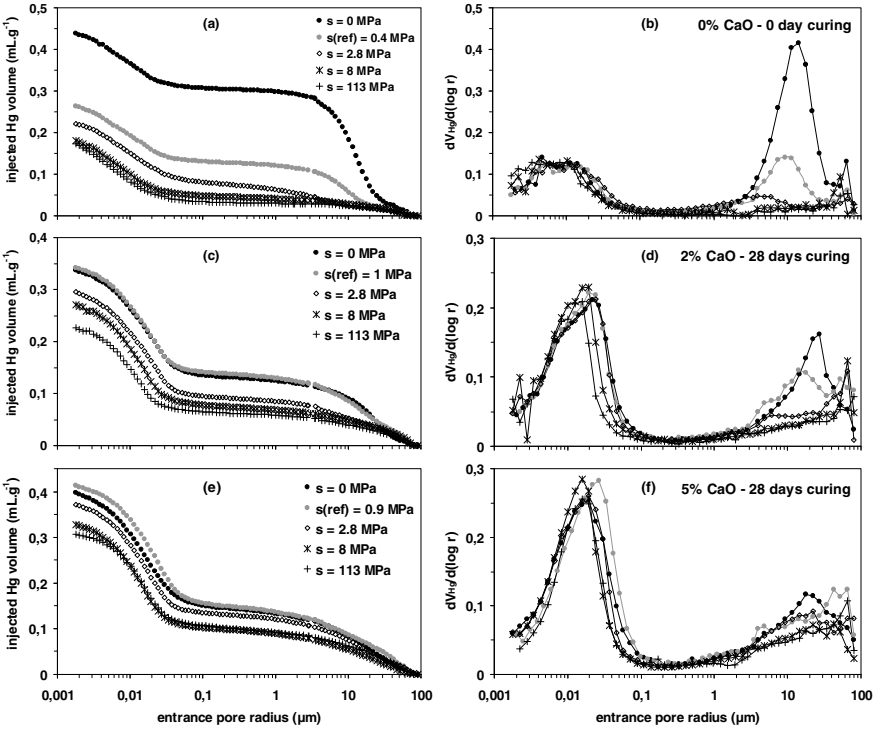

Fig. 2. Influence of saturation (s = 0 MPa) and drying (s = 2.8, 8 and 113 MPa) from the reference state on fabric of the compacted clayey soil treated with 0% lime (a and b) 2 % lime (c and d) and 5 % lime (e and f).

Upon drying, the volumetric shrinkage of the untreated material increased from the initial suction up to 8 MPa (equal to -12% at the suction of 8 MPa), while it was nearly stabilised between the suction of 8 and 113 MPa (Fig 2b). The fabric of the untreated soil subjected to drying exhibited shrinkage that affected the macro-porosity, while the micro-porosity remained almost unchanged despite the range of the suction (Fig 2b). For the soil treated with 2% lime, the increased suction led to a volumetric shrinkage of -5% at 2.8 MPa to -15% at 113 MPa. The volumetric shrinkage of the same orders of magnitude was observed for the material treated with 5% lime. Unlike for the untreated material, the volumetric shrinkage was not stabilised at 8 MPa for either of the lime-treated materials. In conclusion, lime addition to the expansive clayey soil did not prevent the shrinkage induced by drying even if the volume of the lime-treated soil was stabilised at higher suctions than the untreated soil.

Table 3. Void ratio obtained from MIP for compacted lime-treated materials at various suctions

Suction s (MPa)	0	s(ref)	2.8	8	113
0% lime content	1.21	0.69	0.58	0.49	0.47
2% lime content	0.87	0.90	0.81	0.73	0.61
5% lime content	1.06	1.08	0.97	0.85	0.80

5 Conclusion

This study characterised the impact of wetting / drying on the swelling / shrinkage behaviour of a compacted expansive clayey soil treated with lime. The effects of lime content (0, 2% and 5% CaO) and curing periods (0, 28 and 180 days) were considered. From this work, the following conclusions can be drawn:

- Upon wetting, no significant swelling from the initial state of the lime-treated soils, for both lime contents and curing periods, was observed. However, wetting was accompanied by a reorganisation of the microstructure.
- Upon drying, the results showed that the volumetric shrinkage was on the same order of magnitude for both untreated and lime-treated materials. Therefore, lime treatment did not prevent volumetric shrinkage even at high lime content (5% CaO). Moreover, the MIP tests showed an alteration of the lime-treated materials fabric with increasing suction.

Acknowledgements. The results of this research were obtained in the framework of the TerDOUEST programme “sustainable earthworks involving treated soils”, supported by the French National Research Agency.

References

Basma, A.A., Tuncer, E.R.: Effect of lime on volume change and compressibility of expansive clays. Transportation Research Record 1295, 52–61 (1991)

Choquette, M., Berube, M.A., Locat, J.: Mineralogical and microtextural changes associated with lime stabilization of marine clays from eastern Canada. Appl. Clay Sc. 2, 215–232 (1987)

Christensen, A.P.: Cement Modification of Clay Soils, RD002, p. 11. Portland Cement Association, Skokie (1969)

Cuisinier, O., Laloui, L.: Fabric evolution during hydromecanical loading of a compacted silt. Int. J. Num. Ana. Meth. Geom. 28, 483–499 (2004)

Russo, G., Vecchio, S.D., Mascolo, G.: Microstructure of a Lime Stabilised Compacted Silt. Exp. Unsat. Soil Mech.- Springer Proceedings in Physics 112, 49–56 (2007)

Simms, P.H., Yanful, E.K.: Predicting soil–water characteristic curves of compacted plastic soils from measured pore-size distributions. Geotechnique 52(4), 269–278 (2002)

Stoltz, G., Cuisinier, O., Masrouri, F.: Multi-scale analysis of the swelling and shrinkage on a lime-treated expansive soil. Applied Clay Science (in press 2012)

On the Resaturation of Swelling Claystone

Mehrdokht Mohajerani, Pierre Delage, Mohammad Monfared, Anh-Minh Tang, Jean Sulem, and Behrouz Gatmiri

Abstract. The hydration of unsaturated Callovo-Oxfordian (COx) claystone specimens from the 490 m deep URL of Bure in France has been investigated in high stress oedometers by conducting hydration tests on unsaturated specimens under stress values that were lower, equal and higher than the in-situ stress (re-saturation of swelling clays should be done under in-situ stress to avoid any swelling that would affect their structure). Hydration tests always exhibited a swelling behaviour, even under stresses higher than in-situ. Based on other published experimental evidence, it is suggested that this swelling behaviour is due to damage, since the presence of cracks within claystones are known to enhance the swelling properties of claystones. A procedure of saturating claystone samples in the oedometer with limited swelling is then proposed.

Keywords: unsaturated claystone, hydration, swelling properties, effective stress, damage.

Mehrdokht Mohajerani
ENPC, UR Navier/CERMES, Marne la Vallée, France
e-mail: mohajerm@cermes.enpc.fr

Pierre Delage
ENPC, UR Navier/CERMES, Marne la Vallée, France
e-mail: delage@cermes.enpc.fr

Mohammad Monfared
EPFL, LMS, Lausannes, Switzerland
e-mail: mohammad.monfared@epfl.ch

Anh-Minh Tang
ENPC, UR Navier/CERMES, Marne la Vallée, France
e-mail: tang@cermes.enpc.fr

Jean Sulem
ENPC, UR Navier/CERMES, Marne la Vallée, France
e-mail: sulem@cermes.enpc.fr

Behrouz Gatmiri
ANDRA, Châtenay – Malabry, France
e-mail: Behrouz.Gatmiri@andra.fr

1 Introduction

Very low permeability claystones ($k = 10^{-13}$ m/s) are considered as possible host rocks for the storage of high activity radio-active waste at great depth, in particular in France and Switzerland where the claystones considered exhibit some swelling properties. Observations in underground research laboratories (URL) showed that ventilation induced a significant desaturation of the claystone along the gallery walls. Cores also appeared to be significantly desaturated when provided to the lab with values of suction (measured by using a dew point hygrometer) of several tens of MPa.

The process of resaturation of claystone samples prior to testing is of utmost importance given the sensitivity of claystone to changes in water content. Indeed, the results of Pham et al. (2007) showed that decrease in water content (obtained by submitting samples to different values of controlled relative humidity RH) leads to significantly increase the unconfined compressive stress of COx samples (from 27 MPa at 98% RH to 57 MPa at 32% RH). The saturation of low permeability claystone samples (with hydraulic conductivity k around 10^{-20}-10^{-21} m^2) that have been desaturated during the processes of in-situ coring, sample storage, transport to the lab and finally sample trimming is difficult and can be significantly long. Also, saturation under zero stress condition can cause hydraulic damage evidenced by the appearance of cracks resulting from hydration and swelling, as shown by Valès (2008) and Bornert et al. (2010) by using Digital Image Correlation. The quality of the saturation prior to testing is indeed fundamental to investigate the poromechanical behaviour (Bemer et al. 2004) with respect to microstructure effects and induced cracks (Montes et al. 2004).

In this paper, the hydration of unsaturated Callovo-Oxfordian (COx) claystone specimens has been investigated in high stress oedometers by conducting hydration tests on unsaturated specimens under stress values that were lower, equal and higher than the in-situ stress (resaturation of swelling clays should be done under in-situ stress to avoid any swelling that would affect their structure). Hydration tests always exhibited a swelling behaviour, even under stresses higher than in-situ. Based on other published experimental evidence (Mohajerani et al. 2011, Carter et al. 2010, Aversa et al. 1993), it is suggested that this swelling behaviour is due to damage, since the presence of cracks within claystones are known to enhance the swelling properties of claystones. A procedure of saturating claystone samples in the oedometer with limited swelling is then proposed.

2 Studied Material and Sample Preparation

The Callovo-Oxfordian (COx) claystone is an indurated clay of low porosity, low permeability and with a relatively high strength. Its mineralogical composition varies with depth. At a 490 m it contains about 45% clay with 30-35% illite, 0-5% kaolinite and 60-65% interstratified illite\smectite. COx clay also contains about 30% carbonate (calcite), 25% quartz and 5% feldspars, pyrite, iron oxides

(ANDRA, Dossier Argiles, 2005).The smectite percentage in the clay fraction is responsible for the observed swelling capacity.

Three tests of EST27396 n°1, EST27396 n°2, EST27396 n°3 were performed in oedometer rings of 50 mm in diameter whereas the test EST28522 was carried out in a 38 mm diameter ring. Samples were cored to the desired diameter by using a diamond barrel. The cored specimen was afterwards inserted in the ring and its top and bottom faces were carefully polished by using a sand paper sheet placed on a small plane wooden board. The polishing of the upper and down faces of the sample was completed once the wood piece came in contact with the cylindrical section of the metallic ring, thus achieving exactly the required sample thickness with two flat, regular and parallel faces. The loading direction was taken perpendicular to the stratification of samples. The initial degree of saturation was determined by carefully measuring the sample volume (by using a precision calliper). The water content was determined by measuring the initial and final weights of a rock piece before and after drying in the oven at 105°C for one day. The initial suction of the samples was determined by using a chilled mirror dew-point hygrometer (Leong et al. 2003) fabricated by General Eastern. This device is based on the precise measurement of the relative humidity of the sample. It provides the total suction value within a period of time of about 15 min according to Kelvin's law (Fredlund & Rahardjo. 1993):

$$s = u_a - u_w = RT/gM \,.(\ln h) \tag{1}$$

where u_a and u_w are respectively the air and water pressure, s is the total suction, R is the universal (molar) gas constant (R=8.3143 J.mol^{-1}.K^{-1}), T is the absolute temperature (K), g is the gravity acceleration (g=9.81 m.s^{-2}), M is the water molecular mass (M=18.016 g.mol^{-1}) and h is the relative humidity.

As any technique based on vapour exchanges, the dew point hygrometer is suitable at high suctions, preferably higher than 3MPa (Delage et al. 1998). The parameters characterising the initial states of the samples are presented in Table 1. As expected, with initial suctions as high as 17 to 34MPa, the samples were significantly desaturated just after trimming. According to calculations by using Jurin's law based on the pore size distribution (ANDRA documents, 2005) and adopting the hypothesis of cylindrical pores, one can estimate the air entry value of the COx claystone. Jurin's law is written as follows:

$$u_a - u_w = 4\sigma_s \cos\theta / D \tag{2}$$

in which σ_s is the surface tension at the air-water interface and θ is the contact fluid-solid angle (for water, cos θ = 1 and σ_s = 72.75×10^{-3}N/m at 20°C). D is the diameter of the cylinder. With D = 20nm (ANDRA, Dossier Argiles, 2005), the air-entry value of the COx sample can be estimated around 14MPa, indicating probable air continuity within the claystone at higher suction.

Table 1. Initial characteristics of the tested samples.

Sample	EST27396 n°1	EST27396 n°2	EST27396 n°3	EST28522
Depth (m)		483		481
Water content (%)	5.9	6.6	6.3	6.1
Degree of saturation (%)	54.2	60.6	57.8	56
Porosity(%)	22	22	22	22
Measured relative humidity (%)	78	81	80	79
Suction (MPa)	34	28	30	32
Sample diameter (mm)		50		38
Sample height (mm)		15		10
Type of test	Compression followed by swelling under various constant stresses (8, 10 and 12 MPa)			Resaturation test

In this study, a high pressure oedometer developed in CERMES was used. The apparatus has a double lever arm (with one lever arm multiplying the load by 5 and the second one by 10). The specimen is placed on a metallic porous disk inserted in the cell base and connected to two lateral valves that allow satisfactory saturation of the porous disk as described later in more details. Another metallic porous disk is placed on top of the sample to allow vertical drainage through the top and bottom faces. Vertical displacements are monitored by using an electronic LVDT transducer connected to a data acquisition system.

3 Hydration Tests

One of the standard techniques used to estimate the swelling stress of soils consists in running in parallel several oedometric tests in which the samples (at given initial water content) are first loaded under various vertical stresses that are chosen smaller and larger than the estimated swelling stress. The samples are then soaked under these stresses while measuring the volume changes. The swelling stress is interpolated by drawing a curve passing through all the experimental points (either after swelling or compaction) at the intersection of the curve with the no volume change line. This approach has been applied to the COx claystone. Knowing the in-situ condition (approximated by a total vertical stress σ_v= 12.4-12.7MPa and a pore pressure u = 4.9MPa, (Wileveau et al. 2007), three samples were loaded (at given initial water content, see Table 1) to vertical stresses equal to 8, 10 and 12MPa under which they were subsequently soaked. Based on the values of the Biot coefficient between 0.4 and 1 (Bemer et al. 2004), the estimated effective stress could be between 8 and 10.4MPa. Hence, the first load (8MPa) corresponds to the lower bound of the in-situ vertical effective stress, the second value (10MPa) to the upper bound whereas the third one (12MPa) is larger. In such

conditions, one should theoretically observe some swelling under 8MPa, little volume change under 10MPa and some compression under 12MPa.

The initial characteristics of the three samples are presented in Table 1. As expected, the water saturation is far from being complete in the samples. The initial compression was conducted at constant initial water content around 6% (see exact values in Table 1) by following a standard step loading procedure with the load doubled at each step.

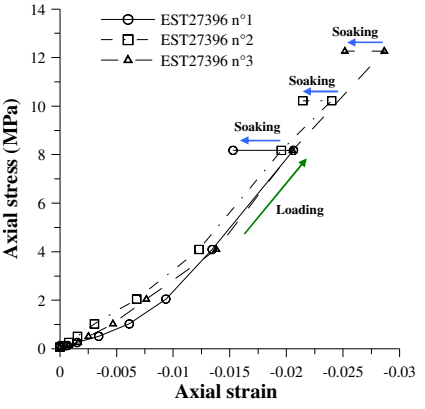

Fig. 1. Oedometric compression curves and hydration test under various vertical loads (EST27396 n°1, 2 and 3).

Results are presented in Fig. 1. in an axial stress versus vertical strain diagram. One can observe that the three compression curves are reasonably similar, probably due to comparable initial unsaturated states (Table 1). Once soaked, swelling is observed under the three stresses applied, including under the higher one (12MPa) that is larger than the in-situ vertical effective stress. The swelling strains are equal to 0.53, 0.26 and 0.35% under 8, 10 and 12MPa respectively. They are not ordered with respect to the stress applied as expected, since a higher strain is observed under 12MPa compared to 10MPa.

It is well known that a sample should not swell under a vertical effective stress higher than the in-situ effective stress in the case of 'perfect sampling' (Skempton, & Sowa 1963). However, the quality of the COx samples has been affected by the excavation, stress release, drying, transport and trimming procedures and all samples hence contain some induced cracks that result in an enhanced swelling behaviour. During the loading phase, some crack closure can occur under low stress level but at higher stress, new cracks can form and propagate. It is thus expected that after loading the swelling properties during hydration would be enhanced. Based on other published experimental evidence, it is suggested that this swelling behaviour is due to damage, since the presence of cracks within claystones are known to enhance the swelling properties of claystones.

4 Resaturation Method

In this proposed resaturation method the swelling of claystone during hydration is limited, so as the disturbance and damage of water sensible claystone due to the free swelling during hydration is minimised. The procedure of saturation is as follows. The sample was placed into the oedometer ring that was previously coated with grease to reduce friction along the lateral surface of the specimen. The porous disks were kept dry so as to ensure a well controlled saturation procedure under in-situ stress conditions close to the natural ones. To ensure good contact between the sample, the porous disks and the piston, a previous low stress loading-unloading cycle was applied prior to injecting pore water up to 1MPa (a value deemed small enough to preserve the sample from any change). During this cycle, all pore water valves were closed to avoid any drying of sample. For the same reason, this preliminary stress cycle was run rapidly, in less than 5 minutes.

The saturation of the bottom porous disk was carried out by infiltrating water under small pressure into the disk. To do so, one of the drainage valves of the cell base was connected to the pore water reservoir whereas the other one was kept open so as to allow the evacuation of the air from the dry porous disk during water infiltration. This valve was closed once water started to flow out.Water was infiltrated under a lower stress of 3.5MPa (a value lower than the interval proposed for the in situ effective stress between 8 and 10.4). As soon as the monitored vertical displacement reached a maximum value of 2 µm, the applied load was doubled.

This procedure was carried out until reaching a load with no further swelling. As shown in Fig. 2. (sample EST28522), swelling is observed up to 1.75MPa with compression starting at 3.5MPa. swelling above the initial sample volume is indeed maintained below 2 µm as planned.

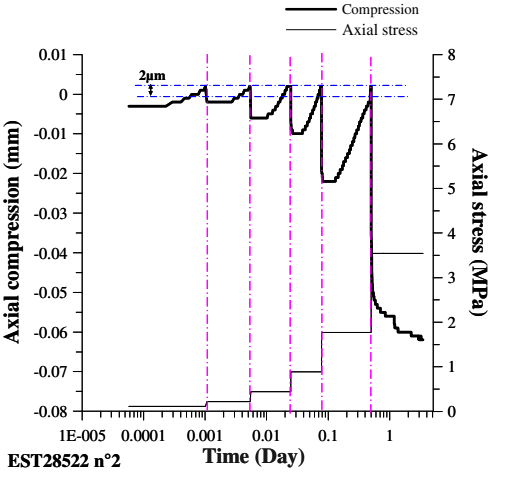

Fig. 2. Saturation phase (EST28522).

5 Conclusion

In this paper the swelling behaviour of COx claystone was observed during the hydration tests under stresses lower, equal and even higher than the in-situ stress. This swelling behaviour is related to the presence of the cracks within the samples, these cracks could be induced during the excavation, stress release, drying, transport and trimming procedures.

In this paper also a resaturation method with a limited swelling for the claystones was proposed. This method consist in limiting the swelling deformation to 2µm by adding the loads once the swelling was observed, so as the disturbance and damage due to the free swelling during hydration was limited.

References

ANDRA. Dossier Argiles, Référentiel du site Meuse/Haute Marne (2005)

Aversa, S., Evangelista, A., Leroueil, S., Picarelli, L.: Some aspects of the mechanical behaviour of structured soils and soft rocks. In: Anagnostopoulos, et al. (eds.) Geotechnical Engineering of Hard soils- Soft Rocks, Balkema, Rotterdam (1993), ISBN 90 54103442

Bemer, E., Longuemare, P., Vincke, O.: Poroelastic parameters of Meuse/Haute Marne argillites: effect of loading and saturation states. Applied Clay Science 26, 359–366 (2004)

Bornert, M., Vales, F., Gharbi, H., Nguyen Minh, D.: Multiscale full-field strain measurements for micromechanical investigations of the hydromechanical behaviour of clayey rocks. Strain 46(1), 33–46 (2010)

Carter, T.G., Castro, S.O., Carvalho, J.L., Hattersley, D., Wood, K., Barone, F.S., Yuen, D., Giraldo, C.M.K.: Tunnelling Issues with Chilean tertiary volcaniclastic rocks. In: Mir conference; Problemi di stabilità nelle opere geotecniche, Capitolo, Torino, vol. 11 (2010)

Delage, P., Howat, M., Cui, Y.J.: The relationship between suction and swelling properties in a heavily compacted unsaturated clay. Engineering Geology 50(1-2), 31–48 (1998)

Fredlund, D.G., Rahardjo, H.: Soil mechanics for unsaturated soils. Wiley (1993)

Leong, E.C., Tripathy, S., Rahardjo, H.: Total suction measurement of unsaturated soils with a device using the chilled-mirror dew-point technique. Géotechnique 53(2), 173–182 (2003)

Marcial, D., Delage, P., Cui, Y.J.: On the high stress compression of bentonites. Canadian Geotechnical Journal 39, 1–9 (2002)

Montes, H.G., Duplay, J., Martinez, L., Escoffier, S., Rousset, D.: Structural modifications of Callovo-Oxfordian argillite under hydration/dehydration conditions. Applied Clay Science 25(3-4), 187–194 (2004)

Mohajerani, M., Delage, P., Monfared, M., Sulem, J., Tang, A.M., Gatmiri, B.: Oedometric compression and swelling behaviour of the Callovo-Oxfordian argillite. International Journal of Rock Mechanics and Mining Sciences 48(4), 606–615 (2011)

Pham, Q.T., Vales, F., Malinsky, L., Nguyen Linh, D., Gharbi, H.: Effects of desaturation-resaturation on mudstone. Physics and Chemistry of the Earth 32, 646–655 (2007)

Wileveau, Y., Cornet, F.H., Desroches, J., Blümling, P.: Complete in situ stress determination in an. argillite sedimentary formation. Physics and Chemistry of the Earth, Parts. A/B/C 32(8-14), 866–878 (2007)

Valès, F.: Modes de déformation et d'endommagement de roches argileuses profondes sous sollicitations hydro-mécaniques. PhD Thesis, Ecole Polytechnique (2008)

Skempton, A.W., Sowa, V.A.: The behaviour of saturated clays during sampling and testing. Géotechnique, 1963; 13 13(4), 269–290 (1963)

Effect of Loading History on Time Dependent Deformation of Rockfill

Enrique Romero, Eduardo E. Alonso, Clara Alvarado, and Felix Wacker

Abstract. The paper explores the time-dependent compressibility of coarse crushed quartzitic slate, focusing on the effects of the previous loading history. Large diameter oedometer tests were performed at different relative humidity (or total suctions) and different overconsolidation ratios (OCR). Preliminary results suggested that pre-compressing the rockfill material at increasing OCRs lead to the progressive vanishing of rockfill delayed deformations.

Keywords: time-dependent compressibility, rockfill, overconsolidation ratio, oedometer tests.

1 Introduction

Rockfill mechanical behaviour is very sensitive to the action of water, which is of particular concern during the design and performance stage of rockfill and zoned dams. These structures also exhibit long term deformations, which tend to depend linearly on the logarithm of time as indicated by field records (see for instance; Oldecop & Alonso 2007). Breakage of rock particles and crack propagation are the main underlying physical mechanisms that explain these phenomena, which depend on the strength of individual particles, the grain size distribution and shape of particles, the stress level and the relative humidity prevailing at the rockfill

Enrique Romero
Universitat Politècnica de Catalunya, Barcelona, Spain
e-mail: enrique.romero-morales@upc.edu

Eduardo E. Alonso
Universitat Politècnica de Catalunya, Barcelona, Spain
e-mail: eduardo.alonso@upc.edu

Clara Alvarado
Universitat Politècnica de Catalunya, Barcelona, Spain
e-mail: alvarado.clara@gmail.com

Felix Wacker
Universitat Politècnica de Catalunya, Barcelona, Spain

voids –or alternatively the activity of the liquid filling these voids– (Oldecop & Alonso 2001, Romero et al. 2005).

The paper specifically explores the time-dependent compressibility, focusing on the effects of the previous loading history –as considered, for instance, by the overconsolidation ratio OCR– on rockfill delayed deformations. A crushed quartzitic slate was tested at constant relative humidity –or total suction– and at different OCR values in special large diameter oedometer cells. The dependency of creep deformation on OCR is by no means an academic issue. In fact, it has practical application, since the long term settlements could be controlled by pre-conditioning techniques (pre-compression).

2 Material Used in the Research

Crushed quartzitic Cambric slate from the Pancrudo River outcrop (Aragón, Spain) and used to build the zoned earth and rockfill Lechago Dam was tested.

Table 1. Properties of quartzitic slate.

Property	Value
Uniaxial compression strength*	14.2-31.9 MPa
Density of solids*	2.75 Mg/m^3
Water absorption*	1.36%
Porosity*	6.3-11.8%
Slake durability (5th cycle) (ASTM D4644)**	96.5%
Flakiness index	19%

* Oldecop & Alonso 2001, Chávez & Alonso 2003; ** Standard test method for slake durability of shales and similar weak rocks.

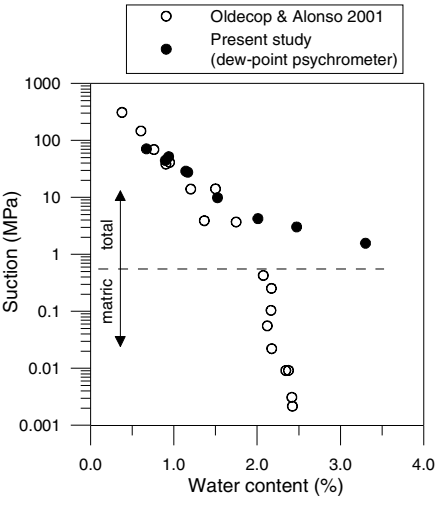

Fig. 1. Retention curve along a drying path for crushed quartzitic slate.

The behaviour of this material has been studied by several authors (see for instance; Oldecop & Alonso 2001, Chávez & Alonso 2003, Chávez et al. 2008). Some properties of the rock material are summarised in Table 1. The material obtained in the quarry was further crushed and sieved. The maximum particle size was fixed at 40mm (before compaction: 10% passing 10-mm sieve and coefficient of uniformity 2.9). The water retention curve of the material along a drying path is shown in Fig. 1.

3 Experimental Program

An oedometer test program was carried out in large diameter cell (300 mm in diameter and approx. 200 mm high). The crushed slate was statically compacted in four layers inside the oedometer ring at a void ratio e_0=0.55±0.03 and water content around w=1% in equilibrium with the relative humidity prevailing at laboratory conditions (approx. 30%). Typical tests involved loading-unloading at saturated state and at constant relative humidity of the air (75% and 30%). The tests performed are summarised in Table 2.

Table 2. Description of the test program performed.

Ref.	Wetting stage	Total suction	Stress applied in long term tests
1	Water at 0.05MPa	0	NC: 0.1; 0.5 and 1 MPa*
			OC: 1.0; 0.87; 0.67 and 0.25 MPa**
2	Vapour	39 MPa	NC: 0.1; 0.5 and 1 MPa*
			OC: 1.0; 0.87; 0.67 and 0.25 MPa**
3	Vapour	160 MPa	NC: 0.1; 0.5 and 1 MPa*
			OC: 1.0; 0.87; 0.67 and 0.25MPa**

*Normally consolidates state. **Overconsolidated states with OCR between 1 and 4.

4 Experimental Results

The evolution of the vertical strain along a loading-unloading path under saturated conditions (ref. 1 in Table 2) is shown in Fig. 2 (on the left). A step loading approach was followed with maximum load duration of 72 hours for overconsolidated states (unloading stages) and 24 hours for normally consolidated conditions. The time evolution of the volume change response under saturated and normally consolidated conditions is presented in the same figure on the right, in which a larger time-dependent compressibility is observed at higher vertical stresses (the different loading steps are indicated in the figure).

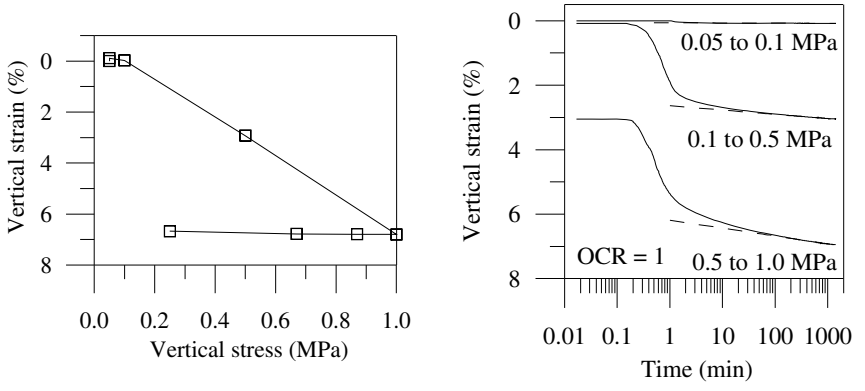

Fig. 2. Volume change results under saturated conditions along a loading-unloading path (left figure). Time evolution of vertical strain in normally consolidated and saturated samples (right figure).

The slope of the vertical strain (ε_v) – log time curves previously presented provides information for the determination of the secondary (time-dependent) compressibility index according to the following equation, which was calculated for elapsed times since load application larger than the reference t_r=100 min

$$C_\alpha = \frac{\Delta\varepsilon_v (1+e_o)}{\Delta \log t} = -\frac{\Delta e}{\Delta \log t} \tag{1}$$

The time dependent compressibility index under normally consolidated conditions $C_{\alpha NC}$ and at different total suctions (refer to Table 2) are plotted in Fig. 3 as a function of the vertical stress σ_v applied, in which the dependency on total suction is readily observed. An equivalent behavioural response was presented by Oldecop & Alonso (2007), in which samples in dry environments displayed nearly null index, consistent with the low crack propagation velocity obtained from the stress corrosion curves at low relative humidity values and with the conceptual model proposed by Oldecop & Alonso (2001). In addition, the compressibility indexes tend to level off at high vertical stresses (usually between 1 and 2 MPa, as shown by Oldecop & Alonso 2007). To limit maximum levelling out, the following empirical expression was used to fit experimental data (Fig. 3) with parameter a, which as a first approximation can depend on total suction

$$C_{\alpha NC} = a\,\sigma_v \Big/ \left(1\text{MPa} + \sigma_v\right) \tag{2}$$

On regarding the time dependent compressibility index under overconsolidated states obtained during the unloading stages, Fig. 4 presents its evolution with OCR. An important reduction in the secondary compressibility was detected at OCR>1, which follows a behavioural response similar to soils (see for instance,

Alonso et al. 2000). The variation of $C_\alpha/C_{\alpha NC}$ for different OCR values was described by the following empirical equation, where α and β are constant parameters that allow reproducing the measured data (α=0 and β=15 are used to plot the curves in Fig. 4).

$$C_\alpha/C_{\alpha NC} = (1-\alpha)\,e^{-\beta(OCR-1)} + \alpha \tag{3}$$

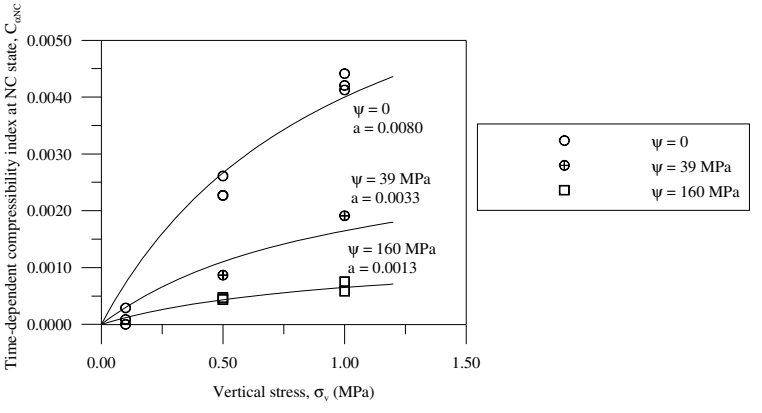

Fig. 3. Time-dependent compressibility index of normally consolidated samples against vertical stress for different constant total suctions.

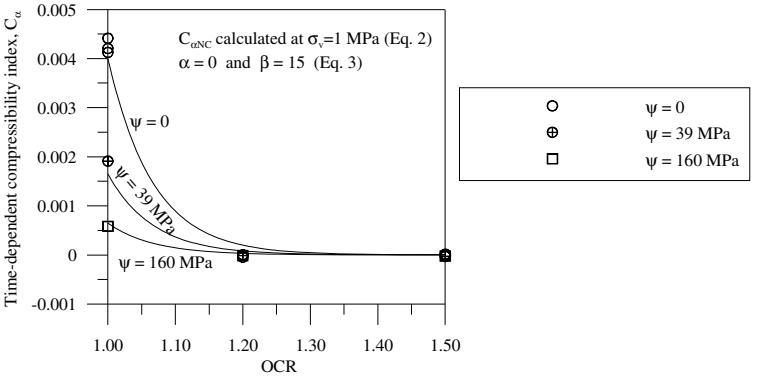

Fig. 4. Time-dependent compressibility index against overconsolidation ratio for different constant total suctions.

5 Conclusions

A crushed quartzitic slate, used in previous investigations on rockfill behaviour, was tested to study the effects of the previous loading history on material delayed

deformations. Typical tests involved loading-unloading samples at constant relative humidity –or total suction– and different OCRs in special large diameter oedometer cells (300 mm in diameter). A finding is that pre-loading the crushed slate at increasing OCRs leads to the progressive vanishing of creep deformations, following a behavioural response similar to soils. The reduction has practical application, since the long term settlements of rockfill materials could be controlled by pre-compression techniques. If at each point of the rockfill embankment an OCR=1.1 is ensured by pre-loading, a reduction to 22% of the normally consolidated long-term settlement would be expected (Eq. (3)).

Acknowledgements. The financial support given by the Universidad de Carabobo (Venezuela) to the third author is greatly acknowledged.

References

Alonso, E.E., Gens, A., Lloret, A.: Precompression design for secondary settlement reduction. Géotechnique 50(6), 645–656 (2000)

Chávez, C., Alonso, E.E.: A constitutive model for crushed granular aggregates which includes suction effects. Soils and Foundations 43(4), 215–227 (2003)

Chávez, C., Romero, E., Alonso, E.E.: A rockfill triaxial cell with suction control. Geotech. Testing J. 32(3), 219–231 (2009)

Oldecop, L.A., Alonso, E.E.: A model for rockfill compressibility. Géotechnique 51(2), 127–139 (2001)

Oldecop, L.A., Alonso, E.E.: Theoretical investigation of the time-dependent behaviour of rockfill. Géotechnique 57(3), 289–301 (2007)

Romero, E., Alonso, E.E., Hueso, O.: Effect of water composition on rockfill compressibility. In: Proc. 16th Int. Conf. on Soil Mechanics and Geotechnical Engineering, Osaka, September 12-16, vol. 3, pp. 1913–1916. Millpress, Rotterdam (2005)

Experimental Study of the Strength and Crushing of Unsaturated Spherical Particles

Bernardo Caicedo and Luis E. Vallejo

Abstract. Numerical models based discrete elements using cylindrical or spherical particles have been used to simulate granular materials. There are few experimental results about the plastic strains on the contacts of the particles, the effect of water content on their strength, and the grain size distribution after crushing. In this study the behaviour of spherical particles under monotonic and cyclic loading is analyzed. The laboratory component of this study involves unsaturated spheres of different diameter made of a mixture of sand and cement and having different strengths.

Keywords: Hertz contact, crushing, granular materials, DEM modelling.

1 Introduction

Granular materials forming part of geotechnical structures like flexible pavements or embankments experience abrasion and crushing as a result of static and dynamic loads applied during the compaction process or during operation.

Numerical models based discrete elements (DEM) using cylindrical or spherical particles has been used to simulate crushing of granular materials; however, to move forward these models in to more realistic conditions it is necessary to provide data of the behaviour of single real particles. Particularly there are few experimental results concerning the plastic strains on the contacts of the particles, the effect of the water content on their strength, and the grain size distribution after crushing.

Bernardo Caicedo
University of Los Andes, Bogotá, Colombia
e-mail: bcaicedo@uniandes.edu.co

Luis E. Vallejo
University of Pittsburgh, Pittsburgh, USA
e-mail: vallejo@pitt.edu

In this study, the behaviour of spherical particles under monotonic and cyclic loading is analyzed. The laboratory component of this study involves unsaturated spheres of different diameter and strength conditioned to different suction levels.

The results of this study provide new experimental data to be implemented in discrete element models to evaluate the behaviour of granular materials in a more realistic way.

2 Experimental Work

2.1 Production of the Spherical Particles

To assess the effect of different parameters like suction, strength and size of the particles in the overall behaviour of granular materials it is crucial to have a method of making particles in a reproducible way. Producing artificial spherical particles allows the control of size, strength, elastic properties, and suction. For the purpose a silicon mould was used, as shown in fig. 1.

The spherical particles were prepared using mortar with increasing different strengths of 12, 20 and 28 MPa; the characteristics of the mortar were chosen to fit the behaviour of sandstones used as a granular material for pavements in Bogotá. Particles were produced with three different diameters of 15, 20 and 25mm.

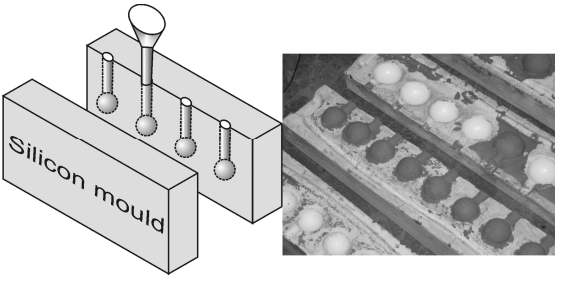

Fig. 1. Silicon mould to prepare spherical particles.

Particles were conditioned at different suction pressures using the vapor equilibrium method, and then their water content was measured. This process allows studying this effect the suction on the strength and stiffness of the spherical particles.

2.2 Experimental Setup

The spherical particles were tested under compression loading using a device that allows the measurement of load and corresponding displacement under compression. This device has the following components (see, fig. 2):

- a set of cylindrical moulds having two windows which allow the location of the LVDT references;
- each mould has rubber cushions located at the top and at the bottom of the two spheres;
- a set of two LVDTs to measure the relative displacement between spheres;
- a loading cell to measure the compression load.

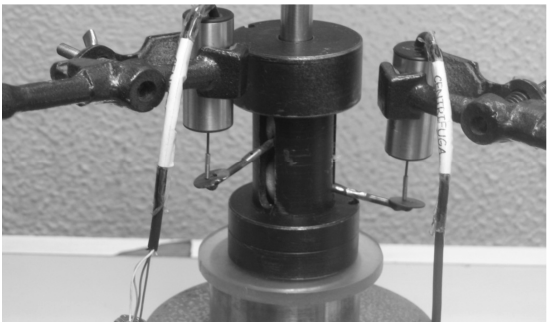

Fig. 2. Experimental setup.

3 Results

Three different aspects are analysed here: load-deformation behaviour under monotonic and cyclic loading, strength and grain size distribution after breakdown.

3.1 Load – Deformation Behaviour

As an example, fig 3(a) presents the load (P)-displacement (α) curves corresponding to a set of particles having 15 mm diameter and conditioned at relative humidity of 10.1%. These curves reveal that the experimental results show a lower stiffness than that predicted by the Hertz theory. This is a clear evidence of plastic strains appearing in the contact between particles at early loads. On the other hand, the Thornton (1997) approach leads to a softer contact between particles compared with the experimental results, the elastoplastic approach proposed by Vu-Quoc & Zhang (1999) allows fitting with good accuracy the experimental results.

Fig. 3(b) presents the experimental results of a set of spheres having the same characteristics than those presented in fig. 3(a). The elastoplastic approach of Vu-Quoc & Zhang (1999) allows fitting the experimental results but only on the loading stage; during unloading the load on the experimental results decrease more rapidly than the decrease of the theoretical model. This discrepancy suggests that during unloading it is necessary to adjust Hertz theory in a similar way than during loading.

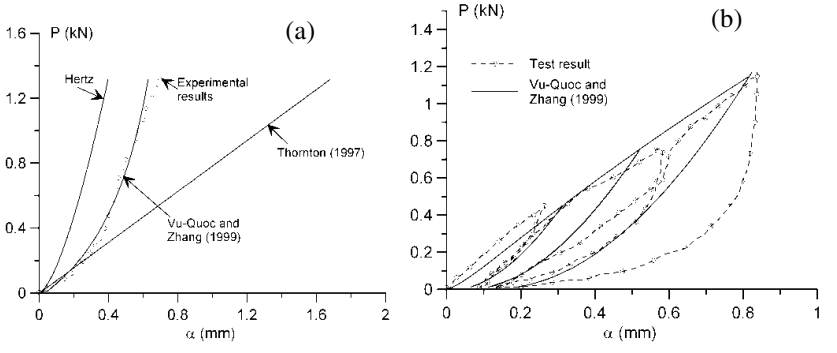

Fig. 3. (a) Monotonic load-deformation curve for 15 mm particles and RH=10.1%, and (b) cyclic load-deformation curve.

3.2 Strength of Particles

Fig. 4 presents the limit compression load at failure upon suction and particle size. As observed, the strength increases with suction; this behaviour is in agreement with the crack growth mechanism proposed by Alonso & Oldecop (2000). To analyze the effect of the particle size it is useful to calculate the characteristic strength defined by Lee (1992) as follows:

$$\sigma = \frac{P}{D^2} \tag{1}$$

Where P is the point load at failure and D is the particle diameter. Lee (1992) also proposes a potential equation to describe the evolution of the strength of particles upon its size:

$$\sigma \propto D^b \tag{2}$$

The parameter b is measured by Lee (1992) is negative, i.e.the strength of the particles reduces as their size increases.

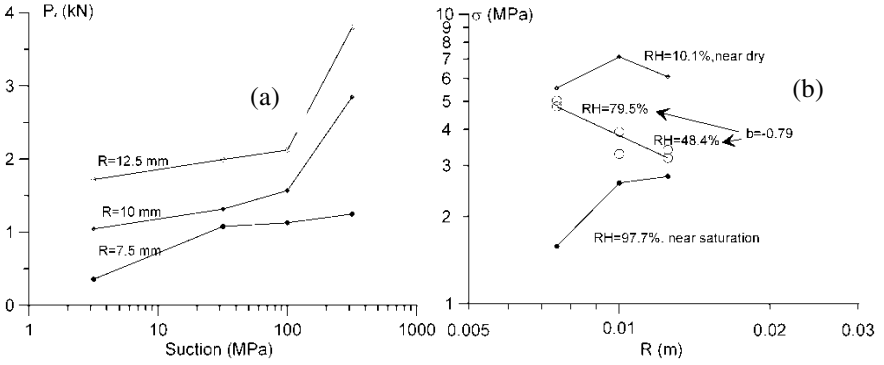

Fig. 4. (a) Limit compression load for particles of different size and suction, (b) limit compression strength for particles of different size and suction.

Fig. 4(b) presents the strength of the particles according with the strength defined by Lee (1992); this figure shows that the trend of particles strength at intermediate relative humidity is in good agreement with the decreasing potential law. However, for particles that approaches the dry or the saturated states the behaviour is different: almost constant strength for dry state and strength increasing with the size for particles near saturation; the source of this discrepancy requires further research.

3.3 Grain size Distribution after Crushing

One of the key points in the analysis of granular materials under crushing is the grain size distribution after particles breakage. Fig. 5 shows the range of grain size distribution after crushing of particles; this range is defined as a function of the relationship between the size of the sub particle and the original size.

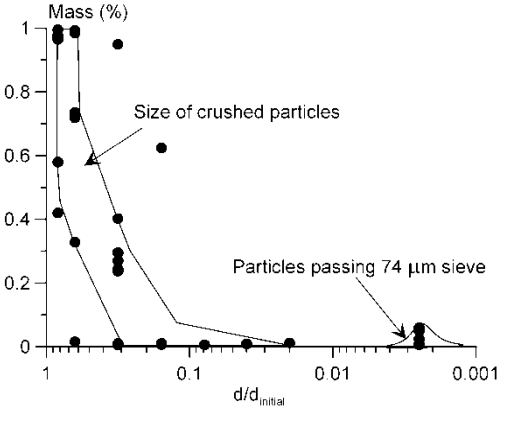

Fig. 5. Grain size distribution of crushed particles.

As observed in fig. 5 the particles after crushing can be grouped in two sets: the first family is made by most of the sub-particles having a size larger than 30% of its original size. On the other hand, a second family of crushed particles has a size lower than 74 μm; these particles are probably coming from the failure surfaces within the particles.

4 Conclusions

This paper presents a research about the behaviour of spherical particles under compression. The following conclusions can be drawn from the experimental results:

- Hertz theory is not a useful theory to describe the behaviour of the contact of particles since plastic strains appears at low loads.
- Using elastoplastic theories it is possible to fit in a better way the loading of spherical particles but modelling unloading requires the development of further theories.
- The effect of suction on the strength of particles is consistent with the sub-critical crack growth propagation proposed by Alonso & Oldecop (2000).
- The results of grain size distribution after crushing provides a useful data to model granular material upon crushing.

References

Alonso, E.E., Oldecop, L.A.: Fundamentals of rockfill collapse. In: 1st Asian Conference on Unsat. Soils., Singapore (2000)

Hertz, H.: “Uber die Ber”uhrung fester elastischer K”orper (On the contact of elastic solids). J. Reine Angewandte Math. 92, 156–171 (1882)

Lee, D.M.: The angles of friction of granular fills, Ph.D. dissertation, University of Cambridge (1992)

Thornton, C.: Coefficient of restitution for collinear collisions of elastic perfectly plastic spheres. ASME Jl. Appl. Mech. 64, 383–386 (1997)

Vu-Quoc, L., Zhang, X.: An elastoplastic contact force–displacement model in the normal direction: displacement-driven version. Proc. R. Soc. Lond. A 455, 4013–4044 (1999)

Author Index